Imperial College of Science, Technology and Medicine

University of London

Behaviour and Design of Transversely Stiffened Plates Subjected to Combined Shear and Direct In-Plane Loading

A thesis submitted for the degree of Doctor of Philosophy
in the Faculty of Engineering of the University of London
and for the Diploma of Imperial College

by

Min Xie

Engineering Structures Section

Department of Civil and Environmental Engineering

August 2000

BIBL. LONDON UNIV.

To:

My Parents

My wife Yiyan Yang

and

our daughter Fangyi

ABSTRACT

Existing design methods for web stiffeners differ widely in concept and in the stiffener size which results. The purpose of this thesis is to further behavioural understanding by experimental, analytical and numerical studies, and to provide a rational, usable and validated design and assessment method for transverse stiffeners, based on the non-linear buckling theory.

Tests were conducted on transversely stiffened plate girders with different geometrical configurations and loading arrangements. The experiments were aimed primarily at validating the elasto-plastic post-buckling behaviour as represented by the finite element program, and at revealing unforeseen phenomena.

The finite element program ABAQUS was used to carry out parametric studies to examine the critical buckling and post-buckling behaviour of stiffened web plates, having a wide range of side and slenderness ratios, subjected to combined shear, compression and bending. External forces acting on the stiffeners were also included.

Analytical studies were undertaken to provide a rational basis for developing a stiffener design model. The internal forces acting on a stiffener were clarified and quantified by the finite element solutions, in conjunction with the simple approximate analytical equations.

The proposed design model for transverse stiffeners takes account of the local panel bending and overall buckling effects, and the stiffener axial force due to the tension field action and to externally applied forces. The design model was validated by reference to finite element solutions and experimental results, and is applicable to concentric and eccentric transverse stiffeners. When compared with the finite element solutions, the proposed model is shown to give more consistent results for stiffener sizes which satisfy the design criteria, than do existing design methods.

ACKNOWLEDGEMENTS

The research presented in this thesis was sponsored by the EPSRC, and was supervised by Professor John C. Chapman. I am deeply grateful to Professor Chapman for his generous and helpful guidance throughout the period of this project, and for the many hours spent in discussions which stimulated plentiful food for thought. I want to thank Professor Chapman sincerely for making my research years educational, informative, and very enjoyable.

My sincere thanks go to Professor Roger E. Hobbs, Dr Paul C. Davidson and Dr Luke A. Louca for their generous support and encouragement. I would also like to thank Dr Graeme S. Stanway for his kind help and the time spent in fruitful discussions.

The experimental work reported in this thesis was facilitated by the skilled team of staff in the Engineering Structures Laboratory. My thanks go to Messrs Tony Boxall, Alan Roberts and Ron Millward for passing freely of their technical expertise in experimental work. In particular, I would like to thank Mr Alan Roberts for the masterly welding skill he exercised in fabricating the test girders, and for his patience and commitment to the test programme.

Other member of staff whom I would like to thank are Mr Colin Kerr, Miss Fionnuala Donovan, Miss Susannah Parry and Mr Mark Soole, for being friendly and helpful.

My thanks go to my fellow research colleagues including Dr Gary Chou, Dr Lionel Fortune, Mr Sengkwan Choi, Dr V. Chinien, Mr J. Friis, Dr K. Nanou, Mr A. Richardson, Dr T. Riginotis, Dr G. Sterrit and Mr L. Gardner. My thanks also go to my friends and colleagues at East China Jiaotong University.

Finally, I am deeply grateful to my wife Yiyan Yang and our daughter Fangyi, not only for their patience, understanding and generous support, but also for enabling me to enjoy our happy family life. Words of thanks also go to my parents and my brother and sister for their continuous support and constant encouragement.

CONTENTS

ABSTRACTS.....3
ACKNOWLEDGEMENTS.....4
CONTENTS.....5
INDEX – TABLES.....12
NOTATION.....13

CHAPTER 1 **INTRODUCTION**

1.1 Background.....18
1.2 Overview of Previous Research.....20
1.2.1 Brief Historical Review.....20
1.2.2 Buckling of Plate Panels.....21
1.2.3 Buckling of Stiffened Plates.....23
1.2.4 Design of Transverse Stiffeners.....26
1.2.5 Experimental Work.....29
1.3 Objectives of Thesis.....31

CHAPTER 2 **EXPERIMENTAL STUDY ON STIFFENED PLATE GIRDERS**

2.1 Introduction.....34
2.2 Test Girders.....35
2.2.1 Dimensions.....35
2.2.2 Manufacture.....38
2.2.3 Reinforcement of Stiffeners.....40
2.3 General Arrangement.....40
2.3.1 Test Rig.....40
2.3.2 Instrumentation.....43
2.3.3 Test Procedure.....44
2.4 Finite Element Models for Test Girders.....45
2.5 Experimental Results and Comparison with FE Solutions.....47
2.5.1 Girder GI.....49
2.5.2 Girder GII.....58
2.5.3 Girder GIII.....68
2.5.4 Girder GIV.....78

2.6 Discussion and Analysis 88
2.6.1 Effects of Flanges on the Required Stiffener 88
2.6.2 Forces in Stiffeners 91
2.6.3 Comparison between single-sided and double-sided stiffeners 91
2.6.4 Failure Mode of Stiffener 93
2.6.5 Effects of Residual Stresses 93
2.7 Conclusions 94

CHAPTER 3 **FINITE ELEMENT MODELLING**

3.1 Introduction 97
3.2 Structural Configuration 98
3.3 Stiffener Type 99
3.4 Material Properties 101
3.5 Boundary Conditions 101
3.6 Initial Imperfections 103
3.6.1 Imperfection Mode 103
3.6.2 Imperfection Magnitude 106
3.7 Residual Stresses 108
3.8 Mesh Size and Convergence Study 109
3.8.1 General 109
3.8.2 Critical Buckling Stress 111
3.8.3 Ultimate Strength 112
3.8.4 Maximum Panel Deflection, w_p 113
3.8.5 Lateral Distributed Forces on the Supported Panel Edges, q_{pn} 115
3.8.6 FE Meshes Adopted for the Parametric Study 115

CHAPTER 4 **PRELIMINARY STUDY ON LATERAL KNIFE EDGE FORCES**

4.1 Introduction 117
4.2 Structure Modelling (Definition of Knife Edge) 118
4.3 Forces Acting on the Knife Edge 119
4.3.1 Distributed Reactive Force on the Knife Edge, q_{pk} 119
4.3.2 Relationship Between q_{pk} and q_{pn}, the Panel Edge Reaction 121
4.4 Determination of q_{pk} and M_{pk} in Finite Element Analyses 124
4.4.1 Reaction at the Supported Edge, q_{Qx} 124
4.4.2 Bending Moment due to the Distributed Reaction 126
4.5 Explicit Equations for the Non-linear Elastic Buckling Behaviour of Plates 127
4.5.1 Analytical Solutions of Uniaxially Compressed Rectangular Plates 127

4.5.2 Proposed Equations 128
4.5.2.1 Maximum Panel Deflection w_p 129
4.5.2.2 Lateral Distributed Force q_{pn} 130
4.6 Non-linear Elastic FE Analyses 130
4.6.1 CUCU Panels 130
4.6.1.1 Panel Deflection w_p/t 130
4.6.1.2 Lateral Distributed force q_{pn} 134
4.6.2 CUCU Plates with an intermediate knife edge 138
4.6.2.1 Deflection in the Plate Panel, w_p/t 138
4.6.2.2 Lateral Distributed Force on the Knife Edge, q_{pk} 142
4.7 Explicit Equations for the Knife Edge Bending Moment 148
4.7.1 Proposed Equations 148
4.7.2 Calibration with Non-linear Elastic Finite Element Results 150
4.8 Conclusions 155

CHAPTER 5 BENDING MOMENTS IN STRAIGHT KNIFE EDGES

5.1 Introduction 157
5.2 Plates subjected to Pure Shear 158
5.2.1 Critical Buckling Behaviour 158
5.2.1.1 Critical Buckling Modes 159
5.2.1.2 Critical Buckling Stresses 162
5.2.2 Non-linear Elastic Buckling Behaviour 163
5.2.2.1 Deflection Modes 163
5.2.2.2 Distribution of q_{pk} and M_{pk} 167
5.2.2.3 Magnitude of Bending Moment in the Knife Edge, M_{pk} 169
5.2.3 Comparison of the Bending Moments in the Knife Edge and the Stiffener 184
5.2.4 Effects of Axial Rigidity of Stiffener on M_{pk} 186
5.2.5 Contribution of M_{pk} to the Stiffener Bending Moment M_s 187
5.2.6 Design Formulae for Predicting M_{pk} 191
5.3 Plates subjected to Combined Loading 194
5.3.1 General 194
5.3.2 Combined Shear and Compression 195
5.3.2.1 Critical Buckling Behaviour 195
5.3.2.2 Non-linear Elastic Buckling Behaviour 201
5.3.2.3 Design Formulae for Predicting M_{pk} 211
5.3.3 Combined Shear and Bending 214
5.3.3.1 Critical Buckling Behaviour 214
5.3.3.2 Non-linear Elastic Buckling Behaviour 220

5.3.3.3 Design Formulae for Predicting M_{pk} 230
5.4 Summary of the Design Formulae for Predicting M_{pk} 233
5.5 Conclusions....234

CHAPTER 6 **AXIAL FORCES IN STIFFENERS**

6.1 Introduction....239
6.2 Structural Modelling 240
6.3 Tension Field Theory 242
6.3.1 Basler's Model 243
6.3.2 Comparison with FE Solutions....244
6.4 Proposed Equation for Predicting P_s....245
6.4.1 Proposed Equation for P_s....245
6.4.2 Discussion on the Proposed Equation....247
6.5 Plates subjected to Pure Shear....248
6.5.1 Distribution of the Axial Force in the Stiffener....249
6.5.2 Magnitude of the Axial Force in the Stiffener....250
6.6 Plates subjected to Combined Loading 252
6.6.1 General 252
6.6.2 Combined Shear and Compression....261
6.6.2.1 Distribution of Axial Force in the Stiffener 261
6.6.2.2 Magnitude of Axial Force in the Stiffener 261
6.6.2.3 Comparison of Proposed Equations with FE Solutions....266
6.6.3 Combined Shear and Bending 267
6.6.3.1 Distribution of Axial Force in the Stiffener 267
6.6.3.2 Magnitude of Axial Force in the Stiffener 276
6.6.3.3 Comparison of Proposed Equations with FE Solutions....277
6.7 Summary of the Design Formulae for Predicting P_s 282
6.8 Conclusions....282

CHAPTER 7 **OVERALL BUCKLING MODELS**

7.1 Introduction....284
7.2 Rigid-Link Model 285
7.2.1 Basis of the Model....285
7.2.2 Pure Shear Condition....286
7.2.2.1 Initially Straight Stiffener, $w_{0s}=0$ 286
7.2.2.2 Initially Imperfect Stiffener, $w_{0s}\neq0$ 289
7.2.3 Compressive Loading Condition 291

7.2.3.1 Initially Straight Stiffener, w_{0s}=0 291
7.2.3.2 Initially Imperfect Stiffener, $w_{0s}\neq0$ 293
7.2.4 Pure Bending Condition 294
7.2.4.1 Initially Straight Stiffener, w_{0s}=0 294
7.2.4.2 Initially Imperfect Stiffener, $w_{0s}\neq0$ 296
7.2.5 Discussion 297
7.3 Beam-Plate Model 298
7.3.1 Basis of the Model 298
7.3.2 Pure Shear Condition 301
7.3.2.1 Initially Straight Stiffener, w_{0s}=0 301
7.3.2.2 Initially Imperfect Stiffener, $w_{0s}\neq0$ 303
7.3.3 Compressive Loading Condition 305
7.3.3.1 Initially Straight Stiffener, w_{0s}=0 305
7.3.3.2 Initially Imperfect Stiffener, $w_{0s}\neq0$ 308
7.3.4 Pure Bending Condition 309
7.3.4.1 Initially Straight Stiffener, w_{0s}=0 309
7.3.4.2 Initially Imperfect Stiffener, $w_{0s}\neq0$ 311
7.3.5 External Stiffener Forces 313
7.3.5.1 External Forces at Both Ends 313
7.3.5.2 External Force at One End 315
7.4 Proposed Interaction Equations for Combined Loading 319
7.5 Conclusions 321

CHAPTER 8 PROPOSED DESIGN MODEL FOR TRANSVERSE STIFFENERS

8.1 Introduction 323
8.2 Effects of Panel Plasticity 325
8.2.1 General 325
8.2.2 Bending Moment due to the Local Panel Bending Effect 325
8.2.3 Axial Force in the Stiffener 329
8.3 Determination of Forces in Stiffeners 331
8.4 Ultimate Strength of Simply Supported Panels 334
8.5 Strength Criterion for Stiffener Design 336
8.5.1 Calculation of Stiffener Stresses 337
8.5.2 Strength Requirement 338
8.5.3 Required Stiffener Size According to the Strength Criterion 339
8.5.3.1 Plates subjected to Pure Shear 340
8.5.3.2 Plates subjected to Combined Shear and Compression 346
8.5.3.3 Plates subjected to Combined Shear and Bending 347

8.6 Stiffness Criterion for Stiffener Design 349
8.6.1 Calculation of Stiffener Deflection 350
8.6.2 Design Limit of Stiffener Deflection 352
8.6.3 Required Stiffener Size According to the Stiffness Criterion 358
8.6.3.1 Plates subjected to Pure Shear 358
8.6.3.2 Plates subjected to Combined Shear and Compression 359
8.6.3.3 Plates subjected to Combined Shear and Bending 362
8.7 Design of Single-sided Stiffeners 363
8.7.1 Modelling of Single-sided Stiffeners 365
8.7.2 Stress Distribution along the Width of Stiffener 365
8.7.3 Calculation of Stiffener Stresses 367
8.7.4 Stiffener Deflection and Its Design Limit 369
8.7.4.1 Calculation of Stiffener Deflection 369
8.7.4.2 Design Limit of Stiffener Deflection 370
8.7.5 Required Stiffener Size 371
8.7.6 Comparison with Double-sided Stiffeners 373
8.8 Proposed Design Procedure 376
8.8.1 Intermediate Stiffeners 377
8.8.2 Special Considerations for Load Bearing Stiffeners 380
8.9 Conclusions 383

CHAPTER 9 COMPARISONS OF THE PROPOSED MODEL WITH EXISTING METHODS AND RESULTS FOR TEST GIRDERS

9.1 Introduction 387
9.2 Existing Design Methods 388
9.2.1 BS5400 388
9.2.2 Eurocode 3 389
9.2.3 AASHTO 390
9.2.4 Horne & Grayson 391
9.2.5 Rahal & Harding 392
9.2.6 Stanway, Chapman & Dowling 393
9.3 Comparison with Existing Design Methods 395
9.3.1 Required Stiffener Sizes 395
9.3.1.1 Double-sided Stiffeners 395
9.3.1.2 Single-sided Stiffeners 402
9.3.2 Comments 404
9.3.2.1 BS5400 404
9.3.2.2 Eurocode 3 405

9.3.2.3 AASHTO 406
9.3.2.4 Horne & Grayson 407
9.3.2.5 Rahal & Harding 407
9.3.2.6 Stanway, Chapman & Dowling 408
9.3.2.7 Proposed Model 408
9.4 Comparison with Results for Test Girders 409
9.4.1 Proposed Model 410
9.4.2 Existing Design Methods 412
9.5 Conclusions 415

CHAPTER 10 **CONCLUSIONS AND RECOMMENDATIONS FOR FUTURE WORK**

10.1 Recapitulation and General Conclusions 418
10.2 Recommendations for Future Work 422

REFERENCES 425

APPENDIX A **FINITE ELEMENT PROGRAM ABAQUS**

A.1 Description of ABAQUS 431
A.2 Numerical Study on Shell Elements 433
A.3 Numerical Study on Beam Elements 439

APPENDIX B **POST-BUCKLING ANALYSIS OF SIMPLY SUPPORTED PLATES IN UNIAXIAL COMPRESSION** 442

APPENDIX C **COMPARISONS OF ABAQUS SOLUTION WITH FINASIC SOLUTION**

C.1 Introduction 448
C.2 Critical Buckling Stress 449
C.3 Ultimate Strength 449

APPENDIX D **FORTRAN PROGRAM FOR STIFFENER DESIGN** 453

INDEX — TABLES

Table ..... Page

2.1a 37
2.1b 37
2.2 38
2.3 49
3.1 110
4.1 131
4.2 131
4.3 134
4.4 143
4.5 144
4.6 150
5.1 167
5.2 169
5.3 188
6.1 250
8.1 328
8.2 334
8.3 335
8.4 336
8.5 336
8.6 336
8.7 356
8.8 360
8.9 363
8.10 367
8.11 372
9.1 396
9.2 400
9.3 403
9.4 404
9.5 410
9.6 414

NOTATION

a	panel width
a_m, A_m	coefficients in deflection functions, m=1, 2, 3, ...
A_s	cross-sectional area of stiffener
b	small panel dimension, b=min{a, d}. *b=540mm* is used in the parametric study presented in this thesis
C, C_i	coefficients used in proposed equations, i=1, 2, 3, ...
CUCU	in-plane boundary conditions, in order of the left, top, right and bottom edges of the plate (Fig. 3.2)
d	panel depth and length of stiffener
D	flexural rigidity of plate, $D=Et^3/12(1-\nu^2)$
e	the distance between the central line of the plate section and the centroidal axis of the cross-section of a single-sided stiffener (Fig. 8.16)
E	modulus of elasticity ($E=2.05\times10^5 N/mm^2$)
F_{pl}	empirical factor for the effect of panel plasticity on the knife edge moment, $F_{pl}=M_{pb}/M_{pk}$ (Fig. 8.2)
G	shear modulus of elasticity, $G=E/2(1+\nu)$
Gi	i^{th} test girder, i=I, II, III, IV (Fig. 2.1 and Table 2.1)
h	$h_s+t/2$ (Fig. 3.1)
h_s	depth of stiffener on one side of plate (Fig. 3.1)
I_s	moment of inertia of stiffener
J_s	torsion constant of stiffener
k_{cr}	critical buckling stress coefficient
k_{cro}	overall buckling stress coefficient for the rigid-link model
k_{ov}	overall buckling stress coefficient for the beam-plate model
k^0_{ov}	overall buckling stress coefficient for unstiffened plates (Ψ=0)
k_{Qov}	overall buckling load coefficient for the beam-plate model subjected to external stiffener forces

M_{ov} stiffener bending moment due to the overall buckling effect, derived from the beam-plate model

M_{pb} stiffener bending moment due to the effect of local panel bending, $M_{pb}=F_{pl}\cdot M_{pk}$

M_{pk} bending moment in straight knife edge, derived from the lateral distributed force on the knife edge

M_{pn} bending moment at the centre of an edge of a simply supported panel

M_{ps} plastic moment capacity of stiffener

M_s stiffener bending moment

M_x, M_y bending moments per unit length of plate section, about the y and x axes, respectively

M_{xy} twisting moment per unit length of plate section perpendicular to the x axis

N Number of FE elements across the smaller panel dimension

P load applied on test girders (Fig. 2.1)

$P_{i-(i+1)}$ web panel located between i^{th} and $(i+1)^{th}$ stiffeners on the test girder

P_s axial force in stiffener, $P_s>0$ for compression

P_{sq} axial squash load of stiffener, $P_{sq}=\sigma_{0s}\cdot A_s$

q distributed lateral force per unit length

q_{Mxy} distributed lateral reaction per unit length due to the twisting moment M_{xy}

q_{pk} distributed lateral force per unit length acting on a straight knife edge

q_{pn} distributed lateral force per unit length acting on an edge of a simply supported panel

q_{Qx} distributed lateral reaction per unit length due to the shearing force Q_x

q_{Vx} distributed lateral reaction per unit length due to the total reactive force V_x

Q_x shearing force, parallel to the z axis, per unit length of plate section perpendicular to the x axis

Q_1 external force acting at one end of the stiffener

$Q_{1,ov}$ overall buckling load for the beam-plate model subjected to external force acting at one end of the stiffener

Q_2 external force acting at both ends of the stiffener

$Q_{2,ov}$ overall buckling load for the beam-plate model subjected to external force acting at both ends of the stiffener

Si	i^{th} stiffener on the test girder, i=1, 2, ..., starting from the left end stiffener (Fig. 2.1)
t	thickness of plate panel
t_s	thickness of stiffener
T	work done by the applied load
u	displacement in x direction
U_{pb}	bending strain energy in plate panel
U_{sb}	bending strain energy in stiffener
v	displacement in y direction
V	shear force
V_x	total reaction, parallel to the z axis, per unit length of plate section along a supported edge perpendicular to the x axis, $V_x = Q_x - \partial M_{xy}/\partial y$
V_u	ultimate shear force
V_u'	$V_u/(\tau_0 dt)$
w	additional deflection (in z direction)
w_p	additional panel deflection
w_s	additional stiffener deflection
w_{sd}	the design limit of the additional stiffener deflection
w_{su}	additional stiffener deflection at the ultimate load of stiffened plates
w_0	initial deflection
w_{0p}	initial panel deflection
w_{0s}	initial stiffener deflection
x,y,z	rectangular coordinates
Z_s	stiffener section modulus
α	panel aspect ratio, α=d/a
β_b	equivalent shear stress factor for bending
β_c	equivalent shear stress factor for compression
δ	vertical deflection of test girder
δ_b	vertical deflection of test girder, due to bending
δ_s	vertical deflection of test girder, due to shear alone
ε	direct strain

ε_x, ε_y	direct strain in the x and y directions, respectively
ε_0	yield strain, $\varepsilon_0=\sigma_0/E$
Γ	stiffener torsional rigidity parameter, $\Gamma=GJ_s/Db$
μ_u	relative shear strength ratio, less than or equal to unity (Eqn. 8.10)
ν	Poisson's ratio ($\nu=0.3$)
Π	total potential energy
θ	inclined angle of rigid-link
θ_x, θ_y, θ_z	rotations about the x, y and z axes, respectively
σ_b	applied bending stress (Fig. 3.1)
$\sigma_{b,cr}$	critical buckling bending stress
$\sigma^0_{b,cr}$	critical bending stress of plate panel, subjected to pure bending
$\sigma_{b,ov}$	overall buckling bending stress for the beam-plate model
σ_{bu}	ultimate bending stress
σ_{bu}'	σ_{bu}/σ_0
σ_c	applied compressive stress (Fig. 3.1)
σ_{cr}	critical buckling stress
$\sigma_{cr,ss}$	critical buckling stress of individual simply supported panel
$\sigma_{c,cr}$	critical buckling compressive stress
$\sigma^0_{c,cr}$	critical compressive stress of plate panel, subjected to compression alone
$\sigma_{c,ov}$	overall buckling compressive stress for the beam-plate model
σ_{cu}	ultimate compressive stress
σ_{cu}'	σ_{cu}/σ_0
σ_s	stress in stiffener
$\sigma_{s,max}$	maximum stress in stiffener
σ_t	tension band stress (Fig. 6.2)
σ_x, σ_y	direct stress in the x and y directions, respectively
σ_0	yield stress
σ_{0p}	yield stress of plate panel
σ_{0s}	yield stress of stiffener
τ	applied shear stress (Fig. 3.1)

τ'	non-dimensional shear stress, $\tau'=\tau/\tau_0$
τ_{cr}	critical buckling shear stress
$\tau_{cr,ss}$	critical buckling shear stress of individual simply supported panel
τ^0_{cr}	critical buckling shear stress of plate panel, subjected to pure shear
τ_{eq}	equivalent shear stress
τ_u	ultimate shear stress
τ_{ov}	overall buckling shear stress for the beam-plate model
τ_u'	τ_u/τ_0
$\tau_{u,ss}$	ultimate shear stress of simply supported panels
$\tau_{u,ss}'$	$\tau_{u,ss}/\tau_0$
τ_0	shear yield stress, $\tau_0=\sigma_0/\sqrt{3}$
Ω	stiffener extensional rigidity parameter, $\Omega=A_s/a\,t$
Ω_d	Ω of the smallest stiffener required
Ψ	stiffener flexural rigidity parameter, $\Psi=EI_s/Db$
Ψ_d	Ψ of the smallest stiffener required, $\Psi_d=\max\{\Psi_{dZ}, \Psi_{dI}\}$
Ψ_{dZ}	Ψ of the smallest stiffener which satisfies the strength criterion (Eqn. 8.7)
Ψ_{dI}	Ψ of the smallest stiffener which satisfies the stiffness criterion (Eqn. 8.11)
Ψ_e	Ψ of the smallest stiffener, of those examined, which remains fully elastic at the ultimate load of stiffened plates
Ψ_p	Ψ of the largest stiffener, of those examined, which has yielded at the ultimate load of stiffened plates
Ψ_{ssu}	the stiffener rigidity required to develop the ultimate strength of simply supported panels
Ψ_w	the stiffener rigidity for which the stiffener deflection at the ultimate load is equal to the deflection limit specified in the stiffness criterion

CHAPTER 1

INTRODUCTION

1.1 BACKGROUND

Stiffened plates can be found in ships, bridges, aircraft, buildings and offshore structures.

Different arrangements of stiffeners are used to reinforce the plate. The geometry commonly used is rectangular plates reinforced by one or two orthogonal directions of stiffeners parallel to the edges. Only transversely stiffened plates are considered in the present investigation.

Stiffeners can be placed on one or both sides of plate. Various stiffener cross-section shapes have been used in engineering practice, such as flat bar, bulb flat, angle, Tee and closed stiffeners. Only open cross section stiffeners will be considered in this study.

Transverse stiffeners are used mainly to enhance the plate strength by subdividing the plating into smaller panels. Some stiffeners carry additional external forces applied to one or both ends of the stiffener. These stiffeners are known as load bearing stiffeners. The stiffeners with no external forces on it are described as intermediate stiffeners. Both will be investigated in the present study.

Following the change from the allowable stress design philosophy to the limit state design philosophy, a considerable amount of research has been conducted to examine the post-buckling and collapse behaviour of steel plated structures. Consequently, many ultimate load methods of design have been produced and several codes of practice were revised, and these have been used to date for the design of bridges and other structures.

Existing limit state design methods differ widely in concept and in the stiffener size which results [1]. Some approaches are based on critical buckling, taking no account of the effects of initial imperfections in the plate and stiffener, or of post-buckling effects. For these reasons, some methods employ an empirical factor to the required stiffener rigidity obtained from the critical buckling criterion [2]. Other approaches, including the current British Standard BS5400 [3] and EUROCODE 3 [4], are based principally on in-plane forces resulting from tension field action and do not give sufficient rational recognition to the out-of-plane forces on the stiffener exerted by panel bending. By designing stiffeners primarily to resist axial forces, the stiffener required by these approaches tends to become progressively more conservative as the panel depth/length ratio increases. In work by Rahal and Harding [5, 6, 7] the importance of out-of-plane forces is recognised, but the empirical formulation for stiffener force is based on a very limited range of panel aspect ratios beyond which significant changes in stiffener and plate behaviour occur.

For webs in shear, recent studies at Imperial College [1,8,9] have demonstrated that the axial forces on the stiffener are of secondary importance, and that out-of-plane forces provide a more rational basis for design. The local panel bending effects and the significance of the tendency for stiffened plates to buckle overall are identified. The studies led to the formulation of a design model, which shows good agreement with elasto-plastic finite element analyses. However, the model has been validated only for concentric flat bar stiffeners on a web having two panels, and only shear is considered.

Plate and box girders are subjected to in-plane bending and compressive stresses in addition to the shear. These stresses exert extra destabilising effects on the transverse stiffener. By further theoretical analysis, numerical parametric studies, and experimental verification, the present investigation aims to develop a design model for both intermediate and load bearing stiffeners with various open cross-section shapes, subjected to combined shear, bending and compression. Possible simplification and modification to the design model [9] will be investigated.

1.2 OVERVIEW OF PREVIOUS RESEARCH

1.2.1 Brief Historical Review

The wide application of stiffened plates in engineering began in the nineteenth century, mainly with the application of steel plates for hulls of ships and with the development of steel bridges.

In the period of 1902 to 1914, Boobnov [10] made a contribution by applying a stress analysis to steel stiffened plates. The stability problem of stiffened plates, and especially the problem of the minimum rigidity of the stiffeners required to restrict buckling in a stiffened plate to the plating between the stiffeners was considered in 1915 by Timoshenko [11,12]. He proposed the energy method to solve the problem.

The extensive use of slender and thin-walled structures in aircraft motivated a considerable amount of research in post-buckling behaviour. The practical interest of a nonlinear theory was recognised in the 1930's (such as the diagonal tension theory proposed in 1931 by Wagner [13] for very thin web panels) and the general post-buckling theory of elastic structures was enunciated by Koiter [14] in 1945. He established that imperfections might result in significant reductions of the critical load, which explained the discrepancy between linear theories and experiments.

The first experimental studies on large scale stiffened plate girders subjected to bending were conducted by Massonnet [15] in 1954. It was observed that the stiffeners worked effectively in the post-buckling range of the plates.

Post-buckling analysis in the plastic range is considerably complicated due to the geometric and material non-linearities. Until computer programs with large displacements and plasticity became available after 1970, relatively little work had been done on the effect of stiffening in the post-buckling range of the plates. Numerical analyses based on non-linear finite difference method were produced at Imperial

College in 1977 for stiffened plates [16]. Crisfield [17] developed both single layer and multi-layer analyses using finite elements, and the method was applied to the analysis of unstiffened and lightly stiffened box girder diaphragms.

Since the late 1970s, by using various established non-linear finite element packages, extensive numerical simulations have been conducted to investigate the plastic post-buckling behaviour and imperfection sensitivity of stiffened plates. In general, the current knowledge about the non-linear buckling behaviour of stiffened plates relies mainly on numerical solutions, although some experimental studies have been carried out.

1.2.2 Buckling of Plate Panels

The governing differential equation for critical buckling of a plate was originally established by Saint Venant [18] in 1883. Bryan [19] presented the expression for strain energy of a plate, and obtained the first solution for critical buckling of plates under uniform in-plane compression. The first exact solution for the critical buckling of plates in shear was provided in 1924 by Southwell and Skan [20] for an infinite strip. Approximate solutions for the shear buckling of rectangular plates have been given by Stein and Neff [21] for the case of simply supported edges, and by Budiansky and Connor [22] for the case of clamped edges. Critical combinations of shear and longitudinal compression were evaluated by Batdorf and Stein [23] for simply supported plates. In their work, a ten terms' series function was used to represent the deflection of the plate. In 1936, Way [24] presented the solutions for simply supported plates under combined shear and bending, using an eight terms series function of deflection. The evaluation of critical buckling stresses of rectangular plates has been undertaken by many researchers, and solutions have been obtained for various loading and boundary conditions [25].

The large deflection theory, which takes account of the stretching of the mid-plane of the plate, is used to study the behaviour of plates in the post-buckling region. In 1910, von Kármán [26] derived the equations governing the elastic post-buckling behaviour of

plate. These equations were generalised by Marguerre [27] to include geometric imperfections and by Skaloud and Donea [28] to take into account the effect of residual stresses. Due to the difficulty in solving these differential equations, post-buckling behaviour is normally investigated by the energy method or numerical techniques. Bulson [29] has reported some post-buckling solutions of plates.

Theoretical treatments of large-deflection elasto-plastic buckling of plates in compression have been conducted by Moxham [30] using a Ritz energy method, Crisfield [17] using a finite element technique, and Frieze et al [31] using a finite difference — dynamic relaxation formulation. The latter work formed the basis of the plate effective width factors in BS5400.

Basler [32] studied the post-buckling behaviour and ultimate strength of plate girder web panels by means of the tension field theory. It was assumed that the flanges do not possess sufficient flexural rigidity to resist the lateral loading imposed by the inclined tension field, and therefore the diagonal tension field does not develop near the web-flange connection and the web collapses after development of an off-diagonal yield band. In contrast, Porter et al [33] developed an ultimate load theory based on the assumption that the flanges are able to anchor the diagonal tension field. As a result, plastic hinges form after development of the yield zone and finally, the web panel fails in a sway mechanism. In design of web panels, the current American AASHTO specification [34] and British Standard BS5400 [3] adopt these two failure theories respectively.

Parametric studies on ultimate strength of simply supported plates under combined shear and direct in-plane loading were carried out by Harding et al [35] using the dynamic relaxation technique. The effects of slenderness, aspect ratio, geometric imperfection, residual stress, material strength, and strain hardening were examined. The loading combinations considered were combined uniform direct and shear loading, combined triangular direct and shear loading, and combined bending and shear loading. The in-plane loading was applied as a combination of axial and shear displacements, and the unloaded panel edges were either unrestrained or restrained. Using the results of

this study, the interaction equation, originally presented by Horne et al [36], was adopted to establish a design formulation [37]. In the British Code BS5400 a revised formula has been introduced to allow redistribution of direct stresses in a shear situation. The background to this formula and its use in design are explained by Harding and Dowling [38].

By using the non-linear elasto-plastic finite element program FINASIC, Chapman and Davidson [39] performed an extensive investigation into the behaviour and design of panels under shear loading. The influence of a realistic range of possible boundary conditions was examined. The initial imperfection was taken as a standard sinusoidal wave with amplitude envisaged in BS5400 for mild steel [51]. Numerical solutions were obtained for a range of aspect ratios and slenderness ratios. Comparisons of panel strength were made with alternative tension field models and several design codes, and significant differences existed between these approaches. It was found that the codes examined considerably overestimate the strength of a tall plate relative to that of a long plate. Based on further elasto-plastic numerical analyses, Davidson et al [40,41] proposed a design model that enables the strength of rectangular plates under uniaxial and biaxial compression, with or without coexistent shear or lateral pressure, to be determined. The interaction relations were compared with existing design rules, which were variously found to be either conservative or non-conservative.

1.2.3 Buckling of Stiffened Plates

Until the early 1960's, work concerning the stability of stiffened plates was based upon elastic plate buckling theory. Different stability problems of stiffened plates have been analysed in the monographs [25, 29]. The general theory of stiffened plates simply supported along their edges, with zero torsional rigidity stiffeners, was developed by Klöppel and Scheer [42]. When the number of parallel stiffeners exceeds three, the orthotropic plate approach was used, where the stiffened plate was considered as an orthotropic plate with smeared rigidities. Based on computer calculations, Klöppel et al [42,43] presented extensive results for practical use.

Theoretical investigation into the elastic post-buckling behaviour of stiffened plates were undertaken by Skaloud et al [44] in 1967. By means of the energy method with a 6-term series function of deflection, a square stiffened plate subjected to uniform shear was analysed, and the stiffeners were found to work in the post-buckling range of the plates.

A parametric finite element study on the ultimate strength of transversely stiffened web panels subjected to shear was carried out by Horne and Grayson [45], with the aim of deriving a simple design rule for transverse web stiffeners. The parameters examined include the panel aspect ratio, the plate slenderness and the stiffener rigidity. The initial geometric imperfections assumed were double sinusoidal in form with magnitudes equal to the tolerance specifications of the British Standard BS5400 [51]. The effects of residual stresses on required stiffener rigidity were found to be negligible, analogous to that found by Harding et al [32] for plate panels in shear. Both concentric and eccentric stiffeners were examined. It was observed that with the stiffener stiffness I_s calculated about an axis at the surface of the plate, the ultimate loads for panels with eccentric stiffeners were close to those for panels with concentric stiffeners for the same value of stiffener rigidity Ψ ($\Psi=EI_s/Db$). Numerical checks were made on panels with three stiffeners. It was assumed that all stiffeners had the same initial displacement in the same direction as each other, and no significant difference in ultimate capacity was observed between panels with either single or three stiffeners.

By means of an established non-linear finite element package, Rahal and Harding [5,7] conducted a similar parametric study to examine the behaviour of transversely stiffened web panels subjected to shear or shear and combined in-plane direct loading, with particular attention to the influence of the geometric parameters on the deflections and stresses in the stiffeners. The analytical model was restricted to an intermediate transverse stiffener and two adjacent plate panels, both of which were modelled with eight-node isoparametric shell elements. All boundaries were simply supported. Plate loading was achieved by means of prescribed boundary displacements. Sinusoidal imperfections with code tolerance amplitude were adopted. Varying parameters were the panel slenderness, aspect ratio and the stiffener rigidity. The results for the slender

panels indicated that an optimum value of stiffener rigidity exists, below which panel strength was sacrificed. It was found that the important panel effect on the stiffener is lateral loading induced by panel buckling, and flexural rigidity rather than axial stiffness is the most important parameter for the design of transverse stiffeners.

The behaviour of a simply supported plate with an intermediate stiffener, subjected to uniform in-plane shear loading, was extensively investigated by Stanway et al. [1, 8, 9] using elastic critical buckling analyses and elasto-plastic large deflection analyses. The critical buckling solutions were obtained by means of an energy method, with the plate deflection being represented by a sinusoidal series. The non-linear elasto-plastic analyses were performed using the Imperial College program FINASIC, the plates being modelled by eight-node isoparametric shell elements and the stiffeners being modelled by three-node space beam elements. In this study, panel slenderness ratios of $80 \leq b/t \leq 180$ (b=small panel dimension), panel aspect ratios d/a from 0.5 (long) to 5 (tall), and flat bar concentric stiffeners with a side ratio of $h/t_s=10$ (h and t_s are depicted in Fig. 3.1) and varying rigidities, were considered. All boundaries were assumed to be unrestrained tangentially. The edges parallel to the stiffener were constrained to remain straight, while those perpendicular to the stiffener were unrestrained in-plane. The initial geometric imperfections considered were part affine to the critical buckling modes, consistent with the tolerances specified in design codes. The analyses showed that in the strength against stiffener rigidity curves, two regions without significant slope changes are joined by a transition region, and this confirmed that an appropriate stiffener rigidity exists. The practical significance of overall buckling in respect of the ultimate strength of stiffened plates was identified. For panel aspect ratios $d/a \leq 3$, the panel bending effect is dominant; while for $d/a \geq 5$, the tendency of overall buckling is of primary importance. For the panel bending effect, it was observed that the stiffener behaviour depends mainly on the bending moments caused predominantly by transverse shear forces in the panels on each side of the stiffener, and that the axial force in the stiffener has a relatively small effect. It was also found that a stiffener that causes a rather small change in buckling mode might result in a large change in ultimate strength.

1.2.4 Design of Transverse Stiffeners

When some time ago the design of plate panels was based on critical loads, an optimum value was used to give the relative flexural rigidity of the stiffener Ψ. According to the critical buckling criterion generally used, the optimum rigidity Ψ^* can be defined as the stiffness at which the critical load of the stiffened plate is equal to the critical load of the most unfavourably loaded plate panel assuming it is simply supported. This criterion forms the basis of some codes of practice for the design of stiffened plates. The advantage of such a criterion is that the design of stiffened plates reduces to the design of the stiffeners and the design of the individual web panels between the stiffeners. Formulae and charts for determination of the optimum rigidity Ψ^* for various kinds of stiffening and loading of plates were published by Klöppel et al [39, 40]. Skaloud [2] listed the formulae for Ψ^* for some frequently encountered cases of stiffened webs and flanges.

Nevertheless, for slender plates whose ultimate load may be much in excess of the critical buckling load, the above criterion will lead to inadequate stiffeners. In addition, the influence of the imperfections cannot be covered by the linear buckling theory. Therefore, the linear buckling theory is unable to describe the actual behaviour of stiffened plates. Based on the available theoretical and experimental results, it was proposed [2] that the optimum rigidity, denoted as $\Psi_{opt,}$ for a stiffener required to be rigid up to collapse, may be taken as

$$\Psi_{opt} = k \cdot \Psi^* \tag{1.1}$$

where k is an empirical correction factor reflecting the effects of initial imperfections and of post-buckling behaviour.

Based on the numerical results of elasto-plastic large deflection analyses, Horne and Grayson [45] proposed a simple minimum rigidity criterion for the transverse stiffeners. It was observed that a minimum value of the stiffener rigidity exists, beyond which further increases of rigidity cause only slight increases in the ultimate capacity of a

stiffened web. An empirical formula was given for this minimum stiffener rigidity for the design of transverse stiffeners, which incorporates the panel slenderness and aspect ratio as variable parameters. It was suggested that the proposed formula might be used as a safe estimate of the required stiffener rigidity for all possible combinations of web loading [46]. One of the shortcomings of this approach arises from the subjective assessment of the minimum stiffener rigidity. Further, no direct reference is made to the stiffener strength, and the availability of the formula presented could be questioned for cases out of the parameter range treated in the parametric study.

Rockey et al [47] proposed a strut model for design of transverse web stiffeners. According to this approach, the stiffener is required to resist stiffener forces calculated from the failure theory by Porter et al [43] for the ultimate strength of web panels. The axial loads arising from the tension field action are assumed to act along the mid-plane of the web panel. To take account of the disturbing action of the web, a critical value of the moment of inertia of the transverse stiffener I_{cr} was introduced. I_{cr} is determined by replacing the applied shear stress with a longitudinal compressive stress of the same magnitude and applying this to a "saw tooth" stiffened plate buckling model, originally proposed by Richmond [48]. The stiffener is then designed as a strut having an reduced moment of inertia ($I-I_{cr}$), subjected to the axial load from tension field action. The method proposed allows the full plastic moment capacity (under bending and compression) of the stiffener section to be developed. This approach is much complicated in application, depending on an estimation of web forces and the plastic design of stiffener itself with explicit allowance for destabilising forces.

BS5400 [3] also uses a strut model for design of the transverse stiffener. The web stiffeners are designed to resist a resolved component of panel tension field force, which was more simply derived than in the approach by Rockey et al, as well as a hypothetical axial force F_{wi} intended to represent the lateral destabilising effect of the deformed web plate. The imaginary force F_{wi} was derived by considering the same "saw tooth" stiffened plate buckling model as used by Rockey et al. The design of transverse web stiffeners according to BS5400 was described in detail by Chatterjee [49].

In the approaches given in BS5400 [3] and by Rockey et al [47], both strength and stiffness criteria for the stiffener are incorporated into the design procedures. In addition, both of them are consistent with the design philosophy for the web panels. On the other hand, the strut model presented in these two approaches employ an empirical effective width approach, where a segment of plate is assumed to act as part of the stiffener. In determining the destabilising action force, both approaches neglect the effect of local panel flexure.

Using the numerical parametric results, Rahal and Harding [6] formulated a linear beam model for the design of transverse stiffeners in girder webs subjected to shear loading. The transverse stiffener was modelled as a simply supported beam subject to a half sine wave distributed load. The magnitude of the load was taken from the non-linear finite element analyses of plates with non-deflecting stiffeners, and expressed as a function of the applied shear stress, the panel yield stress, the panel aspect ratio, and the panel slenderness. It was proposed that the required stiffener rigidity be determined using a criterion of first out-stand yield. Later [7], the model was extended to include coexistent in-plane longitudinal compression and bending. The beam loading was modified to account for the destabilising effects of the in-plane direct loading by introducing a factored combined stress in place of the pure shear stress. The beam cross-section consists of the stiffener itself and an effective width of web plate. The main feature of Rahal and Harding's model is that the lateral force acting on the stiffener is specifically recognised, and it is simple to use. However, the stiffener is designed only to resist this lateral force, and the stiffener rigidity is not accounted for in the formulation for the lateral loading. Besides, the model is based on numerical results for panel aspect ratios up to 2:1 tall, beyond which the assumptions made could be questioned as significant changes in stiffener and plate behaviour would occur. Moreover, the approach proposed makes no reference to the tendency for stiffened plates to buckle overall.

A rational design model for intermediate stiffeners on plates subjected to in-plane shear loading was presented by Stanway et al [9]. In this model, the panels were represented as rigid pin-ended links, inclined to the edges of the plate, and a distributed lateral load was assumed to act on the stiffener to account for the local panel bending effects. The

distribution of the lateral load was taken as the distribution of the reaction on a straight knife edge (no deflection) from critical buckling analyses. The magnitude of the lateral load was taken as the magnitude of the reaction on a straight knife edge from non-linear elastic analyses, with verification by elasto-plastic finite-element analyses. The rigid-link model then enabled the local panel bending and overall buckling effects to be combined. The method proposed for the lateral force is based on the simplification of an "unattached stiffener", where the stiffener only restrains lateral deflection of the plate. No allowance is made for the axial force in stiffener. Both strength and stiffness design criteria were developed to quantify the required stiffener. The strength criterion requires that the bending stress in the stiffener does not exceed the yield stress. The stiffness criterion requires that the stiffener deflection is sufficiently small relative to the panel deflection, to ensure effective subdivision of the stiffened plate. The design model allows distinction to be made between single- and multi-stiffener plates, but it was only tested for single stiffener plates using finite-element analyses. The model takes rational account of the effects of out-of-plane forces and of the tendency for the stiffened plate to buckle overall, and it has been validated by reference to the parametric results for a range of configuration parameters. The validity of the model for parameters out of this range requires further investigations. One disadvantage of this method is that the determination of the stiffener bending moment, due to the panel bending effects, employs some empirical formulae and is not simple to apply. A further disadvantage is that the rigid-link model takes no account of the overall buckling capacity of the plate panels.

1.2.5 Experimental Work

In addition to the theoretical results, experimental evidence is needed to validate the theory about the actual behaviour of stiffeners attached to plated structures. Although much experimental research has been conducted on plate girders, most of the tested girders were fitted with relatively large transverse stiffeners and only a few tests have been specifically conducted to investigate in detail the behaviour of the transverse stiffeners.

Massonnet [15] carried out experimental studies on large-scale plate girders subjected to bending. It was demonstrated that stiffeners proportioned according to the linear buckling criterion, deflected with the web in the post-buckling range of the web panels. He also observed that for stiffeners to remain straight and fully effective up to the collapse of the girder, a higher flexural rigidity was necessary.

In 1981, Rockey et al [47] reported the results of 22 tests on eleven model steel plate girders, differing only in the dimensions of the transverse stiffeners. The panels had an aspect ratio d/a=1, and slenderness d/t=300. Four of the girders had concentric (double sided) flat bar stiffeners while seven had eccentric (single sided) flat bar stiffeners. The stiffener rigidity Ψ varies in a wide range. The test girders were simply supported at each end, and loaded at mid-span. Throughout the tests, the lateral deflections of the stiffeners, the out-of-plane deflection of the web plates and the strains in the intermediate stiffeners were recorded at frequent intervals. The strain gauges were fitted along three sections along the length of the stiffeners, and the measured strains demonstrated that the stiffener was subjected to both axial loads and bending moments. The tests revealed that the use of a relatively small stiffener can result in a significant increase in the ultimate capacity of a girder, but the stiffeners suffer considerable out-of-plane displacement, thereby allowing the buckles in the adjacent panels to merge together. Of the 22 stiffeners tested, seven deflected significantly out-of-plane. It was observed that a stiffener could effectively subdivide the web into two panels even when it has completely yielded over a small length of the stiffener, because the remaining elastic portions are still able to stabilise the web.

Tang and Evans [49] conducted nine tests on two large-scale, transversely stiffened plate girders. The two girders were designed to be identical except for the spacing and dimensions of the transverse stiffeners, which were attached to one side of the web only. The overall span of each girder was 6m, the girder depth was 0.8m and the web thickness was 1mm throughout. The flanges were designed to be adequate to prevent bending failures. The web panel aspect ratio d/a varied from 0.8 to 1.6, and the slenderness d/t =800. Flat bar stiffeners were used, with the width varying from 25mm to 95mm and the thickness from 3.67mm to 6.14mm. The experimental arrangement,

procedure and instrumentation were similar to those adopted by Rockey et al [47]. In seven of the nine tests carried out, the transverse stiffeners proved adequate up to the collapse of the web panels, and the girders failed by the development of a shear sway mechanism. In the other two tests, at a certain level the stiffener suffered considerable displacement in the direction perpendicular to the web and allowed the buckles in the adjacent panels to merge together, followed by the immediate overall collapse of the girder. In all cases it was found that strain values measured at corresponding positions on either face of a stiffener were almost identical, showing that there was virtually no bending of the stiffener in the direction parallel to the plane of the web. The strain values measured also demonstrated the co-existence of axial force and bending moment in the stiffener. It was observed that the yield zone in the stiffener is concentrated near the stiffener/web junction and extends over most of the stiffener width. In Tang and Evans' work, none of the nine stiffeners examined fully satisfied the requirements of BS5400, but only two stiffeners failed in the tests. Four stiffeners also did not match the needs of the design method proposed by Rockey et al [47], but two of these stiffeners behaved adequately in the tests.

1.3 OBJECTIVES OF THESIS

The main objective of this study is to provide a rational and usable design method for transverse web stiffeners. In particular, this study aims:

- To investigate possible simplification and modification to the design model by Stanway et al [9].
- To develop and validate the design model for combined in-plane shear and coexistent longitudinal bending and compression loading.
- To develop the design model which takes account of external stiffener forces.
- To develop and validate the design model for both double-sided (concentric) and single-side (eccentric) stiffeners.
- To extend the numerical solutions to taller and more slender panels.
- To carry out tests on girders with transverse web stiffeners.
- To compare the design model with existing design methods and test results.

To carry out this investigation, the following approaches will be used:

- ***Theoretical Studies***

It is envisaged from the previous study [1] that the transverse force acting on the stiffener due to the local panel bending effect will play an important role in the formulation of the design model for transverse stiffeners, and that it seems impossible to find theoretical solutions for this transverse force. However, the theoretical solutions for some simple cases may form the basis for closed-form equations that could be used to represent the effect of panel bending, enabling a wider range of cases to be covered. For this reason, non-linear elastic buckling behaviour of simply supported plates will be analysed using the energy method and the Galerkin method.

Another important factor in the formulation of the design model for transverse stiffeners is the overall buckling effect of stiffened plates. Rigid-link model by Stanway et al [1,9] will be extended to include compression and pure bending conditions. A beam-plate model, which incorporates the overall buckling capacity of the plate panels, will be proposed and examined using the energy method for each single loading component. Possible application for combined loading will be discussed.

It is expected that the axial force in the stiffener due to the tension field action may become a significant factor for single-sided stiffeners and slender plates. The representation of the stiffener axial force will be explored, on the basis of the Basler tension field theory.

- ***Numerical Analyses***

The finite element program ABAQUS will be used to carry out an extensive parametric study to examine the critical, elastic and elasto-plastic buckling behaviour of the stiffened plates. The investigation will be extended to cover a wider range of the panel aspect ratios d/a and the panel slenderness b/t (b: small panel dimension). Apart from

pure shear, combined shear and longitudinal compression and bending will be considered. Both concentric and eccentric stiffeners will be considered.

- ***Experiments***

A number of tests on transversely stiffened plate girders, with different geometries, will be undertaken to provide verification of the finite element results from ABAQUS, and to validate the proposed design model. The design of the specimens and the instrumentation will be aimed primarily at clarifying stiffener behaviour under shear and bending. In addition, some stiffeners will have external end forces.

- ***Model Development***

By using the theoretical solutions as the basis, design formulae for predicting the forces in transverse stiffeners will be established, with coefficients introduced to be determined by means of the finite element results. The proposed design model will take into account of the local panel bending effect and the tendency for the stiffened plate to buckle overall, as well as the stiffener axial force due to the tension field action. It is intended that the method by Stanway [1] for calculating the lateral stiffener force for pure shear will be simplified. To quantify the required stiffener, both strength and stiffness criteria will be considered.

CHAPTER 2

EXPERIMENTAL STUDY ON STIFFENED PLATE GIRDERS

2.1 INTRODUCTION

Experiments were conducted on four transversely stiffened plate girders. The test girders were designed to be nominally identical in overall dimensions, covering a range of aspect ratios and slenderness ratios of the web panel. The dimensions of the transverse stiffeners were chosen to enable their post-buckling behaviour to be observed. Two different loading arrangements were employed to clarify stiffener behaviour under pure shear (or predominant shear) and combined shear and bending conditions.

The main purpose of the experiments was to substantiate the post-buckling behaviour of plated structures as represented by the finite element program ABAQUS, and to allow calibration of the finite element model for stiffened plates. In this way, the other stiffened plate configurations can be effectively tested through computer simulation, thereby avoiding the expense of large-scale testing and the physical restrictions on the size of the specimen tested.

The second purpose of the experiments was to provide some experimental results on the buckling behaviour of transverse web stiffeners, which will supplement the existing database of test results and may be used to validate the models proposed for design of transverse stiffeners. A further purpose was to reveal any unexpected phenomena.

The details of the experimental girders are given in this chapter. The arrangement of the test rigs, instrumentation, test procedures are described. The experimental results are presented for the test girders, and discussed in relation to the finite element solutions

from ABAQUS. By comparison of the finite element solutions and the test results, the reduction in strength attributable to residual welding stresses can be identified, which is not included in the finite element models.

2.2 TEST GIRDERS

2.2.1 Dimensions

All the four test girders were made from mild steel sheets. Except for the varying stiffener spacings and sizes, the girders were nominally identical to each other in dimensions, having a 2mm×600mm web and 10mm×200mm flanges, and having an overall length of around 2500mm.

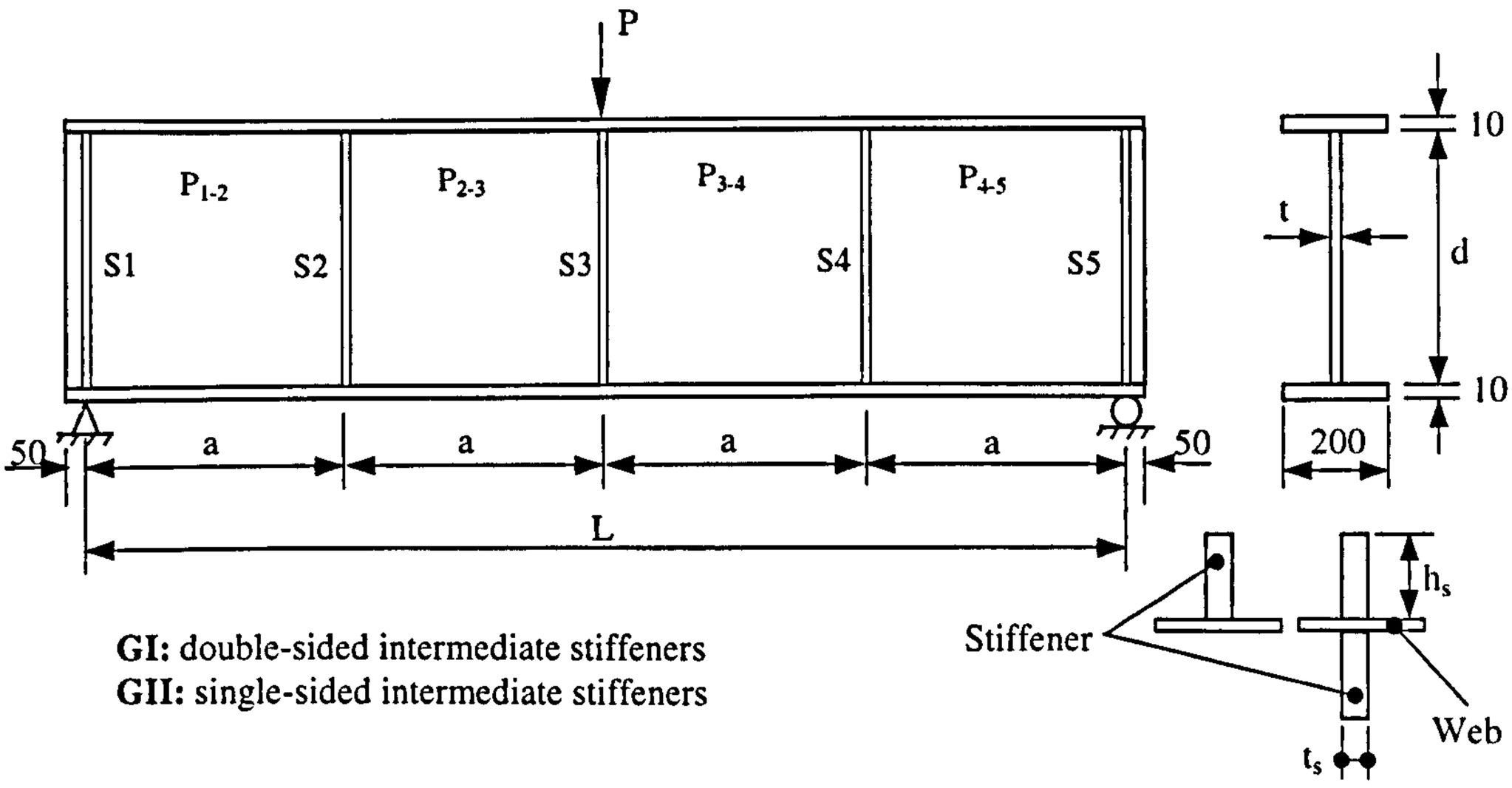
Flat bar stiffeners are used on all the test girders. Half of the girders were fitted with double-sided stiffeners, while single-sided web stiffeners reinforced the remaining girders. The sizes of the intermediate stiffeners were decided on a basis that they are expected to fail according to the existing design methods and according to the finite element analyses by ABAQUS. The bearing stiffeners were designed to meet the yielding strength as required by BS5400, and also checked by ABAQUS.

According to the loading arrangements and web panel dimensions, the test girders can be categorised as follows:

- Group A: d/a=1, central loading
- Group B: d/a=2, loading at both ends, up and down respectively

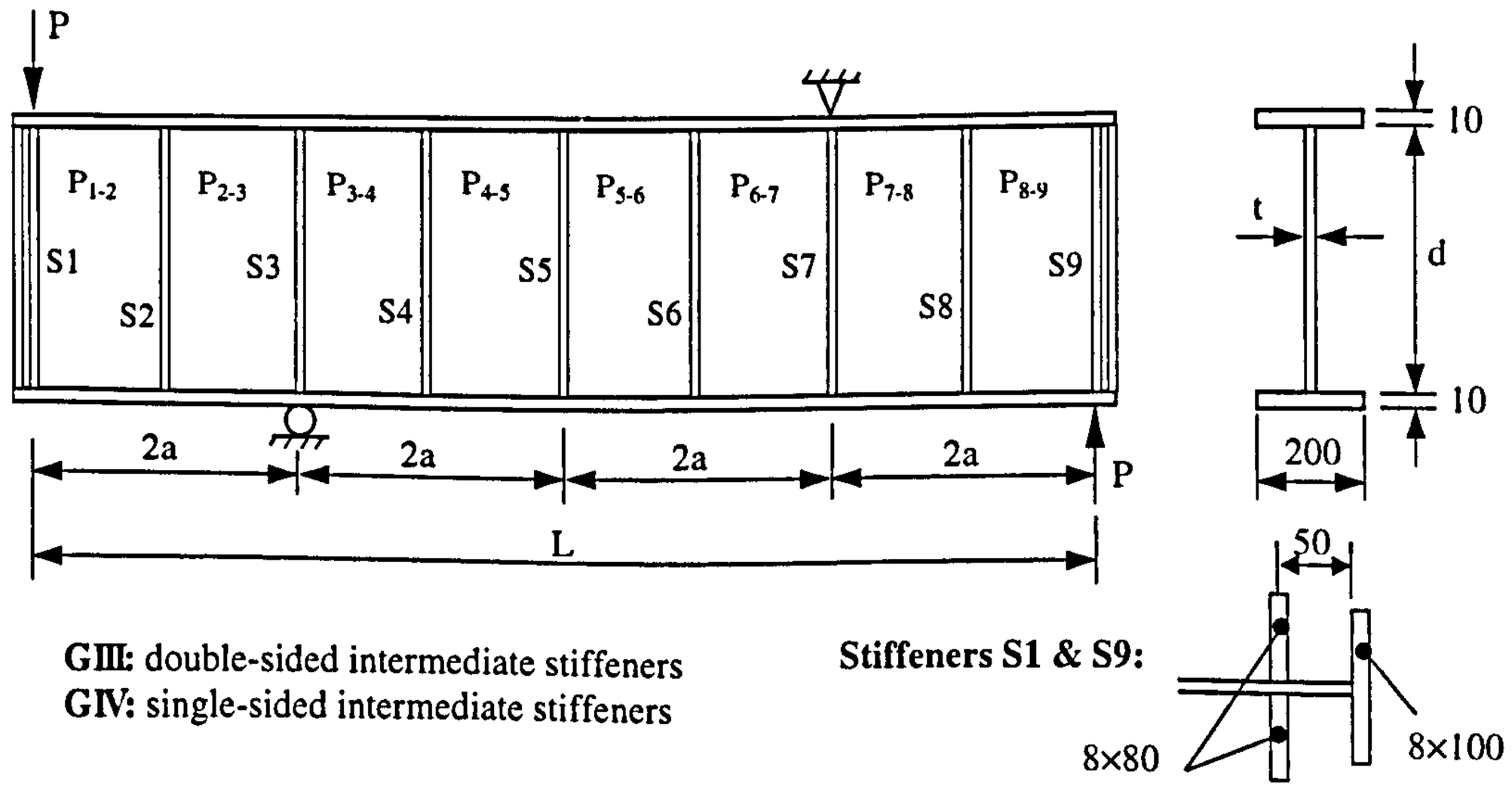
The details of the fabricated girders are given in Fig. 2.1 and Table 2.1a & b. Also included in the table are the yield stresses obtained from the tensile tests of the material for each member.

As shown in Fig. 2.1, the test girders GI and GII had single end stiffeners, while the test girders GIII and GIV had double end stiffeners.



GI: double-sided intermediate stiffeners
GII: single-sided intermediate stiffeners

(a) Group A: Girders GI & GII



GIII: double-sided intermediate stiffeners
GIV: single-sided intermediate stiffeners

Stiffeners S1 & S9:

(b) Group B: Girders GIII and GIV

Figure 2.1 Details of the test girders (see also Table 2.1)

Table 2.1a Properties of the Test Girders GI* and GII* (Units: mm, N/mm^2)

Girder	L	Web				Stiffener S2			Stiffener S3			Stiffener S4			Stfn. Type
		a	d	t	σ_{0p}	h_s	t_s	σ_{0s}	h_s	t_s	σ_{0s}	h_s	t_s	σ_{0s}	
GI	2360	590.0	599.0	2.04	299.5	15.0	5.0	319.9	40.0	6.0	310.9	15.0	3.10	462.7	D.S.
GII	2360	590.0	599.0	2.04	299.3	15.0	4.95	319.9	40.0	7.95	303.5	20.0	5.08	318.8	S.S.

* End stiffeners S1 and S5 were made of double-sided flat bars with t_s=7.95mm, h_s=80mm, σ_{0s}=303.5N/mm^2.

Table 2.1b Properties of the Test Girders GIII* and GIV* (Units: mm, N/mm^2)

Girder	L	Web				Stiffener S2			Stiffeners S4, S5, S6			Stiffener S8			Stfn. Type
		a	d	t	σ_{0p}	h_s	t_s	σ_{0s}	h_s	t_s	σ_{0s}	h_s	t_s	σ_{0s}	
GIII	2360	295.0	599.0	2.05	295.5	16.0	4.97	328.0	16.0	4.97	328.0	20.0	5.10	322.6	D.S.
GIV	2360	295.0	599.0	2.05	295.5	24.90	5.0	329.6	24.90	5.0	329.6	30.20	5.11	284.9	S.S.

* End stiffeners S1 and S9 were double leg stiffeners, and stiffener dimensions are shown in Fig. 2.1, with σ_{0s}=303.5N/mm^2.

Note: 1. D.S.= Double-sided intermediate stiffeners; S.S.= Single-sided intermediate stiffeners

2. The flanges are made of 200mm×10mm flat bars, having a yield stress σ_{0f}=251.6N/mm^2.

As a result of the careful planning of welding technique and sequence, the initial deformation of the fabricated girders was found to be less than the code tolerance. After manufacture and mounting in the test rig, each girder was loaded several times up to the critical buckling load of the girder (about 70KN) predicted by ABAQUS, to develop a stable imperfection pattern. The maximum magnitudes of the initial deformation of the web panels and the stiffeners were then measured using a straight edge, a small steel ruler and feeler gauges, and the results are listed in Table 2.2. The measurements of the initial deformations were also carried out before each subsequent test on the same girder, and these measured values are also included in Table 2.2.

Table 2.2 Maximum magnitudes of the initial geometric imperfection of the test girders [mm]

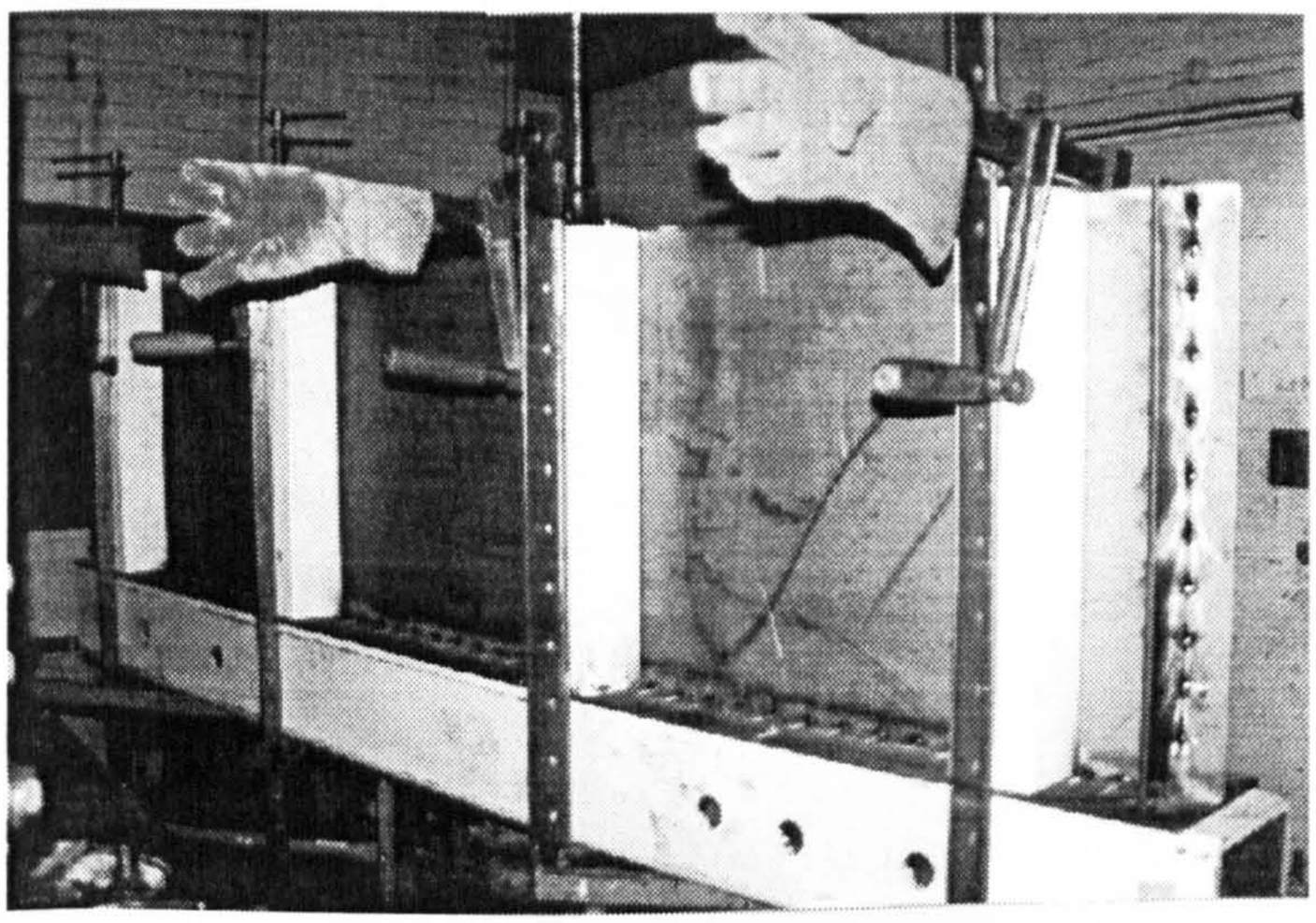
Test No.	Girder	Panels				Stiffeners**		
		P_{1-2}	P_{2-3}	P_{3-4}	P_{4-5}	S2	S3	S4
1	GI	2.0	1.0	1.5	2.0	0.8	0.0	0.8
2		4.0	1.0	1.5	4.0	*	0.1	*
3	GII	0.4	1.1	2.0	1.0	0.6	0.0	0.3
4		3.0	2.5	2.0	2.5	*	0.0	0.4
		P_{1-2}, P_{2-3}, P_{3-4}, P_{4-5}, P_{5-6}, P_{6-7}, P_{7-8}, P_{8-9}				S2	S4, S5, S6	S8
—	GIII	≤0.2				≤0.2		
—	GIV	≤0.3				≤0.2		

Note: * Stiffener was reinforced.
** Load-carrying stiffeners were almost straight, so their initial deflections were taken as zero.

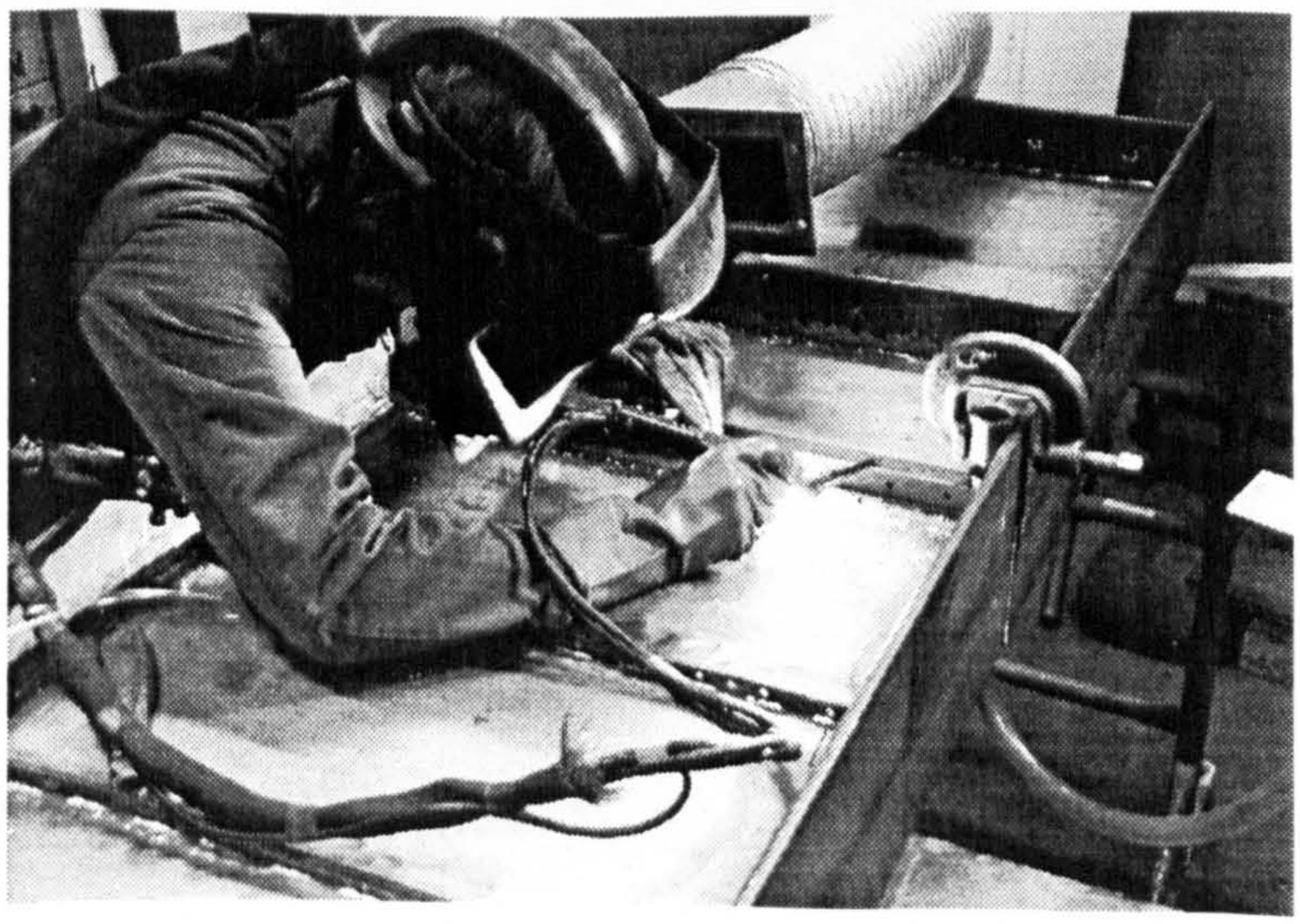
2.2.2 Manufacture

The four test girders were fabricated in the Structures Laboratory of Imperial College. The metal inert gas shielded welding (MIG) process was used to connect web, flanges and bearing stiffeners with continuous welds. The tungsten inert gas shielded welding (TIG) method was used to connect intermediate stiffeners to the web plate, where a much smaller weld was needed. The intermediate stiffeners were intermittently welded to the web plate.

The components were initially fixed by tack welding at 50mm spacing in a jig assembled for the purpose. All the connections were completed by applying a skip-welding procedure which consisted of depositing the staggered weld alternately on either side of the plate at 25mm intervals. For the continuous welds, the spaces were subsequently filled in to complete the weld. During the welding process, temporary bracing members and clamps were employed to restrain the distortion of the plates (Fig. 2.2a). When connecting intermediate stiffeners to web plate, circulating water was used with copper blocks to reduce the heat of welding (Fig. 2.2b).



(a) initial tacking of components



(b) welding of a stiffener

Figure 2.2 Manufacture of the test girder

2.2.3 Reinforcement of Stiffeners

Stiffener sizes were chosen so that one of the intermediate stiffeners would fail before the others. The failed stiffener would then be reinforced in order that further loading could be applied to fail other stiffeners on the same girder.

The failed stiffener was strengthened by two flat bars, which were attached to both sides of the stiffener with fitted pins (6mm in diameter). All the holes were drilled prior to the welding of stiffeners. A view of a reinforced stiffener assembly is shown in Fig. 2.3.

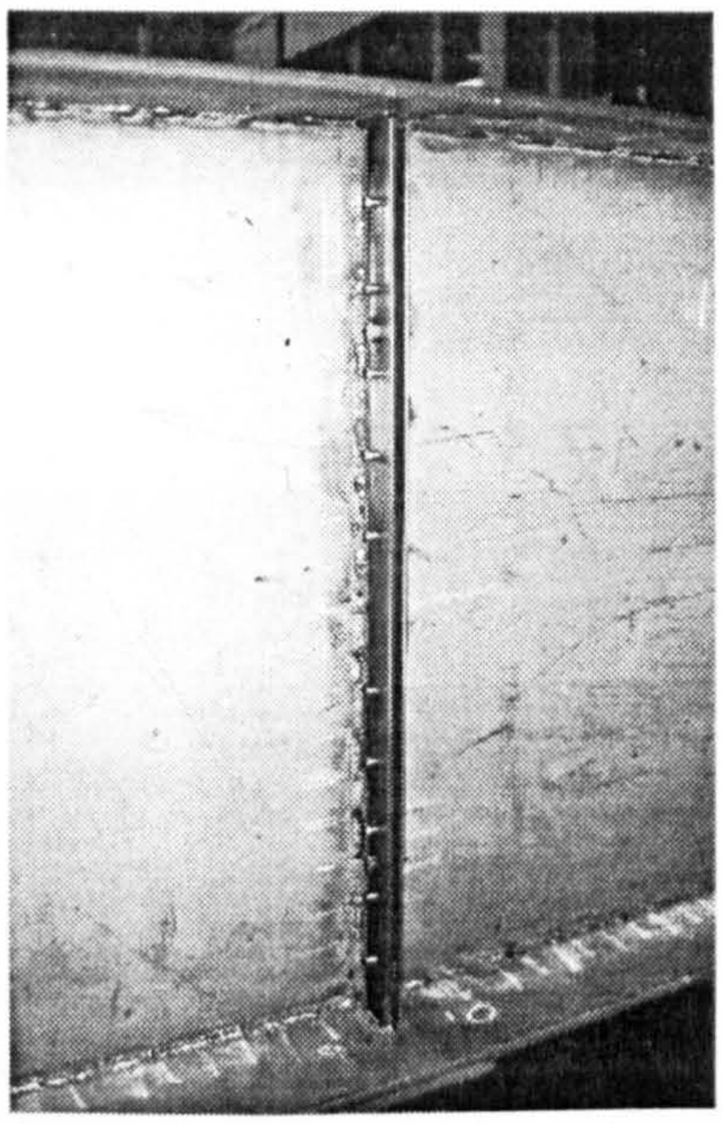
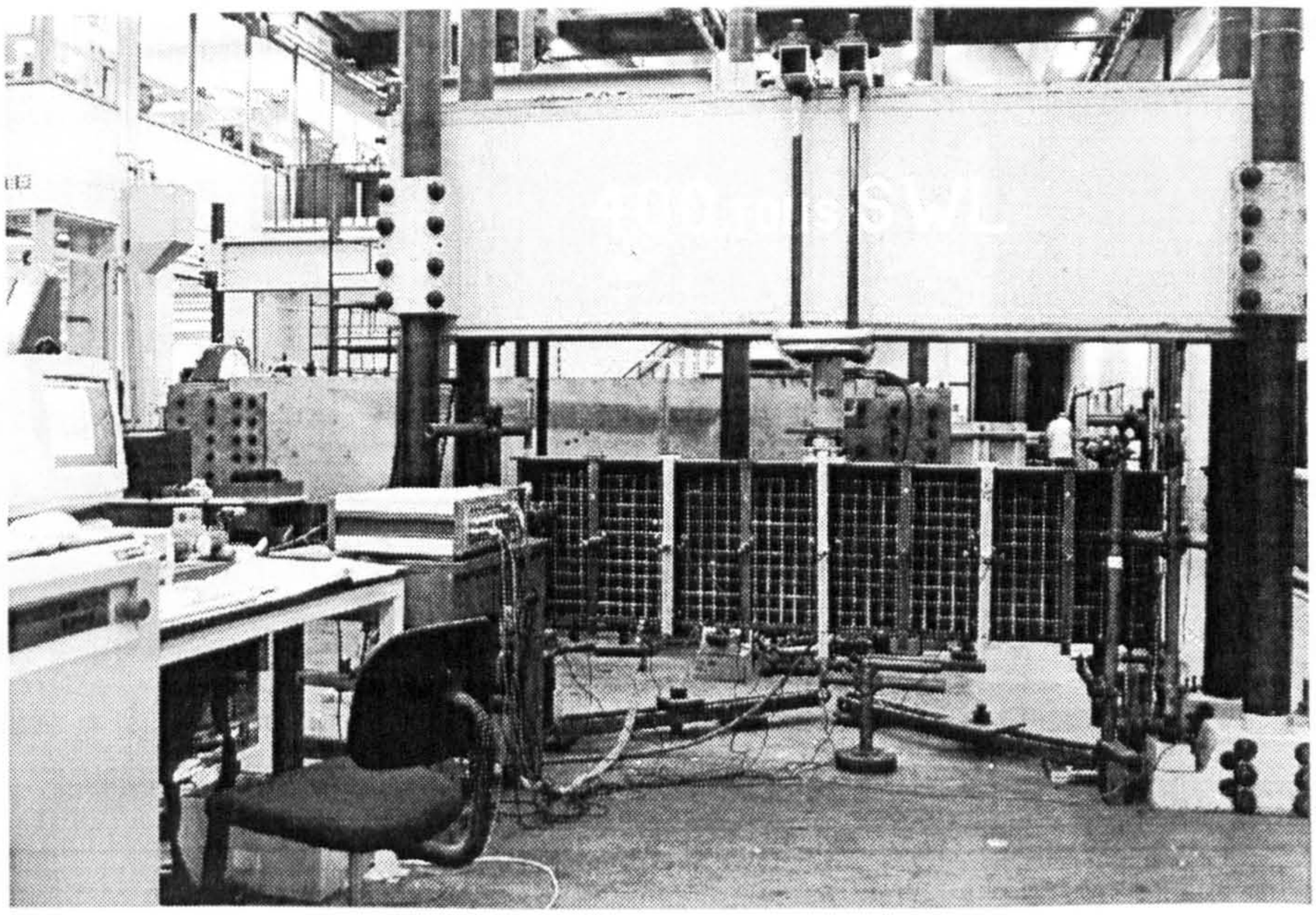


Figure 2.3 Reinforcement of stiffener

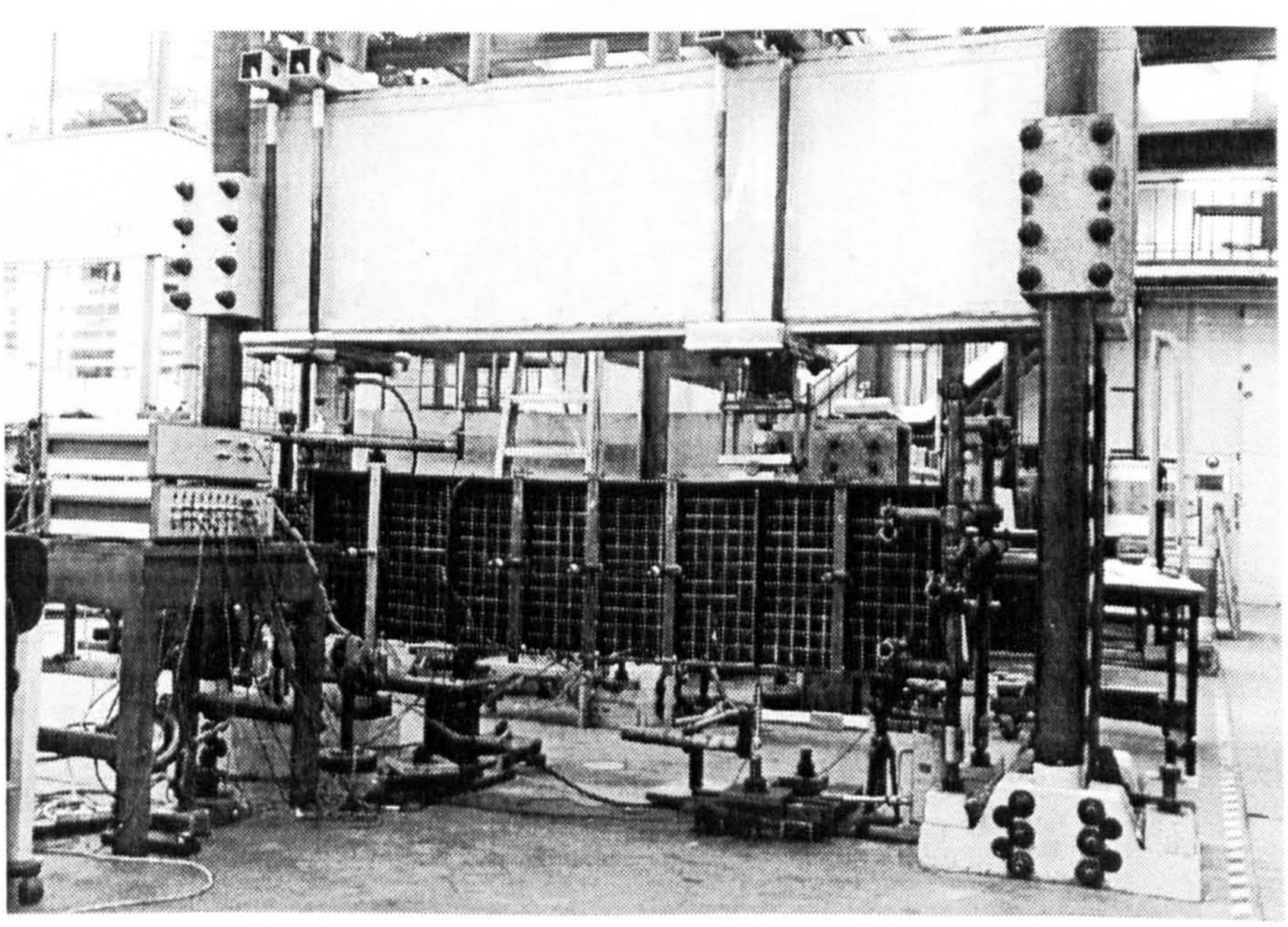
2.3 GENERAL ARRANGEMENT

2.3.1 Test Rig

A general view of the test rig is shown in Fig. 2.4. The rig had a capacity of 4000KN. and was anchored to the strong floor of the laboratory by bolts.



(a) Girders GI and GII



(b) Girders GIII and GIV

Figure 2.4 General view of the test rig

Two of the girders, GI and GII, were supported on a fixed roller at one end and a movable roller at the other end. The two girders were loaded at mid-span respectively (Figs. 2.1a and 2.4a), so that a combination of bending moment and shearing force would exist at the stiffener positions.

The two other girders, GIII and GIV, were loaded equally in opposite directions at both ends. Together with the two supports in between, an up-down-up-down loading condition was formed (Figs. 2.1b and 2.4b). In this arrangement, the girder was subjected to predominant shear forces. The support on the top flange was a fixed roller, while the support on the bottom flange was a movable roller. In order to fit each girder and ensure a tight contact against the flange of the girder when levelled, the height of the top support could be adjusted by adjusting the nuts inside the support, as shown in Fig. 2.5.

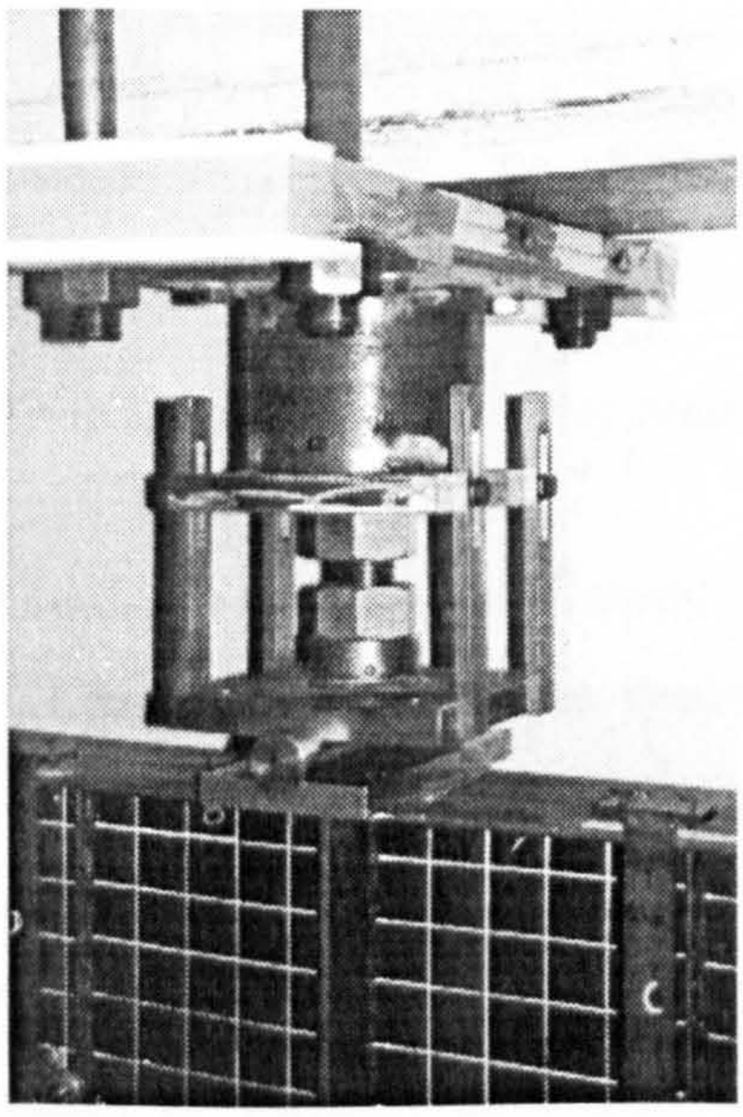
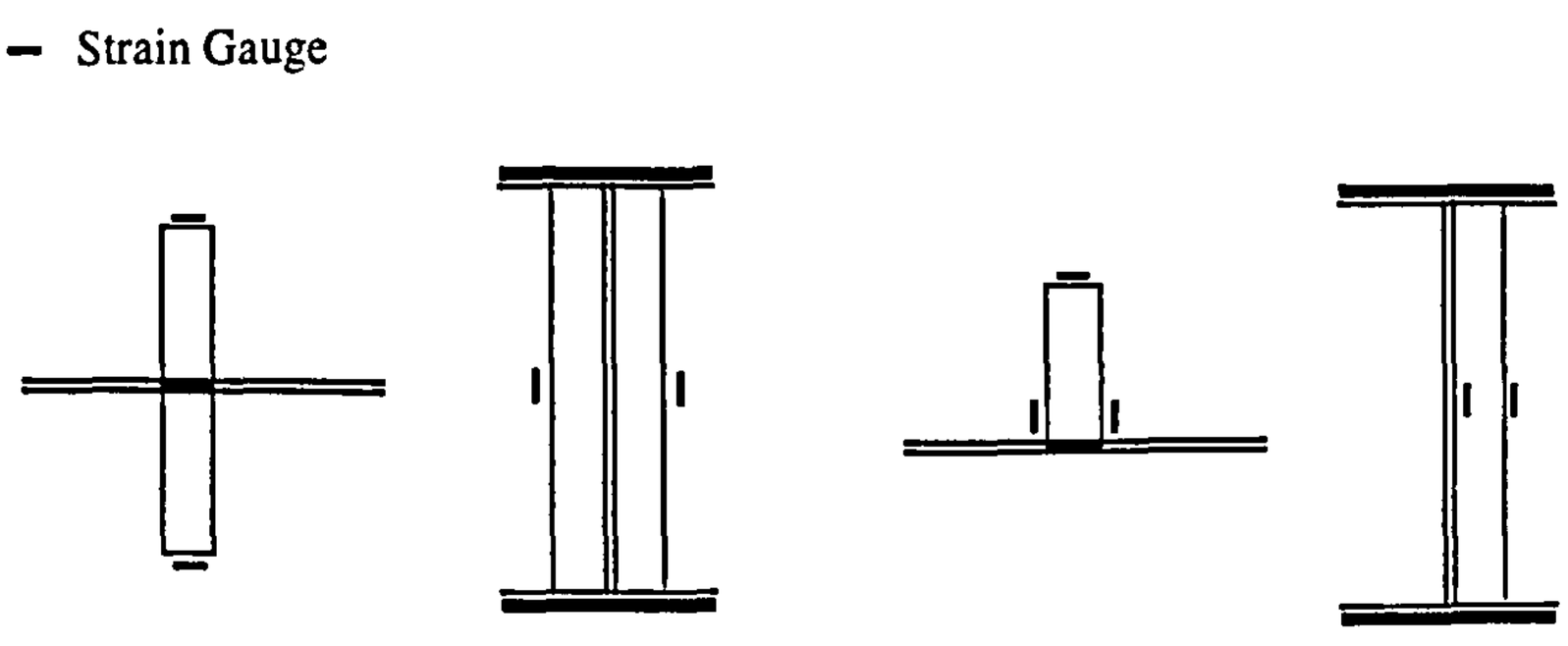


Figure 2.5 Configuration of the adjustable support

500KN capacity hydraulic jacks were used to apply loads. The hydraulic pressure of the interconnected jacks was load-controlled using an Amsler control cabinet. Spherical seats were mounted at the ends of the hydraulic jacks, so the loads were applied concentrically to the test girder.

2.3.2 Instrumentation

Electric resistance strain gauges were affixed at the mid-length of the stiffeners, and detailed locations are shown in Fig. 2.6. The strain gauge used has a base of 3mm in width and 10mm in length. It was expected that the magnitude and the distribution of axial stress on the cross-section of the stiffener could be revealed.



(a) Double-sided stiffener (b) Single-sided stiffener

Figure 2.6 Locations of the strain gauges

Displacement transducers were used to measure the lateral deflections at the mid-length of the stiffeners and (for GI and GII only) at the centre of each web panel. The transducers were fixed on a straight aluminium bar, which hung from a grooved aluminium strip bonded near the edge of the top flange and was hold in contact with the edge of the bottom flange by an elastic band (Fig. 2.7). This arrangement was adopted in order to give a measurement of stiffener deflection relative to the flanges. Also measured was the in-plane deflection of the girder at loading positions (mid-span for GI and GII; ends for GIII and GIV). The small vertical movements at supports were also measured.

Magnitudes of applied load, strain and deflection were recorded by the data acquisition equipment DATASCAN, and logged using the software DALITE which runs on a PC platform. The response of the test girder was monitored using another PC computer, by

plotting the relevant readings of load, deflection and strain from DALITE during the test.

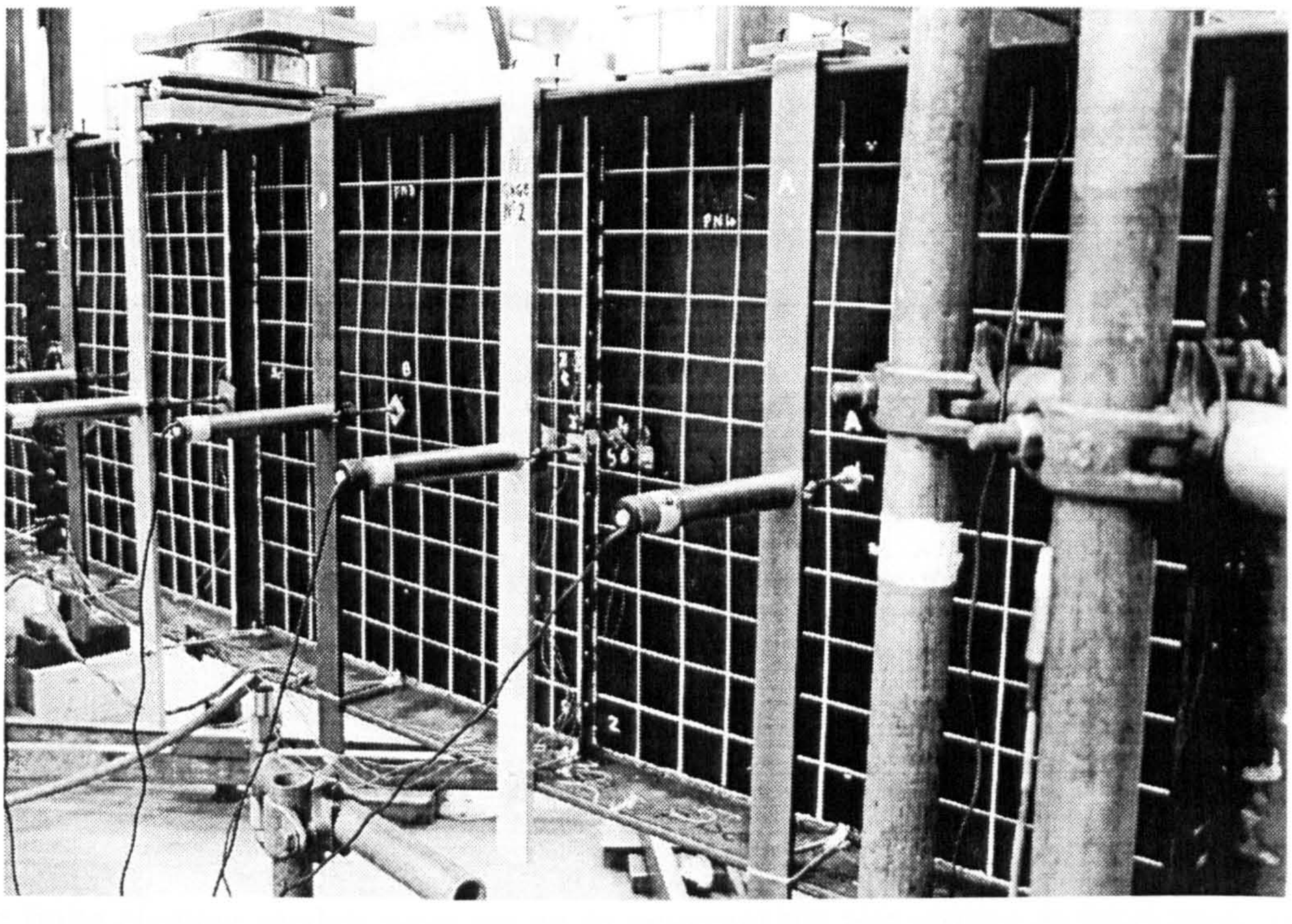


Figure 2.7 Deflection measurement

2.3.3 Test Procedure

The test girder was preliminarily loaded to a small load, close to the estimated critical buckling load of the panels, to check the instrumentation and the setting of the test rig (as any eccentric loading would be undesirable), and then any necessary adjustments were made after unloading. This process was repeated several times until satisfactory. After these static cycles of loading, it was noticed that a stable imperfection pattern was developed. The maximum deflection magnitudes were measured for each web panel and each stiffener at zero load, and were taken as the initial imperfections of the finite element model (Table 2.2).

Initially load was applied to the girder at 10KN increments in a load-and-unload fashion, so as to reveal the load level at which a permanent deformation occurred. As soon as it was evident that the girder deflection became non-linear, the load was applied monotonically in 10KN increments.

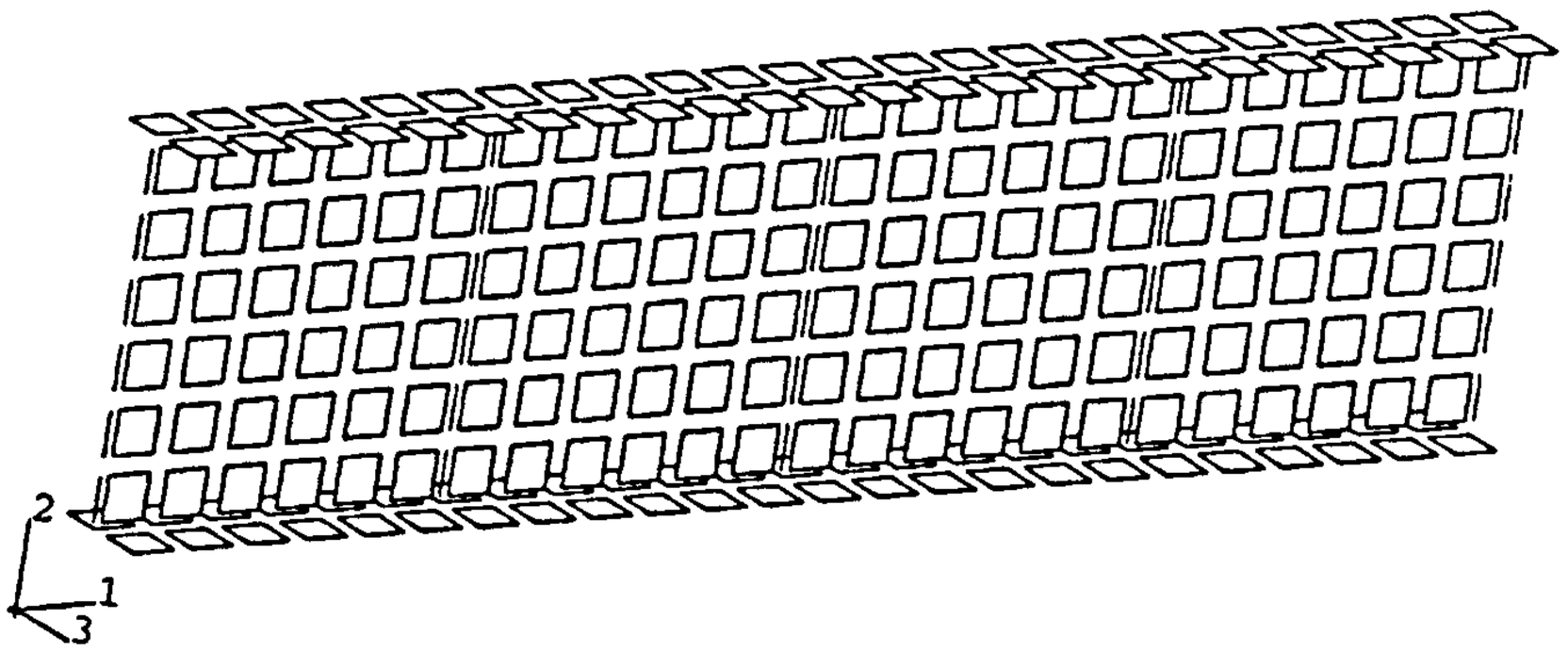
Applied loads, deflections and strains were recorded at all stages. The load vs. deflection curves and the load vs. strain curves were plotted instantaneously on a PC monitor throughout the test. When any of these curves entered the non-linear transition range, suggesting that the incremental displacements were increasing, load increments were reduced gradually (eg 5KN, 2.5KN). When any of the load/deflection curves of the stiffeners, or the load/central displacement curve, reached the plateau area, signifying that the peak load was reached, the test girder was unloaded. The stiffener (or stiffeners) that had failed in the first test was then reinforced and a second test was carried out on the same girder. Finally, the girder was tested to destruction.

2.4 FINITE ELEMENT MODELS FOR TEST GIRDERS

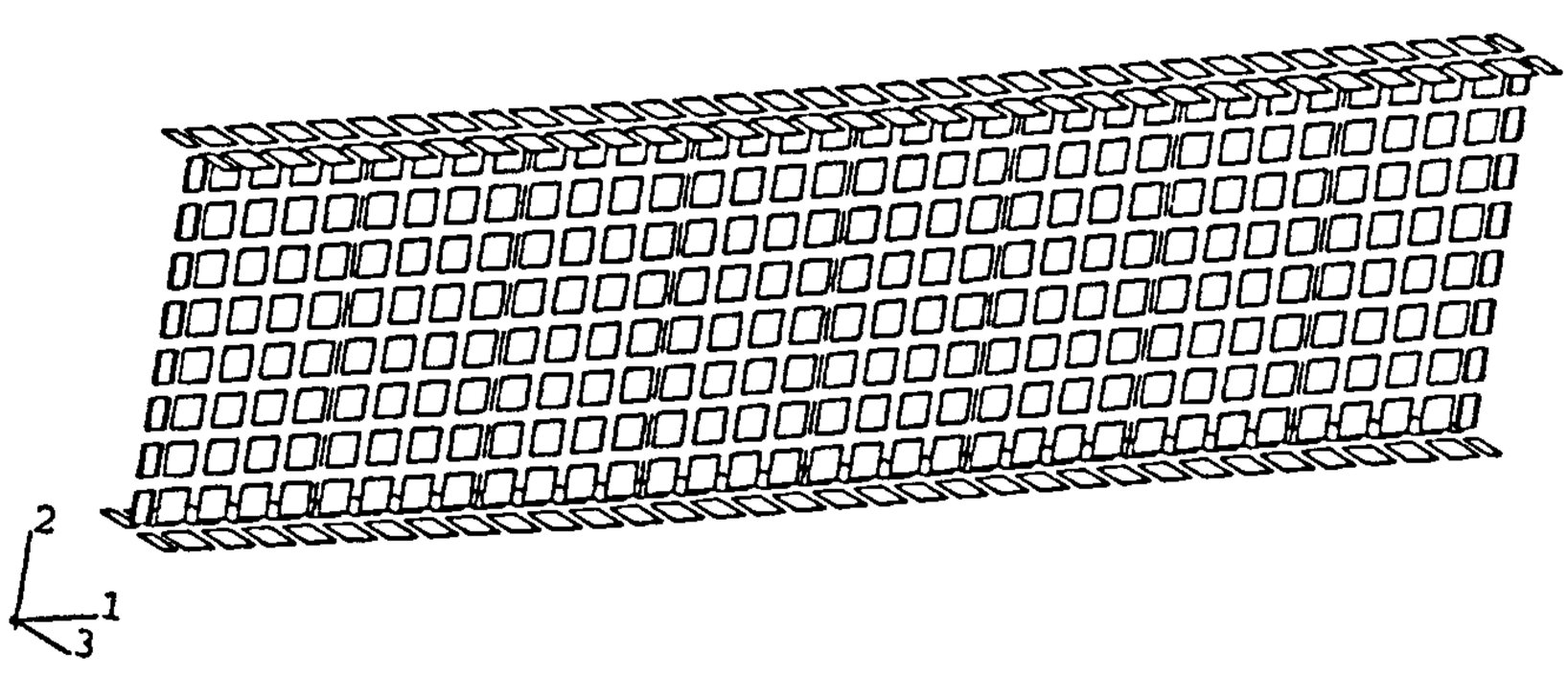
The finite element models were set up to represent the test girders as fabricated, using the parameters listed in Table 2.1. The web plates and flanges were modelled using the ABAQUS S8R5 shell elements, and all stiffeners including bearing stiffeners were modelled using the ABAQUS B32 beam elements.

Square shell elements were used. The number of elements along the small dimension of the panel was 6 for GI and GII (d/a=1), and 4 for GIII and GIV (d/a=2). This mesh size was the same as that used by Stanway [1] for stiffened plates of single stiffener and two adjacent panels, who conducted a convergence study regarding the ultimate shear strength. The mesh was consistent with the criterion that a half-wave should be divided into at least 4 elements.

Boundary condition w=0 was assumed along the perimeter of the web plate, and the in-plane boundary conditions were provided by the attached actual end stiffeners and flanges. The FE models adopted were shown in Fig. 2.8.



(a) Girders GI and GII



(b) Girders GIII and GIV

Figure 2.8 FE models of the test girders

Measured material properties form the basis for the stress vs. strain relationship. A bilinear stress-strain curve was adopted for each member of the girder separately, with the yielding stress obtained from the tensile tests. A linear strain hardening rule of E_t=1%E was selected (Fig. 2.9), which was close to the test results of web material. A modulus of elasticity E of $2.05\times10^5 N/mm^2$ and a Poisson's ratio of 0.3 were adopted.

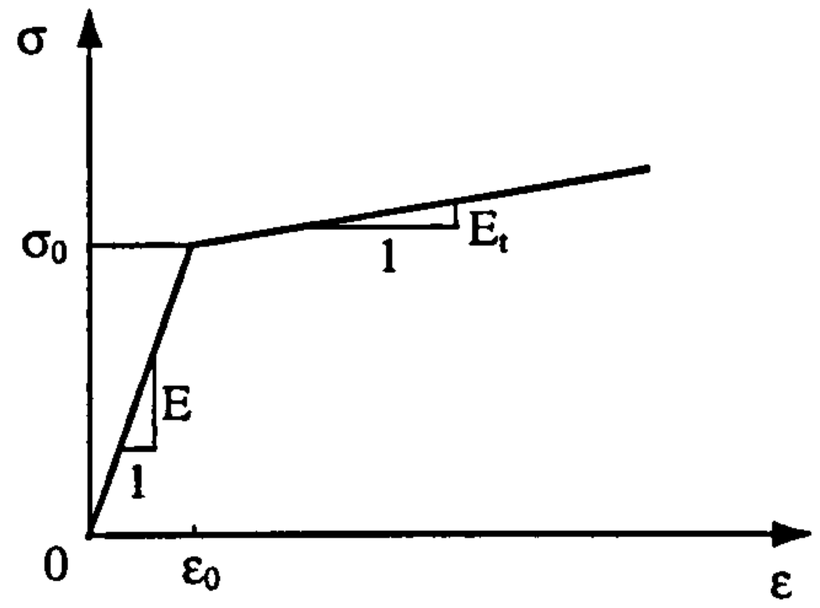


Figure 2.9 Stress-strain relationship adopted in FE models

A series of trial initial geometrical imperfections, which include the first buckling mode of the girder and sinusoidal waves, were used in the finite element analyses of the test girder GI. The results shown in Fig. 2.10 demonstrated that the overall load vs. vertical deflection behaviour is largely independent of the geometry selected, so long as some initial deformed configuration is imposed. However, different initial deformations may result in certain variation in the magnitude and direction of deflection of panel and stiffener, as shown in Fig. 2.10. Therefore, for the comparisons with test results presented in the latter part of this chapter, sinusoidal imperfections with the measured maximum magnitudes (Table 2.2) were adopted for the web panels and stiffeners. Panel imperfections were superimposed on stiffener imperfections. Residual welding stresses were not included in the FE models, because their magnitudes were unknown.

2.5 EXPERIMENTAL RESULTS AND COMPARISON WITH FE SOLUTIONS

In this Chapter, the stiffener failure is defined as that the stiffener failed to perform their functions, either by yielding or by deflecting rapidly. Similarly, the failure load for the test girder is taken as the applied load at which the deflection of the girder started to increase rapidly.

Table 2.3 presents the test results of the first two girders GI and GII. The measured failure loads for stiffeners are listed in the table and compared with the corresponding finite element results. In general, the results agreed quite well, with experimental load

capacity often being less than the numerical values. If allowance is made for the effect of residual welding stresses and for other possible effects, the FE analyses in fact gave good agreement with the test results.

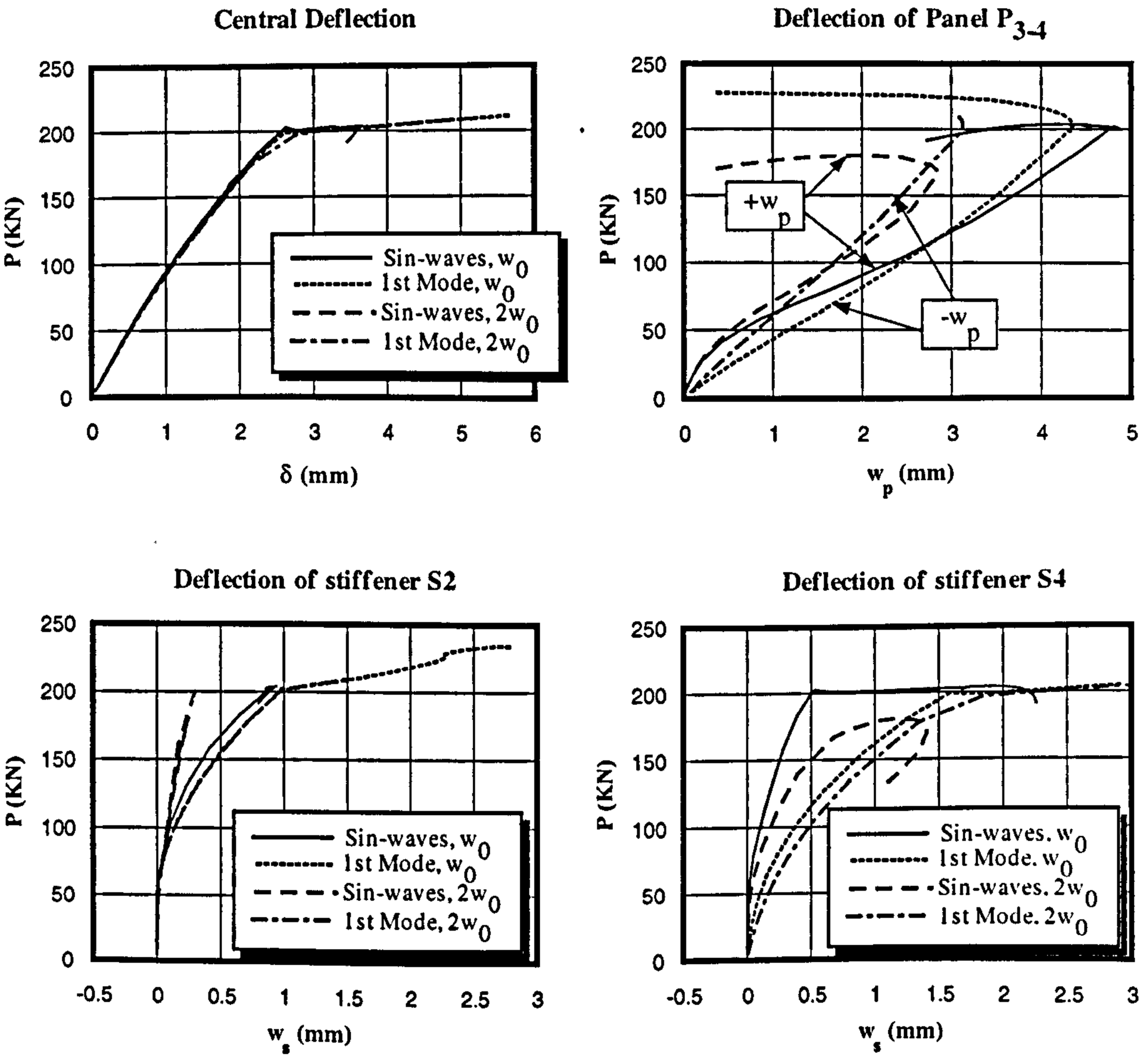


Figure 2.10 Influence of initial imperfections on FE solutions. Girder GI. P as shown in Fig. 2.1(a). w_0 denotes the magnitudes of measured initial imperfection, given in Table 2.2.

The differences between the FE and experimental results are also attributable to the variations in the sizes of the members of the girders and the material strength, and the assumed initial geometrical imperfections.

The behaviour of the test girders will be described below. The load-deflection curves will be presented. The stress distribution on the cross-section of the stiffeners will be

examined, and the axial force and bending moment in the stiffener will be determined. By the time of writing this thesis, the tests on group B (Girders GIII and GIV) have not been fully completed, and therefore only the FE results are presented for these two girders, and the test results will be presented in a separate report in the near future.

Table 2.3 Measured and predicted failure loads for stiffeners

Test No.	Girder	Stiffener	Failure Load P (KN)		$\frac{P_{FE}}{P_{Test}}$	Performance of Stiffener
			Test	FE		
1	GI	S2	182.6	203.9	1.117	Deflecting rapidly
1	GI	S4	177.1	202.6	1.144	Deflecting rapidly
2	GI	S3	216.3	216.6	1.001	Yielding at the top
3	GII	S2	171.4	177.1	1.033	Yielding
4	GII	S4	175.8	209.0	1.189	Deflecting rapidly

2.5.1 Girder GI

Two tests (Test Nos. 1 & 2) were carried out on Girder GI. In *Test 1*, the middle load-carrying stiffener S3 on this girder was reinforced, and the girder was loaded up to 207KN. By then the intermediate stiffeners S2 and S4 had developed considerable deflections, and the central deflection of the girder began to increase rapidly under constant load. The strains measured on the outer edges of the stiffeners S2 and S4 were both below their yield strains. It was noted that the smaller stiffener S4 had a much larger material yield stress (σ_{0s}=462.7N/mm^2). At this stage, the girder was unloaded immediately, and then the two intermediate stiffeners S2 and S4 were strengthened using flat bars, whereas the reinforcement on the middle stiffener S3 was removed. As the second test (*Test 2*), the repaired girder was loaded again, with an intention to test the load-carrying stiffener S3. The test ended at P=216.3KN when the girder collapsed by panel failure and deflection of the end bearing stiffener and flange, without apparent failure of the stiffener S3 and the reinforced stiffeners S2 and S4. This demonstrates the need to design the end stiffener to resist the horizontal component of the tension field force.

BRIT. LONDON

- ***Central Deflection δ***

As illustrated in Fig. 2.11, the load-central deflection relationship is quite linear up to 172.0KN; the curve then continues to rise more slowly reaching a peak load of 207.2KN when the applied load started to drop automatically. By reference to Figs. 2.11 and 2.15, it can be seen that the divergence of the load-central deflection curve from the initial elastic path occurred when the smaller intermediate stiffener S4 began to deflect considerably. The reason for this is that as the stiffener S4 developed a significant deflection, the two adjacent web panels tended to act as a single panel. As a result, the shearing stiffness of the girder was reduced and the shear deformation increased rapidly.

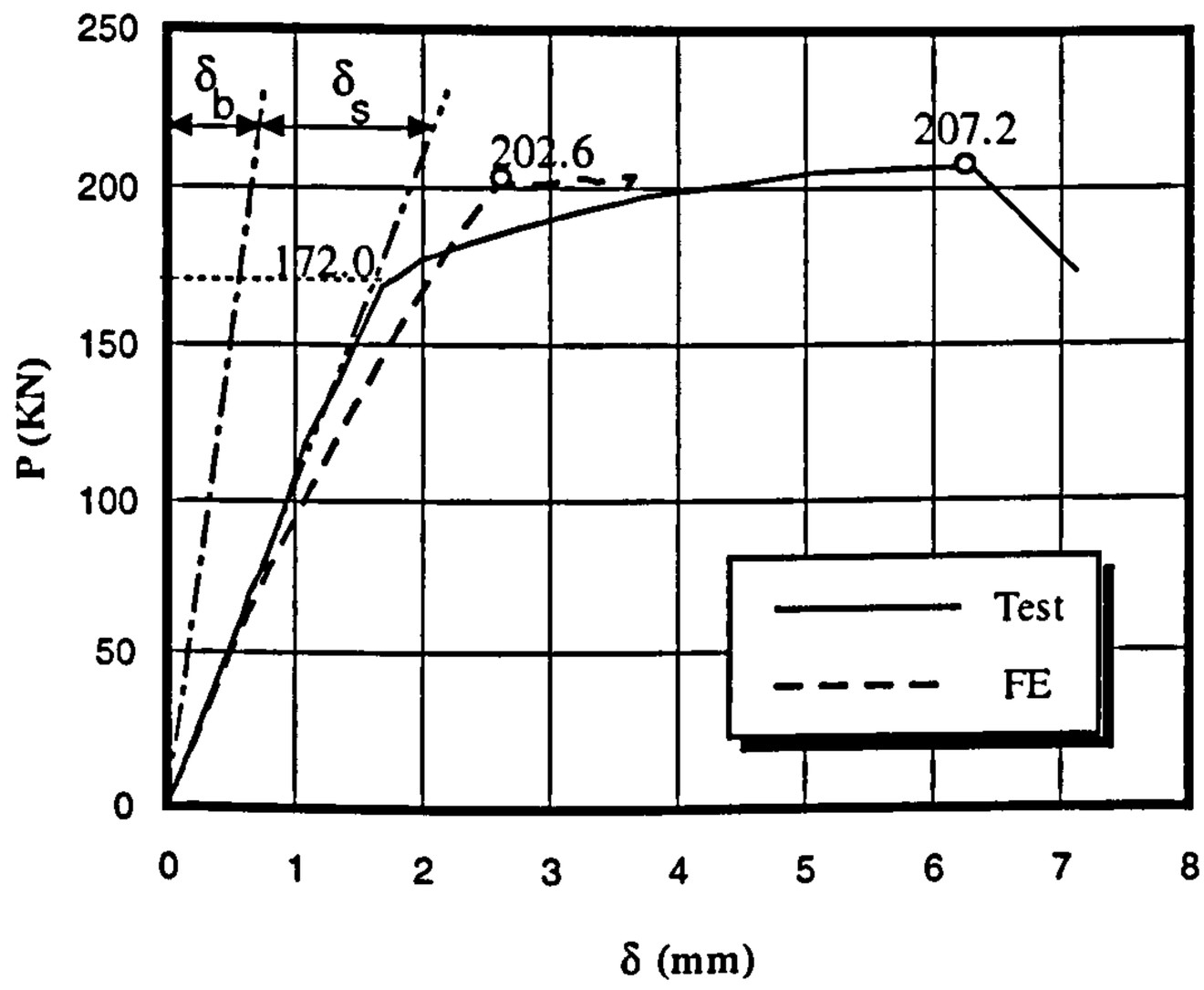


Figure 2.11 Load vs. central deflection curves. Girder GI. Test 1. δ_b and δ_s are given in Eqn. 2.1

The FE load-central deflection curve is also presented in Fig. 2.11. The FE curve is fairly linear initially, but the slope of the curve decreases slightly at about P=70KN, which corresponds to the change in the slope of the panel deflection curve, as can be seen in Fig. 2.13. After reaching a peak load of 202.6KN, there is a slight decrease in load carrying capacity but then the curve quickly develop into a region with a much less

positive slope than the test curve. It is recalled that in the FE analysis, a linear strain hardening rule of E_t=1%E was adopted (Fig. 2.9), and the assumed sinusoidal imperfections may be different from the actual initial deformations. By comparison of the FE results presented in Figs. 2.11 and 2.15, it can be observed that the peak load in the FE P-δ curve (202.6KN) is equal to the load at which the stiffener S4 began to deflect excessively.

According to the simple beam theory, the central deflection of the girder consists of the bending displacement δ_b and the deflection due to shear alone δ_s, and can be written as:

$$\delta \equiv \delta_b + \delta_s = \frac{PL^3}{48EI}\left(1+\frac{12\alpha_s EI}{GAL^2}\right) \tag{2.1}$$

where L is the length of the girder, I is the moment of inertia of the girder, A is the cross-sectional area of the girder, and α_s denotes the shear coefficient. For an I-section beam, α_s is approximately equal to A/A_w, where A_w is the cross-sectional area of the web of the girder. The deflections due to bending and shear alone are also plotted in Fig. 2.11. It is found that the simple beam theory predicts the central deflection of the test girder GI quite accurately up to the point at which the central deflection began to increase rapidly.

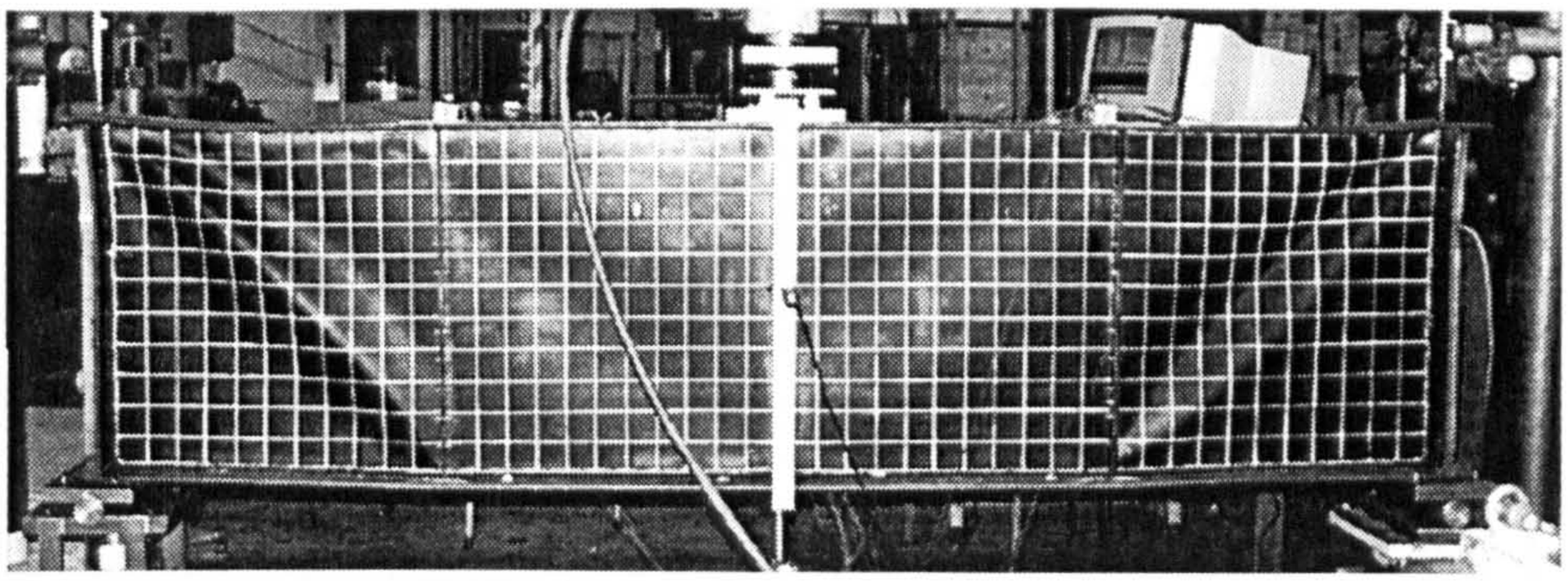
As stated before, the failure load for a test girder is taken as the applied load at which the deflection of the girder began to increase rapidly. For the test girder GI, it is noted that the measured failure load of 172.0KN is about 85% of 202.6KN estimated by ABAQUS without considering the effect of residual welding stresses.

In Fig. 2.12, the contour diagram of the out-of-plane deflection from FE analysis is compared with the deflected shape of the test girder under loading, and good agreement in the panel deflection mode can be seen.

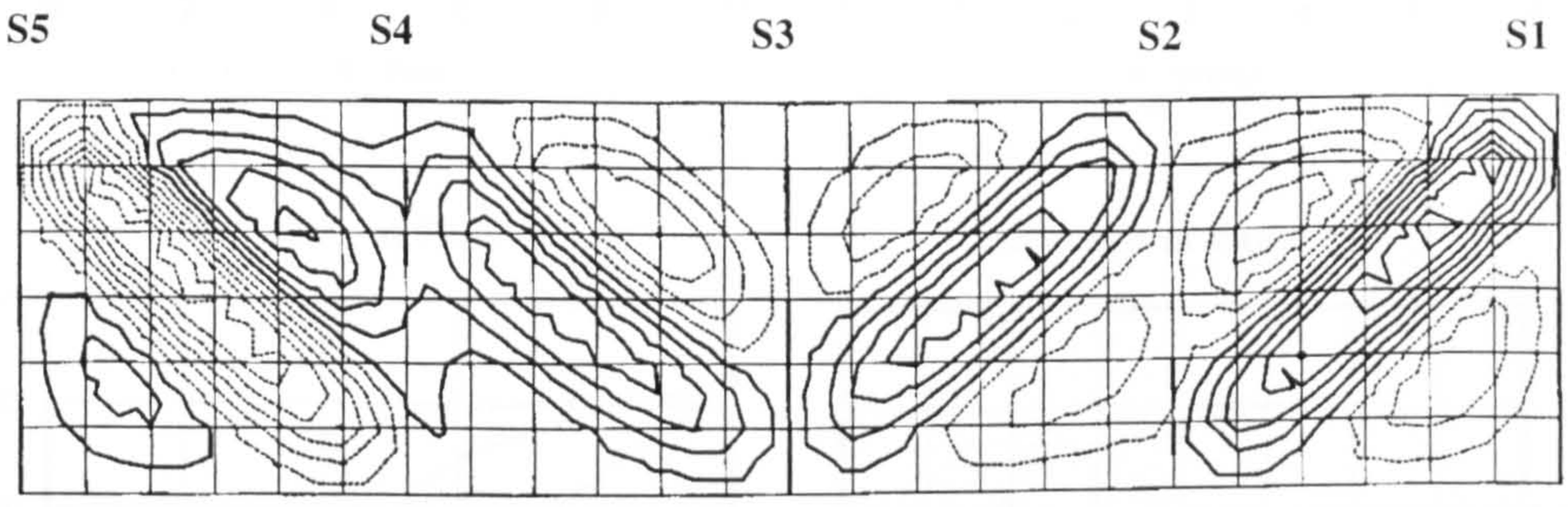
- ***Panel Deflections***

The panel deflection was measured only at the centre of each panel. It was noted that the maximum deflections did not always occur at the centre of each panel. Nevertheless,

in Fig. 2.13 the measured values were compared with the FE results for the same points, and a reasonable agreement can be seen.



(a) Test 2, $w+w_0$



(b) FE for Test 1 (with flanges), w

Figure 2.12 Web deflection of Girder GI. Back view.

The finite element load vs. deflection curves (P vs. w_p) for the panels P_{2-3} and P_{3-4} reveal an apparent panel buckling stage at about P=70KN, which can not be seen in the experimental curves. This can explain the findings in Fig. 2.11 that the experimental load-central deflection curve is linear up to P=172.0KN, while the slope of the FE curves decreases slightly at approximately P=70KN.

- ***Stiffener Deflections***

It was observed both in the test and FE analysis that the intermediate stiffeners S2 and S4 deflect in a half wave with a magnitude much less than the web thickness before the

failure load was achieved. It was also found that the middle load-carrying stiffener S3 kept nearly un-deflected. The stiffener deflection profiles obtained from finite element analysis are shown in Fig. 2.14.

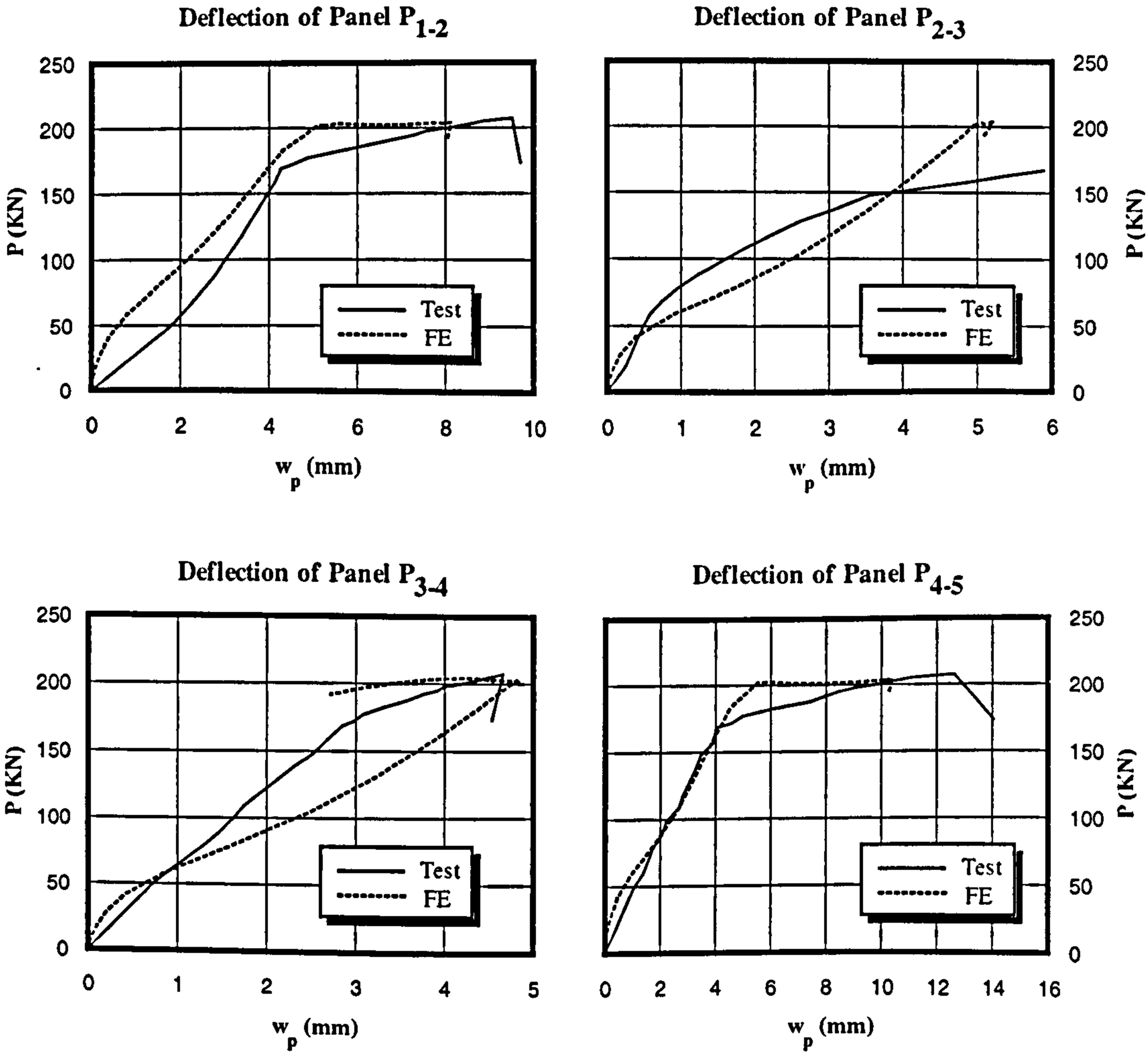


Figure 2.13 Load vs. deflection curves at the centre of the panel. Girder GI. Test 1

The stiffener deflections perpendicular to the web at the mid-length of the stiffener were measured relative to the edge of flanges. The load-deflection curves of the stiffeners are presented in Fig. 2.15. The smaller stiffener S4 (Table 2.1a) hardly deflected at the early stage of loading, and began to deflect slowly from P=70KN. At a load of 177.1KN, the deflection of the stiffener S4 was only 0.31mm, about 1/2000 of its length d or 1/16 of

the panel deflection w_p. After 177.1KN, the deflection increased rapidly to 2.75mm, approximately d/218 or w_p/4.6 at P=207.2KN, so the load of 177.1KN was taken as the failure load of the stiffener S4.

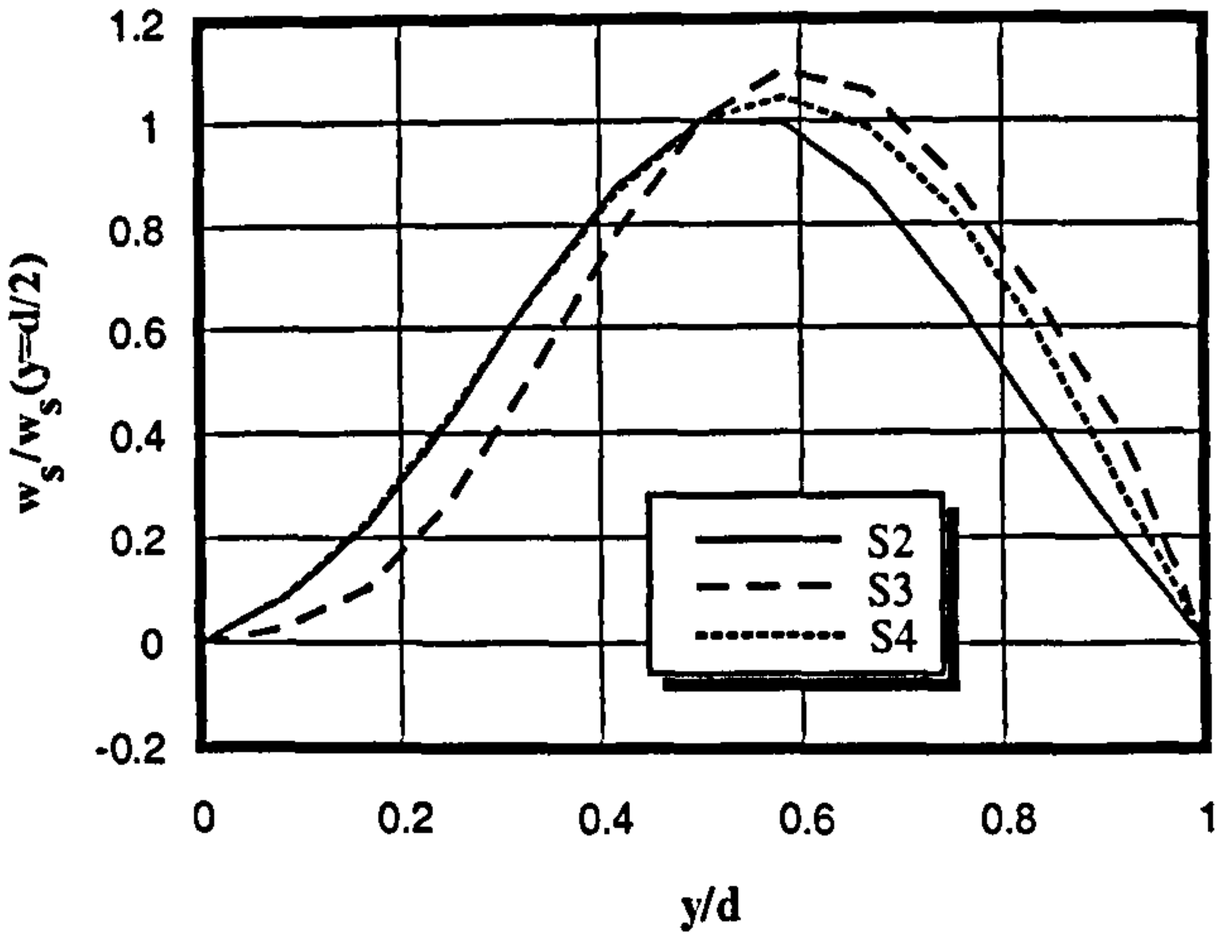


Figure 2.14 Stiffener deflection profiles from FE analysis for Test 1 at P=202.6KN. Girder GI

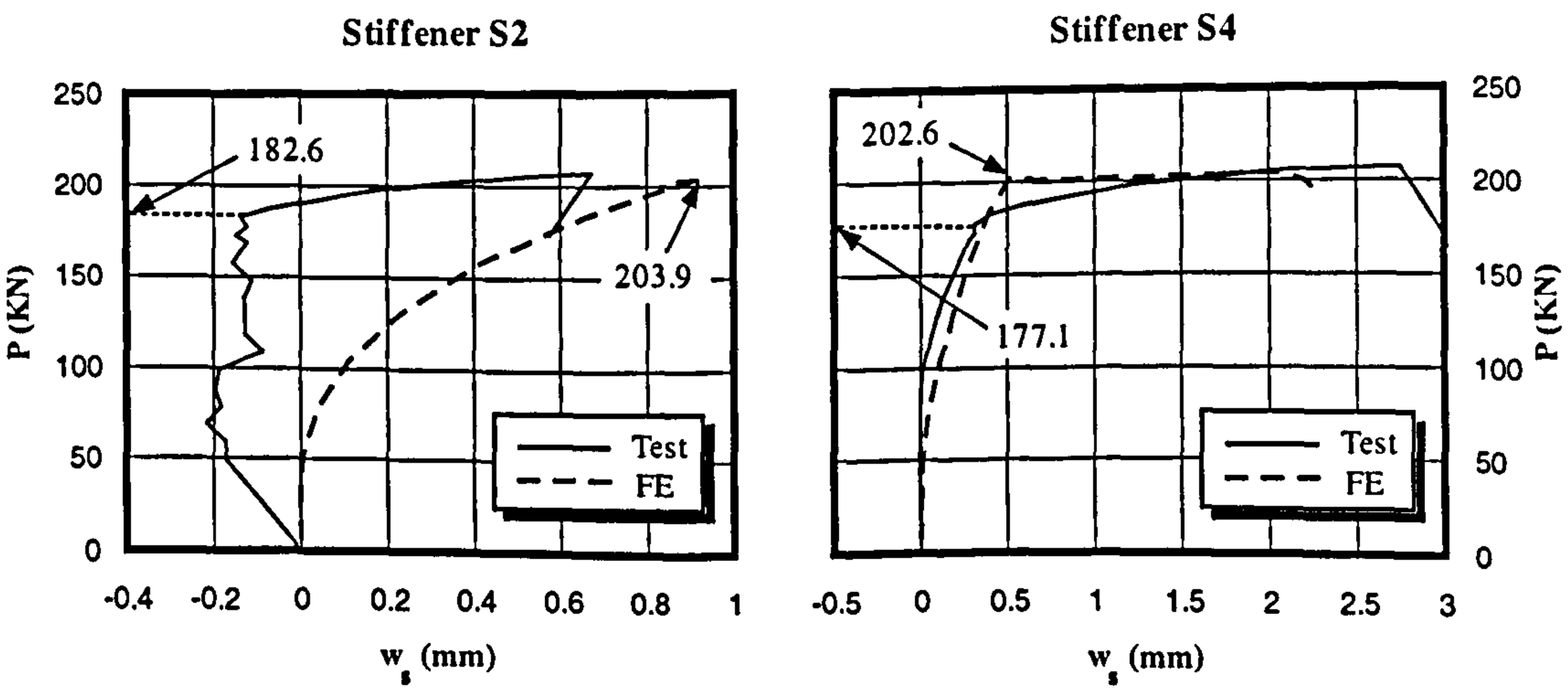


Figure 2.15 Load vs deflection curves of the stiffener. Girder GI. Test 1

The larger stiffener S2 was observed to deflect irregularly in one direction up to a load of 182.6KN, after which the stiffener started to deflect rapidly in the opposite direction.

The stiffener deflection measured at 182.6KN was only 0.14mm, about d/4280 or w_p/40, but it increased to 0.67mm (d/894 or w_p/14) at 207.2KN when the girder began to collapse. Similarly, the failure load of the stiffener S2 was taken as 182.6KN.

- ***Stiffener Forces***

All the stiffeners on the girder GI were double-sided flat bars. The normalised distributions of the axial forces and bending moments along the length of the stiffener were obtained from the non-linear finite element analysis, as given in Fig. 2.16. It was found that the maximum values for the intermediate stiffeners occurred at the mid-length of the stiffener.

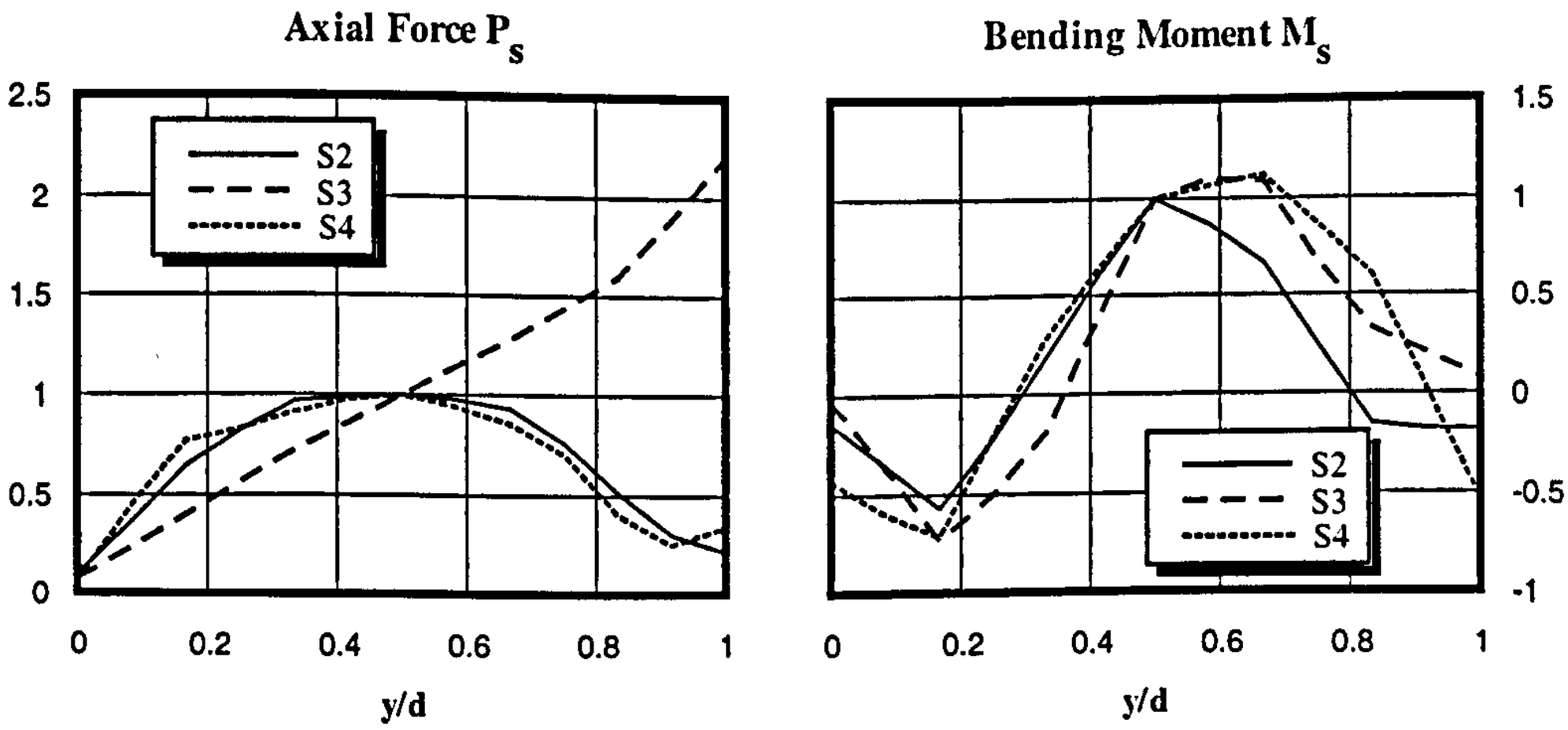


Figure 2.16 Distributions of the axial force and bending moment in the stiffener.
FE results for Test 1, at P=202.6KN. Girder GI

Strain gauges were fitted on the stiffener edges at the mid-length (Fig. 2.6). The strains measured in the stiffeners are plotted in Fig. 2.17. It was found that the strains measured in the stiffeners S2 and S4 were both below the yield strains. It is noted that the smaller stiffener S4 had a much larger yield stress (σ_{0s}=462.7N/mm^2) than the other components of the girder. These strain values show that the two intermediate stiffeners S2 and S4 were subjected to both axial forces and bending moments, whereas the load-

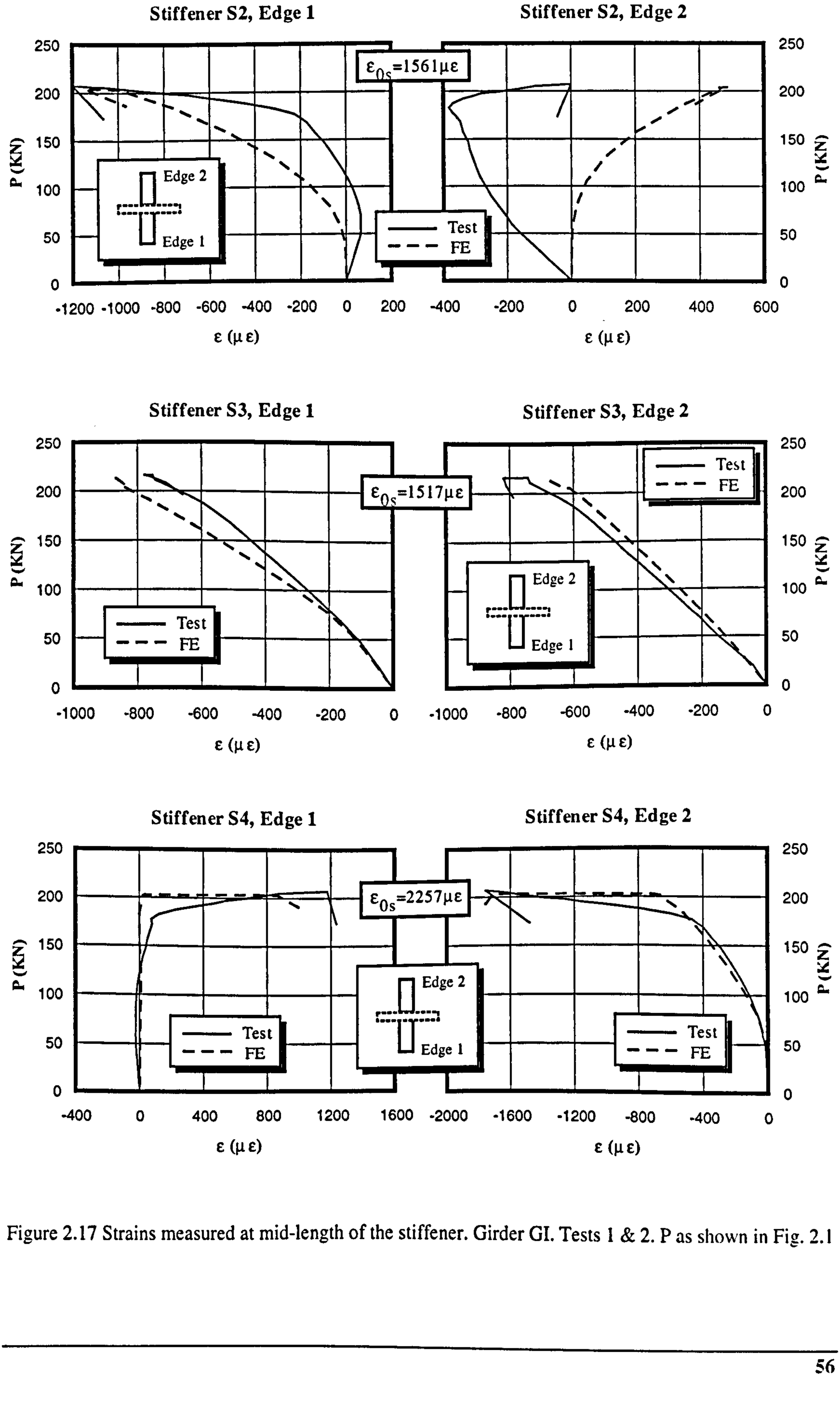
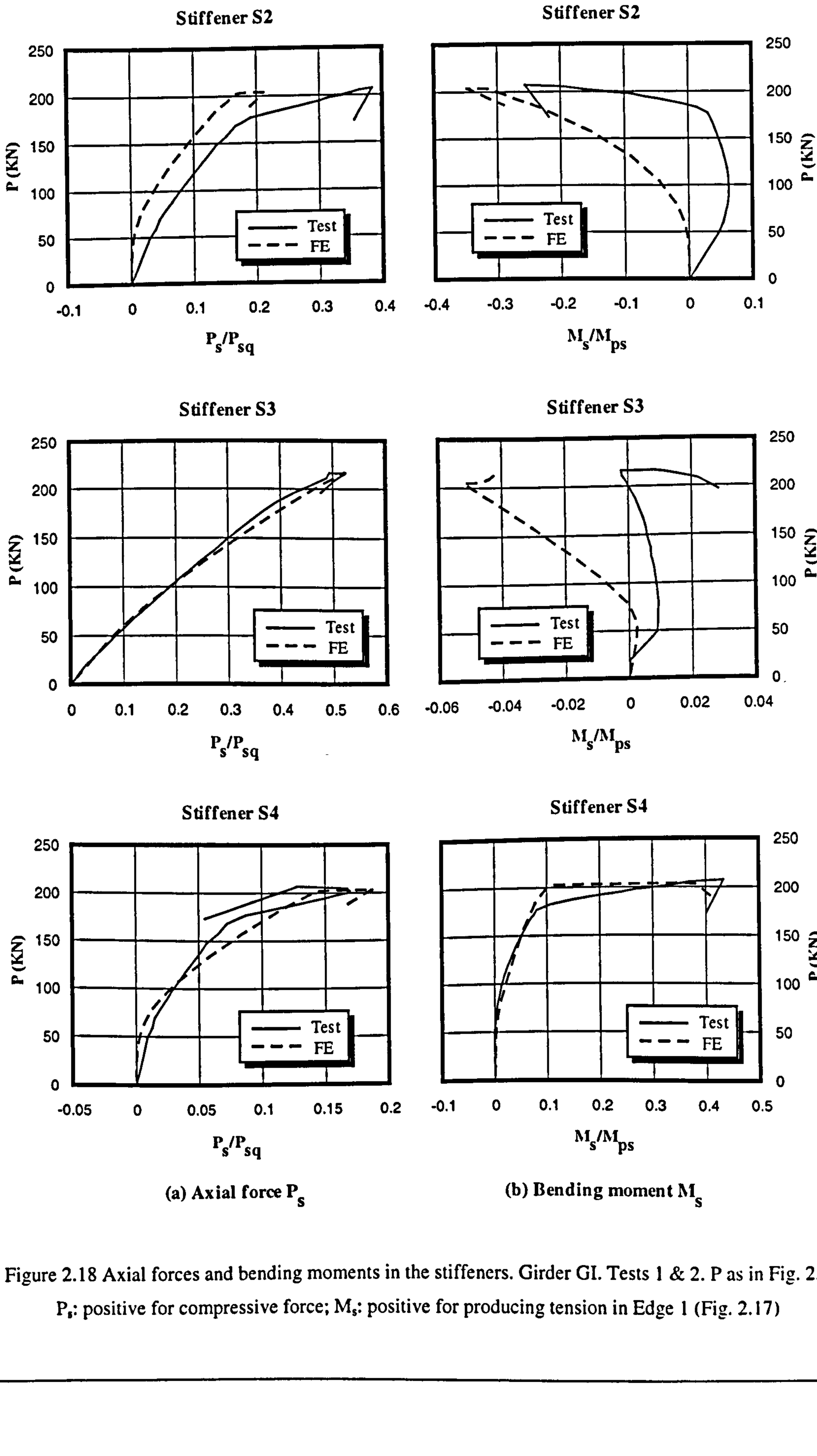


Figure 2.17 Strains measured at mid-length of the stiffener. Girder GI. Tests 1 & 2. P as shown in Fig. 2.1



(a) Axial force P_s **(b) Bending moment M_s**

Figure 2.18 Axial forces and bending moments in the stiffeners. Girder GI. Tests 1 & 2. P as in Fig. 2.1

P_s: positive for compressive force; M_s: positive for producing tension in Edge 1 (Fig. 2.17)

carrying stiffener S3 was virtually only subjected to axial forces. This behaviour is consistent with the measurements of the stiffener deflections.

In terms of the measured strain values, the axial loads and bending moments in the stiffeners were calculated, by assuming a linear distribution of axial stresses on the stiffener section. The values calculated from the test results are compared with the FE solutions in Fig. 2.18. It was found that the internal stiffener forces predicted by ABAQUS agree well with experimental results (M_s/M_{ps} for the stiffener S3 is very small for FE and test). It is reiterated that the results presented in Fig. 2.18 are the values of the stiffener forces at the mid-length of the stiffener.

2.5.2 Girder GII

Two tests (Test Nos. 3 & 4) were carried out on Girder GII. In Test 3, all the stiffeners on this girder were not reinforced, and the girder was loaded up to 171.4KN. By then the strain measured on the outer edge of the smaller intermediate stiffener S2 (Table 2.1a) had reached its yield strain, and the central deflection of the girder began to increase non-linearly. At this stage, the girder was unloaded immediately, and then the intermediate stiffener S2 was strengthened using flat bars. As a second test on GII (Test 4), the repaired girder was loaded again, with an intention to test the larger intermediate stiffener S4. The test ended at P=215.3KN when the girder collapsed, with the failure of the intermediate stiffener S4.

- ***Central Deflection***

As illustrated in Fig. 2.19, the experimental load-central deflection relationship, obtained from Test 4 (i.e., the second test on Girder GII, with the smaller stiffener S2 being reinforced), is nearly linear up to about 175.8KN. At P=181.0KN, the curve becomes to rise more slowly reaching a peak load of 215.3KN when the applied load began to drop automatically. By reference to Figs. 2.19 and 2.23, it can be seen that the divergence of the load-central deflection curve from the initial elastic path occurred when the intermediate stiffener S4 began to deflect considerably. This is because when

the stiffener S4 developed a significant deflection, the two adjacent web panels tended to act as a single panel. As a result, the shearing stiffness of the girder was reduced and the shear deformation increased considerably.

The FE load-central deflection curve is also presented in Fig. 2.19. The FE curve is fairly linear up to a load of P=209.0KN. After P=209.0KN, the slope of the FE curve reduced sharply to a value close to that of the corresponding test curve, and the central deflection δ keeps increasing rapidly. It is noted that in the FE analysis, a linear strain hardening rule of E_t=1%E was adopted (Fig. 2.9). By comparison of the FE results presented in Figs. 2.19 and 2.23, it can be seen that the peak load (P=209KN) in P-δ curve is equal to the load at which the stiffener S4 began to snap.

The deflections due to bending and shear alone, δ_b and δ_s, calculated using Eqn. 2.1, are also plotted in Fig. 2.19. It is found that the simple beam theory predicts the central deflection of the test girder GII quite accurately up to the point at which the central deflection began to increase rapidly.

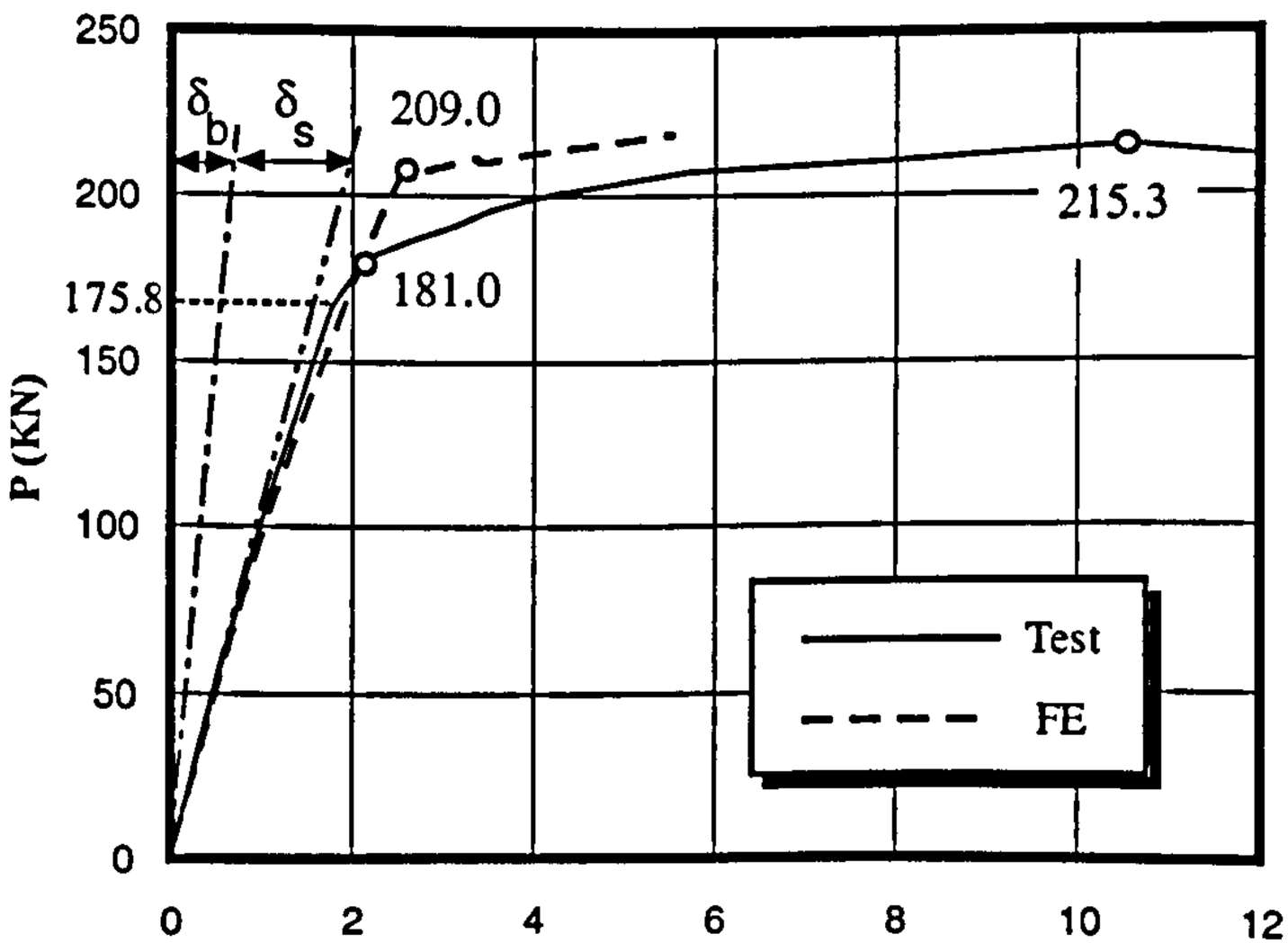
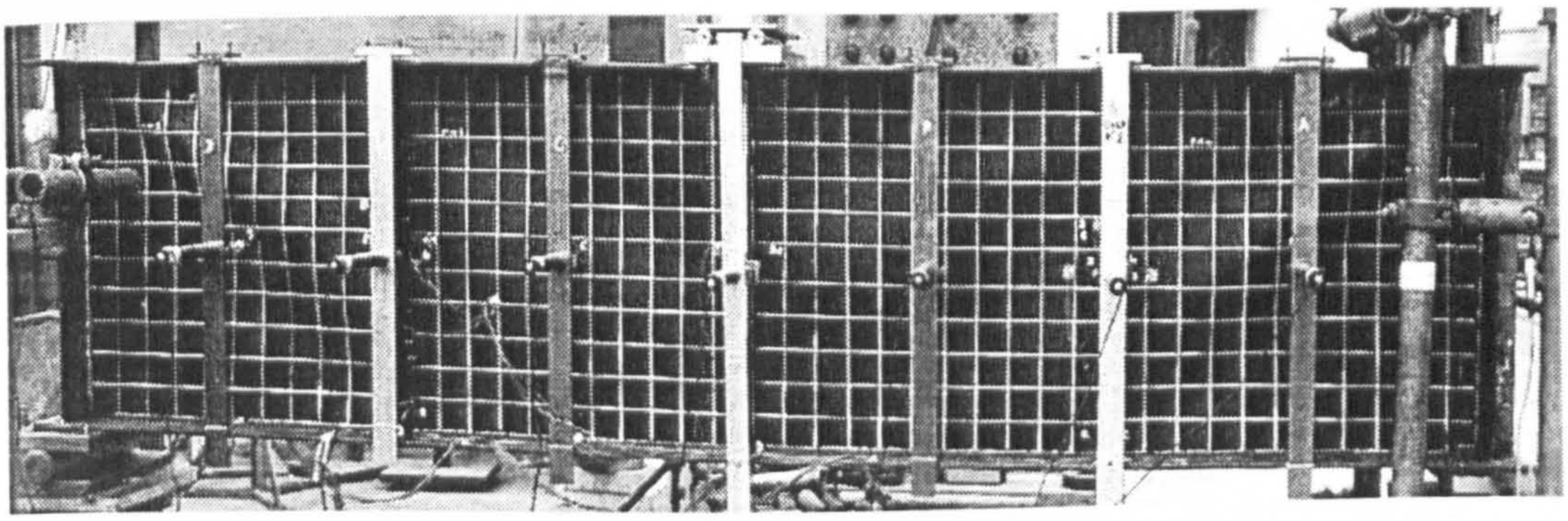


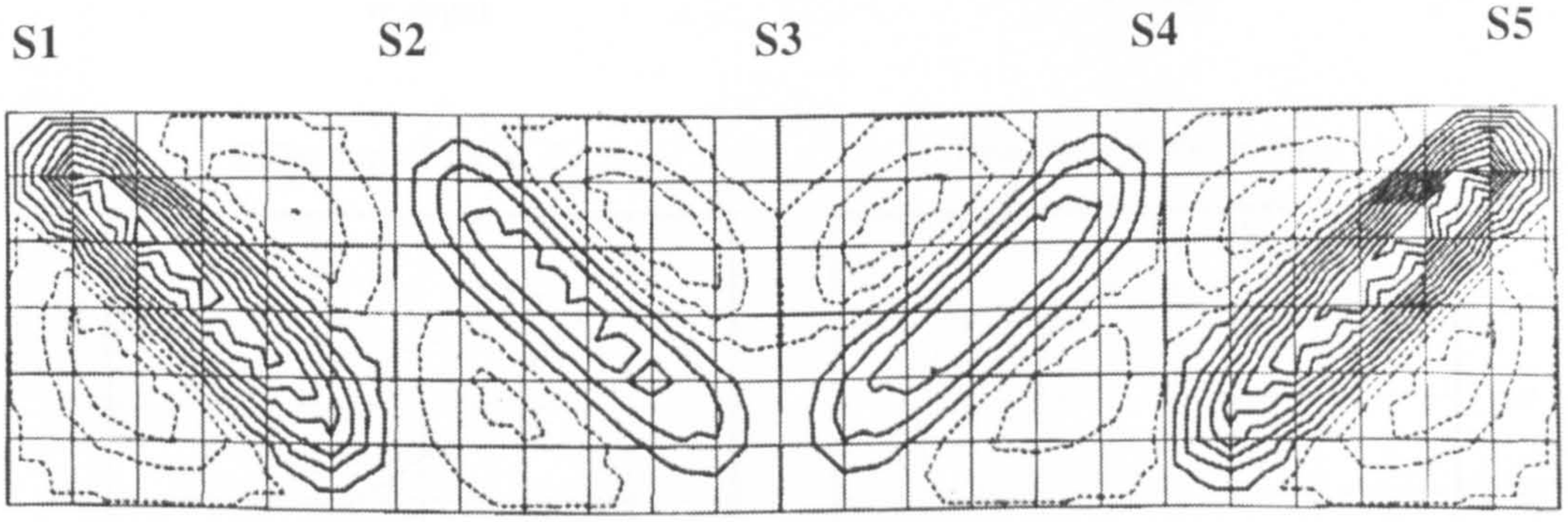
Figure 2.19 Load vs. central deflection curves. Girder GII. Test 4.
δ_b and δ_s are given in Eqn. 2.1. P as shown in Fig. 2.1

As defined before, the failure load for the test girder GII is taken as the applied load at which the deflection of the girder began to increase rapidly. It is noted in Fig. 2.19 that the measured failure load of 181.0KN is about 87% of 209.0KN estimated by ABAQUS without considering the effect of residual welding stresses.

In Fig. 2.20, the contour diagram of the out-of-plane deflection from FE analysis is compared with the deflected shape of the test girder under loading, and good agreement can be seen.



(a) Test , $w+w_0$



(b) FE (with flanges), w

Figure 2.20 Web deflection of Girder GII. 2nd Test on GII (Test 4)

- ***Panel Deflections***

The panel deflection was measured only at the centre of each panel. It was noted that the maximum deflections did not always occur at the centre of each panel. Nevertheless,

in Fig. 2.21 the measured values were compared with the FE results for the same points. For the panels $P_{1\text{-}2}$ and $P_{2\text{-}3}$, the results from the 1st test on this girder (Test 3) are presented, while for the panels $P_{3\text{-}4}$ and $P_{4\text{-}5}$, the results from the 2nd test (Test 4) are shown. As can be seen in Fig. 2.21, the general trends for the panels to buckle indicated by the finite element solutions agree reasonably with the test results. The differences between FE and test results are due to the assumed sinusoidal imperfections, which may be different from the actual initial deformations.

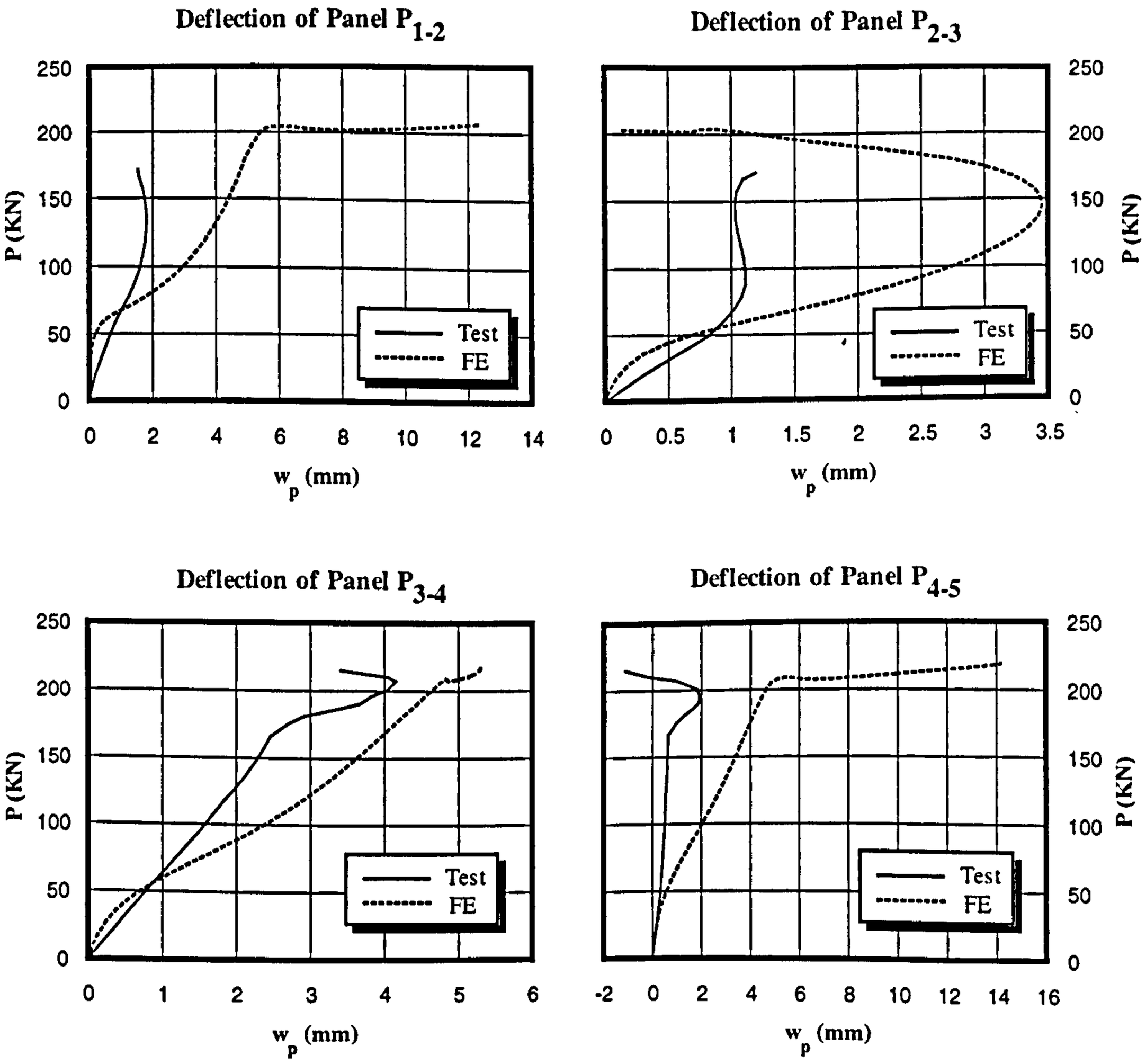


Figure 2.21 Load vs. deflection curves at the centre of the panel. Girder GII. P as shown in Fig. 2.1
Test 3 for the panels $P_{1\text{-}2}$ and $P_{2\text{-}3}$; Test 4 for the panels $P_{3\text{-}4}$ and $P_{4\text{-}5}$.

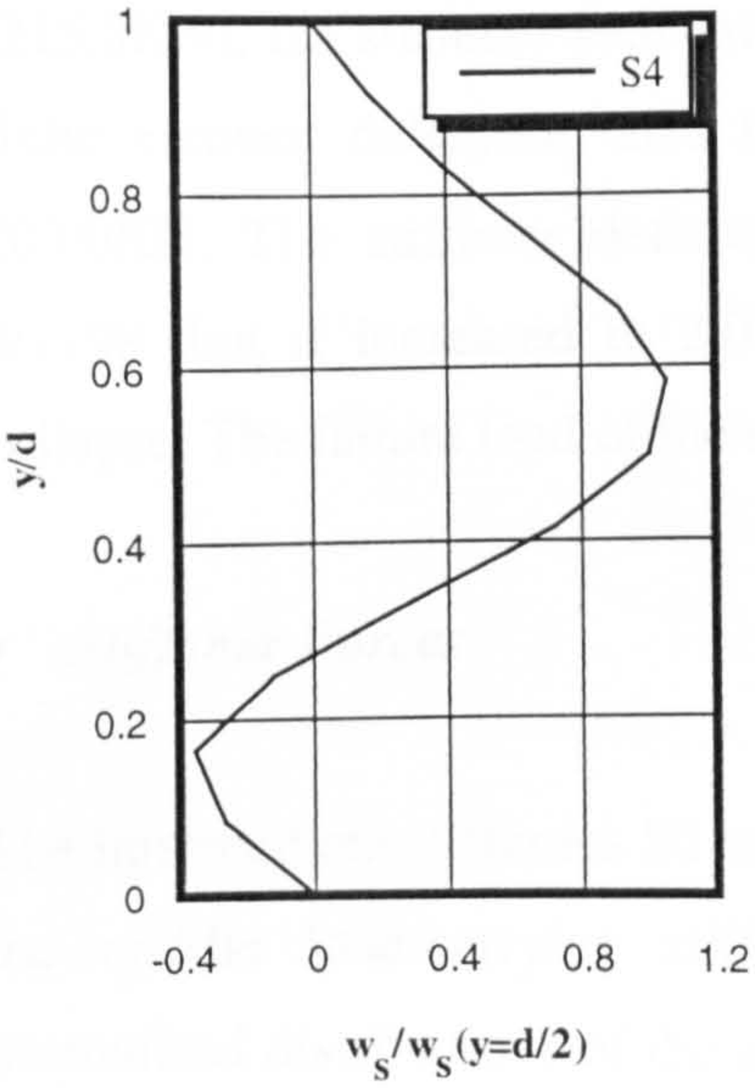
For the panel $P_{2\text{-}3}$, both the experimental and finite element curves of load vs. deflection (P vs. w_p) reveal a significant change in the buckling mode at about P=145KN. It is noted in Fig. 2.23 that when the applied load P approached this value, the deflection of the stiffener S2 began to increase more quickly.

- ***Stiffener Deflections***

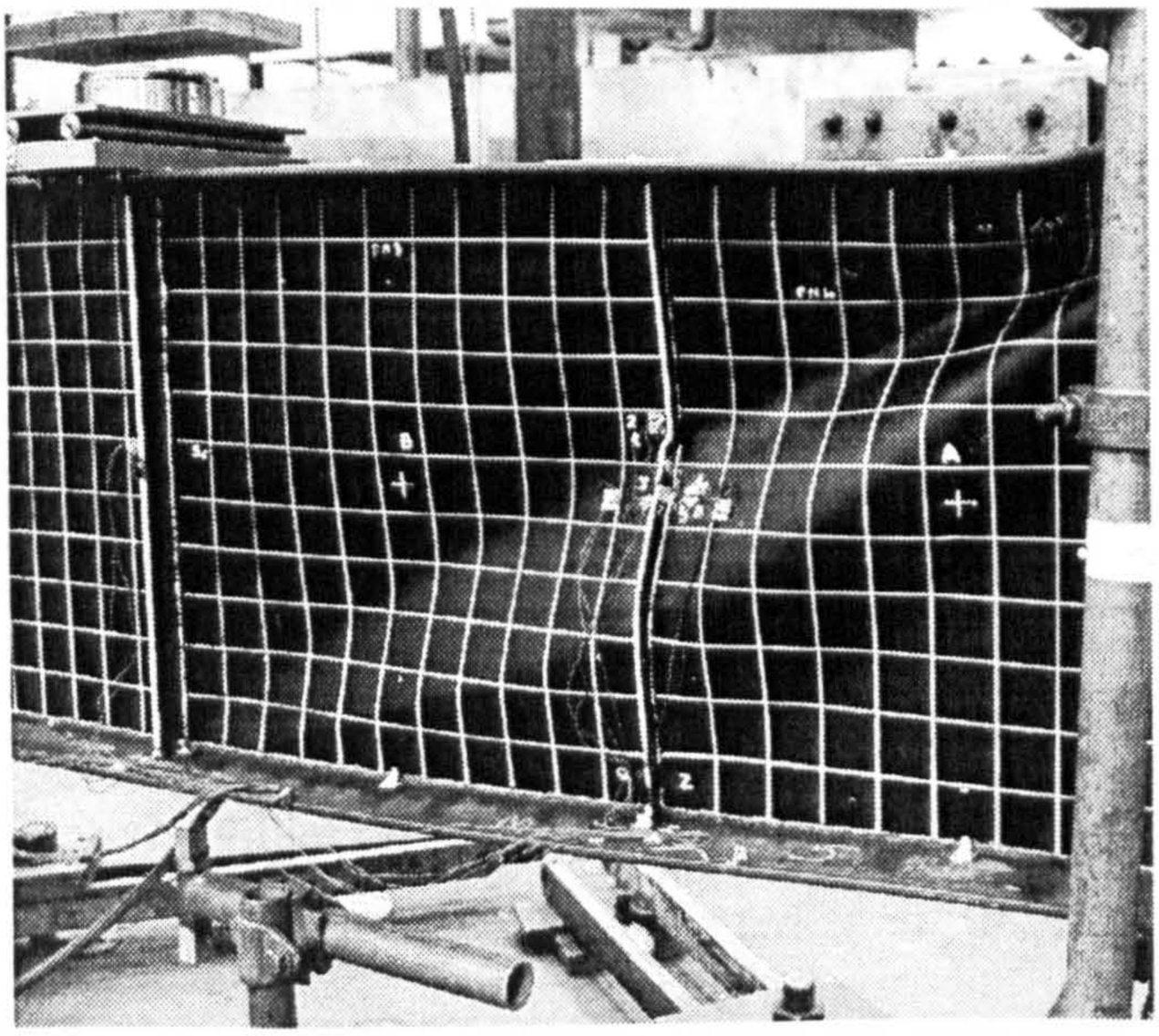
Similar to the observations for Girder GI, it was found that the middle load-carrying stiffener S3 kept nearly un-deflected. In Test 3 (the first test on Girder GII), the intermediate stiffeners S2 and S4 were observed to deflect in a half wave, but the test was stopped before excessive deflection could be developed. In Test 4 (the second test on Girder GII), it was observed that the stiffeners S4 initially deflect in a half wave, but as the load approached the ultimate load of the girder, the stiffener had developed a double-curvature profile. Fig. 2.22a presents the deflected shape of the stiffener S4 at the maximum load obtained from the finite element analysis. In Fig. 2.22b, the deflected stiffener S4 after the test ended is shown. It is apparent that the deflected shape of the stiffener from FE solutions agrees with that shown in the test.

The stiffener deflections perpendicular to the web at the mid-length of the stiffener were measured relative to the edge of flanges. The experimental load-deflection curves of the stiffeners are presented in Fig. 2.23, and compared with the finite element solutions.

It can be seen in Fig. 2.23 that the deflection of the smaller intermediate stiffener S2, measured in Test 3, increases gradually at the early stage of loading, and began to deflect more rapidly after the applied load P reached about 150KN. When the load P approached 171.4KN, it was found that the strain measurement on the outer edge of the stiffener reached the yield strain of the stiffener (Fig. 2.25). At P=171.4KN, the deflection of the stiffener S2 was 3.87mm, about 1/155 of its length d. The load of 171.4KN was taken as the failure load of the stiffener S2. It is seen in Fig. 2.23 that for the stiffener S2, the finite element deflection curve is close to the experimental curve.



(a) FE results



(b) Stiffener S4 after test

Figure 2.22 Deflected shapes for the stiffener S4. Girder GII. Test 4

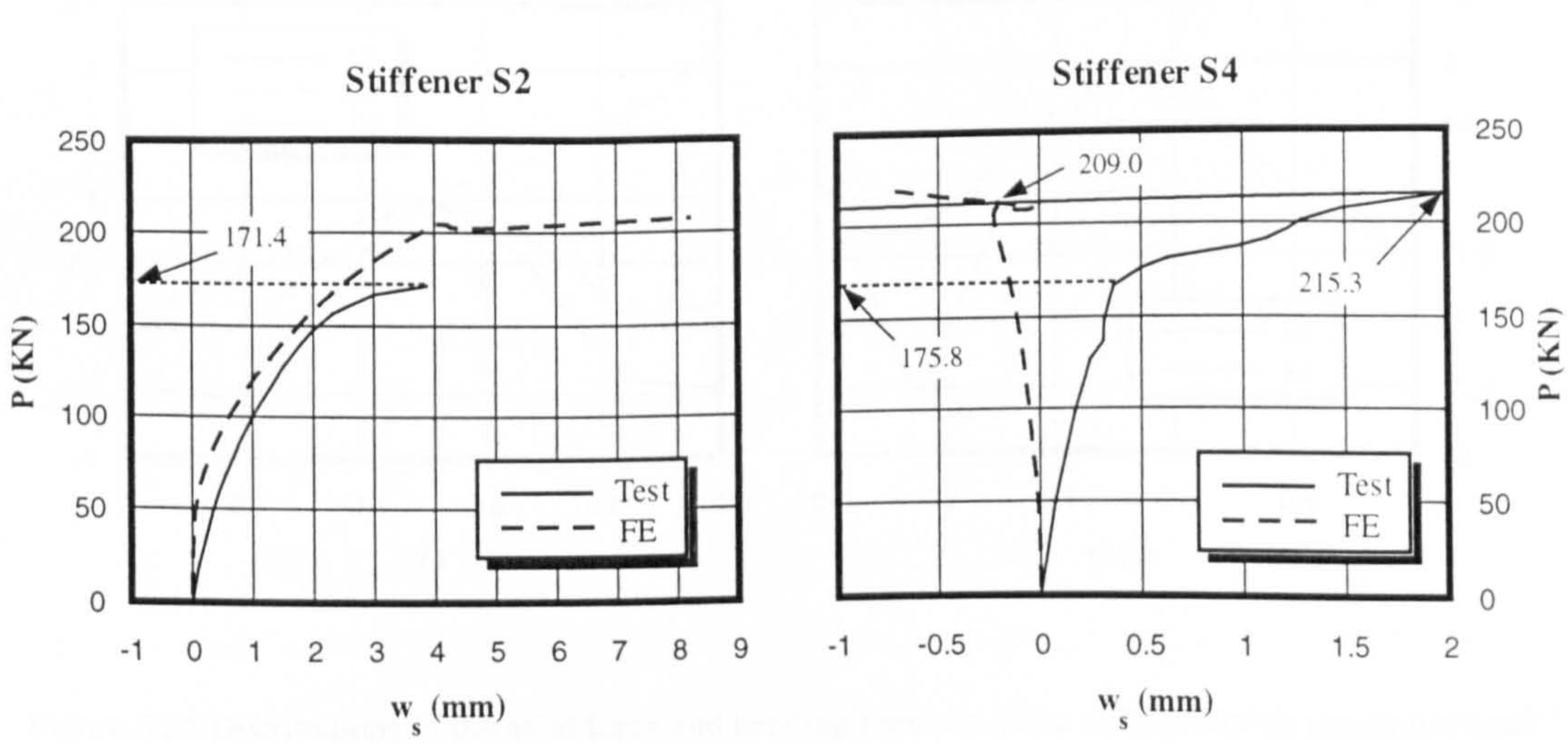


Figure 2.23 Load vs deflection curves of the stiffener. Girder GII. Tests 3 & 4. P as shown in Fig. 2.1

The results shown in Fig. 2.23 for the larger intermediate stiffener S4 are from Test 4. It can be seen that the stiffener S4 deflected slowly up to a load of 175.8KN, after which

the stiffener started to deflect rapidly. As the applied load P reached the maximum load (215.3KN), the stiffener suddenly buckled in the opposite direction. It is noted that the finite element deflection also indicates a similar snapping behaviour, at a load of 209.0KN. The stiffener deflection measured at 175.8KN was only 0.50mm, about d/1198, but it increased to 2.0mm (≈d/300) at 215.3KN when the girder began to collapse. The failure load of the stiffener S2 was taken as 175.8KN.

- ***Stiffener Forces***

The intermediate stiffeners S2 and S4 on the girder GII were single-sided flat bars, and the middle load-carrying stiffener S3 consisted of double-sided flat bars. The normalised distributions of the axial forces and bending moments (about the centroidal axis of the stiffener section) along the length of the stiffener at the maximum load were obtained from the non-linear finite element analysis, as given in Fig. 2.24.

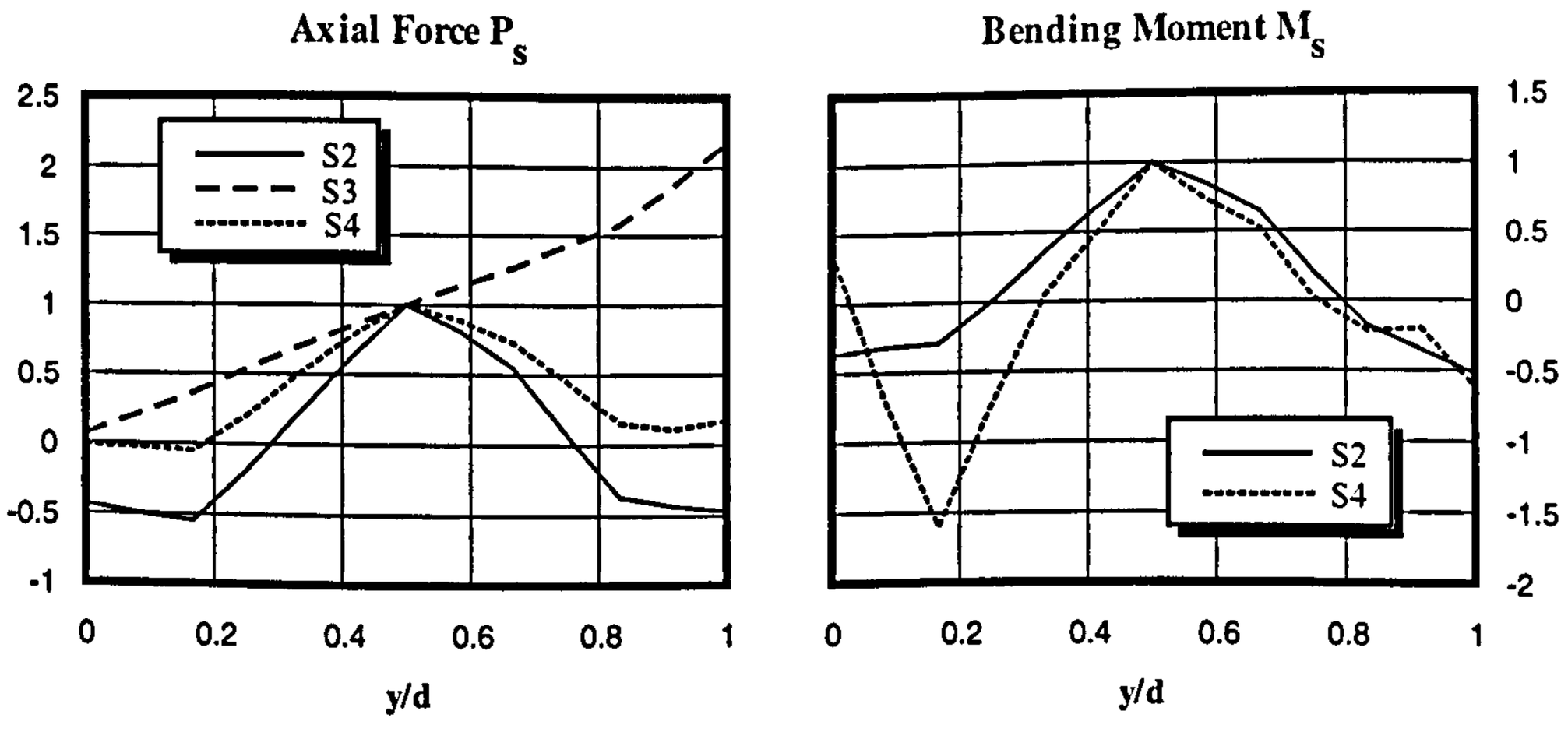


Figure 2.24 Distributions of the axial force and bending moment in the stiffener at the maximum load (P=177.1KN for S2, Test 3; P=209.0KN for S4, Test 4). Girder GII. FE results.

It was found that for the intermediate stiffeners, the maximum values of the axial force P_s occurred at the mid-length of the stiffener, and when the stiffener deflected in a half

wave form, the maximum values of the bending moment M_s also occurred at the mid-length of the stiffener, as shown in Fig. 2.24 for the stiffener S2. The final deflected shape for the stiffener S4 is shown in Fig. 2.22, and the corresponding distribution of M_s is presented in Fig. 2.24, which gives a maximum bending moment at about y/d=0.2. As shown in Fig. 2.26, there is almost no bending in the load-carrying stiffener S3.

Strain gauges were fitted on the stiffener edges at the mid-length (Fig. 2.6). For the single-sided stiffeners S2 and S4, by assuming a linear distribution of the axial stress across the width of the stiffener, the strains in the edge in contact with the web were estimated using the strain values measured on the outer edge and the two sides of the stiffener (see Fig. 2.6). The experimental values of the strains in the stiffeners are presented in Fig. 2.25, where a comparison with the finite element results is made. It is apparent in Fig. 2.25 that the FE analyses produce satisfactory agreement with the test results.

It is shown in Fig. 2.25 that at P=171.4KN, the tensile strain measured on the edge 1 of the stiffener S2 (Test 3) reached the yield strain ε_{0s} of the stiffener material. It is noted in Fig. 2.23 that as the applied load P approached this value, the stiffener had started to deflect rapidly. Therefore, the load of 171.4KN was taken as the failure load for the stiffener S2. It is seen in Fig. 2.25 that the FE results indicate that the stiffener S2 started to yield at P=177.1KN. The strain measurements indicate that the outer edge of the stiffener was in tension, while the edge in contact with the web was in compression, and the tensile strain was significantly greater than the value of compressive strain.

It is evident in Fig. 2.25 that the middle load bearing stiffener S3 was in compression, and the compressive strains on the two opposite edges were almost equal, which indicated that the stiffener S3 was virtually only subjected to axial forces. It is noted that the initial imperfection of the fabricated stiffener S3 was almost zero.

For the single-sided intermediate stiffener S4 (Test 4), the strains measured at the maximum load were below the yield strains, but then the strains increased even at the constant load, because by that time, the stiffener S4 had become unstable and the whole

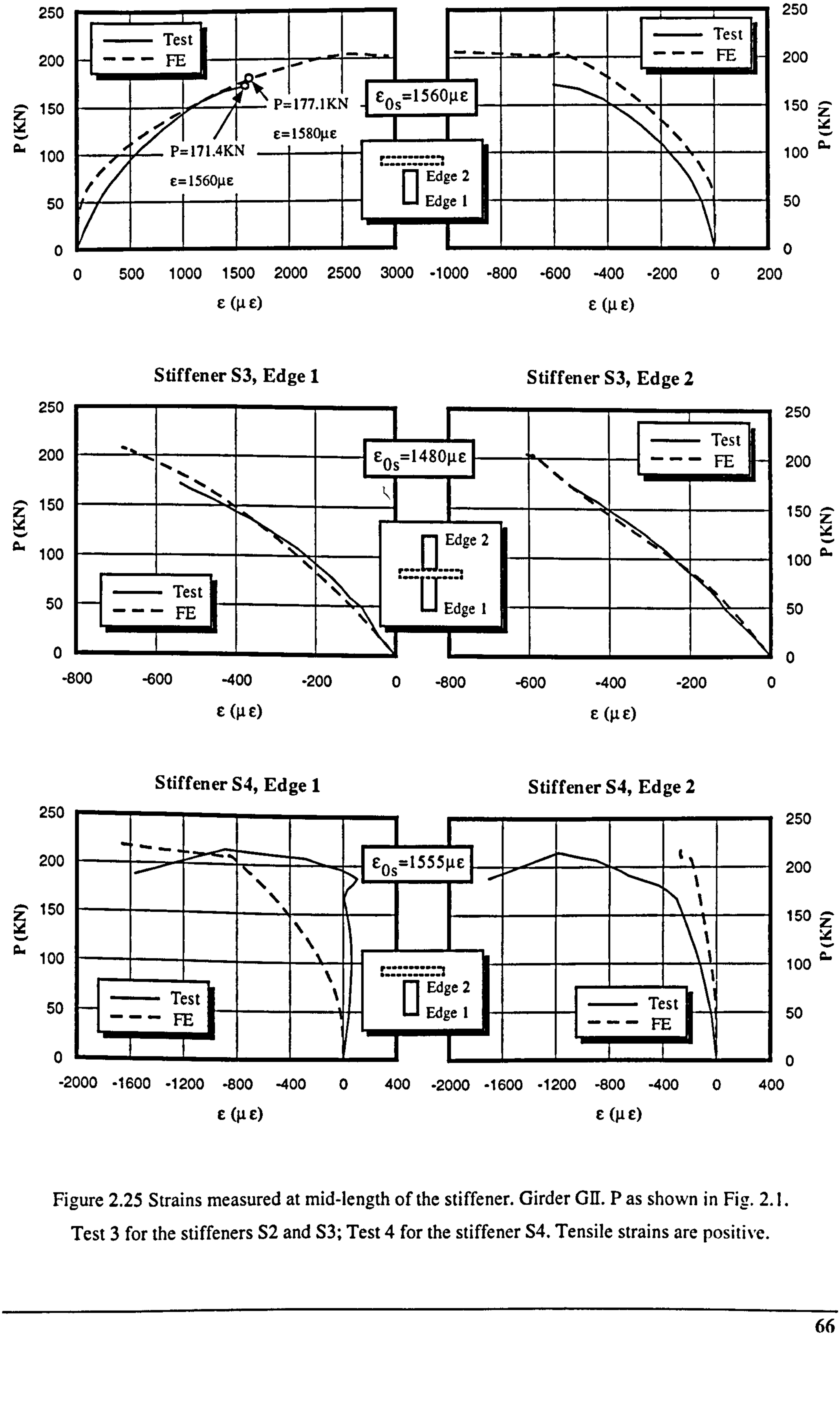
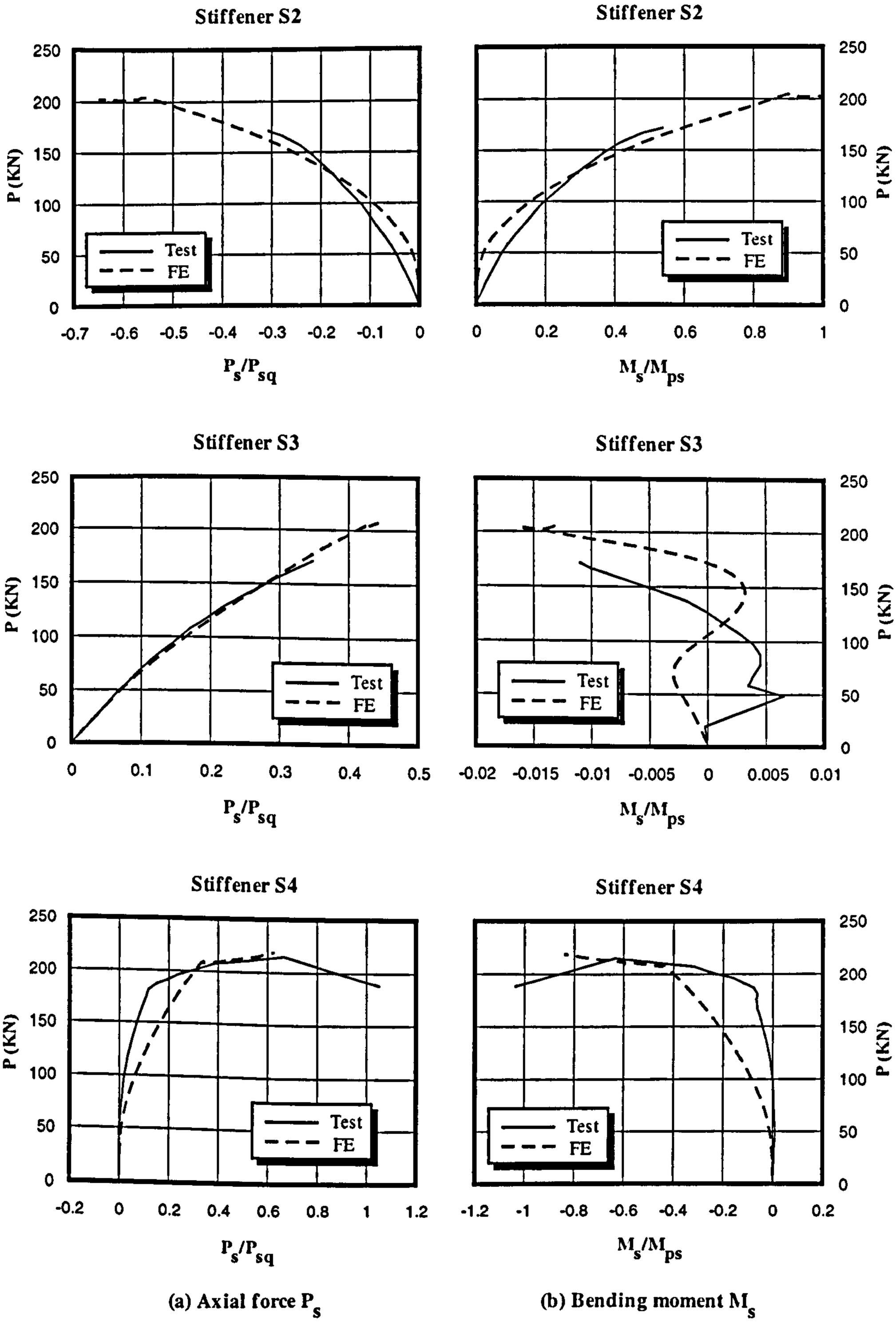


Figure 2.25 Strains measured at mid-length of the stiffener. Girder GII. P as shown in Fig. 2.1. Test 3 for the stiffeners S2 and S3; Test 4 for the stiffener S4. Tensile strains are positive.



(a) Axial force P_s (b) Bending moment M_s

Figure 2.26 Axial forces and bending moments in the stiffeners. Girder GII. P as shown in Fig. 2.1.

P_s: positive for compressive force; M_s: positive for producing tension in Edge 1 (Fig. 2.25)

Test 3 for the stiffeners S2 and S3; Test 4 for the stiffener S4.

girder began to collapse. The measured strain values show that the stiffener S4 was subjected to both axial loads and bending moments. It is observed in Fig. 2.25 that for the initial stage of the test, the finite element solutions indicates that the tip (edge 1) of the stiffener S4 was in tension, while actually it was in compression and also the value of the compressive strain in the tip was greater than that of the edge 2. Referring to Fig. 2.23, the reason for the differences can be seen. That is, the stiffener deflection given by the FE analysis is in the opposite direction of the real deflection of the tested stiffener, caused by the assumed initial imperfection mode.

In terms of the measured strain values, the axial loads and bending moments in the stiffeners were calculated, by assuming a linear distribution of axial stresses on the stiffener section. The values calculated from the test results are compared with the FE solutions in Fig. 2.26. It was found that allowing for the difference in the stiffener deflection caused by the assumed imperfection mode, the internal stiffener forces predicted by ABAQUS agree well with experimental results.

2.5.3 Girder GIII

In this and the next sections, only the finite element results are presented respectively for the test girders GIII and GIV. This is because by the time of writing this thesis, the tests on this group of girders (group B, Fig. 2.1) have not been fully completed. Nevertheless, it has been shown in the preceding sections that the finite element program ABAQUS can well represent the overall behaviour of the stiffened plate girders and the buckling behaviour of their members. Therefore, the FE solutions for these two girders are useful to understand the non-linear buckling behaviour of the plate girders. The experimental results will be presented in a separate report in the near future, and will be compared with the numerical results presented here.

On the test girders GIII and GIV (see Fig. 2.1 and Table 2.1b), there was a single intermediate stiffener (S2 or S8) near each end of the girder. In the middle of the girder, three consecutive intermediate stiffeners (S4, S5 and S6), identical in their dimensions, were used to reveal the buckling behaviour of multiple stiffeners. For the numerical

analyses, the web and stiffener components of the initial imperfection were taken as sine waves, with the code specified magnitudes (Eqns. 3.8 and 3.9), and superimposed on each other. For the middle stiffeners S4, S5 and S6, the initial deflections were taken to be in alternative direction, as assumed by Richmond [48]. For each girder, two analyses were carried out. The first analysis revealed that the stiffener S2 failed before the others (for both GIII and GIV), and the second analysis was run to model the girder after the stiffener S2 was reinforced.

It should be noticed that the stiffener and loading arrangements for GIII and GIV were different from those for GI and GII. Referring to Fig. 2.1, it can be found that for the same magnitude of applied load P, the shear force for GIII and GIV is equal to P, whereas the shear force for GI and GII is P/2. Similarly, the bending moments are also different.

For the test girder GIII, the first analysis indicated that as the applied load P (Fig. 2.1) approaches P=143.9KN, the stiffener S2 reached its yield strain and its deflection started to increase quickly. After increasing the stiffener size of S2, the second analysis was conducted. It was found that the stiffener S8 began to deflect considerably at P=146.8KN, and the yield strain of the stiffener was exceeded at P=149.6KN. It was noted that at P=146.8KN, the vertical end deflection began to increase rapidly. The FE analysis also revealed that of the three middle stiffeners, the stiffener S4 yielded at P=161.9KN, and its deflection started to increase rapidly at this load level.

- ***End Deflection***

In Fig. 2.27, the FE curves of the applied load P against the end vertical deflection at the two ends of the girder (i.e., at the positions of the stiffeners S1 and S9, Fig. 2.1) are presented. It can be seen that the load-deflection relation is nearly linear up to 143.9KN for the left end and 146.8KN for the right end, and then the end deflections began to increase rapidly. It is noted that a linear strain hardening rule of E_t=1%E (Fig. 2.9) was adopted in the FE analysis. By reference to Figs. 2.27 and 2.32, it can be seen that the quick increase in the end deflections is due to the failure of the stiffener S2 or S8,

respectively. It is observed in Fig. 2.32 that the stiffeners S2 and S4 began to deflect considerably and reached their yield strain at P=143.9KN and 148.6KN, respectively. As pointed out previously, when the intermediate stiffener developed a significant deflection, the two adjacent web panels tended to act as a single panel. As a result, the shearing stiffness of the girder was reduced and the shear deformation increased significantly.

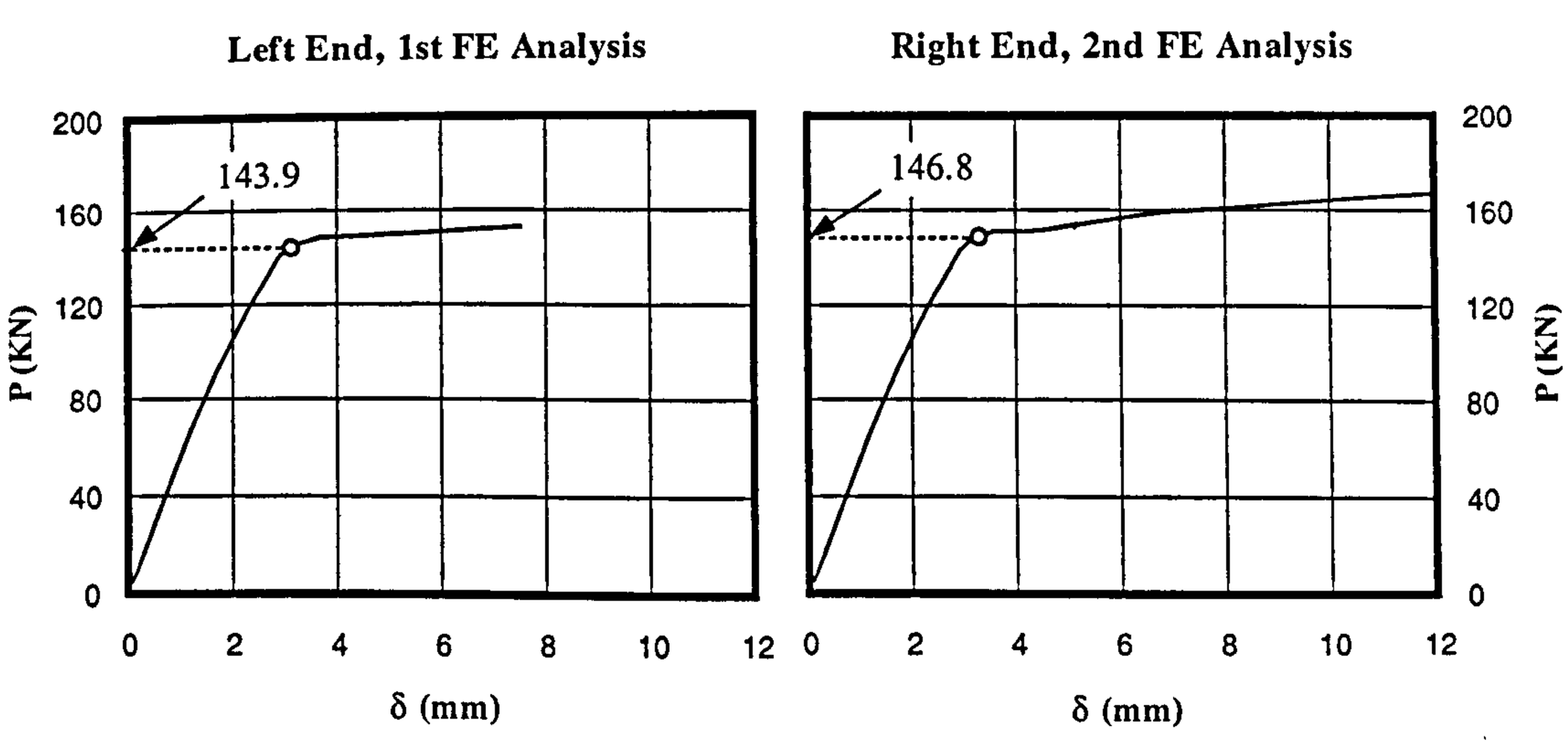


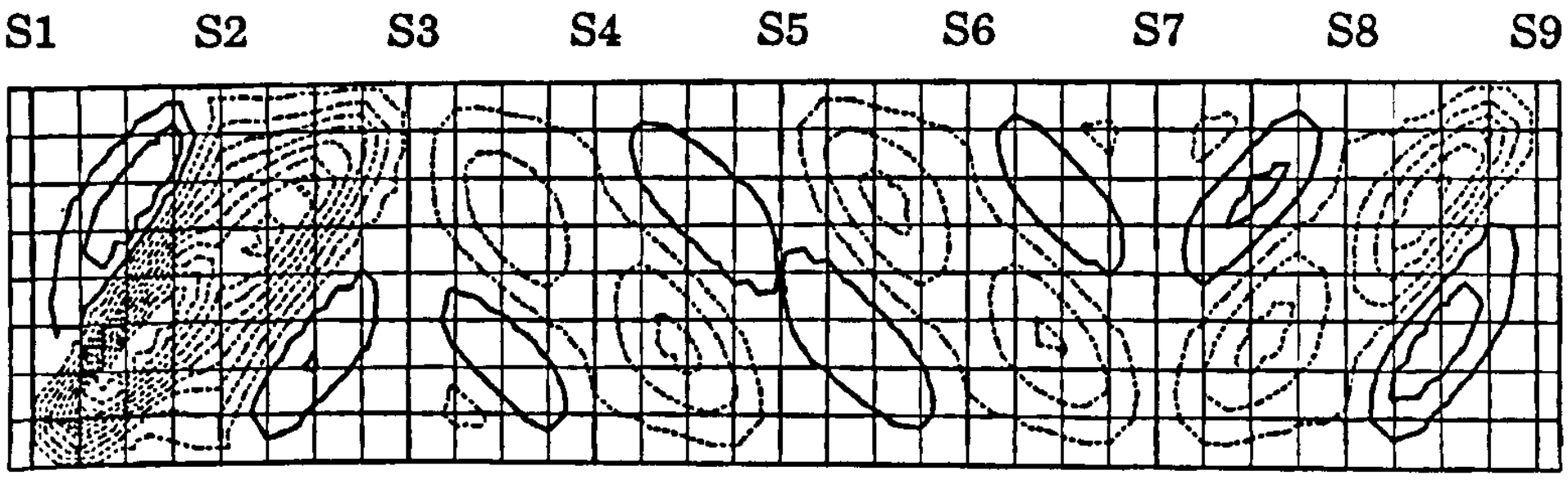
Figure 2.27 Load vs. end deflection curves. Girder GIII P as shown in Fig. 2.1. FE results

Fig. 2.28 shows the contours of the out-of-plane deflection for the stiffened web plate, obtained from the two FE analyses.

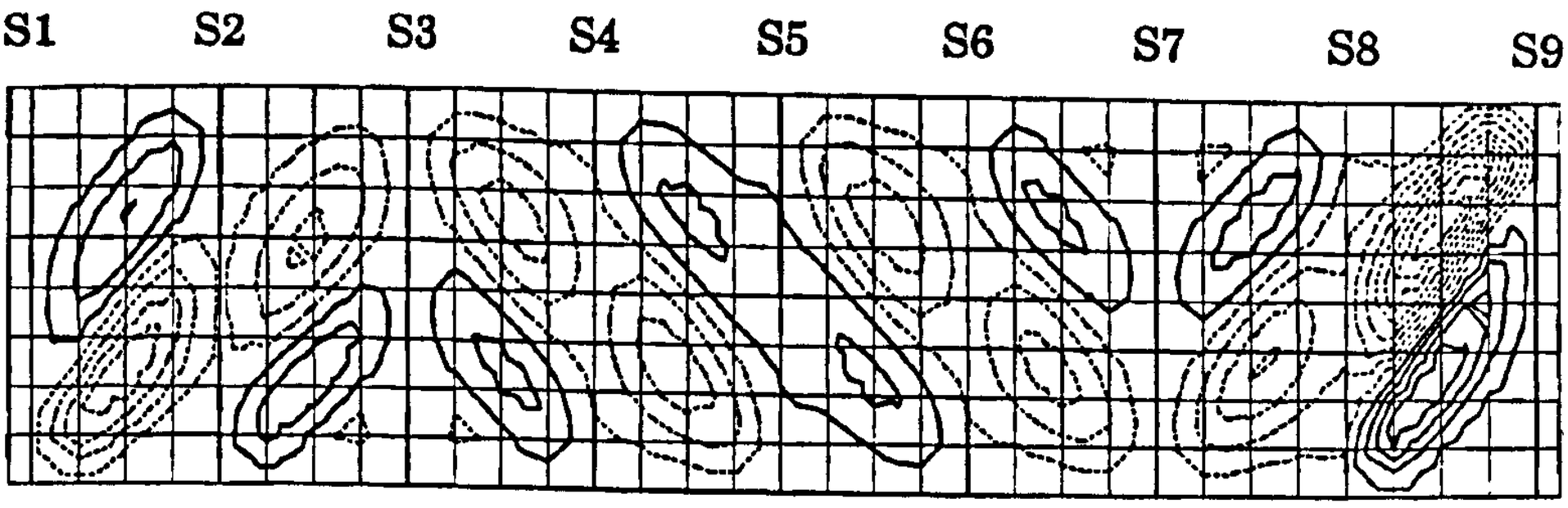
- ***Stiffener Deflections***

The stiffener deflection profiles at the maximum load of the girder, obtained from the finite element analyses for Girder GIII are shown in Fig. 2.29. It can be seen that all the intermediate stiffeners deflect in a half wave.

The magnitudes of the stiffener deflection, perpendicular to the web, at the mid-length of the stiffener are plotted against the applied load P in Fig. 2.30, with the sign of the deflection indicated. Referring to Fig. 2.1, the deflection moving out of the paper is taken as positive.



(a) The 1st FE analysis (with flanges), w at P=143.9KN



(b) The second FE analysis (with flanges), S2 reinforced, w at P=146.8KN

Figure 2.28 Web deflection of Girder GIII FE results

It can be seen in Fig. 2.30 that the deflection of the stiffener S2 started to deflect at about P=60KN, and then increased gradually to 2.14mm (≈d/280) at P=143.9KN. When the load was further increased, the stiffener began to deflect rapidly, and its deflection reached 12.0mm (≈d/50) as the applied load P reached 151.4KN. It is found from Fig. 2.32 that at P=143.9KN, the stiffener S2 had developed yielding. Therefore, the load of 143.9KN is taken as the FE failure load for the stiffener S2.

Similar observations can be made for the stiffener S8. As shown in Fig. 2.30, it was found that at P=146.8KN, the deflection of the stiffener S8 was 1.30mm (≈d/460). After

this load, the stiffener deflection increased rapidly. It is noted in Fig. 2.32 that it was at around this load level, the stiffener S8 began to yield. The FE failure load for the stiffener S8 is taken as P=146.8KN.

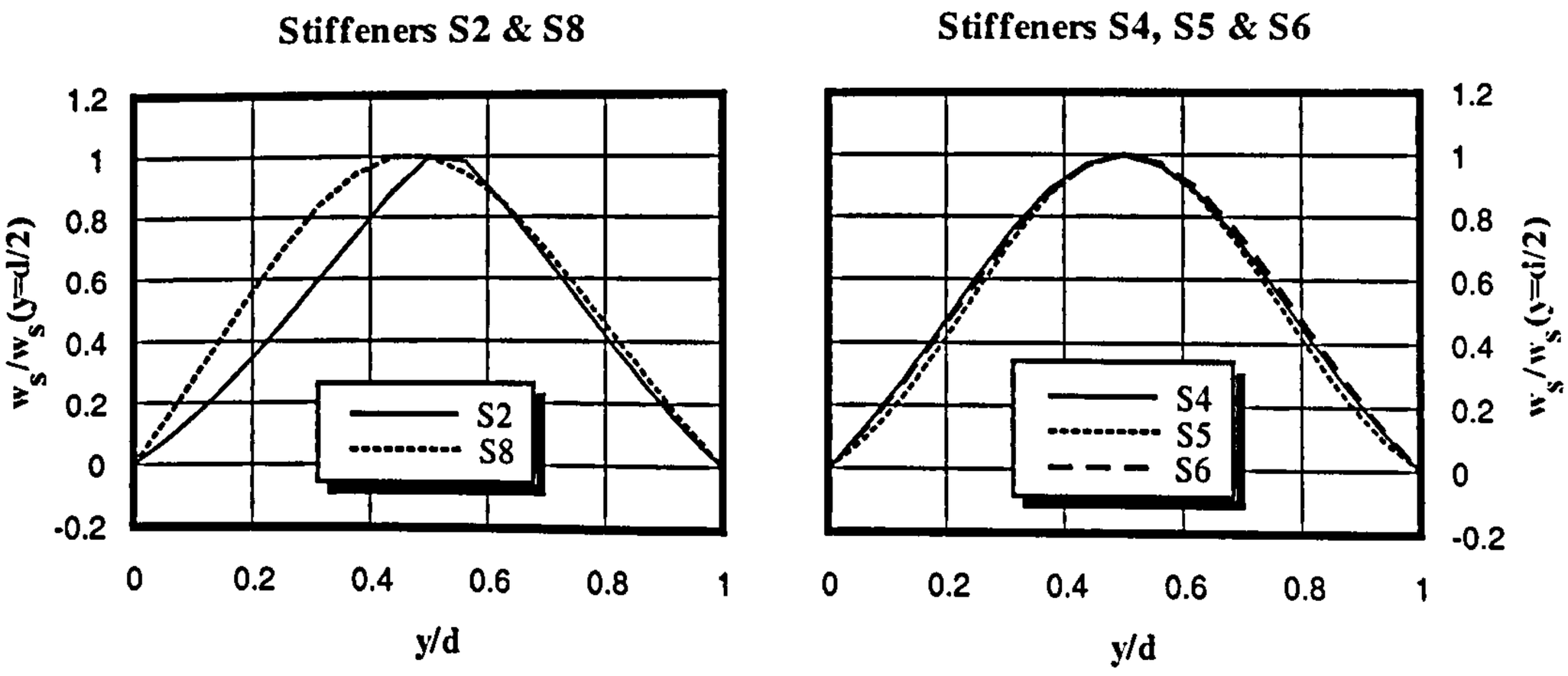


Figure 2.29 Stiffener deflection profiles from FE analyses. Girder GIII
S2 — the 1st FE analysis; S4, S5, S6 and S8 — the 2nd FE analysis

For the three middle stiffeners S4, S5 and S6, having the same size, it is observed in Fig. 2.30 that the stiffener S4 started to deflect considerably at P=161.9KN. When S4 developed significant deflection, the deflection mode of the plate changed, resulting in variations in the deflections of the stiffeners S5 and S6. It is noted that although the three middle stiffeners had the same size as that of the stiffener S2, this group of stiffener failed at a higher load than S2 did. This is mainly attributed to the fact that the boundary conditions for the vertical edges of the web plate between the two supports are provided by the frames, consisting of the stiffeners and flanges, near the ends of the girder (from S1 to S3, and S7 to S9), which is much stronger than the end stiffener itself. The continuity of the web may also contribute to the increase in the strength. It is also noted in Fig. 2.32 that at P=161.9KN, one of the outer edge of the stiffener S4 just grown into plasticity. For the multiple stiffeners S4, S5 and S6, the failure load from ABAQUS is taken as P=161.9KN.

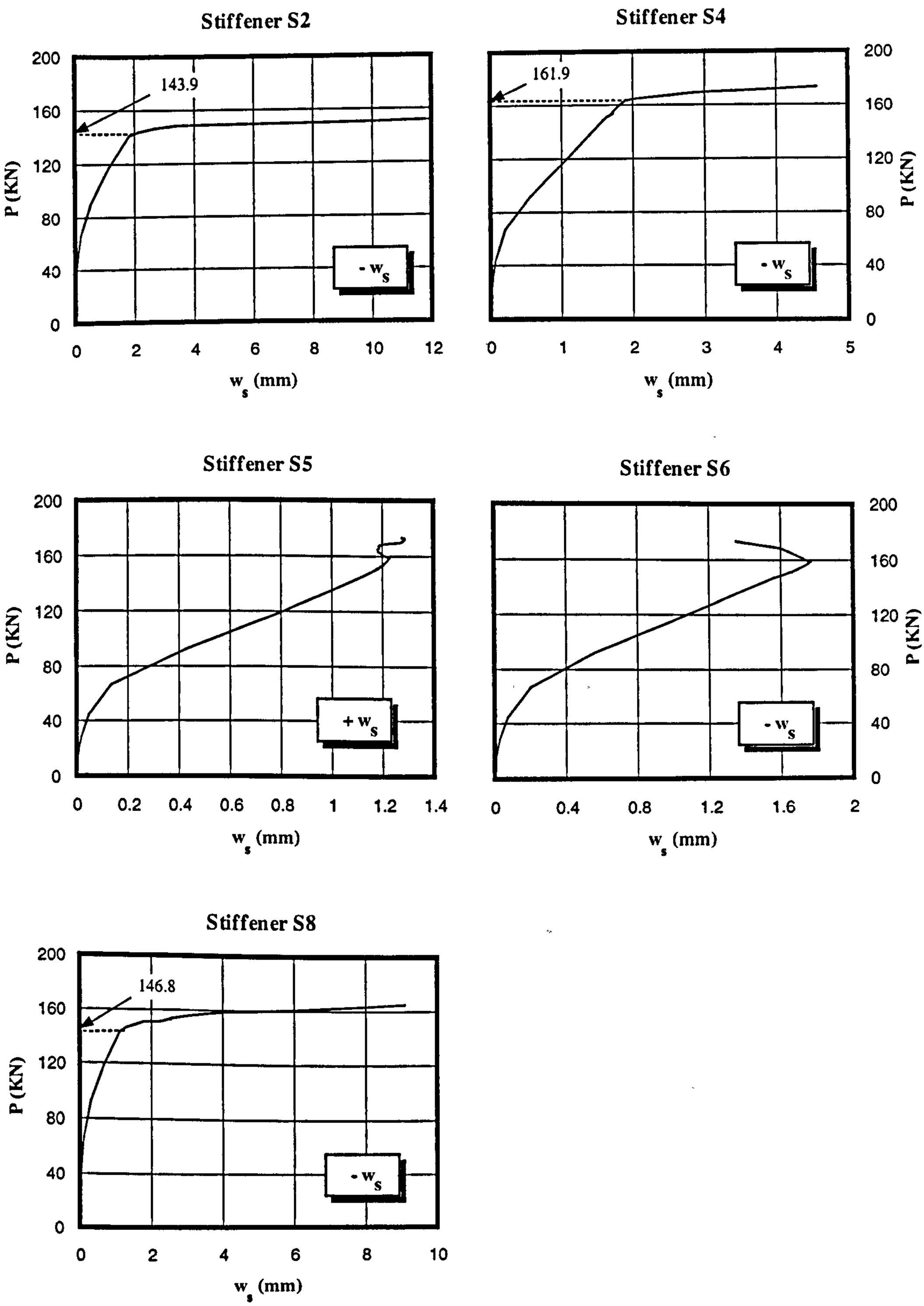
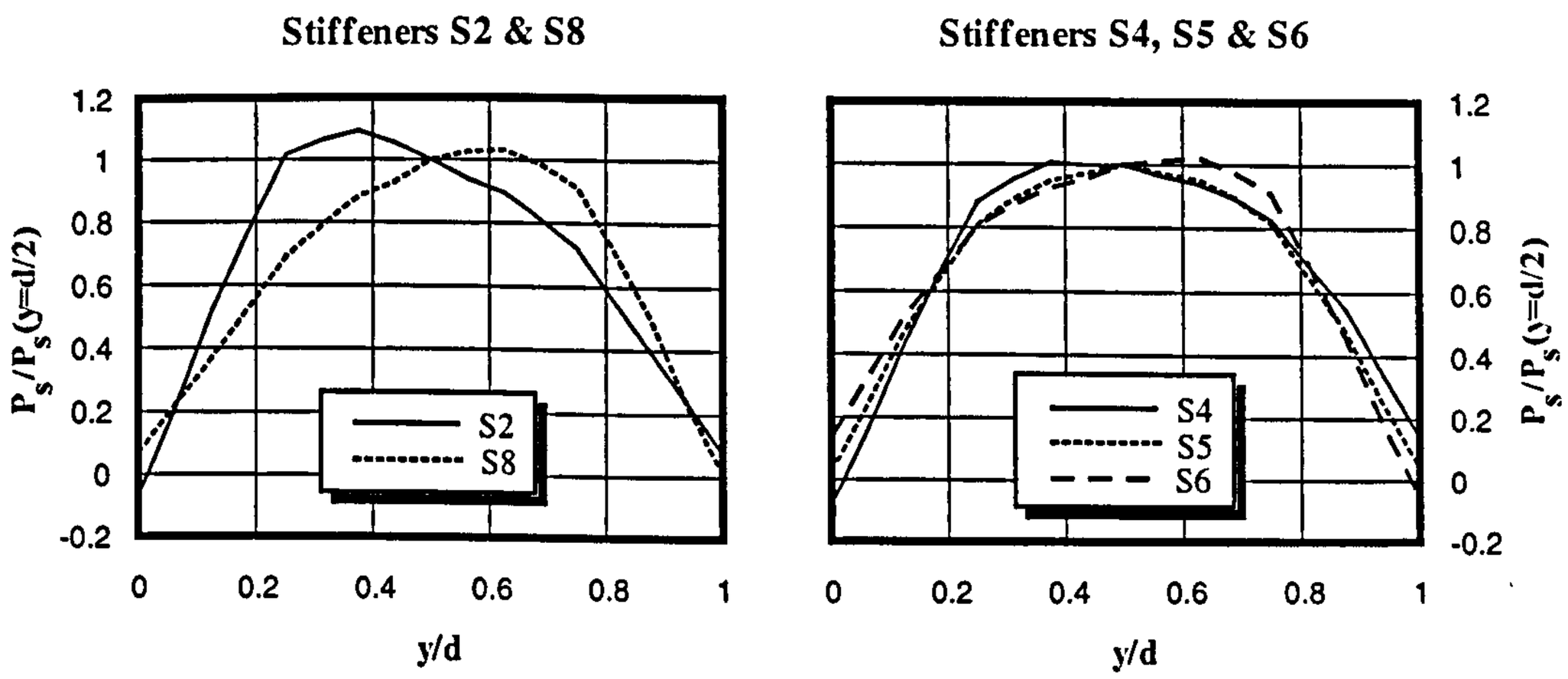


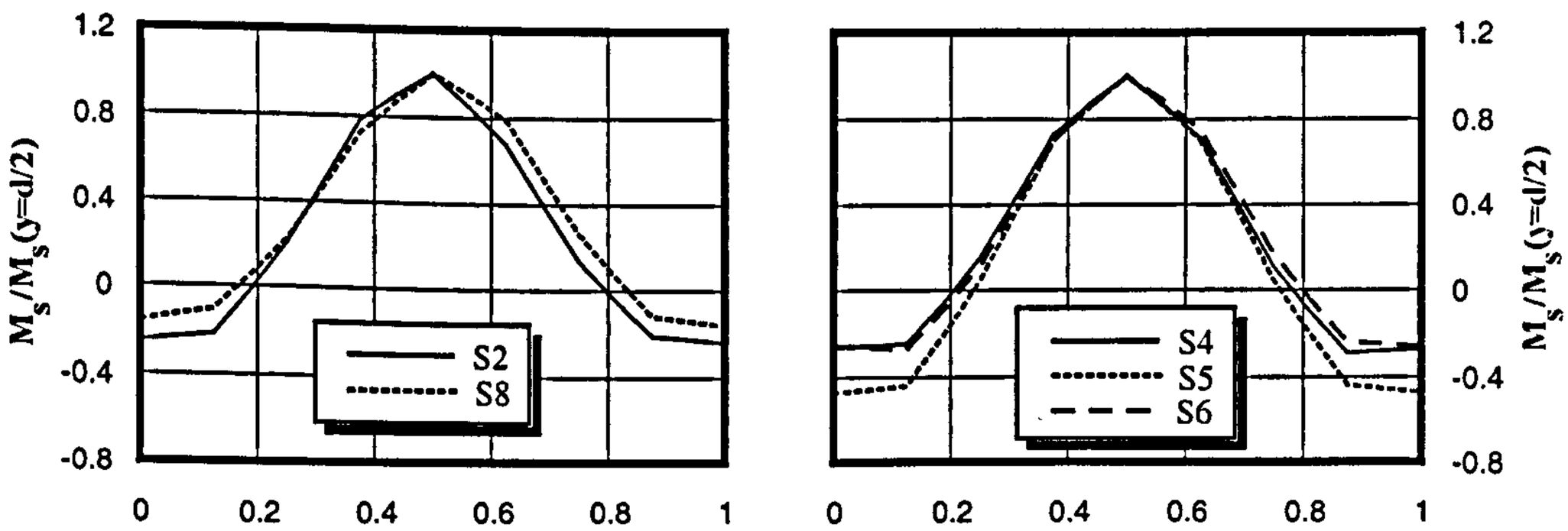
Figure 2.30 Load vs deflection curves of the stiffener. Girder GIII. P as shown in Fig. 2.1. FE results S2 — the 1st FE analysis; S4, S5, S6 and S8 — the 2nd FE analysis

- ***Stiffener Forces***

All the stiffeners on the girder GIII were double-sided flat bars. The normalised distributions of the axial forces and bending moments along the length of the stiffener before the yielding of the stiffener were obtained from the non-linear finite element analyses, as given in Fig. 2.31. It is evident in Fig. 2.31 that for the intermediate stiffeners, the maximum values of the stiffener forces occurred at the mid-length of the stiffener.



(a) Axial Force P_s



(b) Bending Moment M_s

Figure 2.31 Distributions of the axial force and bending moment in the stiffener. Girder GIII. FE results. S2 — the 1st FE analysis; S4, S5, S6 and S8 — the 2nd FE analysis

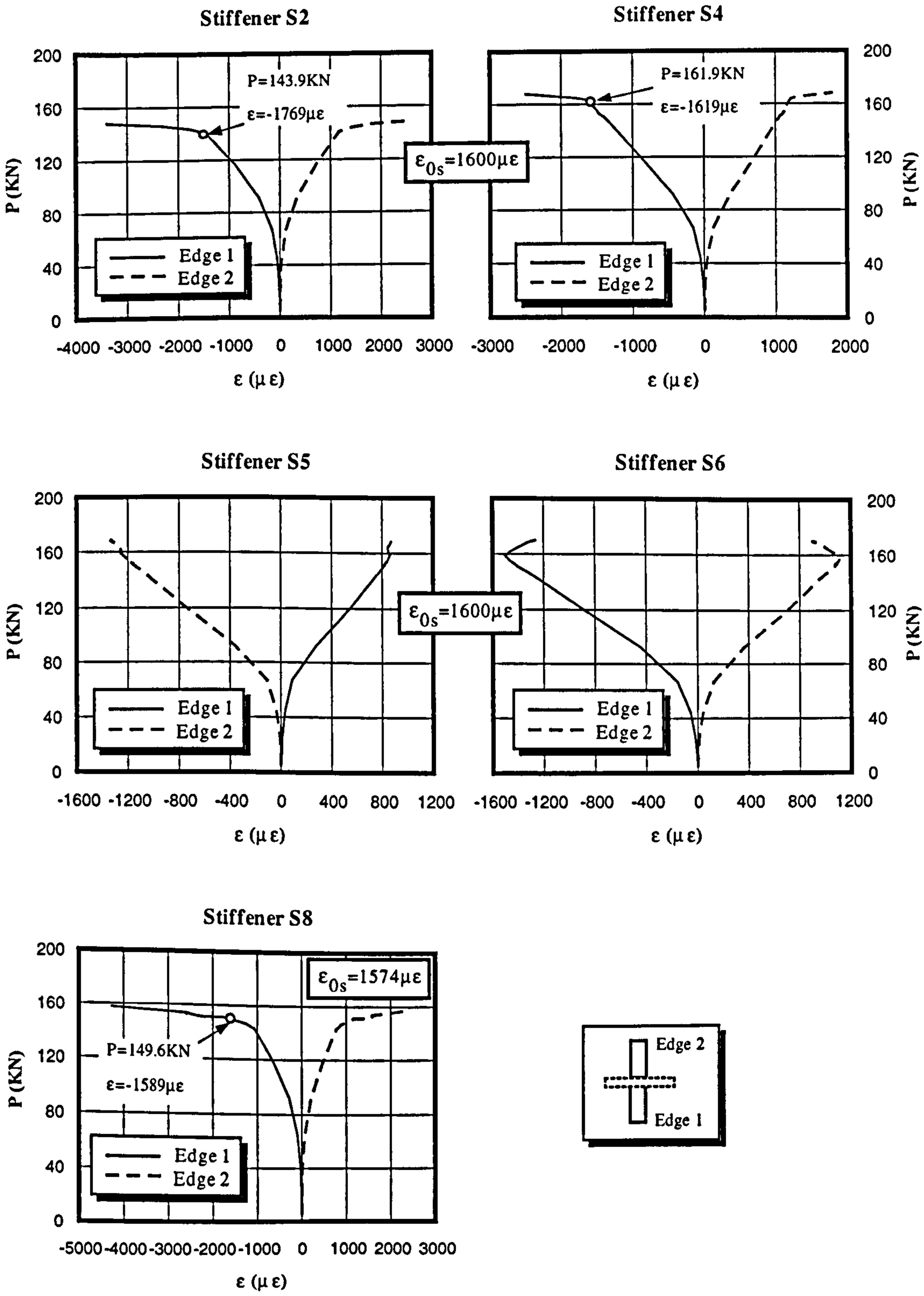


Figure 2.32 Strains at the mid-length of the stiffener. Girder GIII P as shown in Fig. 2.1. FE results S2 – the 1st FE analysis; S4, S5, S6 and S8 – the 2nd FE analysis

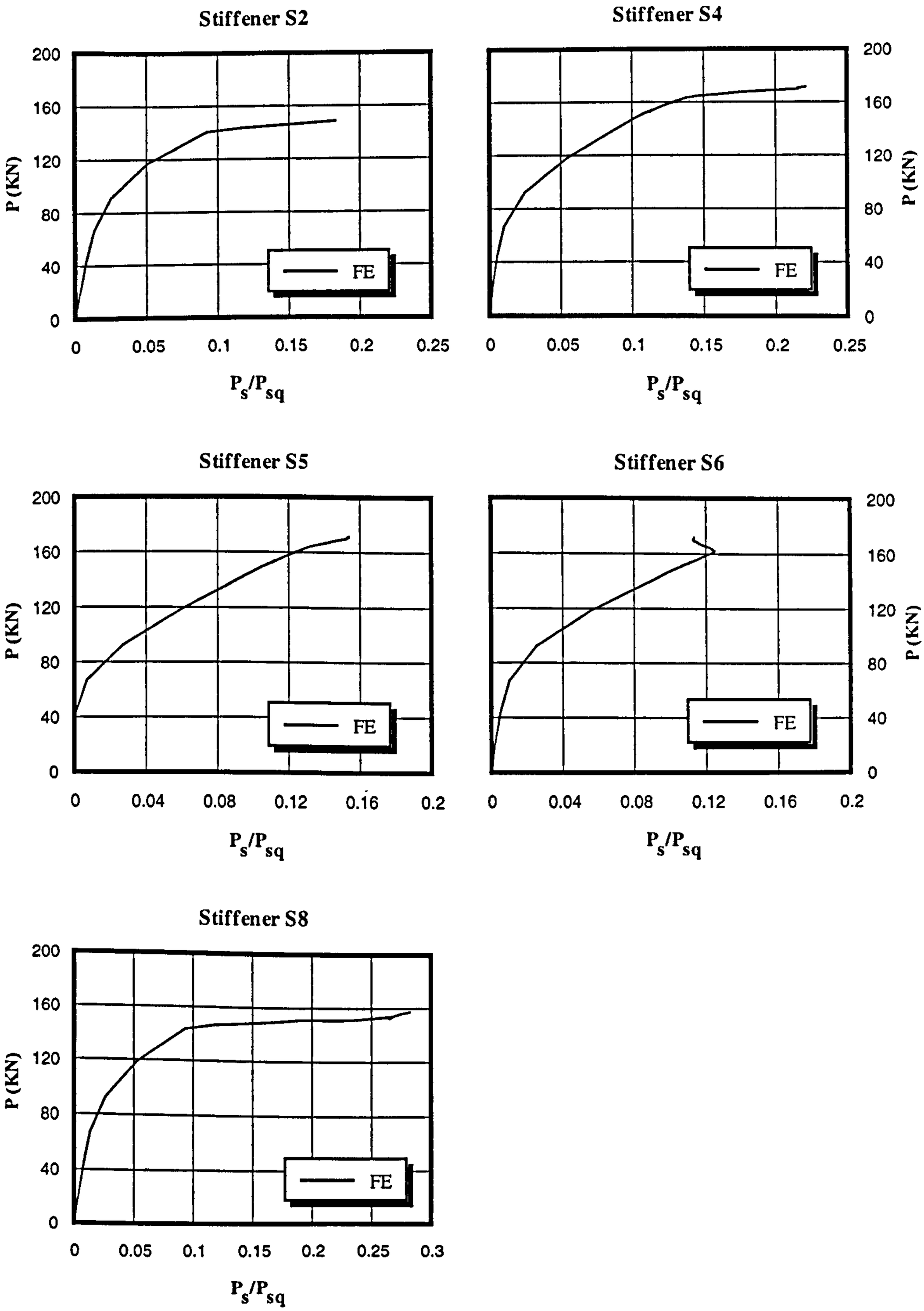


Figure 2.33 Axial forces in the stiffeners. P_s: positive for compressive force. P as shown in Fig. 2.1. Girder GIII. FE results. S2 — the 1st FE analysis; S4, S5, S6 and S8 — the 2nd FE analysis

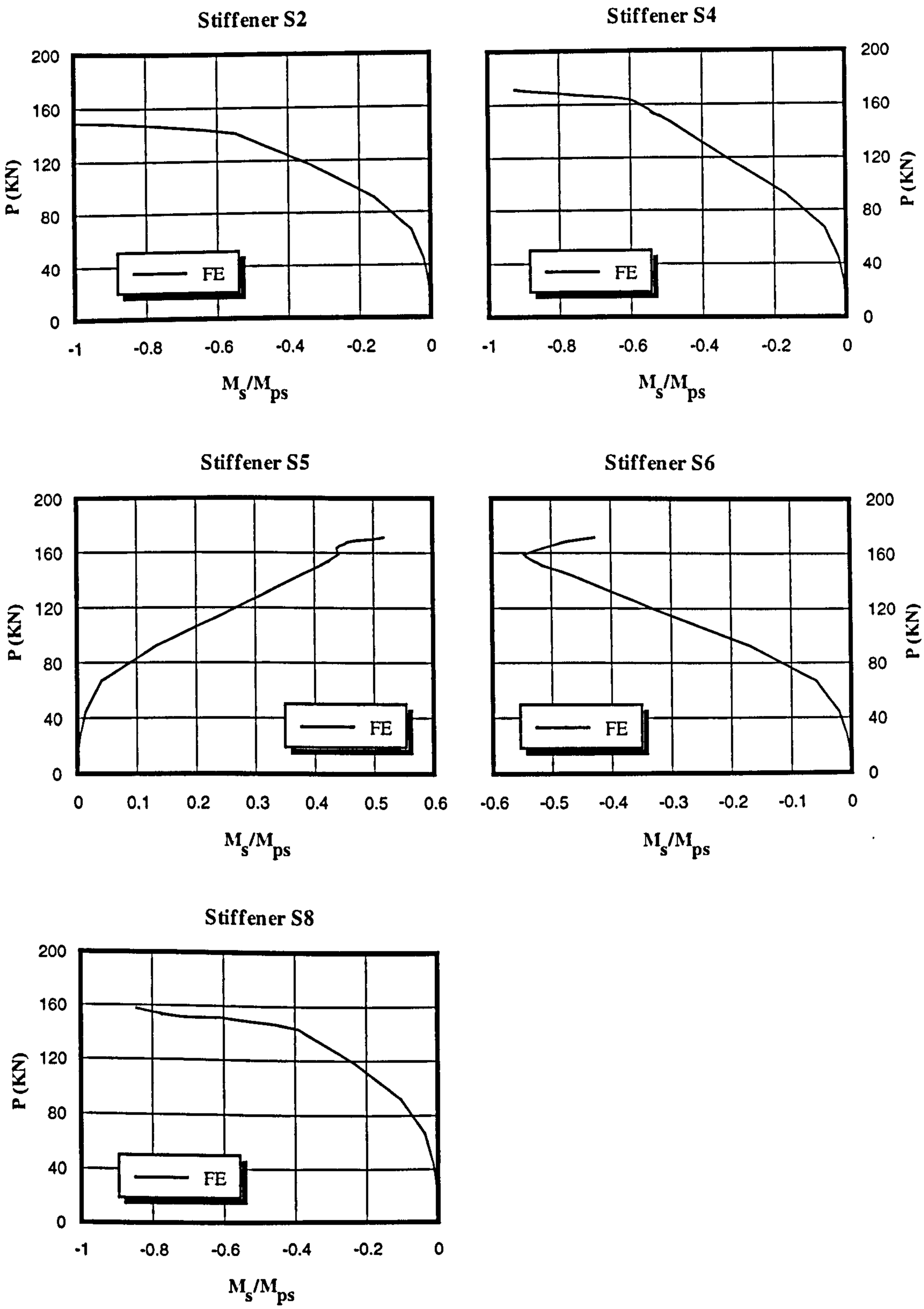


Figure 2.34 Bending moments in the stiffeners. M_s: positive for producing tension in Edge 1 (Fig. 2.32). Girder GIII. P as in Fig. 2.1. FE results. S2 — the 1st FE analysis; S4, S5, S6 and S8 — the 2nd FE analysis

The finite element solutions of the axial strains at the mid-length of the stiffener are shown in Fig. 2.32. It is evident that for all the intermediate stiffeners, one of the outer edges was in tension, with the other in compression, and the strain values for the two edges do not differ considerably. This suggests that the stiffeners were subjected to significant bending moment (Fig. 2.34). As indicated above, the stiffeners S2, S8 and S4 grew into plasticity at P=143.9KN, 149.6KN and 161.9KN, respectively.

The axial force P_s and bending moment M_s were also given by ABAQUS for each intermediate stiffener, and their variations with the applied load P are shown in Fig. 2.33 and 2.34, respectively. It is evident in Fig. 2.33 that for these intermediate double-sided stiffeners, the contribution of the axial force to the total stiffener stress was only about 10~20% when the stiffener failure occurred. As demonstrated in Fig. 2.34, these stiffeners were mainly subjected to a bending moment.

2.5.4 Girder GIV

This section presents the finite element results for the test girder GIV (see Fig. 2.1, and Table 2.1b). As indicated previously, there was a single intermediate stiffener (S2 or S8) near each end of the girder GIV. In the middle of the girder, three consecutive intermediate stiffeners (S4, S5 and S6), identical in their dimensions, were used to reveal the buckling behaviour of multiple stiffeners. All the intermediate stiffeners were single-sided flat bars. For the numerical analyses, the web and stiffener components of the initial imperfection were taken as sine waves, with the code specified magnitudes (Eqns. 3.8 and 3.9), and superimposed on each other. Two finite element analyses were carried out for the girder GIV. The first analysis revealed that the stiffener S2 failed before the others, and the second analysis was run to model the girder after the stiffener S2 was reinforced.

For the test girder GIV, the first FE analysis indicated that as the applied load P (Fig. 2.1) approaches P=148.1KN, the stiffener S2 reached its yield strain and its deflection started to increase quickly. After increasing the stiffener size of S2, the second FE analysis was conducted. It was found that the stiffener S8 began to deflect considerably

at P=149.1KN, and the yield strain of the stiffener was exceeded at P=152.3KN. It was noted that at P=149.1KN, the vertical end deflection began to increase rapidly. The FE analysis also revealed that of the three middle stiffeners, the stiffener S5 started to deflect rapidly at P=160.1KN, and its maximum strain had exceeded the yield strain at P=161.8KN.

- ***End Deflection***

In Fig. 2.35, the FE curves of the applied load P against the end vertical deflection at the two ends of the girder (i.e., at the positions of the stiffeners S1 and S9, Fig. 2.1) are presented. It can be seen that the load-deflection relation is nearly linear up to 148.1KN for the left end and 149.1KN for the right end, and then the end deflections began to increase rapidly. It is recalled that a linear strain hardening rule of E_t=1%E (Fig. 2.9) was adopted in the FE analysis. By reference to Figs. 2.35 and 2.38, it can be seen that the quick increase in the end deflections is due to the failure of the stiffener S2 or S8, respectively. It is observed in Fig. 2.38 that the stiffeners S2 and S4 began to deflect rapidly at P=148.1KN and 149.1KN, respectively. As pointed out previously, when the intermediate stiffener developed a significant deflection, the two adjacent web panels tended to act as a single panel. As a result, the shearing stiffness of the girder was reduced and the shear deformation increased significantly.

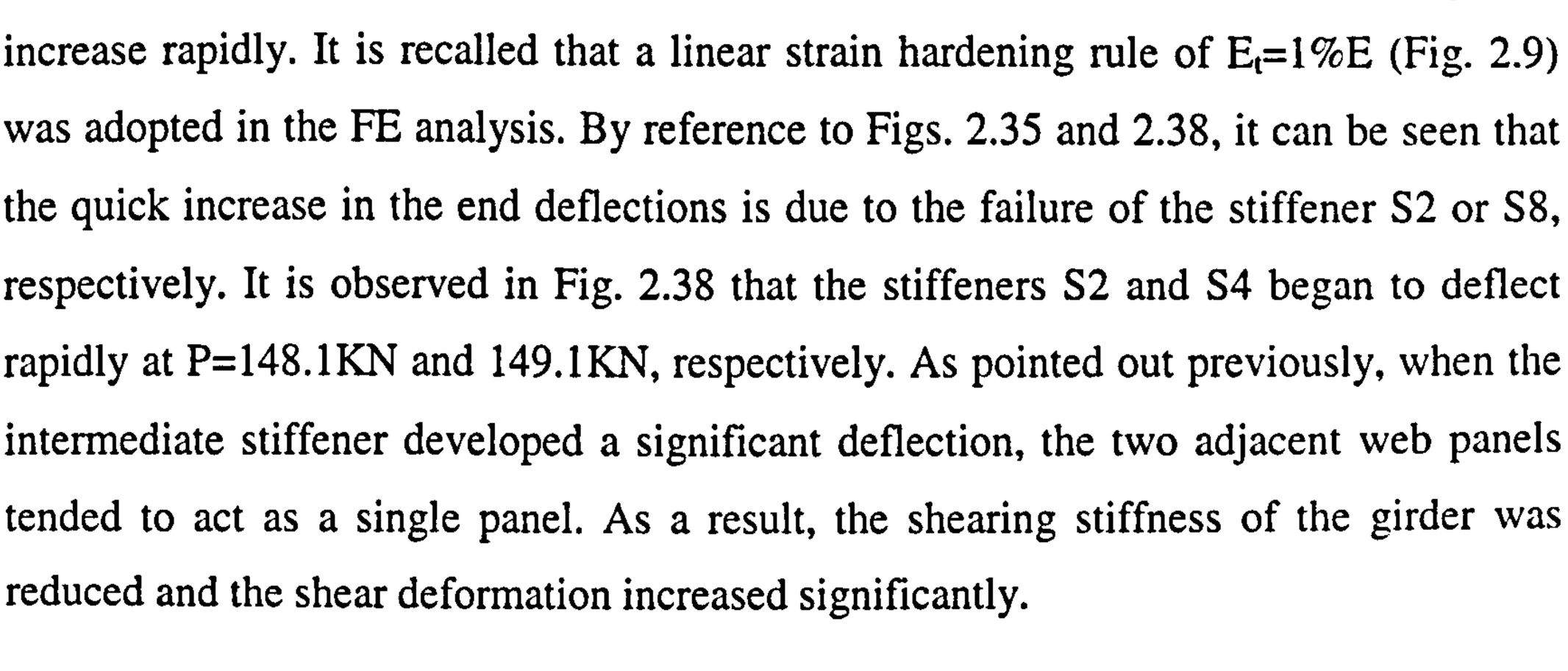
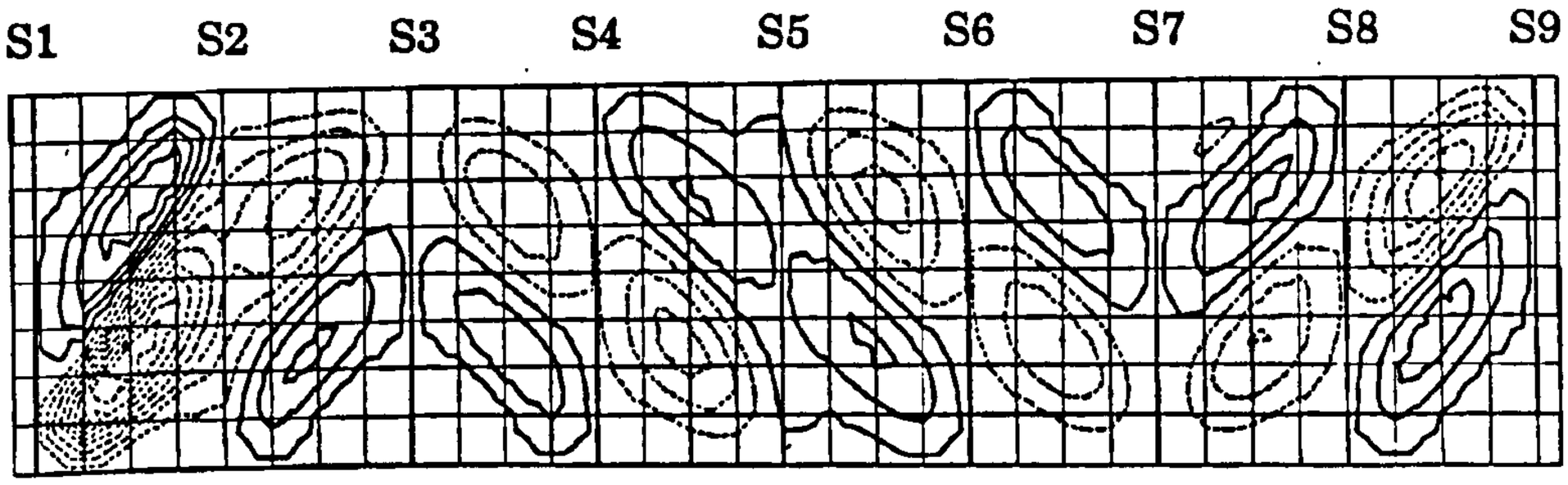
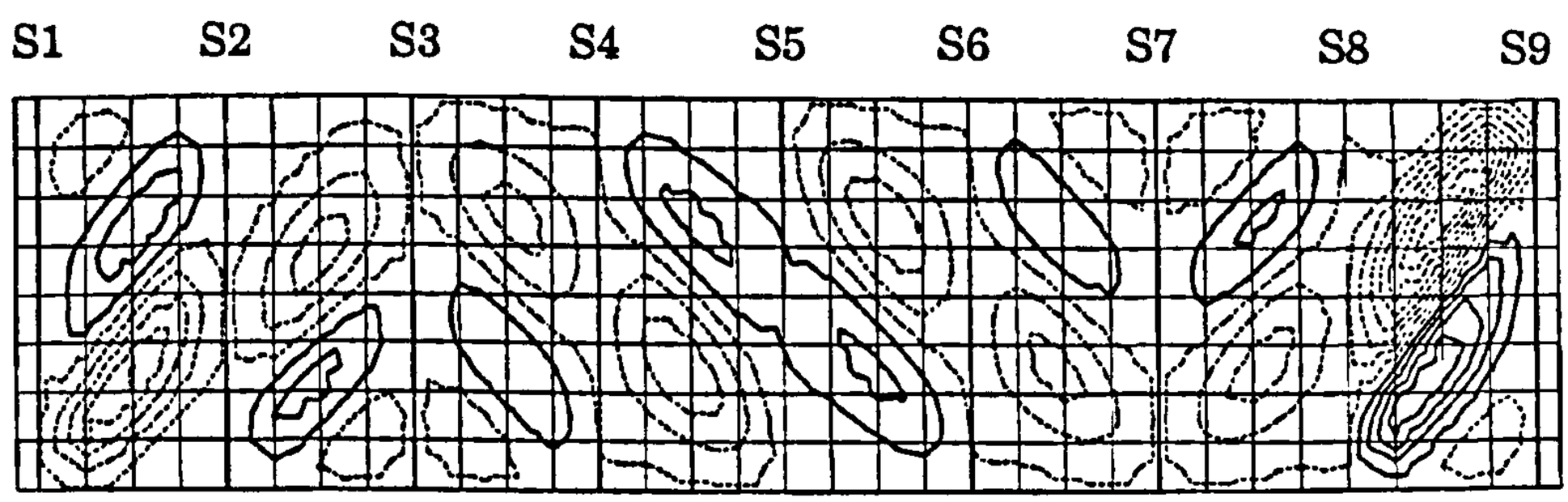


Figure 2.35 Load vs. end deflection curves. Girder GIV. P as shown in Fig. 2.1. FE results

Fig. 2.36 shows the contours of the out-of-plane deflection for the stiffened web plate, obtained from the two FE analyses.



(b) The first FE analysis (with flanges), w at P=148.1KN



(b) The second FE analysis (with flanges), S2 reinforced, w at P=149.1KN

Figure 2.36 Web deflection of Girder GIV. FE results

- ***Stiffener Deflections***

The stiffener deflection profiles at the maximum load of the girder, obtained from the finite element analyses for Girder GIV are shown in Fig. 2.37. It can be seen that all the intermediate stiffeners deflect in a half wave.

The magnitudes of the stiffener deflection, perpendicular to the web, at the mid-length of the stiffener are plotted against the applied load P in Fig. 2.38, with the sign of the

deflection indicated. Referring to Fig. 2.1, the deflection moving out of the paper is taken as positive.

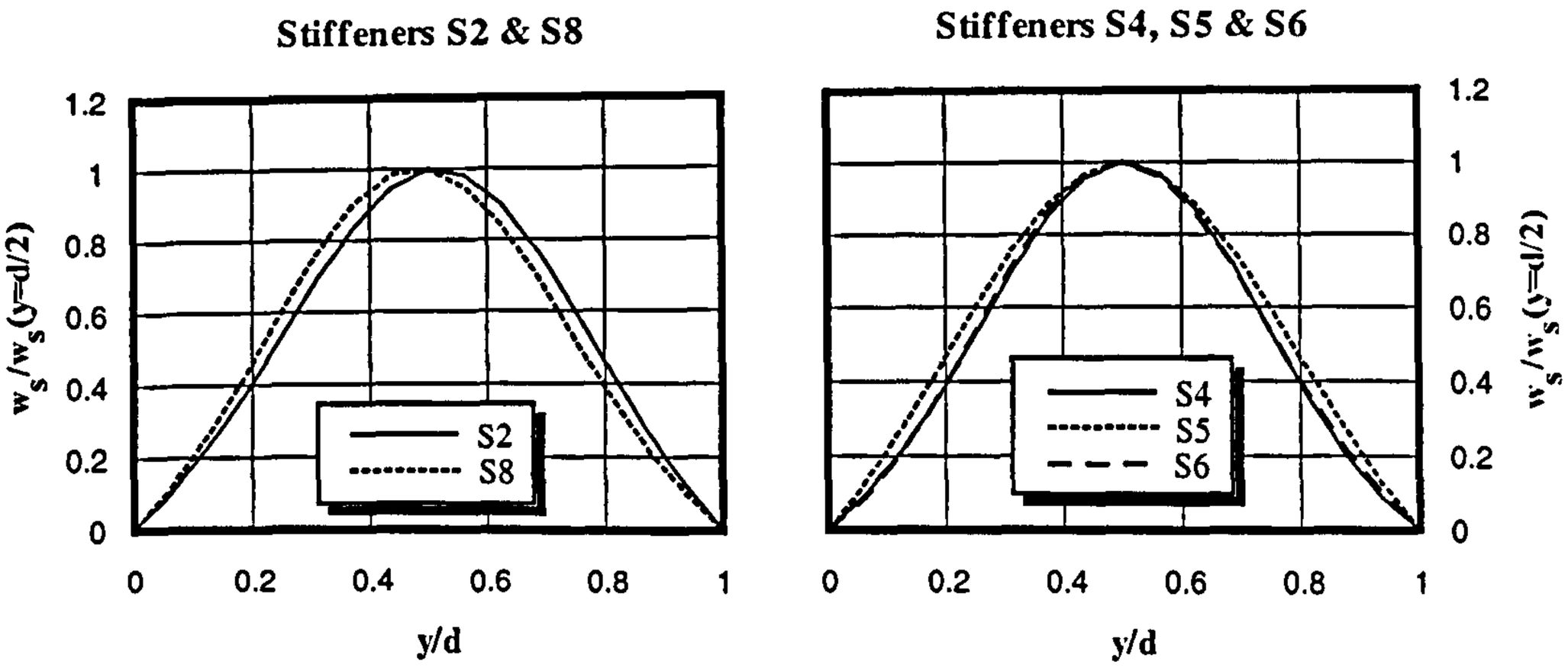
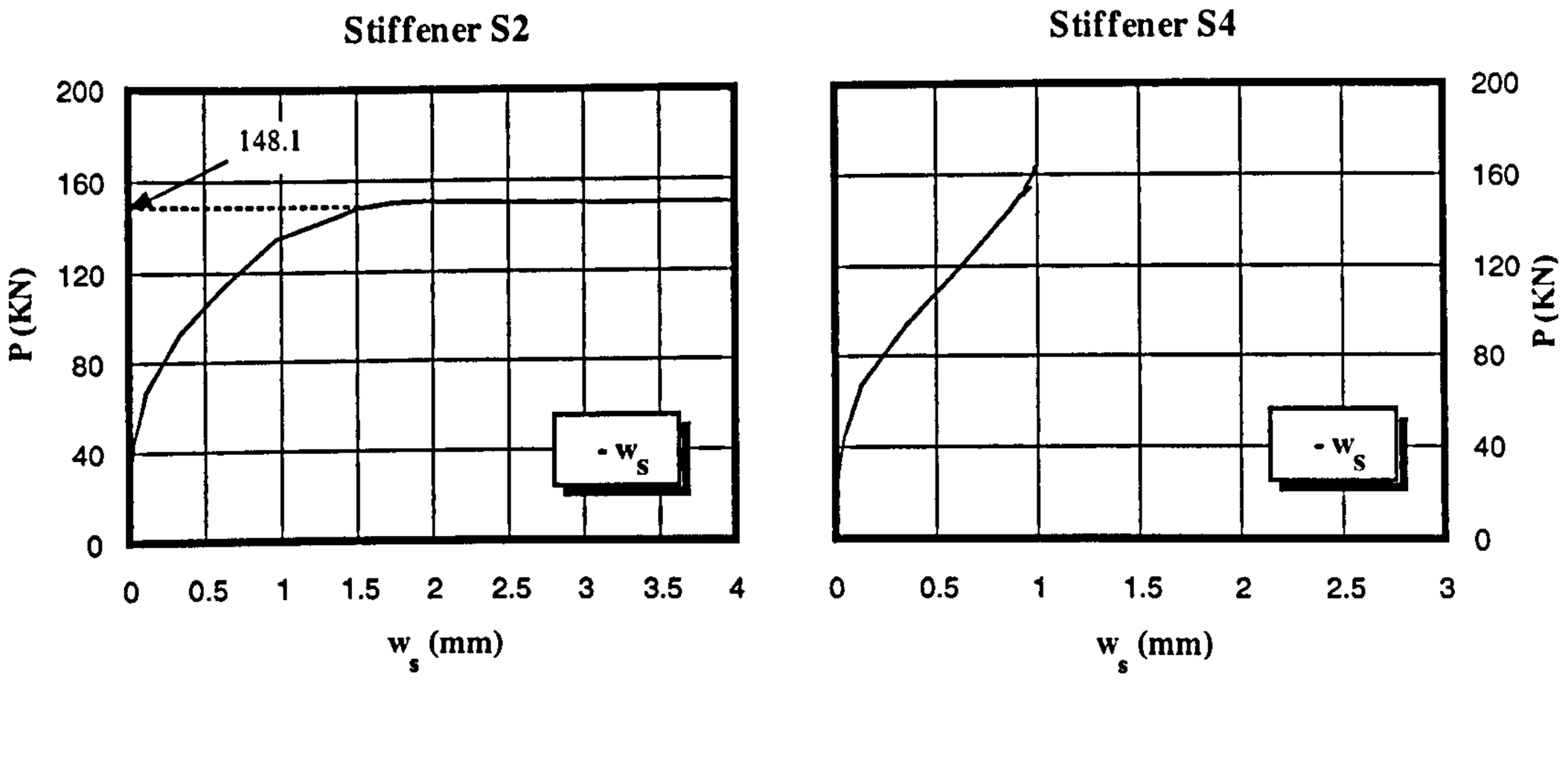


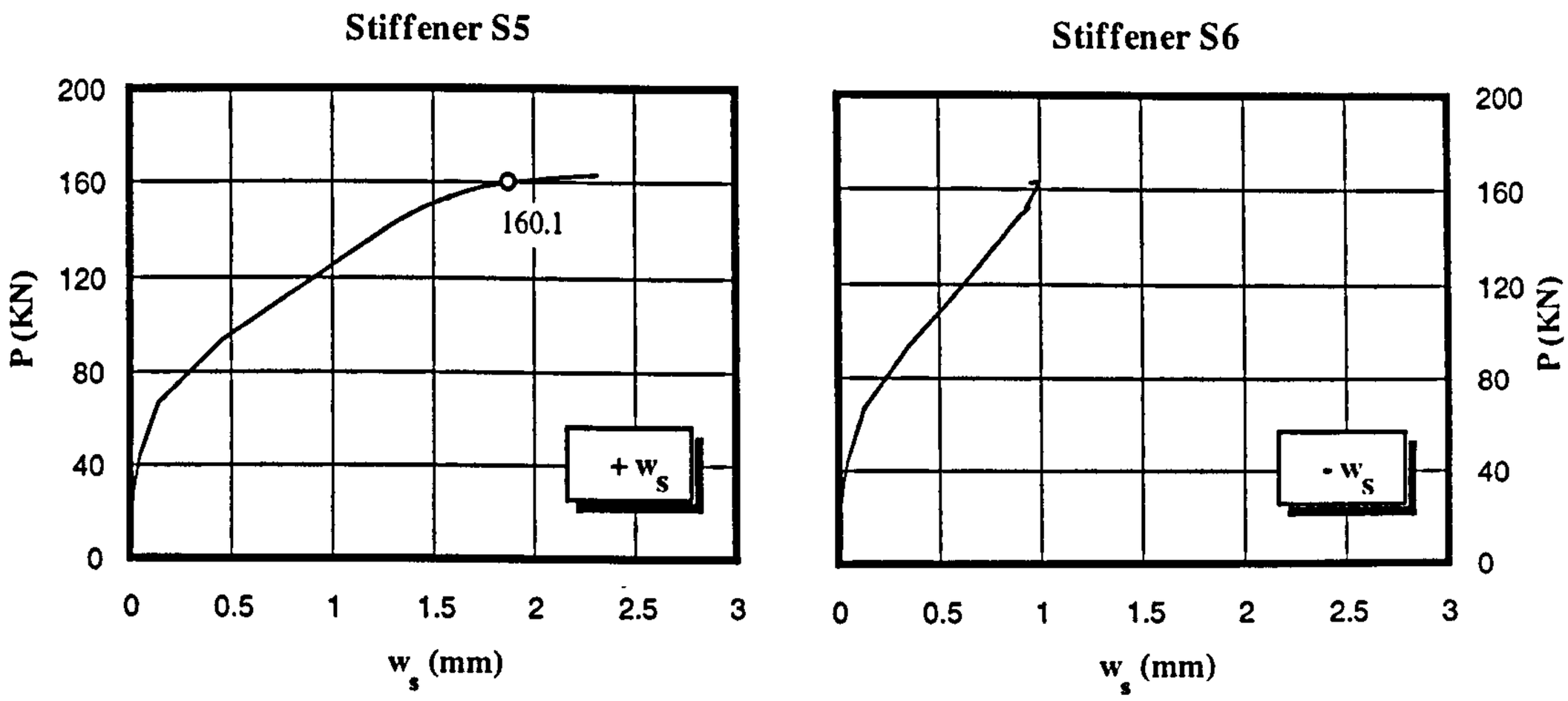
Figure 2.37 Stiffener deflection profiles from FE analyses. Girder GIV

S2 — the 1st FE analysis; S4, S5, S6 and S8 — the 2nd FE analysis

It can be seen in Fig. 2.38 that the deflection of the stiffener S2 started to deflect at about P=40KN, and then increased gradually to 1.51mm (≈d/397) at P=148.1KN. Later the stiffener began to deflect rapidly even at nearly constant load. It is found from Fig. 2.40 that at P=148.1KN, the stiffener S2 had developed plasticity. Therefore, the load of 148.1KN is taken as the FE failure load for the stiffener S2.

Similar observations can be made for the stiffener S8. As shown in Fig. 2.38, it was found that at P=149.1KN, the deflection of the stiffener S8 was 0.74mm (≈d/811). After this load, the stiffener deflection increased rapidly. At the maximum load P=163.2KN, the stiffener deflection was 3.15mm, or d/191. It is noted in Fig. 2.40 that the stiffener S8 began to yield at P=152.3KN. The FE failure load for the stiffener S8 is therefore taken as P=149.1KN.





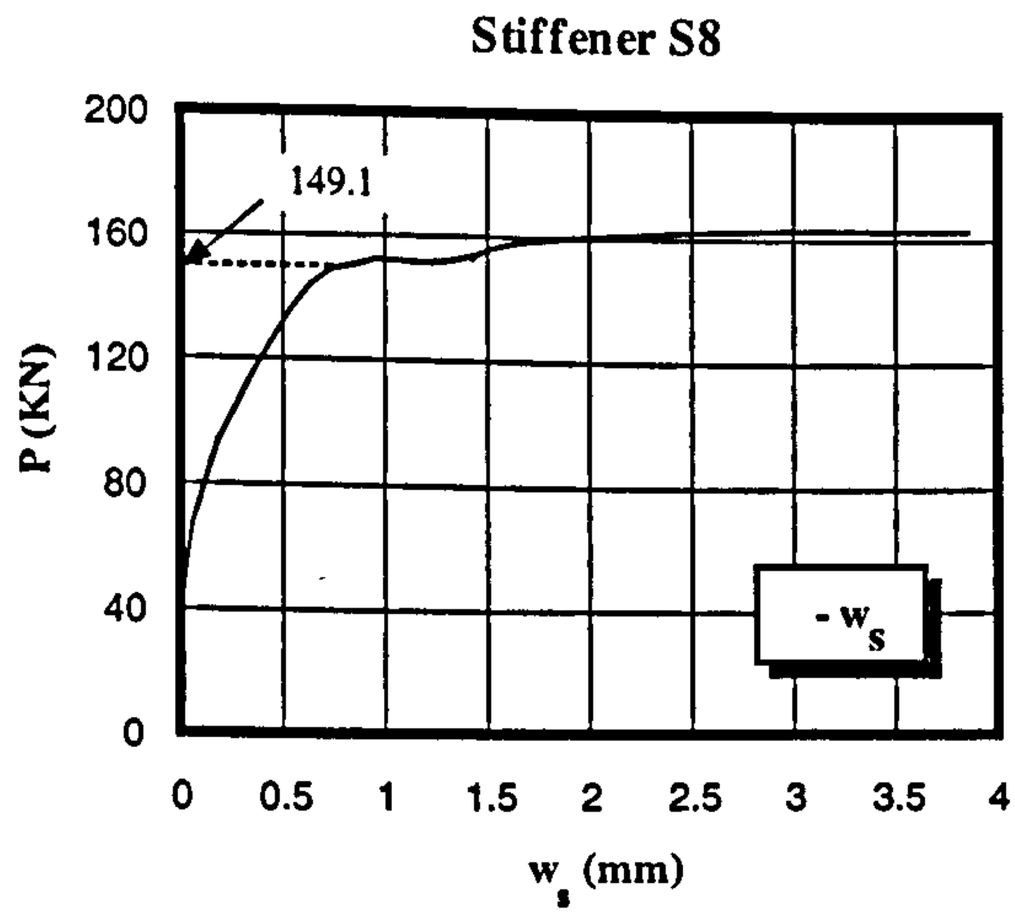


Figure 2.38 Load vs deflection curves of the stiffener. Girder GIV. P as shown in Fig. 2.1. FE results S2 — the 1st FE analysis; S4, S5, S6 and S8 — the 2nd FE analysis

For the three middle stiffeners S4, S5 and S6 which had the same size, it is observed in Fig. 2.38 that the stiffener S5 started to deflect considerably at P=160.1KN. When S5 developed significant deflection, the web deflection mode within the middle span of the girder changed, resulting in variations in the deflections of the stiffeners S4 and S6. As noticed for the test girder GIII, although the three middle stiffeners had the same size as that of the stiffener S2, this group of stiffener failed at a higher load than S2 did. As pointed out before, this is mainly attributed to the fact that the boundary conditions for the vertical edges of the web plate between the two supports are provided by the frames, consisting of the stiffeners and flanges, near the ends of the girder (from S1 to S3, and S7 to S9), which is much stronger than the end stiffener itself. The continuity of the web may also contribute to the increase in the strength. It is also noted in Fig. 2.40 that at P=161.8KN, the outer edge of the stiffener S5 had already grown into plasticity. For the multiple stiffeners S4, S5 and S6, the failure load from ABAQUS is taken as P=160.1KN.

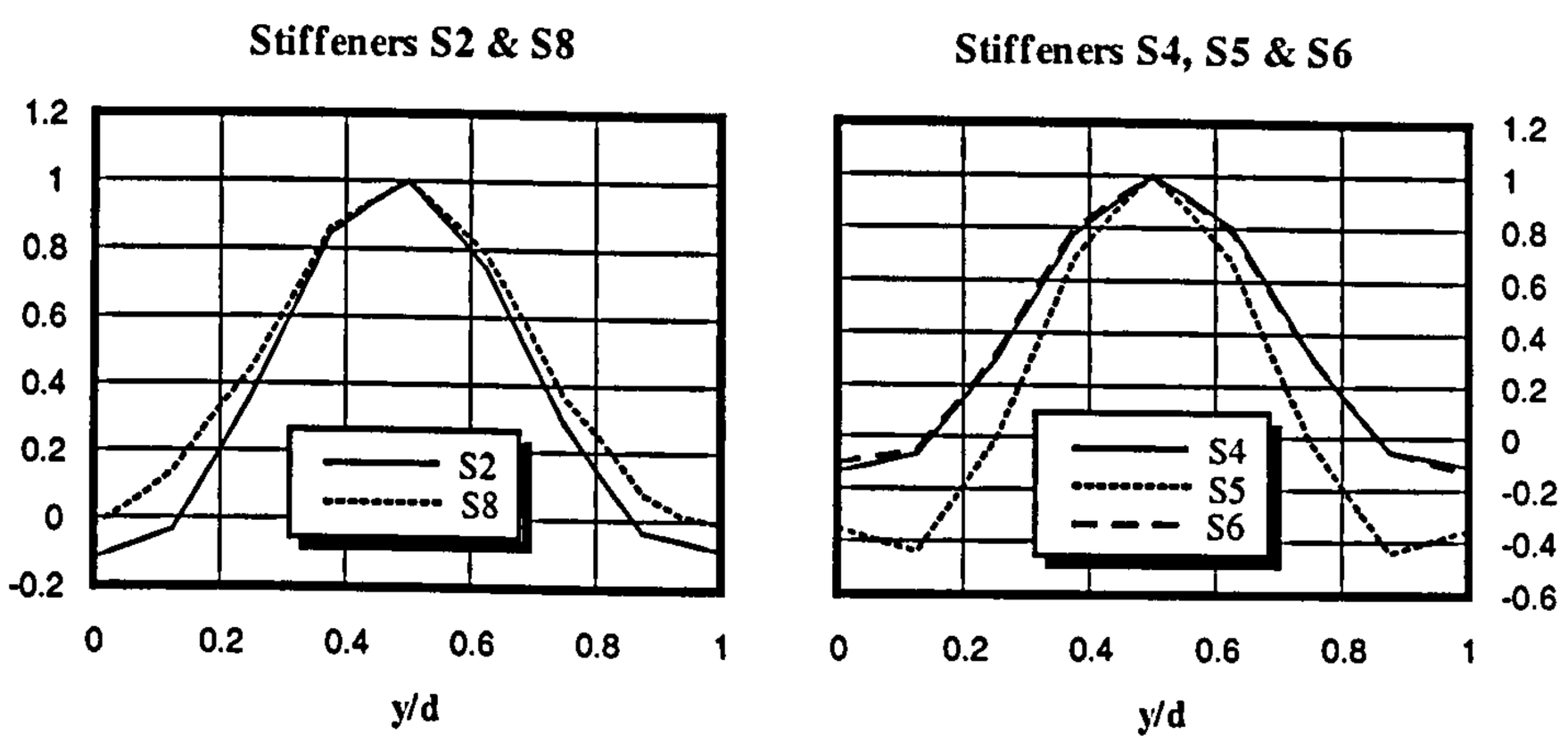
- ***Stiffener Forces***

All the intermediate stiffeners on the girder GIV were single-sided flat bars. The normalised distributions of the axial forces and bending moments (about the centroidal axis of the stiffener section) along the length of the stiffener before the yielding of the stiffener were obtained from the non-linear finite element analyses, as given in Fig. 2.39. It is evident in Fig. 2.39 that for the intermediate stiffeners, the maximum values of the stiffener forces occurred at the mid-length of the stiffener.

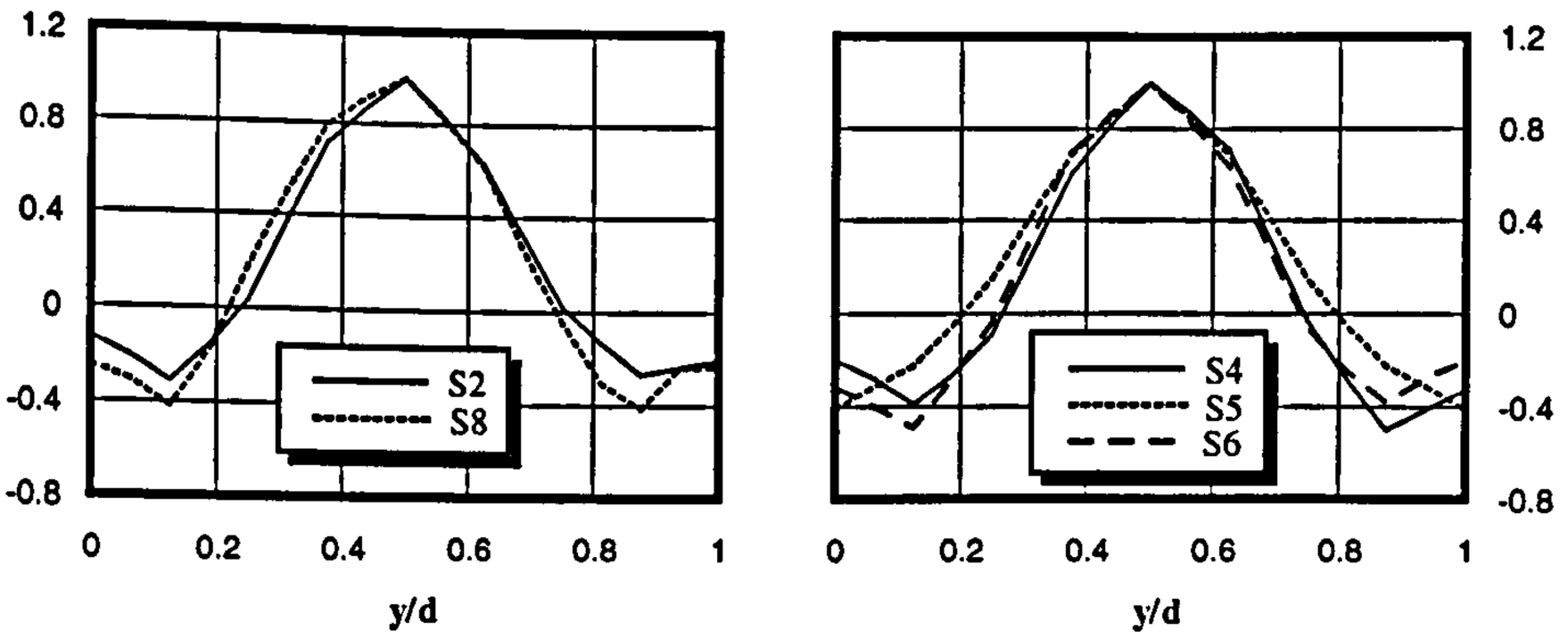
The finite element solutions of the axial strains at the mid-length of the stiffener are shown in Fig. 2.40. It is observed that except for the stiffener S5, the stiffener axial strains at the face in contact with the web were nearly equal to zero, while the tips of these single-sided stiffeners were in compression. This observation may provide a basis for the assumption that for a single-sided stiffener, the neutral axis of the stiffener section occurs at the face in contact with the plate, which was adopted in several existing design methods for transverse stiffeners (e.g., [45] and [9]). However, this assumption can not be applied for the stiffener S5, for which the inner edge of the

stiffener was in significant compression, while the tip was in tension. This suggests that for the design of single-sided stiffeners, different combinations of the axial force and bending moment in the stiffener should be taken into account, and this will be further discussed in Chapter 8.

The axial force P_s and bending moment M_s were also given by ABAQUS for each intermediate stiffener, and their variations with the applied load P are shown in Fig. 2.41 and 2.42, respectively. It is evident in Fig. 2.41 that for these single-sided stiffeners, the contribution of the axial force to the total stiffener stress was much more significant than that for the double-sided stiffeners.

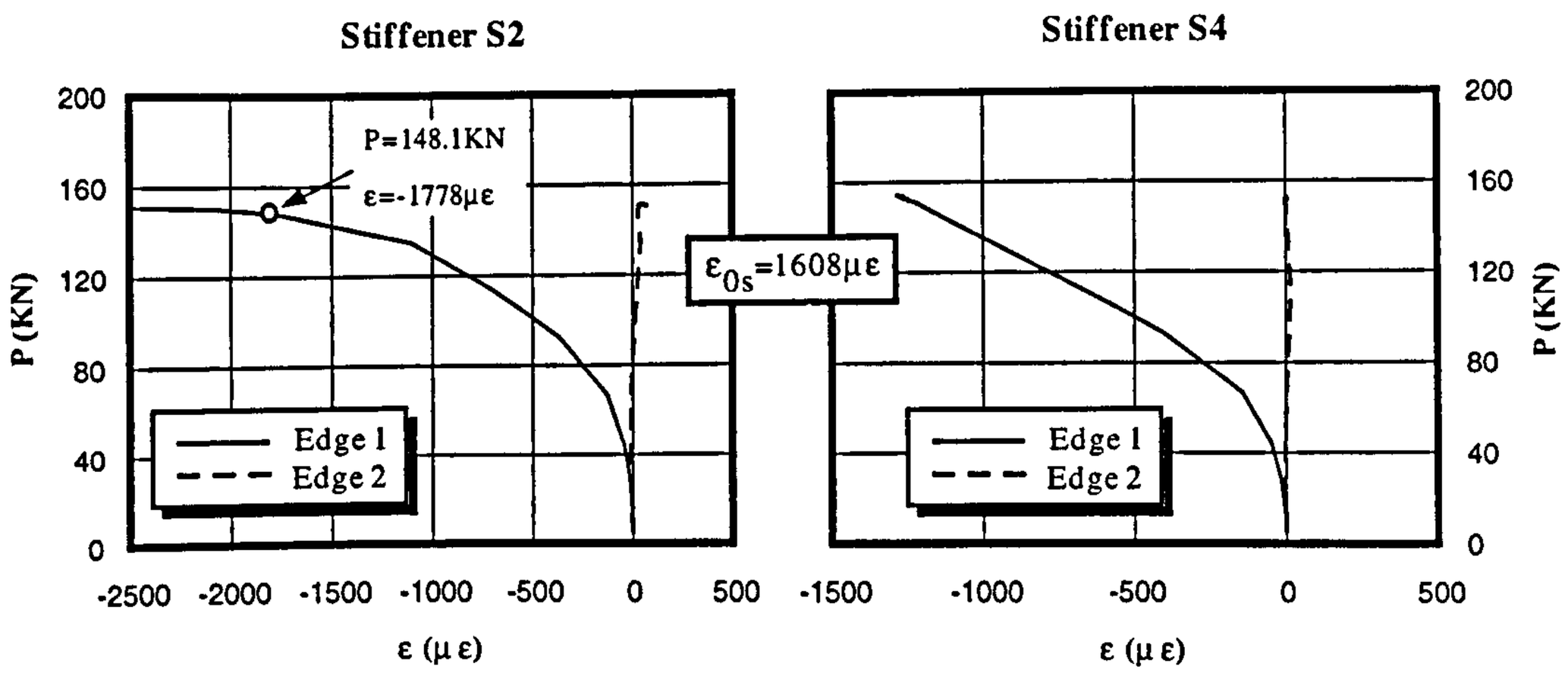


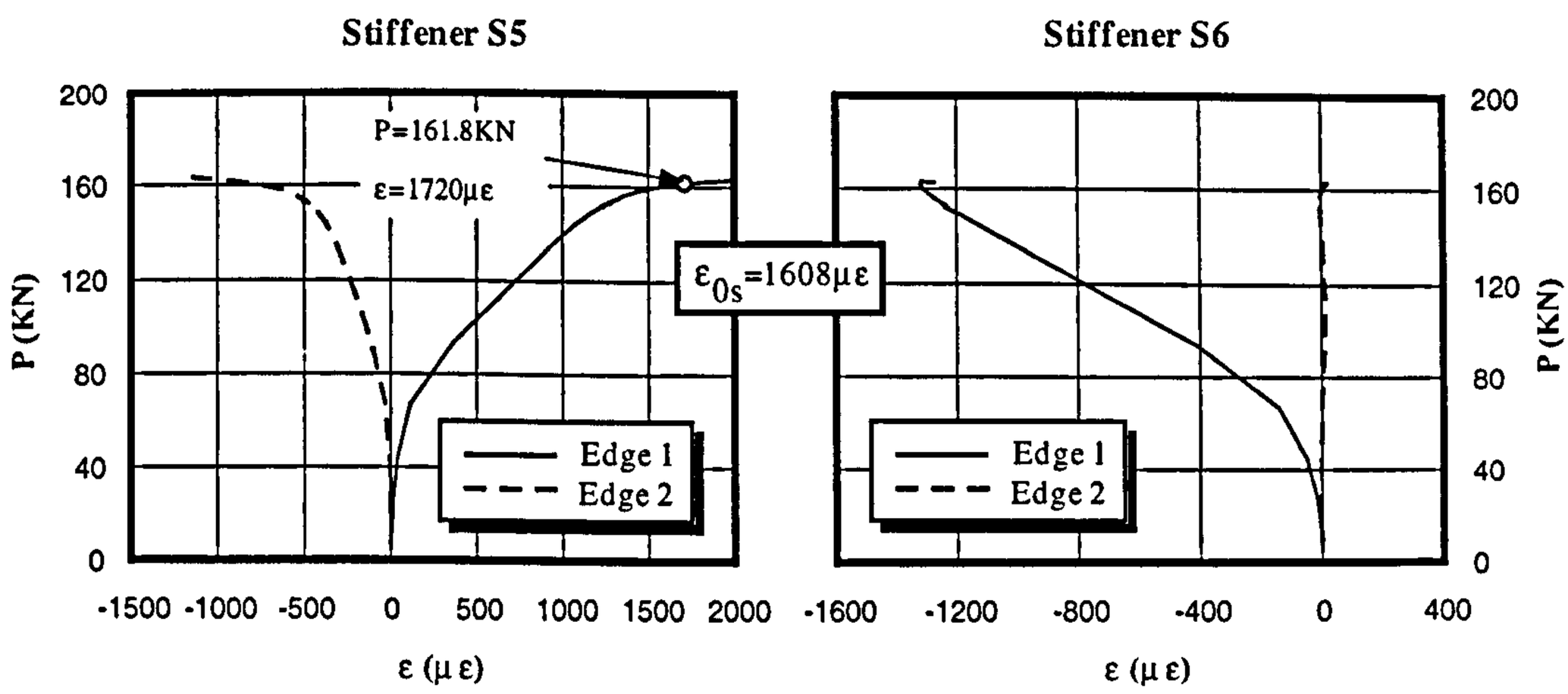
(a) Axial Force P_s



(b) Bending Moment M_s

Figure 2.39 Distributions of the axial force and bending moment in the stiffener. Girder GIV. FE results. FE results. S2 — the 1st FE analysis; S4, S5, S6 and S8 — the 2nd FE analysis





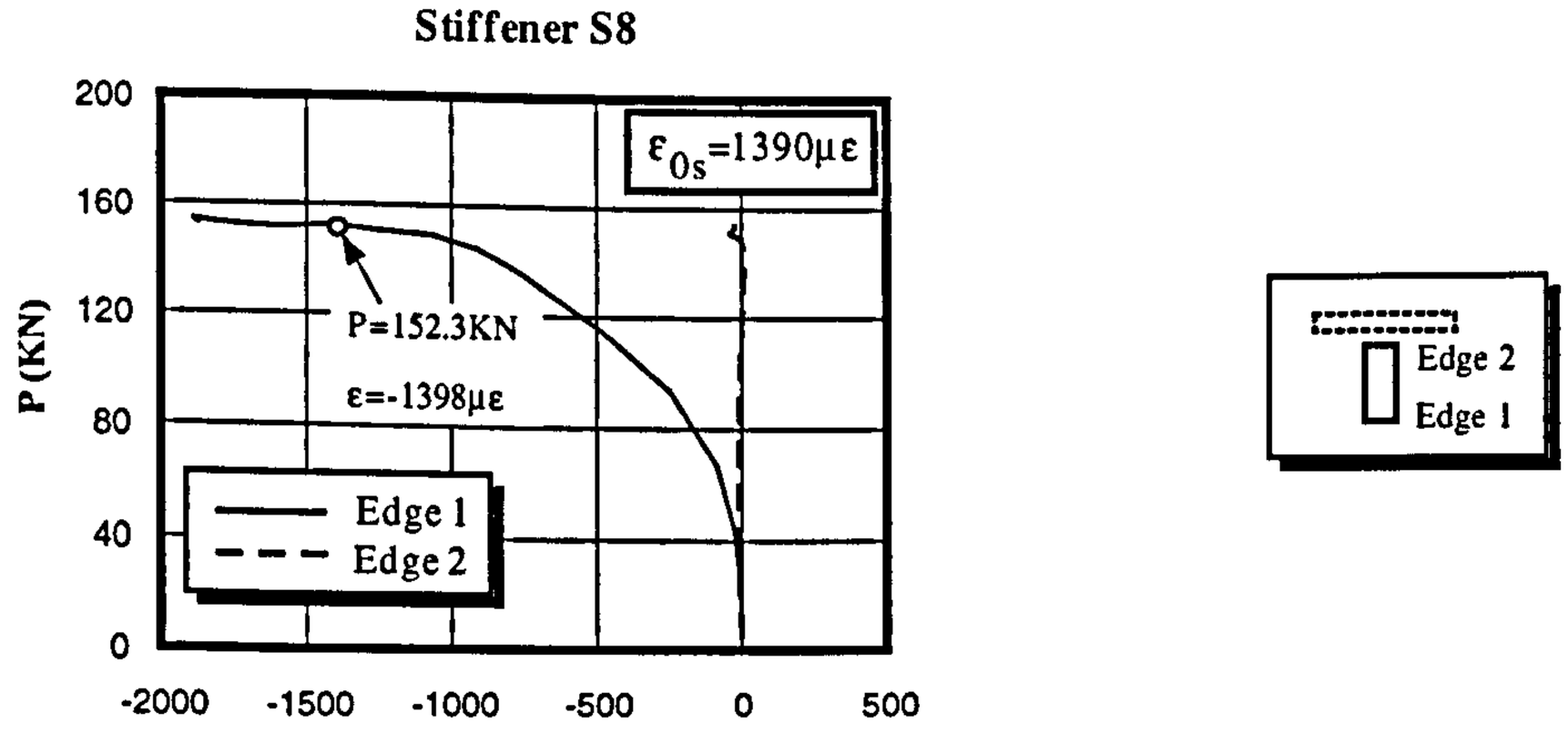


Figure 2.40 Strains at the mid-length of the stiffener. Girder GIV. P as shown in Fig. 2.1. FE results.

FE results. S2 — the 1st FE analysis; S4, S5, S6 and S8 — the 2nd FE analysis

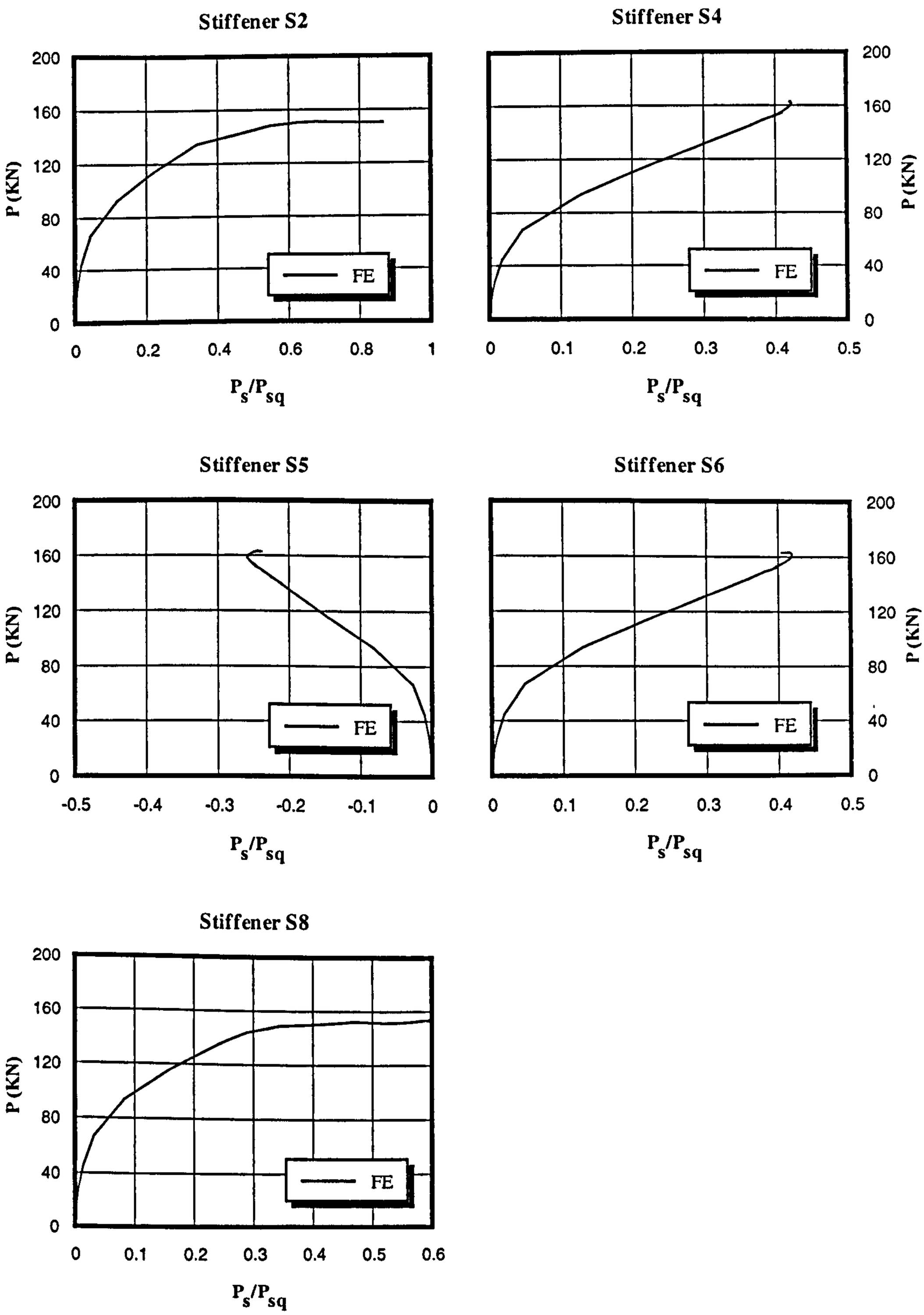


Figure 2.41 Axial forces in the stiffeners. P_s: positive for compressive force. P as shown in Fig. 2.1. Girder GIV. FE results. S2 — the 1st FE analysis; S4, S5, S6 and S8 — the 2nd FE analysis

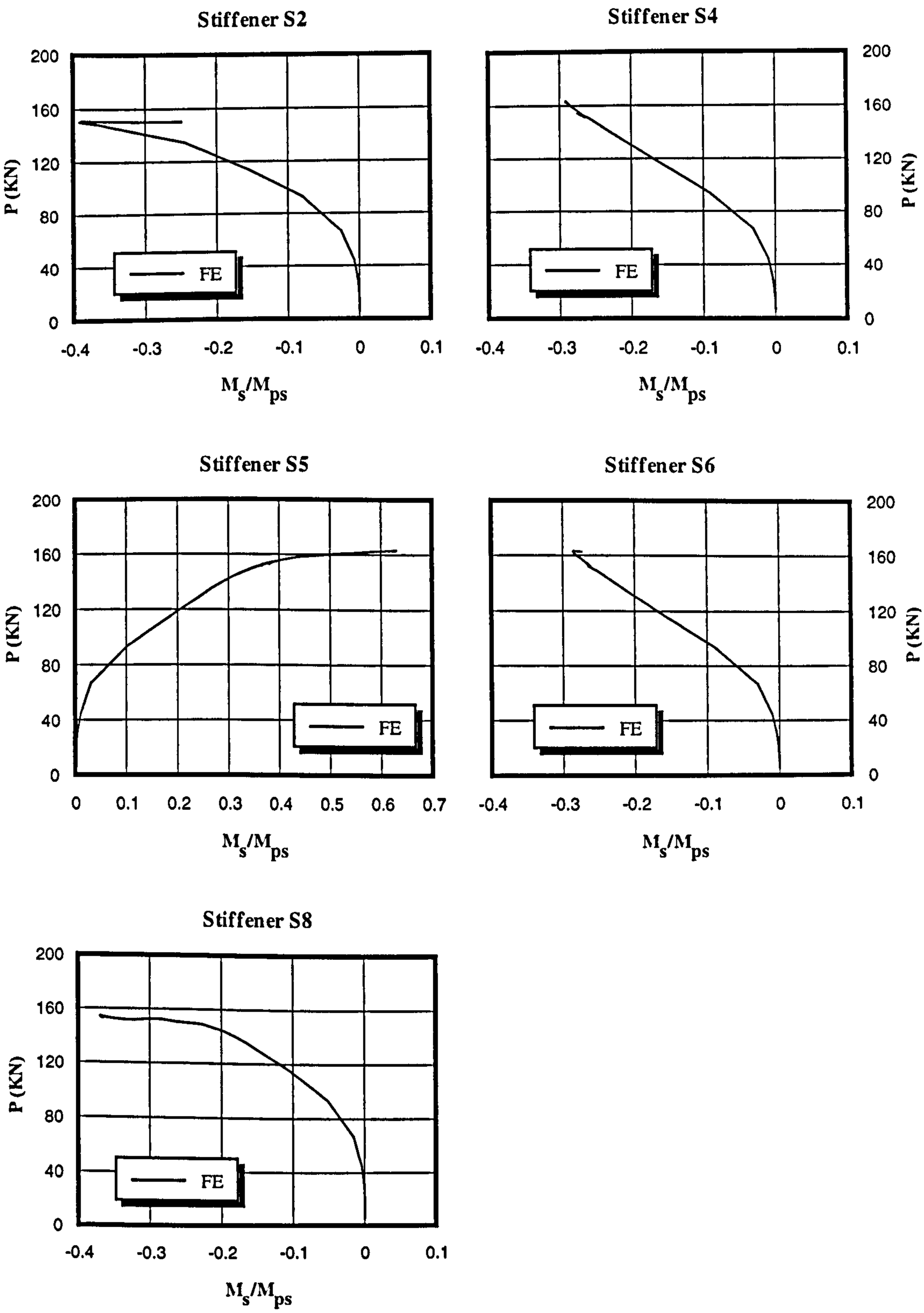


Figure 2.42 Bending moments in the stiffeners. M_s: positive for producing tension in Edge 1 (Fig. 2.40). Girder GIV. P as in Fig. 2.1. FE results. S2 — the 1st FE analysis; S4, S5, S6 and S8 — the 2nd FE analysis

2.6 DISCUSSION AND ANALYSIS

In Section 2.5, the experimental and numerical results for I-section plate girders are presented and compared with each other. It has been pointed out in Section 1.3 that the main objective of the present investigation is to produce a rational and practical design method for transverse web stiffeners. Therefore, it is the purpose of this section to provide rational bases for the development of the design model, by carrying out further analyses on the test girders and discussions on the experimental results.

2.6.1 Effects of Flanges on the Required Stiffener

In design, it is desirable to analyse a structural component in isolation from the surrounding structures. To achieve this simplification, the effects of the surrounding structures on the structural component considered must be approximated as idealised boundary conditions or interactive forces. For I-section plate girders, it is usual to design the web panel as a simply supported plate. The actual restraint afforded by the flanges depends on the flange dimensions and the distance between stiffeners. Chapman and Davidson [39,40] examined the influence of a realistic range of possible boundary conditions on panel shear strength.

Transverse stiffeners are employed to divide the plating into panels. To study the buckling behaviour of the stiffener, a two-panel plate model was adopted separately by several researchers [1,5,45]. In the previous work by Stanway et al [1,8], all the boundaries of the plate are simply supported, and the in-plane boundary conditions are taken as CUCU (Fig. 3.2). It is known that different boundary conditions result in significant variations in the panel strength. Therefore, for design of the transverse stiffeners, it is important to know whether the stiffener size that is adequate for the CUCU plate is also adequate for the plate with flanges. This is one reason for carrying out the tests and finite element analyses for real girders.

Fig. 2.43 presents a comparison of the FE graphs of the ultimate shear strength $V_u'=V_u/V_0$ against the stiffener flexural rigidity parameter Ψ for the plate girders and

for the associated two-panel plates. In the finite element analyses, code specified imperfection magnitudes (Eqns. 3.8 and 3.9) were taken, and the stiffener thickness t_s was kept as 5mm but the width of the stiffener h_s varied. The dimensions of the flanges and web panels were taken as those of the first two test girders. For CUCU plates, the loading conditions considered included pure shear and coexistent shear and bending (Fig. 3.1). In the latter case, the ratio of shear stress to maximum bending stress was taken as $\tau:\sigma_b=1:0.52$, which was the stress ratio at the position of the intermediate stiffeners in the test girders GI and GII. The test results for the intermediate stiffeners listed in Table 2.10 are also shown in Fig. 2.43. Two stiffener sizes are marked on the curves in Fig. 2.43; namely, Ψ_p and Ψ_e. The value of Ψ for which the stiffener just remains elastic at the ultimate load lies between Ψ_p and Ψ_e.

It can be seen in Fig. 2.43 that for both double-sided and single-sided stiffeners, the start of the plateau in the V_u' vs. Ψ curve for the CUCU plates subjected to combined shear and bending is slightly ahead of that for the I-section plate girders. This means that an adequate stiffener for the CUCU plate lies within the plateau of the V_u' vs. Ψ curve for the plates with flanges, but is not overly conservative, and hence is also adequate for the I-section girder. The reason for the earlier start of the plateau in the V_u' vs. Ψ curve for the plate girders than that for the CUCU plates is that for the plate girders, the deflection of buckled web panels is less due to the rotational and extensional restraints provided by the flanges.

By comparison of the V_u' vs. Ψ curves for CUCU plates subjected to shear only and combined shear and bending (Fig. 2.43), it is evident that a larger stiffener is required for plates under pure shear. However, for the cases considered, the difference in the required stiffener size is not large. This confirms the conclusion made by Grayson [46] and by Rahal and Harding [7] that the stiffener rigidity Ψ needed for the maximum panel shear capacity in the absence of other direct stresses is greater than the rigidity needed for any other combination of stresses that is within the panel capacity.

The above comparisons demonstrate that the stiffener required for plates with flanges (I-section girders) can be taken as the required stiffener obtained for the corresponding

CUCU plates. Therefore, it is rational to develop a design approach for transverse web stiffeners by using a CUCU plate model, which will be adopted in the present investigation. It will be useful to verify this conclusion in the future by carrying out a parametric study for plates with different dimensions of flanges or with various boundary conditions other than CUCU.

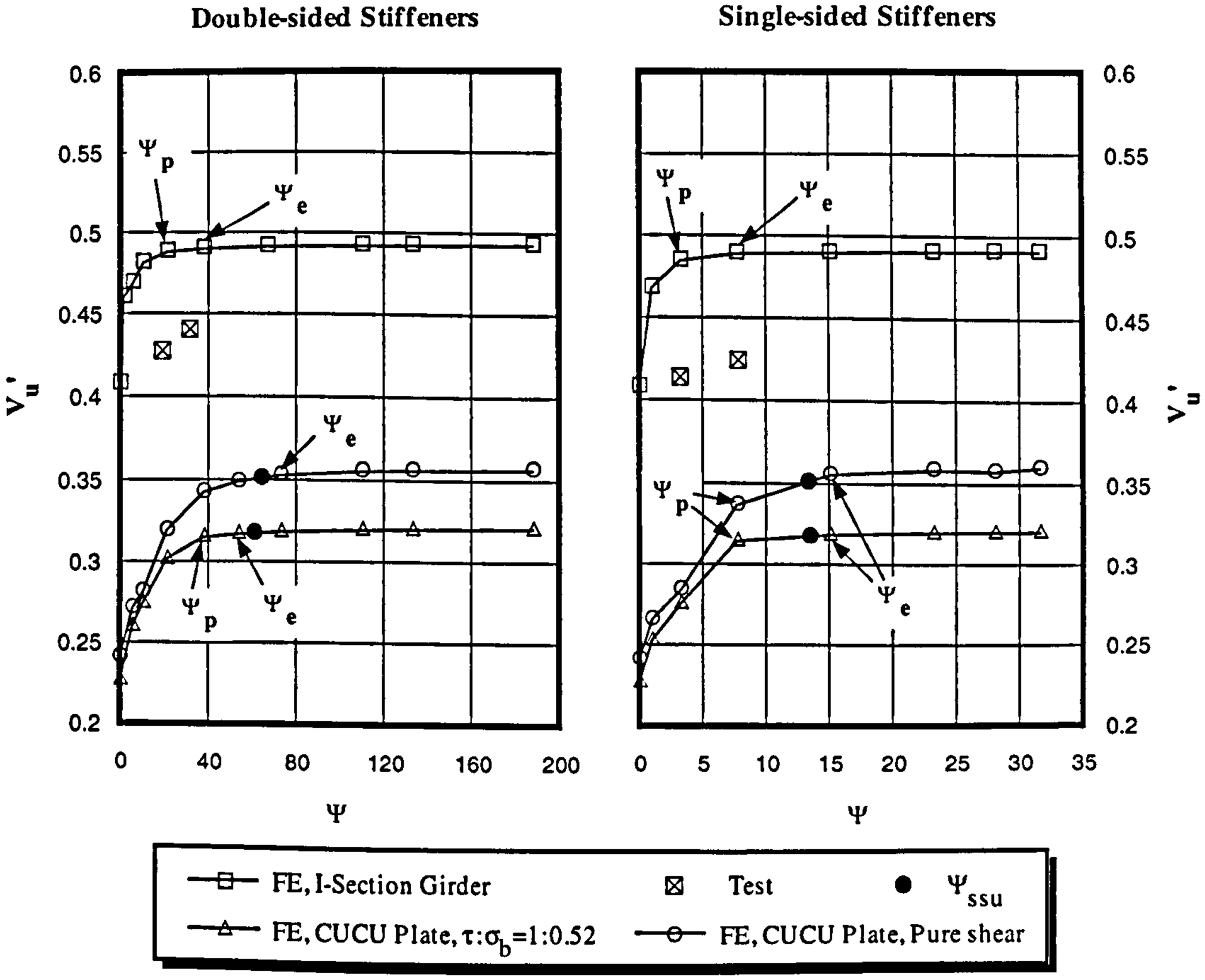


Figure 2.43 Comparison of the shear strength versus stiffener rigidity Ψ curves for plates with and without flanges. Girders GI & GII. a=590mm, d=600mm, t=2mm, t_s=5mm, σ_{0p}=300MPa, σ_{0s}=320MPa.

$\Psi=EI_s/Db$. I_s as given in Eqn. 3.4 for double-sided stiffeners and Eqn. 3.6 for single-sided stiffeners.

Ψ_p: the largest stiffener, of those considered, for which the stiffener has yielded at the ultimate load.

Ψ_e: the smallest stiffener, of those considered, for which the stiffener remains elastic at the ultimate load.

Ψ_{ssu}: the stiffener rigidity required to develop the ultimate load of simply supported panels.

2.6.2 Forces in Stiffeners

The experimental and numerical results show that the intermediate stiffeners were subjected to coexistent axial forces and bending moments. For double-sided stiffeners, the contribution of the axial force to the total stiffener stress at the ultimate load is about 10~20% for the cases tested (Figs. 2.18 and 2.33). For single-sided stiffeners, the stiffener axial force becomes more important, and may contribute up to about 60% of the total stiffener stress at the ultimate load (Figs. 2.26 and 2.41).

It was found that the load bearing stiffeners on the test girders GI and GII were virtually subjected only to axial forces. However, it would be expected that for tall plates and large stiffener initial deformations, the bending moment in the stiffener may become more significant.

In view of the above discussion, it is considered that a rational design model for transverse stiffeners should give an appropriate recognition of both the axial force and bending moment exerted in the stiffener. In the design model proposed in Chapter 8, the stiffener is designed to resist the coexistent axial force and bending moment.

2.6.3 Comparison between single-sided and double-sided stiffeners

It was proposed by Horne and Grayson [45] that with the moment of inertia I_s calculated about the face in contact with the web plate, a single-sided stiffener can be designed to achieve the same flexural rigidity Ψ (i.e., equal I_s) as required for the double-sided stiffener. To verify whether this approach is appropriate for the cases considered, the stiffener rigidities for the single-sided stiffeners shown in Fig. 2.43 were converted by calculating I_s about the face in contact with the web plate, that is, the neutral axis of the stiffener section is assumed to be at the surface of the plate. In Fig. 2.44, the converted V_u' vs. Ψ curves for single-sided stiffeners are compared with those for double-sided stiffeners.

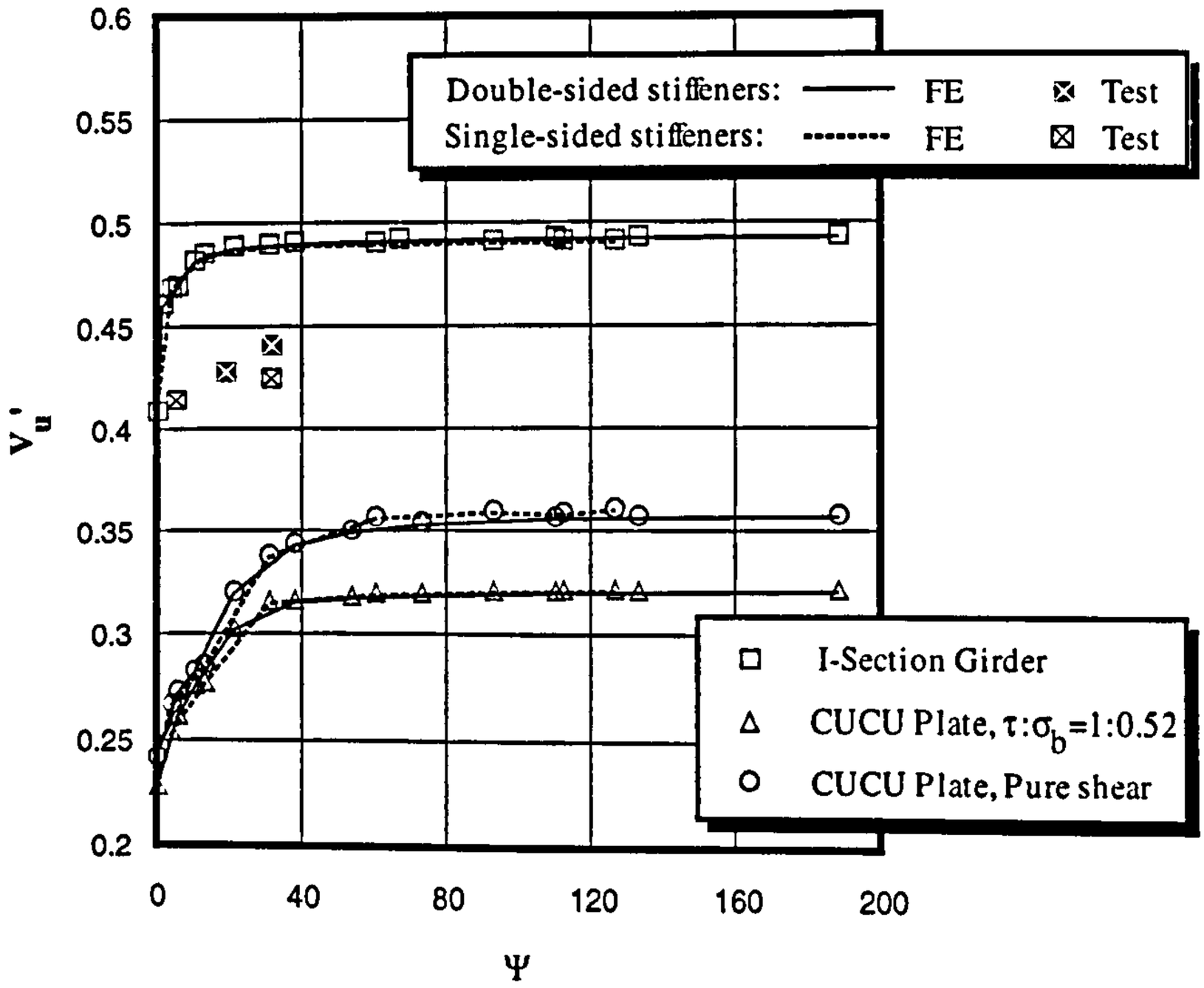


Figure 2.44 Comparison of the V_u' vs. Ψ curves for single-sided and double-sided stiffeners. Girders GI & GII and CUCU plates. a=590mm, d=600mm, t=2mm, t_s=5mm, σ_{0p}=300MPa, σ_{0s}=320MPa. $\Psi=EI_s/Db$, I_s as in Eqn. 8.22 for single-sided stiffeners, and Eqn. 3.4 for double-sided stiffeners

It is apparent in Fig. 2.44 that the converted V_u' vs. Ψ curve for single-sided stiffeners nearly coincide with the corresponding strength curve for double-sided stiffeners. Therefore, for the cases examined, the approach proposed by Horne and Grayson [45] for design of single-sided stiffeners can lead to an adequate stiffener. In Fig. 2.40, the FE results for the test girder GIV also indicate that for the single-sided stiffeners S2, S4, S6 and S8, the stiffener strains in the face in contact with the web are almost equal to zero. However, the FE solutions show that the edge of the stiffener S5 on Girder GIV in contact with the web was in significant tension, and both the experimental and numerical results for the test girder GII (single-sided stiffeners S2 and S4, Fig. 2.25) indicate that the stiffener edge in contact with the web was in significant compression. These observations demonstrate that the approach proposed by Horne and Grayson [45] for design of single-sided stiffeners may only be valid for certain cases. In the design

model proposed in Chapter 8, special features for the single-sided stiffeners are taken into account.

2.6.4 Failure Mode of Stiffener

It has been found in Section 2.5 that the stiffeners fail to perform their functions, either by yielding or by deflecting rapidly. For the test girder GI, it was observed that the intermediate stiffeners S2 and S4 deflected rapidly, even if the maximum strain was still below the yield strain of the stiffener. On the other hand, it was found that the stiffener S2 on Girder GII started to deflect rapidly at the moment that the stiffener reached its yield strain. Similar phenomena were also found for the stiffeners on Girders GIII, GIV. It is noted that the reason for the small stiffener S4 on Girder GI not to yield is because the yield stress of this stiffener was much greater than that of the web panel.

The failure modes of the stiffener indicated above confirm the necessity to introduce both the strength and stiffness criteria in order to determine the required stiffener sizes, as proposed by Stanway et al [1,9]. The strength criterion should ensure that the stiffener will not yield until the required ultimate load of the plate is reached, whereas the stiffness criterion is used to limit the stiffener deflection at the ultimate load. A detailed discussion on the strength and stiffness criteria will be given in Chapter 8.

2.6.5 Effects of Residual Stresses

As indicated before, residual stresses were not included in the finite element models for the test girders. Hence, by comparison of the FE solutions and the experimental results, the effects of residual welding stresses could be identified. It should be pointed out that the differences between FE and test results may also be attributable to other factors, such as initial imperfections, and variations in material strength and geometrical dimensions.

In Table 2.3, the measured loads at which the stiffener failed are compared with the values predicted by the finite element program ABAQUS. It is observed that the failure

load of the stiffener given by ABAQUS is on average about 10% greater than that from the tests. This indicates that the residual stresses will result in a reduction in the plate strength. Nevertheless, it is more important for design of the stiffener that an adequate stiffener stiffness relative to the plate stiffness is attained, so that the plate can be effectively divided into panels. To achieve this, it is necessary that the forces in stiffeners are reasonably accurately predicted. It has been found in Section 2.5 that the measured stiffener forces agree well with the numerical solutions. Therefore, for developing a design model for stiffeners, the effects of residual stresses may be neglected in the parametric study, which will be presented in the subsequent chapters of this thesis.

2.7 CONCLUSIONS

In this chapter, experiments on four transversely stiffened plate girders, categorized into two groups according to the loading arrangements and panel dimensions, are described. Finite element analyses were carried for each test, and for the first group of the test girders (GI and GII), the FE solutions are compared with the test results. The tests on the other group of girders (GIII and GIV) have not been fully completed by the time of writing this thesis, and the experimental results will be presented in a separate report in the near future. But the FE solutions for the test girders GIII and GIV are presented and analysed in this Chapter. The study presented in this Chapter enable the following conclusions to be drawn:

(1) For the test girders GI and GII, comparisons were made between experimental and FE results for the central deflection of the girder, the deflections of each panel and each stiffener, as well as the strains and forces in the stiffeners. Allowing for the presence of residual stresses in the physical girders, imperfection differences, and variations in material and geometrical properties, the FE analyses gave good agreement with the test results.

(2) The comparisons between the experimental and finite element results demonstrated that the overall behaviour of stiffened plate girders and the buckling behaviour of

their members are well represented by the finite element program ABAQUS. This supports the use of ABAQUS for the intensive parametric study carried out in the present investigation.

(3) The experimental and FE results for the applied loads at which the stiffeners failed are tabulated in Table 2.3. It is found that the failure load predicted by the finite element program ABAQUS is on average about 10% greater than that from the tests, and this reduction in the maximum load is mainly attributable to the effects of residual welding stresses. The stiffener failure is defined as that the stiffener failed to perform their functions, either by yielding or by deflecting rapidly.

(4) Although residual stresses result in a reduction in the maximum load for stiffener to fail, and hence the ultimate load of the plate girder, it has been found that the finite element model, in which the residual stresses were not included, gives a satisfactory representation of the buckling behaviour of the stiffener and the forces in the stiffeners. Therefore, for design of the stiffener, the effects of residual stresses may be neglected in the parametric study.

(5) By comparing the ultimate strength versus stiffener rigidity curves from a parametric study for I-section girders and CUCU plates (defined in Fig. 3.2), it is found that the stiffener that is adequate for the CUCU plate is also adequate for the plates with flanges. Therefore, it is rational and useful to develop a design approach for transverse web stiffeners by using a CUCU plate model.

(6) By comparison of the FE results for CUCU plates subjected to shear only and combined shear and bending, it is found that a larger stiffener is required for plates subjected to pure shear. This confirms the conclusion made by Grayson [46] and by Rahal & Harding [7] that the stiffener rigidity Ψ needed for the maximum panel shear capacity is greater than the rigidity needed for any other combination of stresses that is within the panel capacity.

(7) It is found from the experiments and the finite element analyses that the transverse stiffeners were subjected to coexistent axial forces and bending moments. For double-sided intermediate stiffeners, the stiffener stress due to the axial force is about 10~20% of the total stress at the ultimate load. For single-sided intermediate stiffeners, the axial force is more important, and may contribute up to about 60% of the total stiffener stress for the cases tested.

(8) For the test girders GI & GII and associated CUCU stiffened plates, the numerical results show that by calculating the moment of inertia I_s of single-sided stiffeners about the face in contact with the web plate, the single-sided stiffener can be designed to achieve the same flexural rigidity Ψ as required for the double-sided stiffener. However, both the test and FE results have demonstrated that for single-sided stiffeners, the stiffener edge in contact with the plate may also be in significant tension or compression. This implies that it is not generally adequate to assume that the neutral axis of the single-sided stiffener section lies at the edge in contact with the plate. For single-sided stiffeners, further investigation, covering a range of geometrical parameters, is needed to understand their buckling behaviour.

(9) It is found from the experiments and the finite element analyses that the transverse stiffeners fail to perform their functions, either by yielding or by deflecting rapidly, depending on the stiffener sizes and the yield stresses of the web plate and the stiffener. These two failure modes of the stiffener show the necessity to introduce both strength and stiffness criteria in the proposed design model for transverse stiffeners.

CHAPTER 3

FINITE ELEMENT MODELLING

3.1 INTRODUCTION

As one of the approaches to be used in this thesis, a parametric study will be conducted to examine the linear and non-linear buckling behaviour of transversely stiffened plates, subjected to pure shear, and to combined shear and direct in-plane loading. The numerical results are produced using the general-purpose finite element program *ABAQUS*, which is briefly described in Appendix A.

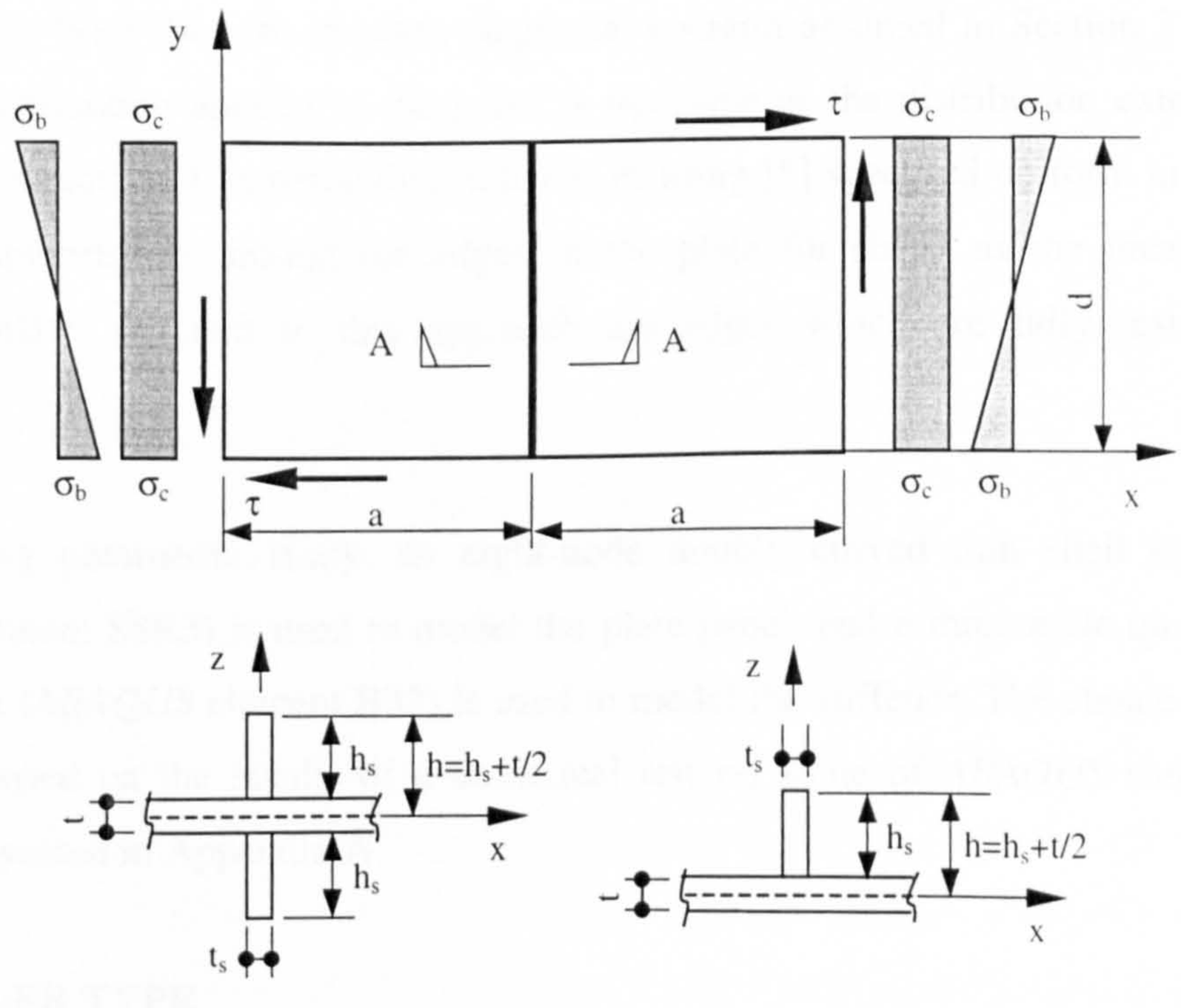
This chapter presents a description of the general features concerning finite element modelling used in this investigation, including structural configuration, material properties, initial imperfections, and boundary conditions. Special features for some particular cases will be described in the relevant chapters of this thesis.

The finite element meshes to be adopted in the investigation are determined with regard to the conflicting requirements of solution accuracy and computational cost and time, based on a mesh convergence study, which will be presented in Section 3.6.

It is contemplated that the present investigation will in some respects be based on the previous study on stiffened plates under pure shear, carried out by Stanway [1]. It is noted that in the previous work, numerical results were provided using the non-linear elasto-plastic finite element program *FINASIC*, developed at Imperial College. In the early stage of the present investigation, the numerical solutions obtained from *ABAQUS* were compared with the FE solutions from *FINASIC*, given by Stanway [1], and good agreement has been found. The detailed comparisons are presented in Appendix C.

3.2 STRUCTURAL CONFIGURATION

As stated in Chapter 1, the main purpose of this investigation is to produce a rational, practical design model for transverse stiffeners on plates subjected to coexistent in-plane shear, compression and bending. The model to be proposed will incorporate the significant effects and parameters. The basic phenomena for stiffened plates under pure shear have been found by Stanway [1] by conducting a parametric study on two-panel plates with an intermediate flat bar stiffener. As an extension of this previous work, the present investigation will also take the two-panel plate with an intermediate stiffener, depicted in Fig. 3.1, as the basic structure to be studied.



Double-sided stiffener Single-sided stiffener

Section A-A

Figure 3.1 Two-panel plate with an intermediate stiffener, subjected to combined shear, compression and bending. The small panel dimension *b=540mm* is adopted in the parametric study

It is considered that the basic phenomena can be revealed by the simple structure in Fig. 3.1. Since the model to be proposed will sufficiently account for these phenomena, structures with other configurations, e.g. multi-stiffener plates, could be treated by considering the effects on the relevant components of the design model.

The effects of the flanges have been studied in Chapter 2, where it is found that for the cases examined, the flanges have an influence on the ultimate strength of the web panel. However, it is observed that the stiffener size which is adequate for the two-panel plate, is also appropriate for the plate with flanges. Therefore, for the purpose of developing a design method for transverse stiffeners, it is reasonable to consider the simple two-panel plate.

The applied shear force is assumed to be uniformly distributed on each boundary of the stiffened plates. With the zero in-plane tangential restraint assumed in Section 3.5, the shear force distribution applied to the panel is the same as the distribution externally applied to the structure. It is noted that Rahal & Harding [5] specified uniform in-plane tangential displacements around the edges of the plate for shear, as the means for loading the plate. Inherent in this approach are edges which are fully restrained tangentially.

In the ensuing parametric study, an eight-node doubly curved thin shell element (*ABAQUS* element S8R5) is used to model the plate panel, and a three-node quadratic beam element (*ABAQUS* element B32) is used to model the stiffener. The choice of the elements is based on the results of a numerical test on some of *ABAQUS* elements, which are presented in Appendix A.

3.3 STIFFENER TYPE

The present investigation aims to develop a design model for transverse stiffeners with open cross-section shapes, whose torsional rigidity is relatively small. In most cases studied in this thesis, double-sided flat bar stiffeners are considered for simplicity, with the out-stand slenderness being taken as:

$$h/t_s = 10 \tag{3.1}$$

This value is used in the previous study carried out by Stanway [1], and complies with the slenderness limit for flat bar stiffeners given in BS5400 [3]:

$$\frac{h_s}{t_s}\sqrt{\frac{\sigma_{0s}}{355}} \le 10 \tag{3.2}$$

The definitions of h, h_s and t_s are illustrated in Fig. 3.1. For double-sided flat bar stiffeners, the stiffener area A_s and the moment of inertia I_s are calculated as follows:

$$A_s = 2h_s t_s \tag{3.3}$$

$$I_s = \frac{1}{12} t_s \left[(2h_s + t)^3 - t^3\right] \tag{3.4}$$

Based on the phenomena found by Stanway et al [1,8,9], the design model will be developed by using some idealised structures, such as the two-panel plate with a knife edge (Fig. 4.1). It is anticipated that a design rule established by means of such idealised structural models might be applicable for various open section stiffeners, either double-sided or single-sided.

For single-sided flat bar stiffeners, as illustrated in Fig. 3.1, the stiffener area A_s and the moment of inertia I_s are taken as:

$$A_s = h_s t_s \tag{3.5}$$

$$I_s = \frac{1}{12} t_s h_s^3 \tag{3.6}$$

Given in Eqns 3.4 and 3.6, the value of I_s is calculated by taking the neutral axis as the centroidal axis of the stiffener cross-section. For double-sided (concentric) stiffeners, the neutral axis occurs at the mid-plane of the plate. For both types of stiffener, only the actual stiffener sections are included, that is, no effective width of the plate is included. The reason for this is that in the proposed design model, only the forces acting in the stiffener itself are considered, and the stiffener is designed as a simple beam, separated from the plate, subjected to an axial force and a bending moment (resulting from a lateral distributed force). Detailed discussions on single-sided stiffeners are presented in Section 8.7. When calculating the cross-sectional properties of other open sections, the same assumptions will be adopted, according to the proposed design model.

In this thesis, the following non-dimensional stiffener rigidity parameters will be used:

- *Ω: stiffener extensional rigidity parameter, $\Omega=A_s/at$*
- *Ψ: stiffener flexural rigidity parameter, $\Psi=EI_s/Db$*
- *Γ: stiffener torsional rigidity parameter, $\Gamma=GJ_s/Db$*

where J_s is the torsion constant of the stiffener. For double-sided flat bar stiffeners, J_s may be approximately taken as:

$$J_s = \frac{2}{3} h_s t_s^3 \tag{3.7}$$

3.4 MATERIAL PROPERTIES

All material is considered to be isotropic. When performing elasto-plastic analyses, the bilinear elastic-perfect plastic stress vs. strain relation is adopted, and the Mises yield surface model is used as the yield criterion. For most of the studies carried out in this investigation, the following material constants are considered:

Young's modulus:	$E=205000\ N/mm^2$
Poisson's ratio:	$\nu=0.3$
Yield stresses:	$\sigma_{0p}=\sigma_{0s}=355\ N/mm^2$
Shear yield stress:	$\tau_0 = \sigma_0/\sqrt{3}$

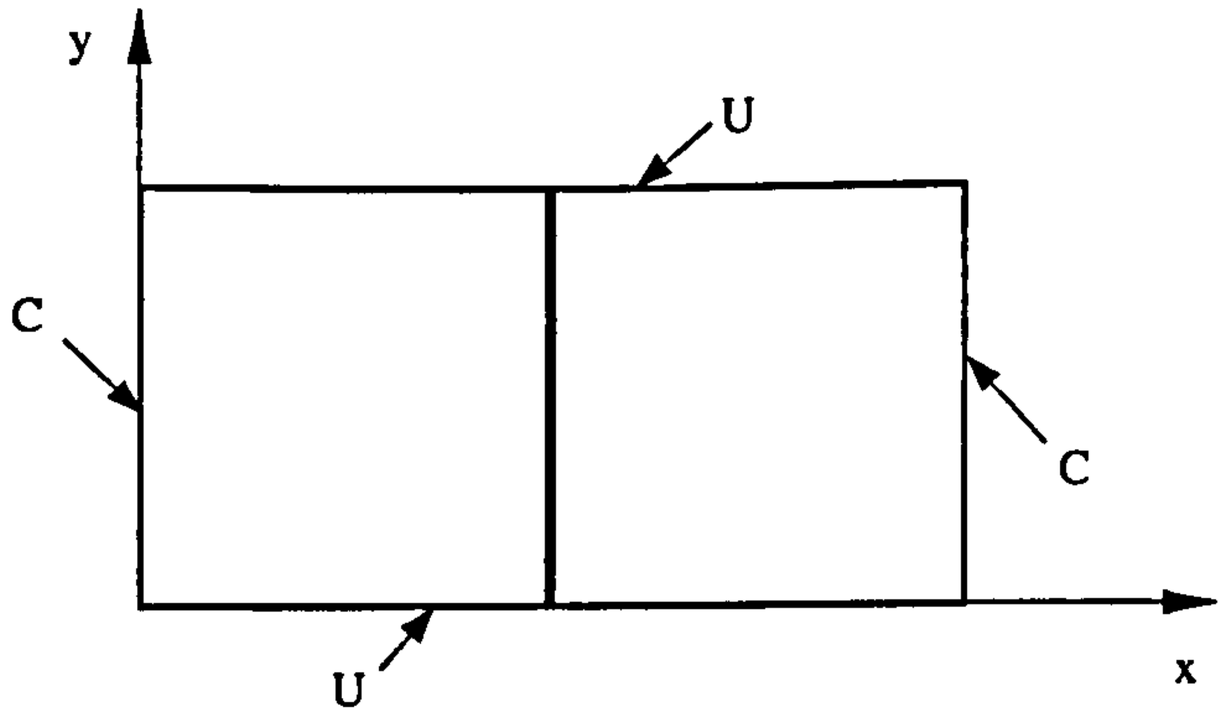
Other values of the yield stresses, such as 245N/mm^2 and 500N/mm^2, are also considered in some instances, which will be indicated in the subsequent sections.

3.5 BOUNDARY CONDITIONS

Due to the complexity and variability of the actual boundary conditions, exact representation is not feasible and assumptions must be made. In Ref. [39], Chapman and Davidson examined the influence of a realistic range of possible boundary conditions on panel shear strength. For design of the transverse stiffeners, Stanway et al [1,8] assumed

that all the boundaries of the plate are simply supported, and the in-plane boundary conditions are represented as CUCU, which will be defined below. In addition, it has been found in Chapter 2 that the stiffener size which is adequate for the CUCU plate, is also appropriate for the plate with flanges. Therefore, in the ensuing non-linear elastic and elasto-plastic buckling analyses, the in-plane boundary conditions will be taken as CUCU. In all finite element analyses presented in this thesis, the out-of–plane boundary conditions are assumed to be simply supported for all the boundaries of the plate. The boundary conditions adopted are depicted in Fig. 3.2, and described below.

For stiffened plates as shown in Fig. 3.1, the edges parallel to the stiffener are constrained to remain straight, denoted by 'C'. The edges perpendicular to the stiffener are unrestrained in-plane, denoted as 'U'. Consequently, the in-plane boundary conditions of the plate, in a sequence of left, top, right and bottom edges, may be simply represented as 'CUCU'.



U: denotes an unrestrained edge where:
- (v) the edge has zero normal restraint, in-plane
- (vi) the edge has zero normal stress (σ_n=0)
- (vii) the edge has zero tangential restraint, in-plane
- (viii) the edge is free to translate and rotate, in-plane

C: denotes a constrained edge where:
- (i) the edge is constrained to remain straight
- (ii) the edge has zero resultant normal stress ($\int \sigma_n dt = 0$)
- (iii) the edge has zero tangential restraint, in-plane
- (iv) the edge is free to translate and rotate, in-plane

All boundaries are simply supported ($w = 0, \quad \frac{\partial^2 w}{\partial n^2} = 0$)

Figure 3.2 Boundary conditions adopted. (from Ref. [1])

For the non-linear buckling analyses, all boundaries are assumed to be unrestrained tangentially. In the design model to be proposed in Chapter 9, the axial forces due to the tension field action are taken into account. However, it has been found by Chapman and Davidson [39,40] that for simply supported panels of d/a=1 and 2, the panel strength is not significantly affected by the tangential boundary condition at the vertical boundaries. They also recommended that it is desirable that the design of the panel should not be dependent on the transfer of membrane forces to the surrounding stiffeners or flanges. The tangentially unrestrained boundary condition is consistent with this recommendation.

In the numerical analyses presented in this thesis, the *ABAQUS* multi-point constraint (*MPC*) type *SLIDER* is used to represent the straight line requirement for the constrained edges. *SLIDER* keeps a node on a straight line defined by two other nodes, but allows the possibility of moving along the line, and the line to change length.

3.6 INITIAL IMPERFECTIONS

3.6.1 Imperfection Mode

Generally, the initial imperfection should comply with the tolerances specified in design codes, and be chosen to produce the most severe effect on resistance. Also, the chosen imperfection should be reasonably representative of practical initial deformation. Imperfections which are affine to the critical buckling modes may reasonably be assumed to give minimum resistance, though this assumption may not always be valid.

For stiffened plates, the initial imperfection consists of two components: that is, the panel imperfection and the stiffener imperfection. In BS5400 [51], the magnitudes of the initial panel deformation w_{0p} and the initial stiffener deformation w_{0s} are specified independently.

On account of the above requirements, it was decided that in the ensuing non-linear buckling analyses, for plates subjected to pure shear, the first point-symmetric (PS)

critical buckling modes of the plates with a straight knife edge, which is defined in Section 4.2 and equivalent to a stiffener of $\Psi=\infty$ and $\Gamma=0$, would be used to define the panel imperfection mode. The stiffener component of initial imperfection is taken as a double sinusoidal wave in all cases where an imperfect stiffener is considered, and is superimposed on the panel component of imperfection.

The reasons for choosing the first point-symmetric critical buckling modes as the panel imperfection shapes have been discussed by Stanway et al [1,8] for plates subjected to pure shear. It was found that for small but non-zero values of Ψ, the most critical mode is always point-symmetric (because the point-anti-symmetric mode causes the stiffener to have zero deflection at its mid-span), and the stiffener moments are greater for the point-symmetric mode. It was also pointed out that the point-symmetric mode is the most severe case for the stiffener required according to the critical buckling stress for plate with an intermediate stiffener, which means a smaller stiffener is needed to attain a divided point-anti-symmetric (PAS) mode than to reach a divided point-symmetric mode.

However, for the knife edge plates, it is demonstrated in Section 5.2 that the difference between the first PS and PAS modes become less distinct for tall plates ($d/a>2$). This is because the mode is less restricted by the boundaries, and plate lines parallel to the nodal lines buckle anti-symmetrically about the knife edge. For very tall plates, the only difference between the first point-symmetric and first point-anti-symmetric modes is the position of the buckle nodal line with respect to the centre of the plate.

For plates under compression or pure bending, the panel imperfection mode adopted is affine to the first symmetric buckling mode of the plate with a straight knife edge. It is foreseen that the symmetric buckling mode would be a higher mode. The symmetric modes are chosen to produce the highest estimate of the stiffener moment, as the main purpose of the present investigation is to develop a design rule for transverse stiffeners. Also, symmetric initial deformations are more likely to be encountered in practice. By similar reasoning, for plates under combined shear and longitudinal direct loading, the panel imperfection is chosen to be affine to the first mode, which is close to the

symmetric or point-symmetric mode, of the knife edge plate under the same loading condition.

It should be pointed out that the initial panel imperfection modes adopted are not consistent with those used for panel design, especially for compression and bending. Panels are designed for simply supported boundary conditions, whereas the symmetric modes assumed for compression and bending for establishing a stiffener design rule imply that one of the vertical edges of the panel is restrained against rotation (at the stiffener position), for which condition the corresponding critical buckling stress is much greater than that for the simply supported condition. Fig. 3.3 presents the critical buckling stresses for plates with an intermediate knife edge subjected to compression and pure bending. It can be seen in Fig. 3.3 that for d/a=5, the critical buckling stress parameter k_{cr} for the first symmetric mode is nearly twice as great as for the lowest buckling mode. However, the symmetric panel imperfections are introduced to obtain the most severe estimate of the lateral forces exerted on the stiffeners.

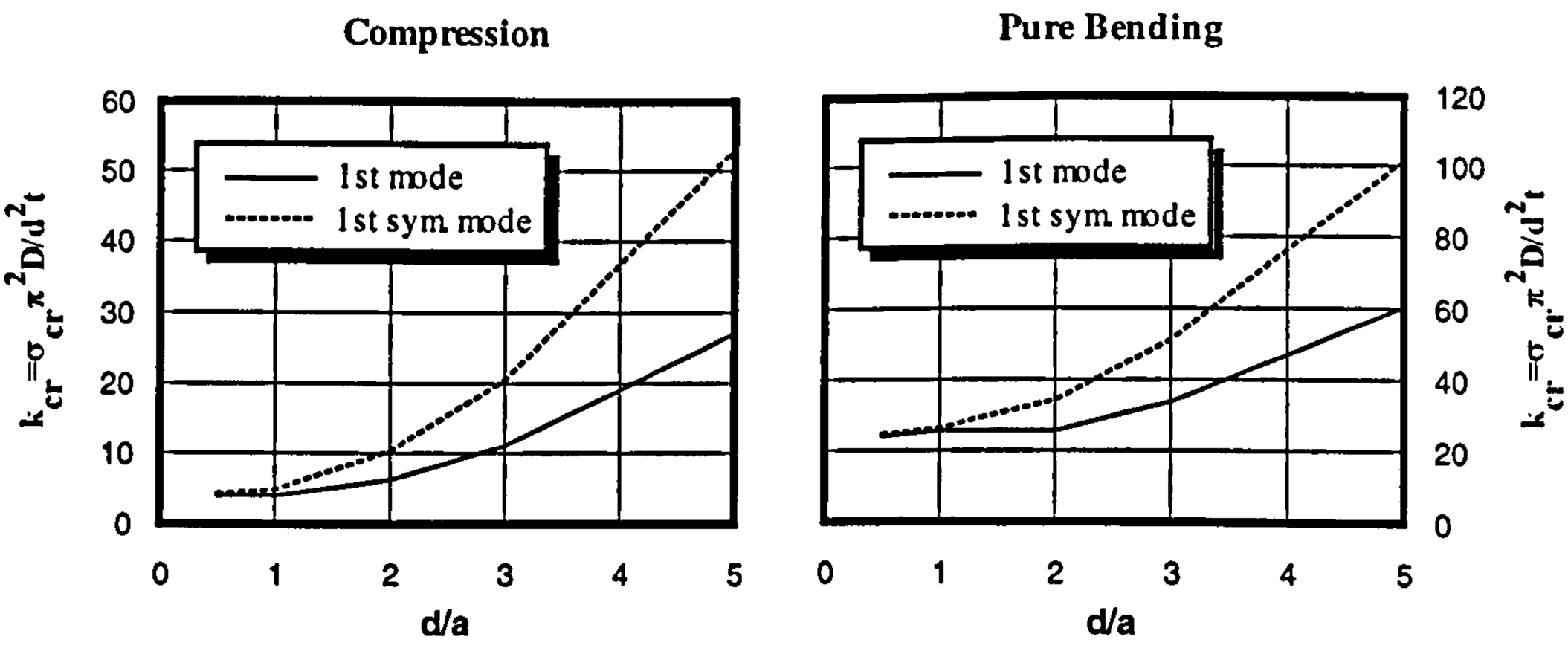


Figure 3.3 Critical buckling stress parameters. Plates with a knife edge (see Fig. 4.1). FE results

The first point-symmetric critical buckling modes of the knife edge plates are presented in Fig. 5.2 for pure shear, in Fig. 5.21 for combined shear and compression, and in Fig. 5.28 for combined shear and bending, respectively.

3.6.2 Imperfection Magnitude

The magnitudes of the initial panel and stiffener imperfections, denoted by w_{0p} and w_{0s} respectively, are taken as:

$$w_{0p} = \frac{b}{165}\sqrt{\frac{\sigma_{0p}}{355}} \tag{3.8}$$

$$w_{0s} = \frac{d}{750} \tag{3.9}$$

These imperfection magnitudes represent the maximum tolerances envisaged by BS5400 [51], and were used in the previous studies [1,5,45]. The measurement of w_{0p} and w_{0s} is shown in Fig. 3.5.

The relative signs of the panel and stiffener components of imperfection are chosen so that the initial deformation has affinity with the buckling mode of the plate with a finite stiffener within the plateau of the critical stress factor k_{cr} vs. Ψ curve. By reference to the critical buckling modes of the stiffened plates with varying Ψ [1,58], the trend in the direction of the stiffener deflection relative to the panel buckles can be identified.

The finite element results of the normalised stiffener and panel deflections for selected stiffener rigidities, obtained by Fortune [58] from the critical buckling analyses, are reproduced in Fig. 3.4. It can be seen in Fig. 3.4 that for $d/a \leq 2$, the maximum stiffener and panel deflections are in opposite directions. However, for $d/a \geq 3$, the magnitudes of the positive and negative panel deflections are nearly equal, and the stiffener deflection could be considered to be in either the same or opposite direction of the maximum panel deflection. For a less stiff stiffener, as shown in Fig. 5.4 for Ψ=300 for d/a=3, and Ψ=600 for d/a=5, the stiffener deflection is in the same direction as the maximum panel deflection. However, for a stiff stiffener, as shown in Fig. 5.4 for Ψ=700 for d/a=3, and Ψ=800 for d/a=5, the stiffener deflection is in the opposite direction to the maximum panel deflection. Therefore, when adding the panel and stiffener components of imperfection together, two types of combination are considered for the non-linear buckling analyses presented in this thesis, as depicted in Fig. 3.5. For $d/a \leq 2$, only type B is adopted, whereas for $d/a > 2$, both type A and type B are adopted.

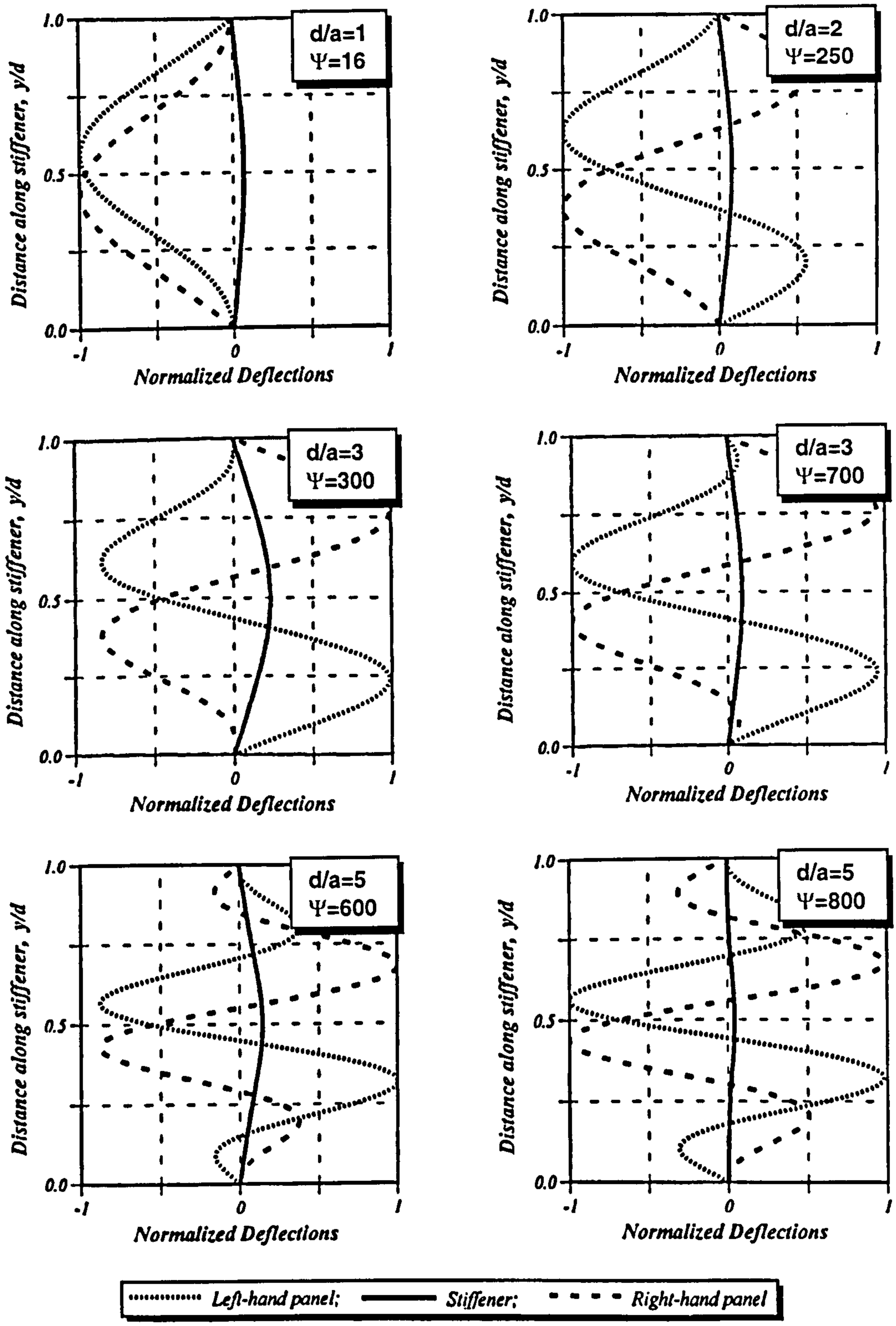
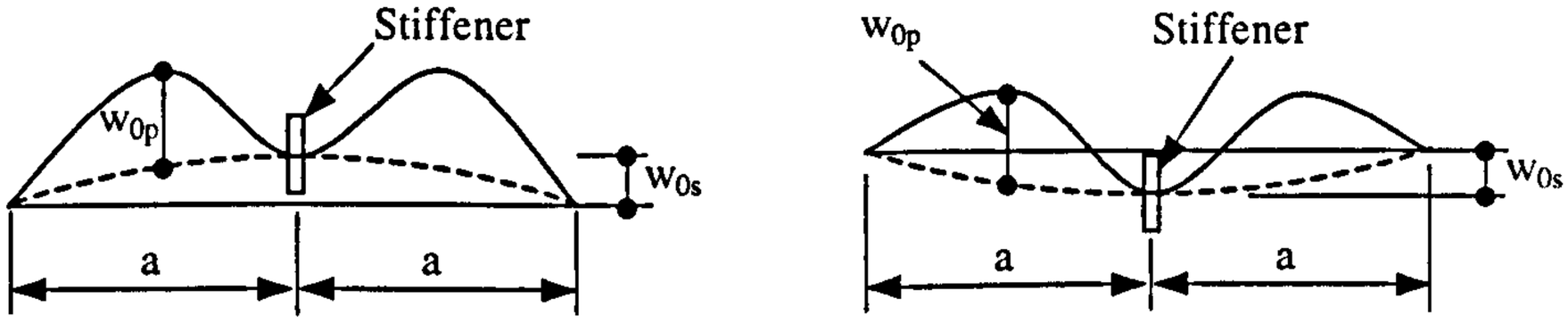


Figure 3.4 Normalised stiffener and panel deflections along the depth of the plate.
CUCU Plates with a stiffener. FE critical buckling analyses. Pure shear (from Ref. [58])

In the ensuing parametric study, imperfections are introduced by perturbations in the geometry, and the perturbed mesh is created by a user program which adds the total initial imperfection to the perfect geometry. The panel imperfection is generated by subtracting the designated eigen-mode from the *ABAQUS* results file obtained in a previous critical buckling analysis, scaled to give a panel imperfection magnitude specified by Eqn. 3.8. The panel component of imperfection is then added to the stiffener component of imperfection, calculated from the sinusoidal function:

$$w_{0s} \sin\left(\frac{\pi x}{2a}\right) \sin\left(\frac{\pi y}{d}\right) \tag{3.10}$$



(a) Type A (b) Type B

For d/a≤2, only type B is adopted.

For d/a>2, both type A and type B are adopted

Figure 3.5 Superimposition of the panel and stiffener components of imperfection

3.7 RESIDUAL STRESSES

The effects of residual stresses were examined by Harding et al. [35] for plate panels subjected to combinations of shear and direct compression. It was found that the residual stresses have negligible effects (less than 5% reduction) on the ultimate capacity of plate panels in shear, but for panels under compression the reduction in the ultimate load was found to be just under 30%. On the basis of a limited parametric study carried out for stiffened plates, Horne and Grayson [45, 46] concluded that the effect of

residual stresses on required stiffener rigidity for all forms of stiffened panel loading could be neglected. This conclusion is reasonable because the stiffener is designed to achieve an ultimate strength of the plate, for which the weakening effect of residual stresses on the plate strength is not considered.

In Chapter 2, by comparison of the experimental results on the test girders, it was found that the finite element model, in which the residual stresses were not included, provided a satisfactory estimate of the load at which the stiffener failed. It was also observed that the measured stiffener forces agree well with the finite element solutions. Therefore, for design of stiffeners, the effects of residual stresses may be neglected in the finite element analysis. It was pointed out in Chapter 2 that the differences between FE and test results were attributable to the effects of residual stresses and other factors, such as initial imperfections and variations in material strength and geometrical dimensions.

The actual distribution and magnitude of residual stresses are unknown. The residual stresses based on some simple assumptions can be incorporated into the finite element model by specifying initial stress states at the integration points of the *ABAQUS* elements. However, the introduction of the residual stresses will make the problem much more complicated.

As indicated previously, the main purpose of this investigation is to establish a design rule for transverse stiffeners. On account of the above discussion, it is decided that residual stresses will not be included in the finite element model in the present investigation, and parameters other than residual stresses will be studied.

3.8 MESH SIZE AND CONVERGENCE STUDY

3.8.1 General

Using the finite element program *FINASIC*, Davidson [40] and Stanway [1] conducted a finite element mesh convergence study for simply supported panels and stiffened plates, respectively. For the panel study carried by Davidson, the accuracy of the ultimate

strength τ_u' was taken as the convergence criterion, while Stanway used the ratio of the stiffener and panel deflections at the ultimate load, w_{su}/w_{pu}, as a convergence criterion for stiffened plates. In their studies, square shell elements were used to represent the plate panels. The mesh sizes adopted in their parametric study are listed in Table 3.1.

With the increasing computational capacity of computers and the more powerful finite element programs (eg. *ABAQUS*), it is possible to use much finer meshes without increasing the cost and time of the solution. Therefore, a mesh convergence study is carried out to assess the necessity and practicability of using finer meshes for the present parametric study.

Table 3.1 The number of square FE elements across the smaller panel dimension (b taken as 540mm). N

d/a	Davidson [40]	Stanway [1]	Present Study
<1	6	6	8
=1	8	6	8
>1	6	4	8*

* Note: For d/a≥5, the number of elements across the greater panel dimension is taken as 40.

In the ensuing parametric study, the behaviour of both plate panels and stiffened plates will be investigated. For the stiffened plates, due to the greater local plate bending curvature, the least accurate solution for a given mesh is for the case of $\Psi=\infty$ or the knife-edge stiffened plate, which is expected to be close to a simply supported panel. Hence, an appropriate mesh size required for an individual panel is expected to be satisfactory for a stiffened plate having the same panel dimensions.

Referring to the contour diagrams of the critical buckling modes shown in Fig. 4.4, the smallest buckle wavelength occurs for d/a=1. The solution for a square panel is therefore expected to be the least accurate for a given square mesh. For this reason, the present convergence study is conducted for square panels (d/a=1). 2:1 panels (d/a=2) are also considered to assess the effect of a slightly increased buckling wavelength in the long panel dimension. Because shear buckling requires a finer mesh than compressive

buckling (see Appendix A.2.4) and for reasons of simplification, only panels under pure shear are considered.

The increase of panel slenderness ratio b/t is expected to produce a less accurate solution, since a greater bending curvature of panels occurs. In this convergence study, b/t=180 is considered.

It is anticipated that in addition to the panel critical buckling strength and the ultimate strength, the non-linear elastic solutions of the maximum panel deflection w_p and the lateral distributed force acting on the supported edge of the panel may be used to formulate a method for the design of the transverse stiffeners. Therefore, the accuracy of these parameters is important for choosing the mesh size, and these parameters are taken as the convergence criteria for the present study.

3.8.2 Critical Buckling Stress

The critical buckling analysis results are presented in Fig. 3.6. It is evident that the errors in k_{cr}, relative to the converged k_{cr} obtained from a much finer mesh (N=20), are less than 0.5% for the meshes of N≥6.

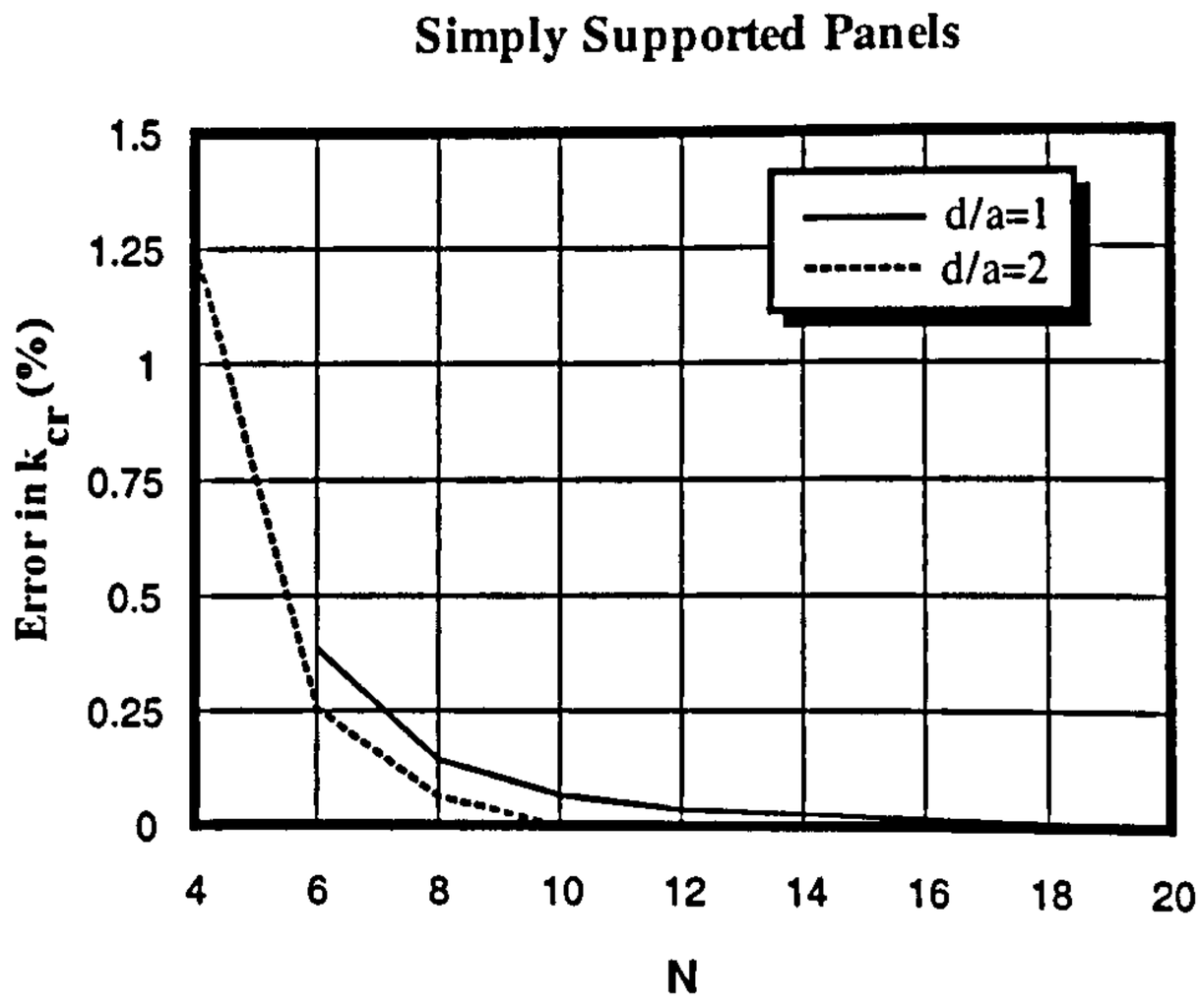


Figure 3.6 Convergence of the critical buckling stress coefficient k_{cr}. Pure shear

3.8.3 Ultimate Strength

Fig. 3.7 presents elasto-plastic shear stress versus overall shear strain and panel deflection curves for the square and 2:1 CUCU panels with different mesh sizes. It is evident that τ' converges much more quickly for the lower strain values.

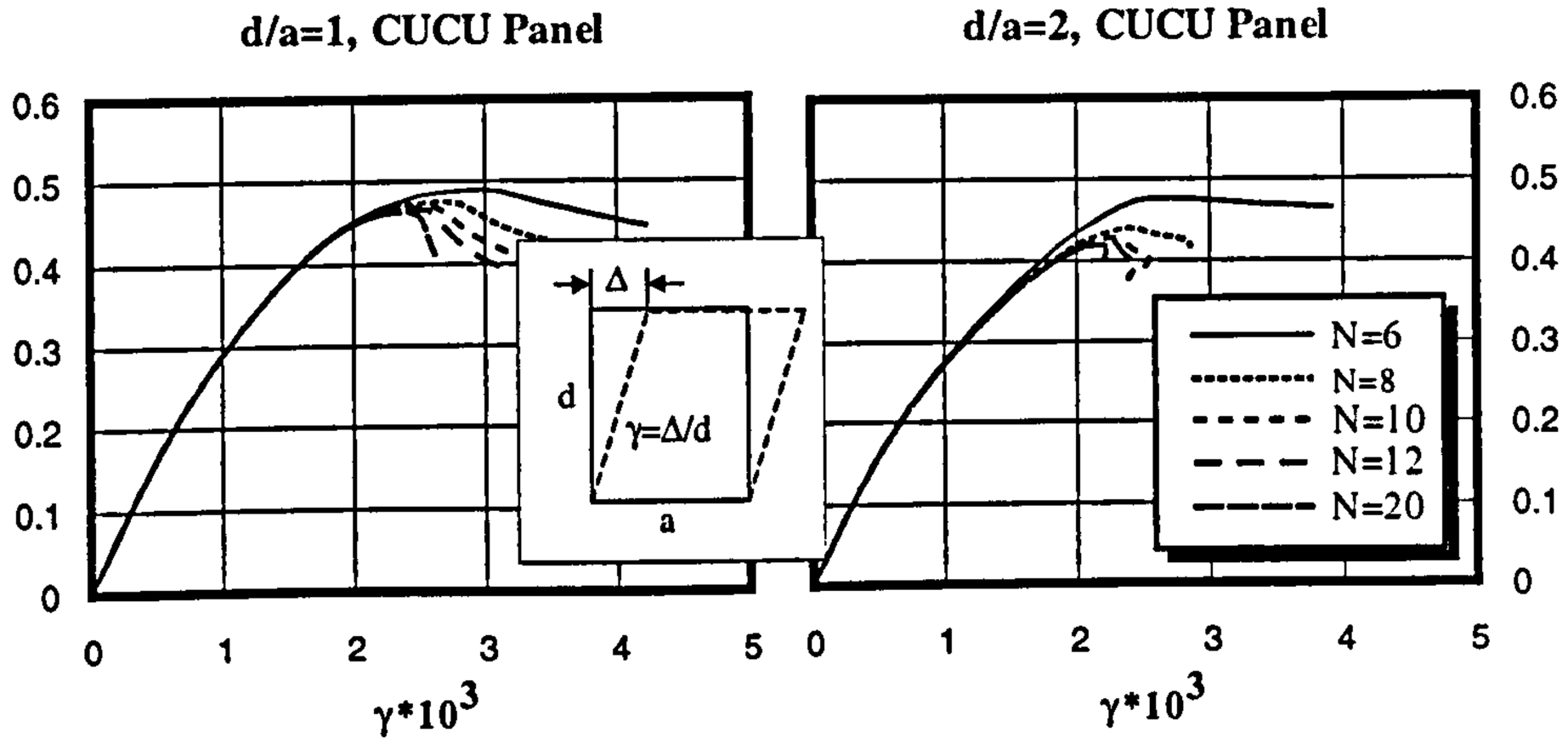


Figure 3.7 Non-linear elasto-plastic behaviour of simply supported panels for varying FE mesh sizes. Point symmetric imperfection, $w_{0p}/t=1.091$. $a/t=180$, $t=3mm$, $\sigma_0=355N/mm^2$. Pure shear

It is noted in Fig. 3.7(a) that in the post-ultimate region, the shear stress vs. strain curves seem not to converge, which may be due to the kinks formed locally in the unrestrained edges and the more localised bending curvatures. Therefore, it is considered that a

uniform mesh may not be suitable for the post-ultimate analyses, and a much finer graded mesh may be necessary to describe the local shear deformation. It is noted in Fig. 3.7(b) that the shear stress vs. panel deflection curves show better convergence with the increasing number of square elements, because the maximum out-of-plane deflection may not be affected significantly by the local shear deformation.

The errors in non-dimensional panel ultimate strength τ_u', relative to the converged value of τ_u' obtained from a much finer mesh (N=20), are illustrated in Fig. 3.8 for various FE mesh sizes. It is apparent that the relative error in τ_u' is less than 6% if a mesh of N≥6 is used.

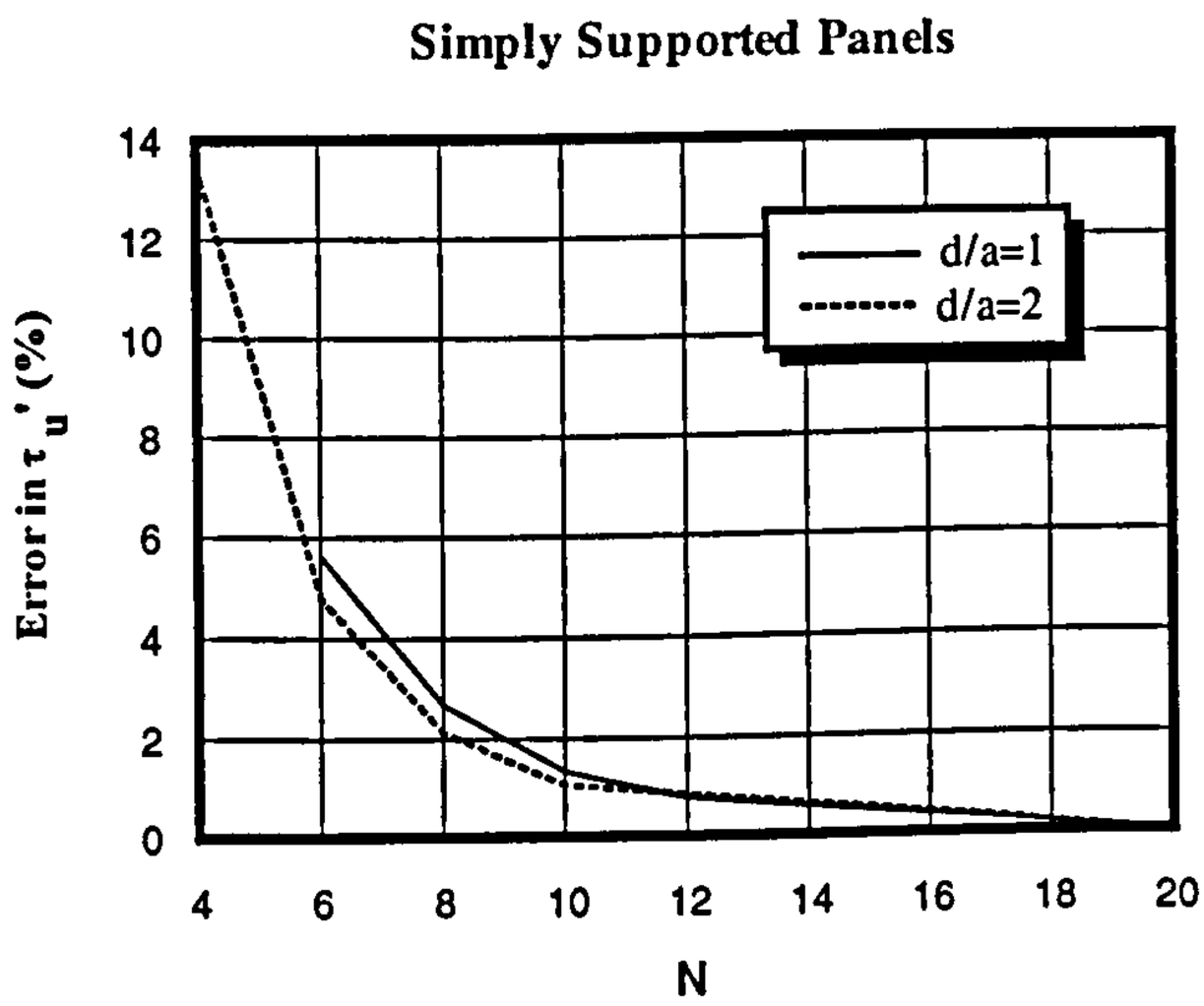


Figure 3.8 Convergence of the non-dimensional ultimate shear strength τ_u'. Pure shear

3.8.4 Maximum Panel Deflection, w_p

The non-linear elastic finite element solutions of the maximum panel deflection w_p are presented in Fig. 3.9. It can be seen in Fig. 3.9 that the ratio of w_p/t converges quickly.

In Fig. 3.10, the comparisons of w_p/t for different mesh sizes are made at the shear stress τ'=0.489, which is in the vicinity of the ultimate shear strength τ_u' (Fig. 3.8). By taking the values of w_p/t for the finest mesh examined (N=20) as the converged value,

the estimated errors in w_p/t for different mesh sizes at $\tau'=0.489$ are shown in Fig. 3.10. It is observed that for a mesh of $N \geq 6$, the error in w_p/t will be less than 1.5%.

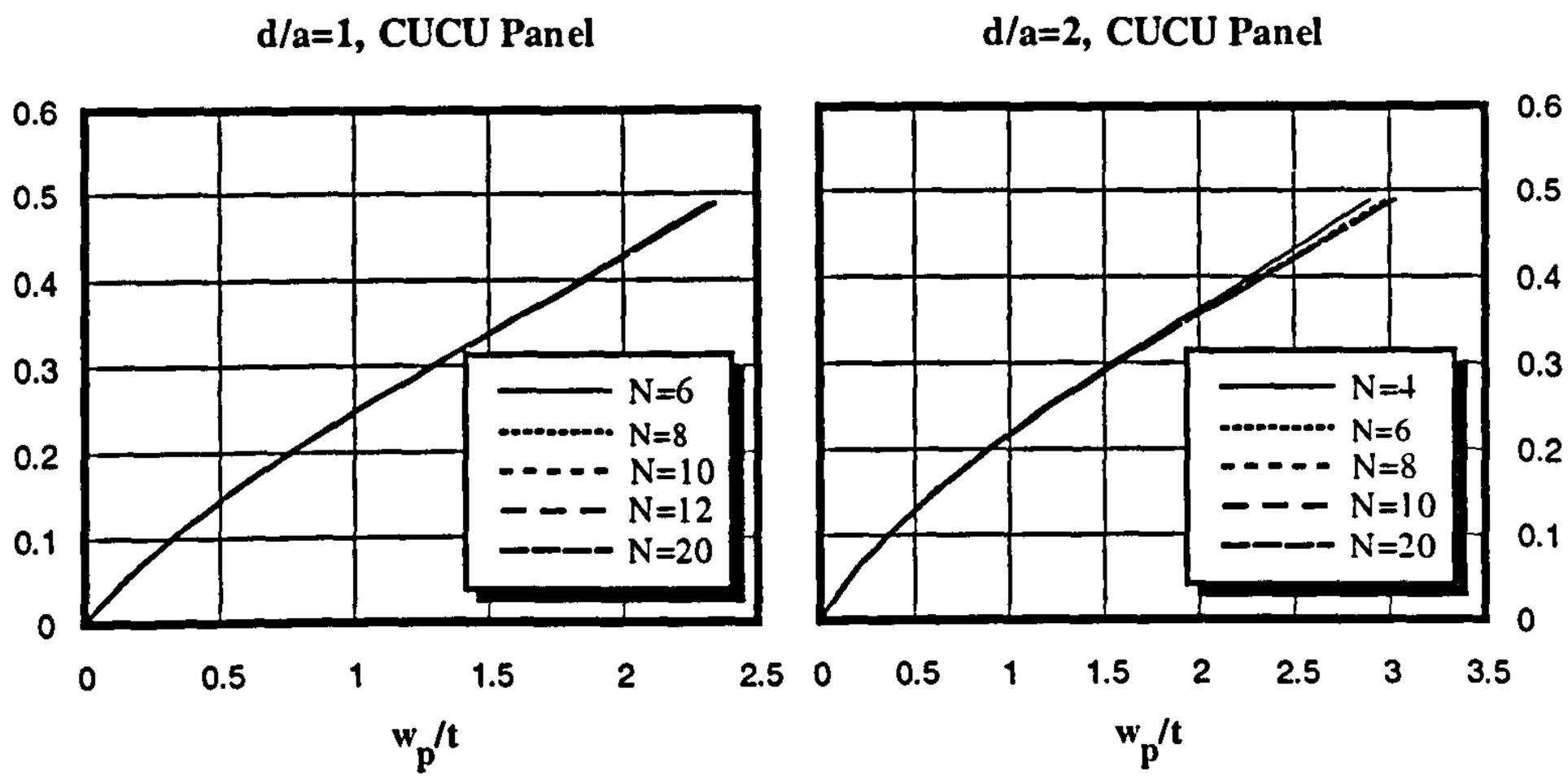


Figure 3.9 Shear stress versus maximum panel deflection for varying FE mesh sizes. Pure shear Non-linear elastic FE results. Point symmetric imperfection, $w_{0p}/t=1.091$. $a/t=180$, $t=3mm$

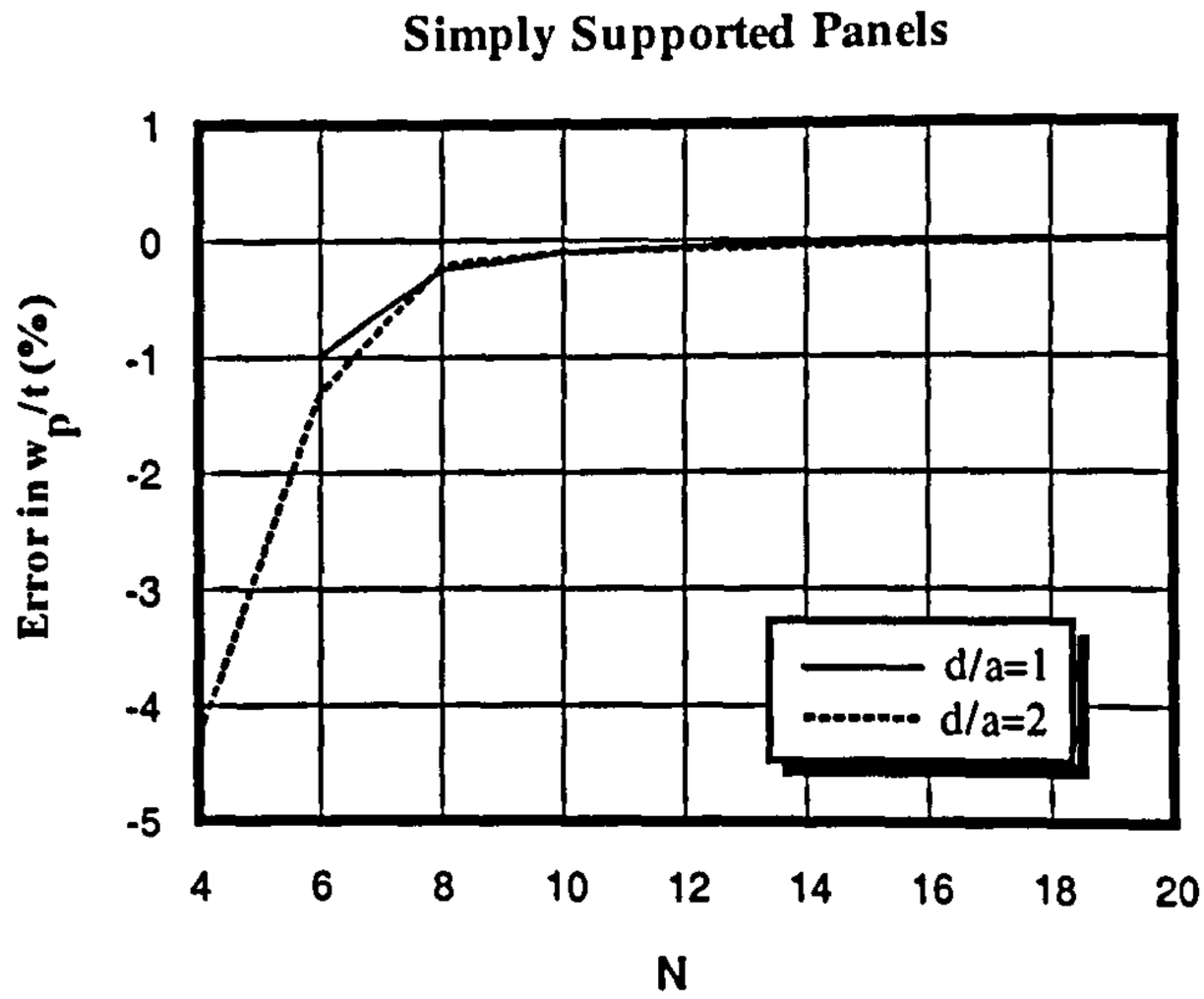


Figure 3.10 Convergence of the maximum panel deflection, w_p/t. Pure shear

3.8.5 Lateral Distributed Forces on the Supported Panel Edges, q_{pn}

The lateral distributed reactive forces acting on the left-hand supported edge of simply supported panels were calculated using the equivalent nodal force method presented in Section 4.4.1. The magnitude of the lateral force at the mid-length of the edge, denoted as q_{pn}, is plotted against the applied shear stress, τ' in Fig. 3.11. For τ'=0.489, the relative errors in $q_{pn}b^3/Dt$, with respect to the value for the finest mesh examined (N=20), for different mesh sizes are presented in Fig. 3.12. It can be seen in Fig. 3.12 that to allow a relative error less than 5%, a mesh of N≥6 is required for d/a=1, and N≥8 for d/a=2.

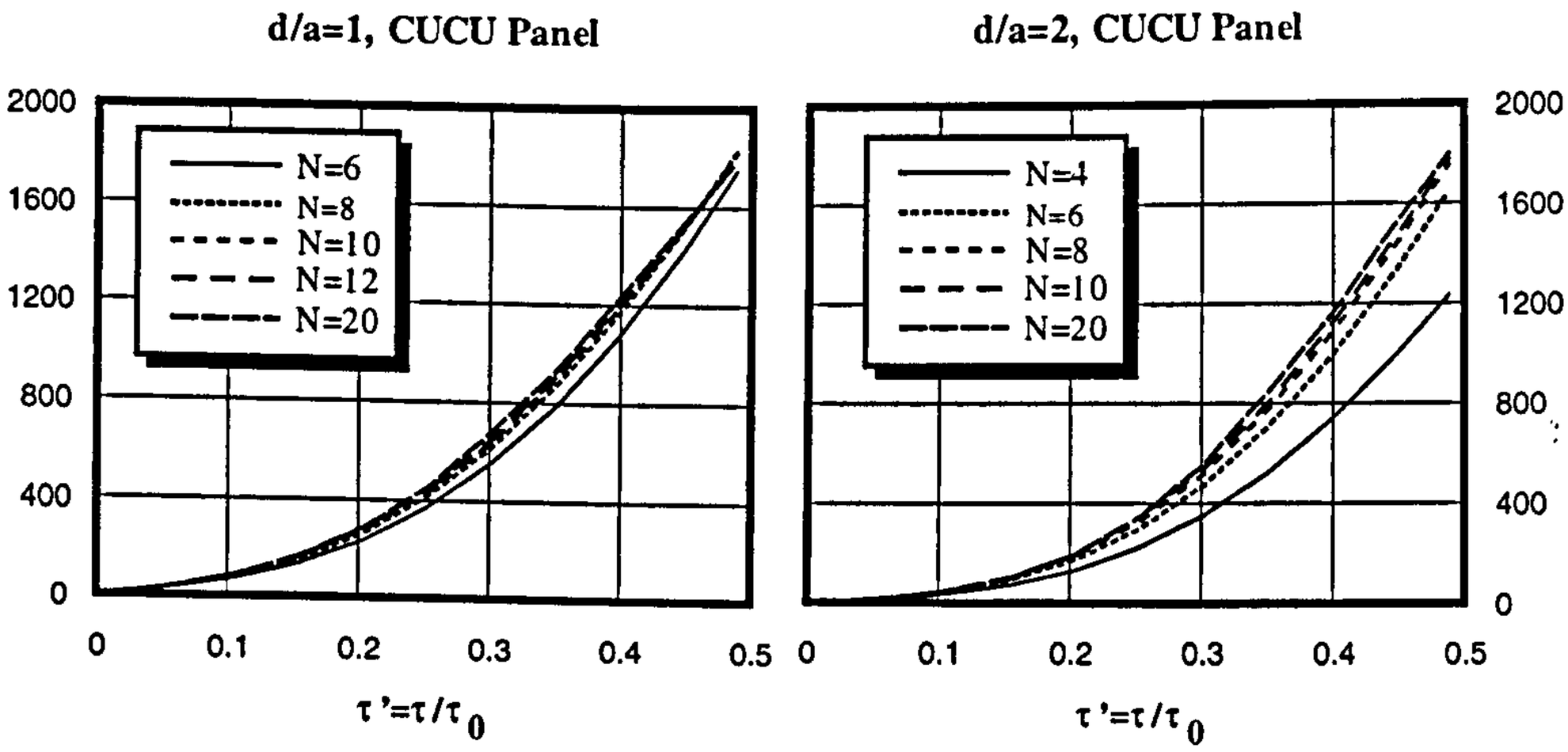


Figure 3.11 Shear stress versus lateral distributed edge force for varying FE mesh sizes. Non-linear elastic FE results. Point symmetric imperfection, w_{0p}/t=1.091. Pure shear

It is noted that the mesh size adopted by Stanway [1] is N=6 for d/a=1, and N=4 for d/a≥2. It is observed in Fig. 3.12 that for N=4, the relative error in $q_{pn}b^3/Dt$ for d/a=2 can be as high as 31%.

3.8.6 FE Meshes Adopted for the Parametric Study

The FE meshes to be used for the ensuing parametric study are chosen to ensure that the relative errors in k_{cr}, τ_u', w_p/t and $q_{pn}b^3/Dt$ are all less than 5%. On account of the above

discussion, it is noted that a mesh of N=8 can meet such a requirement. Therefore, for the ensuing parametric study, the number of shell elements across the small panel dimension is taken as N=8 for all panel aspect ratios. Square shell elements will be used for d/a≤5, while rectangular shell elements will be used for d/a>5 with the number of elements across the greater panel dimension being kept as 40, resulting in a side ratio of the shell elements equal to 1:2 for d/a=10. The mesh sizes for very tall plates are chosen on account of the computing time and the size of the disk space. The adopted mesh sizes are summarized in Table 3.1.

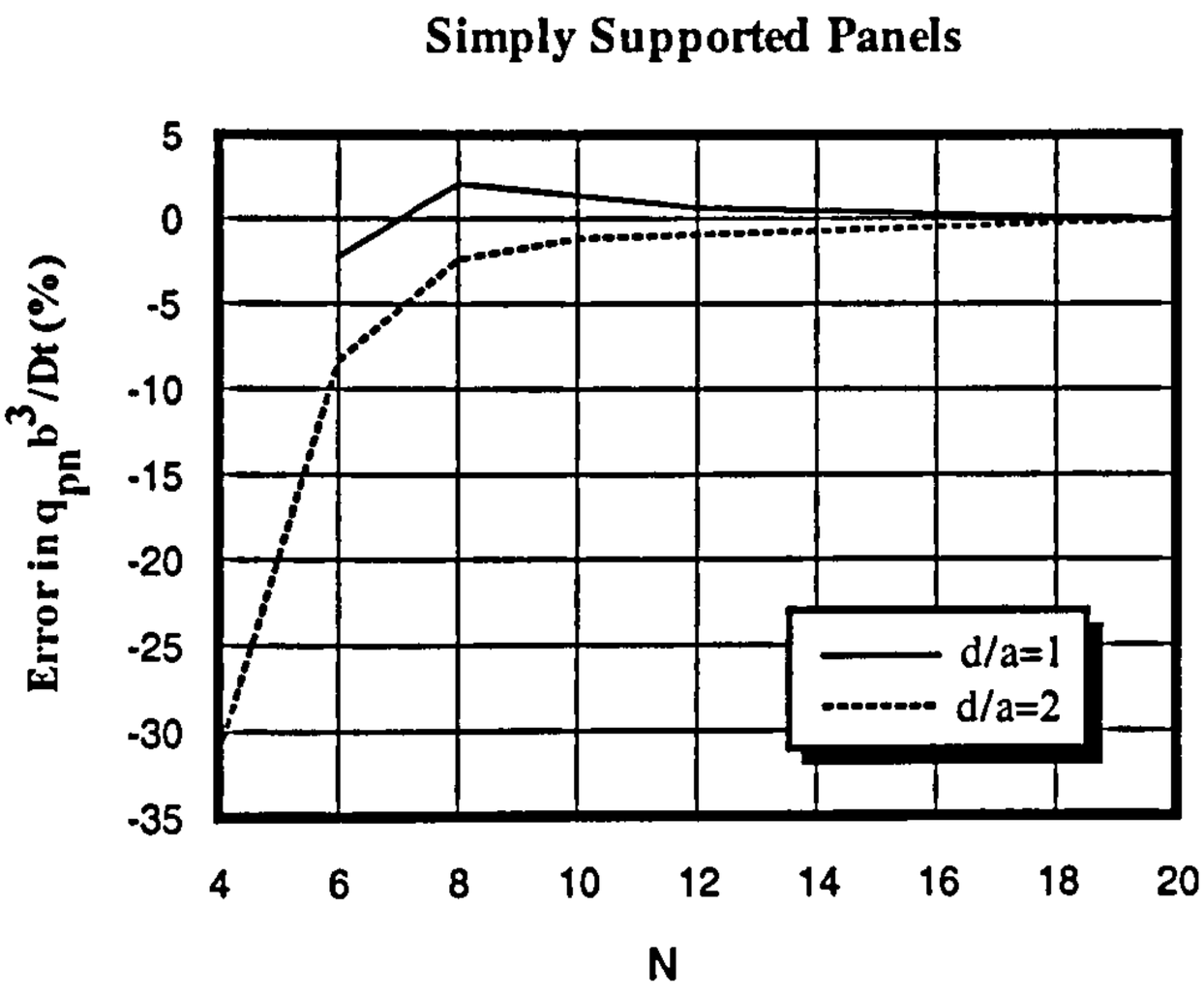


Figure 3.12 Convergence of the lateral distributed force on the supported edge. Pure shear. τ'=0.489

In the parametric study presented in this thesis, the small panel dimension *b* was taken to be 540mm. Panel aspect ratios d/a from 0.5 to 10, and panel slenderness ratios b/t from 80 to 300, were considered.

CHAPTER 4

PRELIMINARY STUDY ON LATERAL KNIFE EDGE FORCES

4.1 INTRODUCTION

It has been shown by Stanway [1] that the bending moment in the knife edge M_{pk}, due to the distributed knife edge reaction q_{pk}, can provide a reasonably accurate estimate of the attached stiffener moment due to the effect of local panel bending of stiffened plates. In his stiffener design model, the distribution of the lateral knife edge reaction q_{pk} was obtained from critical buckling analysis, while the magnitude of the lateral load q_{pk} was determined in terms of the non-linear elastic finite element results, with verification by elasto-plastic numerical analysis. The formulae for the calculation of M_{pk} were obtained from the curve-fitting of FE and series analyses results, and are not simple to use.

By carrying out numerical analyses on simply supported plates subjected to in-plane compression and lateral load respectively, it is verified that the reactions given by the FE program ABAQUS for critical buckling analysis are calculated using an equivalent lateral load approach. The equivalent lateral load is assumed to produce the same deflection as the critical buckling mode. As a result, the reactions are not in equilibrium with either themselves or the actual applied loads. Therefore, it is considered to be logical and necessary for the determination of the knife edge moment M_{pk} to be based directly on the results of non-linear elastic analyses.

In this chapter, a possible simplification to the method proposed by Stanway et al [9] is investigated. Starting from the non-linear elastic analytical solutions of a simply supported panel under compression, explicit equations are proposed to represent the

non-linear elastic buckling behaviour of plates, subjected to in-plane shearing forces. The non-linear elastic finite element results are used to determine the coefficients in the explicit equations. In this way, the simplicity and generality of the approximate analytical equations is combined with the wide availability and accuracy of numerical results to provide design formulae. Several possible approaches to represent the knife edge forces are examined. Eventually, a simple formula is recommended for the calculation of the knife edge moment M_{pk}, which will be used in the next chapter to establish the design formulae for predicting the knife edge moment for plates subjected to pure shear, combination of shear, compression and bending.

4.2 STRUCTURE MODELLING (DEFINITION OF KNIFE EDGE)

The two-panel plates subjected to uniform in-plane shear forces, shown in Fig. 4.1, are considered in this chapter. The plate is equally divided by a straight knife edge. The knife edge is unattached to the plate, and is defined by the constraint:

$$w\big|_{x=a} = 0 \tag{4.1}$$

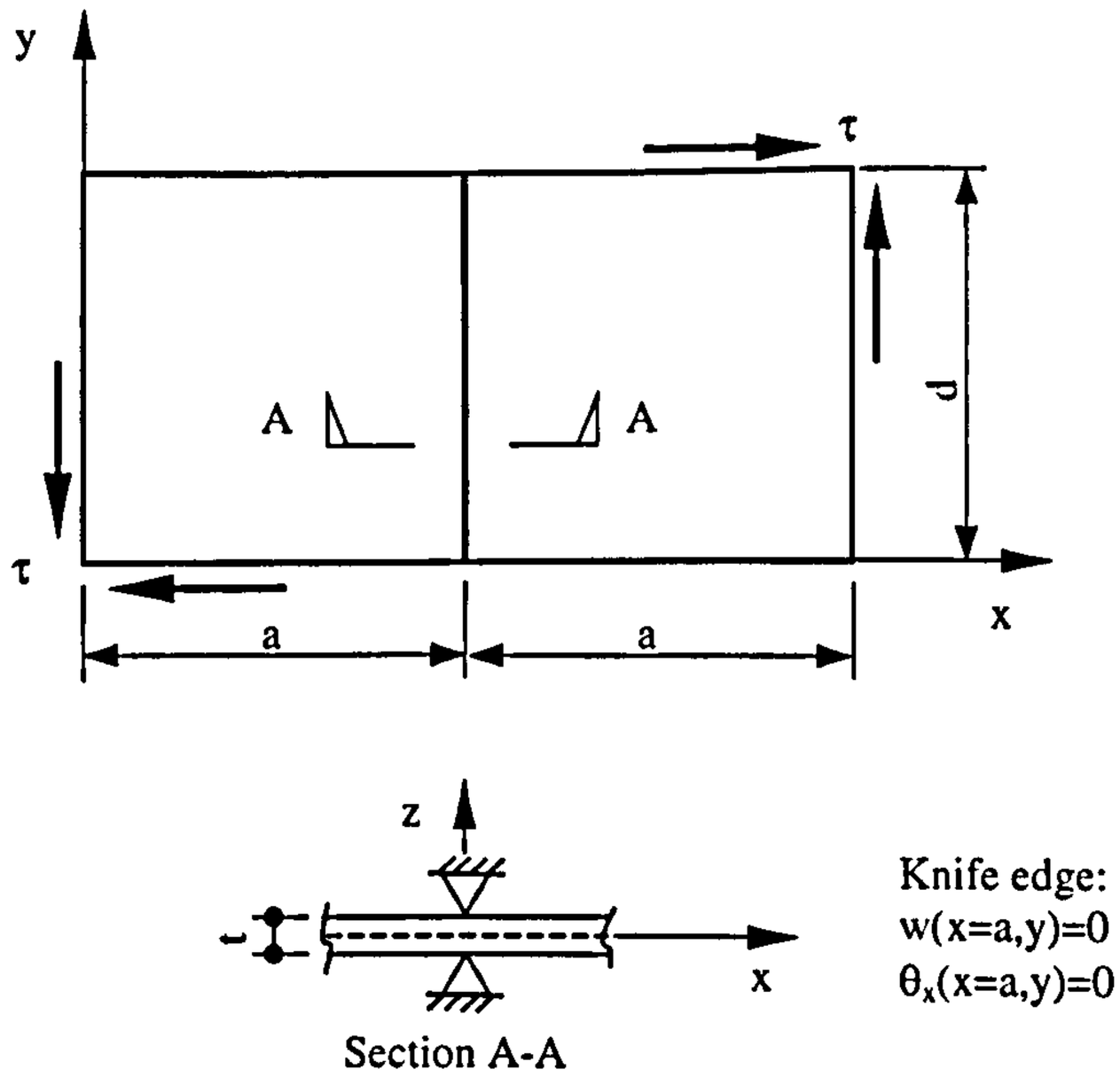


Figure 4.1 Two-panel plate with an intermediate knife edge

Implied in Eqn. 4.1 is the constraint:

$$\theta_x\big|_{x=a} = 0 \tag{4.2}$$

The remaining panel degrees of freedom, u, v, θ_y and θ_z, along the knife edge (x=a), are unrestrained by the knife edge.

All the boundaries of the plate are simply supported. The in-plane boundary conditions are assumed to be CUCU, as defined in Chapter 2, and the tangential in-plane boundary conditions are taken as being unrestrained.

The panel imperfections are fully affine to the first point-symmetric critical buckling modes of the plate, which are presented in Fig. 4.2. The reason for this is that the point-symmetric mode gives the greater value of the knife edge force for a given applied shear stress. A more detailed discussion is given in Chapter 3.

4.3 FORCES ACTING ON THE KNIFE EDGE

4.3.1 Distributed Reactive Force on the Knife Edge, q_{pk}

In general, the total reaction V_x on a simply supported edge, e.g. x=constant, includes the shearing force Q_x and the contribution of the twisting moment M_{xy}, and can be expressed as:

$$V_x = Q_x - \partial M_{xy}/\partial y \tag{4.3}$$

The finite element program ABAQUS can provide directly the total reactive force V_x if the simply supported condition is represented as w=0 only. If both w=0 and θ_x=0 are specified for a simply supported edge, the shearing force Q_x and the twisting moment M_{xy} acting along the edge can be obtained separately from ABAQUS. This is illustrated in Fig. 4.6.

The knife edge is subjected to the distributed reactive force q_{pk}, which results only from the difference in the panel transverse shear forces Q_x across the knife edge. The contribution of the panel twisting moment M_{xy} to the lateral force q_{pk} is zero, because

the continuity of the panel slope $\partial w/\partial x$ across the knife edge ensures that the twisting moments M_{xy} in the left and right hand panels, immediately adjacent to the knife edge are equal in magnitude. A detailed discussion can be found in Section 3.6.3 (P.428) of Stanway's thesis [1].

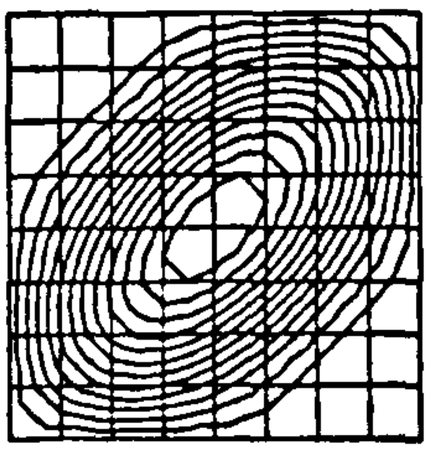
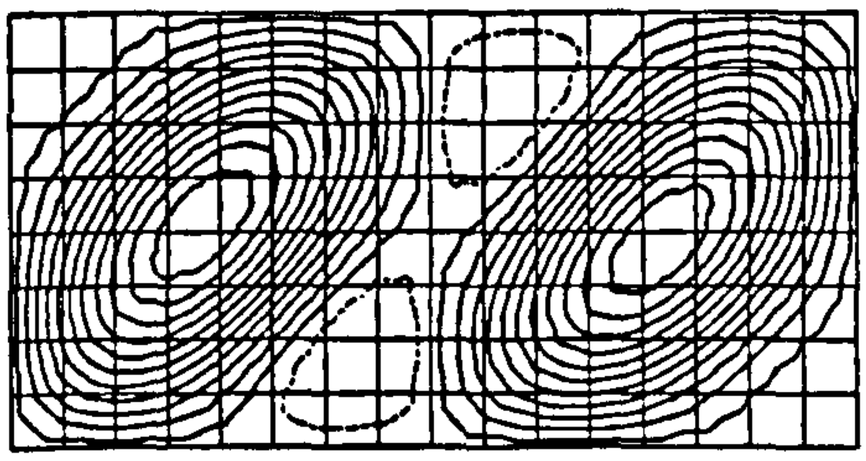
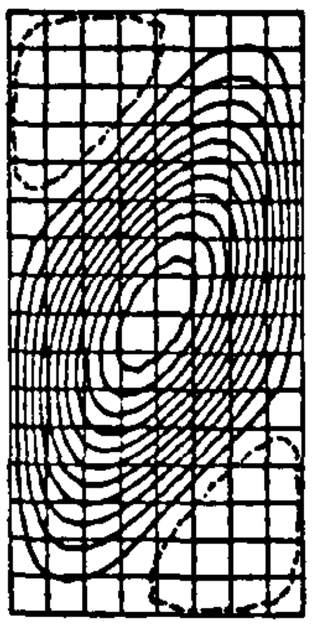
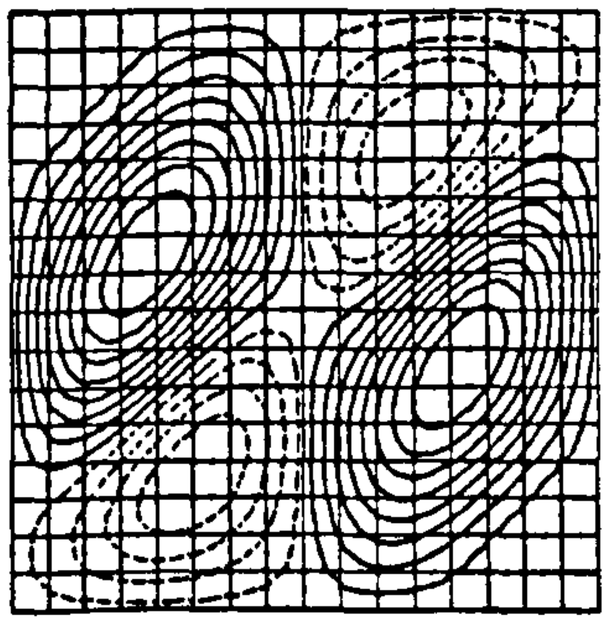
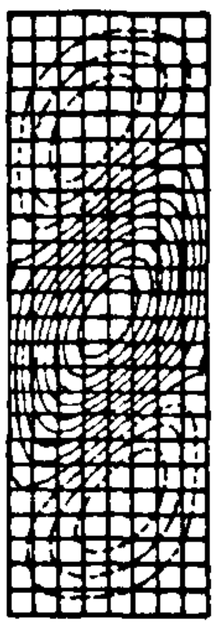
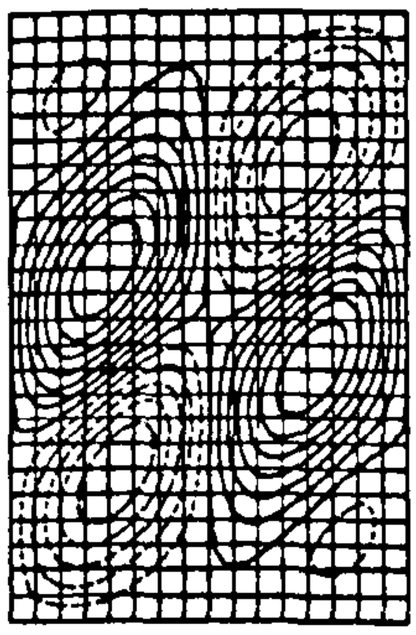
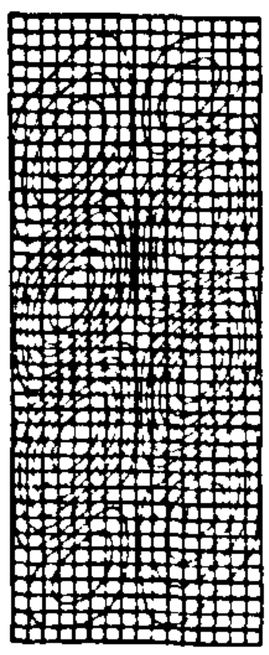
d/a	Panels	Plates with a straight knife edge
1	 kcr=9.3335	 kcr=9.9013
2	 kcr=6.5517	 kcr=6.7529
3, 5	d/a=3  kcr=5.8448 d/a=5  kcr=5.5612	d/a=3  kcr=5.9087 d/a=5  kcr=5.5598

Figure 4.2 First point-symmetric buckling modes, used as initial panel imperfection modes. Pure shear

To support the above conclusion, non-linear elastic FE analyses were carried out for a knife-edge stiffened plate with d/a=1 and a/t=180, subjected to in-plane shearing forces. The condition at the knife edge was modelled numerically as (1) w=0 only and (2) w=0 and θ_x=0, respectively. The magnitude of distributed lateral force, q_{pk}, was calculated from the nodal reactive forces given by ABAQUS, using the method given in the next section, and the results are shown in Fig. 4.3. It is apparent that the lateral force including the effect of M_{xy} is almost equal to that considering the shearing force Q_x only, that is:

$$q_{pk} = q_{Qx} = q_{Vx}, \quad and \; q_{Mxy} = 0 \tag{4.4}$$

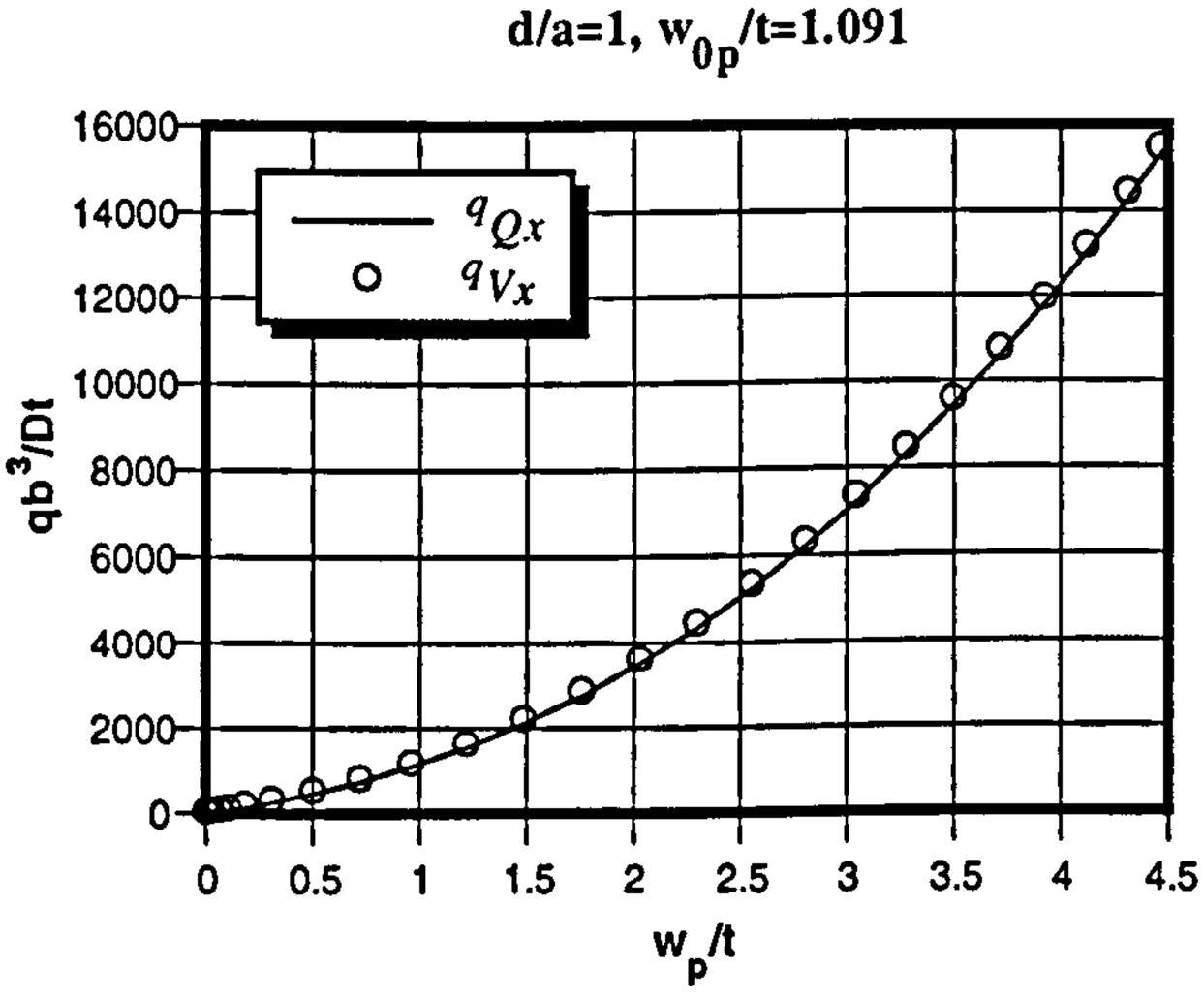


Figure 4.3 Magnitudes of the distributed lateral forces acting on the knife edge. FE results

4.3.2 Relationship Between q_{pk} and q_{pn}, the Panel Edge Reaction

The structure in Fig. 4.1 may be considered as two separate simply supported panels, as illustrated in Fig. 4.4, with continuity being enforced between the two panels at the adjacent edges, x_1=a and x_2=0. The continuity constraints between the two panels for the slope $\partial w/\partial x$ and the bending moment M_x are:

$$\left.\frac{\partial w_1}{\partial x_1}\right|_{x_1=a} = \left.\frac{\partial w_2}{\partial x_2}\right|_{x_2=0} \tag{4.5}$$

$$\left.\frac{\partial^2 w_1}{\partial x_1^{\,2}}\right|_{x_1=a} = \left.\frac{\partial^2 w_2}{\partial x_2^{\,2}}\right|_{x_2=0} \tag{4.6}$$

where w_1 and w_2 represent the out-of-plane deflections in the left and right hand panels, respectively.

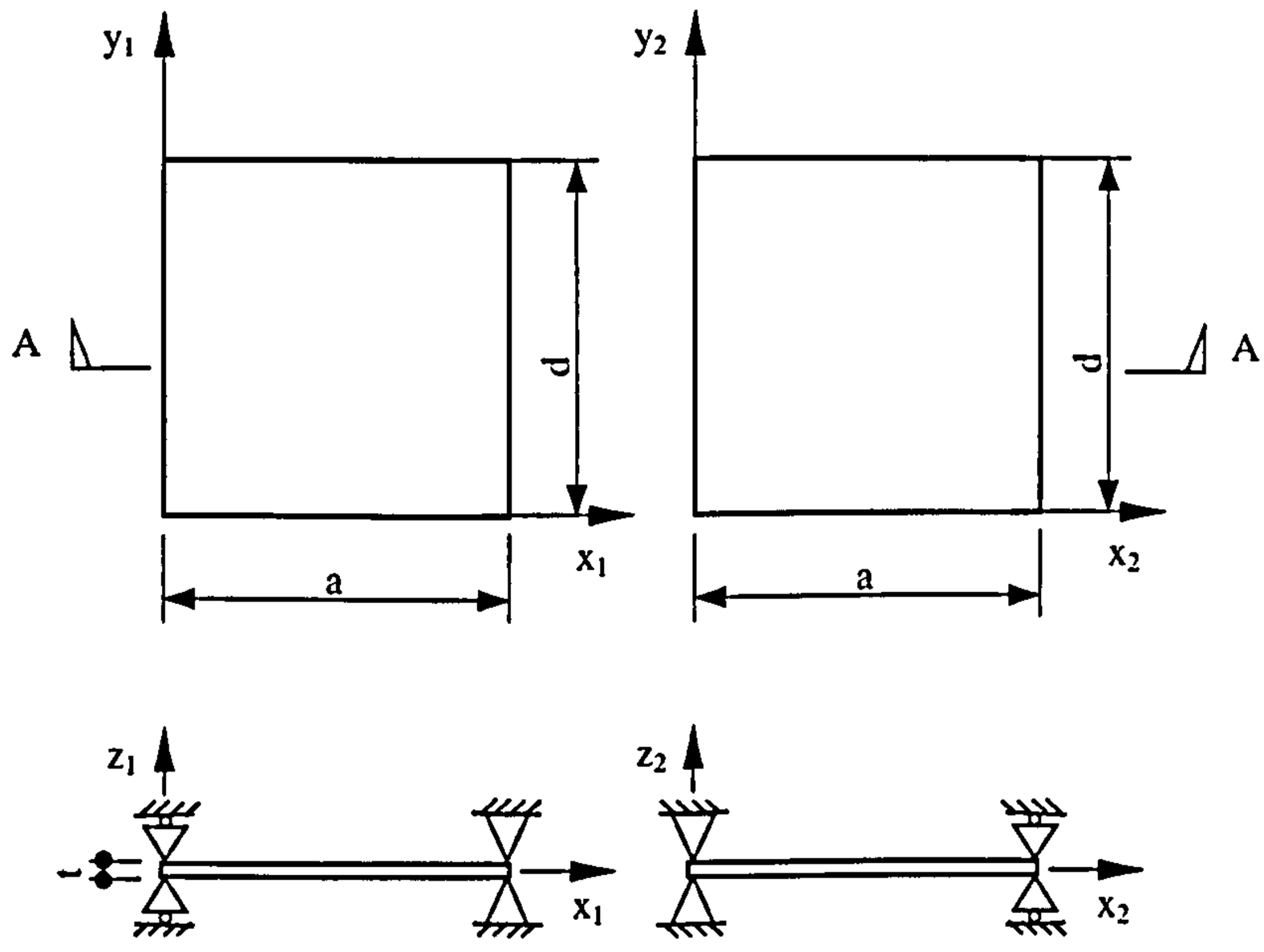


Figure 4.4 Two separate simply supported panels, as a representation of the continuous plate in Fig. 4.1 Continuity constraints given by Eqns. 4.5 and 4.6. (from ref. [1])

In terms of the model shown in Fig. 4.4, the knife edge reaction q_{pk} can be obtained by adding the reactions acting on the adjacent edges, x_1=a and x_2=0. However, it is quite difficult to determine the reactions on the edges of each panel when the continuity constraints (Eqns. 4.5 and 4.6) are enforced. By neglecting the plate continuity across the knife edge, the model shown in Fig. 4.4 becomes two isolated simply supported

panels, where $q_{Mxy} \neq 0$. Furthermore, provided that the deflection in the isolated panels is the same as that in the continuous plate panels, the knife edge reaction q_{pk} could be taken as the sum of the reactive forces q_{Qx} on the left and right edges of an isolated panel, that is:

$$q_{pk} = q_{Qx}\Big|_{left} + q_{Qx}\Big|_{right} \tag{4.7}$$

Since the deflection mode of interest is point-symmetric, the lateral reactive forces on the two opposite edges are anti-symmetric to each other, as shown in Fig. 4.11. Therefore, the magnitude of q_{pk} at the mid-length of the knife edge may be expressed as:

$$q_{pk} = 2q_{pn} \tag{4.8}$$

where q_{pn} denotes the magnitude of the reaction q_{Qx} at the mid length of the left-hand edge of an isolated simply supported panel.

On account of the influence of the panel continuity across the knife edge, it is proposed that the lateral force at the middle of the knife edge, q_{pk} be represented as:

$$q_{pk} = C \cdot q_{pn} \tag{4.9}$$

where C is a coefficient which may varies with the panel aspect ratio d/a. The coefficient C may be obtained by the curve-fitting of FE results.

The reason for the analysis presented in this section is that by establishing a relationship between the knife edge reaction and the panel edge reaction, the magnitude of the knife edge reaction, q_{pk} could be obtained from the analysis of an isolated simply supported panel. It was initially expected that approximate non-linear elastic theoretical solutions could be obtained for an isolated panel, which would be much simpler to analyse than a plate with a knife edge.

The bending moment due to the knife edge reaction, denoted as M_{pk}, can be easily calculated when the magnitude and distribution of the distributed knife edge reaction are known.

4.4 DETERMINATION OF q_{pk} AND M_{pk} IN FINITE ELEMENT ANALYSES

4.4.1 Reaction at the Supported Edge, q_{Qx}

The finite element program ABAQUS outputs equivalent nodal reactive forces Q_x associated with the constraint w=0 along the supported edge (eg. x=constant). The nodal forces given by ABAQUS are oscillatory point forces and must be converted to a smoothly distributed force to obtain q_{Qx}.

In 1984, Jirousek and Bouberguig [53] presented a simple formula for an estimate of reactions from computed equivalent nodal forces at the plate boundary, and this method is adopted in the present study for calculating q_{Qx} at the supported edge of a simply supported panel and q_{pk} at the knife edge. Stanway [1] also employed this method in his investigation. The method is presented below.

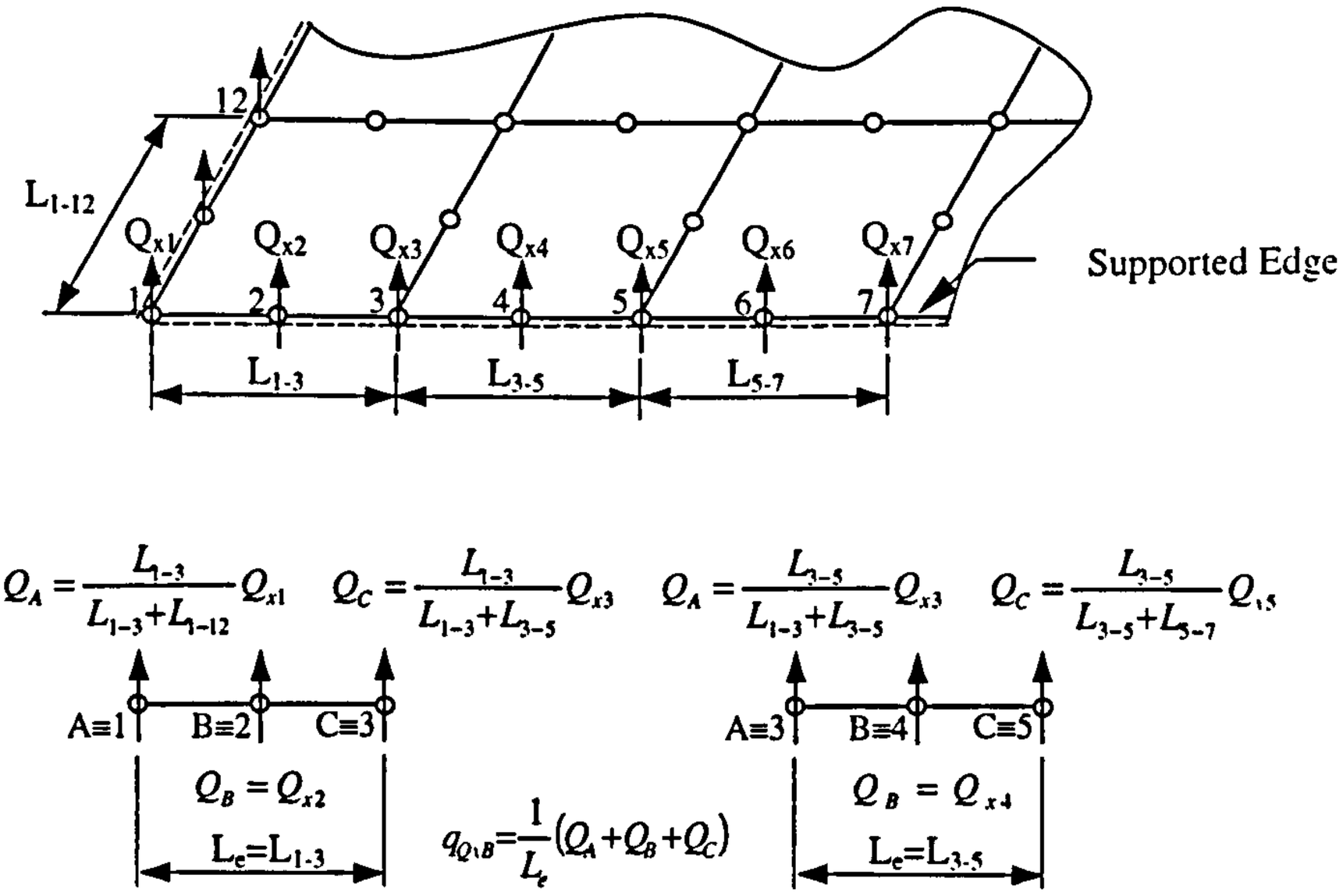


Figure 4.5 Evaluation of reactions at supported edges from equivalent nodal forces (from ref. [53])

As shown in Fig. 4.5, the computed equivalent nodal force at node i is denoted as Q_{xi} (i=1,2,3,...). To evaluate the reaction intensities q_{QxB} at the mid node B of each element

side situated at the supported edge, the equivalent nodal force at nodes shared by two adjacent element sides, such as at node 3, should be divided into two parts:

$$Q_{x3} = (Q_C)_{1-3} + (Q_A)_{3-5}$$

belonging to the end points C and A of the two adjacent sides. The evaluation of such nodal forces Q_A, Q_B and Q_C allotted to each particular element edge is illustrated in Fig. 4.5. The intensity of the distributed reactions at the mid node is then calculated as

$$q_{QxB} = (Q_A + Q_B + Q_C)/L_e \tag{4.10}$$

where L_e is the length of the element side along the supported edge.

Estimates of q_{Qx} at the nodes shared by adjacent element edges may be obtained, for a regular mesh with a constant L_e, by the cubic interpolation of the known intensities at mid nodes:

$$q_{Qxi} = \frac{1}{16}\left[-(q_{QxB})_{i-3} + 9(q_{QxB})_{i-1} + 9(q_{QxB})_{i+1} - (q_{QxB})_{i+3}\right] \tag{4.11}$$

To assess the accuracy of this method, a simply supported square plate, subjected to a uniform lateral pressure q, was analysed using ABAQUS. Values of q_{Qx}, calculated using the equivalent nodal forces and Eqns. 4.10 and 4.11, are compared in Fig. 4.6 with the theoretical distributions (see p.120 of reference [52]). It can be observed that the equivalent nodal force method is very accurate.

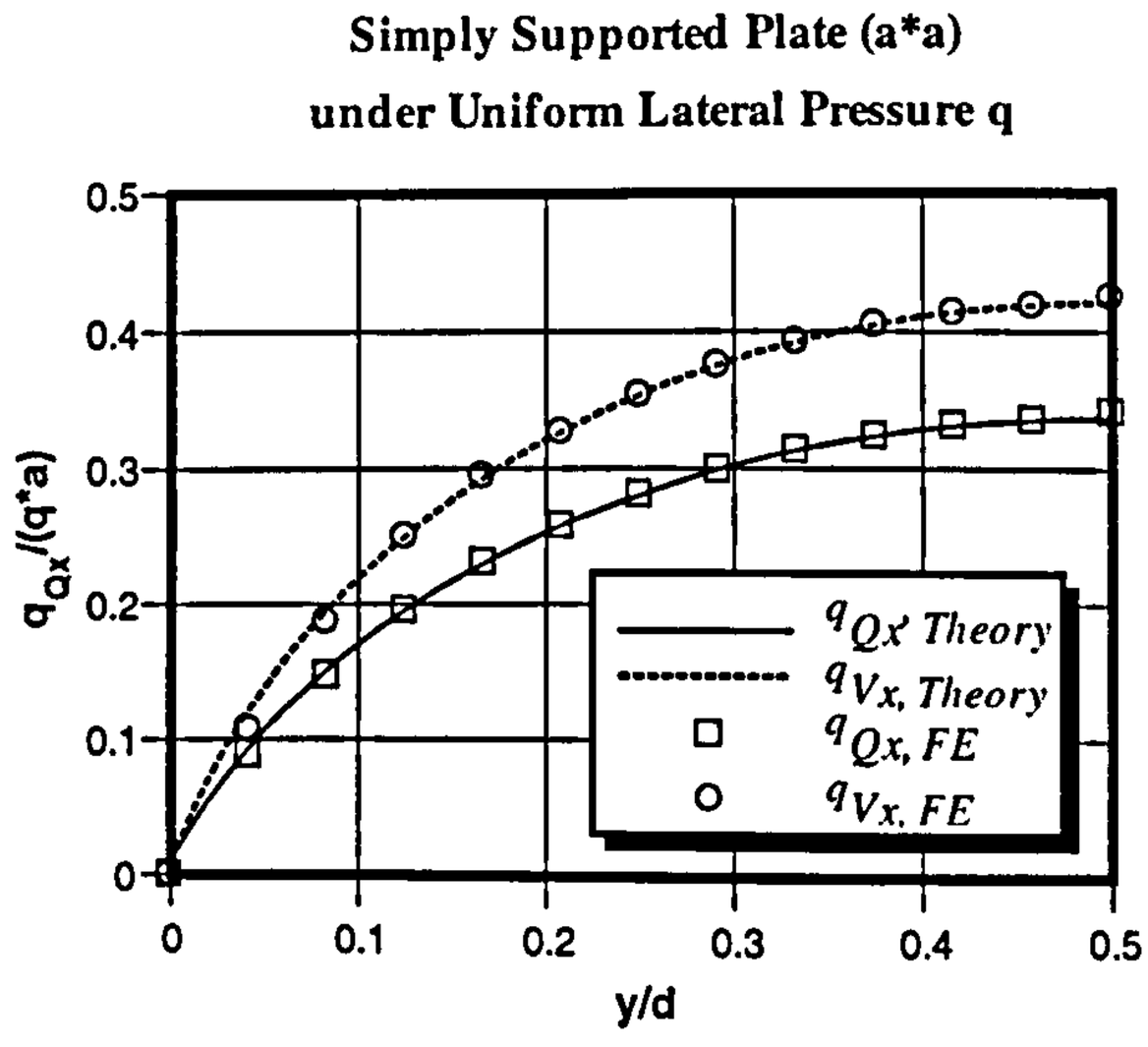


Figure 4.6 Distributions of reactions along simply supported edge x=0 or x=a. 6X6 mesh in FE

Shown in Fig. 4.6, values of q_{Vx} were obtained from the output reactive forces when the simply supported edges were represented as w=0 only. Alternatively, when both w=0 and θ_x=0 were specified for the supported edges, values of q_{Qx} were obtained.

4.4.2 Bending Moment due to the Distributed Reaction

With respect to design of the stiffener, the major axis bending moment M_s is one of the important internal stiffener forces. Bending moment, M, resulting from the distributed edge reaction, q, may be calculated using the simple beam model presented in Fig. 4.7.

Figure 4.7 Beam model for the calculation of bending moment acting on the supported edges

Referring to Fig. 4.7, the supported edge is represented as a simply supported beam subjected to a distributed lateral load. The magnitude of the lateral load at each node is taken as the reaction intensity, obtained using the equivalent nodal force method presented in Section 4.4.1. A linear interpolation of the lateral load is assumed between two adjacent nodes. By means of this simple model, the bending moment acting along the supported edges can be determined by the following recurrent equations:

$$M_{i+1} = M_i + Q_i \cdot \Delta L - \left(\frac{1}{3}q_i + \frac{1}{6}q_{i+1}\right) \cdot (\Delta L)^2 \quad , \quad i = 1, 2, 3, \cdots, n \tag{4.12}$$

where M_1=0, and

$$Q_1 = \int_0^L q(y_1)\,dy_1 - \frac{1}{L}\int_0^L y_1 q(y_1)\,dy_1 \tag{4.13}$$

$$Q_{i+1} = Q_i - \frac{1}{2}(q_i + q_{i+1}) \cdot \Delta L \tag{4.14}$$

4.5 EXPLICIT EQUATIONS FOR THE NON-LINEAR ELASTIC BUCKLING BEHAVIOUR OF PLATES

4.5.1 Analytical Solutions of Uniaxially Compressed Rectangular Plates

To find out the distributed reaction and resulting bending moment at the supported panel edge, the non-linear elastic buckling behaviour of simply supported rectangular plates was analysed using the energy method and the Galerkin method, respectively. The theoretical analyses were carried out for two reasons. Firstly, it was thought that a theoretical analysis might be more efficient in enabling a wider range of cases to be covered, on account of the fact that the finite element method is mainly for detailed appraisal rather than design. Secondly, analytical solutions may offer the distinct advantages of simplicity and flexibility of presentation, and therefore can form the basis for closed-form equations which could be used to predict the knife edge moment M_{pk} for the design model.

Since pure shear is the basic loading condition considered in the present study, a rectangular plate under shear was initially investigated using several different approaches, such as the energy method and the Galerkin method. However, no closed-form solutions could be obtained. For this reason, theoretical analysis on plates under shear was not pursued further. Instead, an approximate solution for uniaxially compressed constrained (CCCC) plates was derived using the von Kármán equations and Galerkin's method. It was expected that the approximate theoretical solutions for

this simple case may be extended to develop explicit equations, which may be fitted to finite element results, for predicting the knife edge forces caused by shear.

Appendix B presents a relatively simple solution of the non-linear differential equations of the elastic problem of a rectangular simply supported constrained plate subjected to uniaxial compression. In deriving the analytical solution, it is assumed that both the initial imperfection, w_{0p}, and the additional deflection due to the applied load, w_p, take the form of a single half sine-wave in both the longitudinal and transverse directions.

To determine the panel deflection magnitude, w_p, Eqn. B.23 can be re-ordered as follows:

$$\left[\left(\frac{w_p + w_{0p}}{t}\right)^2 - \left(\frac{w_{0p}}{t}\right)^2\right] = C \cdot \left[\frac{\sigma_c}{\sigma_{c,cr}} - \frac{w_p}{w_p + w_{0p}}\right] \tag{4.15}$$

where:

$$C = \frac{\left(\alpha + \alpha^{-1}\right)^2}{\frac{3}{4}\left(1 - \nu^2\right)\left(\alpha^2 + \alpha^{-2}\right)} \tag{4.16}$$

and α denotes the aspect ratio d/a. $\sigma_{c,cr}$ is the critical compressive stress of the panel.

By replacing y=d/2 into Eqn. B.26, the magnitude of the distributed reactive force at the mid length of the supported edge, q_{pn}, may be expressed as:

$$\frac{q_{pn} b^3}{Dt} = \pi^3 \left(1 + \alpha^{-2}\right) \cdot \frac{w_p}{t} \tag{4.17}$$

4.5.2 Proposed Equations

The approximate solution given in Eqns. 4.15 and 4.17 was obtained by assuming that both the initial imperfection and the additional deflection under load can be represented by a single sinusoidal function. It is known from the finite element analysis that the deflected profile of the plate is not an exact sinusoidal surface and in addition, the deflection mode changes with the magnitude of the applied load, due to the effect of the

in-plane forces. Further, it is recalled that Eqns. 4.15 and 4.17 were derived for the simple case of uniaxially compressed constrained plates.

To be used for more general cases, such as plates under pure shear, Eqns. 4.15 and 4.17 are formulated to include higher order terms. The proposed explicit equations for panel deflection, w_p, and lateral distributed force at the mid-length of the supported edge, q_{pn}, are summarised below.

4.5.2.1 Maximum Panel Deflection w_p

The maximum panel deflection w_p, additional to the imperfection w_{0p}, can be represented as:

$$\eta^{\frac{1}{2}} = C_1\xi + C_2\xi^2 + C_3\xi^3 \tag{4.18}$$

where:

$$\eta = \left(\frac{w_p + w_{0p}}{t}\right)^2 - \left(\frac{w_{0p}}{t}\right)^2 \tag{4.19}$$

$$\xi = \left(\frac{\tau}{\tau_{cr}} - \frac{w_p}{w_p + w_{0p}}\right)^{\frac{1}{2}} \tag{4.20}$$

and C_1, C_2 and C_3 are coefficients which will be determined by the curve fitting of FE results. τ_{cr} is the critical shear stress of the isolated panel. By comparison with the analytical equations obtained in Section 4.5.1, these coefficients are expected to vary with the panel aspect ratio d/a only.

It was noted that an equation, which takes the same form of Eqn. 4.18 but C_2=0, was presented by Williams and Walker [54] in 1977 to describe the lateral deflection of square plates subjected to compression, shear, and combined compression and shear. In their work, the coefficients C_1 and C_3 were determined by means of the finite difference analysis results.

4.5.2.2 Lateral Distributed Force q_{pn}

The magnitude of the lateral distributed reactive force at the mid length of the supported edge is expressed as:

$$\frac{q_{pn}b^3}{Dt} = C_1\frac{w_p}{t} + C_2\eta + C_3\kappa \tag{4.21}$$

where q_{pn} is the force per unit length, η and κ are defined as follows:

$$\eta = \left(\frac{w_p + w_{0p}}{t}\right)^2 - \left(\frac{w_{0p}}{t}\right)^2 \tag{4.22}$$

$$\kappa = \left(\frac{w_p + w_{0p}}{t}\right)^3 - \left(\frac{w_{0p}}{t}\right)^3 \tag{4.23}$$

and C_1, C_2 and C_3 are coefficients which will be determined by the curve fitting of FE results. By comparison with the analytical solution Eqn. 4.17, the coefficients in Eqn. 4.21 are expected to vary with the panel aspect ratio d/a only.

Eqn. 4.21 may also be used for representing the lateral distributed force q_{pk}, acting at the mid length of the knife edge for plates with an intermediate knife edge.

4.6 NON-LINEAR ELASTIC FE ANALYSES

4.6.1 CUCU Panels

4.6.1.1 Panel Deflection w_p/t

Non-linear elastic parametric studies were carried out for CUCU panels of d/a=1 and 2, with an initial imperfection in the form of the first point-symmetric buckling mode, subjected to pure shear. In terms of the numerical results obtained, the coefficients C_1, C_2 and C_3 in Eqn. 4.18 were calculated by the least squares method, and their values are listed in Table 4.1.

Table 4.1 Coefficients for panel deflections, Eqn. 4.18

d/a	C_1	C_2	C_3
1.0	1.680	1.713	-0.482
2.0	0.606	2.389	-0.543

The deflection curves shown in Fig. 4.8 cover a range of τ/τ_{cr}=1~4. This region is adopted on account of the possible values of τ_u/τ_{cr} for simply supported panels (see Table 4.2), and will also be used for relevant figures in the latter part of this thesis.

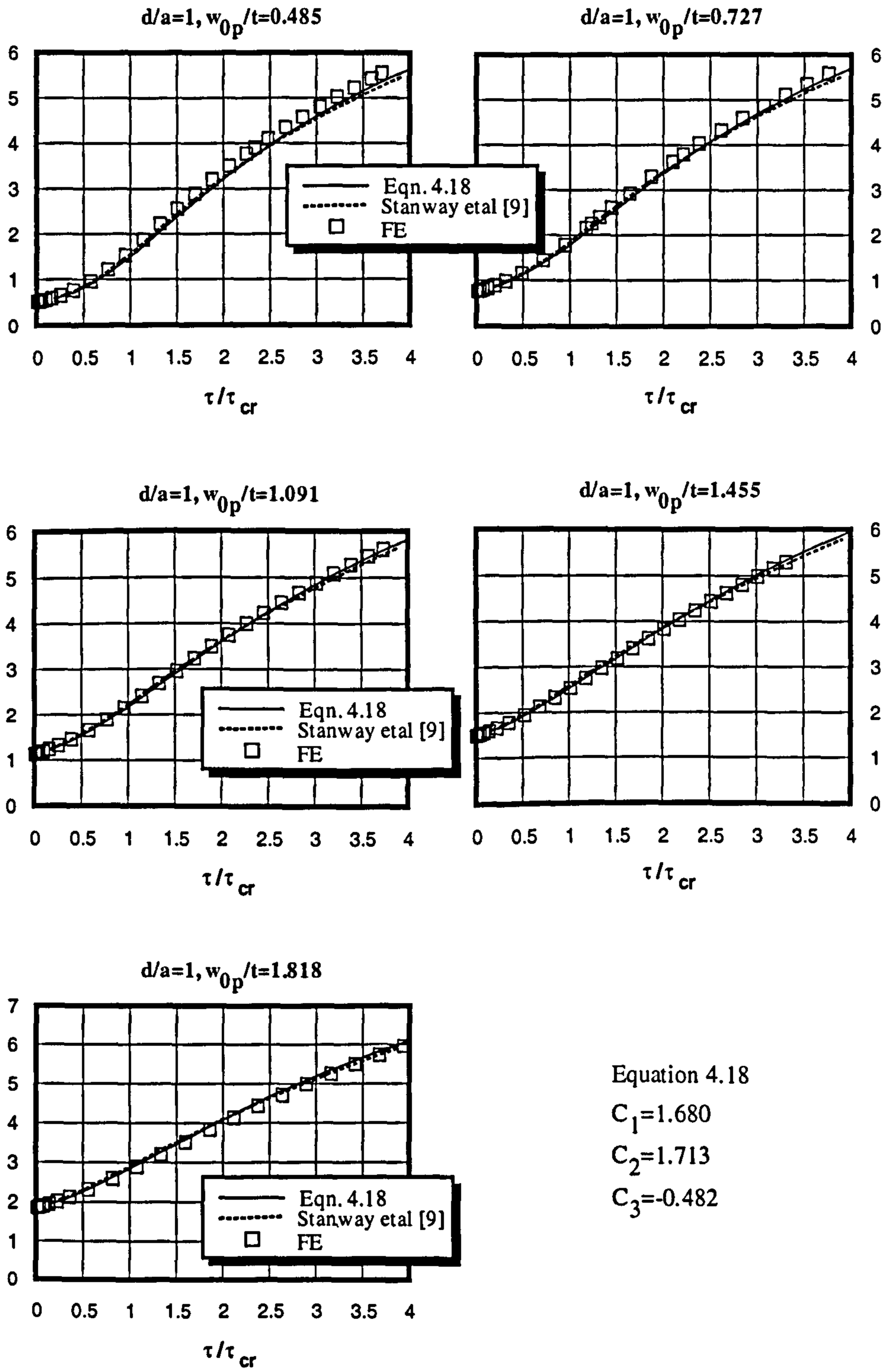
Table 4.2 Ratio of ultimate shear stress to critical shear stress, τ_u/τ_{cr}*

d/a	b/t=80	b/t=180	b/t=300
1	0.688	1.915	3.379
2	0.888	2.296	3.986

* σ_{0p}=355N/mm^2, τ_u from Davidson's model [40]

In Fig. 4.8, the panel deflections estimated by Eqn. 4.18 are compared with the finite element results, and a good agreement between them is observed. The panel deflection calculated from the equation proposed by Stanway et al [9] are also shown in Fig. 4.8. The deflection modes are illustrated in Fig. 4.13, where a comparison to the deflection modes of knife-edge plates is made.

The deflection modes for d/a=3 and 5 are also included in Fig. 4.13. It is noted that for tall panels (d/a≥3), the main difference in the panel deflection modes is the number of half waves accommodated along the depth of panel. The maximum panel deflections in tall panels are presented in Fig. 4.9, in comparison with the results for d/a=1 and 2. It is observed that the maximum panel deflection lies between the curves for d/a=2 and 7. By determining the coefficients in Eqn. 4.18 for each aspect ratio d/a, Eqn. 4.18 is adequate for representing the non-linear elastic values of the maximum panel deflection. As a rough estimate, the magnitudes of deflection for simply supported panels can be calculated using the deflection curve for d/a=1, or by linear interpolation between the values for d/a=2 and very tall panel. For more accurate estimation of panel deflection, Eqn. 4.18 should be established for each aspect ratio.



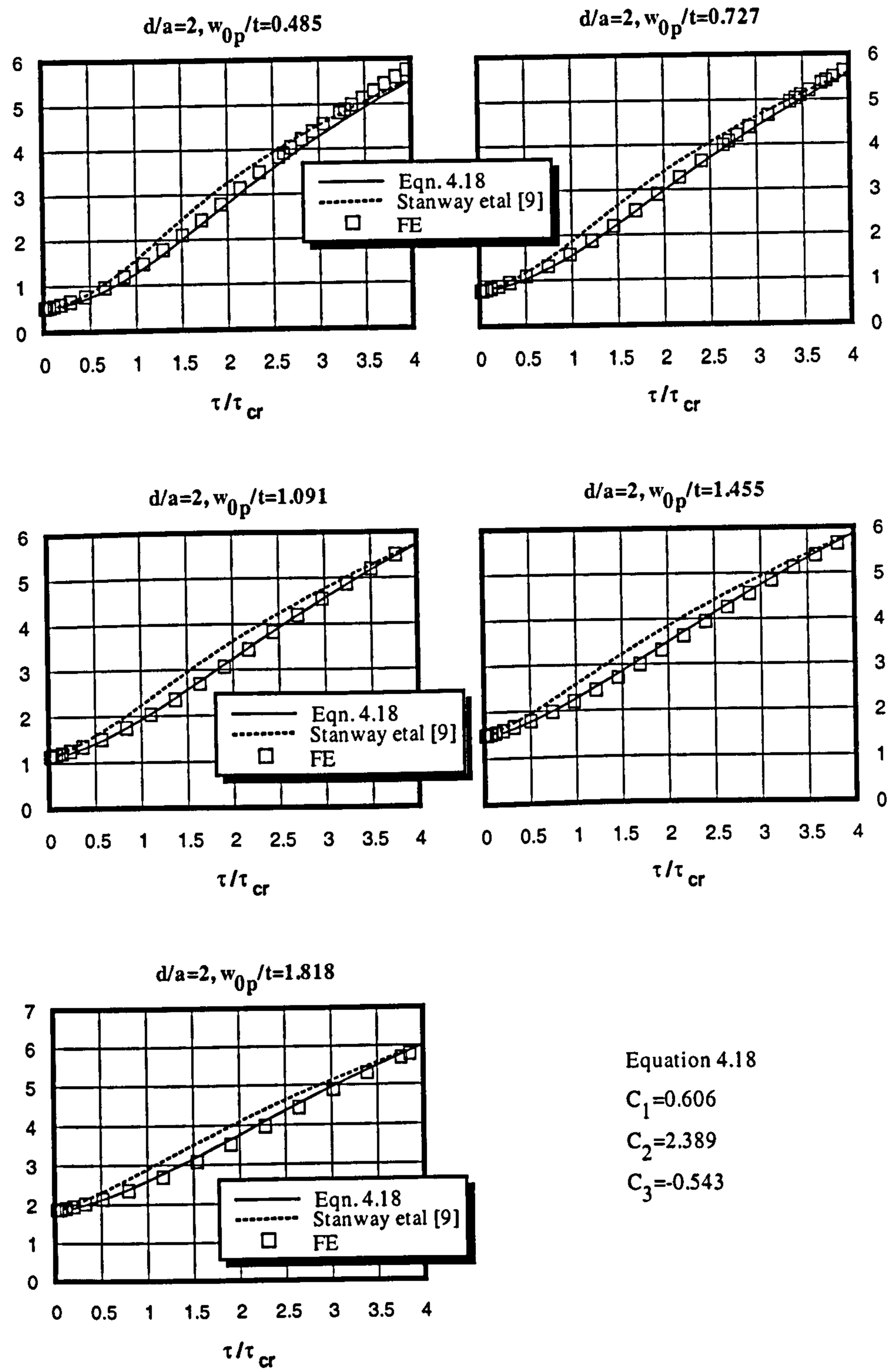
Equation 4.18

C_1=1.680

C_2=1.713

C_3=-0.482

Figure 4.8 Maximum panel deflection w_p/t. CUCU Simply supported panels. Pure shear



Equation 4.18

C_1=0.606

C_2=2.389

C_3=-0.543

Figure 4.8 (Cont.) Maximum panel deflection w_p/t. CUCU Simply supported panels. Pure shear

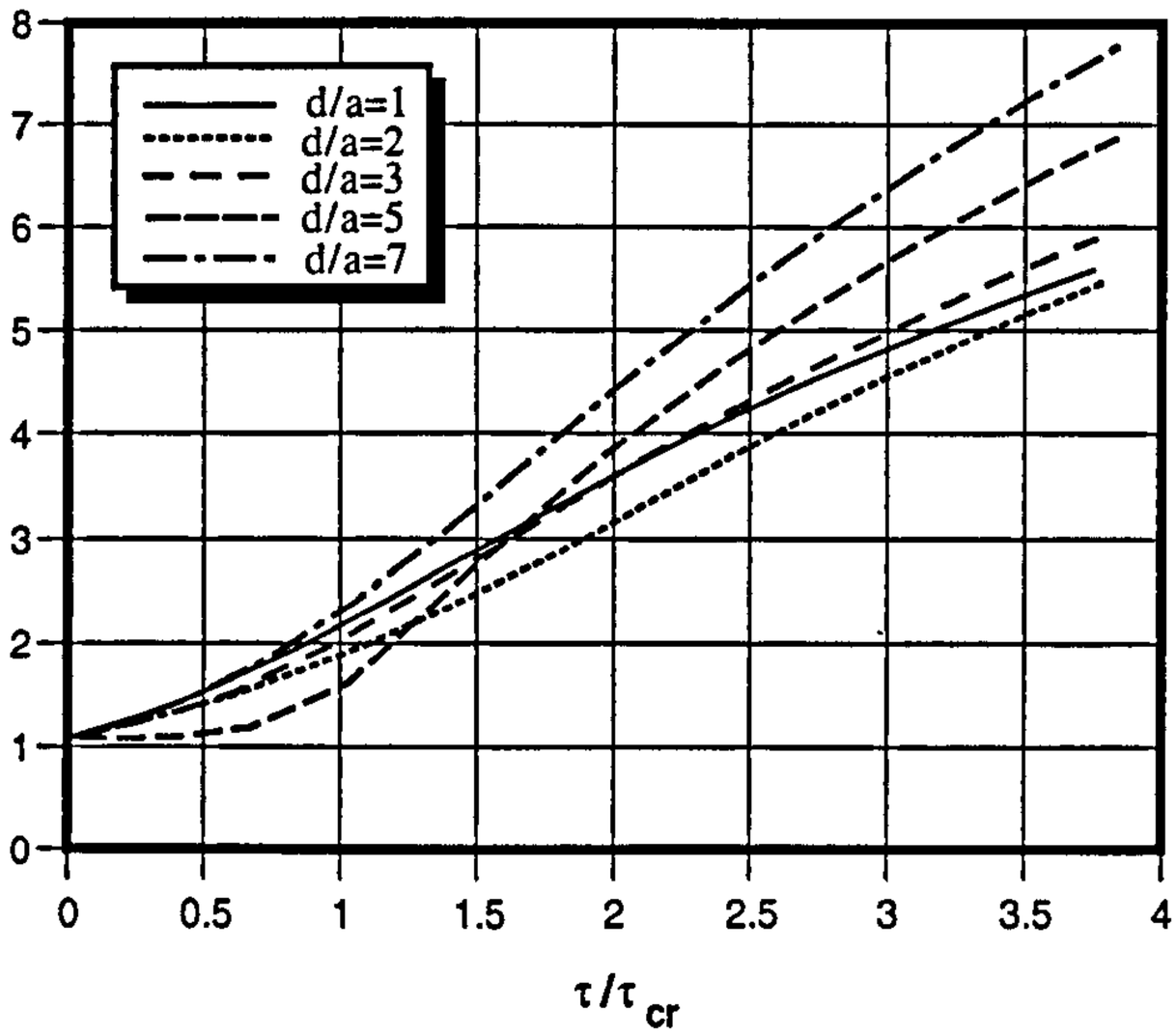


Figure 4.9 Comparison of the maximum panel deflection for tall panels. Pure shear. FE results

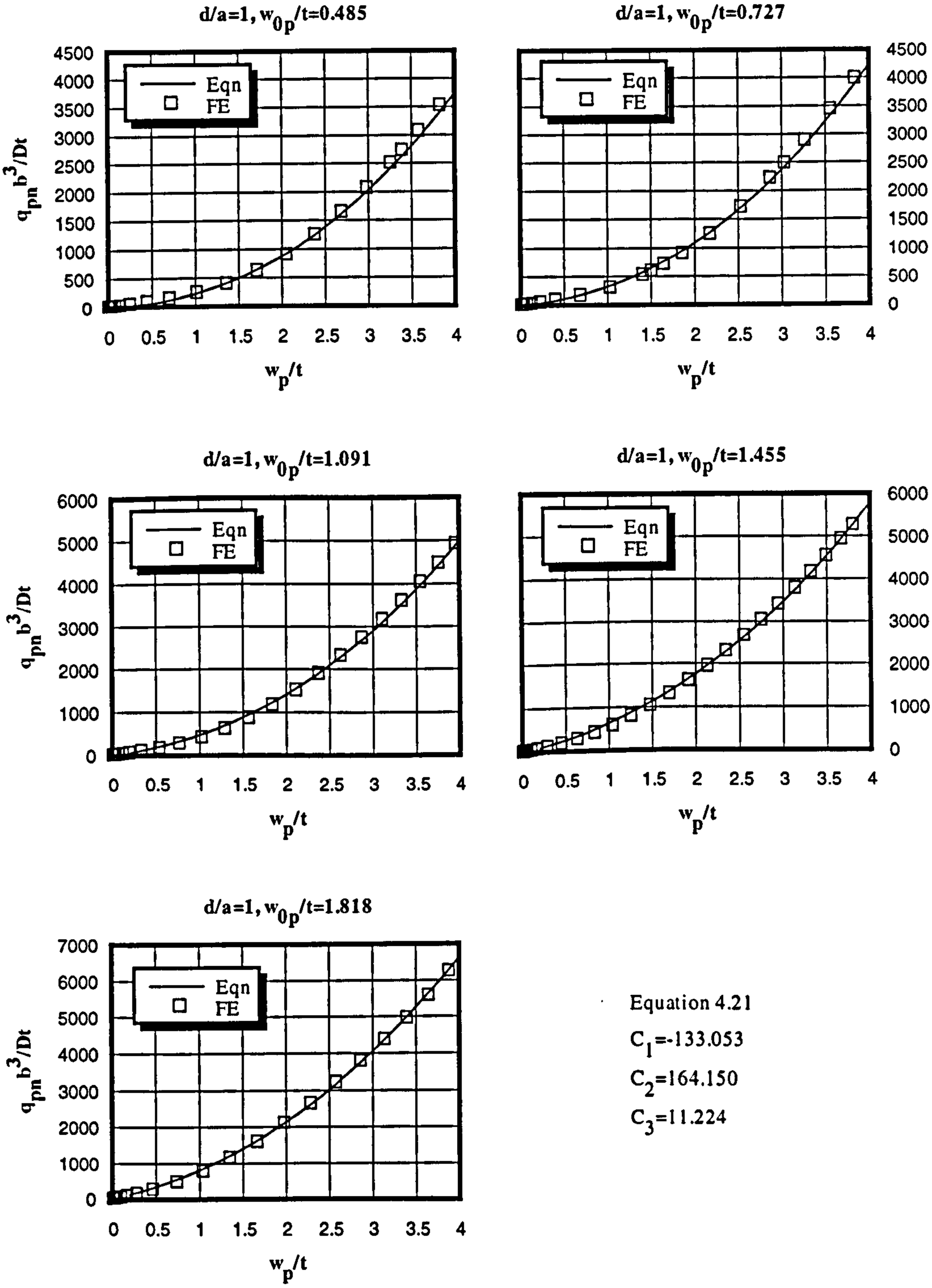
4.6.1.2 Lateral Distributed force q_{pn}

In terms of the non-linear elastic FE results for CUCU panels subjected to pure shear, the coefficients C_1, C_2 and C_3 in Eqn. 4.21 are obtained by the least squares method, and their values are summarised in Table 4.3.

Table 4.3 Coefficients for distributed panel edge forces, Eqn. 4.21

d/a	C_1	C_2	C_3
1.0	-133.053	164.150	11.224
2.0	-250.009	176.975	-3.749

The values of the lateral distributed force estimated by Eqn. 4.21 are presented in Fig. 4.10. Good agreement is observed between the predicted values and the finite element results.



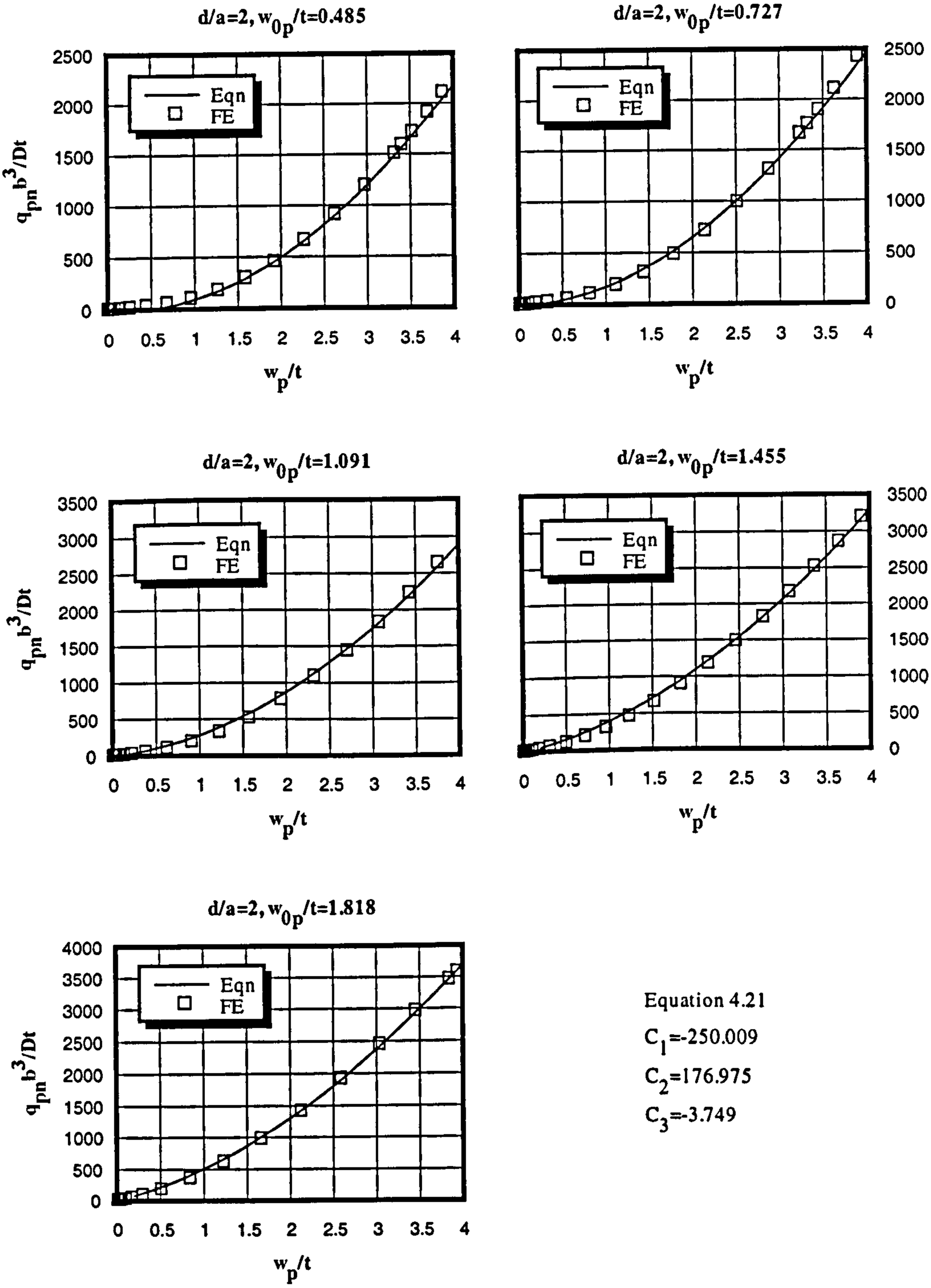
Equation 4.21

C_1=-133.053

C_2=164.150

C_3=11.224

Figure 4.10 Lateral distributed force acting at the mid-edge. CUCU panels. Pure shear



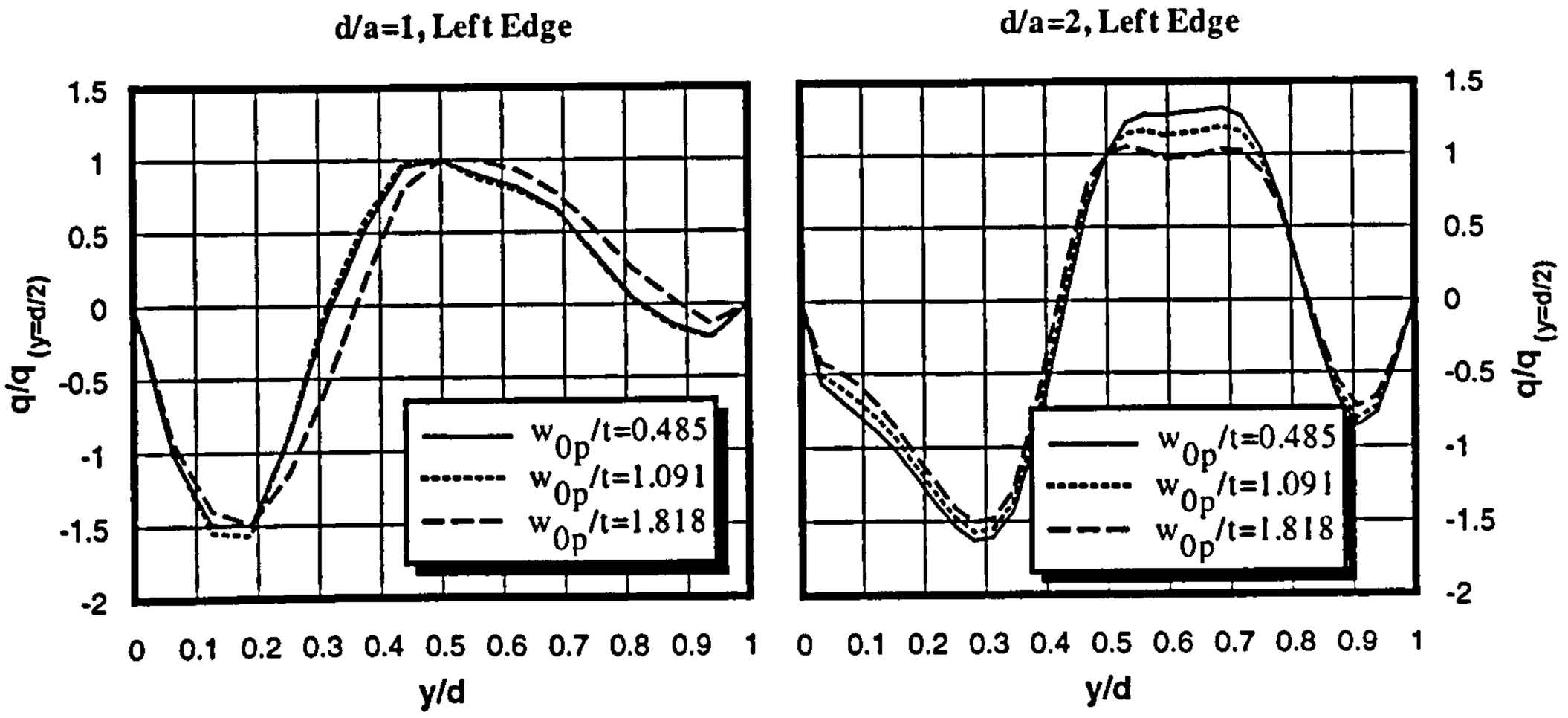
Equation 4.21

C_1=-250.009

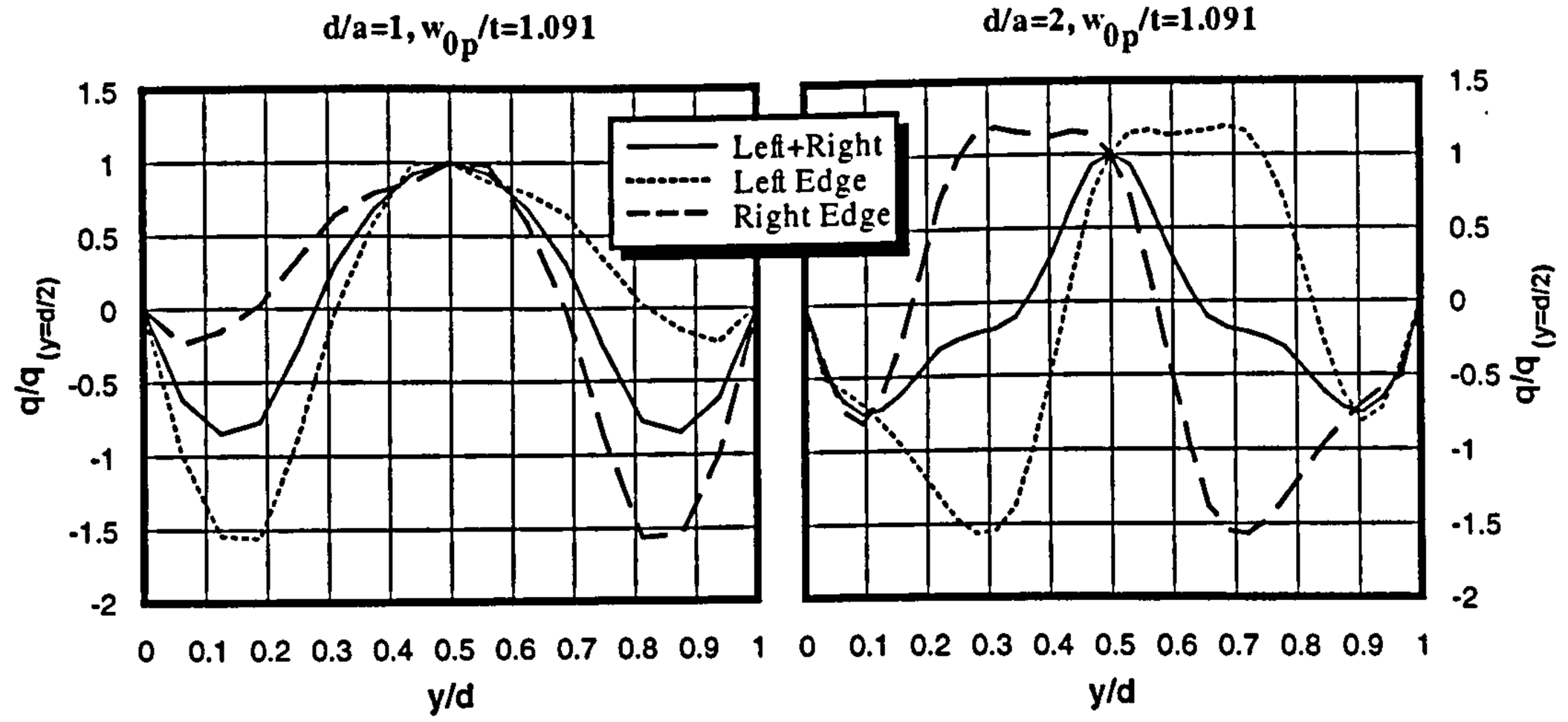
C_2=176.975

C_3=-3.749

Figure 4.10 (Cont.) Lateral distributed force acting at the mid-edge. CUCU panels. Pure shear



(a) Variation with w_{0p}/t



(b) Distribution of q along two opposite edges

Figure 4.11 Distribution of lateral forces along the supported edges. Non-linear elastic FE analyses. CUCU Simply supported panels. Pure shear

The distribution of the lateral force along the left supported edge is illustrated in Fig. 4.11(a). It is apparent that the distribution of the edge reactions hardly varies with the magnitude of initial imperfection, w_{0p}/t.

It is observed in Fig. 4.11(b) that the lateral forces on the two opposite edges of the panel are anti-symmetric. Also shown in Fig. 4.11(b) is the distribution of the lateral forces obtained by adding together the reactions on the left and right edges. As indicated in Eqn. 4.7, the sum of the reactions on the two opposite edges may represent the reaction along the knife edge, and this will be further examined in the next section.

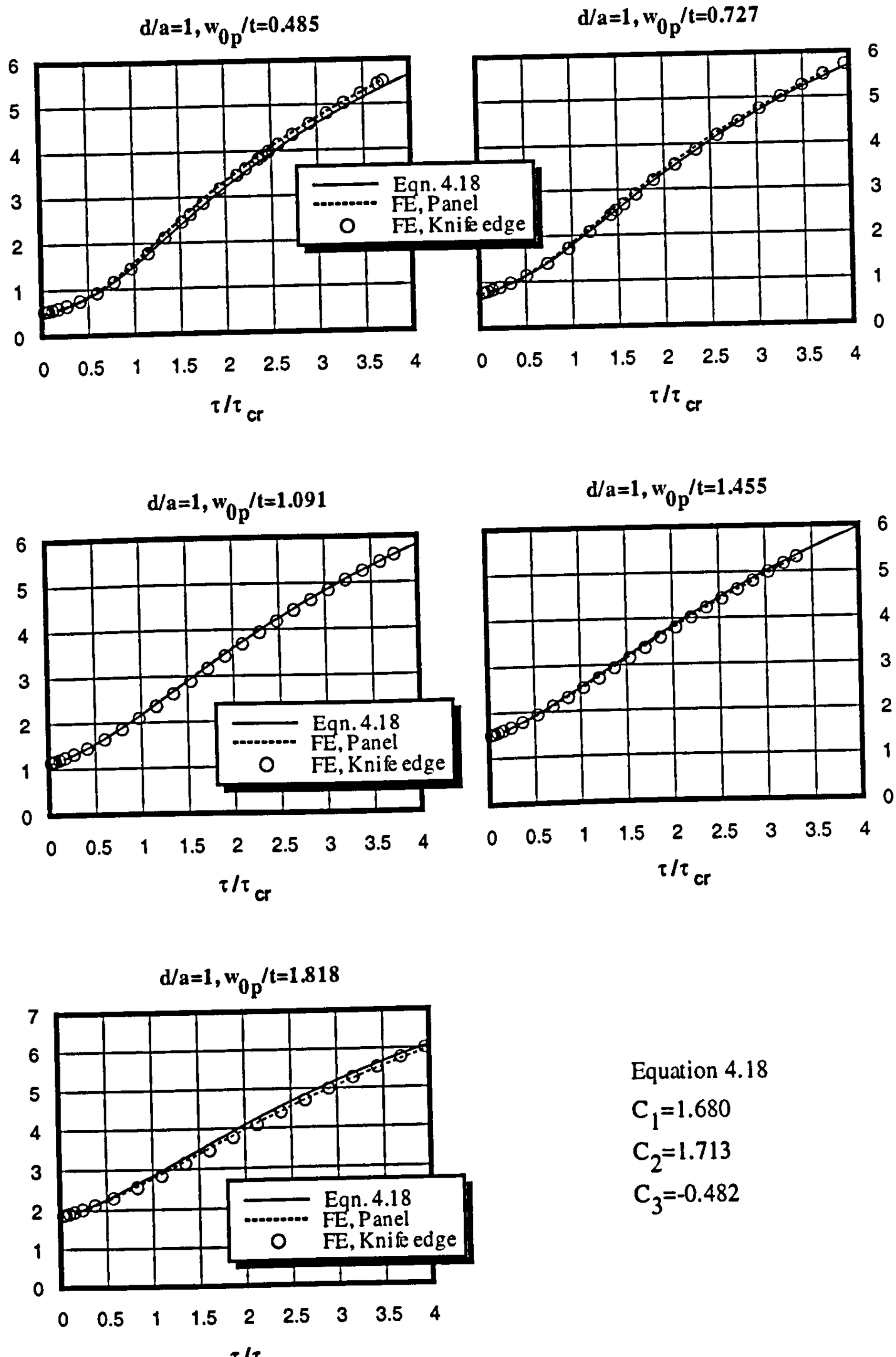
4.6.2 CUCU PLATES WITH AN INTERMEDIATE KNIFE EDGE

4.6.2.1 Deflection in the Plate Panel, w_p/t

Non-linear elastic parametric studies were carried out for CUCU plates having d/a=1, 2 with an intermediate straight knife edge, subjected to pure shear. As stated in Section 4.2, the initial imperfection is taken in the form of the first point-symmetric critical buckling mode. The numerical results of the maximum deflection in the panels are shown in Fig. 4.12. It is noted that for the range of aspect ratios considered here, the deflection equation obtained for the isolated panel can also be used to represent the maximum deflection in the panels of plates with an intermediate knife edge.

By comparing the contour plots of the out-of-plane deflection, w, between isolated panels and plates with a knife edge, as presented in Fig. 4.13, it can be seen that the deflection modes in the corresponding panels are quite similar, especially for d/a=1. This can explain why the deflection equation for the isolated panel can provide accurate estimates of the maximum panel deflection for the knife edge cases.

It is found that the similarity indicated above is still true for tall plates by examining the deflection modes for d/a=3 and 5, which are also included in Fig. 4.13. This implies that the plate continuity across the knife edge does not affect the panel deflection profiles



Equation 4.18

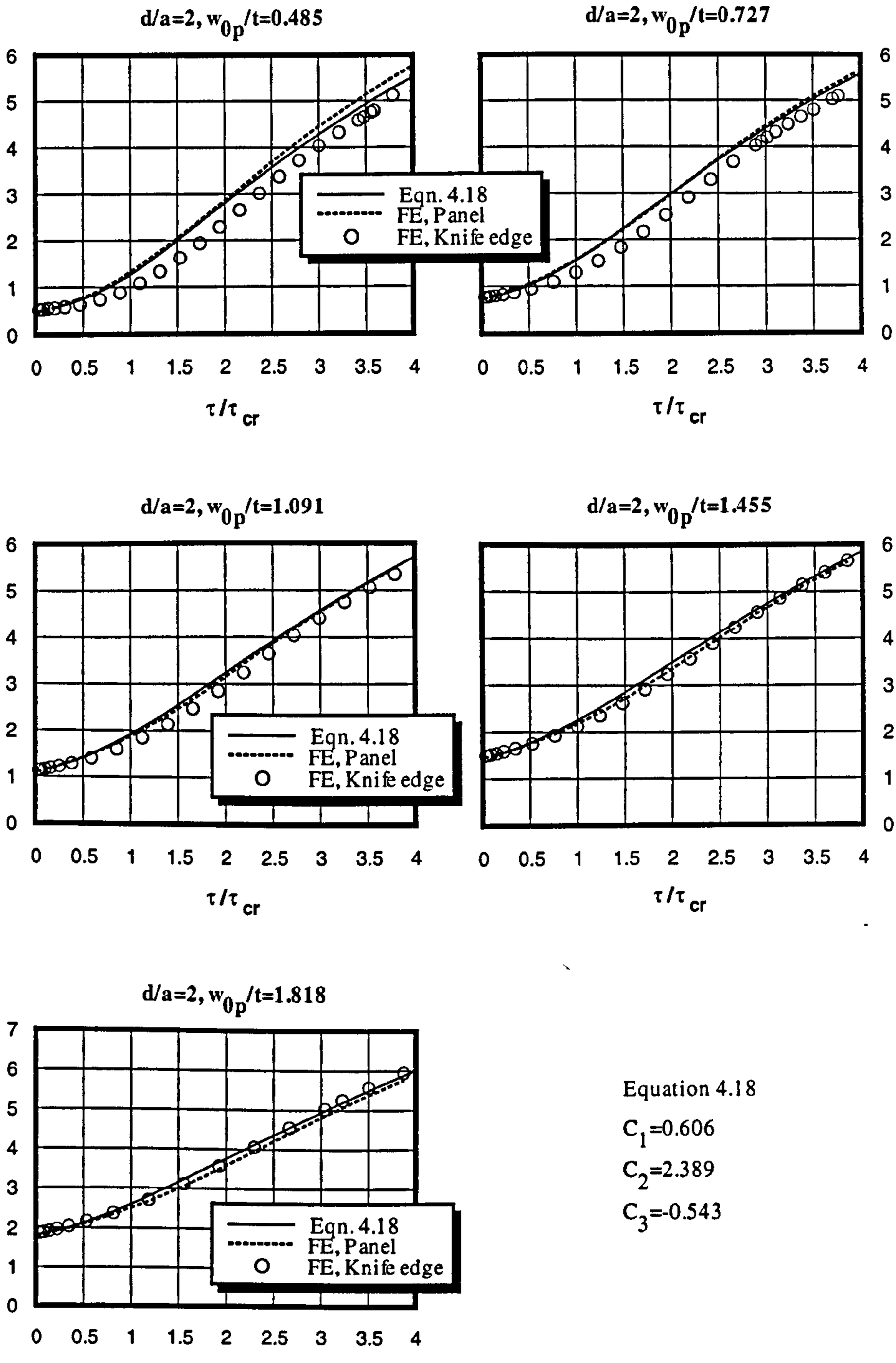
C_1=1.680

C_2=1.713

C_3=-0.482

Figure 4.12 Maximum panel deflection w_p/t. Pure shear.

CUCU plates with an intermediate straight knife edge



Equation 4.18

C_1=0.606

C_2=2.389

C_3=-0.543

Figure 4.12 (Cont.) Maximum panel deflection w_p/t. Pure shear.
CUCU plates with an intermediate straight knife edge

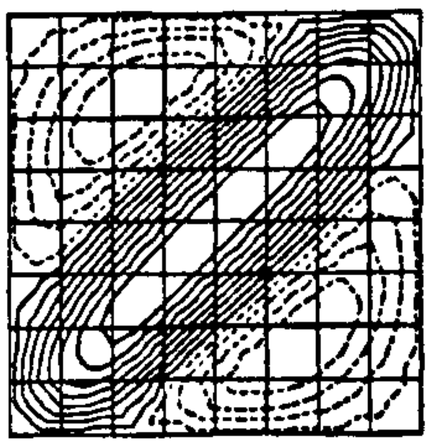
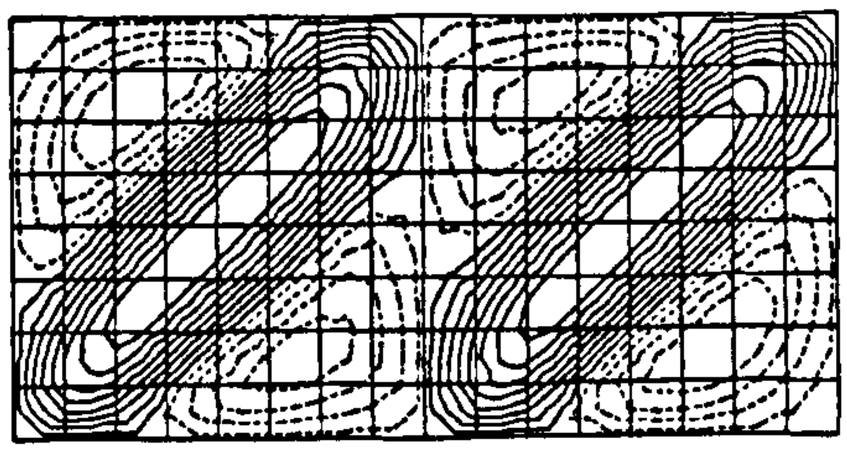
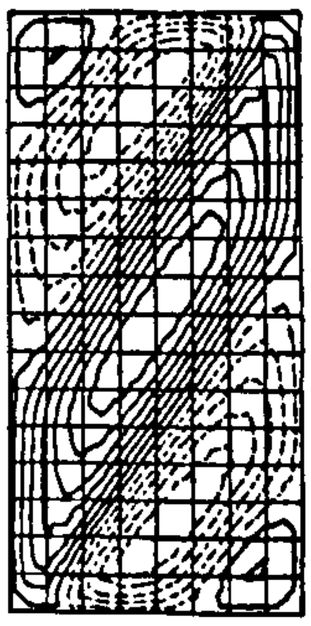
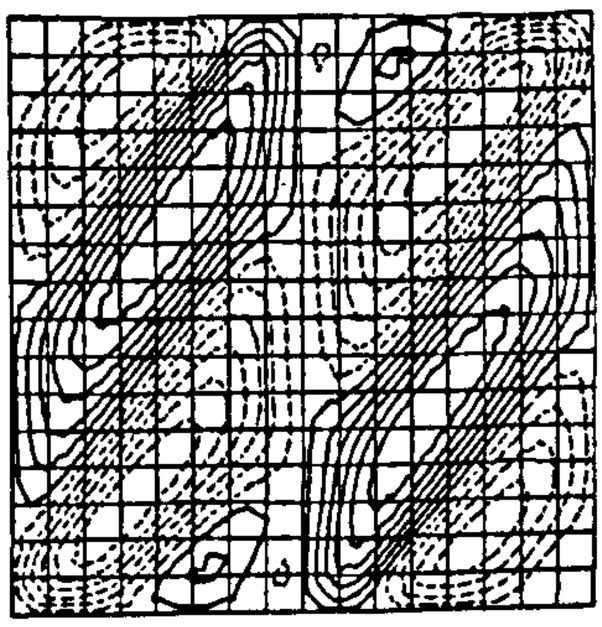
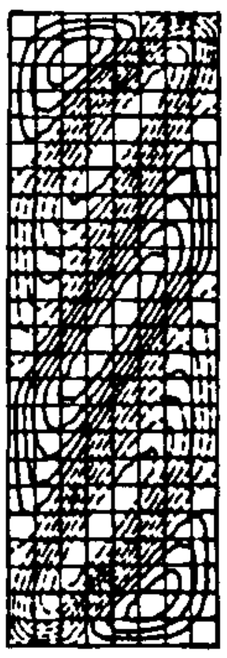
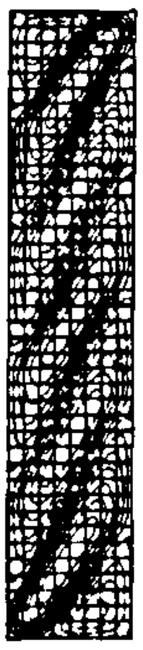
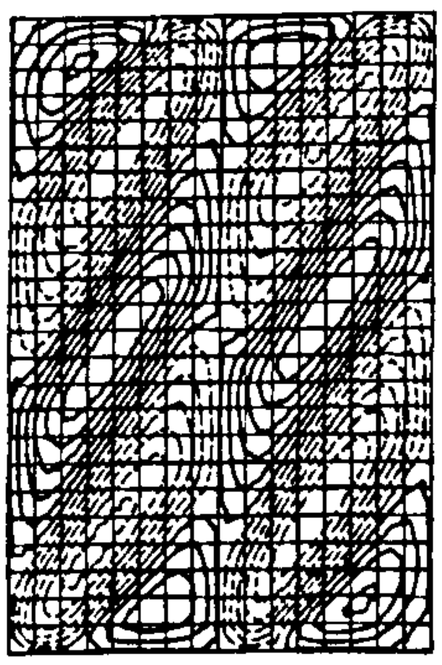
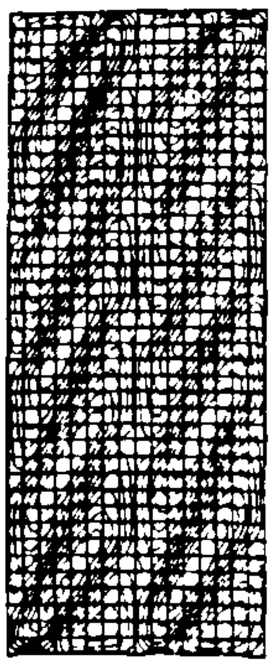
d/a	Panels	Plates with a straight knife edge
1	 τ/τ_{cr}=3.7	 τ/τ_{cr}=3.7
2	 τ/τ_{cr}=4.3	 τ/τ_{cr}=4.3
3, 5	d/a=3  τ/τ_{cr}=4.5 d/a=5  τ/τ_{cr}=4.7	d/a=3  τ/τ_{cr}=4.5 d/a=5  τ/τ_{cr}=4.7

Figure 4.13 Deflection modes from non-linear elastic buckling analyses. Pure shear.
Point-symmetric panel imperfections, w_{0p}/t=1.091. CUCU Panels and plates with a straight knife edge

significantly, and the likely reason is that plate lines parallel to the nodal lines deflect nearly anti-symmetrically about the knife edge, as demonstrated in Fig. 4.13. This observation can also be applied for the critical buckling modes, for which the critical buckling stresses of panels and plates with a knife edge becomes less distinct as d/a is increased from unity, as shown in Fig. 5.3.

By means of the ABAQUS POST program, the deflection modes at different load levels can be plotted. It was observed that as the applied shear stresses are increased, the deflected profiles change from the initial mode (i.e., the first point-symmetric buckling mode, see Fig. 4.2) to the preferred well-developed mode (see Fig. 4.13). It was noted that for d/a=1, the main buckles keep in the diagonal direction, with only their widths decreasing as the load increased, as occurred in the isolated panels. This may be the reason why better prediction is obtained for the cases of d/a=1. For the tall plates, both the location and the number of buckles change with the applied shear stresses, and the mode changes for the knife edge plate are not in accordance with those of the isolated panel, especially before the preferred shear modes are well-developed. Therefore, it is expected that the difference between plate with a knife edge and the associated isolated panel may become greater, as can be seen in the FE results presented in Fig. 4.14. It is noted that the maximum difference occurs at a small load, where the modes change significantly. Nevertheless, as this difference is relatively small, it is considered to be reasonable to use the deflection equations obtained for the isolated panels to predict the maximum panel deflection for plates with an intermediate knife edge.

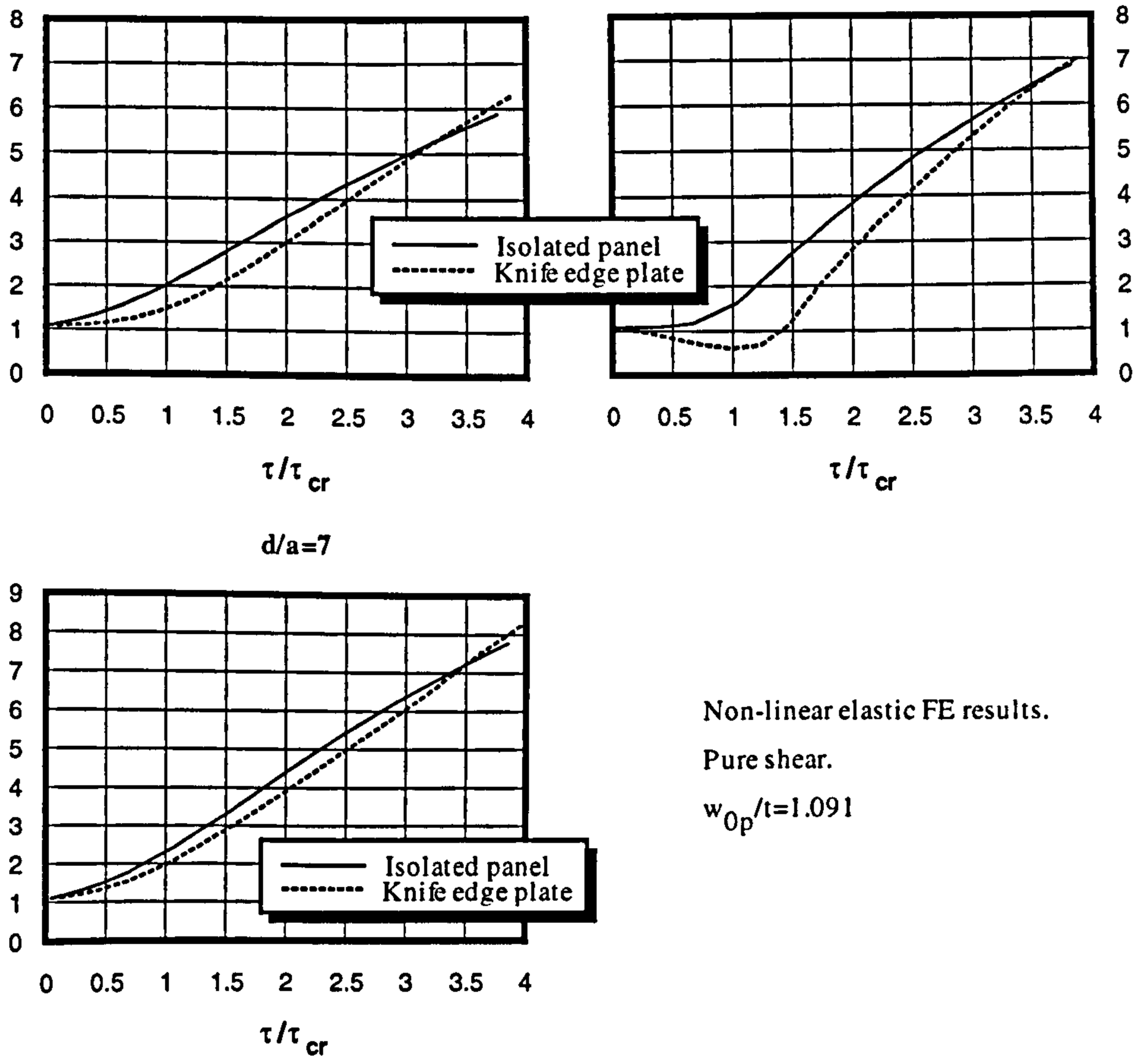
4.6.2.2 Lateral Distributed Force on the Knife Edge, q_{pk}

- **Approach 1: $q_{pk}=f(w_p/t)$**

In this approach, the lateral force on the knife edge, q_{pk}, is determined directly by means of its relationship with w_p/t, as defined in Eqn.4.21. In terms of the non-linear elastic FE results of plates with a straight knife edge, the coefficients C_1, C_2 and C_3 in Eqn.4.21 are obtained by the least squares method, and they are summarised in Table 4.4.

Table 4.4 Coefficients for lateral knife edge forces, Eqn. 4.21

d/a	C_1	C_2	C_3
1.0	-23.611	280.194	41.017
2.0	1301.075	20.725	27.959



Non-linear elastic FE results.

Pure shear.

$w_{0p}/t=1.091$

Figure 4.14 Comparison of deflections between CUCU panels and plates with a straight knife edge

- **Approach 2: $q_{pk}=C\cdot q_{pn}$**

In this approach, the lateral force on the knife edge q_{pk} is calculated, using Eqn. 4.9 given in Section 4.3.2, from the lateral force on the edge of the simply supported panel q_{pn}. The magnitude of q_{pn} is obtained by means of its relationship with w_p/t, that is, Eqn. 4.21 with the coefficients determined from the FE results of isolated panels.

The coefficient C in Eqn. 4.9 is determined by the curve-fitting of FE results. To calculate the coefficient C, FE results of q_{pk} vs. w_p/t curves are required, together with q_{pn} calculated from Eqn. 4.21 for the same value of w_p/t.

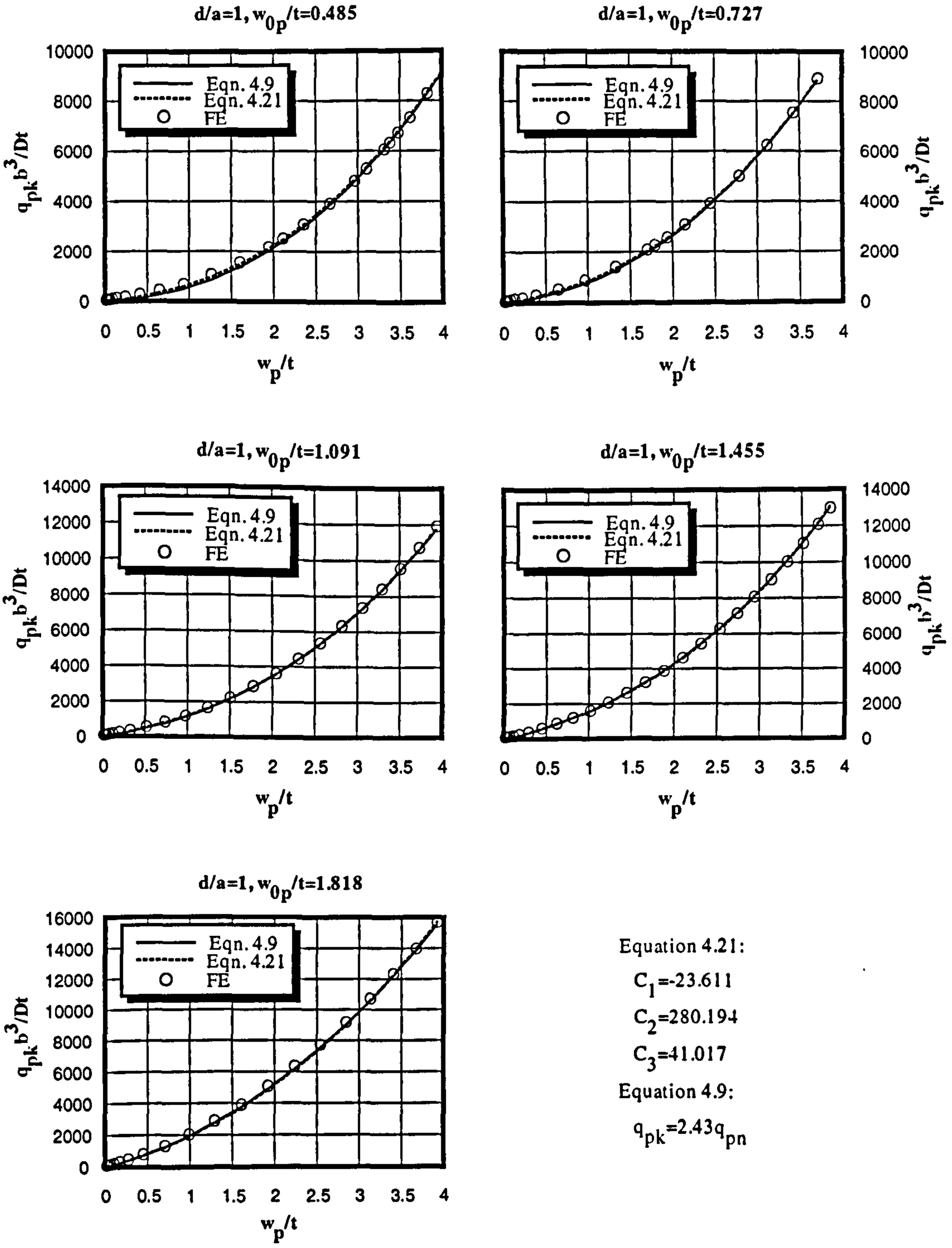
Table 4.5 Coefficient C in Eqn. 4.9

d/a	C
1.0	2.43
2.0	3.38

The values of lateral distributed force estimated by Eqns. 4.21 and 4.9 are presented in Fig. 4.15. It is evident that the values obtained from the first approach agree quite well with the FE results. As for the second approach, accurate estimates can still be attained for d/a=1, but for d/a=2, the differences between the FE and predicted values are found to vary with the magnitude of initial imperfection, w_{0p}/t. This means that the relationship of the panel edge force with w_{0p}/t may not be extended to the knife edge forces simply by multiplying by a constant. The possible reason for this is that as the applied shear stresses are increased, the deflection mode changes more significantly for d/a=2 than for d/a=1, as indicated in Section 4.6.2.1, and the change in the deflection modes is related to the initial imperfection.

Fig. 4.16 presents the distribution of the lateral force along the knife edges, obtained from the finite element analyses. It is observed that the distribution of the lateral force obtained by adding the forces on the two opposite edges is more close to the distribution of the lateral knife edge force for d/a=1 than for d/a=2. It is also noted in Fig. 4.16 that the distribution of the lateral knife edge force does not vary with the magnitude of initial imperfection, w_{0p}/t.

Based on the above discussion, it is considered that the first approach is more suitable for representing the lateral knife edge force. To say it more clearly, the knife edge force can take the same form of equation initially proposed for the simply supported panel edge force, but the coefficients in the equation are to be determined directly using the elastic large deflection FE results of plates with a knife edge.



Equation 4.21:

C_1=-23.611

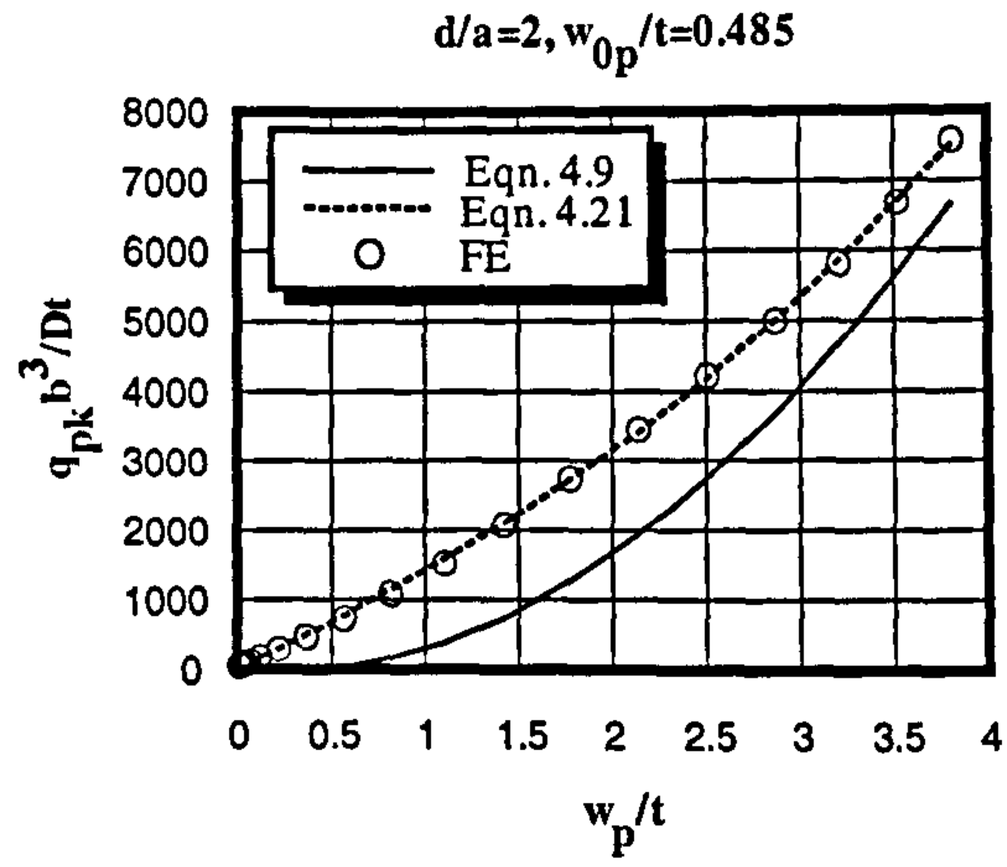
C_2=280.194

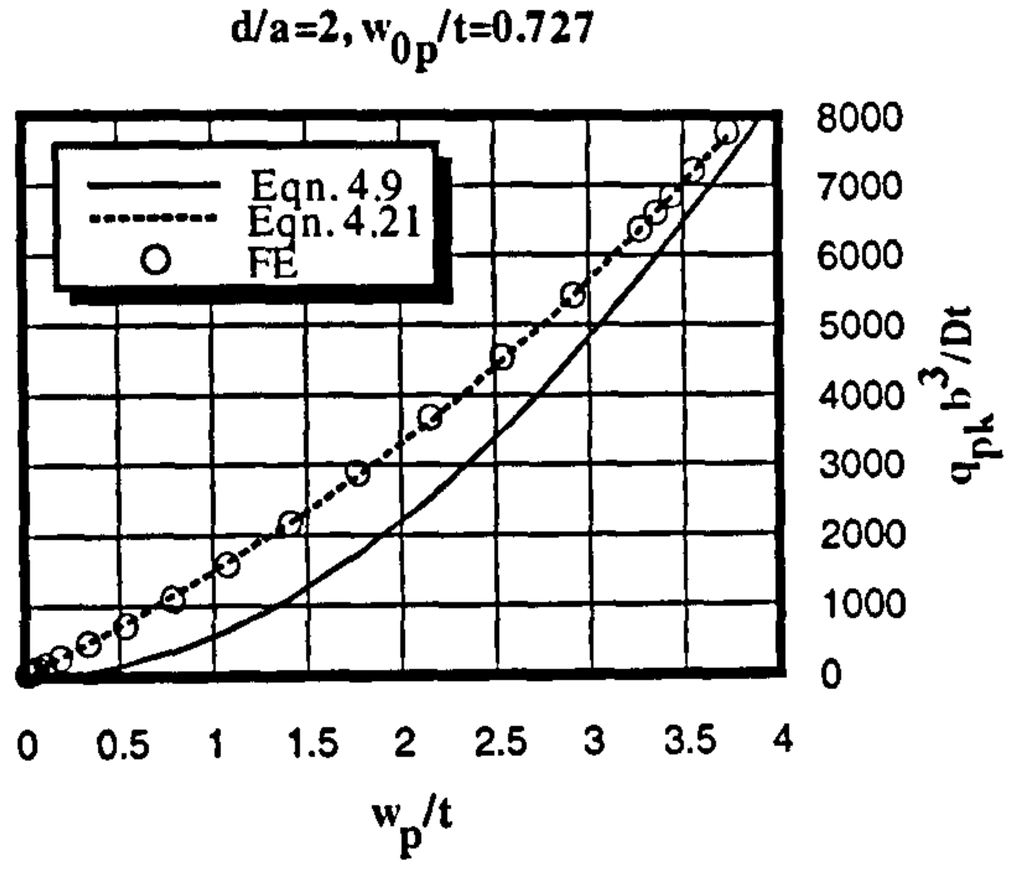
C_3=41.017

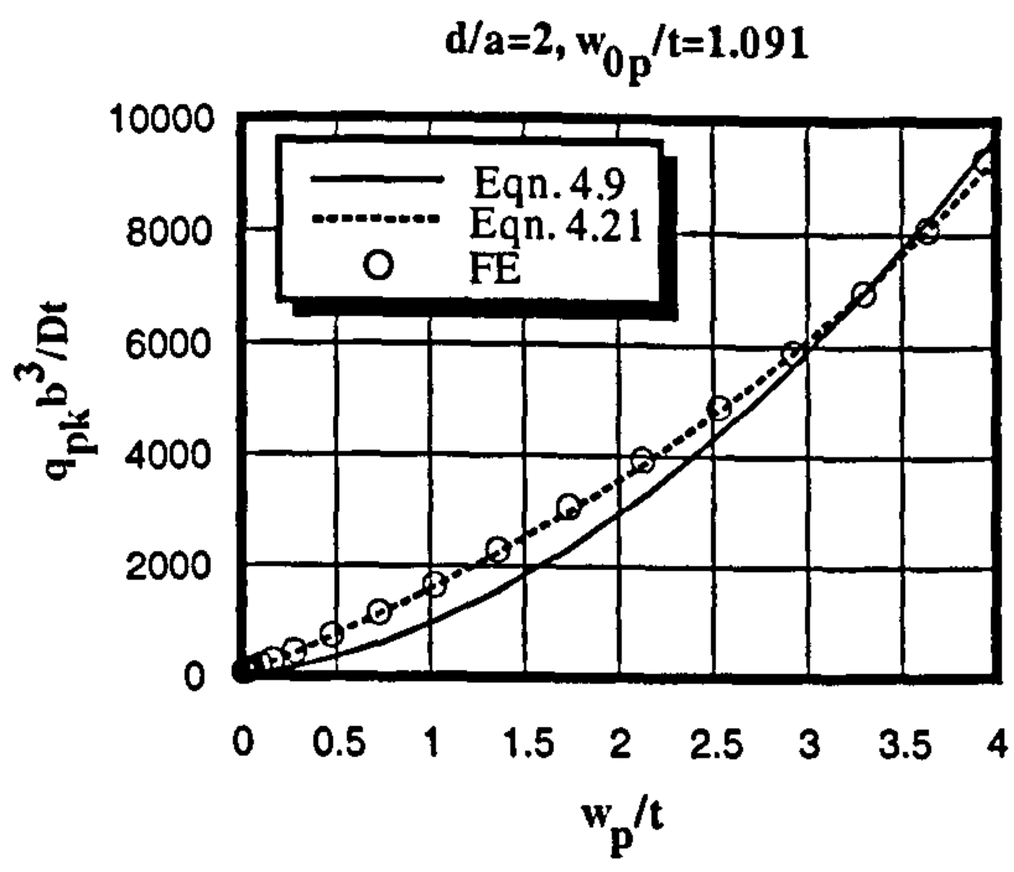
Equation 4.9:

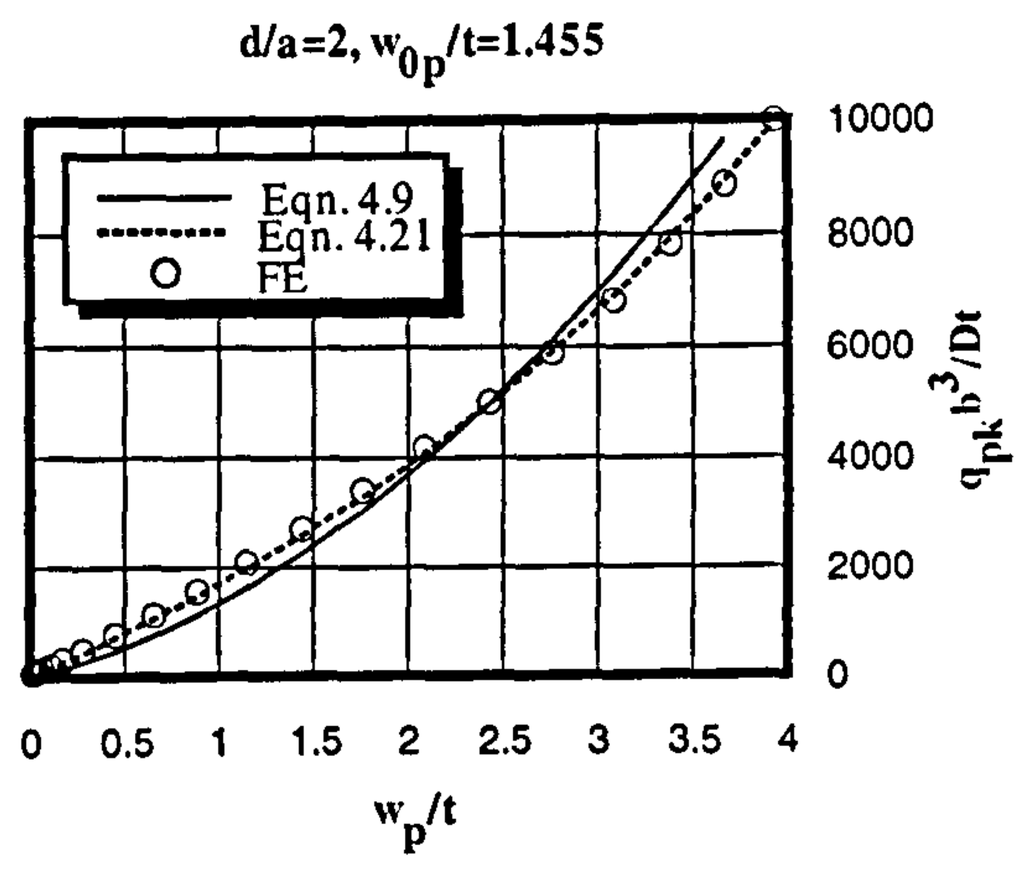
$q_{pk}=2.43q_{pn}$

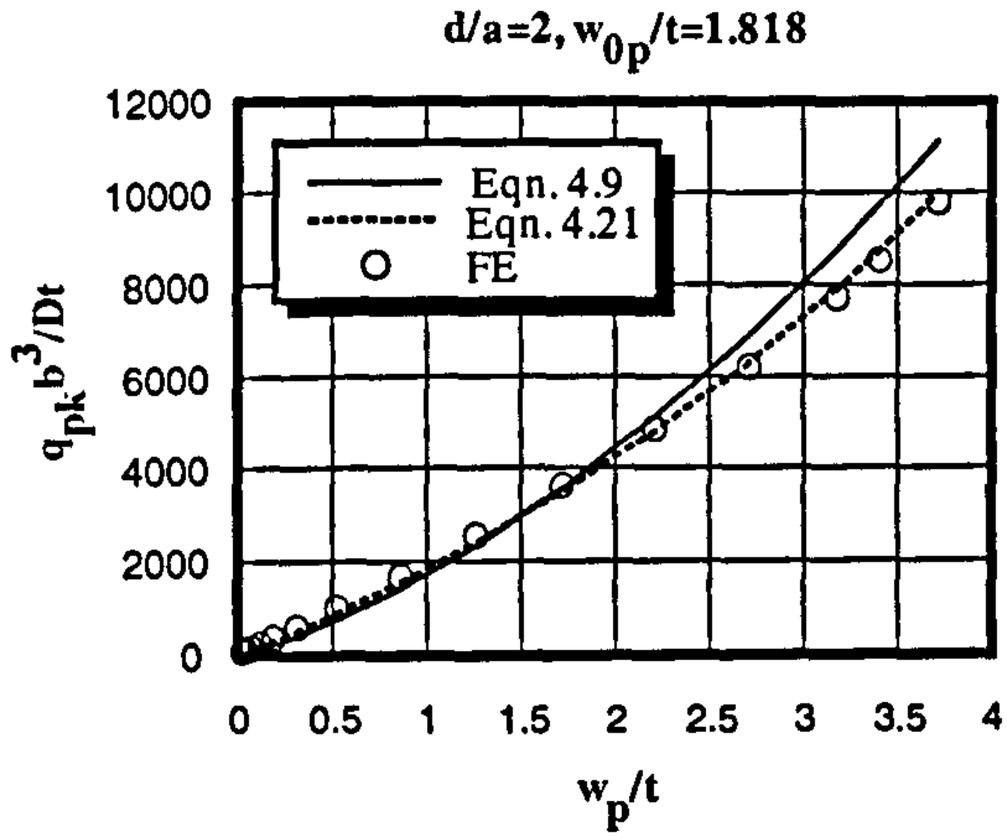
Figure 4.15 Lateral distributed force acting at the mid-edge. Pure shear.
CUCU plates with an intermediate straight knife edge











Equation 4.21:

C_1=1301.075

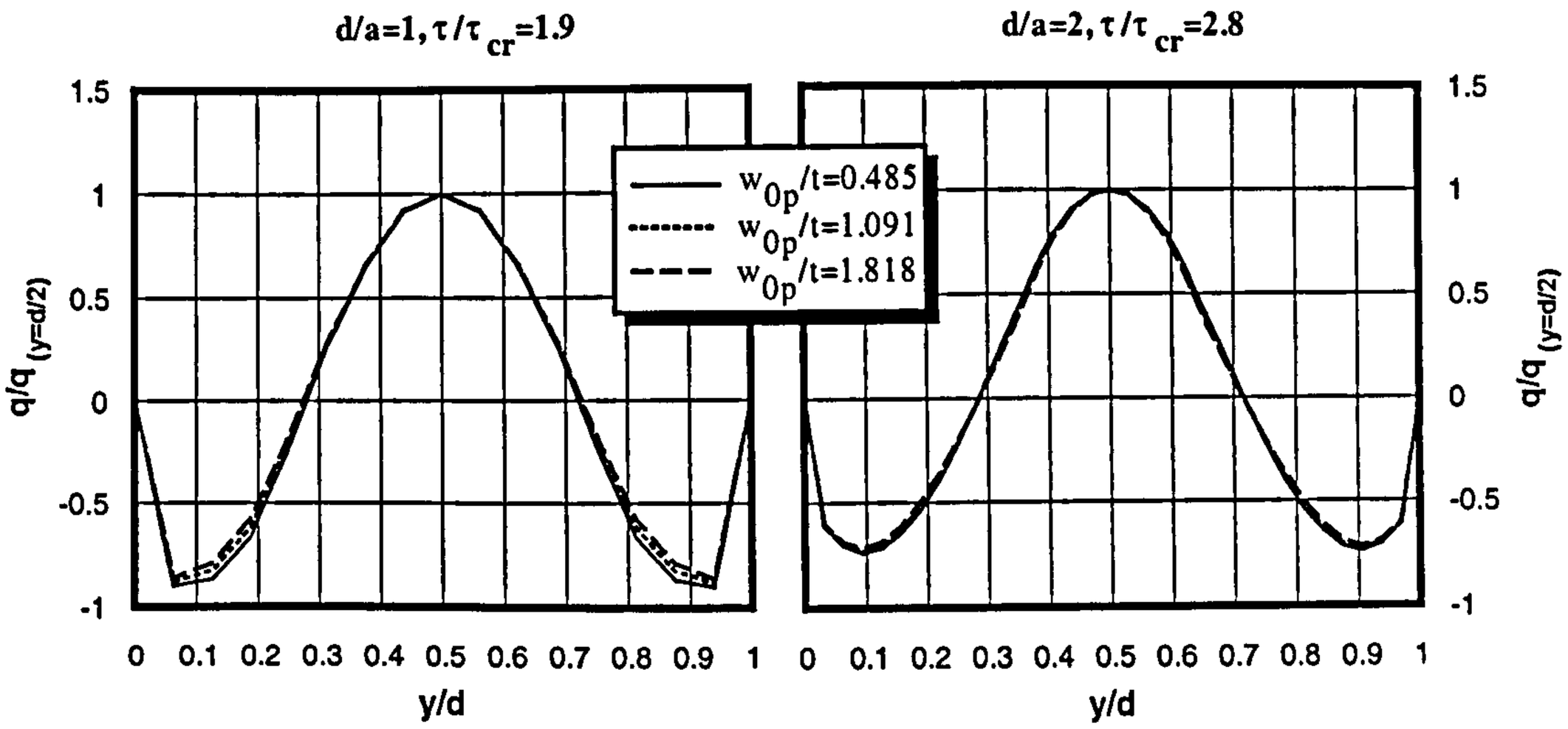
C_2=20.725

C_3=27.959

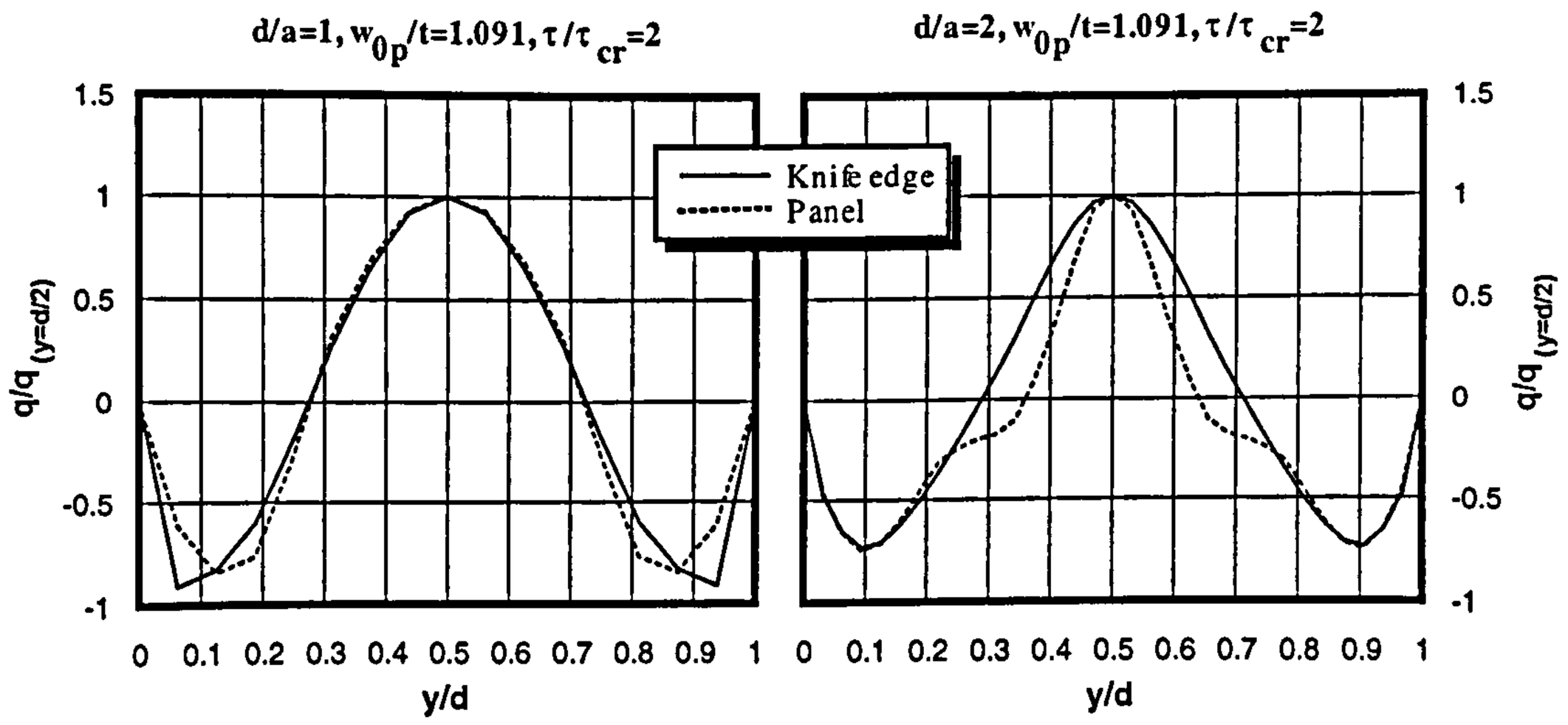
Equation 4.9:

$q_{pk}=3.38q_{pn}$

Figure 4.15 (Cont.) Lateral distributed force acting at the mid-edge. Pure shear CUCU plates with an intermediate straight knife edge



(a) Variation with w_{0p}/t



(b) Distribution of knife edge forces and panel edge forces

Figure 4.16 Distribution of the lateral force along the knife edge. FE results. Pure shear CUCU plates with an intermediate straight knife edge

However, it is the maximum bending moment in the knife edge that will be used for the design of stiffeners. To calculate the bending moment due to the lateral knife edge forces, it is required that both the maximum magnitude and the distribution of the lateral knife edge forces should be known. It is found in Fig. 4.16 that the distribution of q_{pk} varies with d/a, and may not be represented accurately using a simple function. On the other hand, in comparison with the calculation of q_{pk}, the bending moment in the knife edge can be calculated directly from the nodal reactions along the knife edge without additional difficulties, using the methods presented in Section 4.4.2. Therefore, an equation for the calculation of the knife edge moment is proposed and examined in the next section.

4.7 EXPLICIT EQUATIONS FOR THE KNIFE EDGE BENDING MOMENT

In this section, using the approximate analytical solutions for a simply supported panel under uniaxial compression as the basis, an equation for the calculation of the knife edge moment is proposed and calibrated against the finite element results of plates of d/a=1 and 2 under pure shear. The proposed equation presents a direct relationship of the knife edge moment with the applied load and initial imperfection, avoiding the calculation of the panel deflection.

4.7.1 Proposed Equations

For the uniaxially compressed panels, referring to Eqn. B.26, the reaction at the supported edge, q_{Qx}, has a half sine-wave distribution, with its maximum value denoted as q_{pn}. The bending moment caused by the distributed force q_{Qx} may be expressed as:

$$M = \left(\frac{d}{\pi}\right)^2 \cdot q_{pn} \sin\left(\frac{\pi y}{d}\right) \tag{4.24}$$

From Eqns. 4.24 and 4.17, the maximum value of the bending moment, M_{pn}, can be obtained:

$$\frac{M_{pn} b^3}{Dt} = \pi\left(1+\alpha^{-2}\right)\left(\frac{d}{b}\right)^2 \cdot \frac{w_p}{t} \tag{4.25}$$

The dimensionless additional panel deflection w_p/t, as given in Eqn. 4.15, is a function of the applied stress ratio, $\sigma_c/\sigma_{c,cr}$, and the initial deflection, w_{0p}/t. In order to present a direct relationship between the bending moment and the applied stress, a modified Young's equation 4.26 obtained from small deflection theory [25] is considered:

$$\frac{w_p}{t} = \frac{\sigma_c/\sigma_{c,cr}}{1-\sigma_c/\sigma_{c,cr}} \cdot \frac{w_{0p}}{t} \tag{4.26}$$

Replacing equation 4.26 into Eqn. 4.25 and assuming $1-\sigma_c/\sigma_{c,cr} \approx 1$ leads to:

$$\frac{M_{pn}b^3}{Dt} = \pi\left(1+\alpha^{-2}\right)\left(\frac{d}{b}\right)^2 \cdot \frac{w_{0p}}{t} \cdot \frac{\sigma_c}{\sigma_{c,cr}} \tag{4.27}$$

In Section 4.6.2, elastic large deflection finite element analyses were carried out on plates with an intermediate knife edge. It was found that the lateral distributed force at the mid length of the knife edge, q_{pk}, can be well represented using the explicit equation 4.21, which was initially proposed for the reaction on the supported edge of a simply supported panel, q_{pn}. Analogously, it is expected that the knife edge moment M_{pk} can be expressed in the same form of the equation as Eqn. 4.27 used for the bending moment on the panel edge, M_{pn}.

On the other hand, according to Eqns. 4.24 and 4.25, it is obvious that the value of the knife edge bending moment, M_{pk} is proportional to the magnitude of the distributed lateral force on the knife edge. It has been demonstrated in Section 4.6.2 that the normalised knife edge force $q_{pk}b^3/Dt$, via the panel deflection w_p/t, can be well described using the applied stress ratio τ/τ_{cr} and the dimensionless initial deflection w_{0p}/t, for cases of pure shear.

On account of the fact that Eqn. 4.27 is derived from small deflection theory and that the proposed equation should reveal the non-linear characteristics as implied in Eqns. 4.18 and 4.21, the following equation is formulated to give the non-linear elastic relationship of the knife edge bending moment with the applied shear stresses:

$$\frac{M_{pk}b}{Dt} = \frac{w_{0p}}{t} \cdot \sum_{i=1}^{2} C_i \cdot \left(\frac{\tau}{\tau_{cr}}\right)^i + \sum_{j=1}^{4} C_{j+2} \cdot \left(\frac{\tau}{\tau_{cr}}\right)^j \tag{4.28}$$

where C_k, (k=1, 2, ..., 6) are coefficients which will be determined by the curve fitting of FE results. By comparison with the analytical solution Eqn. 4.27, the coefficients in Eqn. 4.28 are expected to vary with the panel aspect ratio d/a only.

4.7.2 Calibration with Non-linear Elastic Finite Element Results

As mentioned in Section 4.6.2, non-linear elastic parametric studies were carried out for CUCU plates of d/a=1, 2 with an intermediate straight knife edge, subjected to pure shear. In this section, the nodal reactions along the knife edge, obtained from ABAQUS, were used to calculate the knife edge bending moments using the methods presented in Section 4.4.2. The numerical results of the bending moments were then used to calibrate the proposed equation 4.28.

It is noted in Eqn. 4.28 that for a fixed value of d/a, the normalised knife edge bending moment, $M_{pk}b/Dt$, is related to the values of w_{0p}/t and τ/τ_{cr} only, and will not vary directly with the panel slenderness ratio, b/t. This conclusion is confirmed by comparison of the numerical results of parametric studies. As presented in Fig. 4.17, the curves of $M_{pk}b/Dt$ versus τ/τ_{cr} for the cases of equal w_{0p}/t but different b/t are almost coincident. It is also noted in Fig. 4.18 that the distribution of the bending moment along the knife edge does not vary with the magnitude of initial imperfection, w_{0p}/t.

In terms of the numerical results of the knife edge moment, the coefficients C_k, (k=1, 2, ..., 6) in Eqn. 4.28 are obtained by the least squares method, and they are summarised in Table 4.6.

Table 4.6 Coefficients C_k (k=1,2, ..., 6) for knife edge moment M_{pk}, Eqn. 4.28

d/a	C_1	C_2	C_3	C_4	C_5	C_6
1.0	29.71	-0.524	-6.960	4.962	21.37	-2.865
2.0	83.62	-16.59	-14.03	19.70	54.99	-7.676

Fig. 4.19 presents a comparison between the numerical results and the values predicted using Eqn. 4.28 with the coefficients given in Table 4.6, and a good agreement can be

seen. This suggests that for the aspect ratios d/a=1 and 2, the proposed equation 4.28 can be used to represent the maximum bending moment in knife edges. Also, it seems quite likely that Eqn. 4.28 may be applied for more general cases including plates of a wide range of aspect ratios, subjected to pure shear and in-plane combined loading conditions, and this will be further investigated in Chapter 5.

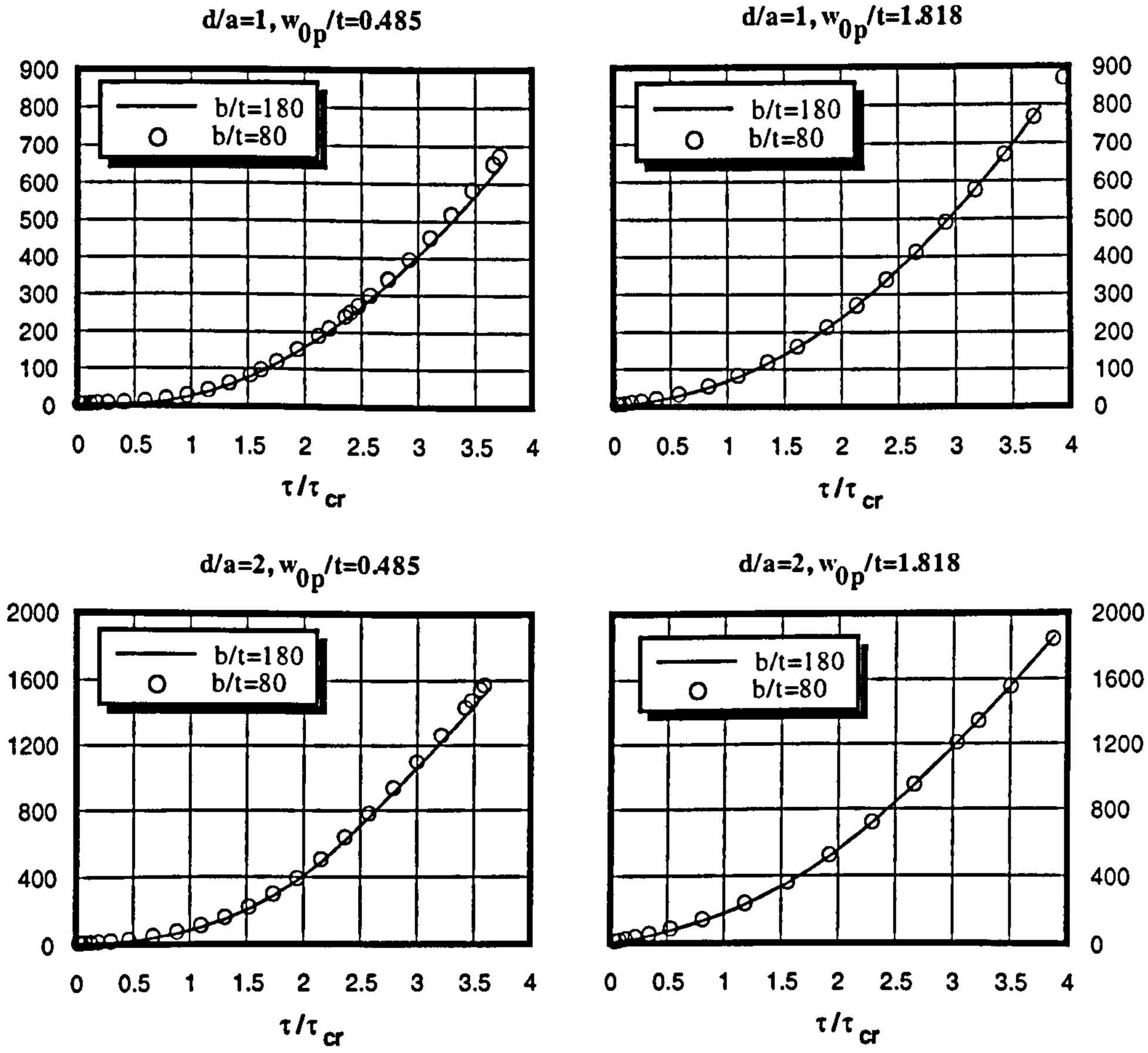


Figure 4.17 Variation of the knife edge bending moment M_{pk} with w_{0p}/t and b/t. FE results. CUCU plates with an intermediate straight knife edge. Pure shear

The knife edge bending moments calculated from the equation proposed by Stanway et al [9] are also shown in Fig. 4.19. It can be seen that for d/a=1, the values obtained from Stanway et al [9] agree quite well with the FE results from ABAQUS; whereas for d/a=2, there are significant differences between them. Referring to the mesh

convergence study presented in Section 3.8, it is considered that the main reason for the differences is the mesh size used in the finite element analyses. In Stanway's work [1], the number of square elements along the small panel dimension is 6 for d/a=1 and 4 for d/a≥2, respectively. It was observed in Fig. 3.12 that compared to the converged values (20 square elements along the small panel dimension), such mesh sizes would cause an error of 2.2% for d/a=1 and 31.3% for d/a=2 in the magnitude of lateral panel edge forces. In this thesis, eight square elements across the small panel dimension are used, which may result in relative errors of panel edge forces less than 2.5%. It is also noted that Stanway had to use spring elements with stiffness great enough to obtain the nodal reactions along the knife edge when he used the FINASIC program to carry out finite element analyses.

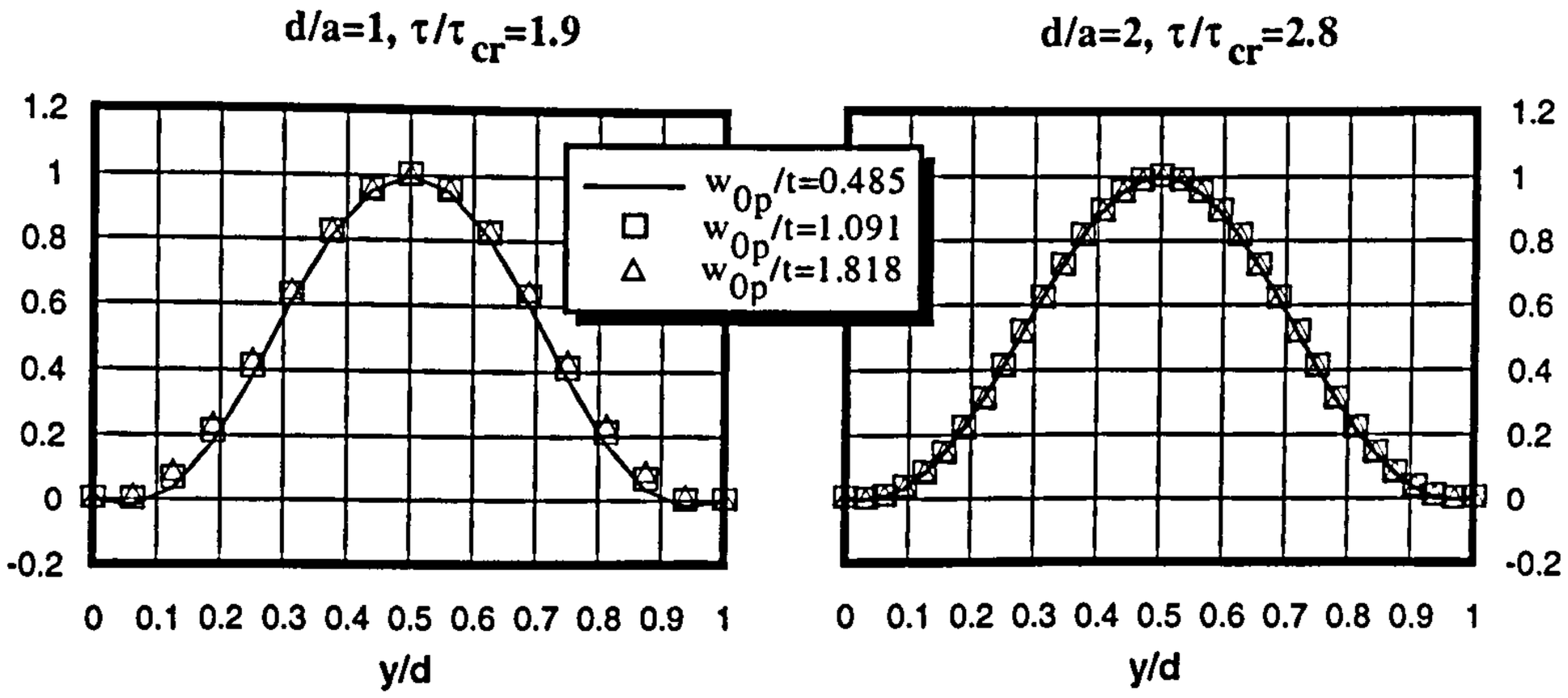
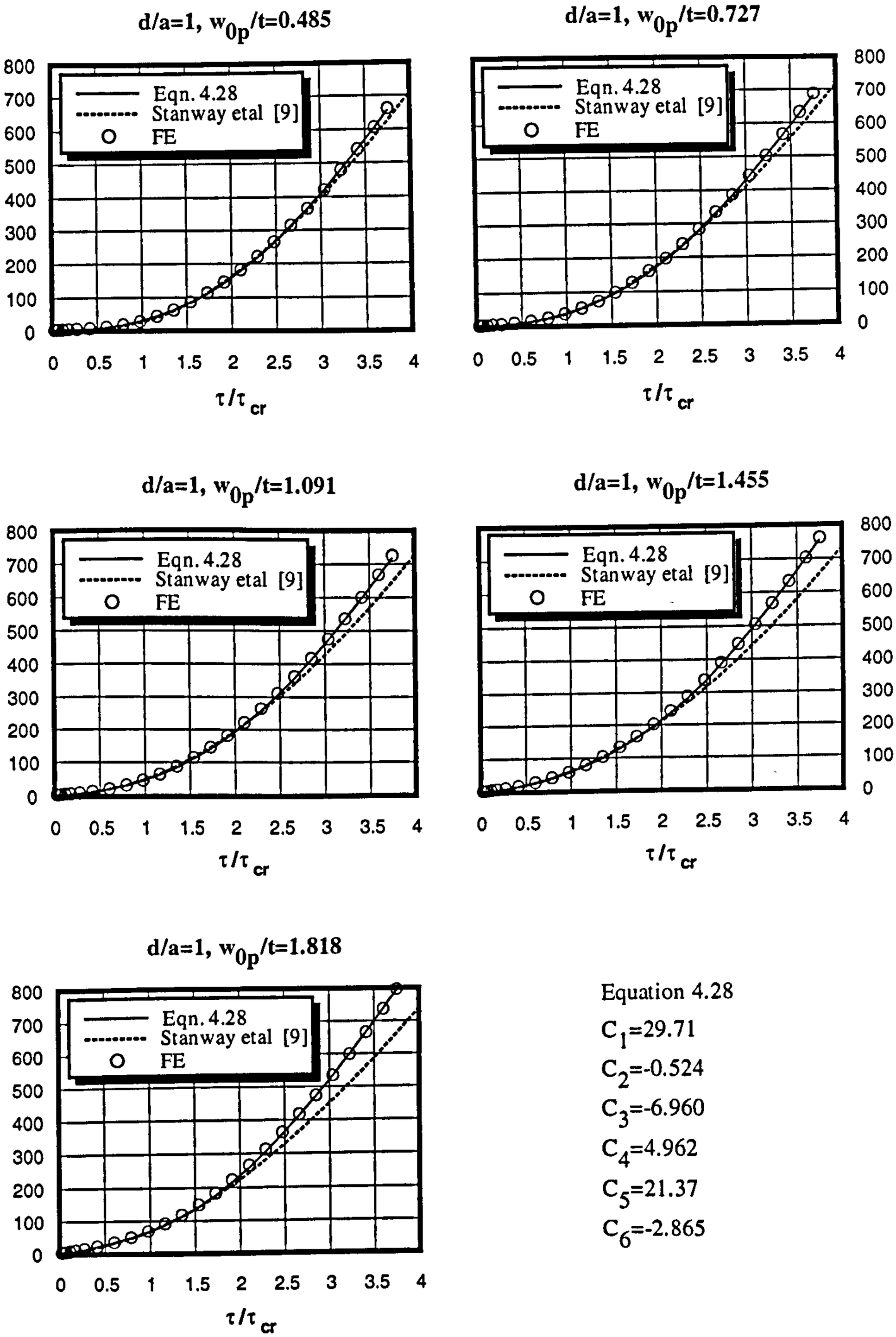


Figure 4.18 Distribution of the bending moment along the knife edge. FE results. Pure shear CUCU plates with an intermediate straight knife edge

Fig. 4.18 presents the distribution of the bending moments along the knife edge, obtained from the finite element analyses. It is observed that for d/a=1 and 2, the knife edge moment due to the distributed lateral knife edge forces has a distribution close to a single half wave, with its maximum value at the mid length of the knife edge.



Equation 4.28

C_1=29.71

C_2=-0.524

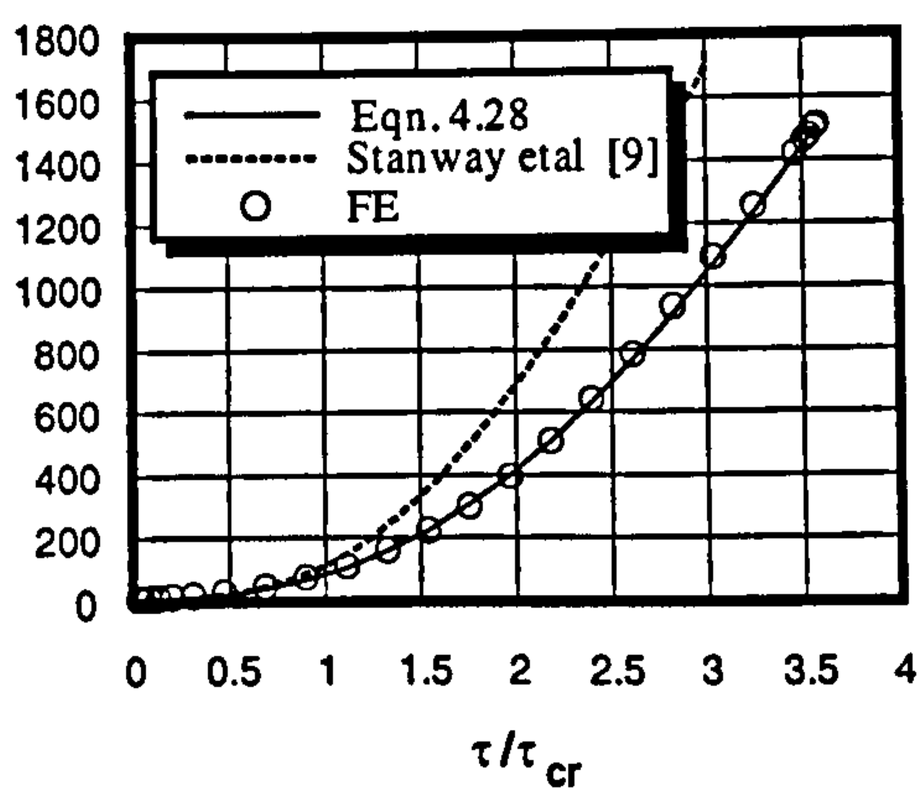
C_3=-6.960

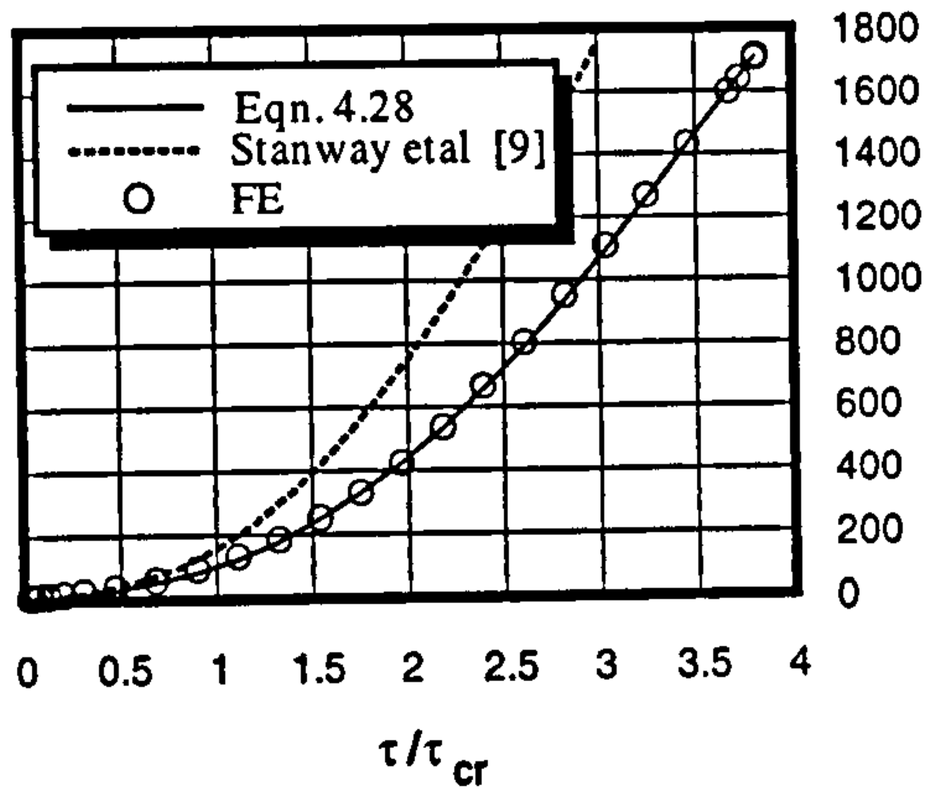
C_4=4.962

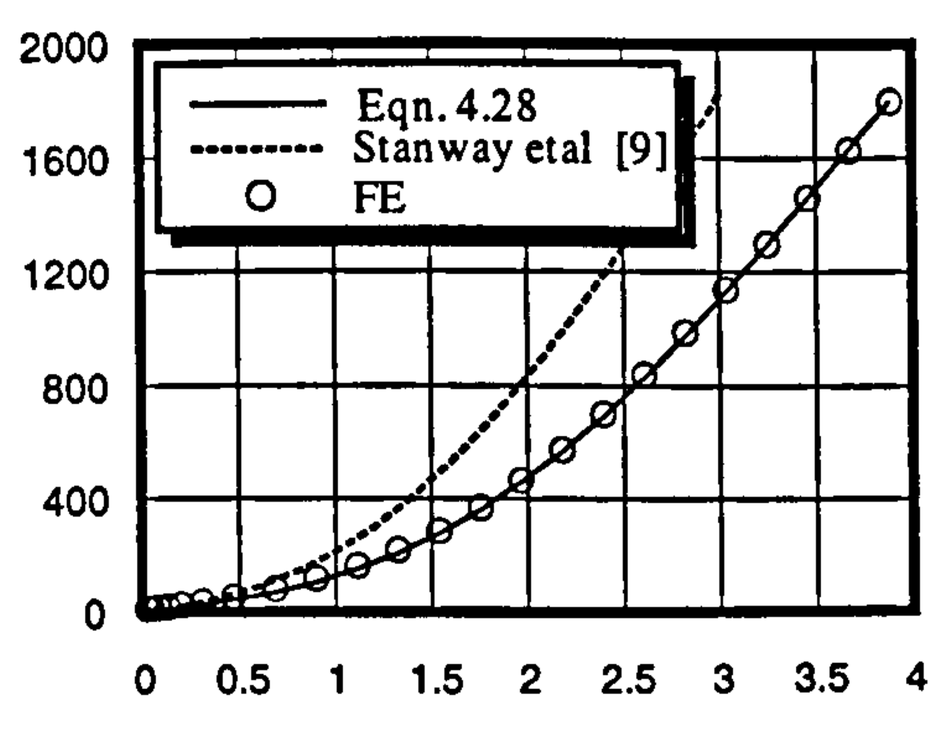
C_5=21.37

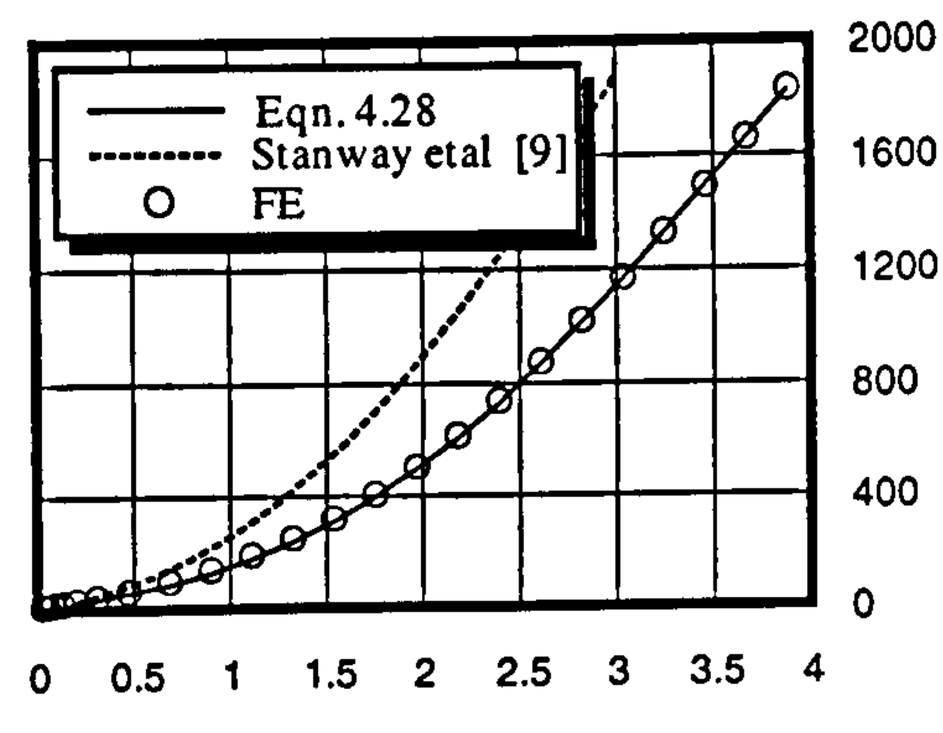
C_6=-2.865

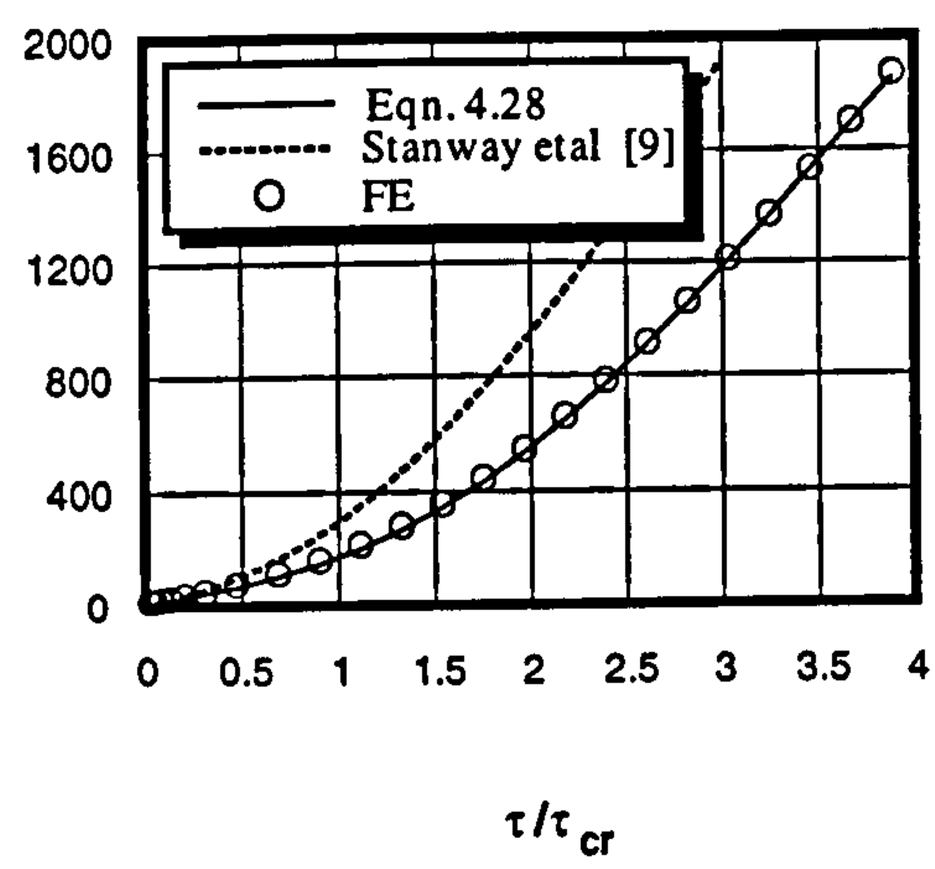
Figure 4.19 Maximum bending moments in the knife edge. Pure shear.
CUCU plates with an intermediate straight knife edge. Non-linear elastic FE results











Equation 4.28

C_1=83.62

C_2=-16.59

C_3=-14.03

C_4=19.70

C_5=54.99

C_6=-7.676

Figure 4.19 (Cont.) Maximum bending moments in the knife edge. Pure shear CUCU plates with an intermediate straight knife edge. Non-linear elastic FE results

4.8 CONCLUSIONS

In this chapter, several possible approaches to representing the knife edge forces have been investigated, and calibrated against the finite element results of plates of d/a=1 and 2 under pure shear. As a result of this preliminary study, the following conclusions can be made:

(1) A practical and logical approach to providing design formulae is to use simple analytical solutions as the basis, and then to establish explicit equations with coefficients to be determined by means of finite element results.

(2) A knife edge may be represented by the constraint equations 4.1 and 4.2. The knife edge is subjected to the distributed reactive force q_{pk}, which results from the difference in the panel transverse shear forces Q_x across the knife edge. The panel twisting moment M_{xy} does not contribute to the lateral distributed force q_{pk} (Fig. 4.3).

(3) In the finite element models of plates with a knife edge, the panel imperfections should be fully affine to the first point-symmetric critical buckling mode of the knife edge plate, which gives the greatest value of the knife edge force for a given applied shear stress.

(4) The lateral distributed forces acting on the supported edges, as well as knife edges, can be obtained using the equivalent nodal force method presented in Section 4.4.1. The bending moment, resulting from the distributed lateral forces, may be calculated using the recurrent equations 4.12 to 4.14.

(5) The plate continuity across the knife edge does not affect the panel deflection profiles significantly. The difference in the maximum panel deflection between plates with a knife edge and the associated isolated panels is relatively small, so it reasonable to use the deflection equations obtained for the isolated panels to predict the maximum panel deflection of plates with an intermediate knife edge (Fig. 4.12).

(6) It is not practicable to calculate the knife edge forces solely from the individual panel edge forces, although certain relationship exists between them, especially for d/a=1 (Fig. 4.15). This is because their relationship varies with the aspect ratio d/a and the initial deflection magnitude w_{0p}/t and hence the coefficients in Eqn. 4.9 need to be given for each individual case.

(7) The proposed equations 4.18 and 4.21 can well represent the non-linear elastic behaviour of panels and plates with a straight knife edge, provided that the coefficients are determined for each d/a. As a rough estimate, the magnitudes of deflection for simply supported panels may be calculated using the deflection equation for d/a=1.

(8) Eqn. 4.18 is adequate for representing the non-linear elastic values of the maximum panel deflection. For moderately tall panels, the panel deflections can be estimated by linear interpolation between the values for d/a=2 and for a very tall panel, e.g. d/a=7 (Fig. 4.9).

(9) Eqn. 4.28 is recommended as the basic formula for the calculation of the knife edge moment, M_{pk}. More general cases, including plates of other aspect ratios, subjected to pure shear and to combined in-plane loading will be further investigated in Chapter 5.

CHAPTER 5

BENDING MOMENTS IN STRAIGHT KNIFE EDGES

5.1 INTRODUCTION

According to the proposed design model presented in Chapter 8, the maximum stiffener bending moment is one of the internal stiffener forces required in order to size the stiffener. It has been found by Stanway [1] that for stiffened plates, the stiffener moment due to the local panel bending effect can be represented by the bending moment in a straight knife edge, M_{pk}. In this chapter, the knife edge moments for non-linear elastic cases are examined. The stiffener bending moment due to the effect of overall buckling tendency will be studied in Chapter 7, and the determination of the total stiffener moment, including the effect of plate plasticity, will be discussed in Chapter 8. In Chapter 6, the axial forces in stiffeners are investigated.

In Chapter 4, a simple formula, Eqn. 4.28, has been proposed for calculating the bending moment due to the reaction acting on a straight knife edge, which is equivalent to an unattached straight stiffener of infinite rigidity, $\Psi=\infty$, and $\Gamma=0$. Equation 4.28 presents a direct relationship of the knife edge moment with the applied load and initial imperfection, and is quoted as follows:

$$\frac{M_{pk}b}{Dt}=\frac{w_{0p}}{t}\cdot\sum_{i=1}^{2}C_i\cdot\left(\frac{\tau}{\tau_{cr}}\right)^i+\sum_{j=1}^{4}C_{j+2}\cdot\left(\frac{\tau}{\tau_{cr}}\right)^j \tag{5.1}$$

where τ_{cr} is the critical shear stress of a simply supported panel; C_k (k=1,2, ..., 6) are coefficients which are to be determined by the curve fitting of FE results, and they are expected to vary with the panel aspect ratio d/a only.

In this chapter, a parametric study is carried out to examine the non-linear elastic behaviour of plates with a straight knife edge (Fig. 5.1), with particular attention to the knife edge moment M_{pk}, due to the distributed reaction q_{pk} along the knife edge. Eqn. 5.1 is used as the basic formula for the calculation of the knife edge moment for plates subjected to pure shear and combined shear, compression and bending. As a result, design formulae for predicting the knife edge moment will be established. The finite element model and the method to convert the nodal reactions along the knife edge into the knife edge moments are described in Chapter 4. The numerical results are produced using the finite element program ABAQUS.

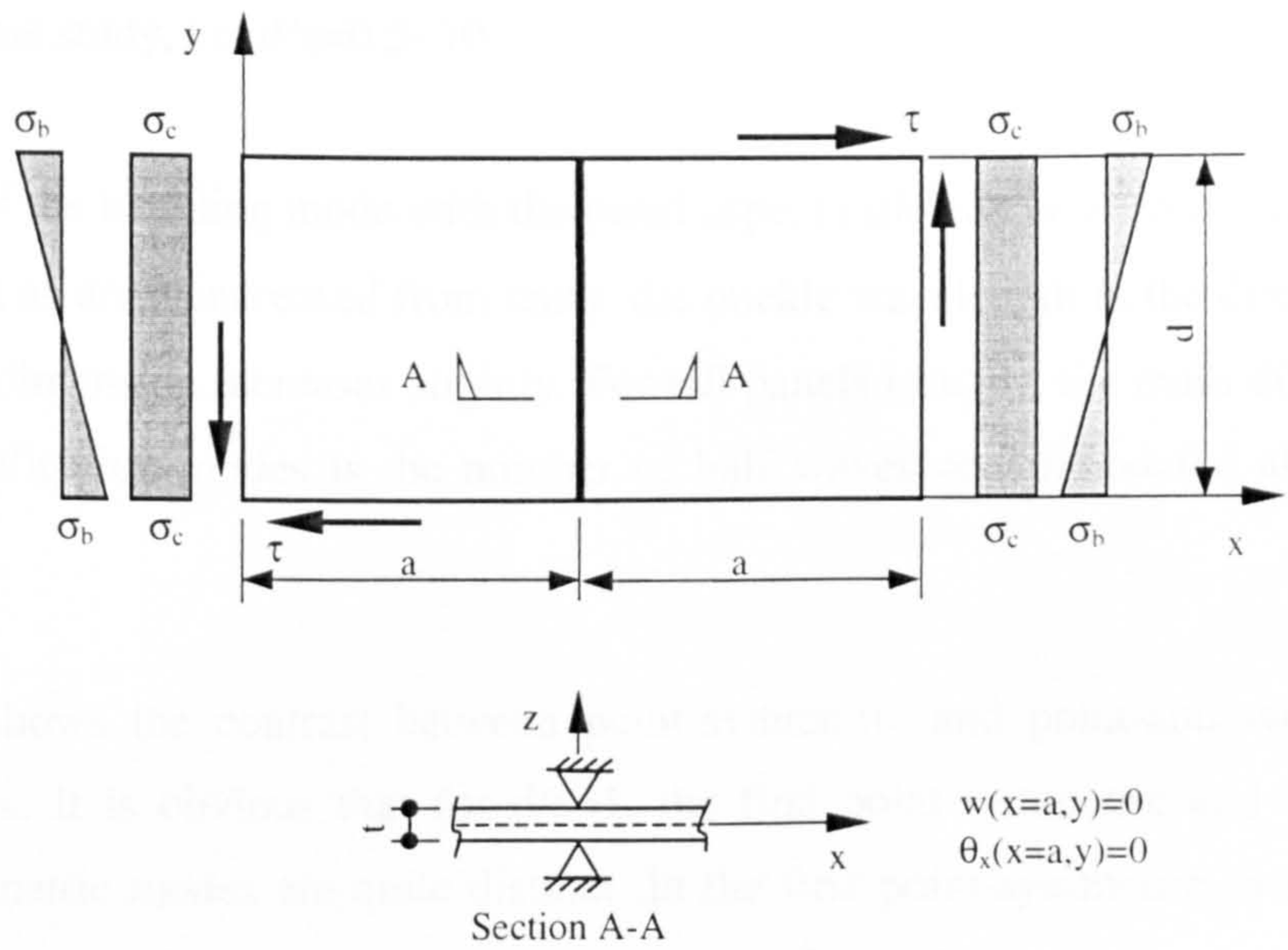


Figure 5.1 Two-panel plate with a straight knife edge, subjected to combined shear, compression and bending

5.2 PLATES SUBJECTED TO PURE SHEAR

5.2.1 Critical Buckling Behaviour

Before studying the non-linear elastic buckling behaviour of plates with a straight knife edge, critical buckling analyses are carried out using the finite element program

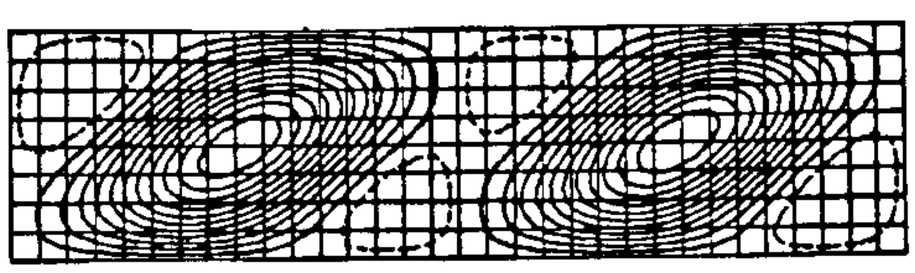
ABAQUS. The main purpose of these analyses is to find the critical buckling modes, of which the first point-symmetric modes will be used to form the initial imperfections for the non-linear buckling analyses. The numerical results of the critical buckling analysis are presented below.

5.2.1.1 Critical Buckling Modes

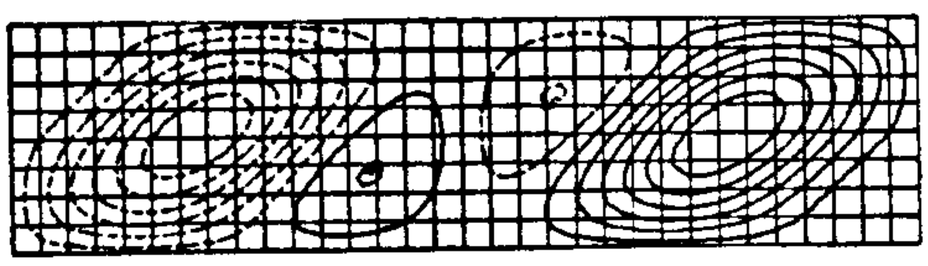
The contour plots of the first point-symmetric and first point-anti-symmetric critical buckling modes are given in Fig. 5.2, covering the range of panel aspect ratios considered in this study, i.e. d/a=0.5~10.

The variation of the buckling mode with the panel aspect ratio can be seen in Fig. 5.2. It is observed that as d/a is increased from unity, the buckle wavelength in the direction of the long panel dimension increases slightly. For tall panels (d/a≥5), the main difference in the panel deflection modes is the number of half waves accommodated along the depth of panel.

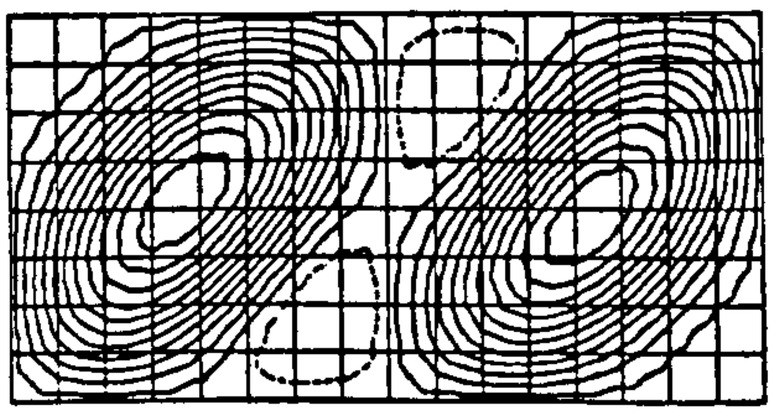
Fig. 5.2 also shows the contrast between point-symmetric and point-anti-symmetric buckling modes. It is obvious that for d/a=1, the first point-symmetric and the first point-anti-symmetric modes are quite distinct. In the first point-symmetric modes, the two panels deflect in the same direction, while in the first point-anti-symmetric mode, the two panels buckle in the opposite direction. As d/a is increased from unity the difference between the two buckling modes becomes less distinct. This is because the mode is less restricted by the boundaries, and plate lines parallel to the nodal lines buckle anti-symmetrically about the knife edge. For very tall plates, the only difference between the first point-symmetric and first point-anti-symmetric modes is the position of the buckle nodal line with respect to the centre of the plate, as can be seen for d/a≥5.



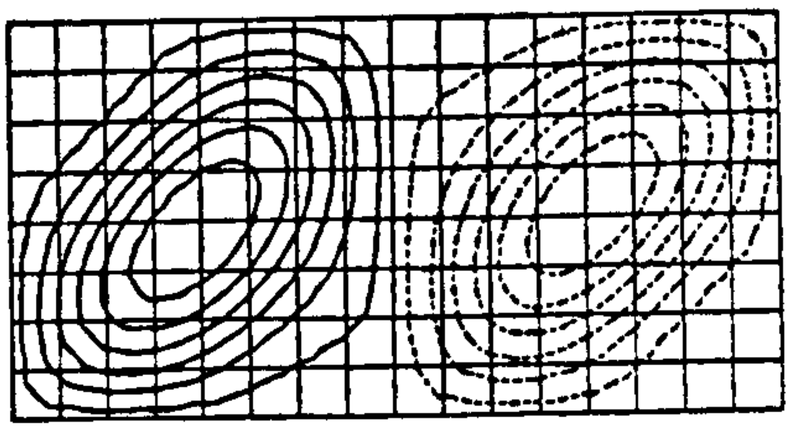
d/a=0.5, kcr=6.566



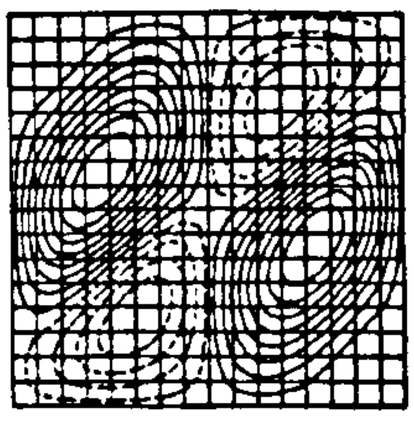
d/a=0.5, kcr=6.560



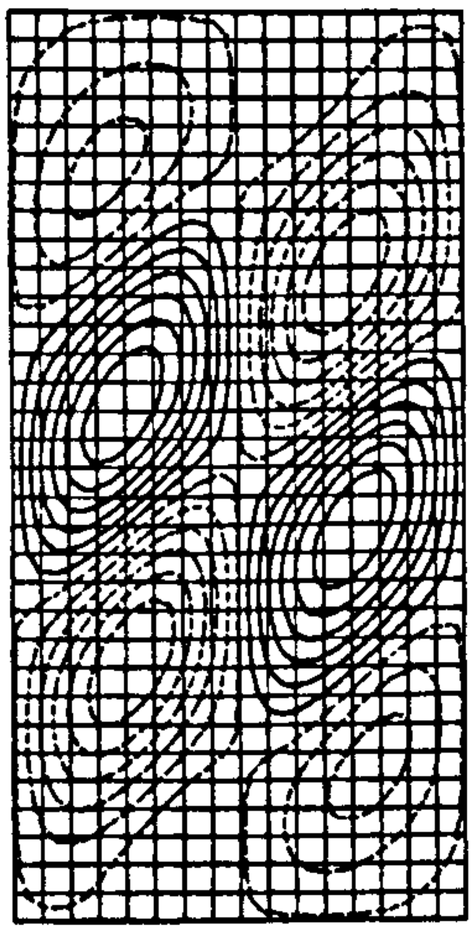
d/a=1, kcr=9.901



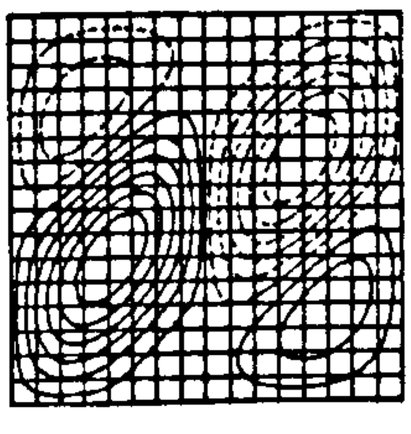
d/a=1, kcr=10.247



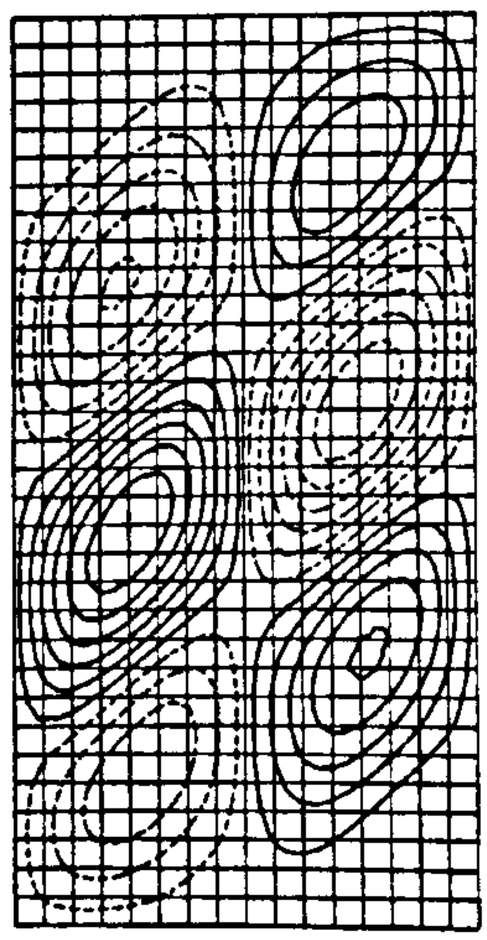
d/a=2, kcr=6.753



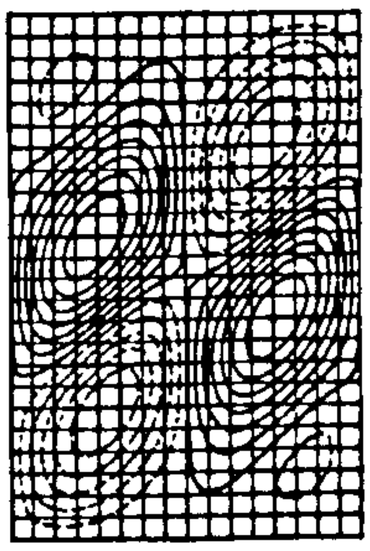
d/a=4
kcr=5.679



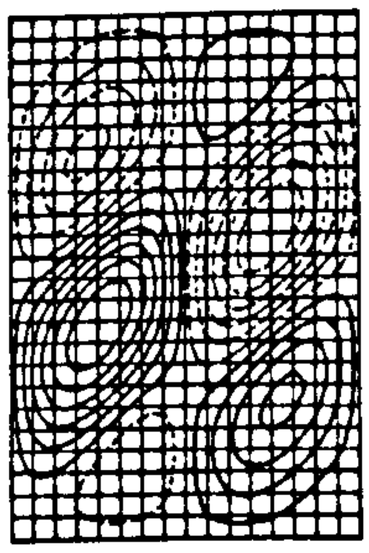
d/a=2, kcr=6.574



d/a=4
kcr=5.673



d/a=3
kcr=5.909

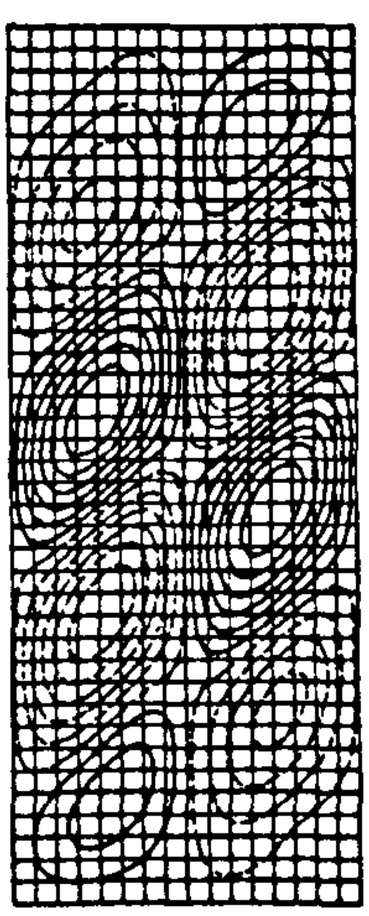


d/a=3
kcr=5.961

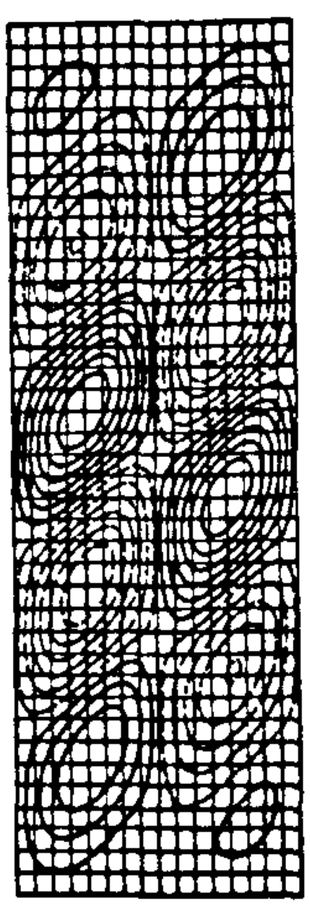
1st Point-symmetric modes

1st Point-anti-symmetric modes

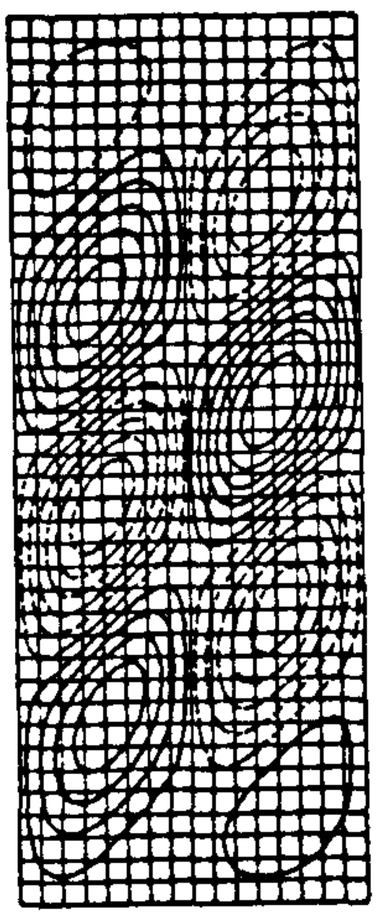
Figure 5.2 Critical buckling modes of plates with a knife edge. Pure shear



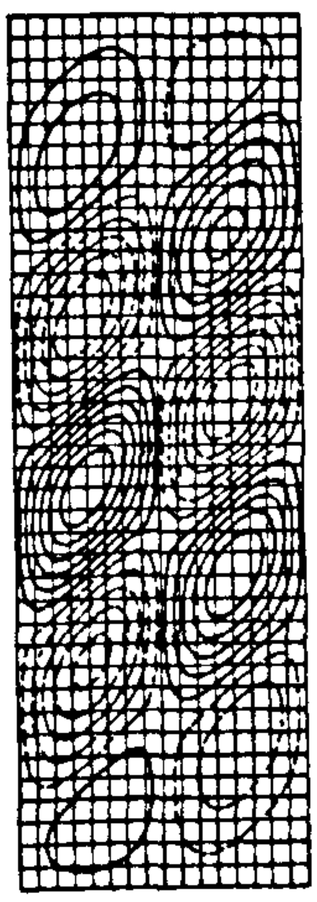
d/a=5
kcr=5.560



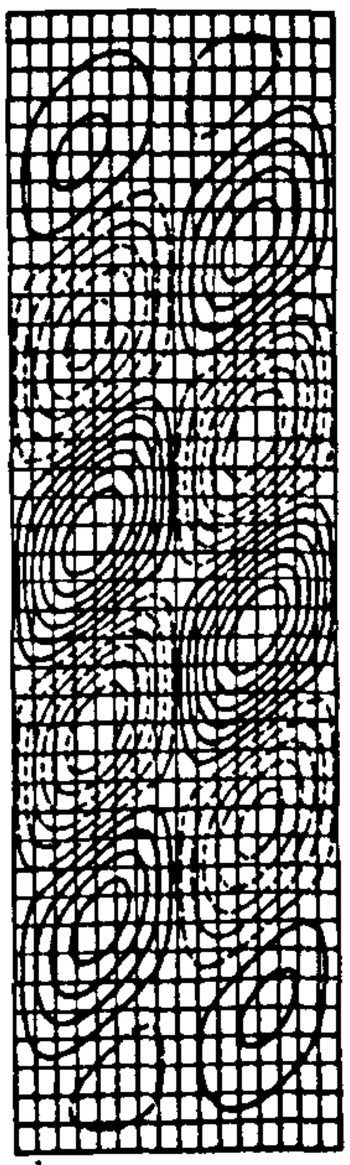
d/a=6
kcr=5.486



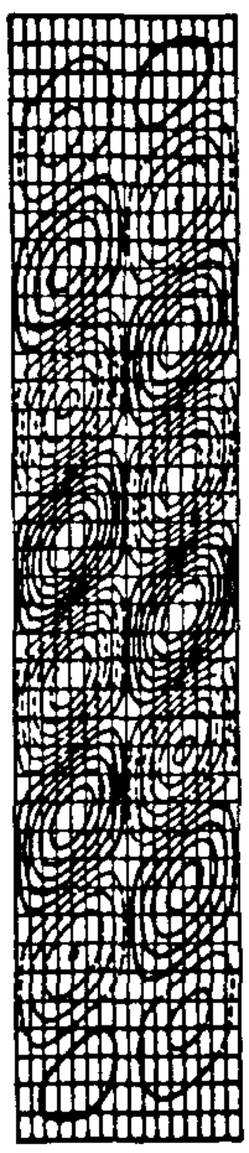
d/a=5
kcr=5.552



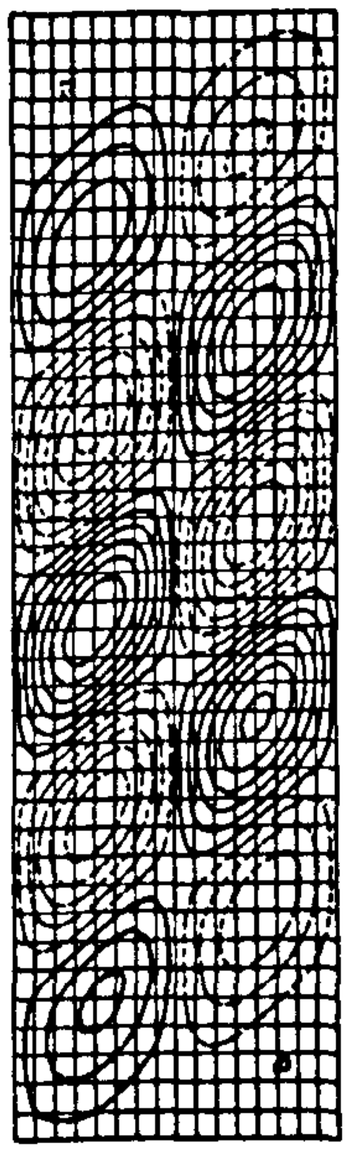
d/a=6
kcr=5.495



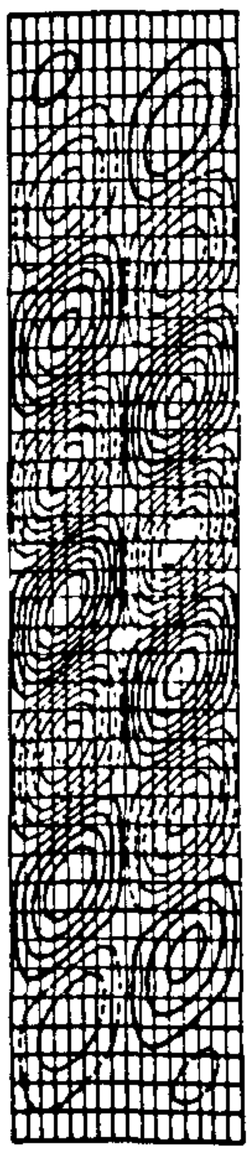
d/a=7
kcr=5.454



d/a=10
kcr=5.396



d/a=7
kcr=5.448



d/a=10
kcr=5.395

1st Point-symmetric modes

1st Point-anti-symmetric modes

Figure 5.2 (Cont.) Critical buckling modes of plates with a knife edge. Pure shear

5.2.1.2 Critical Buckling Stresses

The variation of the critical buckling stress coefficient k_{cr} with the panel aspect ratio d/a is presented in Fig. 5.3. It is apparent that the difference between the critical buckling stresses for the first point-symmetric and first point-anti-symmetric modes diminishes as d/a is away from one. This is consistent with the observation on the critical buckling modes, stated in Section 5.2.1.1.

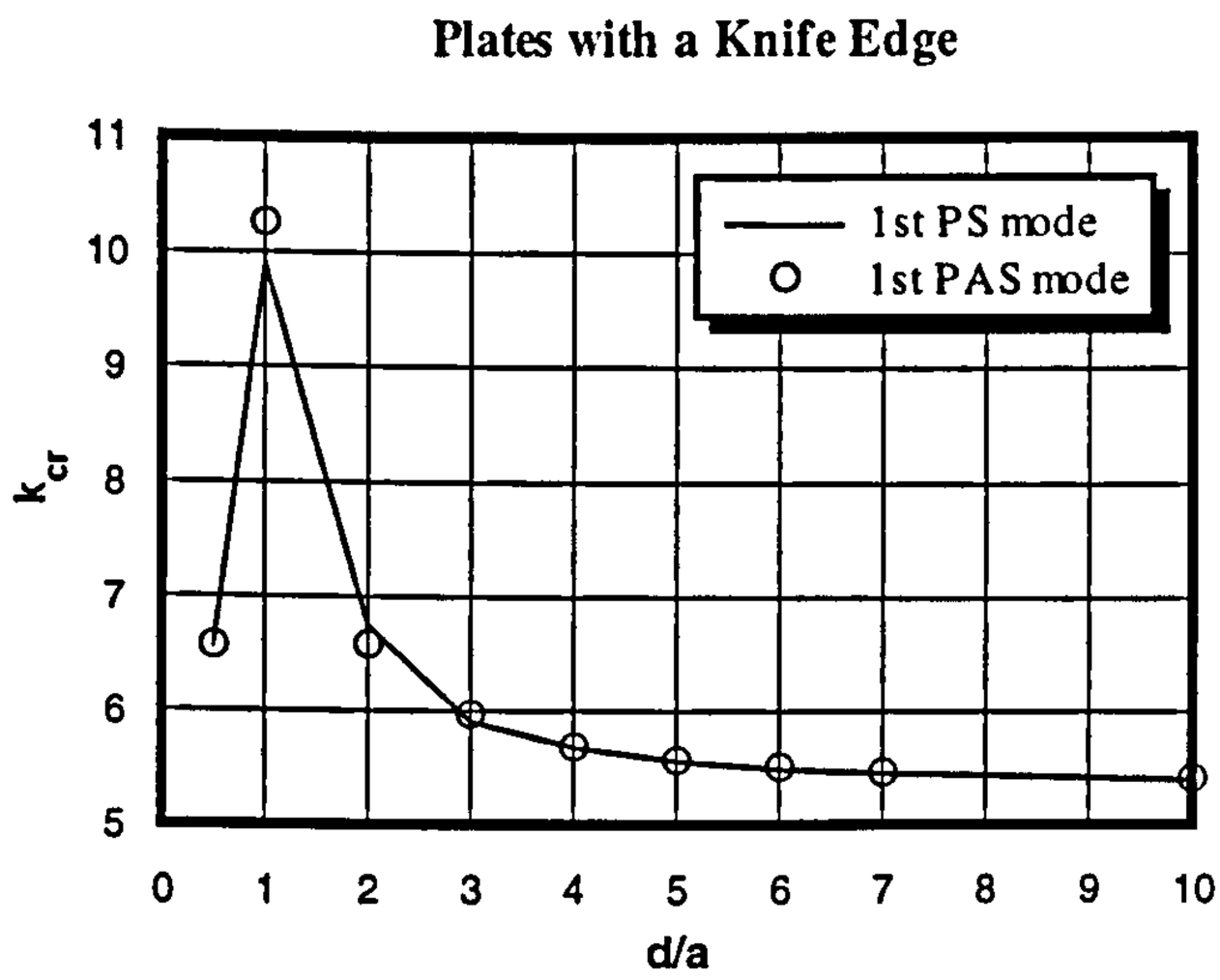


Figure 5.3 Variation in critical buckling stress coefficient k_{cr} with panel aspect ratio d/a.
Pure shear. FE results

Comparison of the contour plots of buckling modes, between plates with a knife edge and isolated simply supported panels, as presented in Fig. 4.2, demonstrates that as d/a is increased from unity, the deflection modes in the corresponding panels are quite similar. Therefore, it is expected that the lowest critical buckling stress for plates with a knife edge will be close to the simply supported panel buckling stress, which may be calculated using the following equation:

$$k_{cr} = 5.35 + 4/\alpha^2 \quad , \quad \alpha = \min\left(\frac{d}{a}, \frac{a}{d}\right) \geq 1 \tag{5.2}$$

This expectation is confirmed by the comparison in k_{cr} between the knife edge plate and the isolated simply supported panel, as illustrated in Fig. 5.4. Consequently, it is considered that the critical buckling stress for plates with a knife edge can also be

estimated using Eqn. 5.2. This conclusion also supports the formation of Eqn. 5.1, where τ_{cr} is taken as the critical shear stress of an isolated simply supported panel.

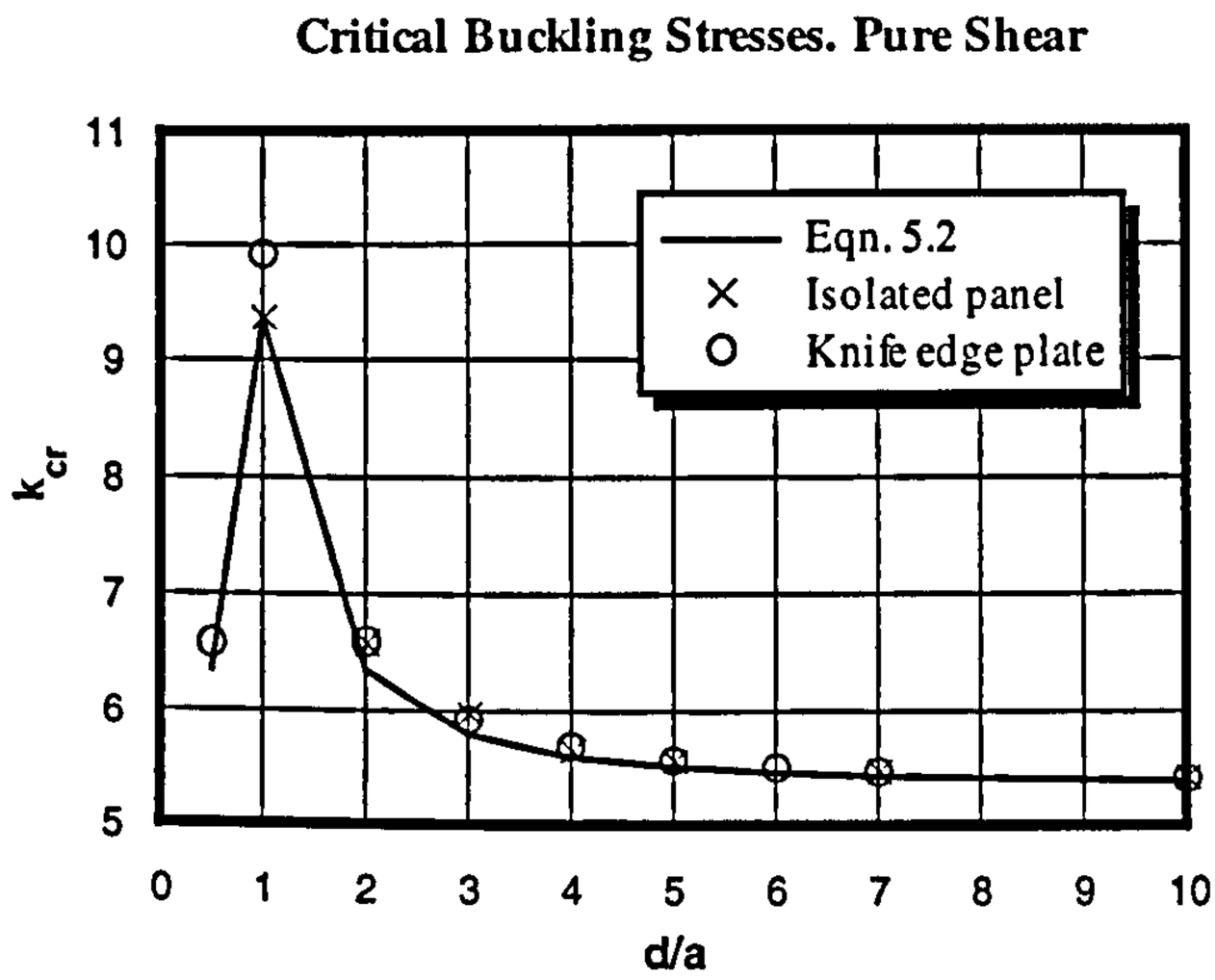


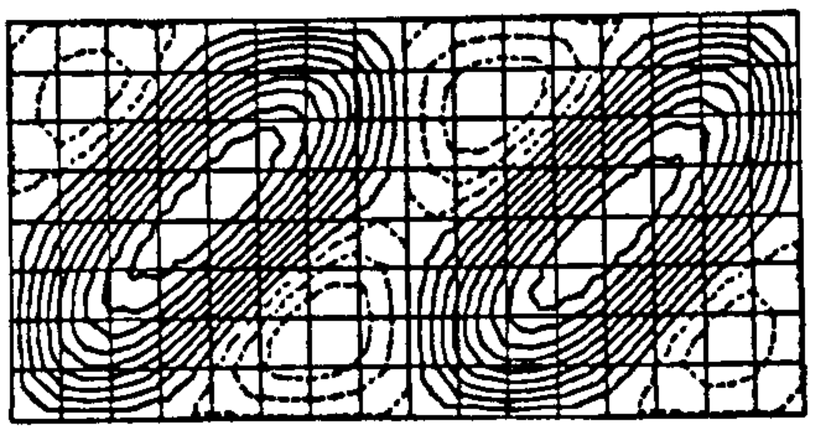
Figure 5.4 Comparison of critical buckling stress coefficients between panels and plates with a knife edge. 1st critical buckling modes. FE results. Equation for kcr: $kcr=5.35+4/\alpha^2$, $\alpha \geq 1$

5.2.2 Non-Linear Elastic Buckling Behaviour

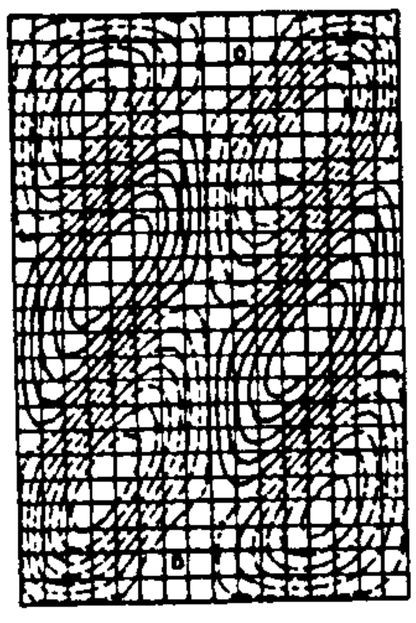
This section presents the numerical results of a non-linear elastic parametric study for plates with an intermediate straight knife edge, subjected to pure shear, as shown in Fig. 4.1. In this study, panel aspect ratios d/a from 0.5 to 10 are considered, and the non-dimensional magnitude of panel imperfection, w_{0p}/t, varies from 0.485 to 1.818, which corresponds to a range of panel slenderness ratio b/t=80 to 300 when w_{0p} is taken as code specified values with $\sigma_{0p}=355N/mm^2$. Initial panel imperfection is affine to the first point-symmetric buckling mode. For tall panels, other imperfection modes are also considered, and this is indicated in the relevant sections.

5.2.2.1 Deflection Modes

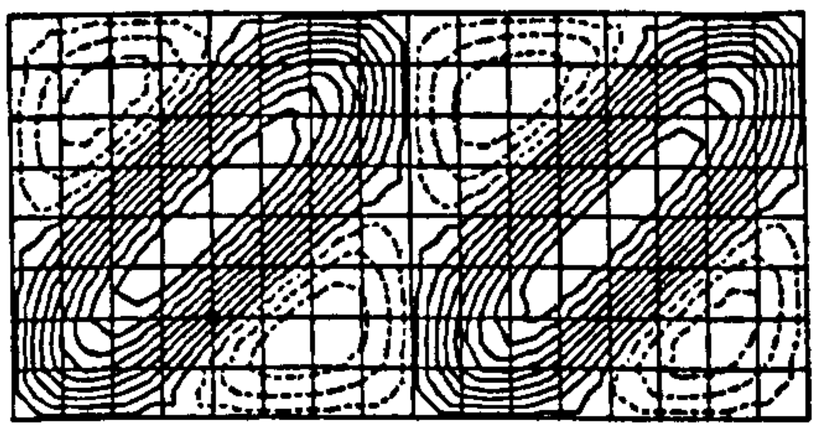
The contour diagrams of deflection mode at different load levels for the cases of d/a=1 and 3 are shown in Fig.5.5. It is observed that as the applied shear stresses are increased,



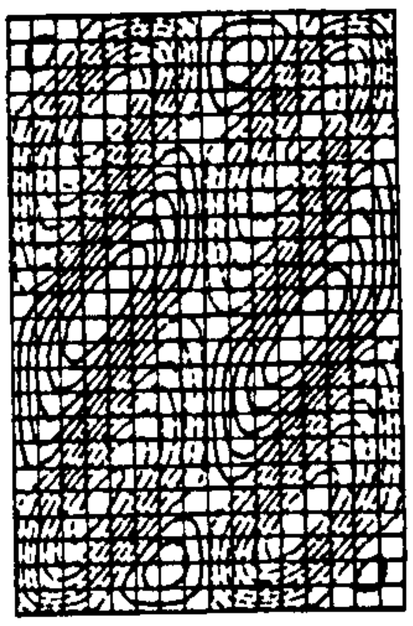
$\tau/\tau_{cr}=1.0$



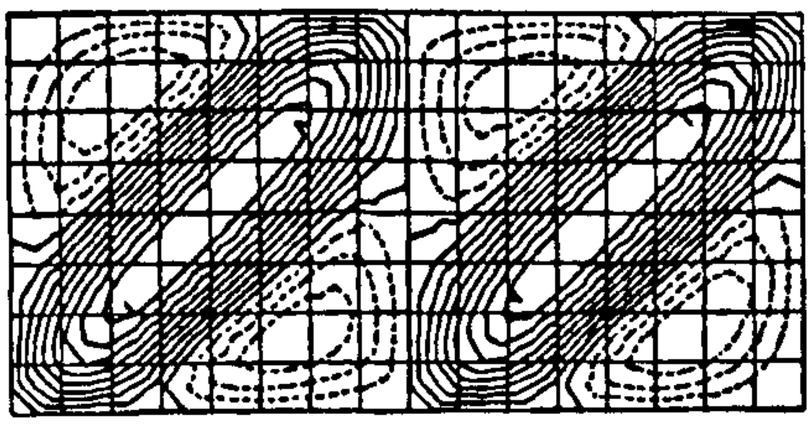
$\tau/\tau_{cr}=1.0$



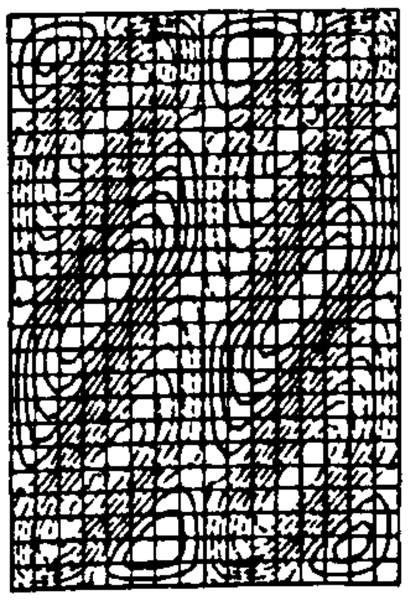
$\tau/\tau_{cr}=2.0$



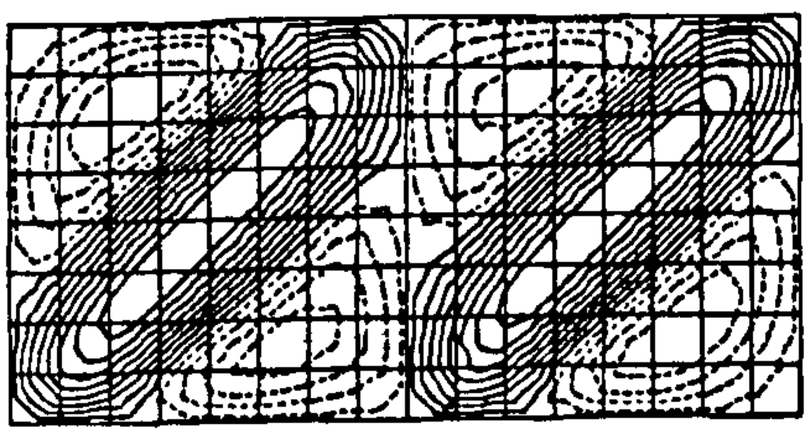
$\tau/\tau_{cr}=2.0$



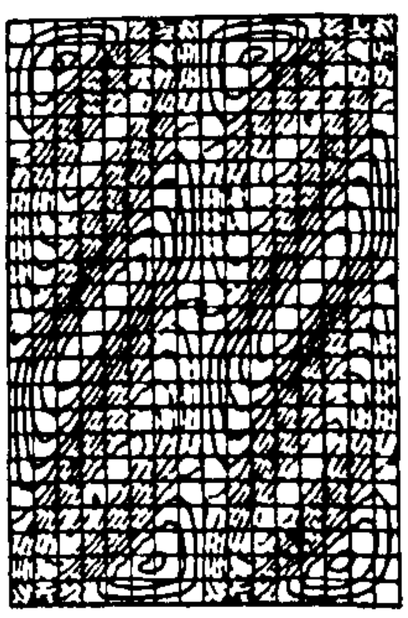
$\tau/\tau_{cr}=3.0$



$\tau/\tau_{cr}=3.0$



$\tau/\tau_{cr}=3.7$

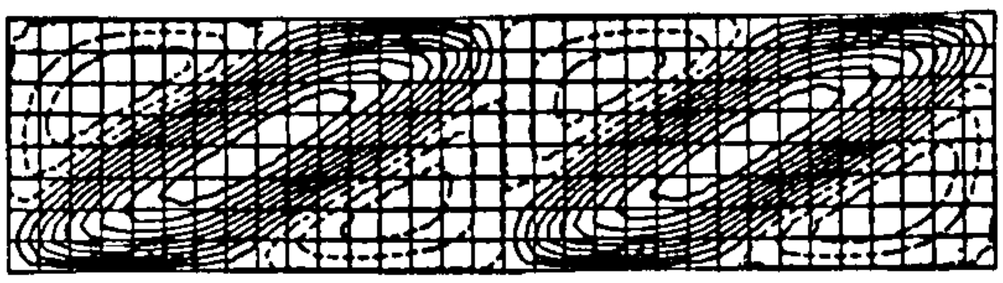


$\tau/\tau_{cr}=4.0$

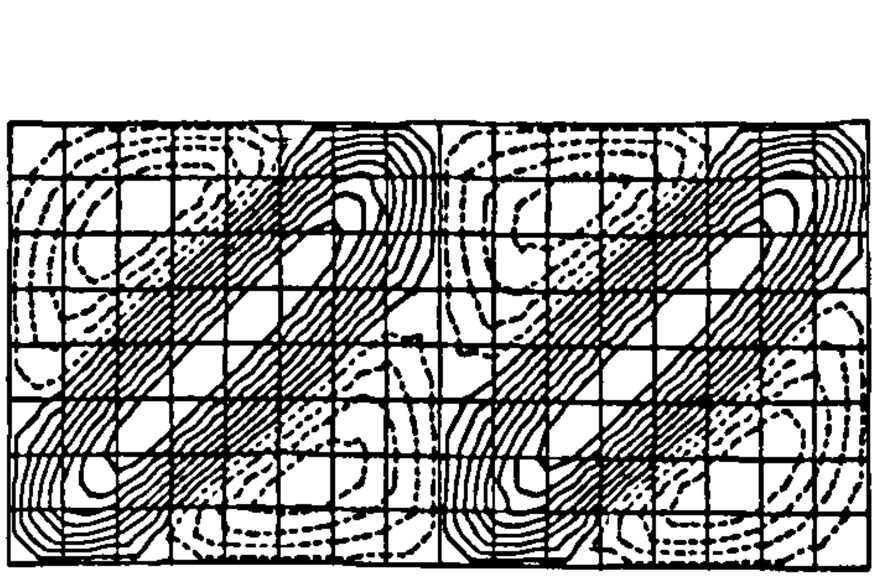
(a) d/a=1

(b) d/a=3

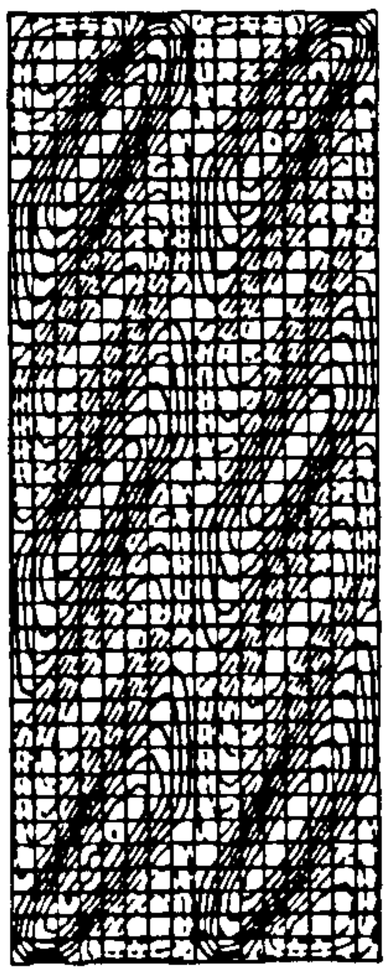
Figure 5.5 Load-deflection history of plates with a straight knife edge. Non-linear elastic FE results. Pure shear. Point-symmetric panel imperfections, $w_{0p}/t=1.091$



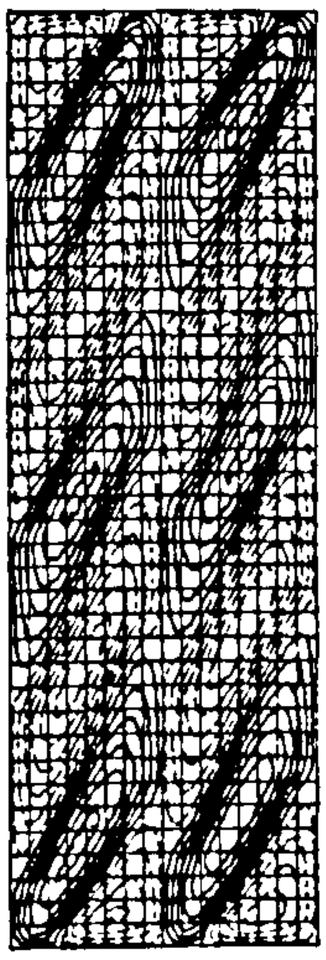
d/a=0.5



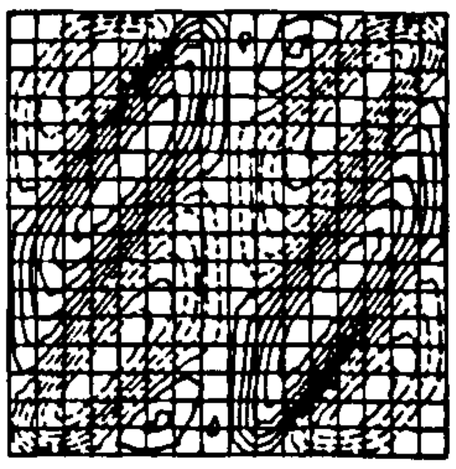
d/a=1



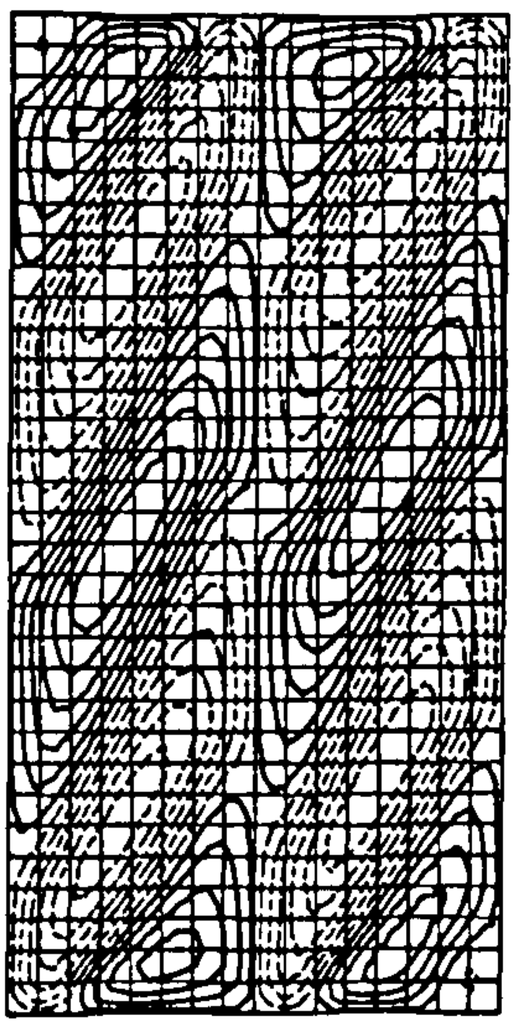
d/a=5



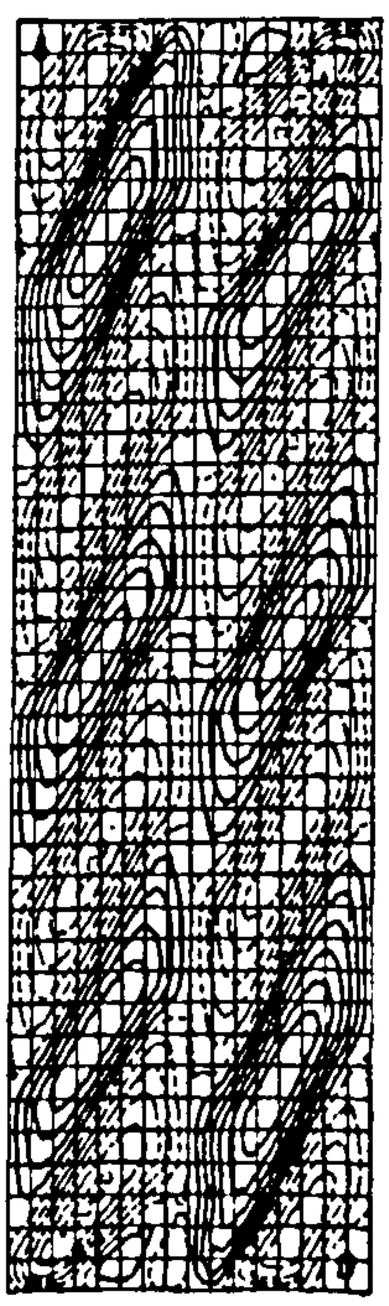
d/a=6



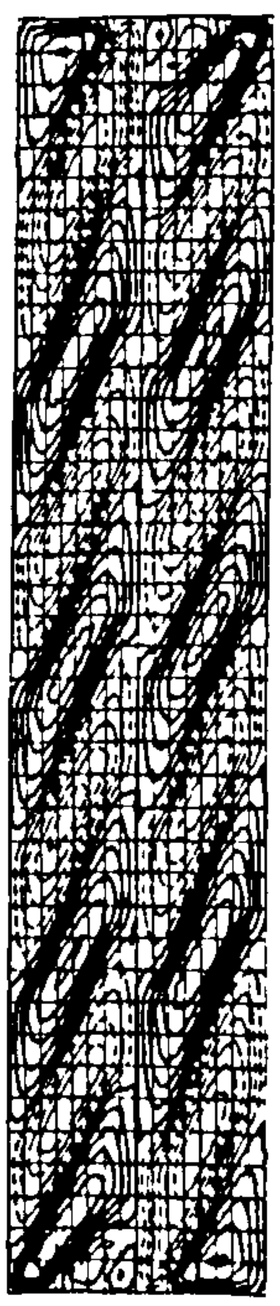
d/a=2



d/a=4



d/a=7



d/a=10



d/a=3

Figure 5.6 Deflection modes of plates with a knife edge. Non-linear elastic FE results.
Pure shear. Point-symmetric panel imperfections, $w_{0p}/t=1.091$

the deflected profiles change from the initial mode (i.e., the first point-symmetric buckling mode, see Fig. 5.2) to the preferred well-developed (sharper) mode. It is also noted that for d/a=1, the main buckles keep in the diagonal direction, with a wavelength, taken as perpendicular to the centre of the nodal line, decreasing as the load is increased. For the tall plates, both the location and the number of buckles are found to change with the applied shear stresses. The reason for the change in mode shape is the membrane effects developed in the plate.

In Fig. 5.6, contour plots of out-of-plane deflection are presented for each aspect ratio considered. By comparing the modes shown in Figs. 5.2 and 5.6, the differences between the critical buckling and elastic large-deflection modes can be observed.

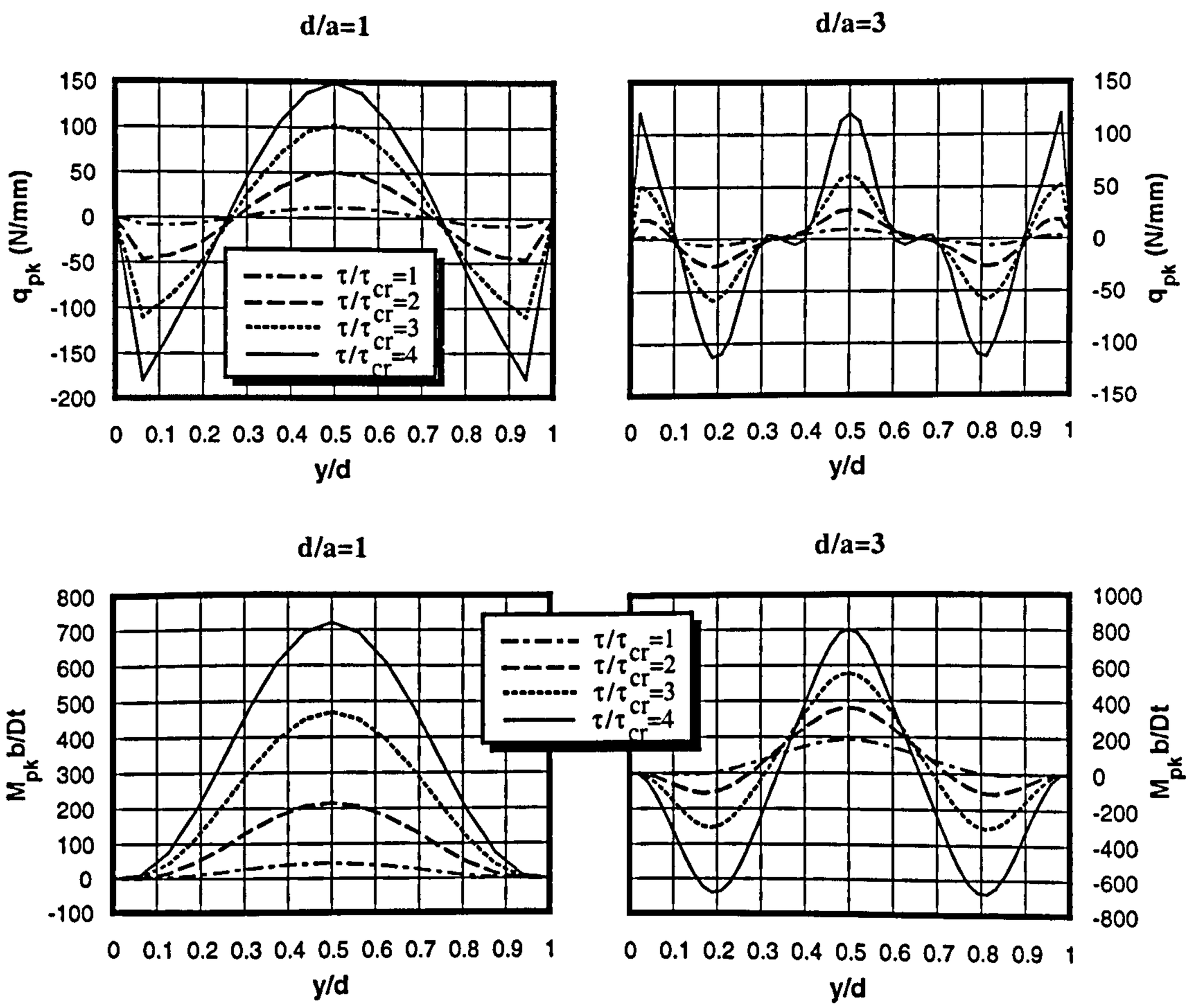


Figure 5.7 Variation in the distributions of q_{pk} and M_{pk} with the applied shear stresses. Plates with a straight knife edge. w_{0p}/t=1.091. Non-linear elastic FE results. Pure shear

5.2.2.2 Distribution of q_{pk} and M_{pk}

It has been found in Section 5.2.2.1 that the deflection modes change with the applied load. On account of the fact that the lateral reaction along the knife edge, q_{pk}, is related to the panel deflections, it is expected that the distribution of q_{pk} will also vary with the applied stresses. This is confirmed by the elastic large-deflection finite element analysis results for the distributions of q_{pk} and M_{pk} for d/a=1 and 3, as presented in Fig. 5.7 (p.5.10).

In order to illustrate how the distributions of q_{pk} and M_{pk} vary with the panel aspect ratio, the values of q_{pk} and M_{pk} along the knife edge at $\tau/\tau_{cr}\approx 4$ for $w_{0p}/t=1.091$ are presented in Figs. 5.8 and 5.9 (pp.170-171), respectively. The maximum amplitudes of q_{pk} and M_{pk} are listed in Table 5.1.

Table 5.1 Maximum values of q_{pk} and M_{pk}. $w_{0p}/t=1.091$. Pure shear

d/a	τ/τ_{cr}	τ (N/mm^2)	q_{pk} (N/mm)	$M_{pk}b/Dt$
0.5	3.16	118.5	89.3	580.8
1	3.75	200.0	178.9	721.3
2	4.09	153.4	117.2	1958.2
3	4.09	136.6	120.7	802.1
4	3.95	128.1	107.5	1017.6
5	3.90	123.4	117.9	830.3
6	3.98	124.9	116.8	1049.8
7	4.05	126.0	115.1	2836.5
10	3.96	122.2	109.2	3266.7

It is found in Table 5.1 that apart from d/a=1, the amplitude of q_{pk} does not vary significantly with the panel aspect ratio d/a, and seems to depend mainly on the applied shear stress τ. On the other hand, it can be seen in Fig. 4.9 that the panel deflection at

$\tau/\tau_{cr}\approx4$ varies with the panel aspect ratio d/a, with $w_p/t\approx6\sim8$. Therefore, it may be more reasonable to establish a direct relationship between the knife edge force q_{pk}, and hence the knife edge moment M_{pk}, and the applied shear stress, rather than to calculate q_{pk} and M_{pk} from the panel deflection w_p/t. Such a direct relationship is given by Eqn. 5.1, and will be used to present design formulae for calculating the knife edge moment M_{pk}.

It is noted that due to the variation in the distribution of q_{pk}, both the distribution and amplitude of the resulting knife edge bending moment M_{pk} vary significantly with the aspect ratio d/a. For the purpose of stiffener design, only the maximum magnitudes of the knife edge bending moment M_{pk} are considered.

For the cases of d/a=10, it is found that the distribution of q_{pk} is sensitive to the magnitude and mode pattern of the initial panel imperfection, w_{0p}/t. As a result, M_{pk} takes two different types of distribution, as shown in Fig. 5.10. When the initial panel imperfection is in the form of the first point-symmetric critical buckling mode (Fig. 5.11a), it is observed that for $w_{0p}/t=0.485$ and 0.727, the distribution curves are similar to those for d/a=6, while for $w_{0p}/t=1.091$ to 1.818, the distribution curves are similar to those for d/a=7. The reason for the variation in the distribution of q_{pk} is because for d/a=10, the panels took different deflection shapes for the different imperfection magnitudes, as can be seen in Figs. 5.11.

It can be seen that the deflection mode for $w_{0p}/t=1.091$ (Fig. 5.11c) is more close to the initial imperfection mode imposed (Fig. 5.11a) than the mode for $w_{0p}/t=0.485$ (Fig. 5.11b). This is because for a greater imperfection magnitude, it is more difficult for the deflection mode to change from the initial shape.

To further demonstrate the sensitivity of the deflection mode to the initial imperfection for such tall plates, non-linear elastic buckling analyses were carried out, by adopting an initial imperfection in the form of the non-linear elastic deflection mode obtained for $w_{0p}/t=0.485$ (Fig. 5.11b), with a normalised magnitude of $w_{0p}/t=1.091$ and 1.818, respectively. As shown in Fig. 5.11d, it is found that the deflection modes for these greater imperfections stay in the same form of the initial mode, namely, Fig. 5.11b.

Also, it is shown in Fig. 5.10 that the distributions of q_{pk} and M_{pk} associated with such deflection modes are almost coincident with the distribution curves found for w_{0p}/t=0.485, for which a very similar deflection mode is obtained. This confirms that the variations in the distributions of q_{pk} and M_{pk} for d/a=10 are due to the differences in the deflection modes, and the resulting differences in the magnitudes of M_{pk} will be discussed in the next section.

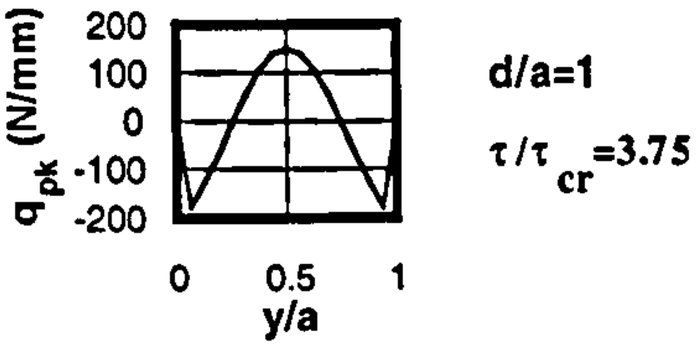
A similar analysis was conducted for d/a=7. As shown in Fig. 5.12, when the second point-symmetric (PS) mode is used as the initial imperfection mode, the distribution of M_{pk} is close to those for d/a=3~6 (Fig. 5.9), which are different from the distribution curve for d/a=7 when the initial mode is in the form of the first PS mode (Fig. 5.9).

5.2.2.3 Magnitude of Bending Moment in the Knife Edge, M_{pk}

In this section, the relationship between the magnitudes of non-dimensional knife edge moment $M_{pk}b/Dt$ and applied shear stresses are represented in the form of Eqn. 5.1. The coefficients C_k (k=1, 2, ..., 6) in Eqn. 5.1 are determined for each aspect ratio, respectively, by the curve fitting of the non-linear elastic finite element results using the least squares method. The values of C_k obtained are listed in Table 5.2.

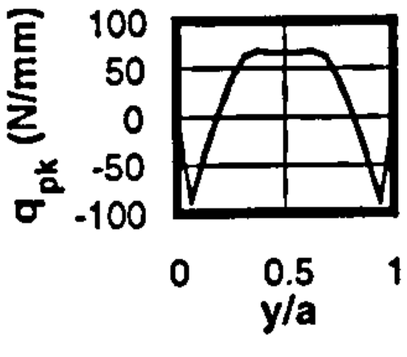
Table 5.2 Coefficients C_k (k=1,2, ..., 6) for Mpk, Eqn. 5.1

d/a	C_1	C_2	C_3	C_4	C_5	C_6
0.5	21.64	-4.065	-1.060	-24.13	51.52	-8.341
1.0	29.71	-0.524	-6.960	4.962	21.37	-2.865
2.0	83.62	-16.59	-14.03	19.70	54.99	-7.676
3.0	82.78	-3.654	-19.32	106.9	-31.72	3.433
4.0	53.05	6.702	-10.12	69.30	-0.422	-1.474
5.0	56.94	-0.939	-15.81	114.9	-37.44	4.334
6.0	12.43	15.21	13.94	-41.28	41.28	-5.124
7.0	24.70	17.04	11.12	16.71	80.03	-12.18



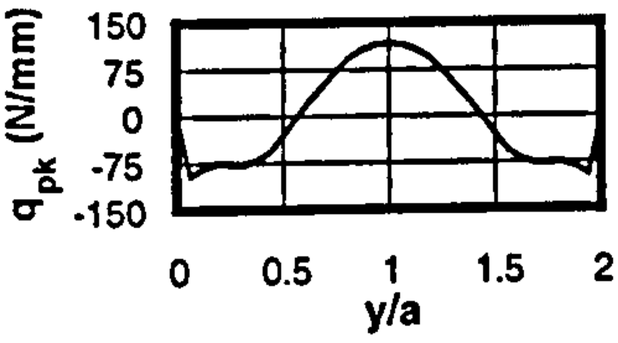
d/a=1

τ/τ_{cr}=3.75



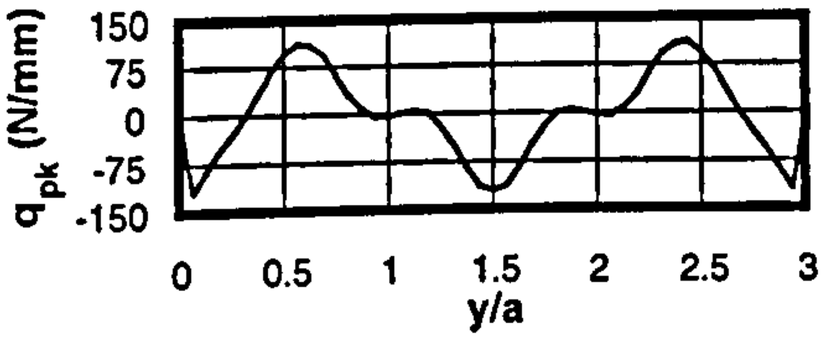
d/a=0.5

τ/τ_{cr}=3.16



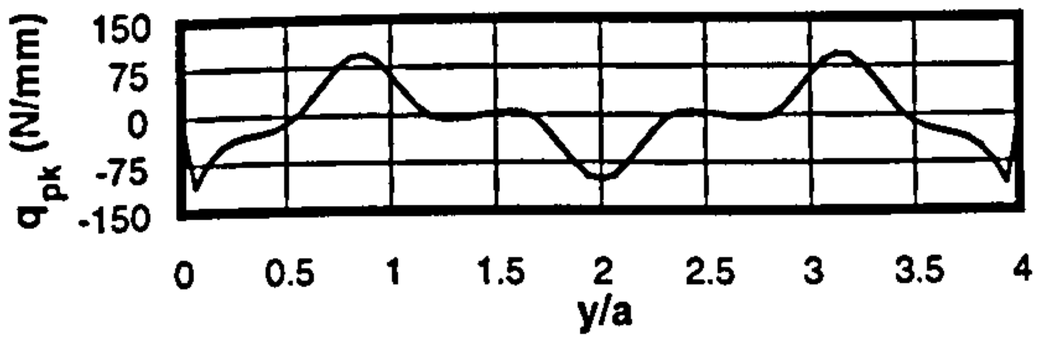
d/a=2

τ/τ_{cr}=4.09



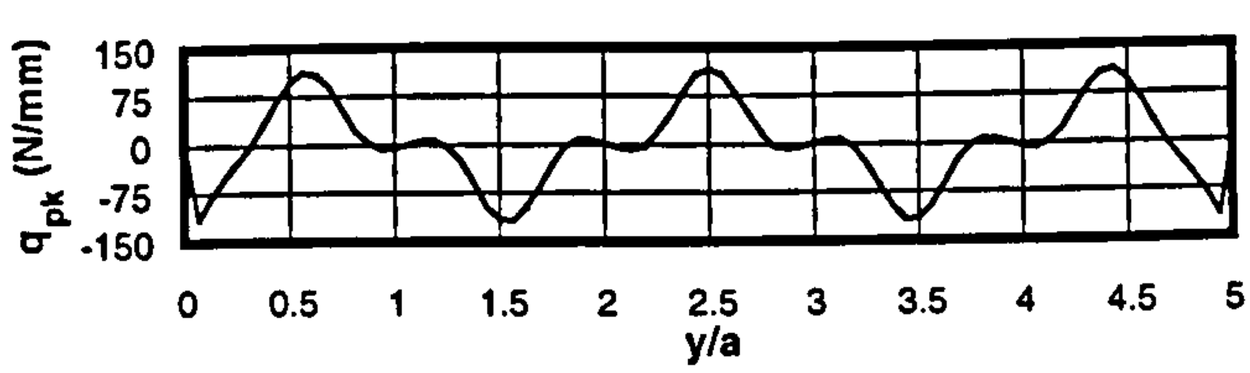
d/a=3

τ/τ_{cr}=4.09



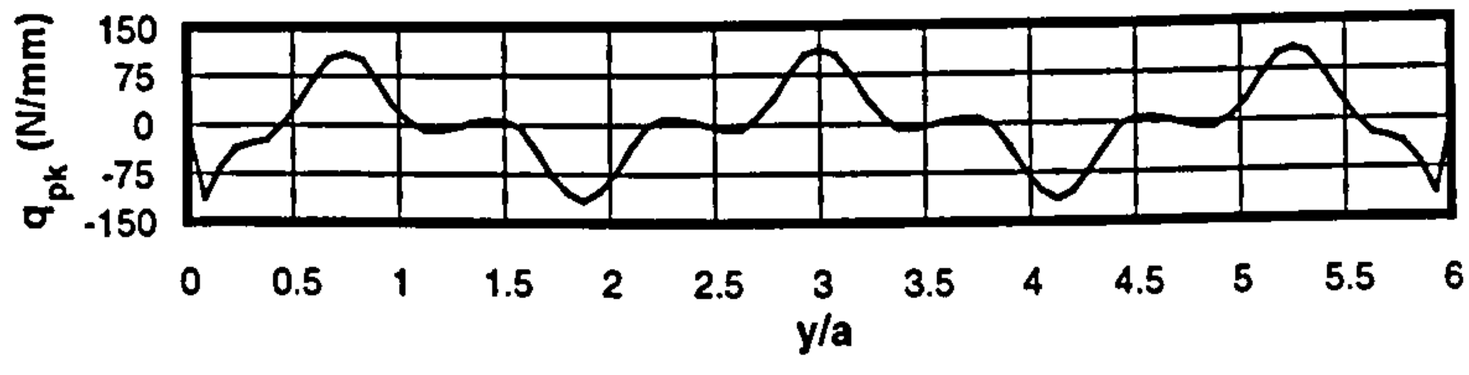
d/a=4

τ/τ_{cr}=3.95



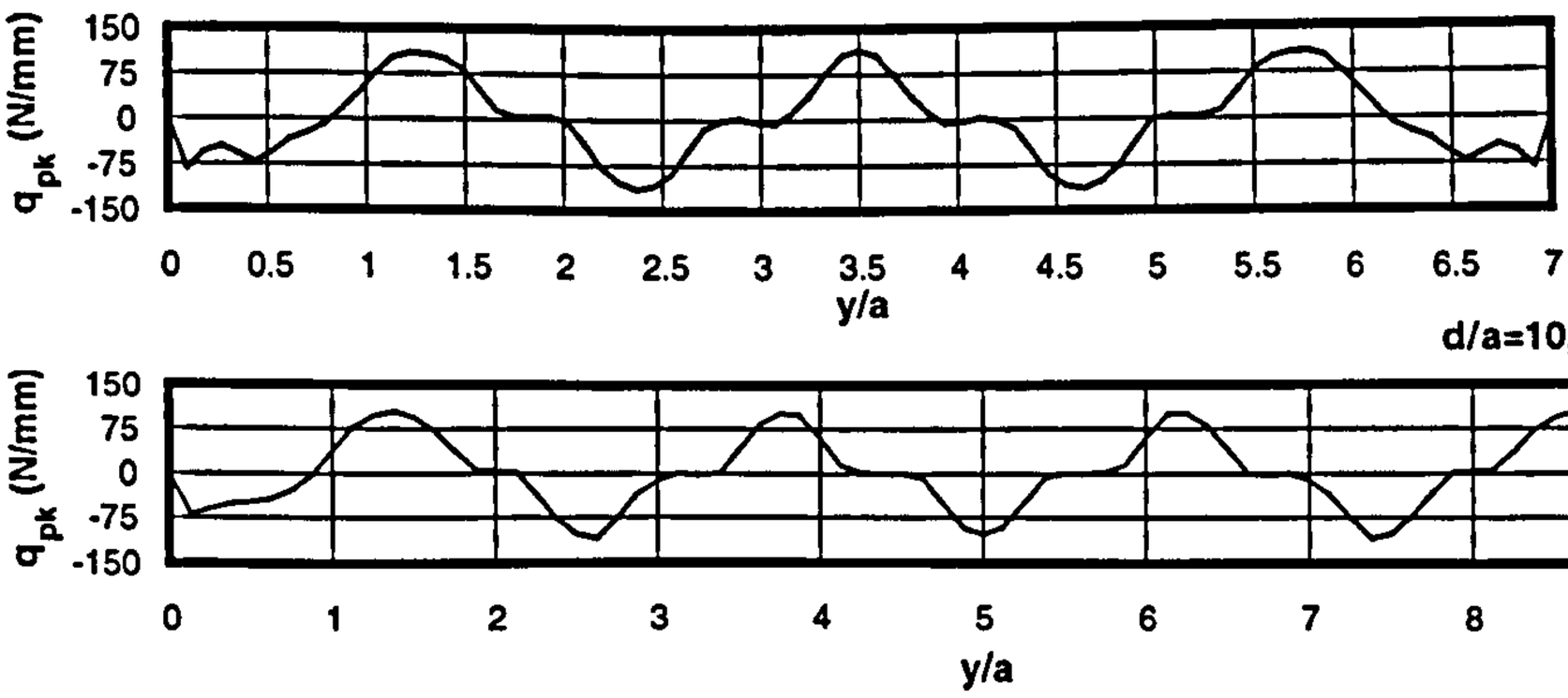
d/a=5

τ/τ_{cr}=3.90



d/a=6

τ/τ_{cr}=3.98

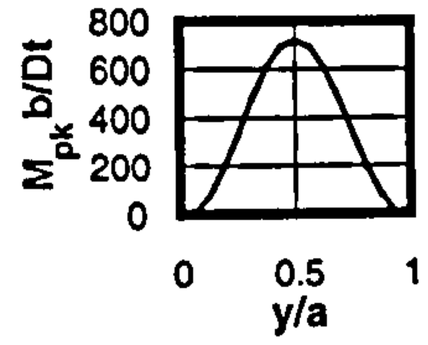


d/a=7

τ/τ_{cr}=4.05

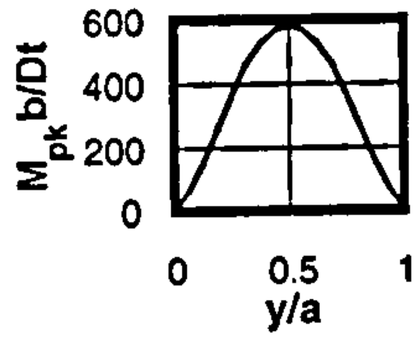
Figure 5.8 Distribution of q_{pk} along the knife edge for d/a=0.5~10, w_{0p}/t=1.091.

Plates with a straight knife edge. Non-linear elastic FE results. Pure shear



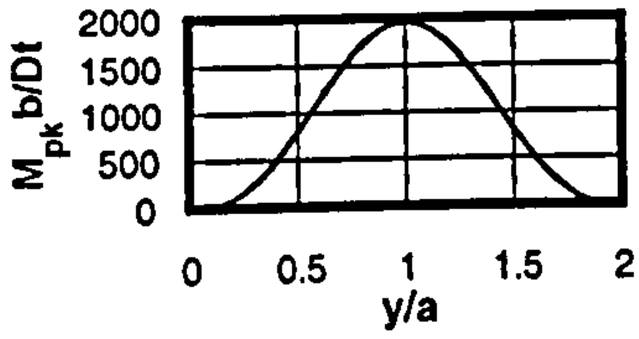
d/a=1

τ/τ_{cr}=3.75



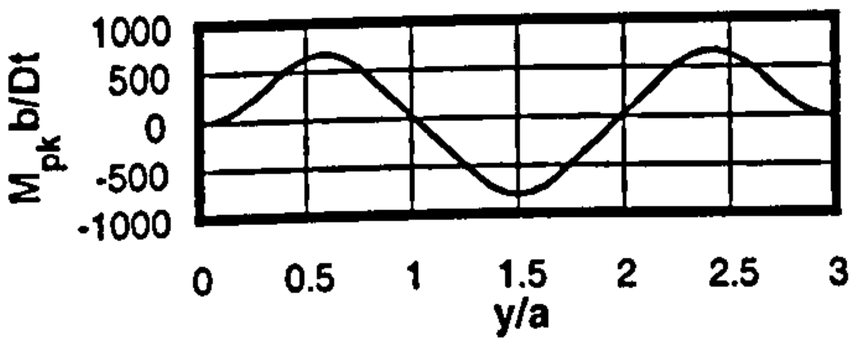
d/a=0.5

τ/τ_{cr}=3.16



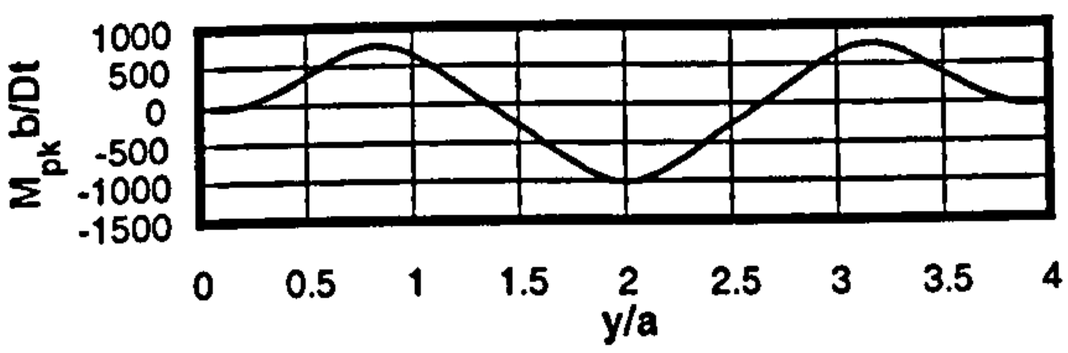
d/a=2

τ/τ_{cr}=4.09



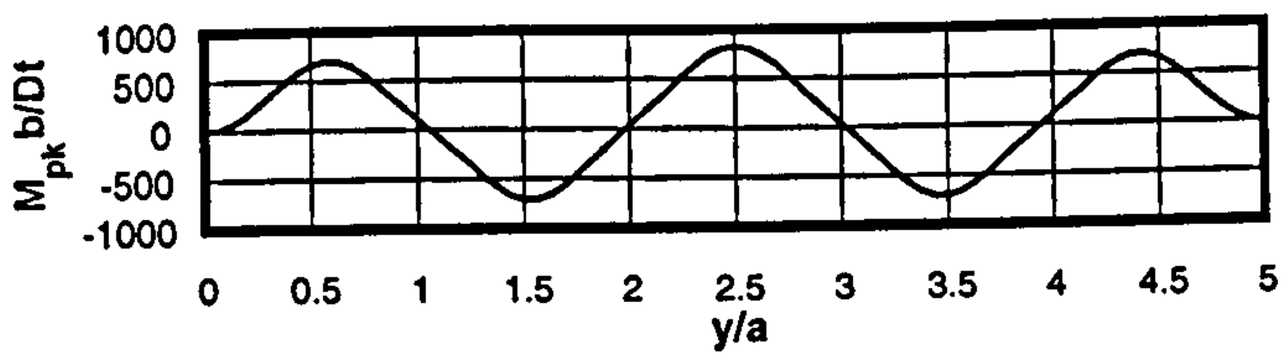
d/a=3

τ/τ_{cr}=4.09



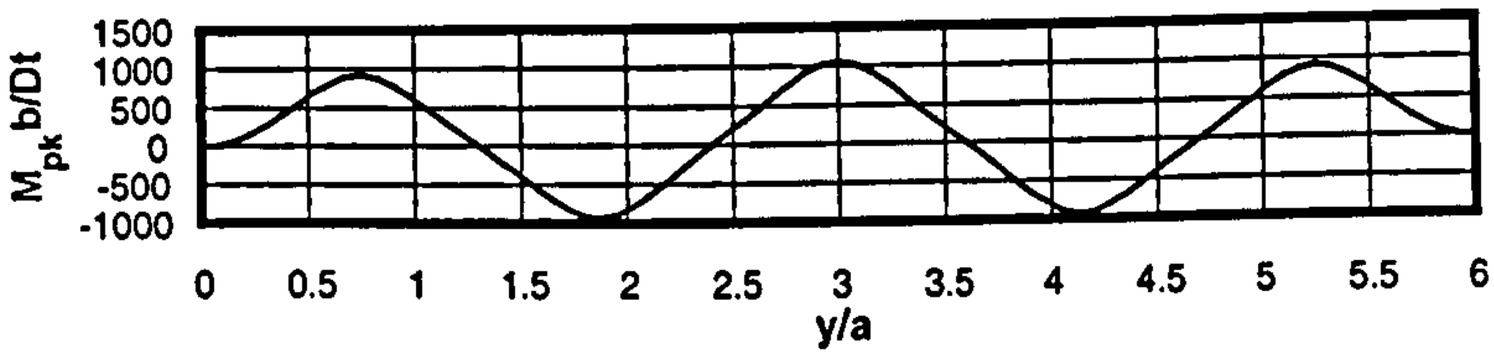
d/a=4

τ/τ_{cr}=3.95



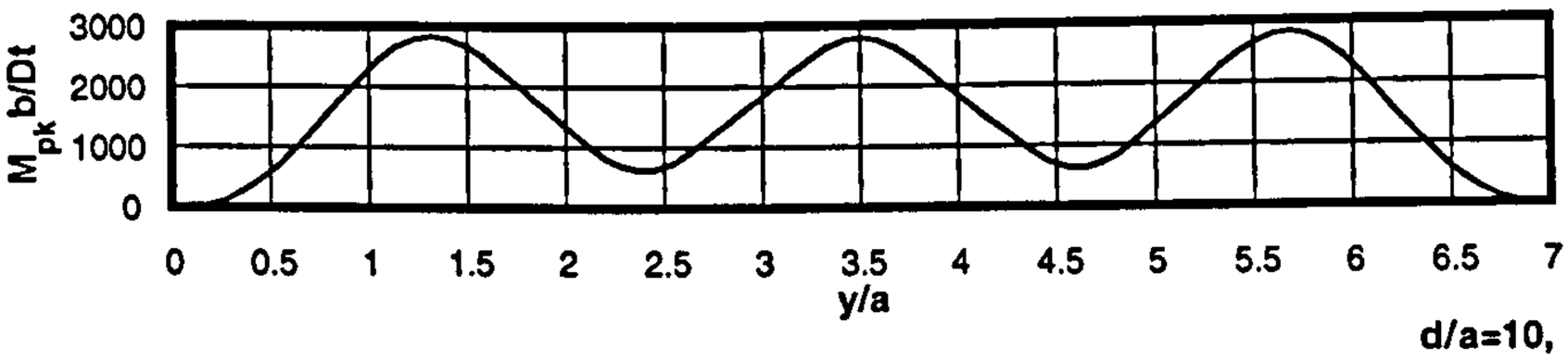
d/a=5

τ/τ_{cr}=3.90



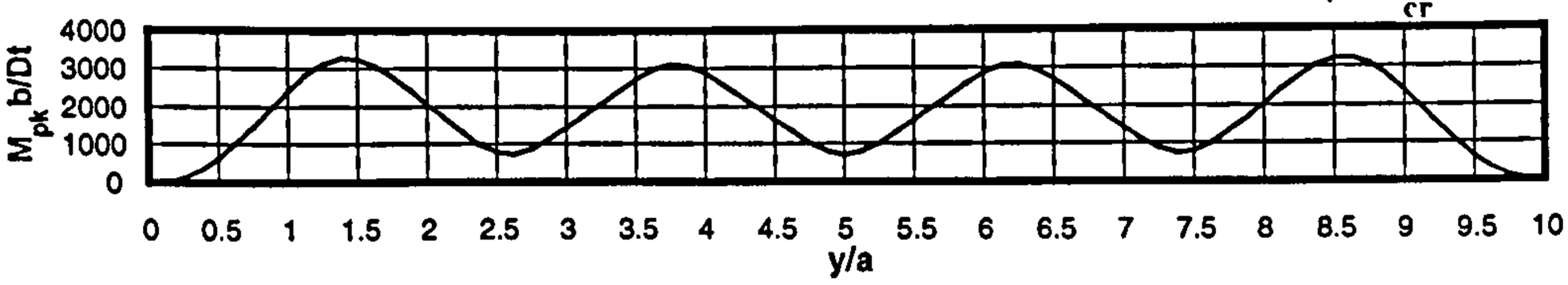
d/a=6

τ/τ_{cr}=3.98



d/a=7

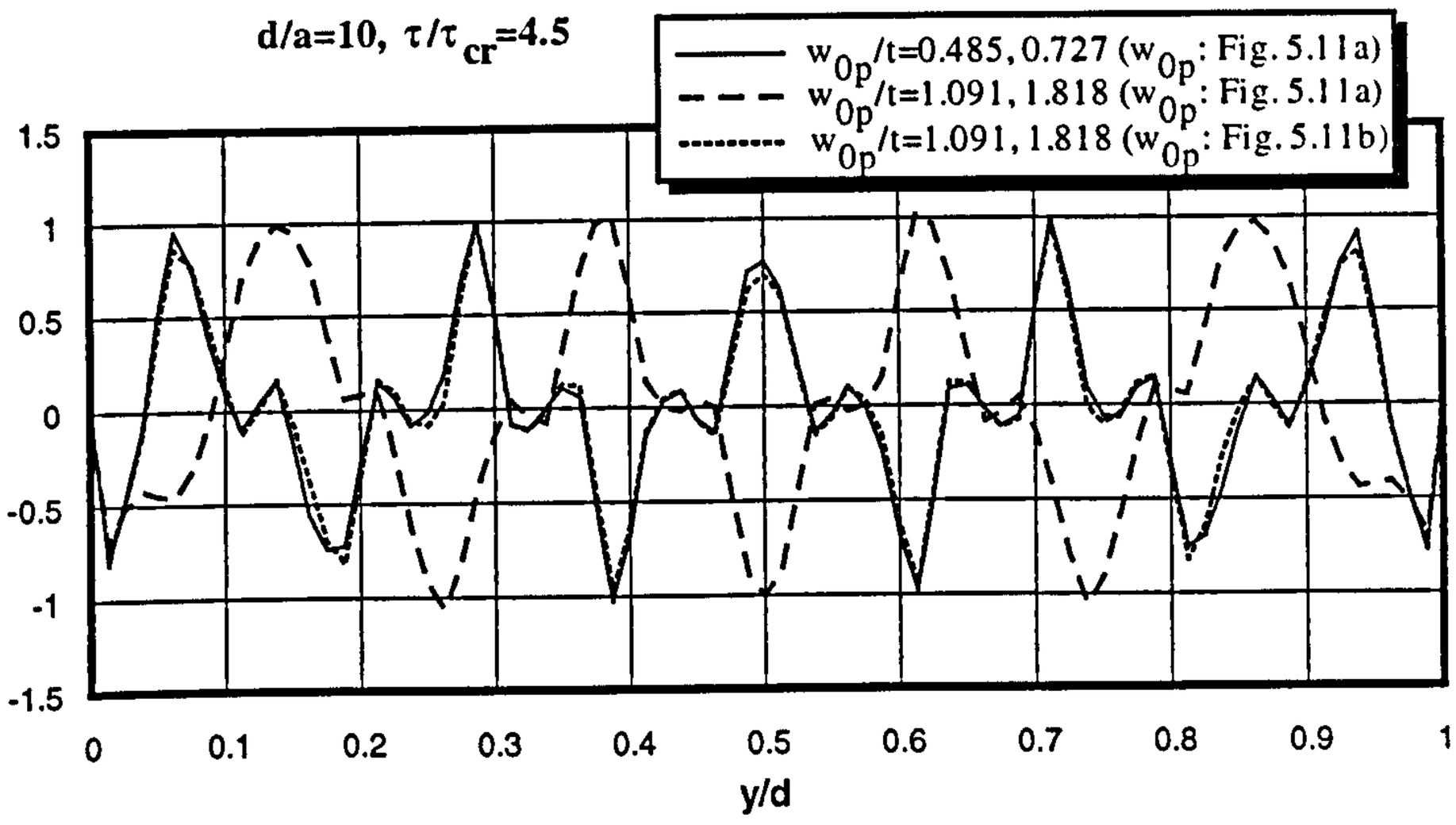
τ/τ_{cr}=4.05



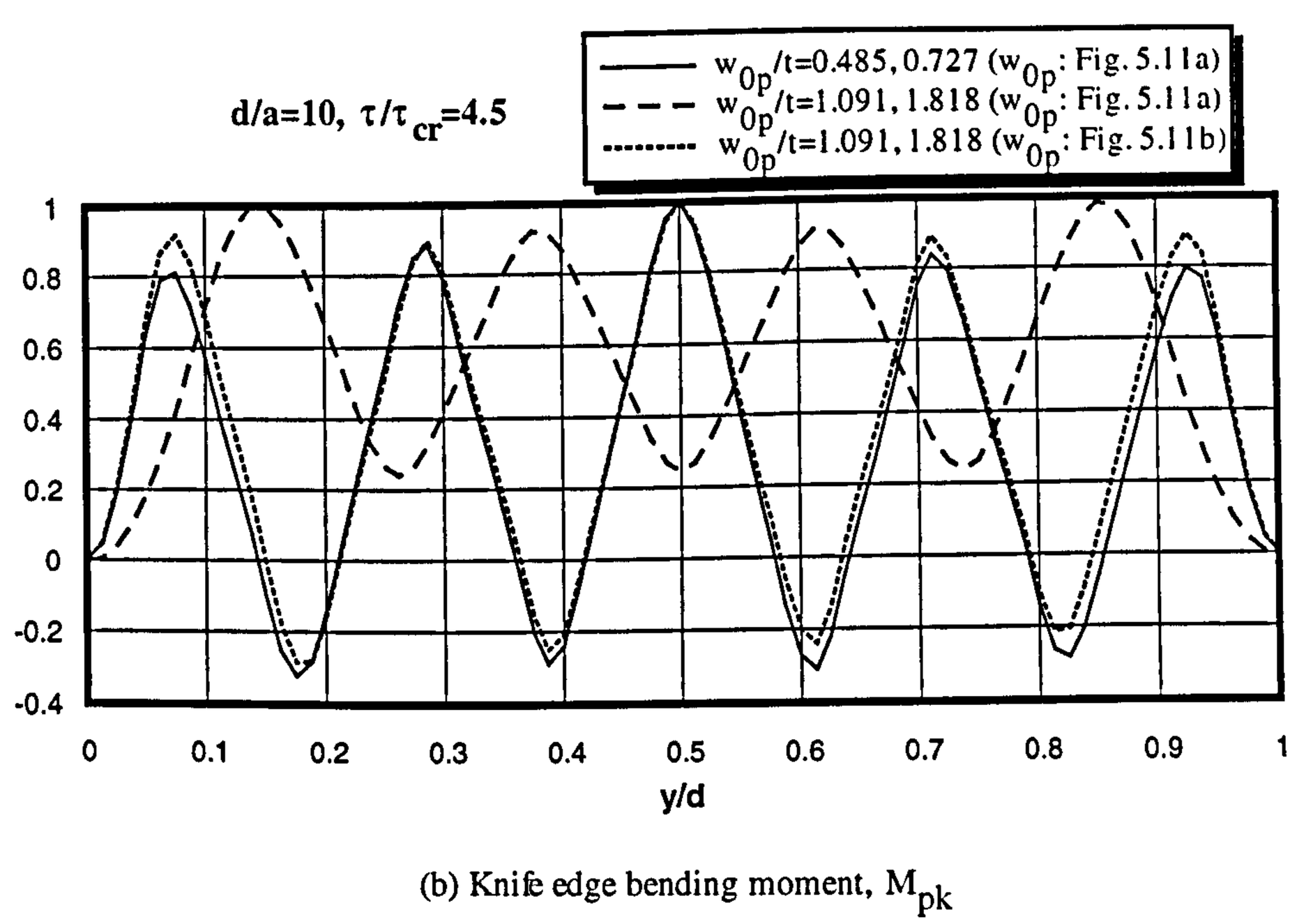
d/a=10, τ/τ_{cr}=3.96

Figure 5.9 Distribution of M_{pk} along the knife edge for d/a=0.5~10, w_{0p}/t=1.091.

Plates with a straight knife edge. Non-linear elastic FE results. Pure shear

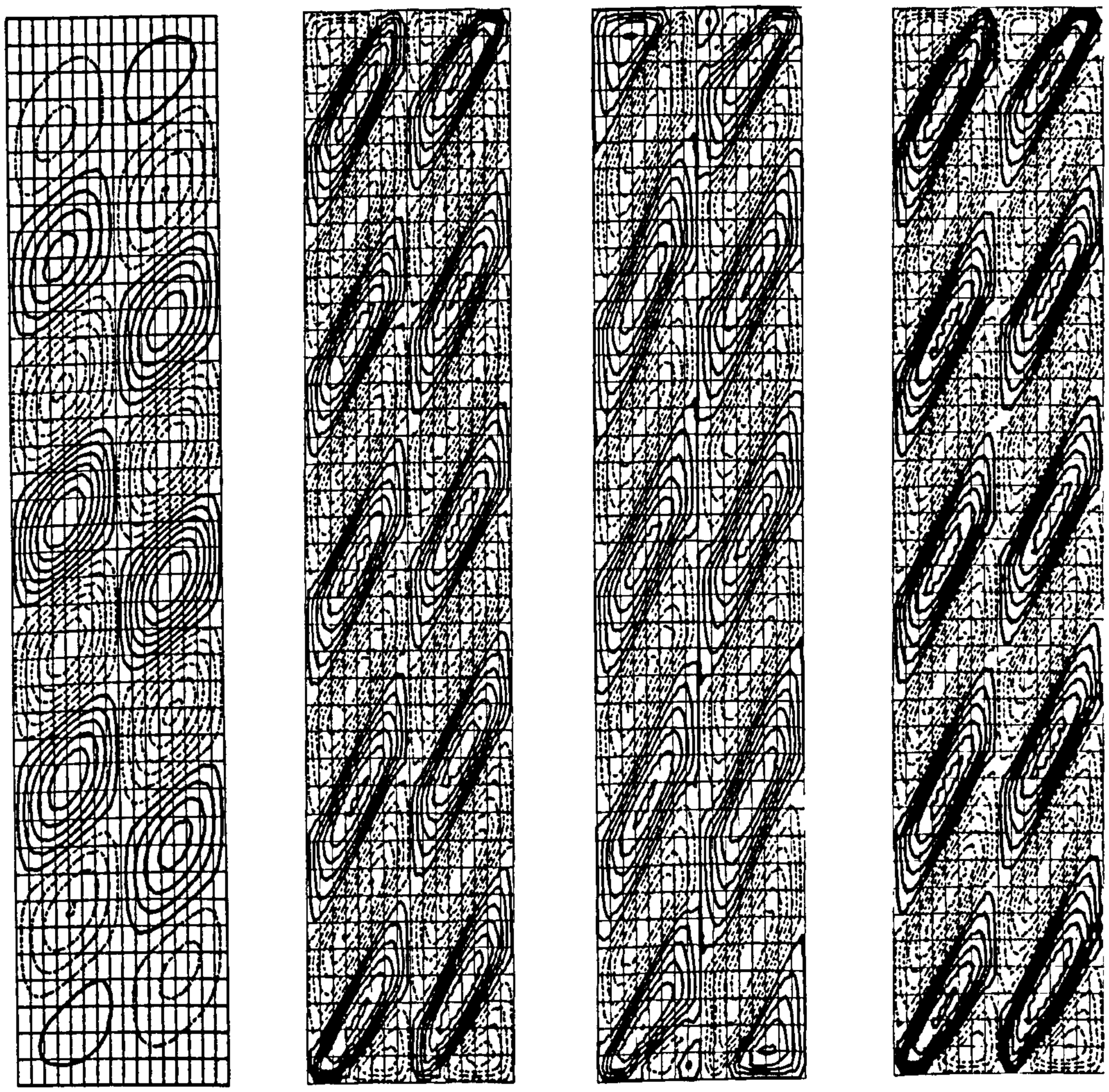


(a) Lateral force on knife edge, q_{pk}



(b) Knife edge bending moment, M_{pk}

Figure 5.10 Variation in the distributions of q_{pk} and M_{pk} with the initial panel imperfection w_{0p}/t.
Knife edge plates of d/a=10. Non-linear elastic FE results. Pure shear



1st PS Buckling Mode

(a)

NLEL Mode w0p/t=0.485 w0p: Fig. (a)

(b)

NLEL Mode w0p/t=1.091 w0p: Fig. (a)

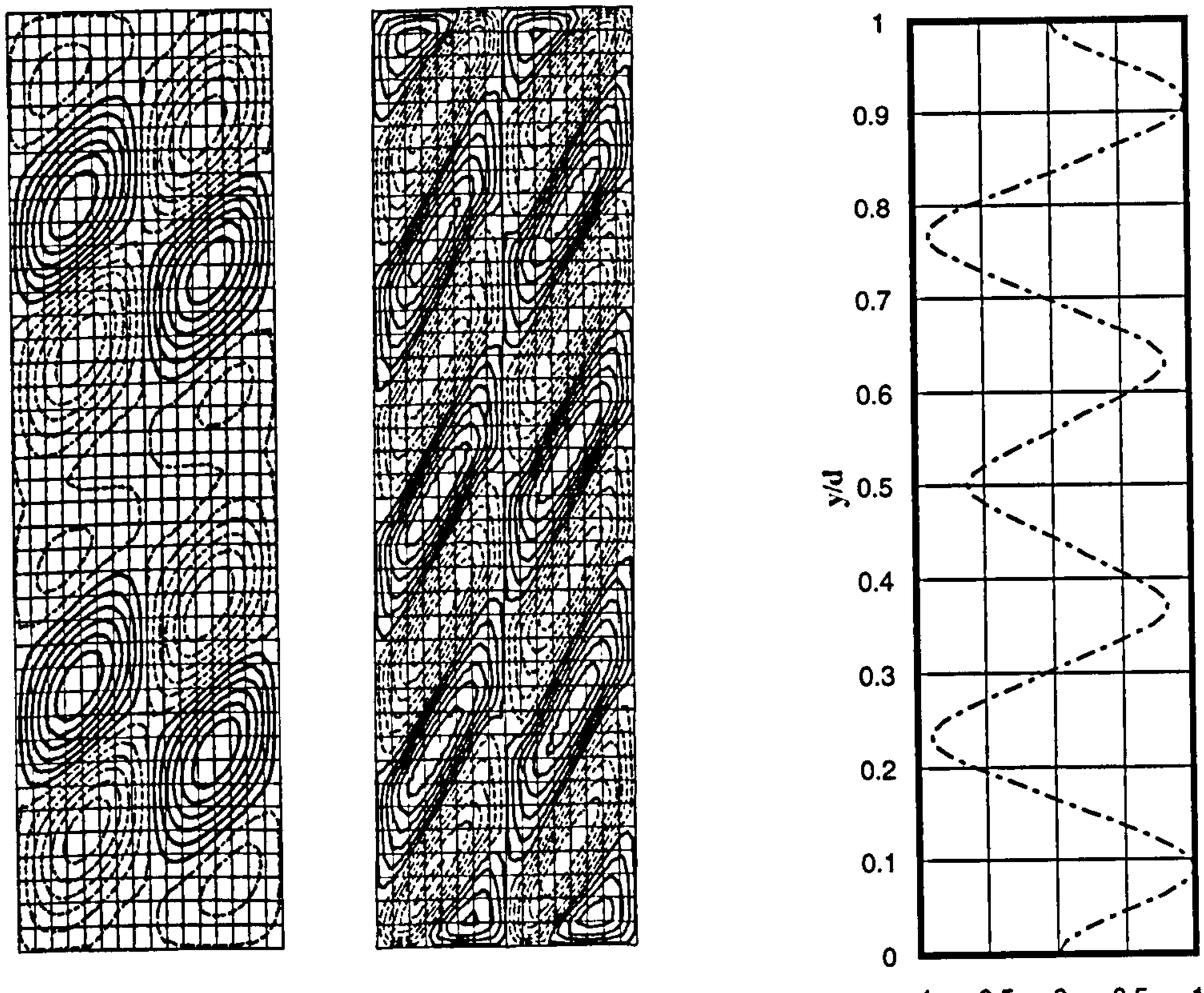
(c)

NLEL Mode w0p/t=1.091 w0p: Fig. (b)

(d)

*** NLEL = Non-linear elastic analysis.**

Figure 5.11 Variation of the deflection modes with the initial panel imperfection w_{0p}/t, found for the knife edge plates of d/a=10. Non-linear elastic FE results. Pure shear



2nd PS Buckling Mode

NLEL Mode w0p: 2nd PS mode

(a)

(b)

(c)

Figure 5.12 Deflection mode & distribution of M_{pk} for a of d/a=7, with a straight knife edge. 2^{nd} PS initial imperfection mode, w_{0p}/t=1.091. Non-linear elastic FE results. Pure shear

Fig. 5.13 presents a comparison between the numerical results and the values predicted using Eqn. 5.1 with the coefficients given in Table 5.2, and good agreement can be seen. Fig. 5.13 does not include the diagrams for d/a=1 and 2, since they are already given in Fig. 4.19. By comparison with the finite element results, it can be concluded that for plates with a straight knife edge under pure shear, the proposed equation 5.1 is adequate for representing the magnitudes of the knife edge bending moment M_{pk}. Nevertheless,

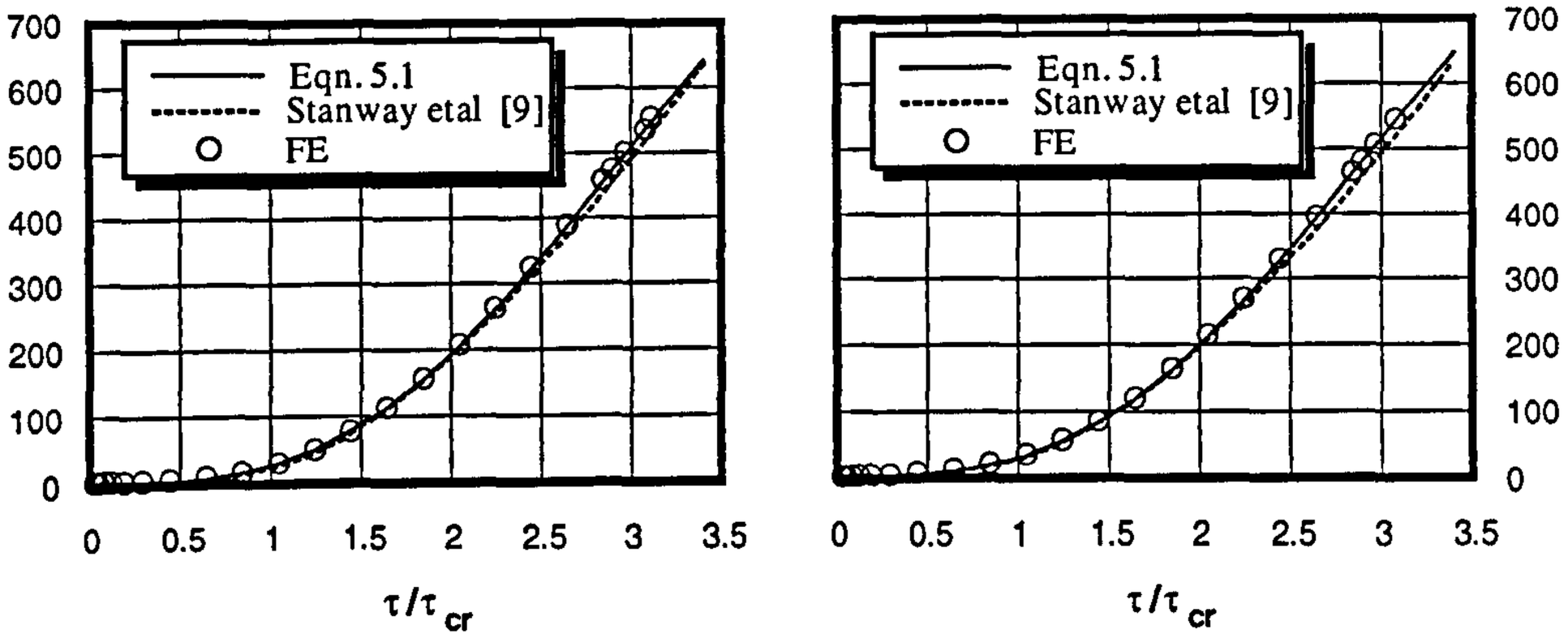
for the purpose of design, the above relationship between the knife edge moment and panel aspect ratio will be further simplified in Section 5.2.6.

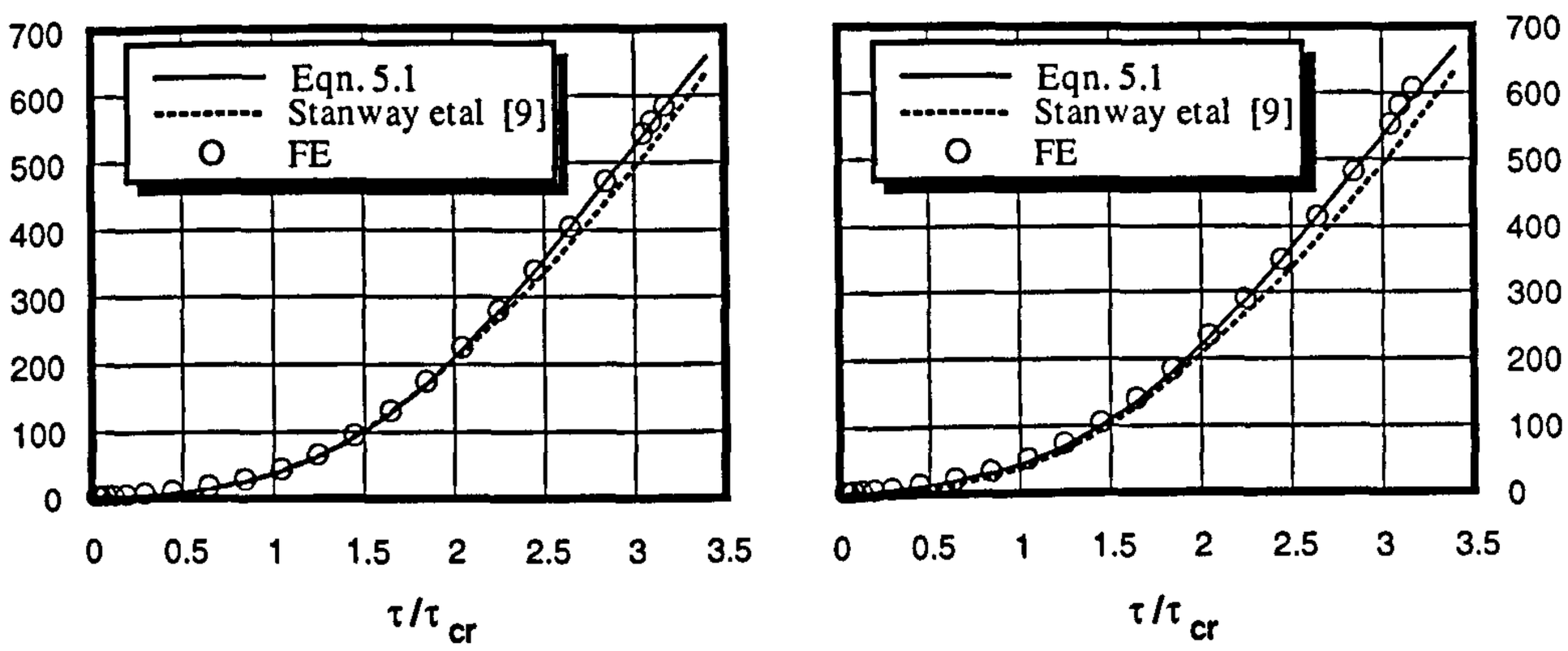
The knife edge bending moments calculated from the equations proposed by Stanway et al [9] are also shown in Fig. 5.13, and the possible reasons for its differences from FE results are stated in Section 4.7.2. It is also noted that in Stanway's model, the knife edge moments for d/a>5 are assumed to be equal to that for d/a=5.

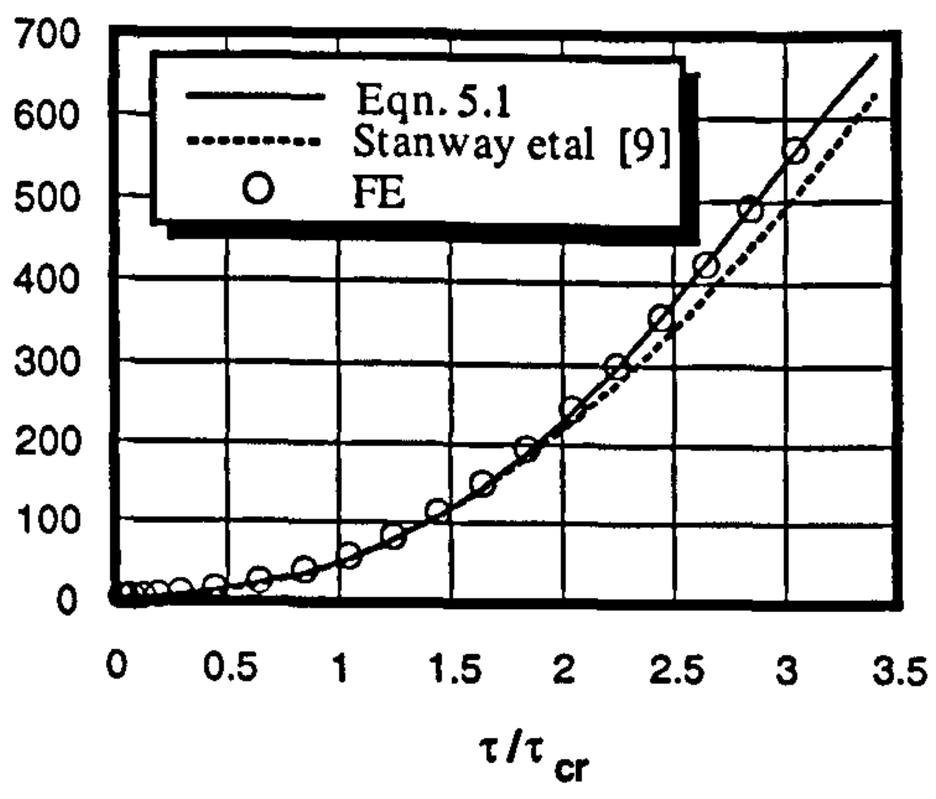
For d/a=10, as indicated in Section 5.2.2.2, two different distributions of M_{pk} were observed, depending on whether the deflection mode is free to change from the initial imperfection mode. Correspondingly, it is found that the maximum amplitudes of the bending moments along the knife edge differ greatly between the cases where different distributions of M_{pk} take place, and for this reason, the coefficients in Eqn. 5.1 are not given for d/a=10. As shown in Fig. 5.13(g), the magnitudes of the knife edge moments for w_{0p}/t=0.485 and 0.727 are only about half of the knife edge moments for w_{0p}/t=1.091, 1.455 and 1.818. It can also be found in Fig. 5.13(g) that the magnitudes of M_{pk} for w_{0p}/t=0.485 and 0.727 are close to the values of M_{pk} for d/a=6, whereas the knife edge moments for w_{0p}/t=1.091, 1.455 and 1.818 are close to those obtained for d/a=7. It is noted that this agreement is in parallel to the similarity observed on the distributions of M_{pk}.

For the imperfection magnitudes of w_{0p}/t=1.091 and 1.818 for d/a=10, a deflection mode similar to the mode of w_{0p}/t=0.485 can be achieved by imposing an initial imperfection mode affine to the non-linear elastic mode of w_{0p}/t=0.485 (Fig. 5.11). As a result, as illustrated in Fig. 5.14, the magnitudes of M_{pk} for w_{0p}/t=1.091 and 1.818 are found to be in the same range as the knife edge moment obtained for w_{0p}/t=0.485, and hence the knife edge moments for d/a=6.

For d/a=7, it is observed in Fig. 5.12 that when the second point-symmetric buckling mode is used as the initial imperfection mode, the distribution of M_{pk} is close to those for d/a=3~6 (Fig. 5.9). The magnitude of M_{pk} for this case is shown in Fig. 5.14(a), and is found to be also close to the knife edge moments for d/a=6.







Equation 5.1

C_1=21.64

C_2=-4.065

C_3=-1.060

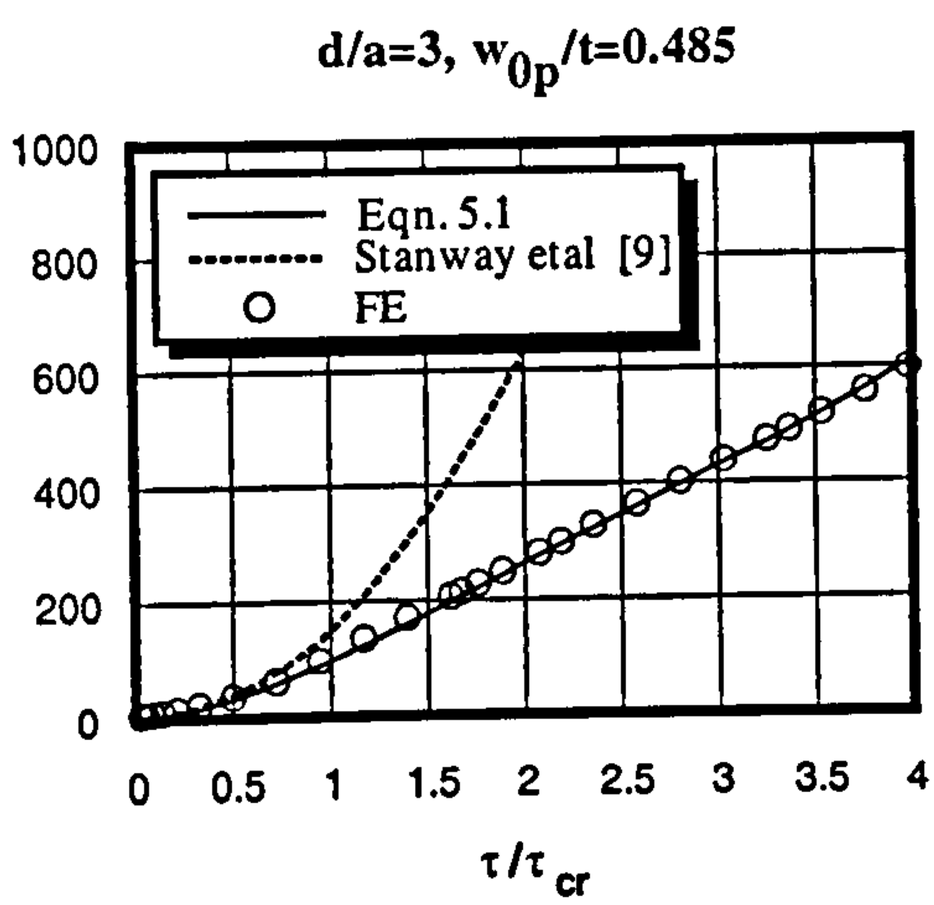
C_4=-24.13

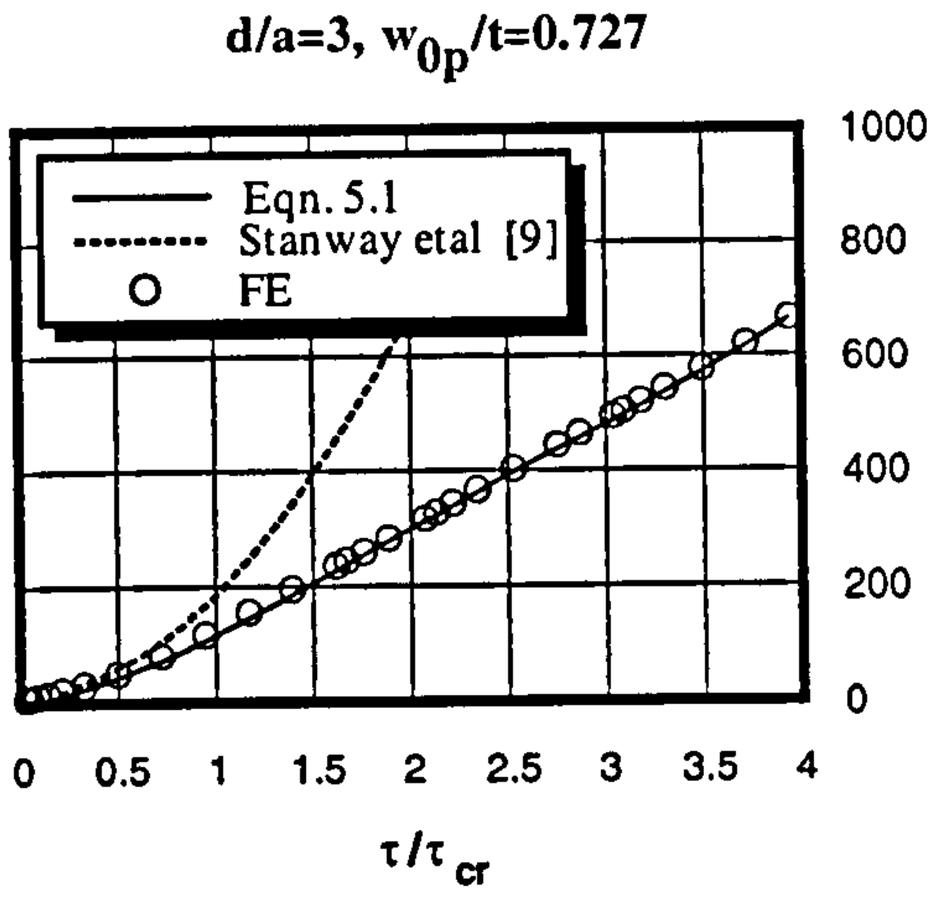
C_5=51.52

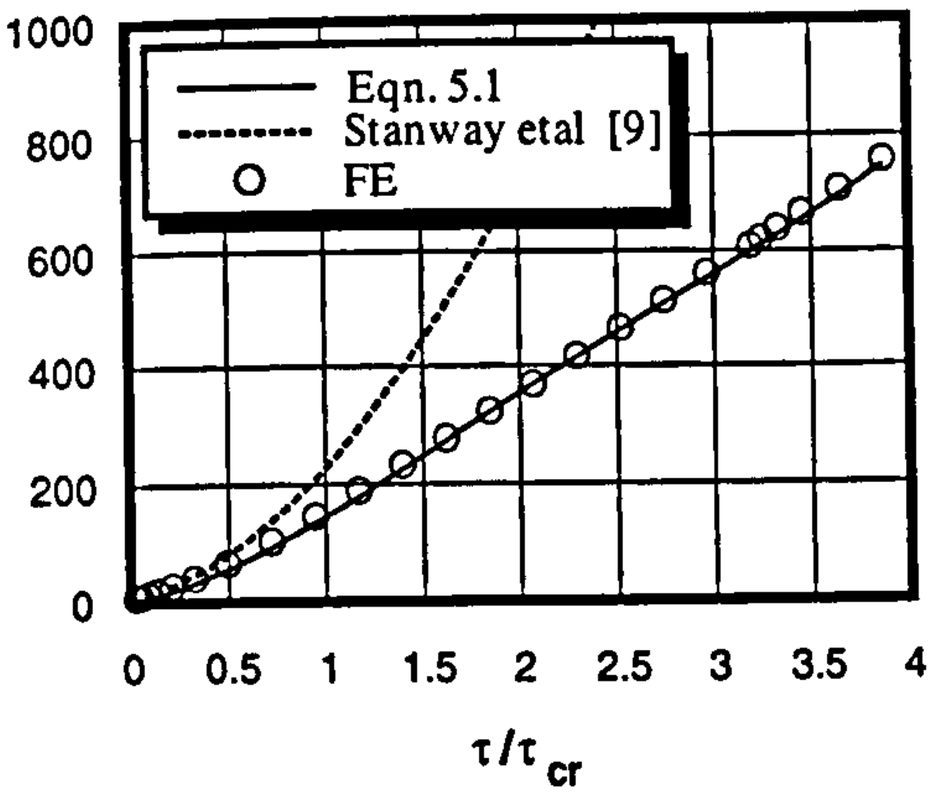
C_6=-8.341

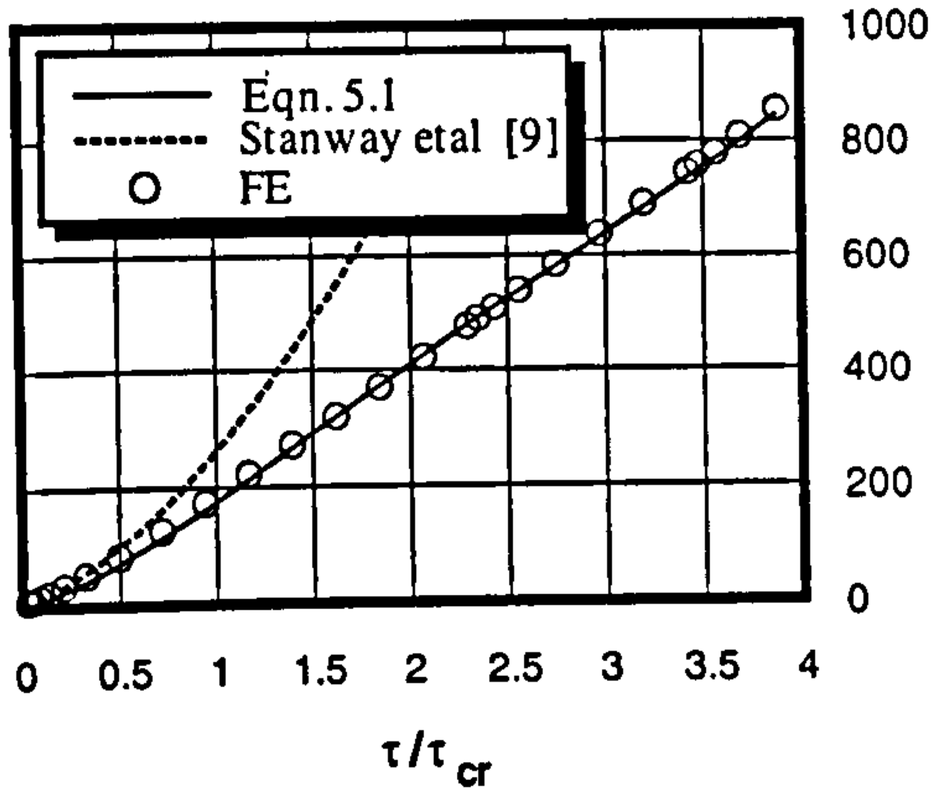
(a) d/a=0.5

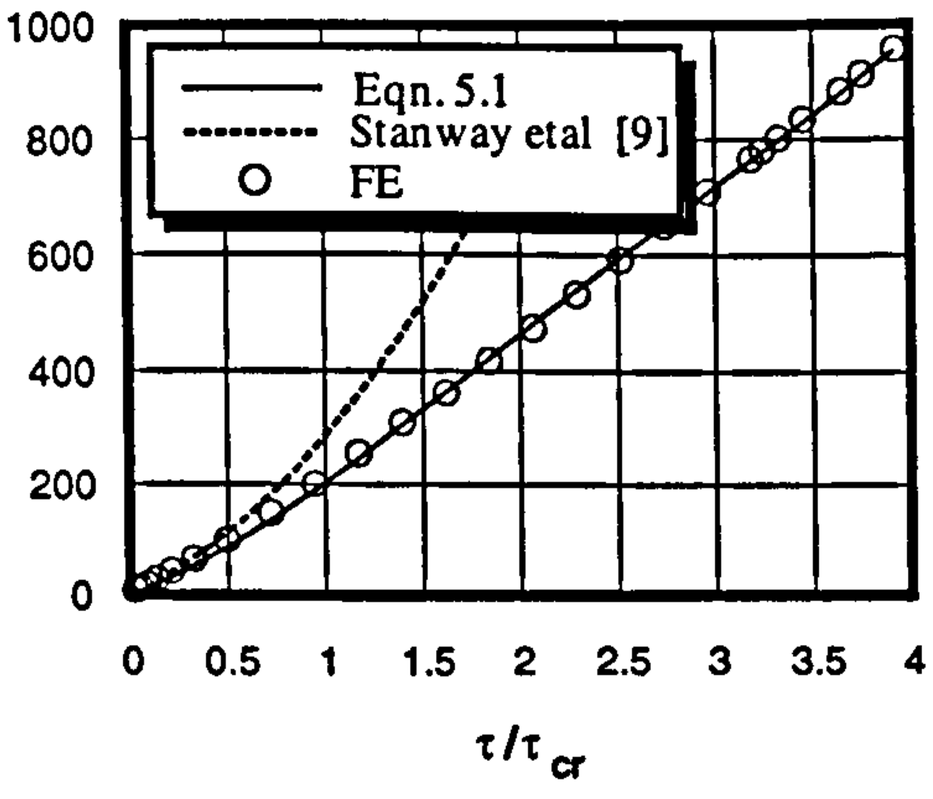
Figure 5.13 Maximum bending moments in the knife edge. Non-linear elastic FE results. CUCU plates with a straight knife edge. Imperfection affine to the 1st PS buckling mode. Pure shear











Equation 5.1

C_1=82.78

C_2=-3.654

C_3=-19.32

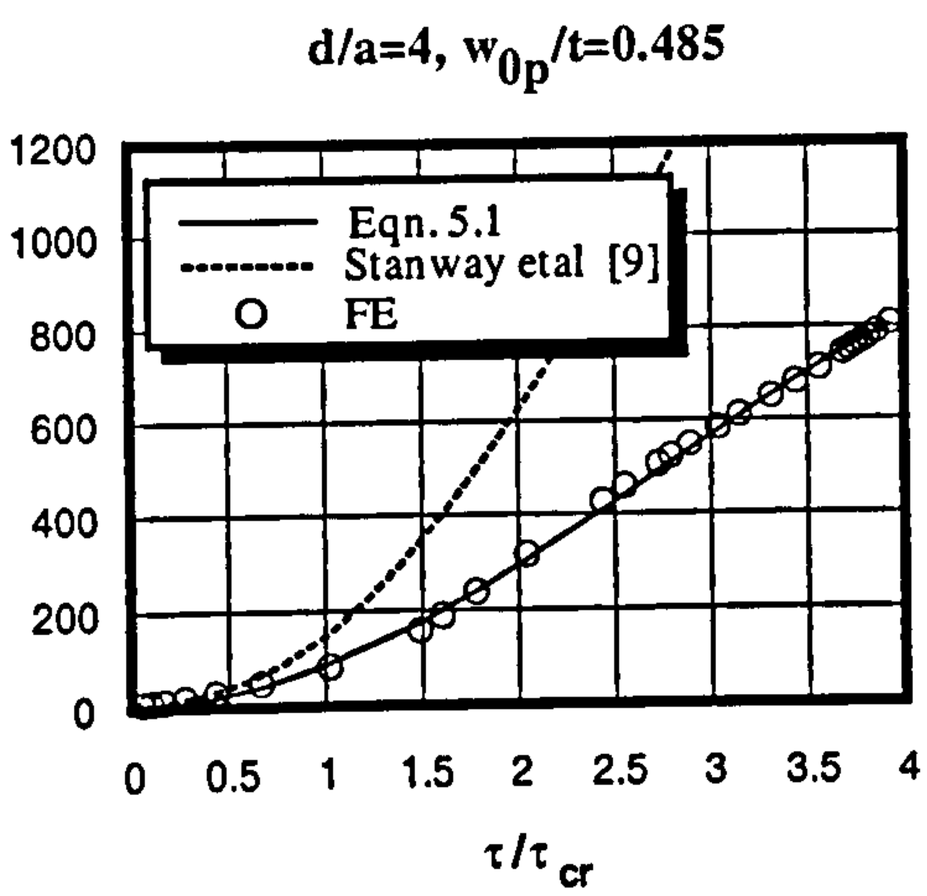
C_4=106.9

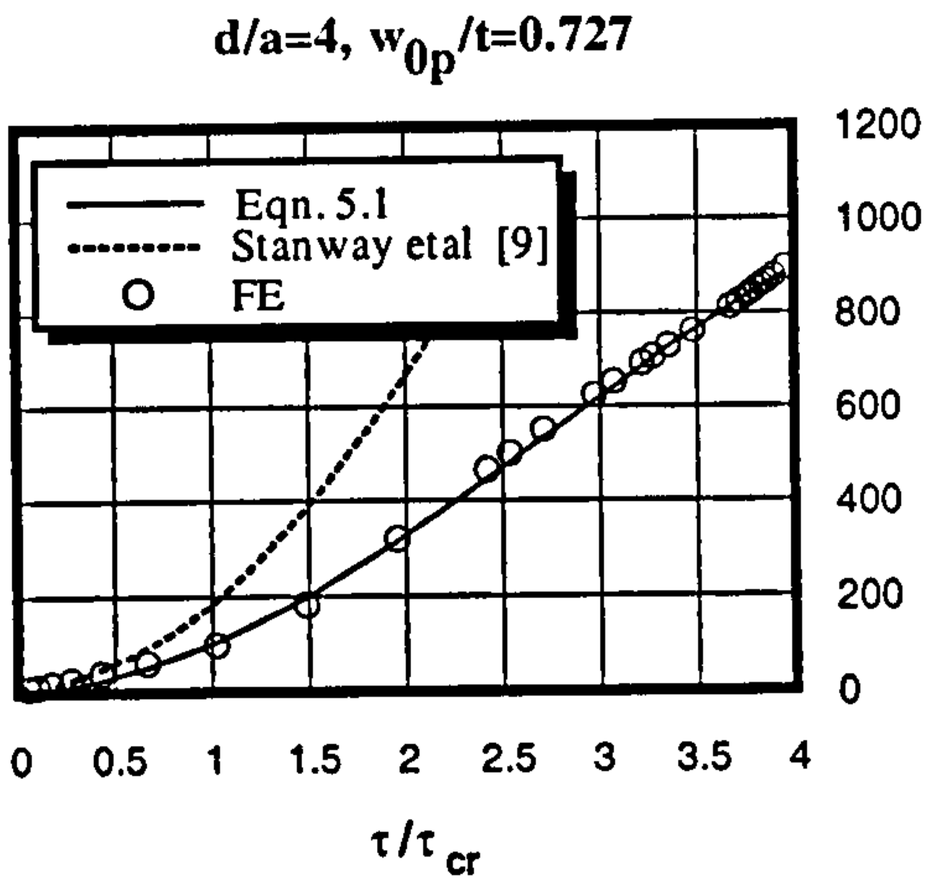
C_5=-31.72

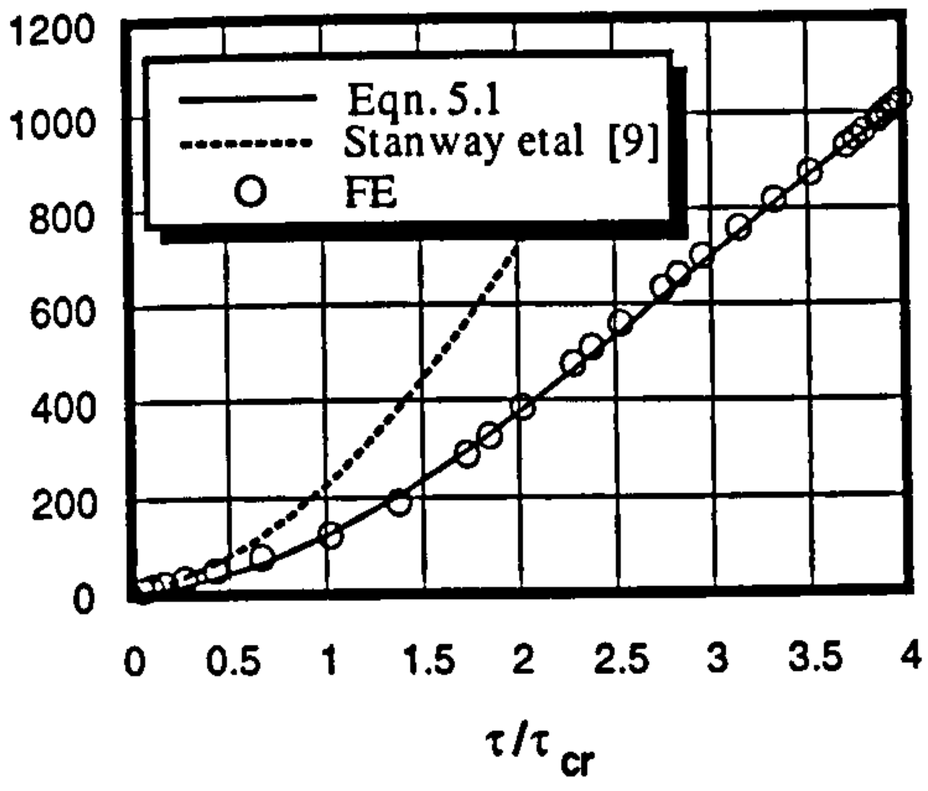
C_6=3.433

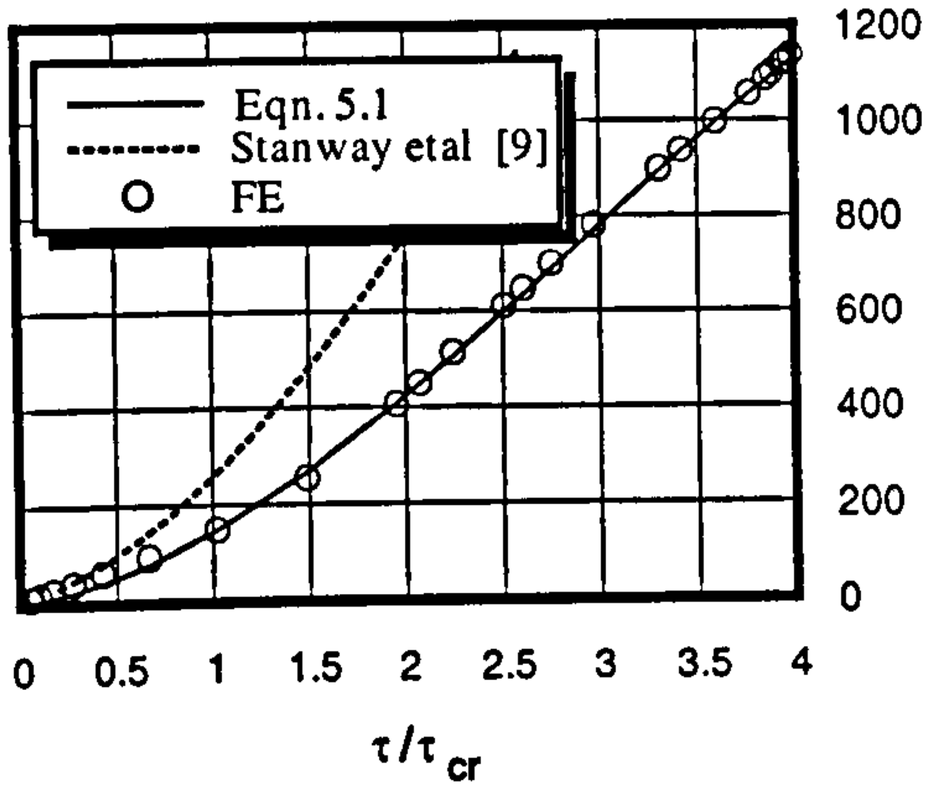
(b) d/a=3

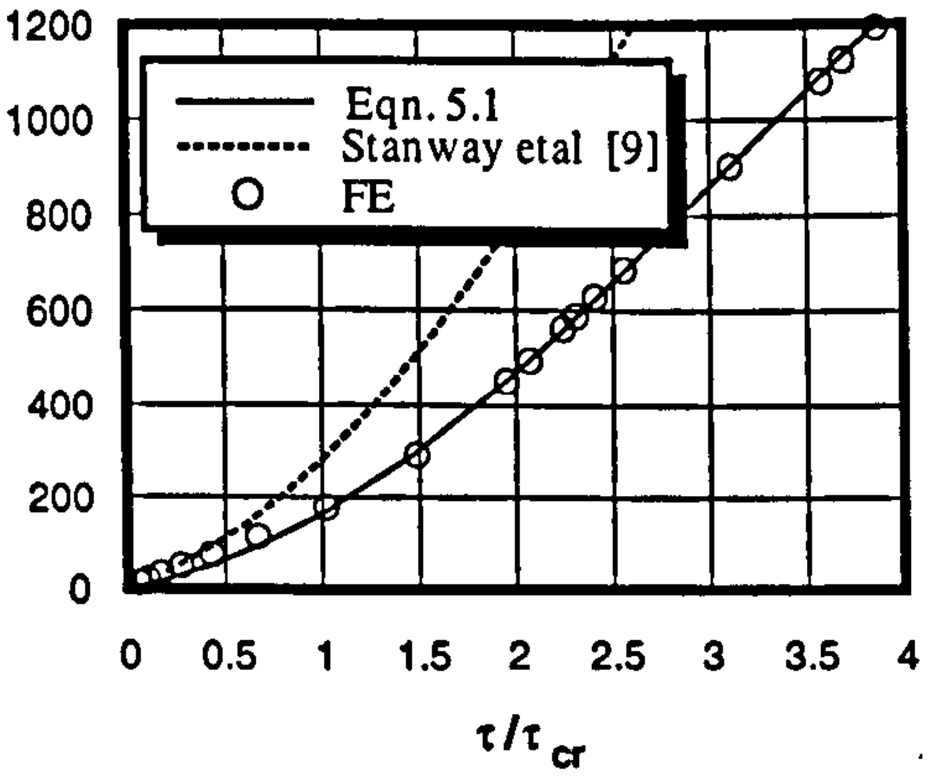
Figure 5.13 (Cont.) Maximum bending moments in the knife edge. Non-linear elastic FE results. CUCU plates with a straight knife edge. Imperfection affine to the 1st PS buckling mode. Pure shear











Equation 5.1

C_1=53.05

C_2=6.702

C_3=-10.12

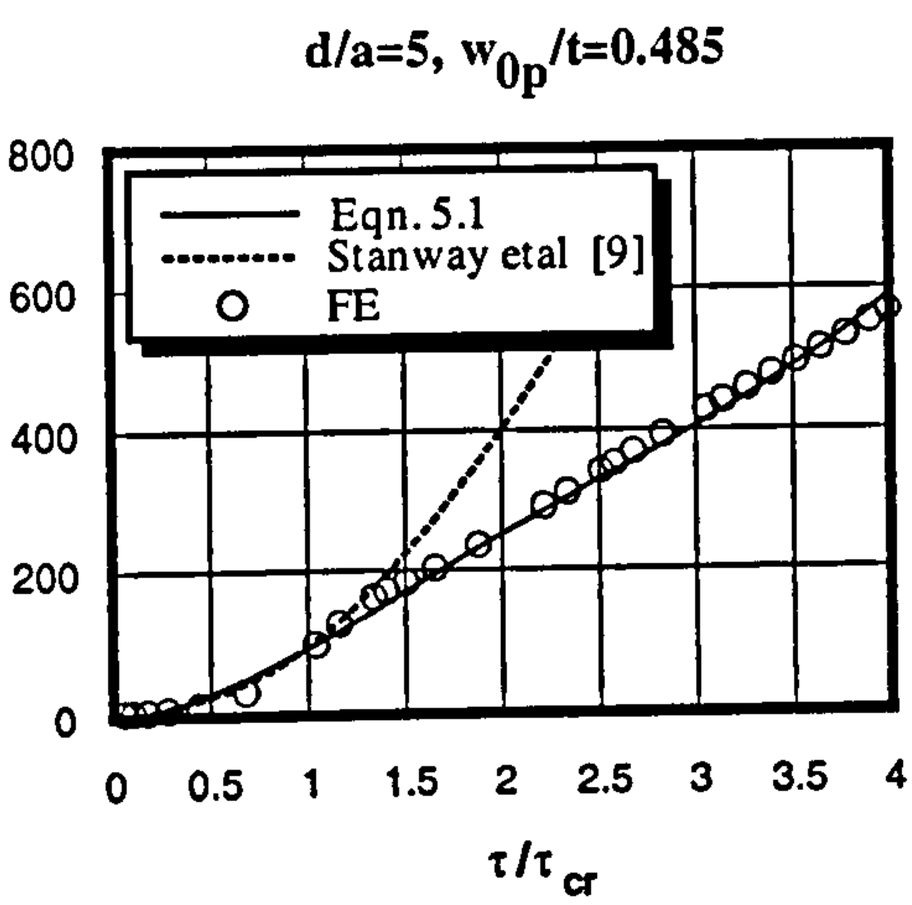
C_4=69.30

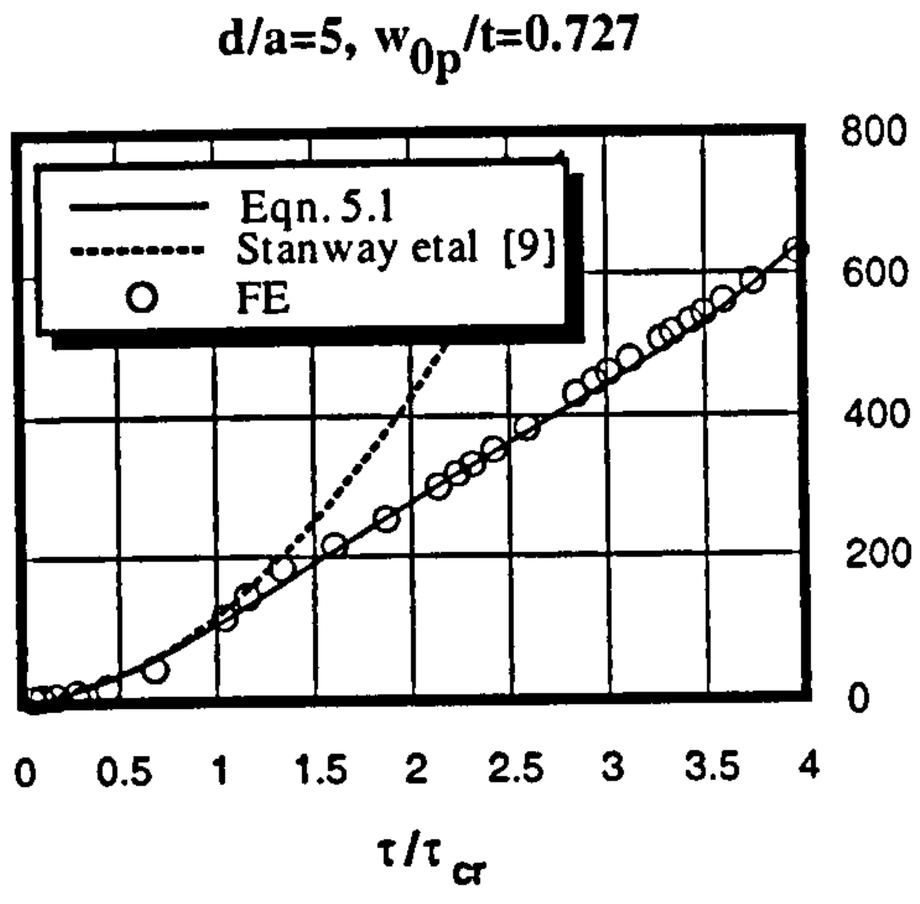
C_5=-0.422

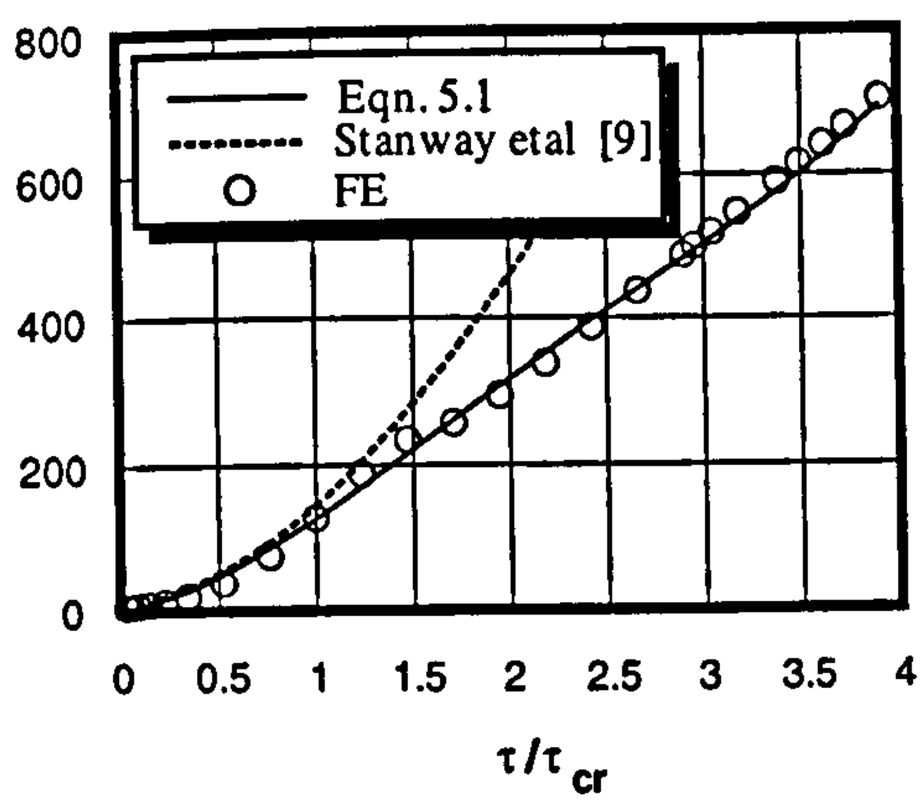
C_6=-1.474

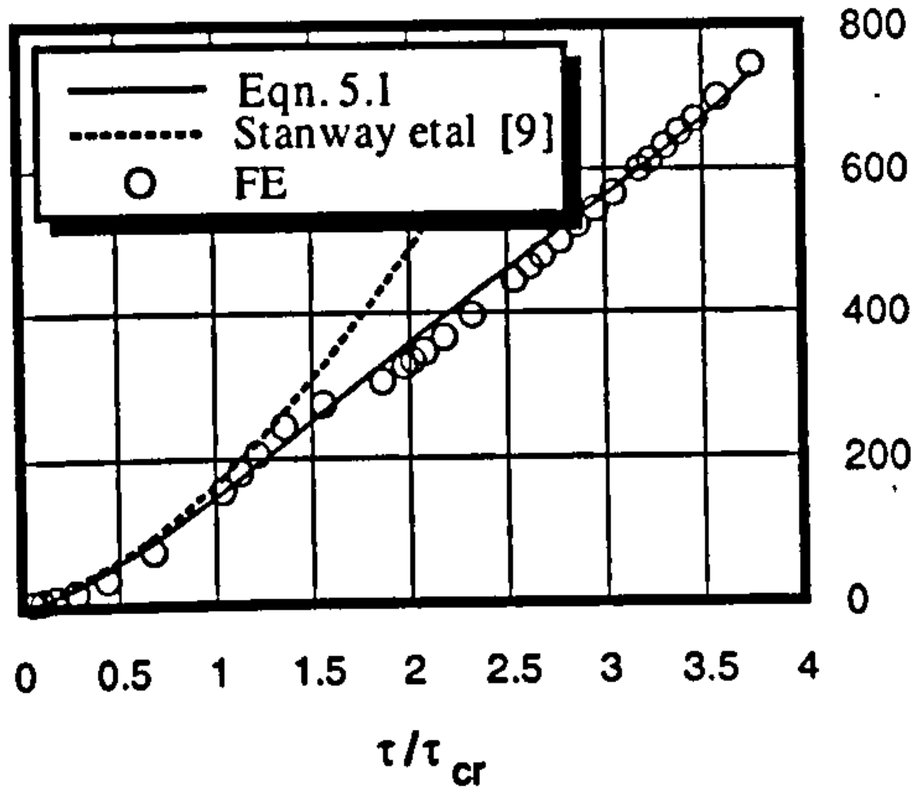
(c) d/a=4

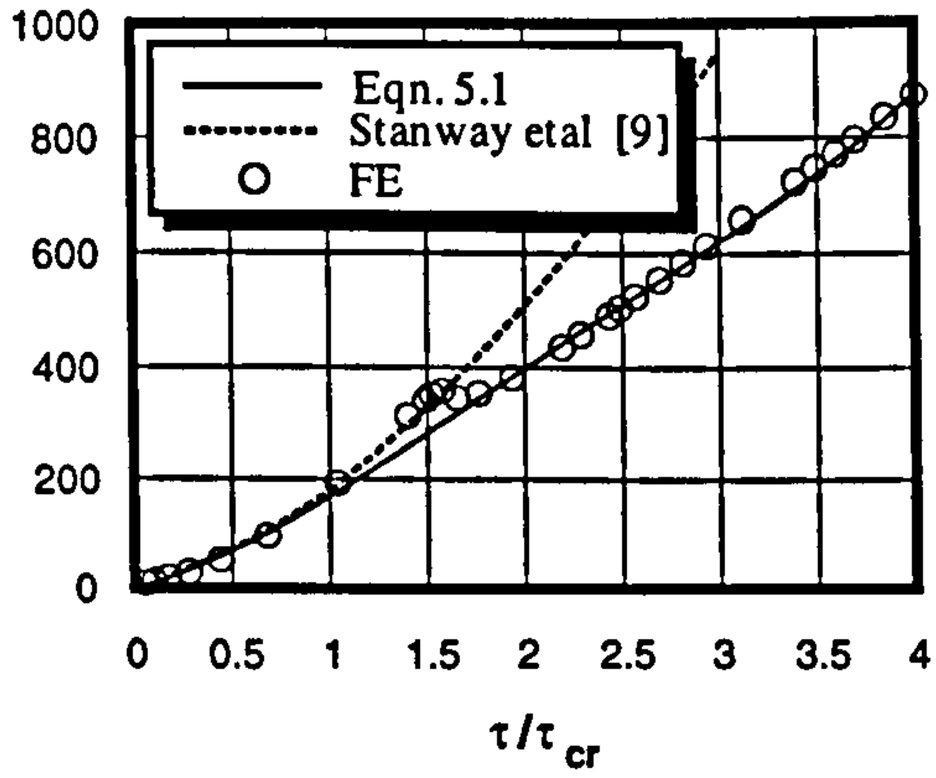
Figure 5.13 (Cont.) Maximum bending moments in the knife edge. Non-linear elastic FE results. CUCU plates with a straight knife edge. Imperfection affine to the 1st PS buckling mode. Pure shear











Equation 5.1

C_1=56.94

C_2=-0.939

C_3=-15.81

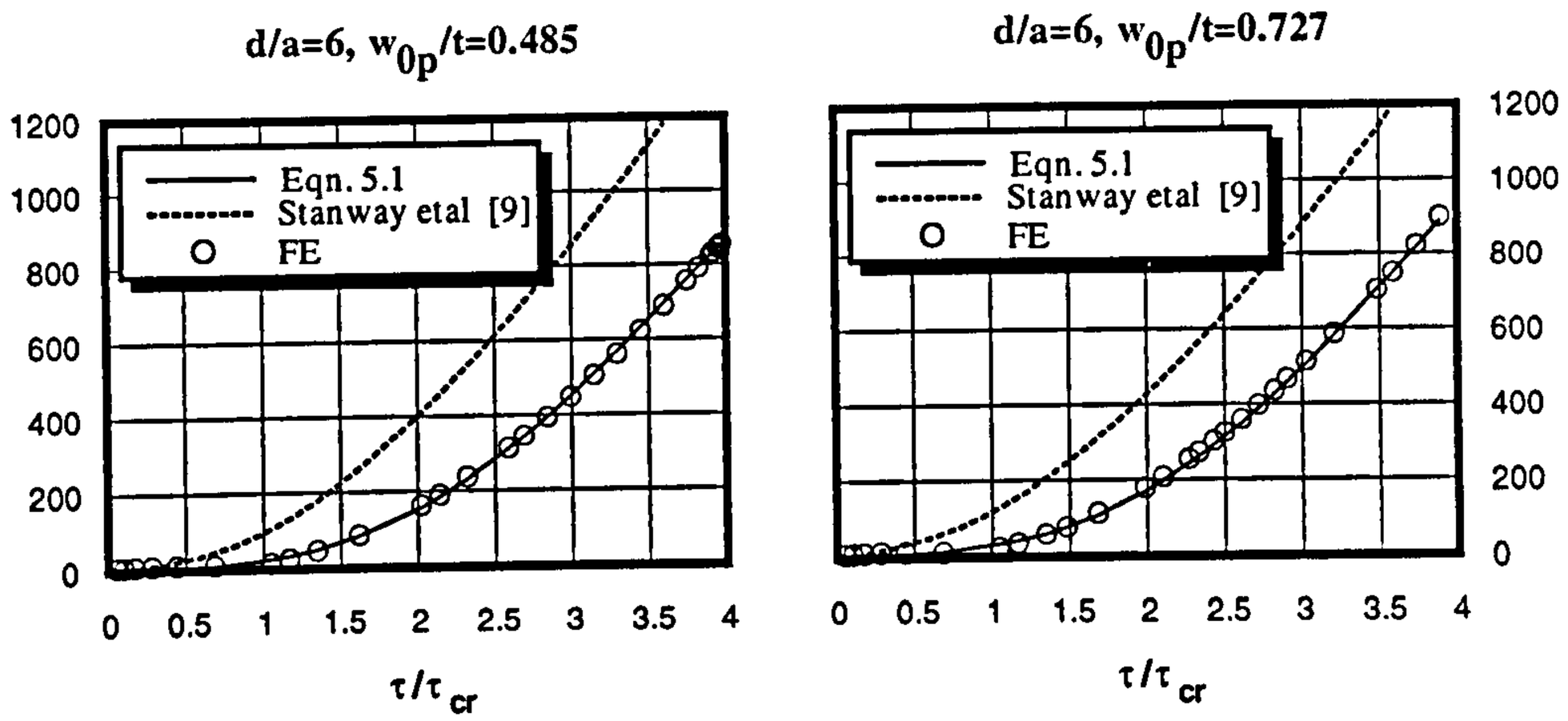
C_4=114.9

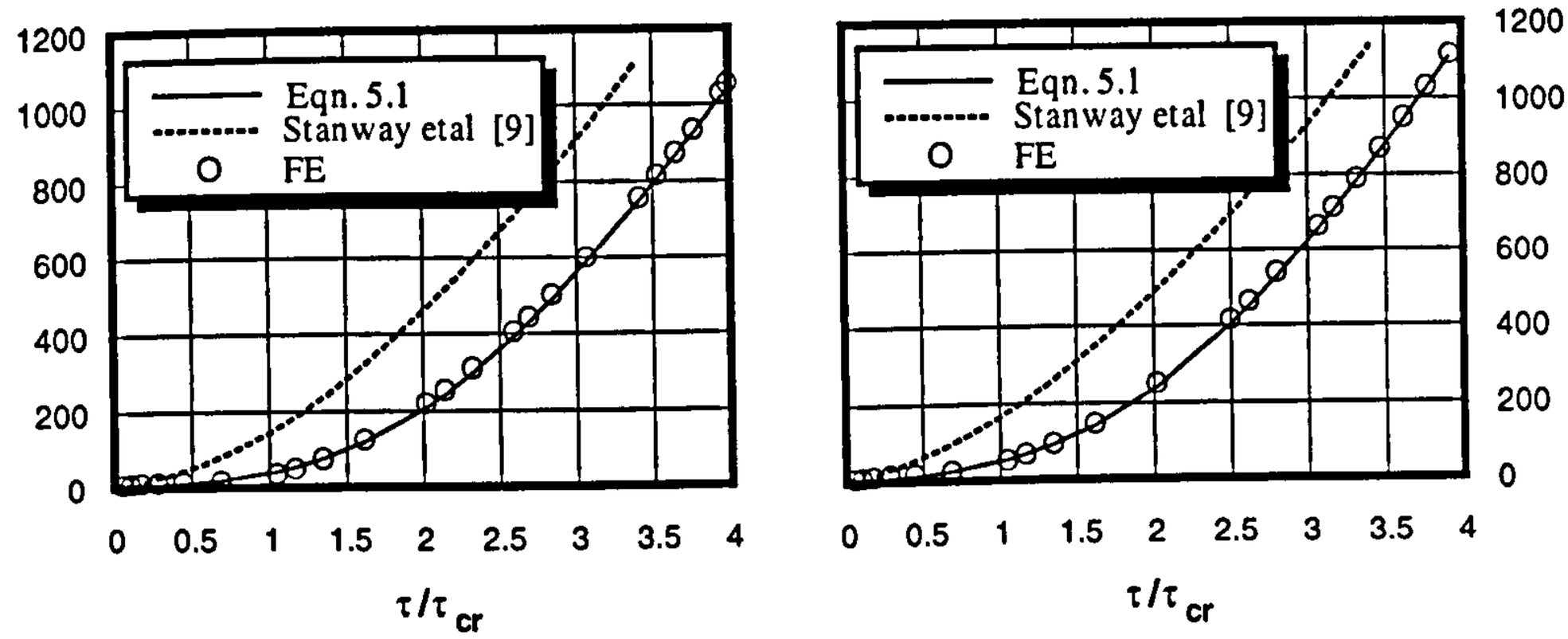
C_5=-37.44

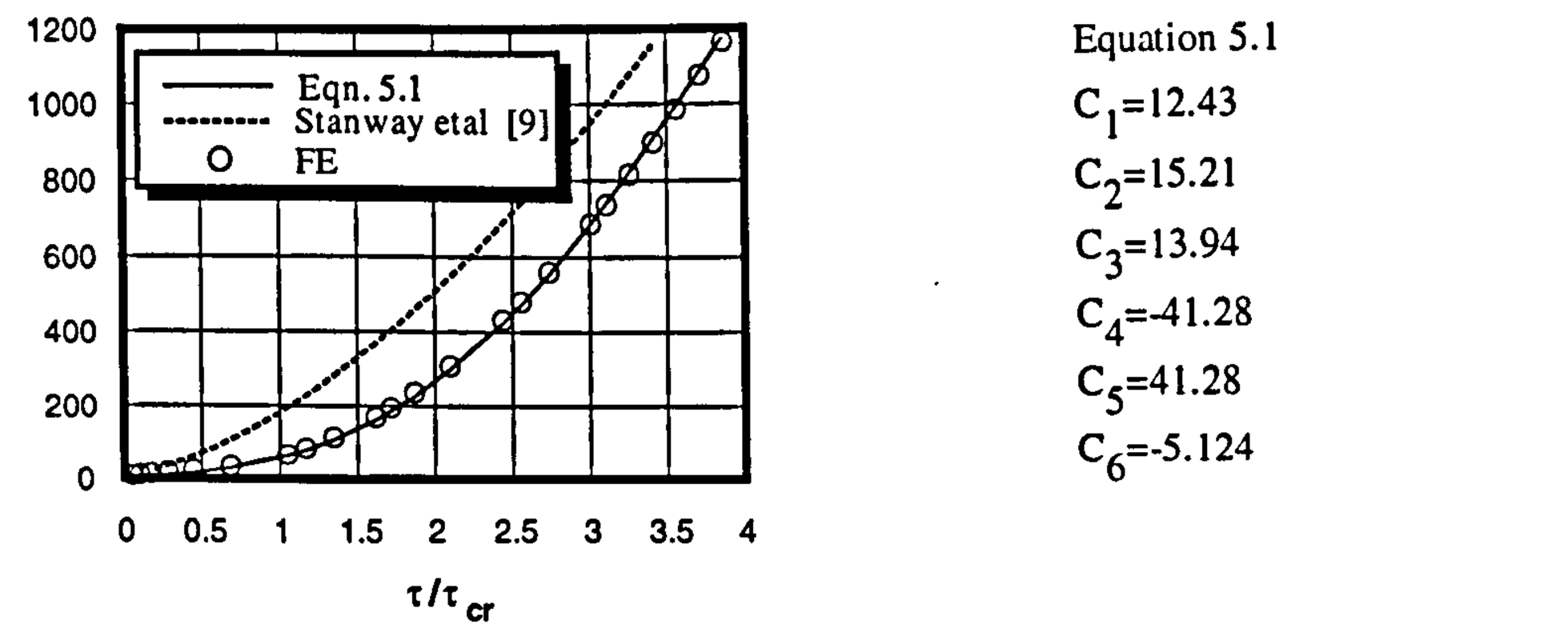
C_6=4.334

(d) d/a=5

Figure 5.13 (Cont.) Maximum bending moments in the knife edge. Non-linear elastic FE results. CUCU plates with a straight knife edge. Imperfection affine to the 1st PS buckling mode. Pure shear







Equation 5.1

C_1=12.43

C_2=15.21

C_3=13.94

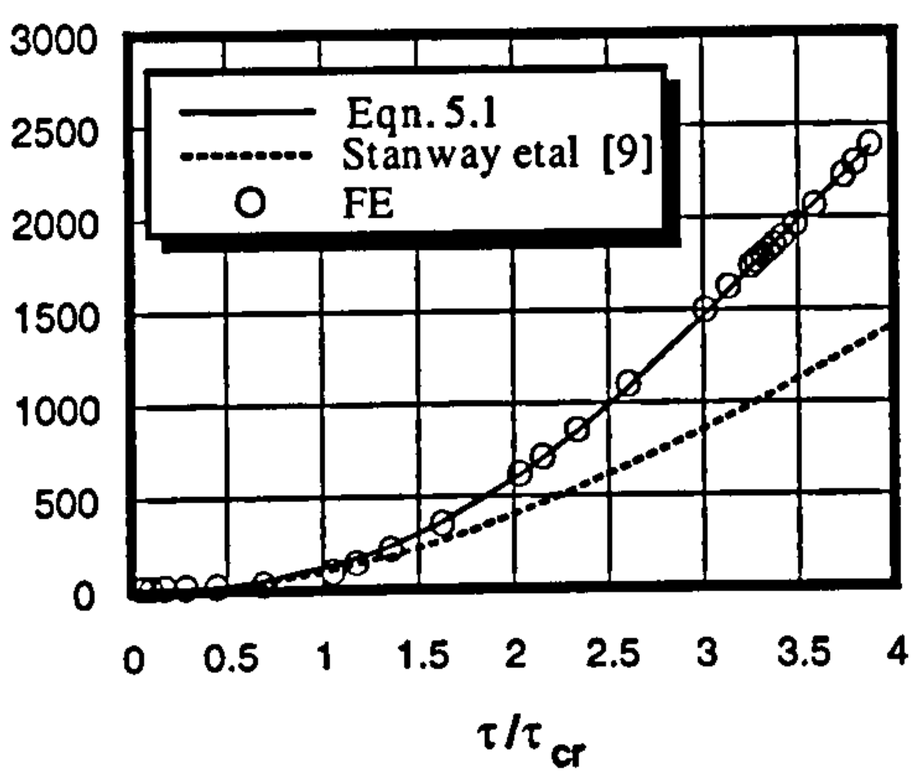
C_4=-41.28

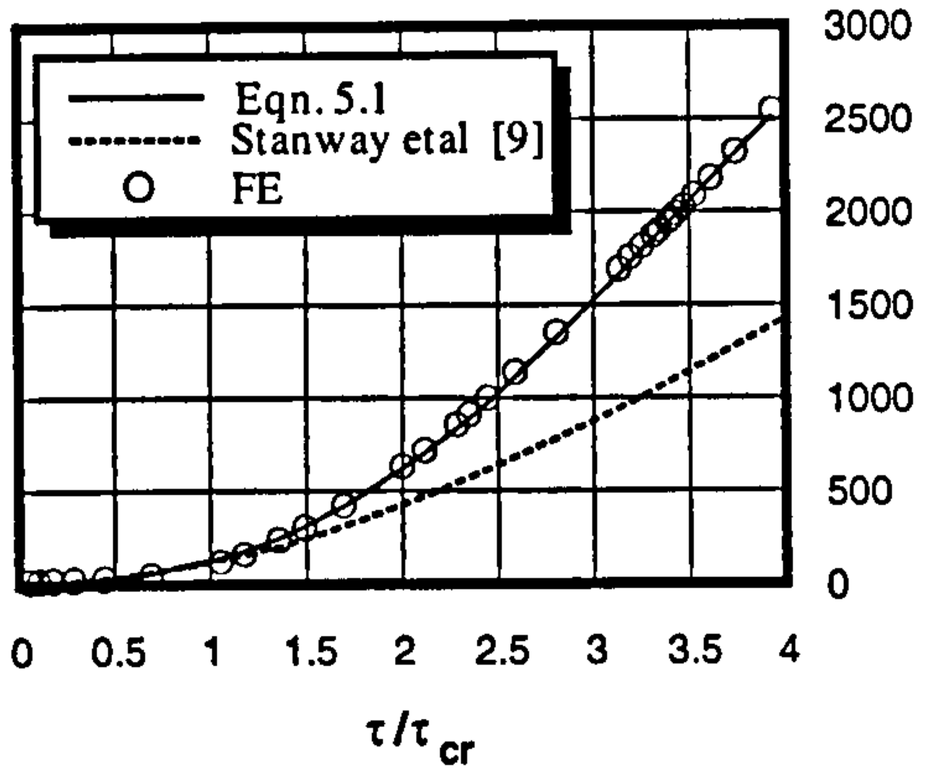
C_5=41.28

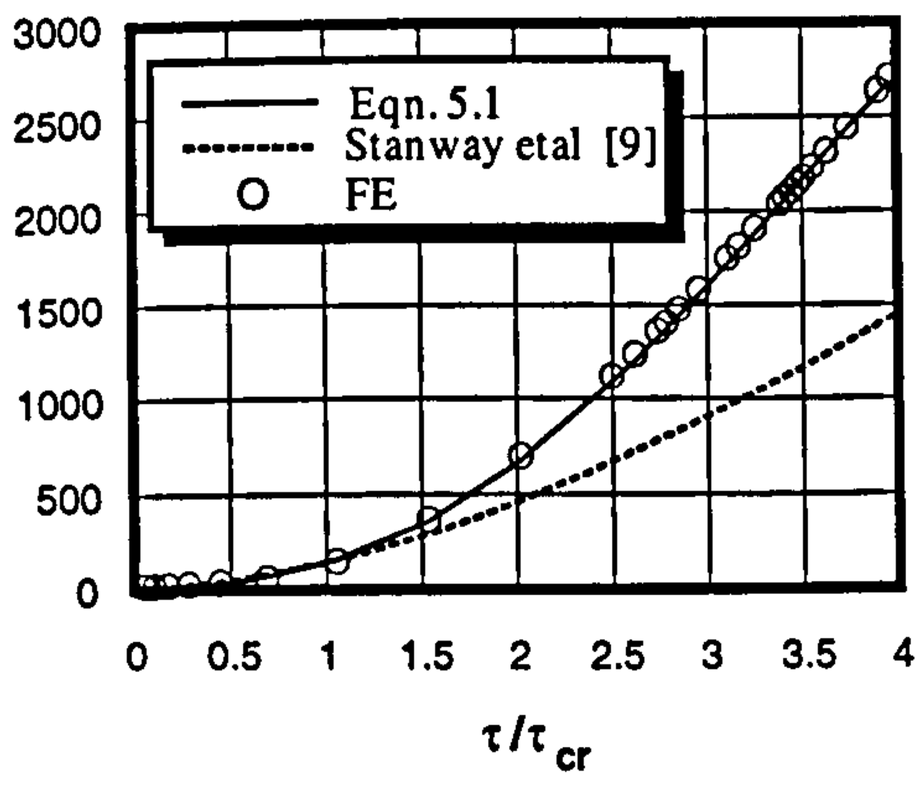
C_6=-5.124

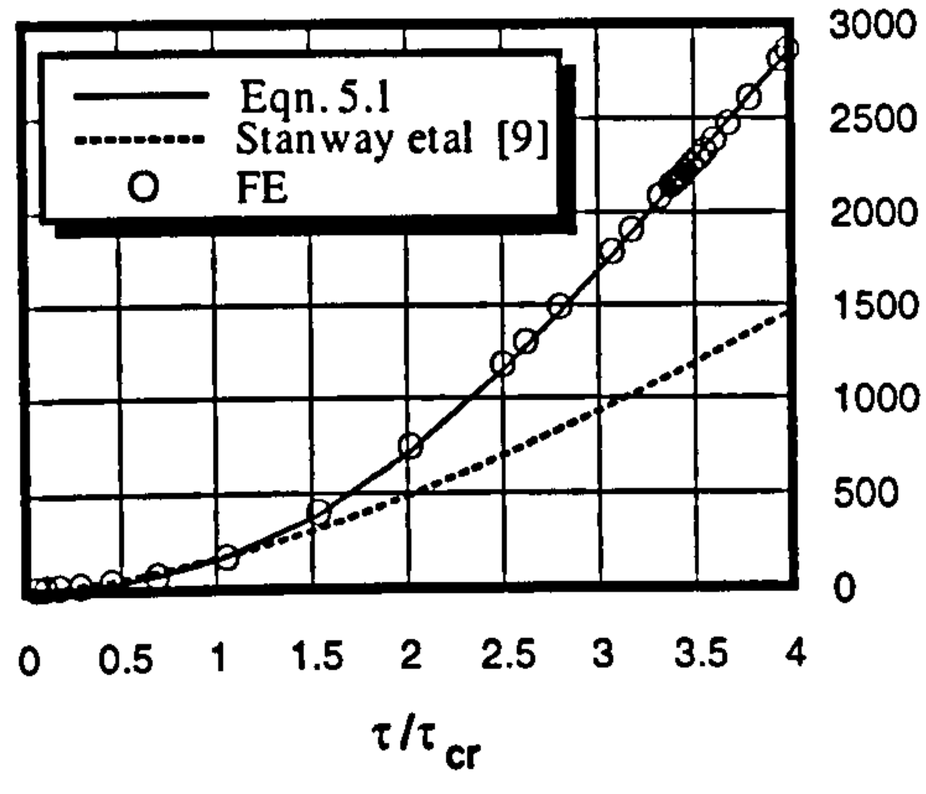
(e) d/a=6

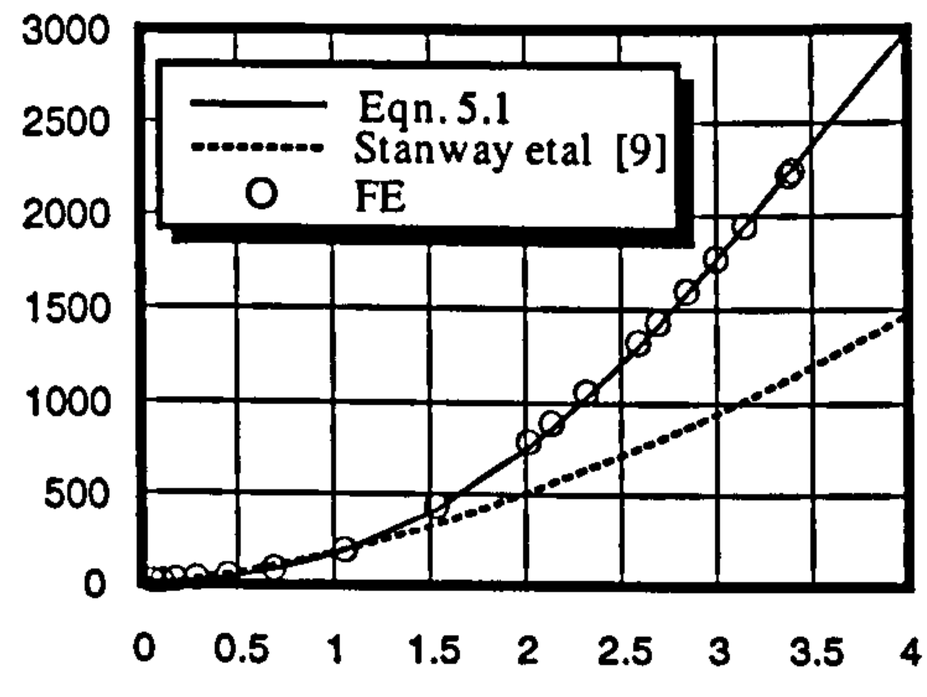
Figure 5.13 (Cont.) Maximum bending moments in the knife edge. Non-linear elastic FE results. CUCU plates with a straight knife edge. Imperfection affine to the 1st PS buckling mode. Pure shear











Equation 5.1

C_1=24.70

C_2=17.04

C_3=11.12

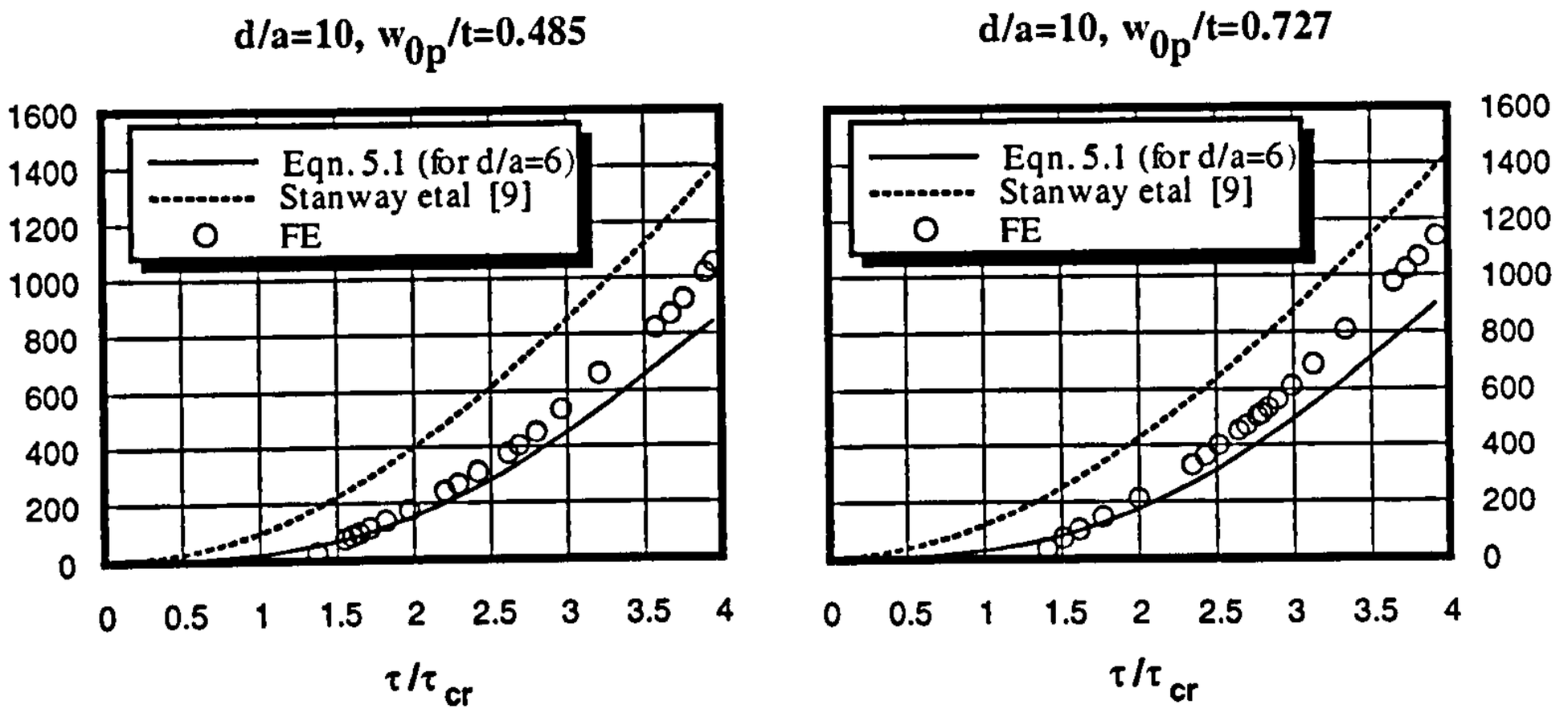
C_4=16.71

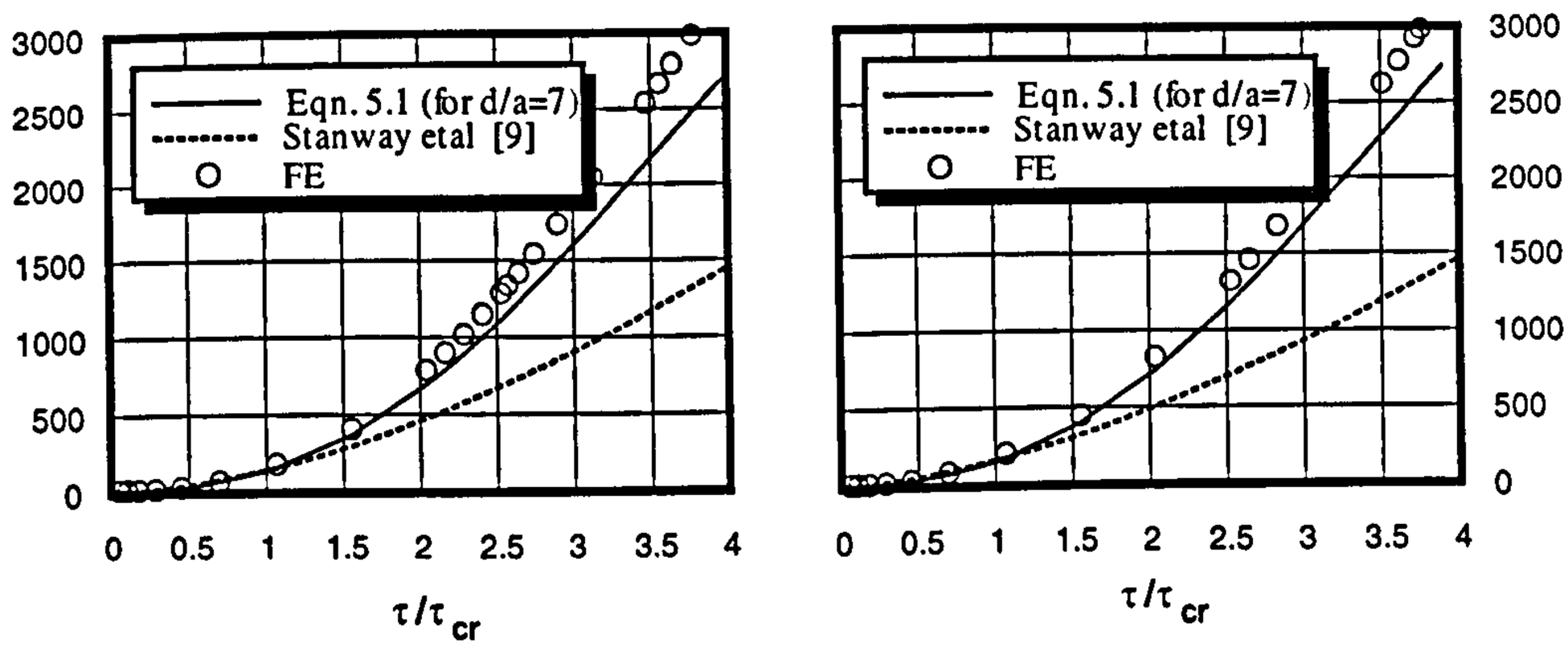
C_5=80.03

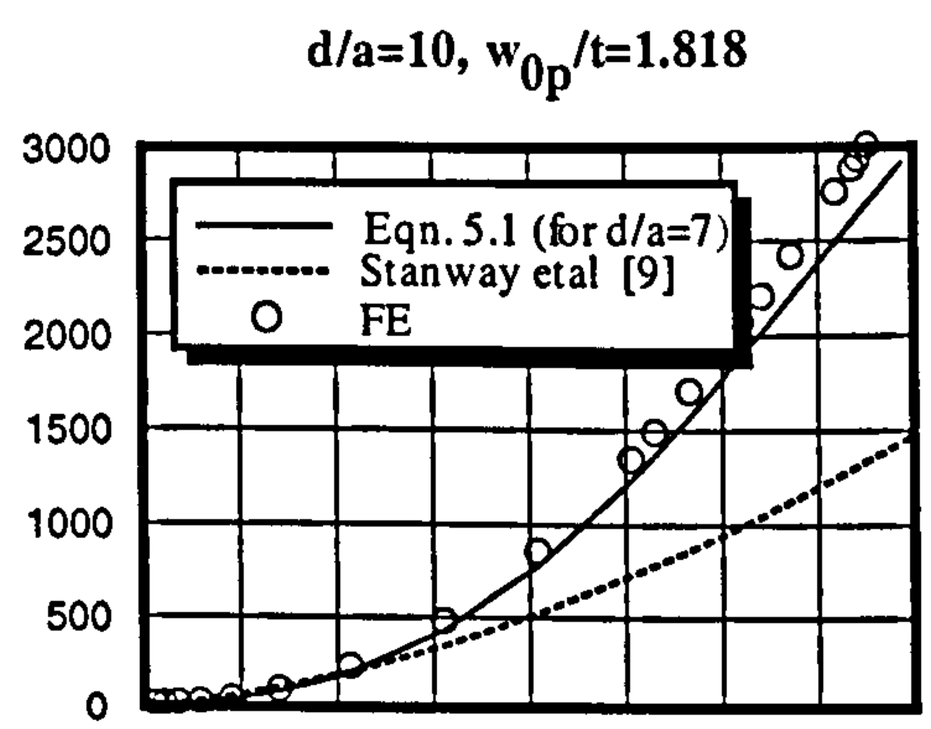
C_6=-12.18

(f) d/a=7

Figure 5.13 (Cont.) Maximum bending moments in the knife edge. Non-linear elastic FE results. CUCU plates with a straight knife edge. Imperfection affine to the 1st PS buckling mode. Pure shear

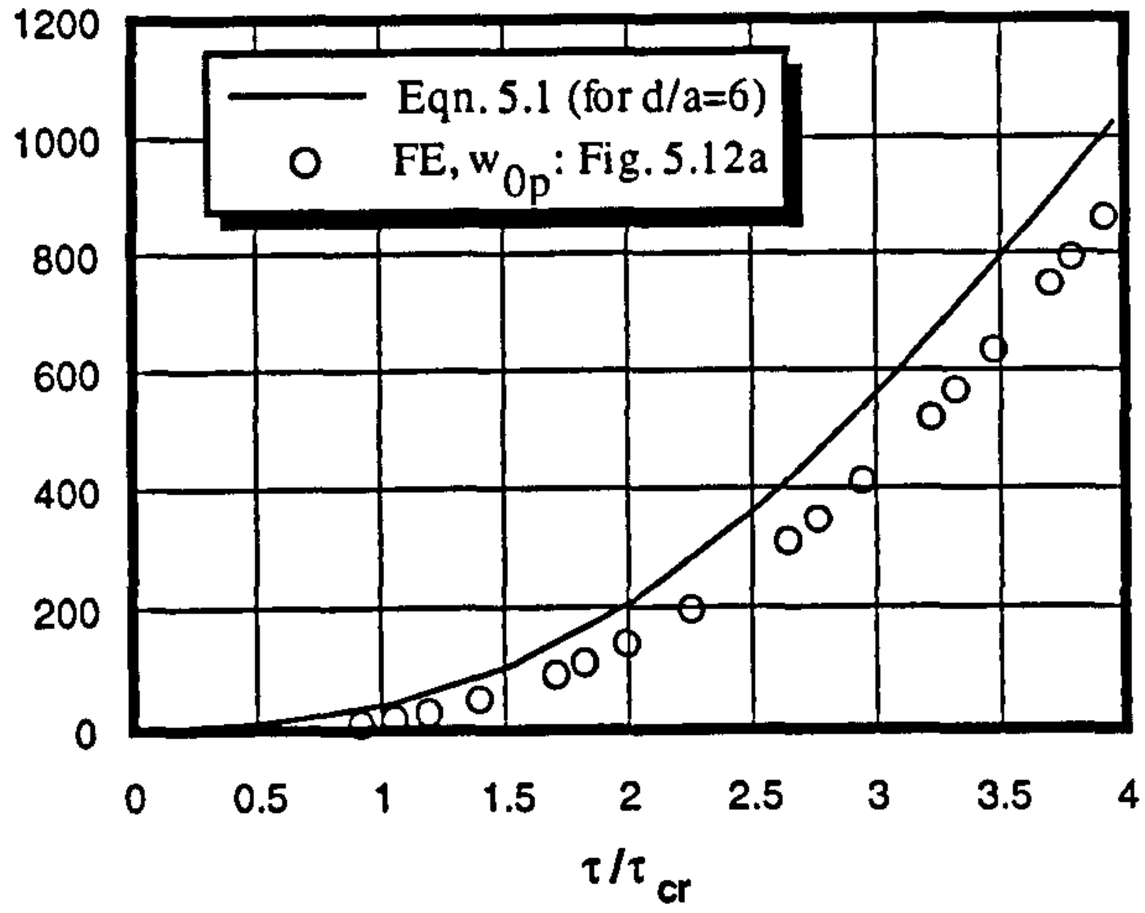






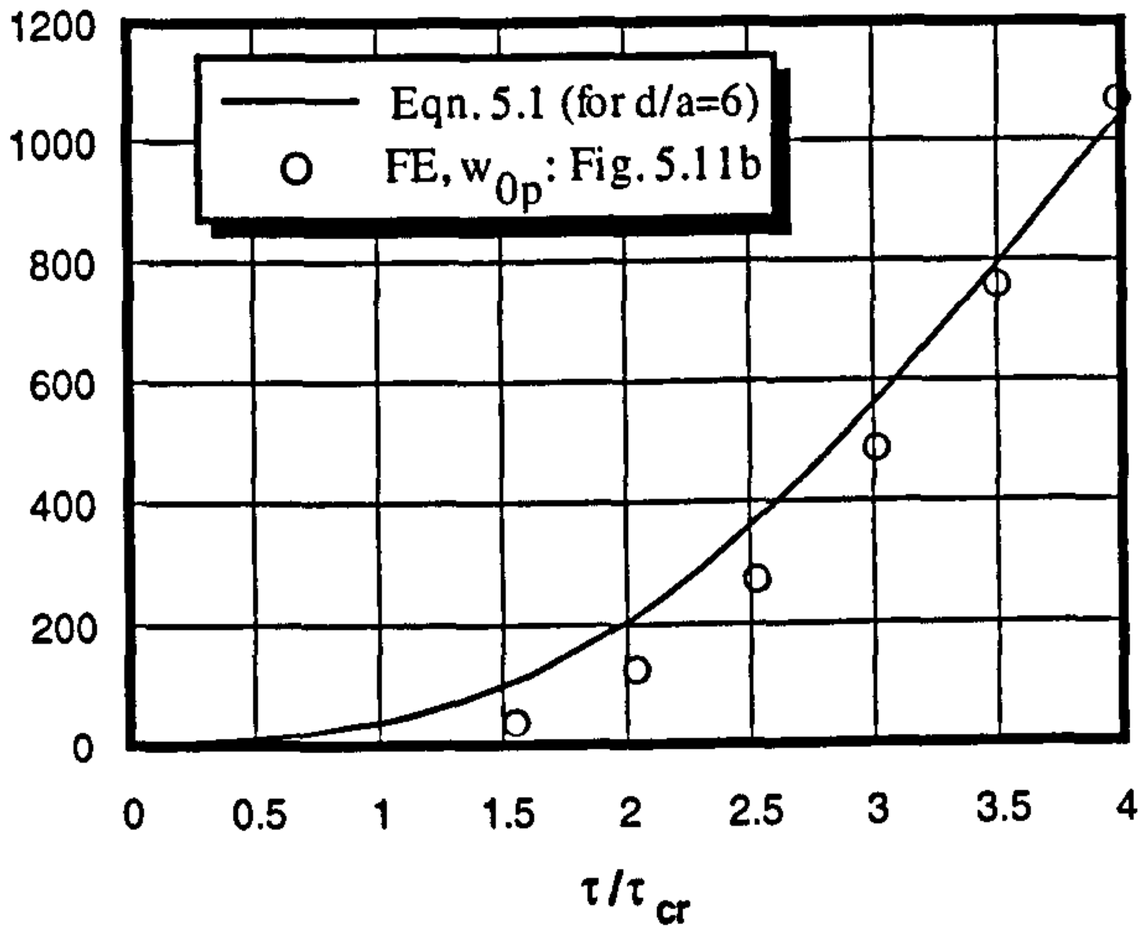
(g) d/a=10

Figure 5.13 (Cont.) Maximum bending moments in the knife edge. Non-linear elastic FE results. CUCU plates with a straight knife edge. Imperfection affine to the 1st PS buckling mode. Pure shear



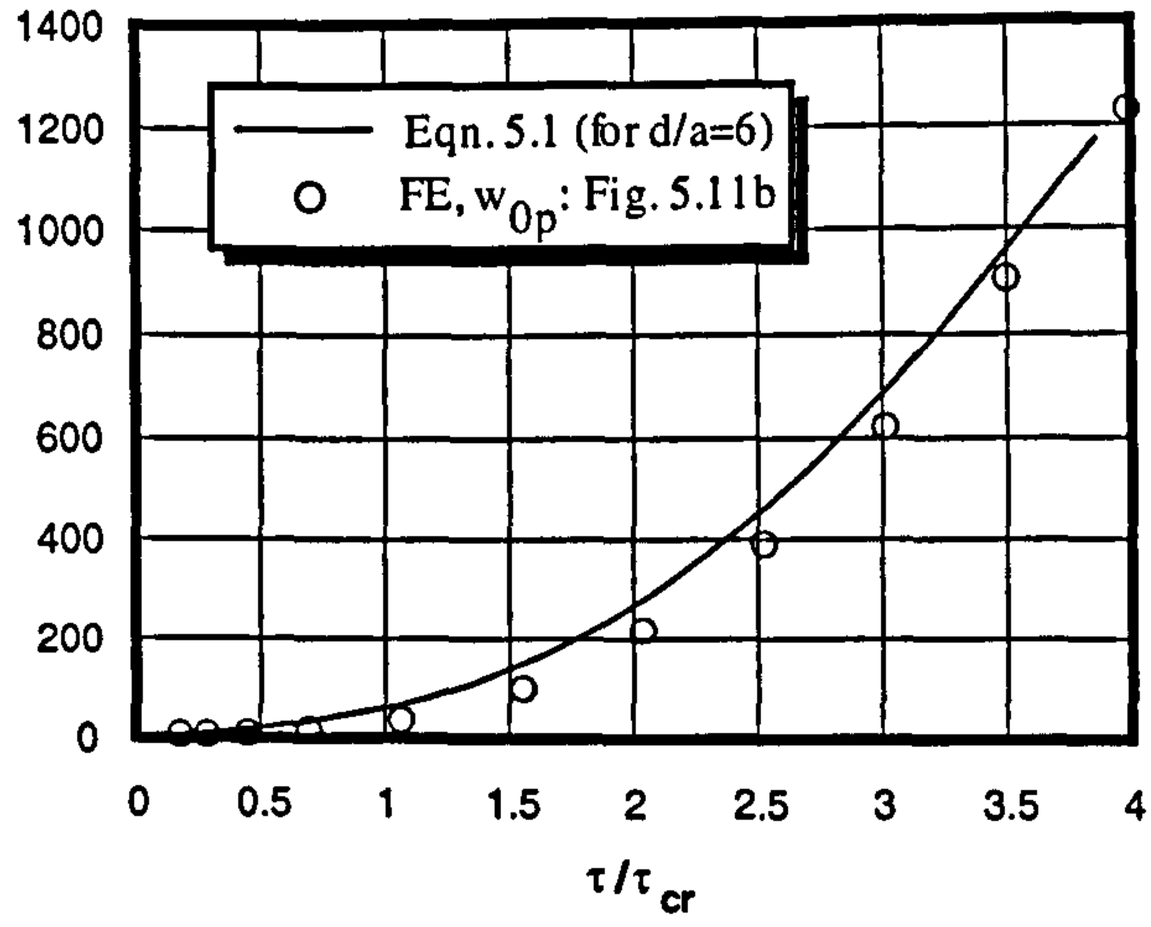
(a) d/a=7

w_{0p}/t=1.091



(b) d/a=10

w_{0p}/t=1.091



(c) d/a=10

w_{0p}/t=1.818

Figure 5.14 Maximum bending moments in the knife edge . Non-linear elastic FE results.
CUCU plates with a straight knife edge. Imperfection affine to the 1st PS buckling mode. Pure shear

5.2.3 Comparison of the Bending Moments in the Knife Edge and the Stiffener

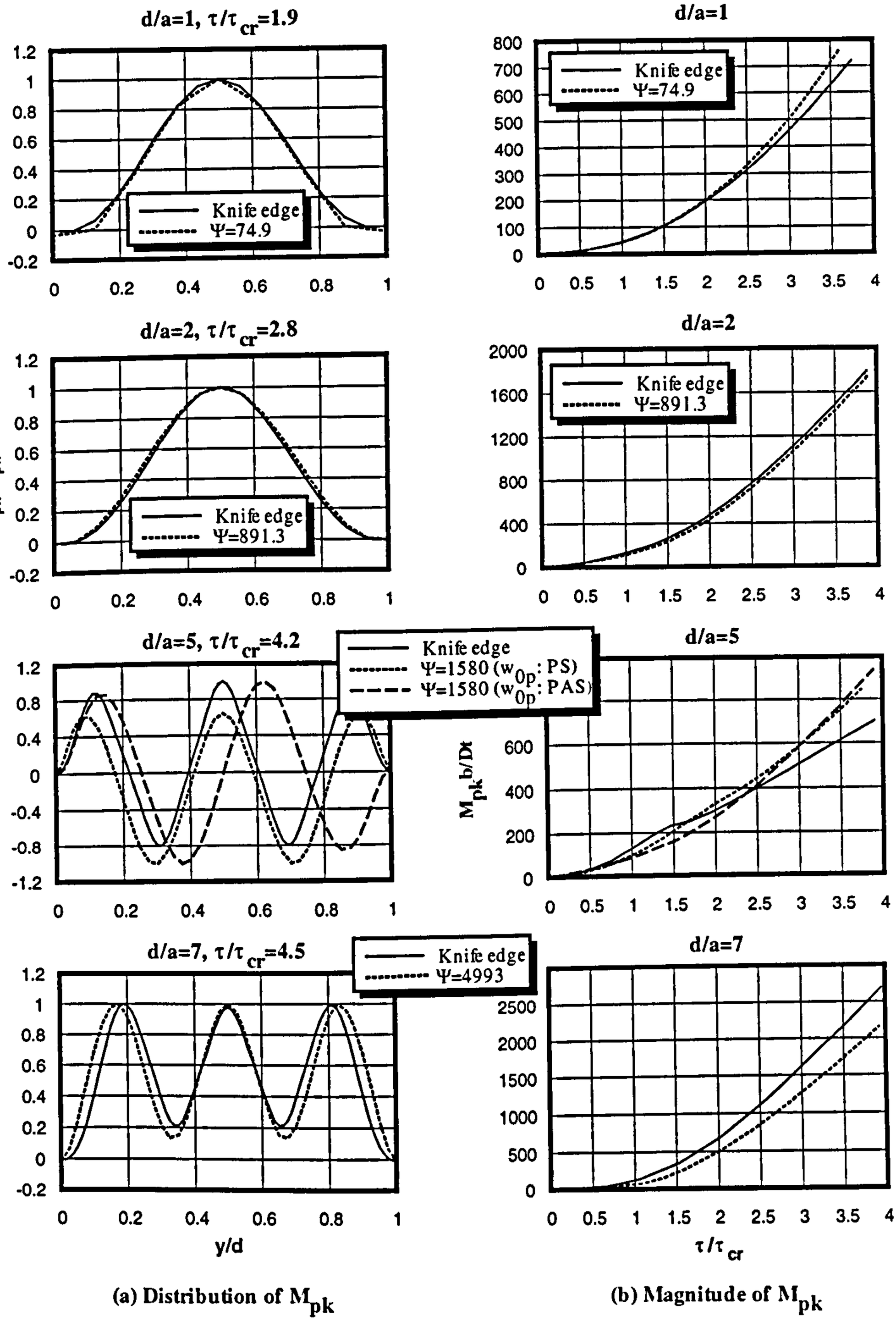
For the cases of d/a=1, 2, 5 and 7 with w_{0p}/t=1.091, non-linear elastic finite element analyses were also carried out on CUCU plates with an intermediate straight flat bar stiffener (w_{0s}=0). The values of stiffener flexural rigidity Ψ adopted are in the practical range, which are chosen to be stiff enough to divide the panels. The stiffener is modelled using quadratic beam elements, so the bending moments in the stiffener can be directly provided by ABAQUS program.

Fig. 5.15 presents a comparison of the bending moments between the knife edge and the stiffener. It is evident that for these two stiffening forms, both the distributions and the maximum amplitudes of the bending moments are respectively quite close to each other. This observation confirms that:

- *The knife edge moment can be taken as an estimate of the stiffener bending moment due to the panel bending effect.*
- *The equivalent nodal force method described in Section 4.4 can be used to convert the nodal reactions along the knife edge into the knife edge moment.*

For d/a=5, both point symmetric and point-anti-symmetric panel imperfections were examined, but no significant difference in the maximum magnitudes of M_{pk} was found (Fig. 5.15).

As discussed previously, for very tall plates, namely, d/a=7 and 10, the bending moments in straight knife edges are sensitive to the initial panel imperfections. It will be demonstrated in Section 5.2.5 that the bending moment for d/a=7, presented in Fig. 5.15, for a straight knife edge or stiff stiffener is almost equal to the bending moment found in an imperfect stiffener, when the first PS mode is used as the imperfection mode. However, when a different initial deflection mode is imposed, the values of M_{pk} are significantly reduced, to become close to those obtained for d/a=6, as can be seen by comparing Fig. 5.14(a) with Fig. 5.13(f). Similar results are also found for d/a=10 for w_{0p}/t=1.091~1.818. A detailed discussion is given in Section 5.2.5.



(a) Distribution of M_{pk}

(b) Magnitude of M_{pk}

Figure 5.15 Comparison of bending moments between the knife edge and a stiffener. Pure shear. CUCU plates with an straight knife edge or flat bar stiffener. Non-linear elastic FE results. Initial imperfection affine to the 1st PS buckling mode, $w_{0p}/t=1.091$. $w_{0s}/t=0$. $\Psi=EI_s/Db$

5.2.4 Effects of Axial Rigidity of Stiffener on M_{pk}

In the stiffener design model presented in Chapter 8, the axial force resulting from the tension field action is also taken into account. In Chapter 6, plates with a straight non-deflecting stiffener are used to investigate the in-plane axial forces exerted on the stiffeners. By contrast, it is noted that the knife edge plate model, shown in Fig. 5.1, corresponds to a zero cross-sectional area of the stiffener. In this subsection, the effects of the stiffener axial rigidity, $\Omega=A_s/at$, on the knife edge moment are examined. The finite element model used for this purpose is based on the knife edge model (Fig. 5.1), but with added axial spring elements (SPRINGA) along the knife edge, and the spring stiffness is assigned a value great enough to be considered as $\Omega=\infty$.

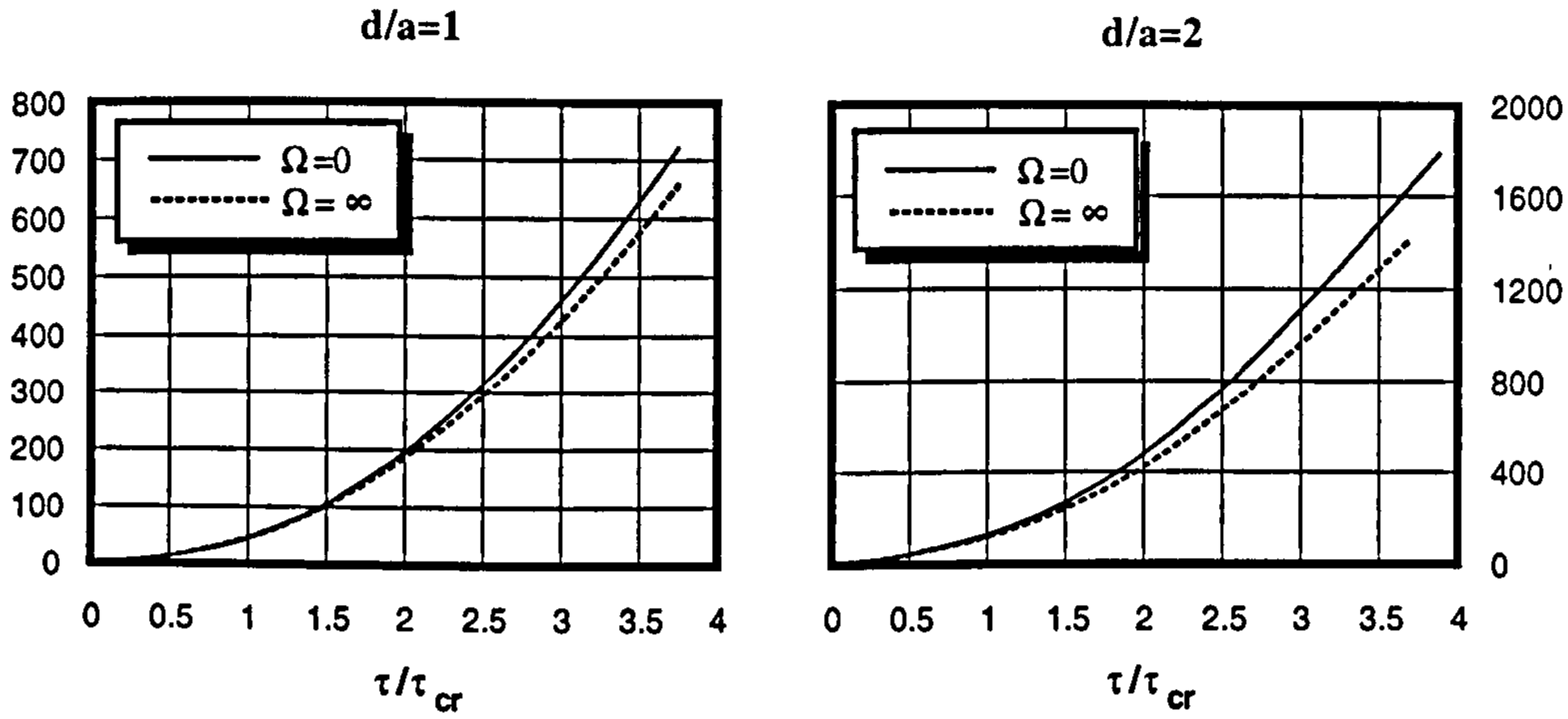


Figure 5.16 Variation in the knife edge moment with the stiffener axial rigidity. Pure shear. CUCU plates with a straight knife edge, with axial springs arranged along the knife edge. Non-linear elastic FE results. $w_{0p}/t=1.091$. $w_{0s}=0$. $\Omega=A_s/at$

Fig. 5.16 presents the non-linear elastic finite element results for the cases of d/a=1 and 2 with $w_{0p}/t=1.091$. It is evident that the knife edge bending moment does not vary significantly with the axial rigidity of the stiffener. However, it is expected that with the increase of panel aspect ratio d/a, the effects of the axial constraints provided by the stiffener may also increase. This tendency can be seen in Fig. 5.15, where comparisons between the knife edge and a practical stiffener were made. Nevertheless, the

differences illustrated in Fig. 5.15 for tall plates are considered to be negligible, since it is found in Section 5.2.5 and also in Ref [1] that as d/a is increased, the local panel bending effect becomes less important, and conversely the effect of the overall buckling tendency becomes much more significant. This conclusion provides further justification for the knife edge model to be used to evaluate the bending moments in the stiffeners.

5.2.5 Contribution of M_{pk} to the Stiffener Bending Moment M_s

In Section 5.2.3, a comparison of the bending moments was made between the knife edge and a stiffener of large flexural rigidity, and both were straight (w_{0s}=0). Such a comparison provides verification in the modeling of the local panel bending effects. In this section, the contribution of the knife edge moment M_{pk} to the total bending moment in a non-straight stiffener, M_s, is investigated. The purpose of doing this is to provide a behavioural understanding, so the relationship between the knife edge moment and panel aspect ratio, defined by Eqn. 5.1 and Table 5.2, can be further simplified, which will be discussed in Section 5.2.6. Further, by carrying out such a comparative study, the implication of the two different sets of the bending moments in straight knife edges, corresponding to the different magnitudes or mode pattern of the initial imperfection, observed in Section 5.2.2.3 for d/a=7 and 10, can be clarified.

Non-linear elastic finite element analyses were carried out on CUCU plates with an intermediate stiffener for d/a=1, 2, 5, 7 and 10 with w_{0p}/t=1.091, and as mentioned previously, the values of stiffener flexural rigidity Ψ used are in the practical range. In Fig. 5.17, the bending moments in both straight and initially imperfect stiffeners are compared with the moments in a straight knife edge, and the values at the ultimate shear stresses for simply supported panels with $\sigma_{0p}=\sigma_{0s}=355N/mm^2$ are tabulated in Table 5.3.

It is shown in Table 5.3 that for d/a=1 and 2, the knife edge moment M_{pk} accounts for nearly 92% of the bending moment M_s in an imperfect stiffener for the cases studied. Consequently, the accuracy of representing the panel bending effect, namely, M_{pk}, is quite important for d/a≤2 for design of the stiffeners. The ratios of the bending moments between straight stiffeners and imperfect stiffeners are around 91% for d/a=1 and 2.

Table 5.3 Comparison of the bending moments in the knife edge and stiffeners.

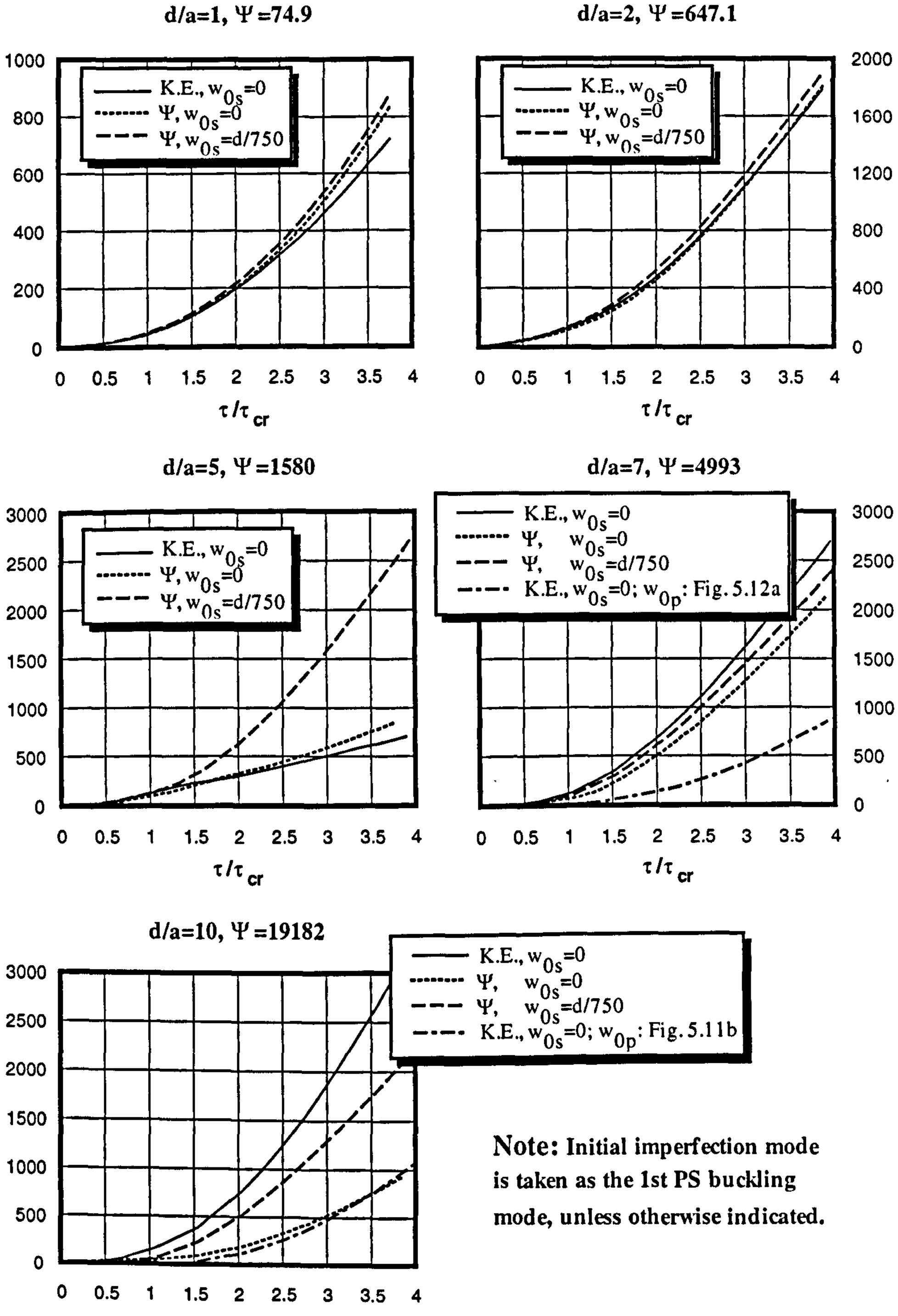
Non-linear elastic buckling analyses. FE results. Pure shear b=540mm, t=3mm, $w_{0t}/t=1.091$*

d/a	Ψ	$\tau_{u,ss}/\tau_{cr,ss}$	$\frac{M_{pk}b}{Dt}(w_{0s}=0)$	$\frac{M_s b}{Dt}(w_{0s}=0)$	$\frac{M_s b}{Dt}(w_{0s}=\frac{d}{750})$	$\frac{M_{pk}(w_{0s}=0)}{M_s(w_{0s}=d/750)}$	$\frac{M_s(w_{0s}=0)}{M_s(w_{0s}=d/750)}$
1	74.9	1.827	162.1	164.4	177.1	0.915	0.928
2	647.1	2.342	665.4	649	723.1	0.920	0.898
5	1580	2.227	344.7	379.1	820.3	0.420	0.462
7	4993	2.229	872.2	657.4	779.7	1.119	0.843
			187.4**	352.8**	779.7	0.240	0.452
10	19182	2.271	1000.2	260.3	697.8	1.433	0.373
			192.8***	260.3	697.8	0.276	0.373

Notes: * Imperfection modes affine to the first point-symmetric buckling mode, unless otherwise indicated.

**Imperfection mode as in Fig. 5.12(a).

***Imperfection mode as in Fig. 5.11(b).



Note: Initial imperfection mode is taken as the 1st PS buckling mode, unless otherwise indicated.

Figure 5.17 Comparison of the knife edge moments with the bending moments in stiffeners.
CUCU plates with an intermediate straight knife edge or flat bar stiffener.
Non-linear elastic FE results. Pure shear. $w_{0p}/t=1.091$. $\Psi=EI_s/Db$

For d/a=5, it is seen that the panel bending effect, represented by M_{pk}, only accounts for about 42% of the total stiffener bending moment. Hence, the accuracy of M_{pk} become less important as d/a is increased from d/a=2. By contrast, the contribution of the effect of overall buckling tendency becomes more important, which accounts for about 54% of the total stiffener moment.

It is noticed that for the cases of d/a=7 and 10 investigated, when the initial imperfection mode is taken as the first point-symmetric buckling mode, the knife edge moment M_{pk} is even greater than the total bending moment M_s in a non-straight stiffener. By examining the contour plots of out-of-plane deflection, it is found that for this imperfection mode, the non-linear elastic deflection modes for both the straight knife edge and the imperfect stiffener are quite similar. However, when the modes shown in Figs. 5.12a and 5.11b are used as the initial deflection modes for d/a=7 and 10, respectively, the knife edge moments drop to about 25% of the total stiffener moments. Furthermore, it is observed in Fig. 5.17 that for d/a=10, the knife edge moment associated with the imperfection mode of Fig. 5.11b, is quite close to the bending moment in a straight stiff stiffener. Therefore, it is considered that for this case, the knife edge moment obtained by employing the imperfection mode Fig. 5.11b, represents the local panel bending effect. On the other hand, the knife edge moment obtained by using the 1st PS buckling mode as the imperfection mode, may characterise the total stiffener moment, and as discussed previously, this is because the deflection mode in this case is not free to change away from the initial imperfection mode.

Based on the above discussions on the behaviour of very tall plates, it may be concluded that for d/a≥7, the bending moment in a straight knife edge may either represent the stiffener moment due to the local panel bending effect, or the total stiffener moment, which includes both the panel bending effect and the overall buckling effect. The key factors that determine which occurs, are the mode profile and the magnitude of the initial panel imperfection.

By referring to Figs. 5.14 and 5.17, it can be seen that for d/a=7 and 10, the knife edge moments, which may represent the local panel bending effect, are close to the values of

M_{pk} for d/a=6. Therefore, for the reason of simplicity, it is assumed that for d/a≥7, M_{pk} can be taken as the same values of M_{pk} for d/a=6, and the differences between M_{pk} and the total stiffener moment M_s can be accounted for by the bending moments calculated from the overall buckling model presented in Chapter 7, as for d/a=6. In Chapter 8, this assumption will be adopted in the proposed design model for transverse stiffeners, and the bending moments calculated from the proposed model will be compared with the numerical solutions (see Section 8.3), where satisfactory agreement can be seen.

5.2.6 Design Formulae for Predicting M_{pk}

It has been found in Section 5.2.2.3 that for plates with a straight knife edge under pure shear, Equation 5.1, together with its coefficients defined in Table 5.2, can accurately represent the magnitudes of the knife edge bending moment M_{pk}. However, it has been found that the predicting of M_{pk} for very tall plates (d/a≥7) is very complicated. Also, in order to make the prediction of M_{pk} as simple as possible, it is considered that the relationship between M_{pk} and panel aspect ratio d/a could be further simplified. In Fig 5.18, $M_{pk}b/Dt$ versus τ/τ_{cr} curves for d/a=0.5~6 with w_{0p}/t=1.091 are plotted together, the curves for other ratios of w_{0p}/t are not shown as they are quite similar. On account of the different requirements in predicting M_{pk} for different aspect ratios d/a, as discussed in Section 5.2.6, it is considered that the knife edge moment M_{pk} for different panel aspect ratios can be represented by three design curves, which are shown in Fig. 5.18.

For the design of transverse stiffeners on plates subjected to pure shear, it is proposed that the panel bending effect, M_{pk}, can be calculated in terms of these three curves. The proposed design formulae for calculating M_{pk} can be written as:

- *Curve A:*

$$\frac{M_{pk}b}{Dt} = 29.71\left(\frac{w_{0p}}{t}\right)\left(\frac{\tau}{\tau_{cr}}\right) - 0.524\left(\frac{w_{0p}}{t}\right)\left(\frac{\tau}{\tau_{cr}}\right)^2 \qquad \text{for d/a}\leq 1$$
$$-6.96\left(\frac{\tau}{\tau_{cr}}\right) + 4.962\left(\frac{\tau}{\tau_{cr}}\right)^2 + 21.37\left(\frac{\tau}{\tau_{cr}}\right)^3 - 2.865\left(\frac{\tau}{\tau_{cr}}\right)^4$$

- *Curve B:*

$$\frac{M_{pk}b}{Dt} = 83.62\left(\frac{w_{0p}}{t}\right)\left(\frac{\tau}{\tau_{cr}}\right) - 16.59\left(\frac{w_{0p}}{t}\right)\left(\frac{\tau}{\tau_{cr}}\right)^2 \qquad \text{for d/a=2}$$
$$-14.03\left(\frac{\tau}{\tau_{cr}}\right) + 19.70\left(\frac{\tau}{\tau_{cr}}\right)^2 + 54.99\left(\frac{\tau}{\tau_{cr}}\right)^3 - 7.676\left(\frac{\tau}{\tau_{cr}}\right)^4$$

- *Curve C:*

$$\frac{M_{pk}b}{Dt} = 69.47\left(\frac{w_{0p}}{t}\right)\left(\frac{\tau}{\tau_{cr}}\right) + 1.942\left(\frac{w_{0p}}{t}\right)\left(\frac{\tau}{\tau_{cr}}\right)^2 \qquad \text{for d/a}\geq 3$$
$$-16.96\left(\frac{\tau}{\tau_{cr}}\right) + 80.11\left(\frac{\tau}{\tau_{cr}}\right)^2 - 7.281\left(\frac{\tau}{\tau_{cr}}\right)^3 - 0.264\left(\frac{\tau}{\tau_{cr}}\right)^4$$

(5.3)

where τ_{cr} is the critical shear stress for simply supported panel, and can be determined using Eqn. 5.2. The values of M_{pk} for 1<d/a<2 and 2<d/a<3 can be obtained by linear interpolation, as illustrated in Fig.5.19.

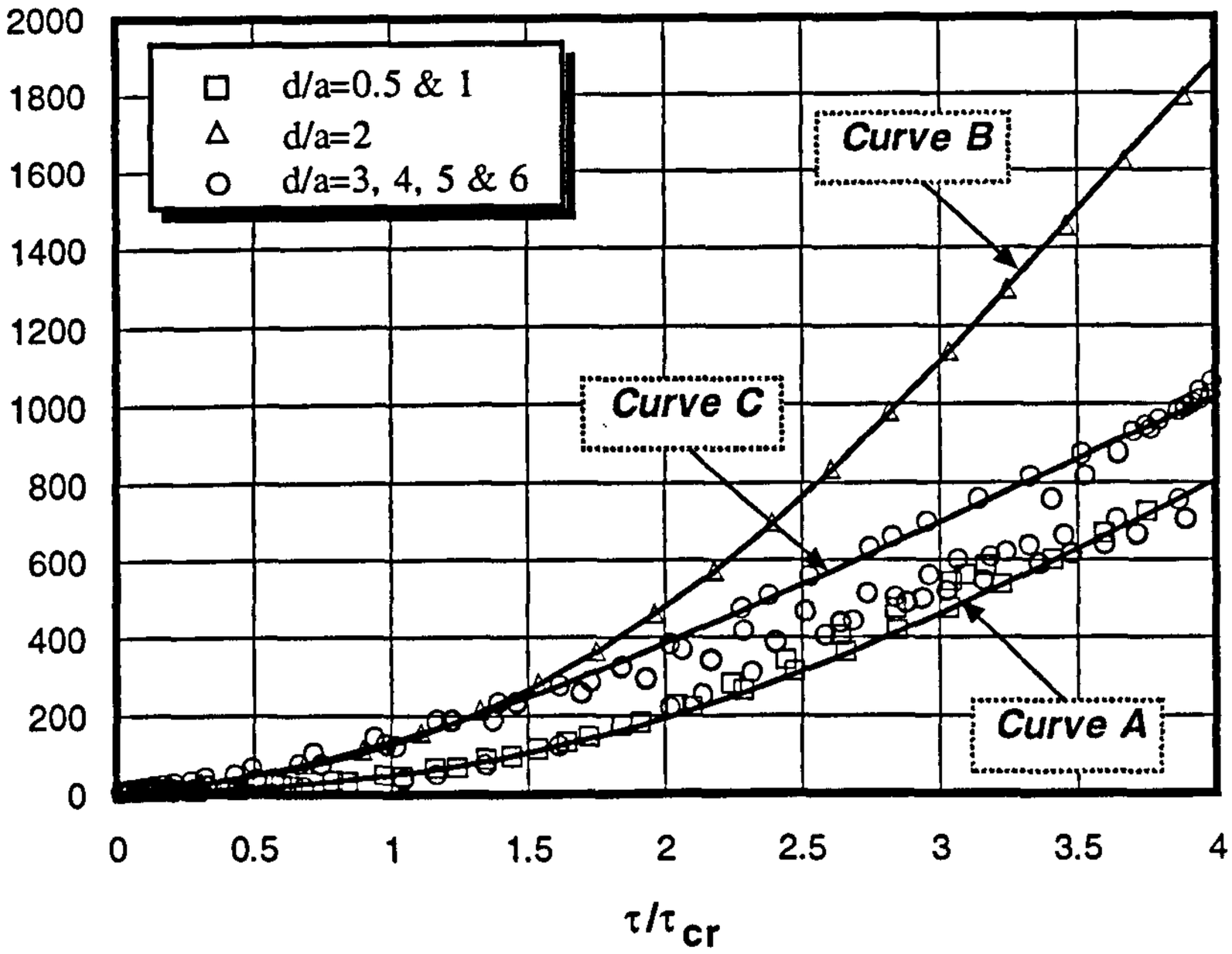


Figure 5.18 Knife edge moment M_{pk} for different panel aspect ratios d/a. Pure shear. CUCU plates with a straight knife edge. Non-linear elastic FE results

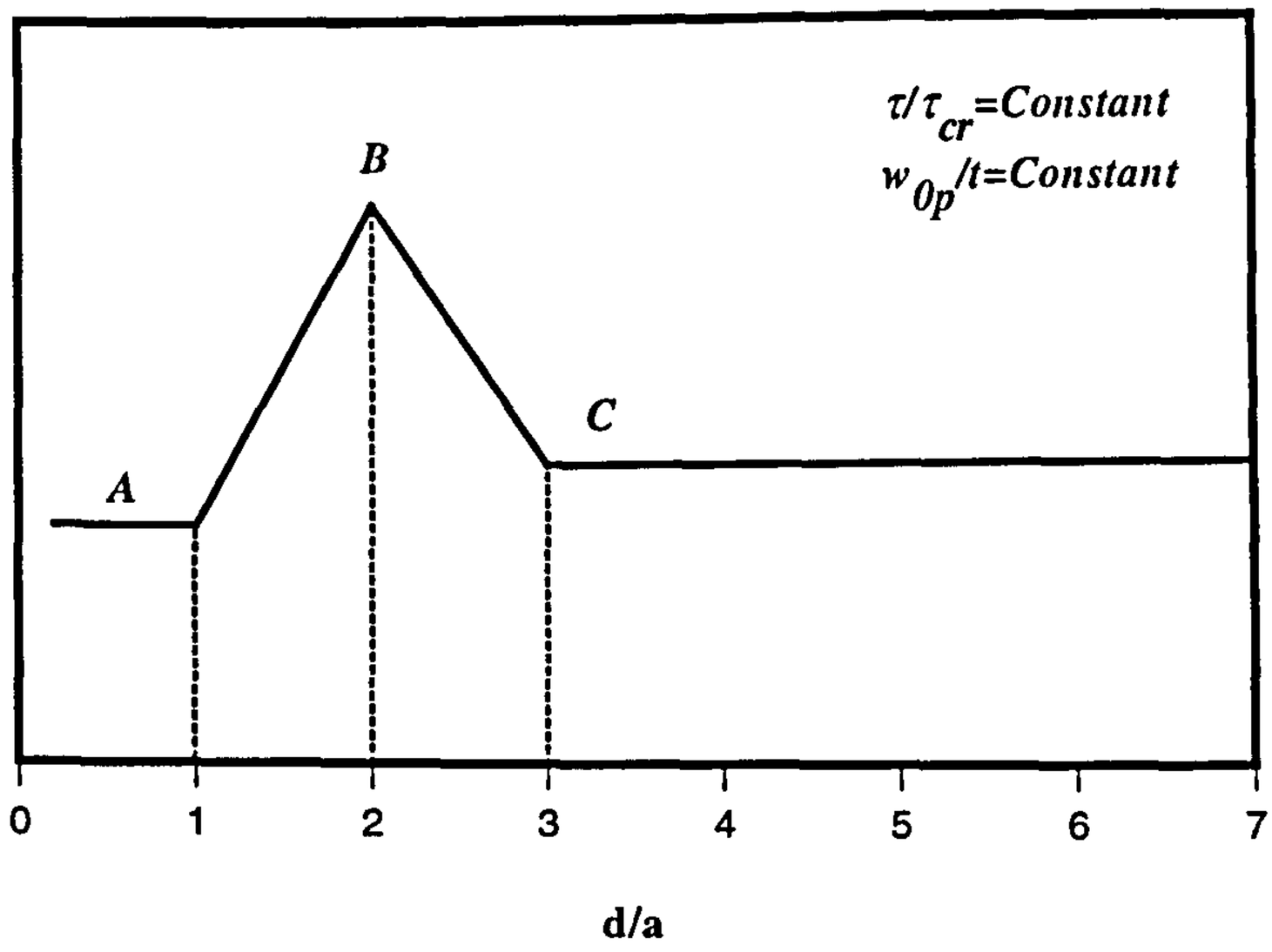


Figure 5.19 Schematic representation of the knife edge moment M_{pk}, varying with aspect ratio d/a

5.3 PLATES SUBJECTED TO COMBINED LOADING

5.3.1 General

In this section, plates with a straight knife edge, subjected to coexistent shear, compression and bending (Fig. 5.1), are considered. The bending moment in the knife edge is investigated by carrying out a non-linear elastic parametric study for plates subjected to different proportions of compression and shear, or of bending and shear.

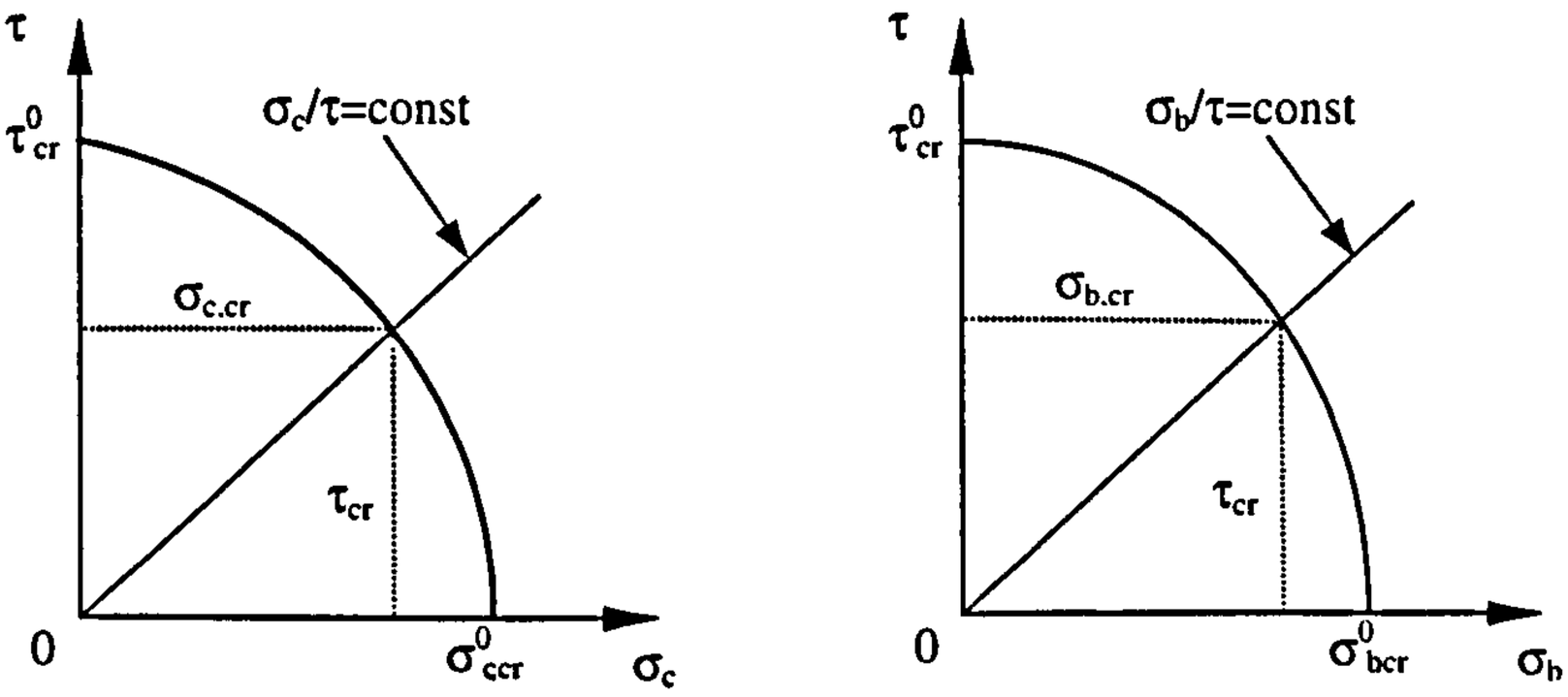
It would be impracticable to conduct a parametric study which covers a wide range of cases corresponding to the different combinations of the parameters such as the ratio of individual load components, panel aspect ratio and initial panel imperfection, with which the knife edge moment would vary. However, it is noted that Grayson [46] has suggested that the design value of the stiffener rigidity determined for pure shear (Eqns. 9.8 and 9.9, [45]) might be used as a safe estimate of the required stiffener rigidity for all possible combinations of web loading. A similar conclusion was also made by Rahal and Harding [7] who stated that the stiffener rigidity needed for the maximum panel shear capacity in the absence of other direct stresses is always greater than the rigidity needed for any other combination of stresses that is within the panel capacity. Therefore, the intention of this parametric study is to examine the relations in the knife edge moments for pure shear and for combined loading. It is anticipated that with some modifications, the predicting formulae obtained for the pure shear condition could be approximately extended to the combined loading conditions, possibly by introducing an equivalent shear stress. To justify the adequacy of this anticipation for predicting the knife edge moments for plates subjected to combined shear and longitudinal stresses, the following parameters were considered in the parametric study:

- $d/a=0.5, 1, 2, 5$
- $\sigma_c:\tau$ *or* $\sigma_b:\tau=1:0, 5:1, 2:1, 1:1, 1:2, 1:5, 0:1$

For the non-linear buckling analyses, the load components were applied proportionally.

The initial imperfection is affine to the first buckling mode for the combined loading, which is, or is close to, a symmetric or point-symmetric buckling mode. The imperfection magnitude is taken as $w_{0p}/t=0.485$ (b/t=80) for shear and compression, and $w_{0p}/t=1.091$ (b/t=180) for shear and bending.

In the latter part of this chapter, τ^0_{cr}, $\sigma^0_{c,cr}$ and $\sigma^0_{b,cr}$ stand for the critical stresses of the plates, subjected to shear, compression or bending alone, respectively. The stresses which produce buckling when acting simultaneously are denoted as τ_{cr}, $\sigma_{c.cr}$ and $\sigma_{b.cr}$, as illustrated in Fig. 5.20.



(a) Shear & Compression

(b) Shear & Bending

Figure 5.20 Schematic representations of the critical stresses for combined loading conditions

5.3.2 Combined Shear and Compression

5.3.2.1 Critical Buckling Behaviour

The critical buckling analysis is carried out mainly to obtain the critical buckling modes, and the first mode which is, or is close to, a symmetric or point-symmetric buckling mode, is used to form the initial imperfections for the non-linear buckling analyses. The numerical results of the critical buckling analysis are summarised below.

The contour plots of the first two critical buckling modes for plates with a straight knife edge are given in Fig. 5.21, covering the range of panel aspect ratios considered in this study, i.e. d/a=0.5, 1, 2, and 5. It can be observed in Fig. 5.21 that for the plates of d/a≤1, the variation in the buckling modes with the load ratio σ_c/τ is quite regular, which lies mainly in the progressive change of the inclination of buckles. However, for tall panels, the buckling modes for different values of the load ratio σ_c/τ differ from each other in both the buckle inclination and the number of buckles along the depth of the plate.

The interaction curves of the lowest critical buckling stresses for the knife edge plates of d/a=0.5, 1, 2 and 5, subjected to combined shear and compression are presented in Fig. 5.22. As can be seen in Fig. 5.22, the interaction curve between shear and compression can be represented approximately by the equation:

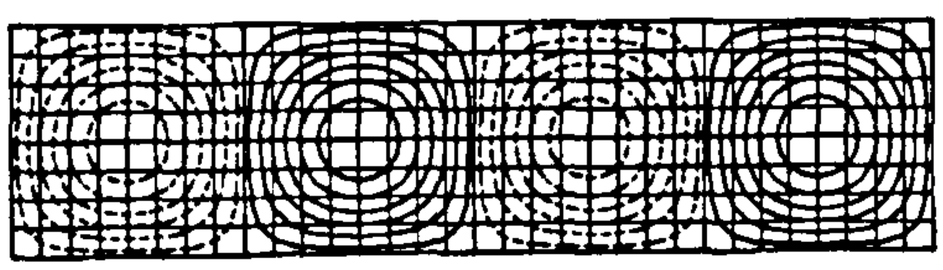
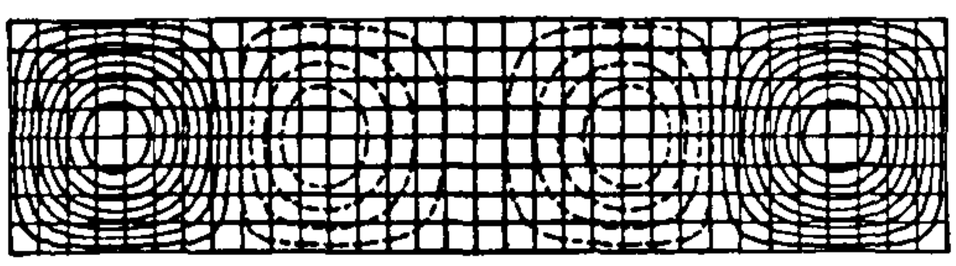
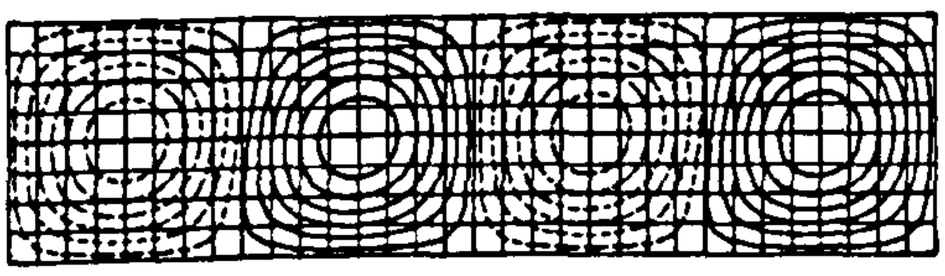
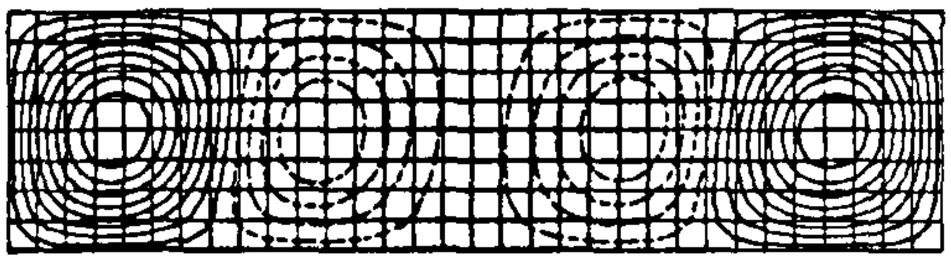
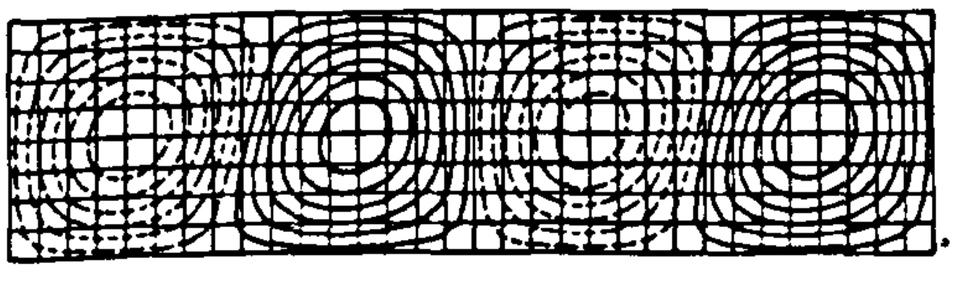
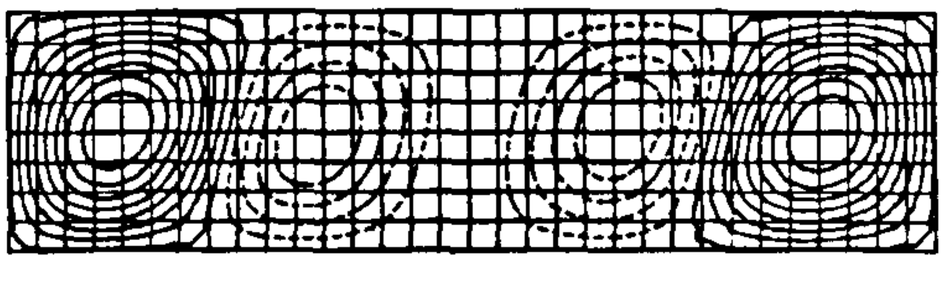
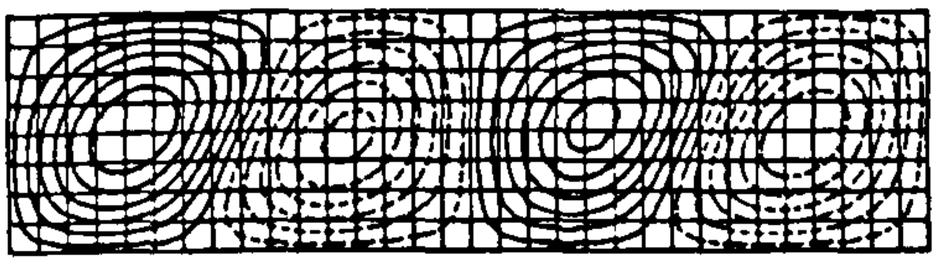
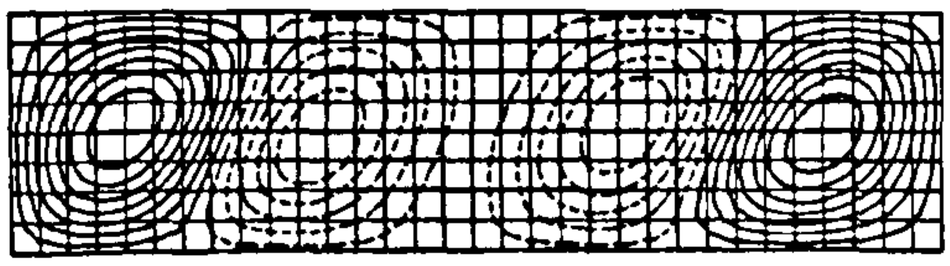
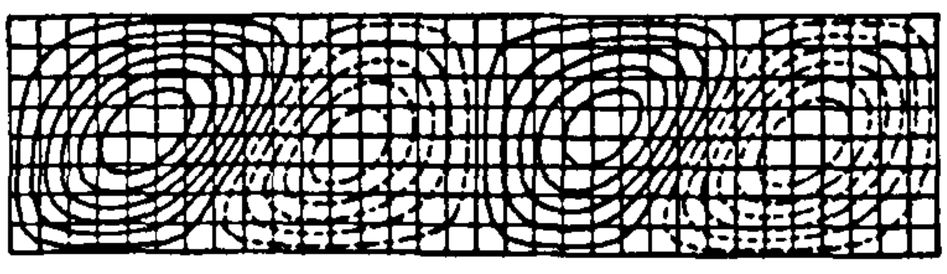
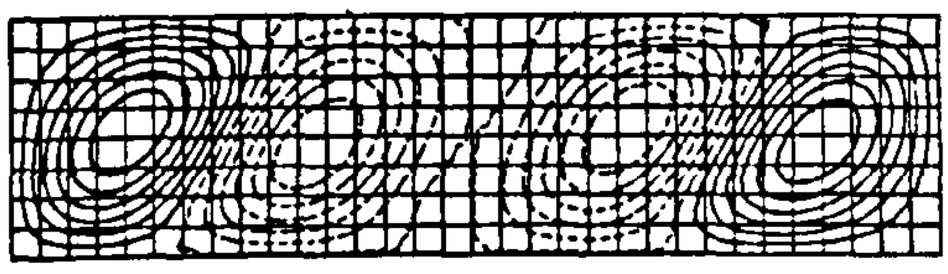
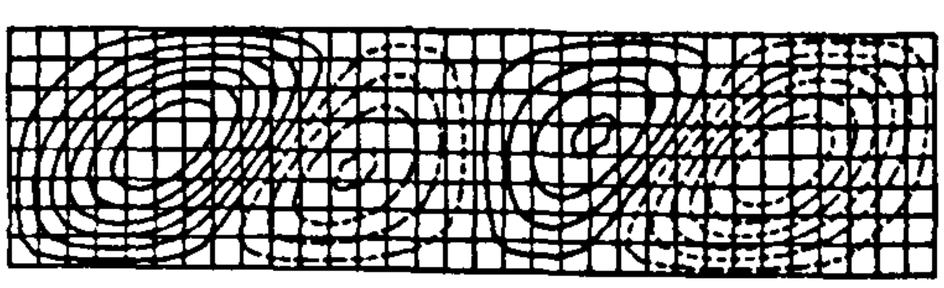
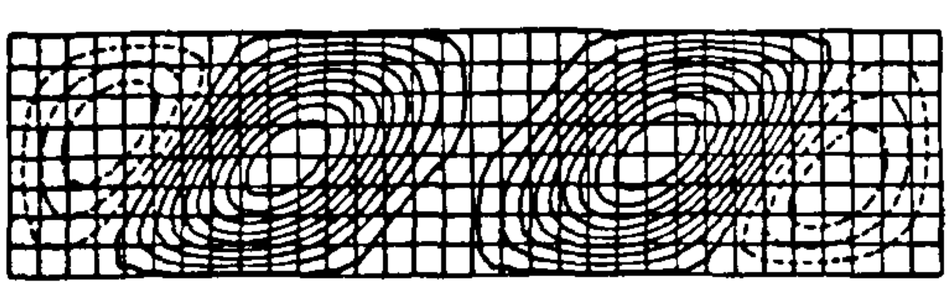
$$\frac{\sigma_{c,cr}}{\sigma^0_{c,cr}}+\left(\frac{\tau_{cr}}{\tau^0_{cr}}\right)^2=1 \tag{5.4}$$

It is noted in Fig. 5.22 that due to the effect of mode changes, as d/a is increased from 1 to 5, the difference between the finite element results and Eqn. 5.4 becomes gradually larger

It has been found in Section 5.2.1.2 that the lowest critical buckling stress for plates with a knife edge under pure shear, τ^0_{cr}, may be taken as the simply supported panel buckling stress, which can be calculated using Eqn. 5.2. Similarly, it is suggested that the critical compressive stress $\sigma^0_{c,cr}$ can be determined by the equation:

$$\sigma^0_{c,cr}=k_{cr}\frac{\pi^2 D}{d^2 t},\quad k_{cr}=\begin{cases}4, & for\quad d/a\le 1\\ \left(\dfrac{a}{d}+\dfrac{d}{a}\right)^2, & for\quad d/a\ge 1\end{cases} \tag{5.5}$$

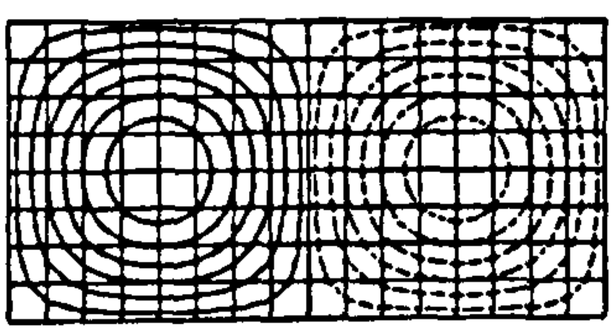
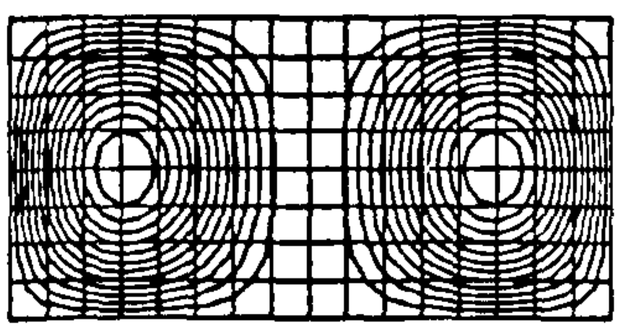
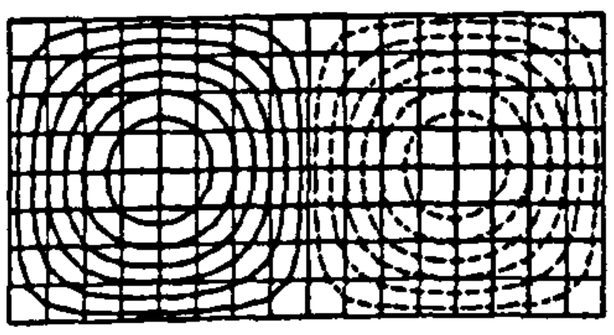
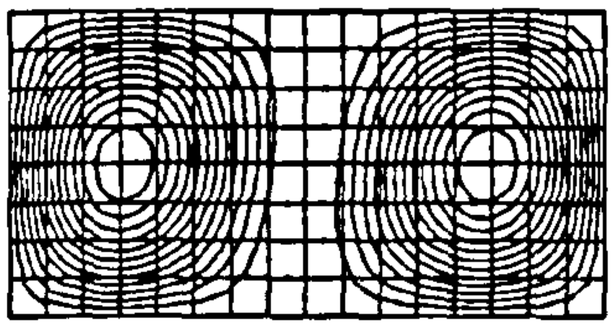
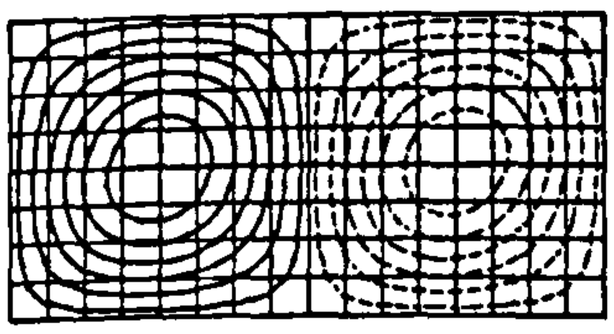
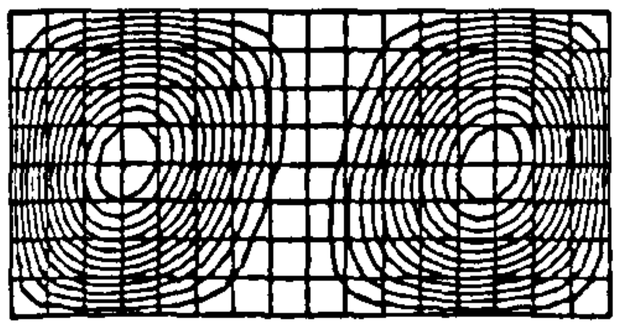
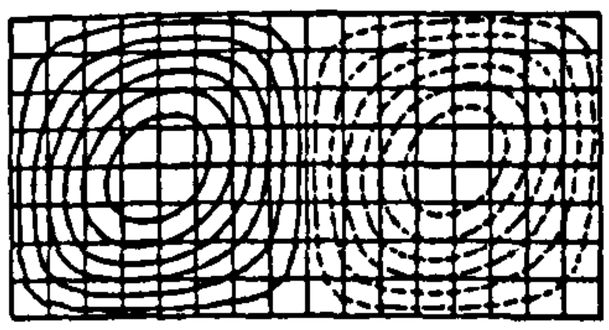
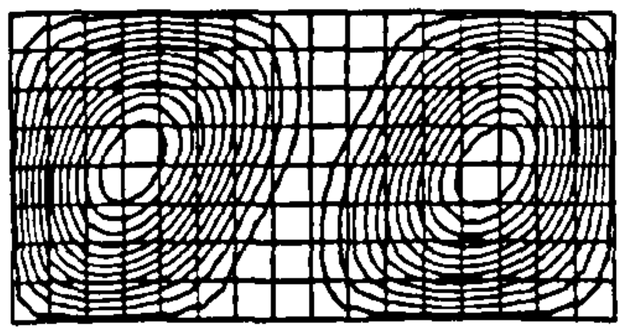
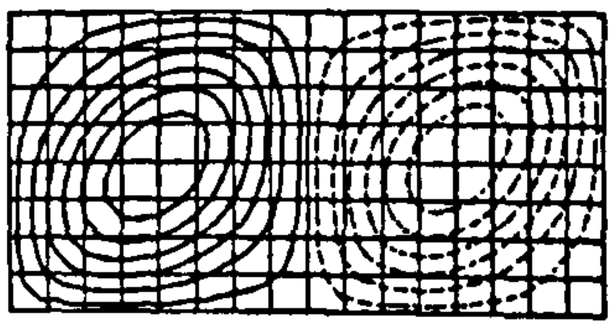
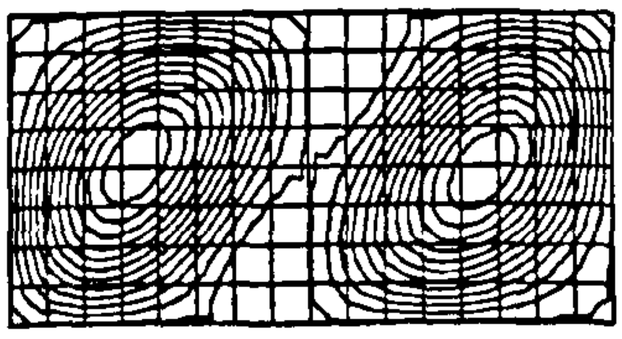
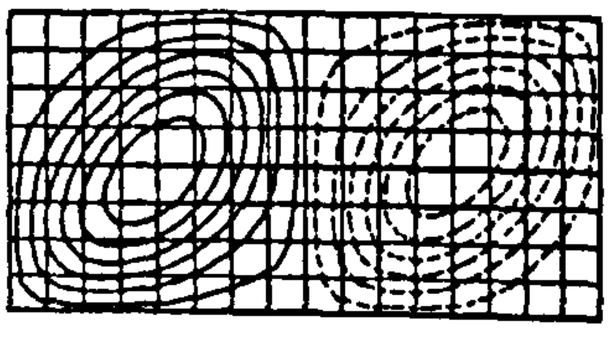
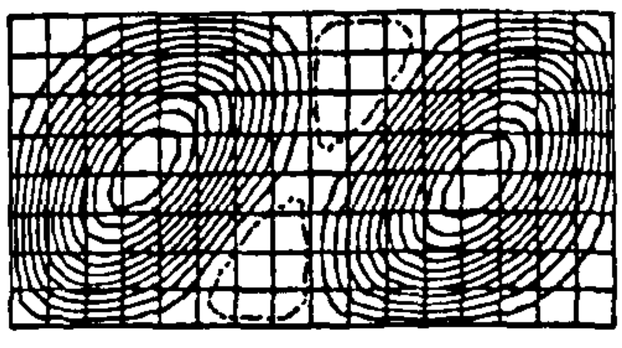
Eqn. 5.5 is generally used for calculating the compressive buckling stresses for simply supported panels [56].

1st Buckling Mode	2nd Buckling Mode
	
σ_c:τ=1:0, $k_{cr,c}$=3.997, $k_{cr,s}$=0	σ_c:τ=1:0, $k_{cr,c}$=4.233, $k_{cr,s}$=0
	
σ_c:τ=5:1, $k_{cr,c}$=3.943, $k_{cr,s}$=0.789	σ_c:τ=5:1, $k_{cr,c}$=4.172, $k_{cr,s}$=0.834
	
σ_c:τ=2:1, $k_{cr,c}$=3.699, $k_{cr,s}$=1.849	σ_c:τ=2:1, $k_{cr,c}$=3.892, $k_{cr,s}$=1.946
	
σ_c:τ=1:1, $k_{cr,c}$=3.130, $k_{cr,s}$=3.130	σ_c:τ=1:1, $k_{cr,c}$=3.258, $k_{cr,s}$=3.258
	
σ_c:τ=1:2, $k_{cr,c}$=2.224, $k_{cr,s}$=4.448	σ_c:τ=1:2, $k_{cr,c}$=2.286, $k_{cr,s}$=4.572
	
σ_c:τ=1:5, $k_{cr,c}$=1.126, $k_{cr,s}$=5.629	σ_c:τ=1:5, $k_{cr,c}$=1.146, $k_{cr,s}$=5.731

(a) d/a=0.5

$$Note: \quad k_{cr,c} = \sigma_{c,cr}\frac{b^2 t}{\pi^2 D} \quad , \quad k_{cr,s} = \tau_{cr}\frac{b^2 t}{\pi^2 D}$$

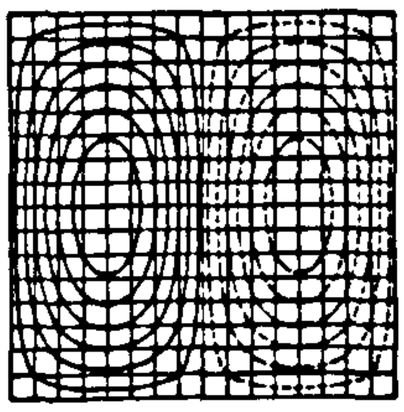
Figure 5.21 Critical buckling modes of plates with a knife edge. Shear and compression

1st Buckling Mode		2nd Buckling Mode	
	σ_c:τ=1:0 $k_{cr,c}$=3.997 $k_{cr,s}$=0		σ_c:τ=1:0 $k_{cr,c}$=4.843 $k_{cr,s}$=0
	σ_c:τ=5:1 $k_{cr,c}$=3.975 $k_{cr,s}$=0.795		σ_c:τ=5:1 $k_{cr,c}$=4.795 $k_{cr,s}$=0.959
	σ_c:τ=2:1 $k_{cr,c}$=3.866 $k_{cr,s}$=1.933		σ_c:τ=2:1 $k_{cr,c}$=4.573 $k_{cr,s}$=2.287
	σ_c:τ=1:1 $k_{cr,c}$=3.550 $k_{cr,s}$=3.550		σ_c:τ=1:1 $k_{cr,c}$=4.012 $k_{cr,s}$=4.012
	σ_c:τ=1:2 $k_{cr,c}$=2.830 $k_{cr,s}$=5.661		σ_c:τ=1:2 $k_{cr,c}$=2.998 $k_{cr,s}$=5.996
	σ_c:τ=1:5 $k_{cr,c}$=1.599 $k_{cr,s}$=7.997		σ_c:τ=1:5 $k_{cr,c}$=1.601 $k_{cr,s}$=8.003

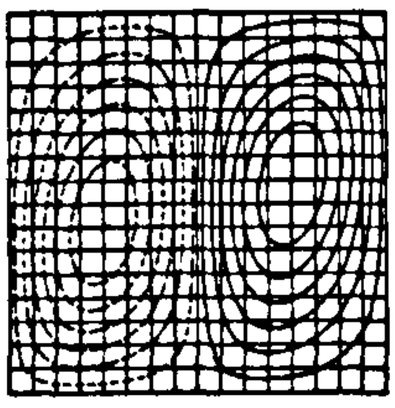
(b) d/a=1

$$Note: \quad k_{cr,c} = \sigma_{c,cr} \frac{b^2 t}{\pi^2 D} \quad , \quad k_{cr,s} = \tau_{cr} \frac{b^2 t}{\pi^2 D}$$

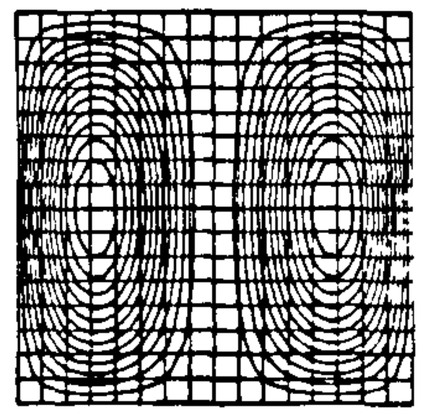
Figure 5.21 (Cont) Critical buckling modes of plates with a knife edge. Shear and compression



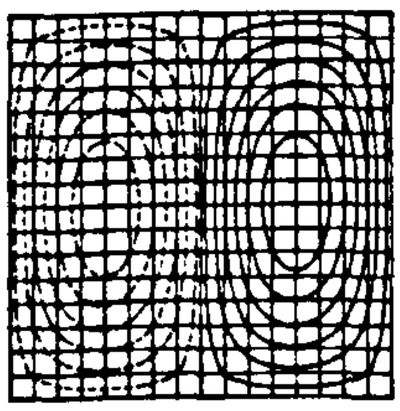
σ_c:τ=1:0, 1st Mode
$k_{cr,c}$=1.562, $k_{cr,s}$=0



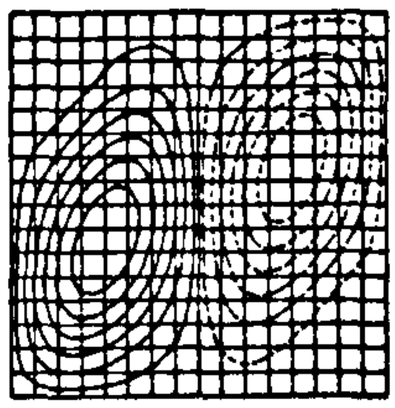
σ_c:τ=1:2, 1st Mode
$k_{cr,c}$=1.380, $k_{cr,s}$=2.759



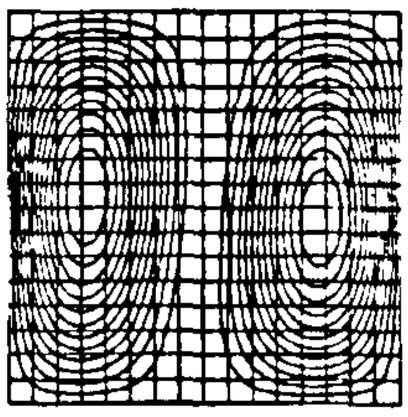
σ_c:τ=1:0, 2nd Mode
$k_{cr,c}$=2.595, $k_{cr,s}$=0



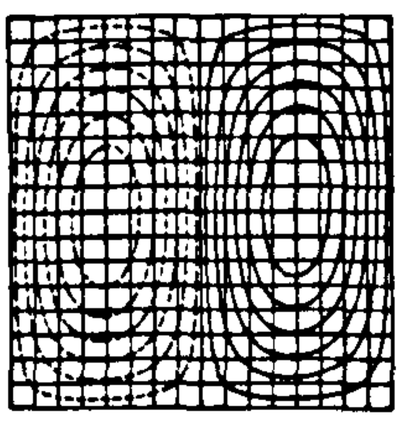
σ_c:τ=5:1, 1st Mode
$k_{cr,c}$=1.560, $k_{cr,s}$=0.312



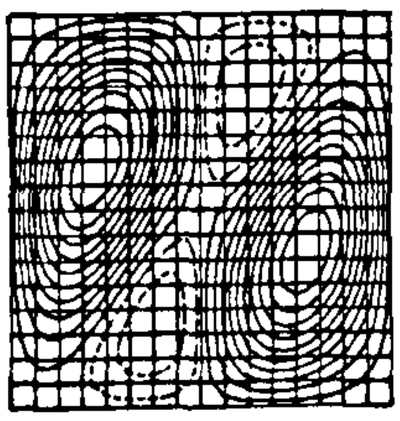
σ_c:τ=1:5, 1st Mode
$k_{cr,c}$=0.946, $k_{cr,s}$=4.728



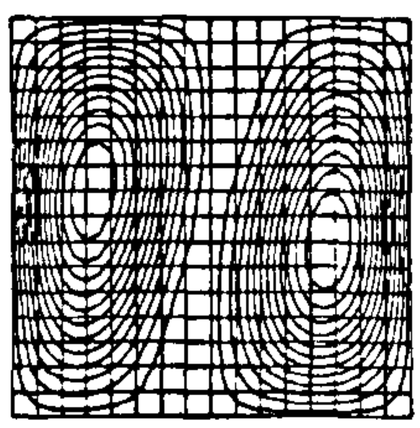
σ_c:τ=5:1, 2nd Mode
$k_{cr,c}$=2.580, $k_{cr,s}$=0.516



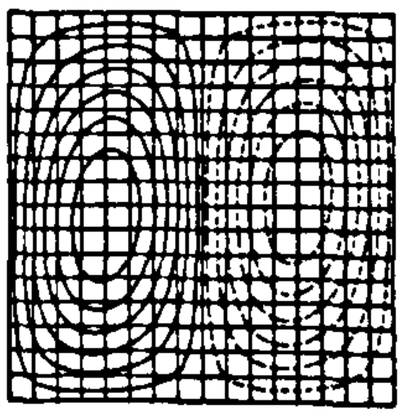
σ_c:τ=2:1, 1st Mode
$k_{cr,c}$=1.548, $k_{cr,s}$=0.774



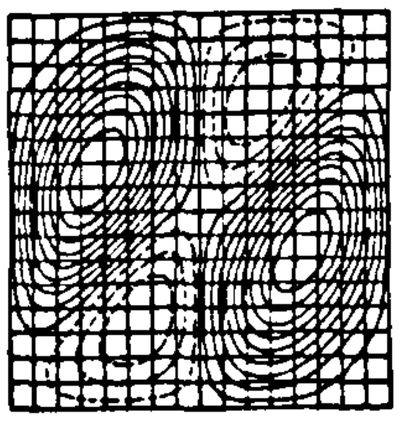
σ_c:τ=1:2, 2nd Mode
$k_{cr,c}$=1.830, $k_{cr,s}$=3.661



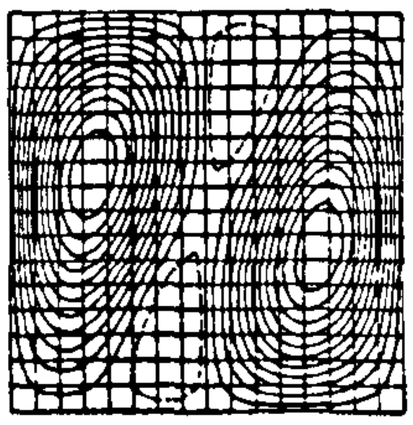
σ_c:τ=2:1, 2nd Mode
$k_{cr,c}$=2.505, $k_{cr,s}$=1.253



σ_c:τ=1:1, 1st Mode
$k_{cr,c}$=1.509, $k_{cr,s}$=1.509



σ_c:τ=1:5, 2nd Mode
$k_{cr,c}$=1.044, $k_{cr,s}$=5.218

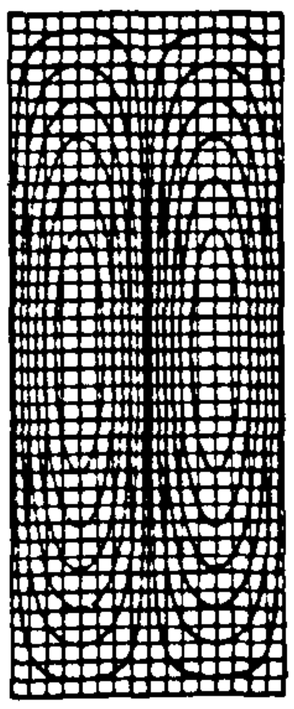


σ_c:τ=1:1, 2nd Mode
$k_{cr,c}$=2.294, $k_{cr,s}$=2.294

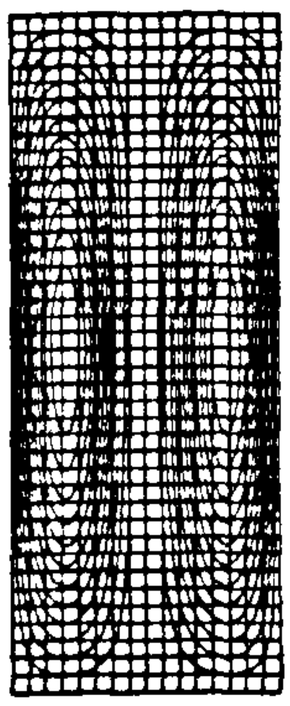
(c) d/a=2

$$Note: \quad k_{cr,c} = \sigma_{c,cr}\frac{b^2 t}{\pi^2 D} \quad , \quad k_{cr,s} = \tau_{cr}\frac{b^2 t}{\pi^2 D}$$

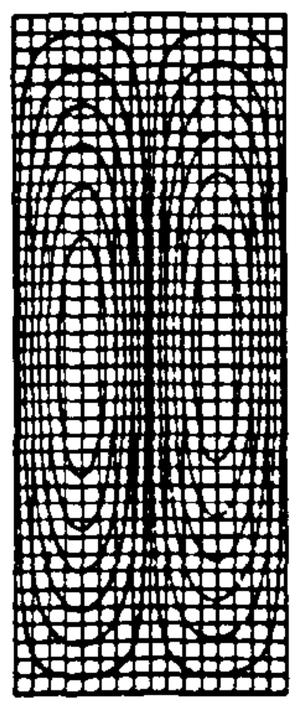
Figure 5.21 (Cont) Critical buckling modes of plates with a knife edge. Shear and compression



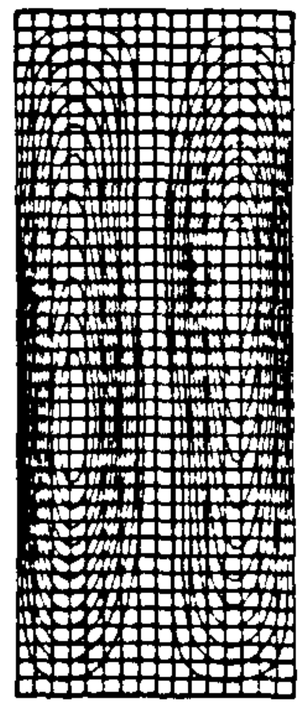
σ_c:τ=1:0, 1st Mode
$k_{\sigma,c}$=1.081, $k_{\sigma,s}$=0



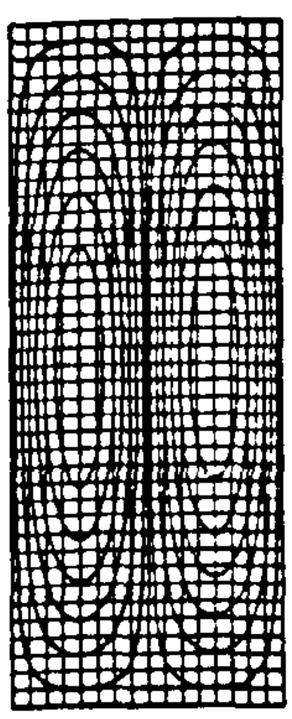
σ_c:τ=1:0, 4th Mode
$k_{\sigma,c}$=2.126, $k_{\sigma,s}$=0



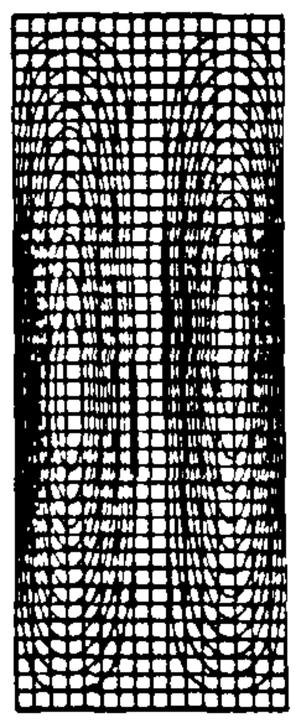
σ_c:τ=2:1, 1st Mode
$k_{\sigma,c}$=1.079, $k_{\sigma,s}$=0.540



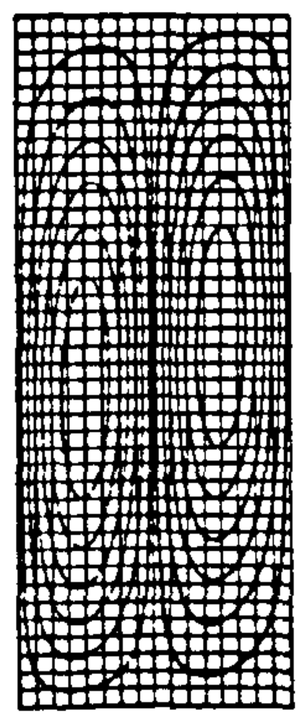
σ_c:τ=2:1, 4th Mode
$k_{\sigma,c}$=2.119, $k_{\sigma,s}$=1.060



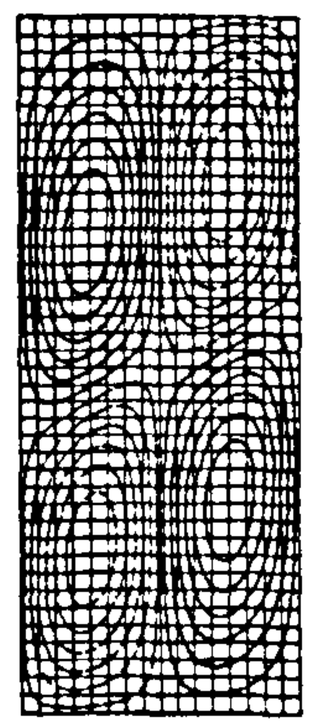
σ_c:τ=5:1, 1st Mode
$k_{\sigma,c}$=1.081, $k_{\sigma,s}$=0.216



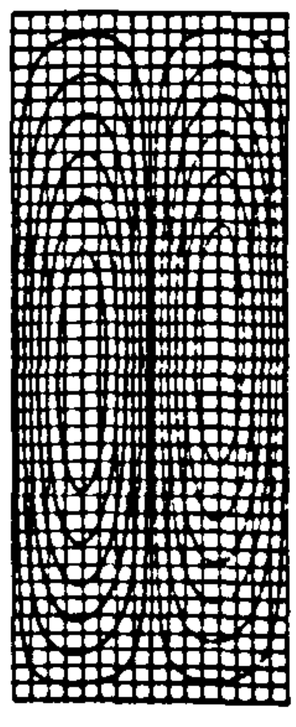
σ_c:τ=5:1, 4th Mode
$k_{\sigma,c}$=2.125, $k_{\sigma,s}$=0.425



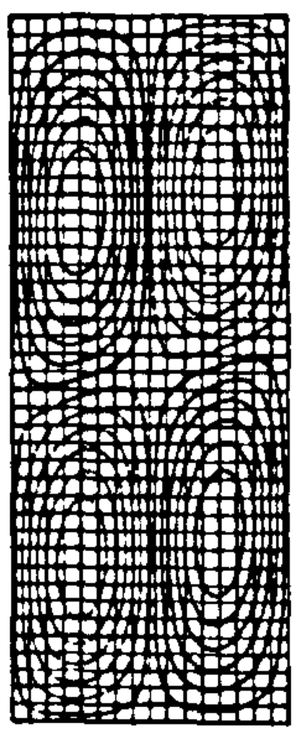
σ_c:τ=1:2, 1st Mode
$k_{\sigma,c}$=1.049, $k_{\sigma,s}$=2.098



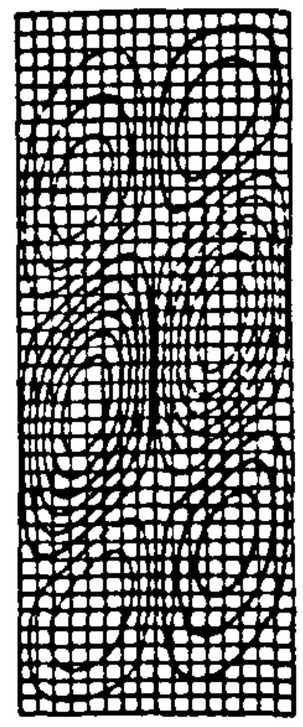
σ_c:τ=1:2, 2nd Mode
$k_{\sigma,c}$=1.183, $k_{\sigma,s}$=2.366



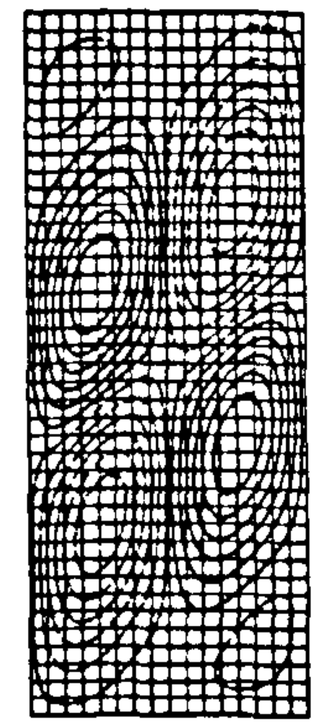
σ_c:τ=1:1, 1st Mode
$k_{\sigma,c}$=1.073, $k_{\sigma,s}$=1.073



σ_c:τ=1:1, 2nd Mode
$k_{\sigma,c}$=1.297, $k_{\sigma,s}$=1.297



σ_c:τ=1:5, 2nd Mode
$k_{\sigma,c}$=0.818, $k_{\sigma,s}$=4.088



σ_c:τ=1:5, 1st Mode
$k_{\sigma,c}$=0.812, $k_{\sigma,s}$=4.059

(d) d/a=5

$$Note: \quad k_{cr,c} = \sigma_{c,cr}\frac{b^2 t}{\pi^2 D} \quad , \quad k_{cr,s} = \tau_{cr}\frac{b^2 t}{\pi^2 D}$$

Figure 5.21 (Cont) Critical buckling modes of plates with a knife edge. Shear and compression

For a given ratio of applied load components, σ_c/τ, the critical shear stress τ_{cr} in the presence of compression can be obtained from Eqn. 5.4, and may be written as:

$$\frac{\tau_{cr}}{\tau_{cr}^0} = \frac{2}{r_c + \sqrt{r_c^2 + 4}} \tag{5.6}$$

where r_c represents the ratio of applied compressive load to the shear load, defined as:

$$r_c = \frac{\sigma_c/\sigma_{c.cr}^0}{\tau/\tau_{cr}^0} \tag{5.7}$$

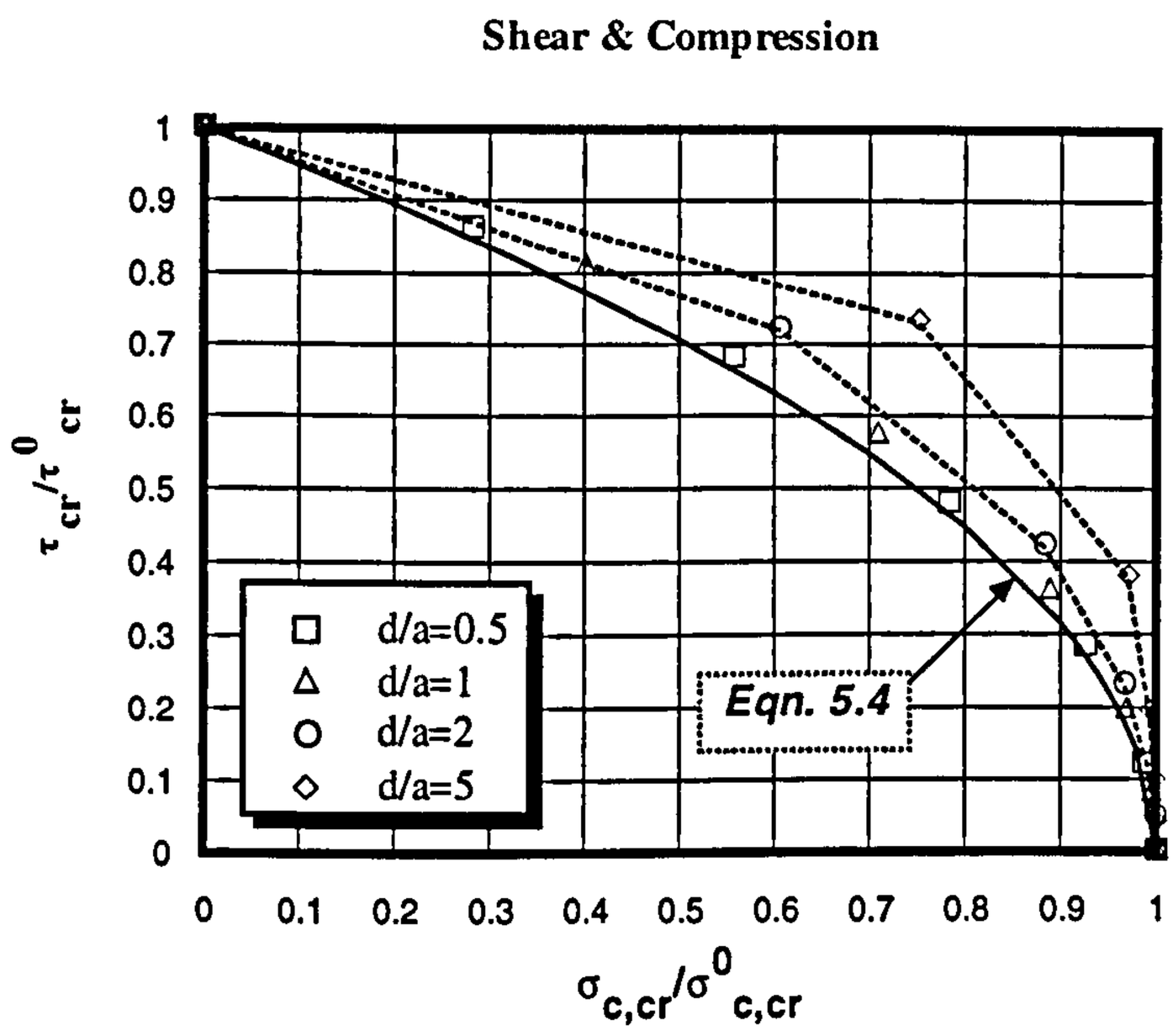


Figure 5.22 Interaction curves of the critical stresses for combined shear and compression. Plates with a straight knife edge. FE results. Eqn. 5.4

5.3.2.2 Non-Linear Elastic Buckling Behaviour

- ***Deflection Modes***

In Fig. 5.23, contour plots of out-of-plane deflection are presented for different combinations of applied shear and compressive stresses. As for the critical buckling

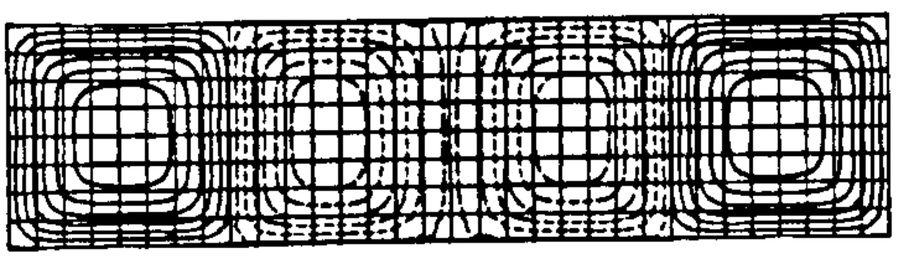
modes, it is observed that as the relative magnitude of the applied shear stress τ is increased, the inclined angle of the buckle increases progressively, with the buckling modes changing from the compressive (symmetric) modes to the shear (point-symmetric) modes. For tall panels, the number of buckles along the depth of the plate also varies with the load ratio σ_c/τ. By comparing the modes shown in Figs. 5.21 and 5.23, the differences between the critical buckling modes and the elastic large-deflection modes can be seen. Further, by means of the ABAQUS POST program, it was found that the deflection modes also vary with the magnitudes of applied loads.

As discussed in Section 5.2.2.2, the lateral forces acting on the knife edge, and hence the knife edge moments, are related to the panel deflections. Therefore, due to the wide variations in the deflection modes, it is expected that the modelling of the knife edge forces for combined loading conditions will be much more complicated than for single loading component, such as pure shear. The accurate representations of the knife edge moment M_{pk} by closed-form expressions for combined loading conditions is not feasible.

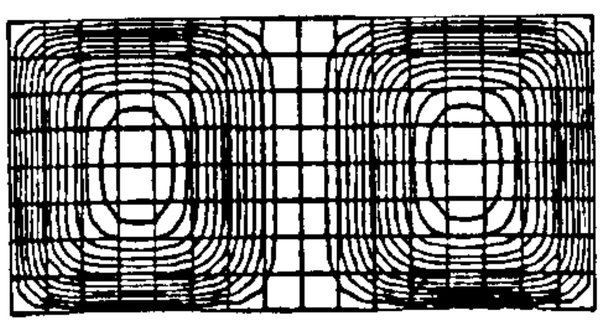
- ***Distribution of the Knife Edge Moment***

For plates subjected to coexistent shear and compressive stresses, τ and σ_c, the distribution curves of the bending moments along the knife edge, obtained from the non-linear elastic finite element analyses, are presented in Fig. 5.24. For each case, the knife edge moments at three different load levels, represented by τ/τ_{cr} for cases in the presence of shear and σ_c/σ^0_{ccr} for compression alone, are illustrated in Fig. 5.24.

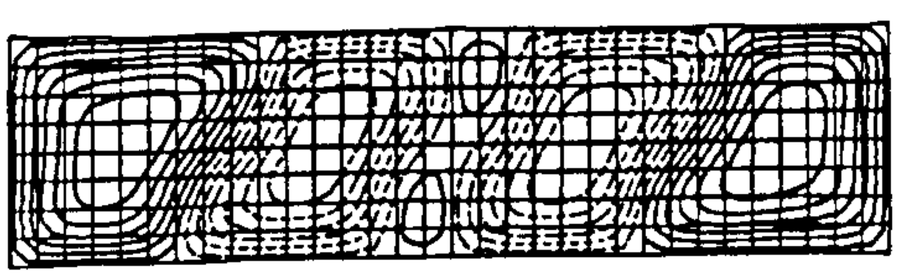
It is observed in Fig. 5.24 that for combined shear and compression, the knife edge moments generally distribute in a form similar to a single half wave, with the maximum magnitude at the mid-length of the knife edge. This is because the distribution of the knife edge moment for pure shear is quite similar to that for compression alone, as shown in Fig. 5.24.



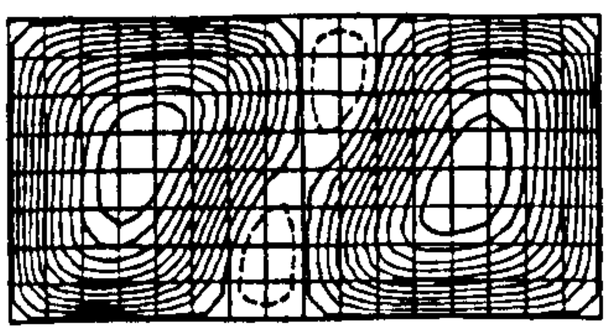
σ_c:τ=1:0



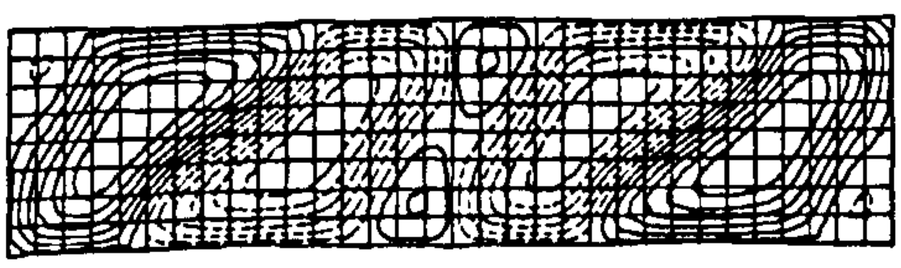
σ_c:τ=1:0



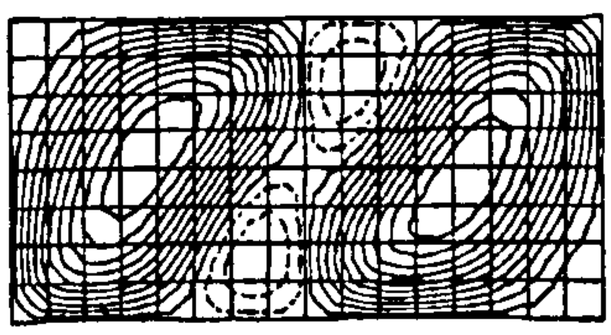
σ_c:τ=5:1



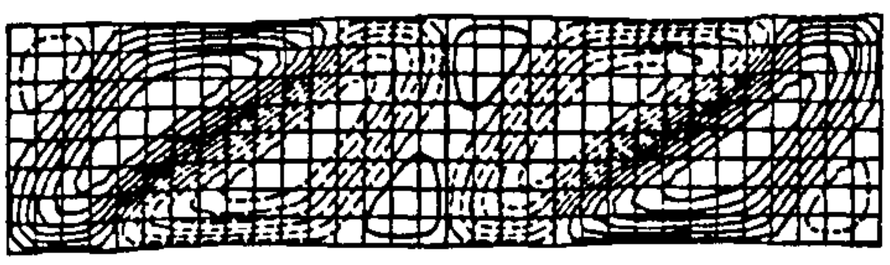
σ_c:τ=5:1



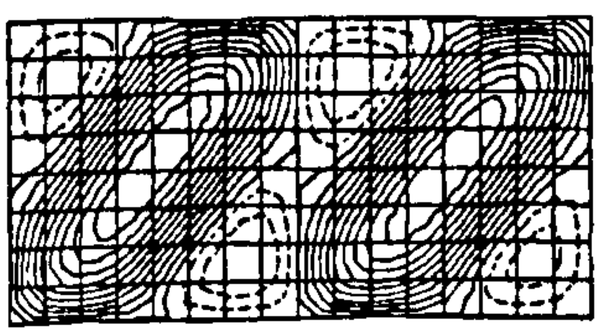
σ_c:τ=2:1



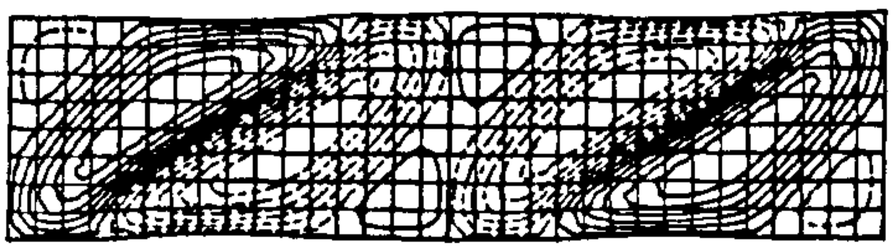
σ_c:τ=2:1



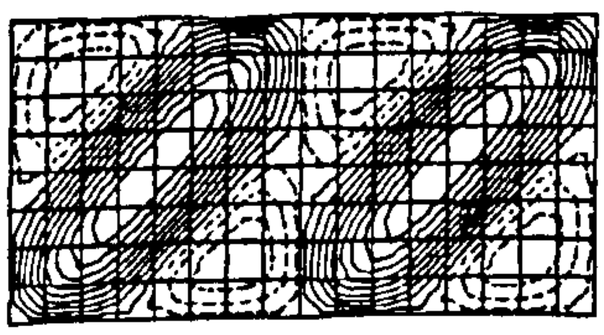
σ_c:τ=1:1



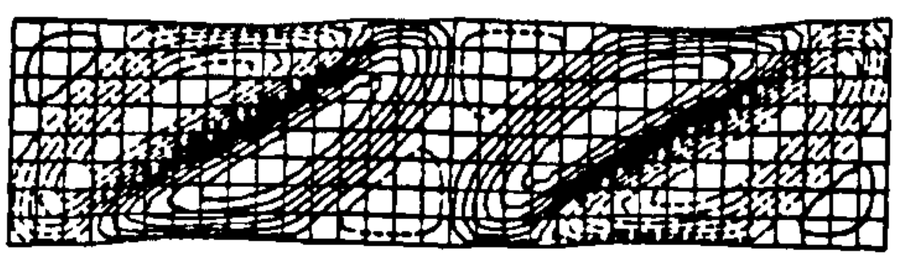
σ_c:τ=1:1



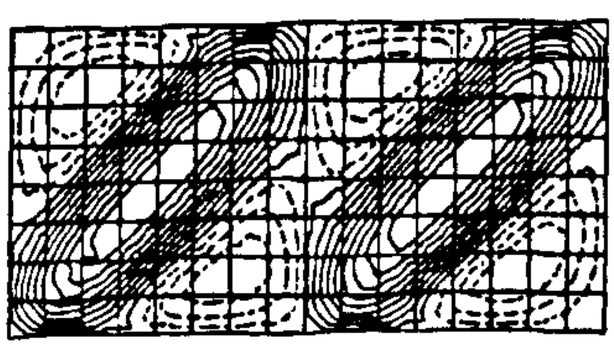
σ_c:τ=1:2



σ_c:τ=1:2



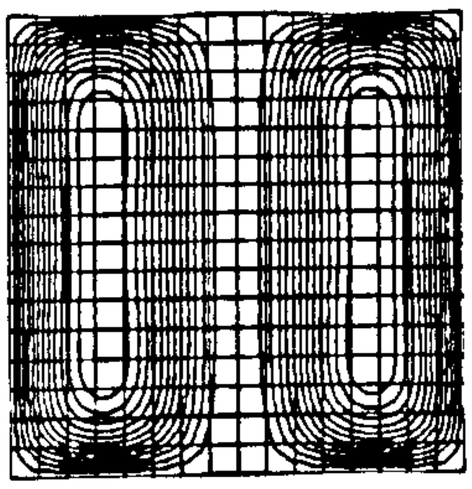
σ_c:τ=1:5



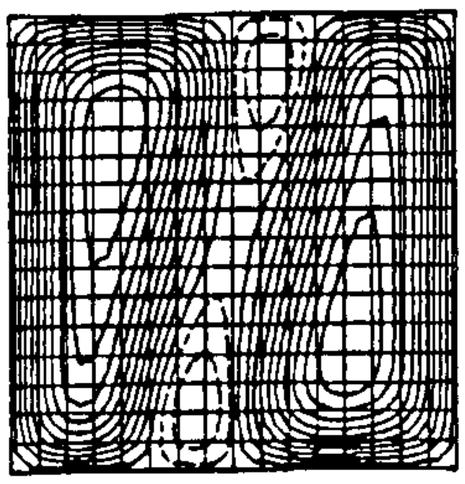
σ_c:τ=1:5

(a) d/a=0.5 **(b) d/a=1**

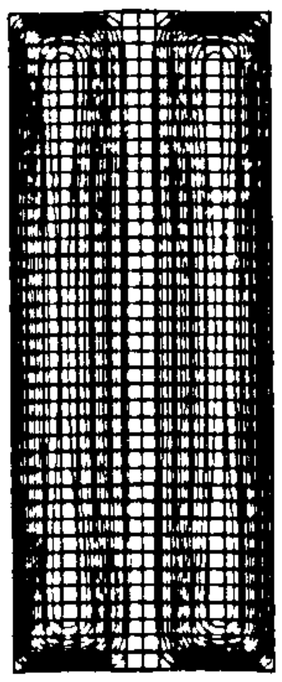
Figure 5.23 Deflection modes of plates with a straight knife edge.
Combined shear and compression. Non-linear elastic FE results. w_{0p}/t=0.485



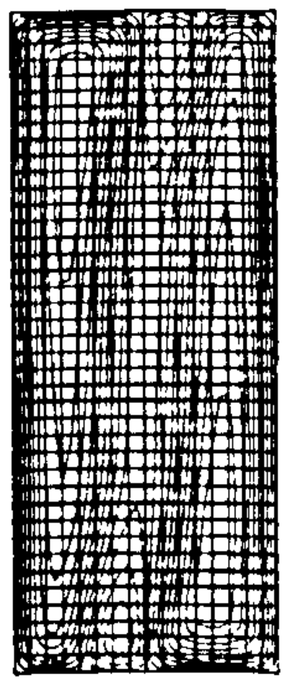
σ_c:τ=1:0



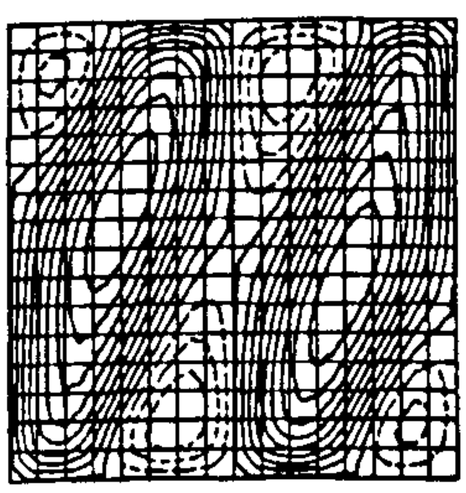
σ_c:τ=5:1



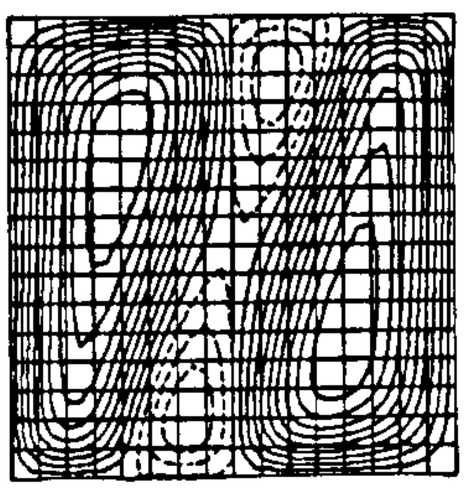
σ_c:τ=1:0



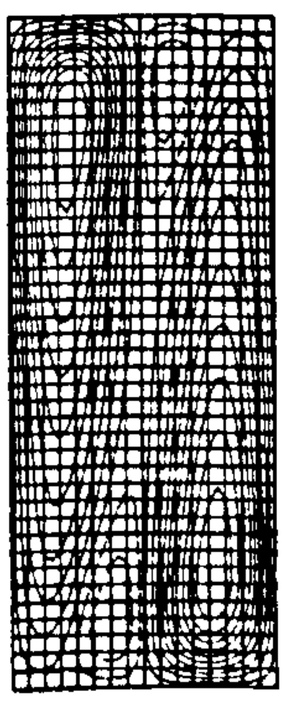
σ_c:τ=5:1



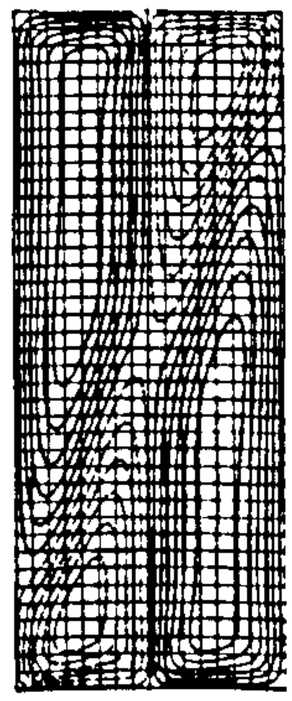
σ_c:τ=1:1



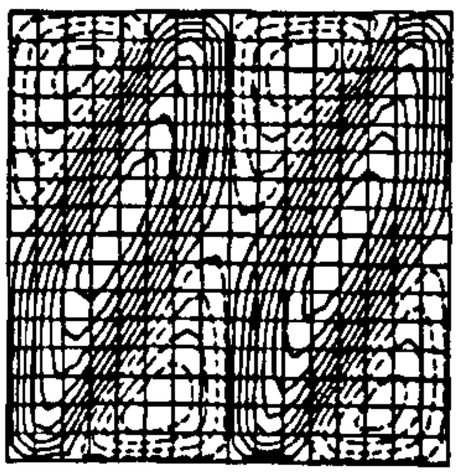
σ_c:τ=2:1



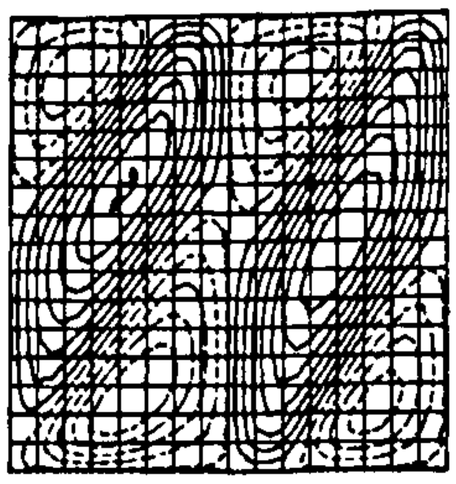
σ_c:τ=2:1



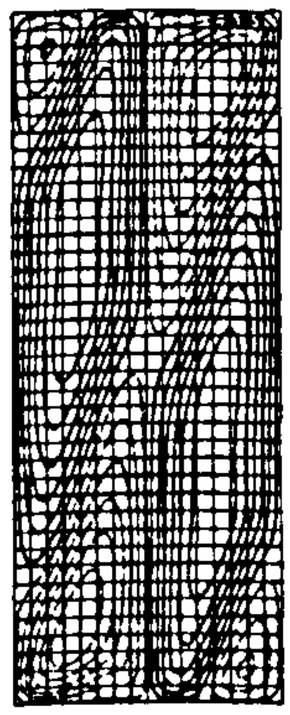
σ_c:τ=1:1



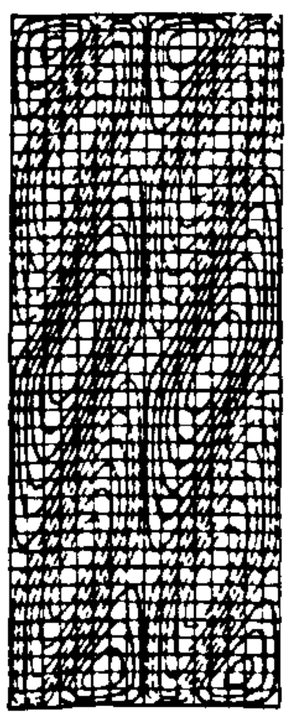
σ_c:τ=1:2



σ_c:τ=1:5



σ_c:τ=1:2

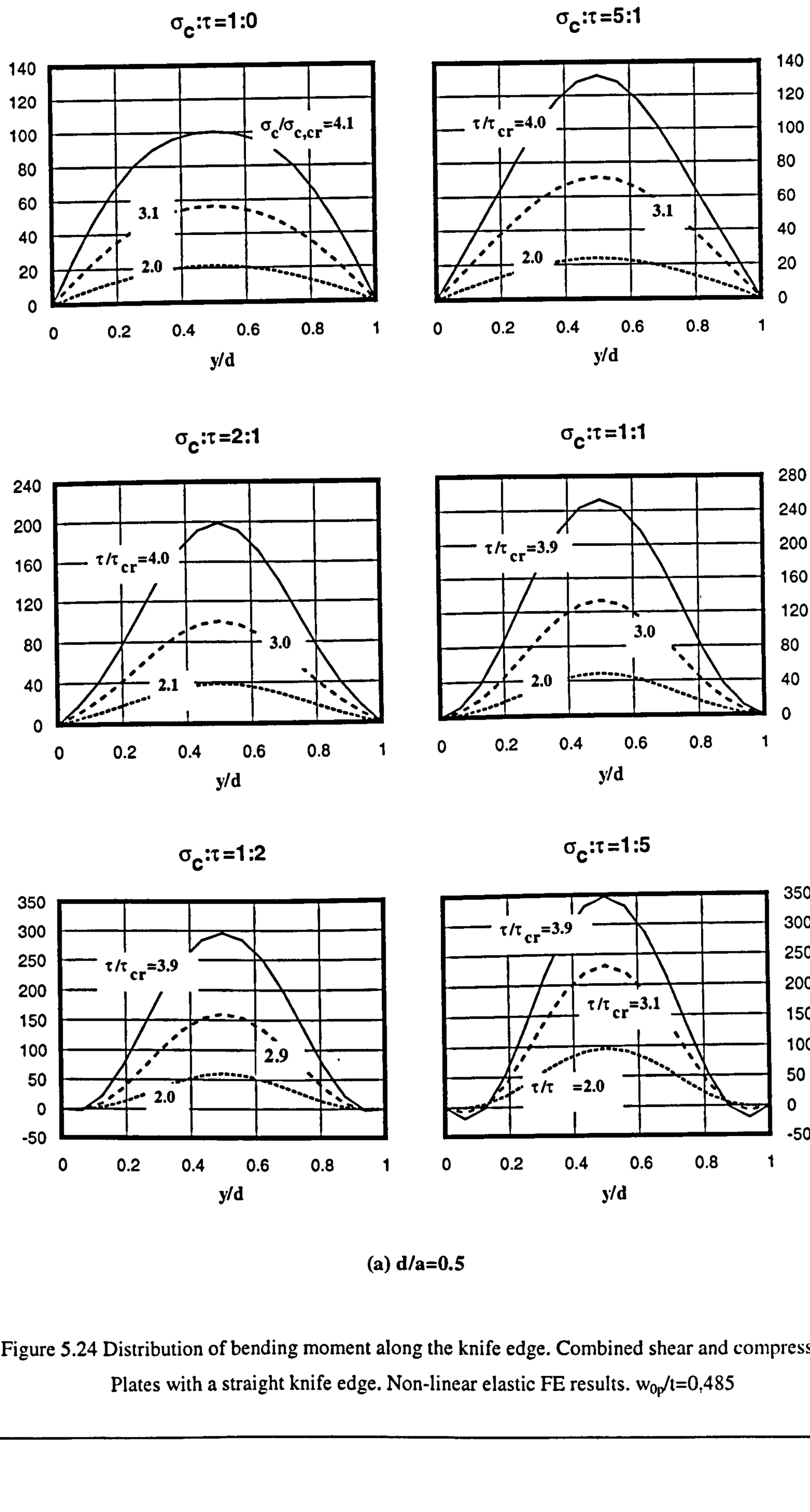


σ_c:τ=1:5

(c) d/a=2

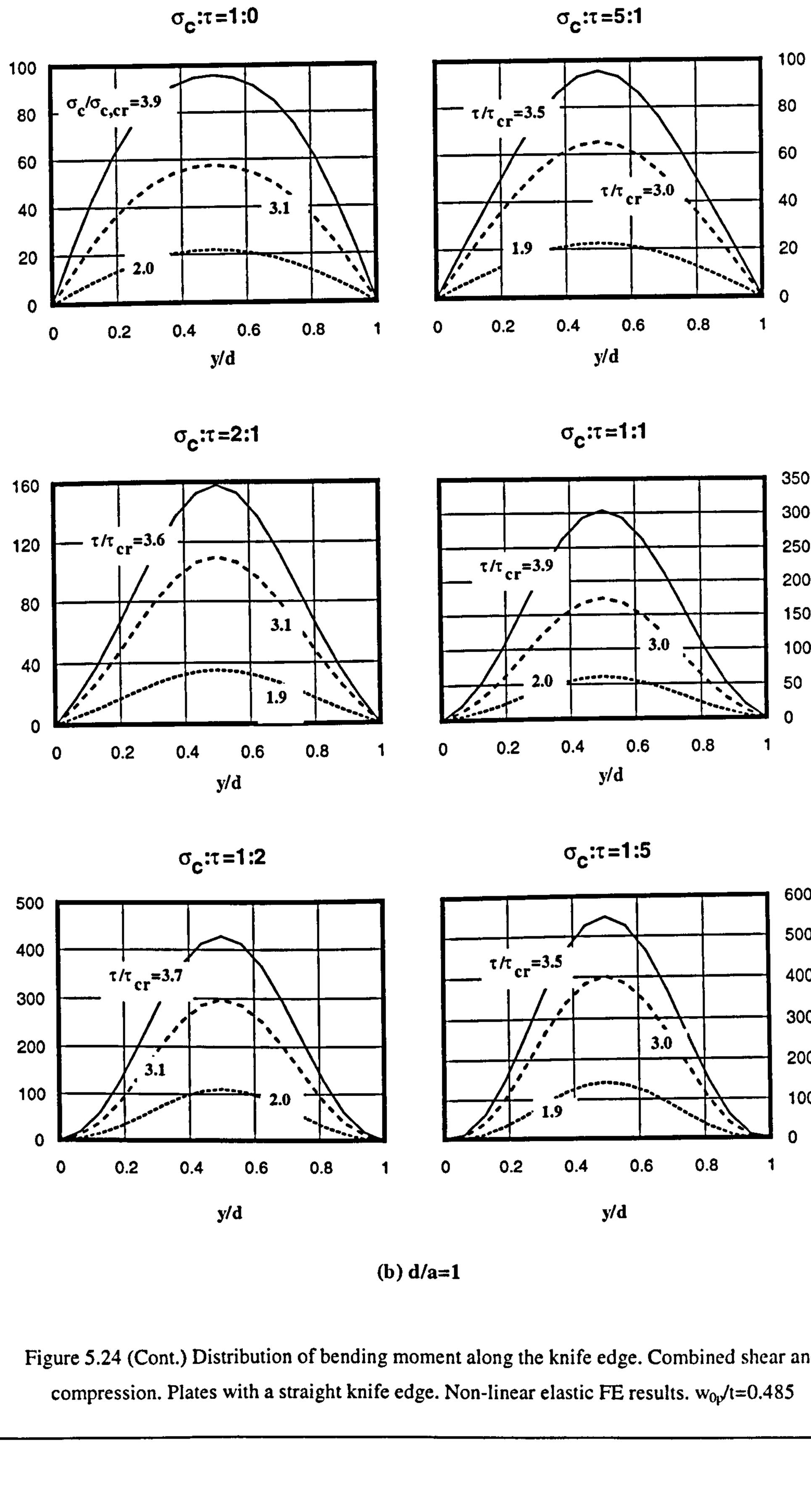
(d) d/a=5

Figure 5.23 (Cont) Deflection modes of plates with a straight knife edge.
Combined shear and compression. Non-linear elastic FE results. w_{0p}/t=0.485



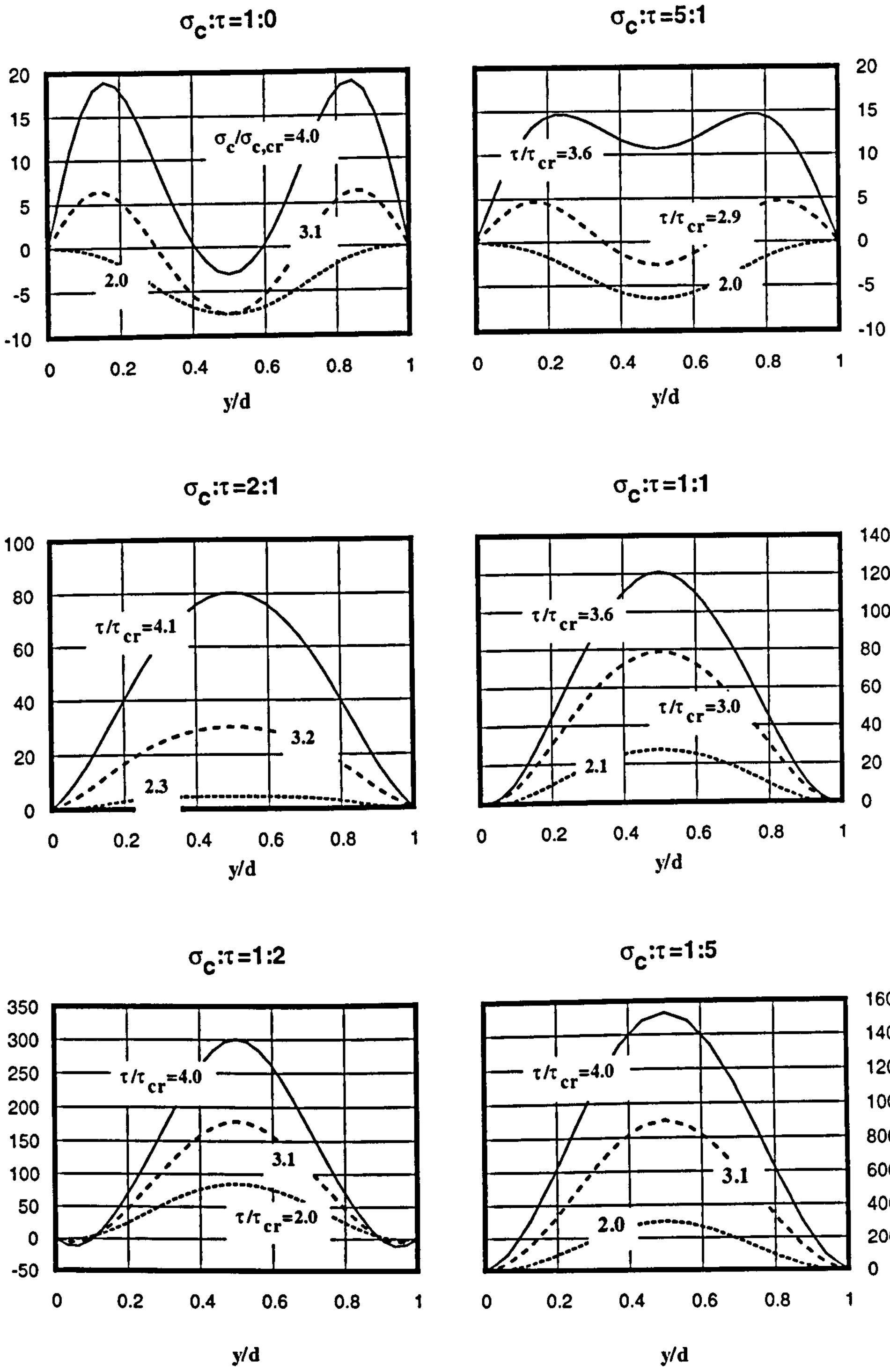
(a) d/a=0.5

Figure 5.24 Distribution of bending moment along the knife edge. Combined shear and compression. Plates with a straight knife edge. Non-linear elastic FE results. w_{0p}/t=0,485



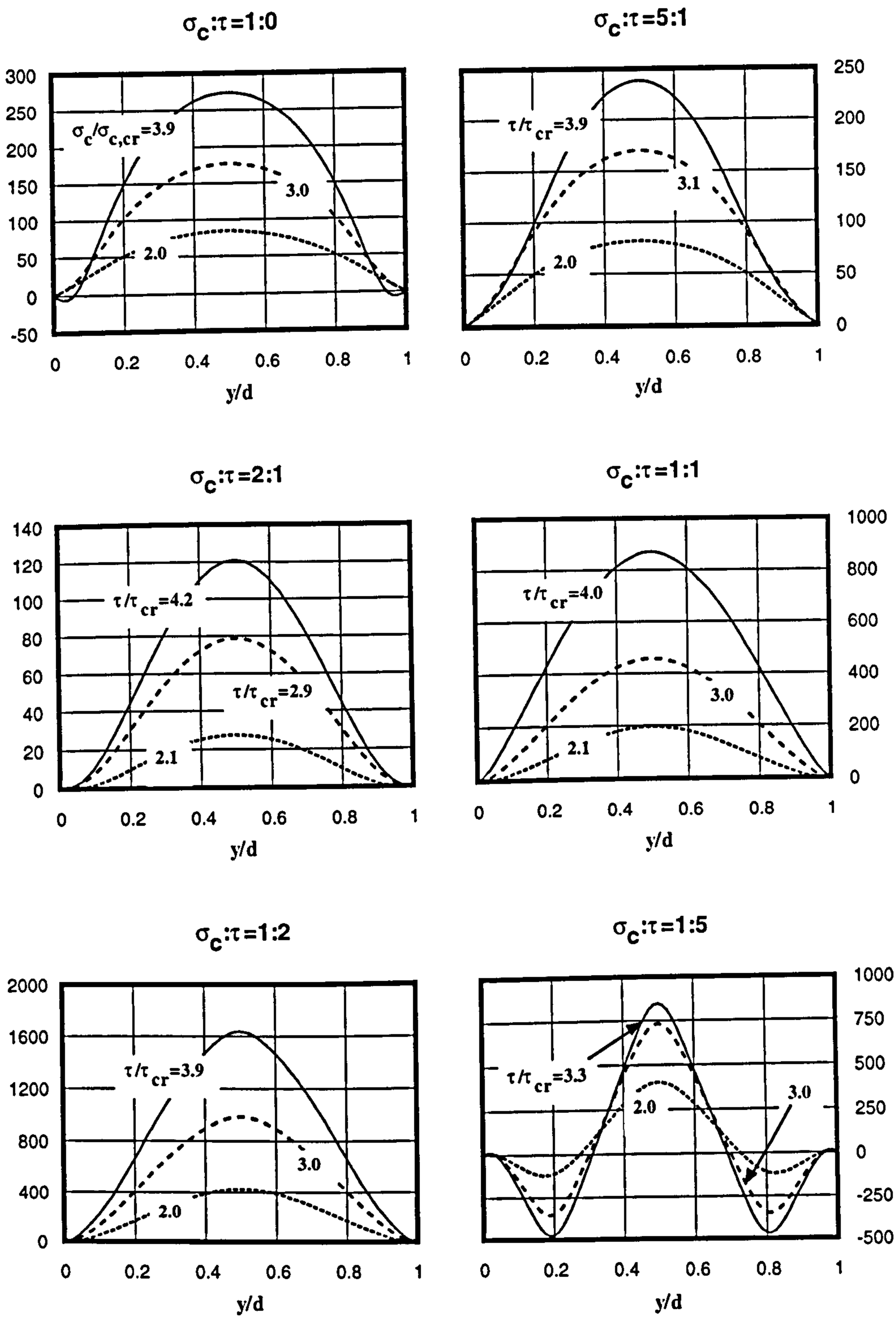
(b) d/a=1

Figure 5.24 (Cont.) Distribution of bending moment along the knife edge. Combined shear and compression. Plates with a straight knife edge. Non-linear elastic FE results. $w_{0p}/t=0.485$



(c) d/a=2

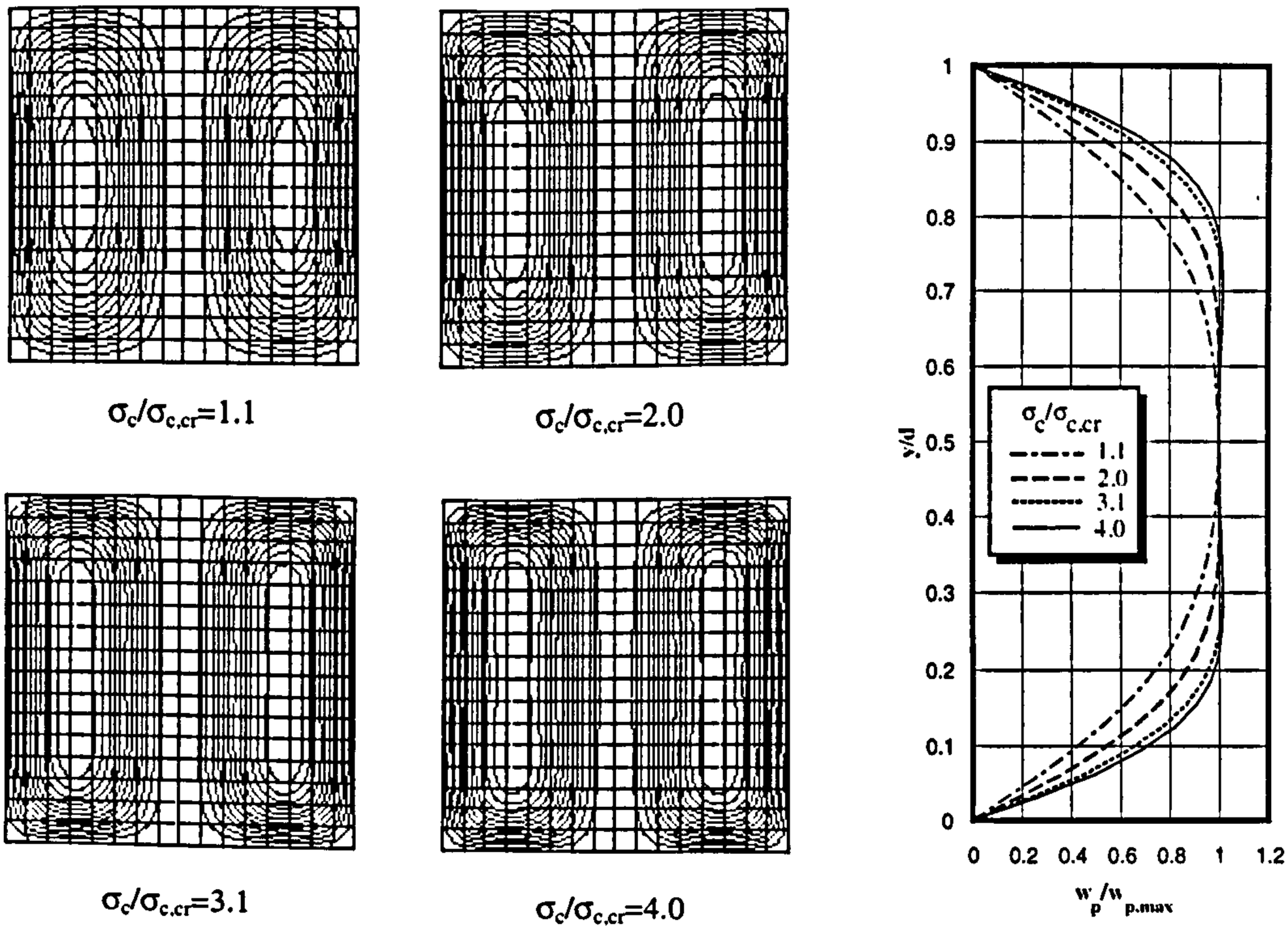
Figure 5.24 (Cont.) Distribution of bending moment along the knife edge. Combined shear and compression. Plates with a straight knife edge. Non-linear elastic FE results. $w_{0p}/t=0.485$



(d) d/a=5

Figure 5.24 (Cont.) Distribution of bending moment along the knife edge. Combined shear and compression. Plates with a straight knife edge. Non-linear elastic FE results. $w_{0p}/t=0.485$

It is demonstrated in Fig. 5.24(c) that for plates subjected to compression or compression dominated, the shape of the knife edge moment changes with the magnitude of the applied load. The reason for this alternation is also associated with the panel deflection modes, which are shown in Fig. 5.25(a), together with the panel deflection profiles along a vertical line passing through the maximum deflection point (Fig. 5.25b). It is also noted that for these loading conditions, the knife edge moment change its sign as the magnitude of the applied load is increased. The possible reason for this is that the natural lowest buckling mode for the knife edge plate of d/a=2 under compression is anti-symmetric about the knife edge (Fig. 5.21), so when the deflections in the sub-panels are relatively small, the panels may tend to deflect the knife edge in the opposite direction. However, as the deflections in the two sub-panels are great enough, which are equal, the whole plate may tend to deflect in the same direction.



(a) Contour diagrams

(b) Panel deflection profiles

Figure 5.25 Load-deflection history of plates with a straight knife edge. Non-linear elastic FE results. Compression. Symmetric panel imperfection, $w_{0p}/t=0.485$. d/a=2

- ***Magnitude of the Knife Edge Moment, M_{pk}***

With respect to design of the transverse stiffeners, the maximum amplitude of the bending moment along the knife edge is of interest. For the cases of different ratios of σ_c/τ, investigated for each aspect ratio d/a, the maximum values of the non-dimensional knife edge moment, $M_{pk}b/Dt$, are plotted in the same diagram, as shown in Fig. 5.26.

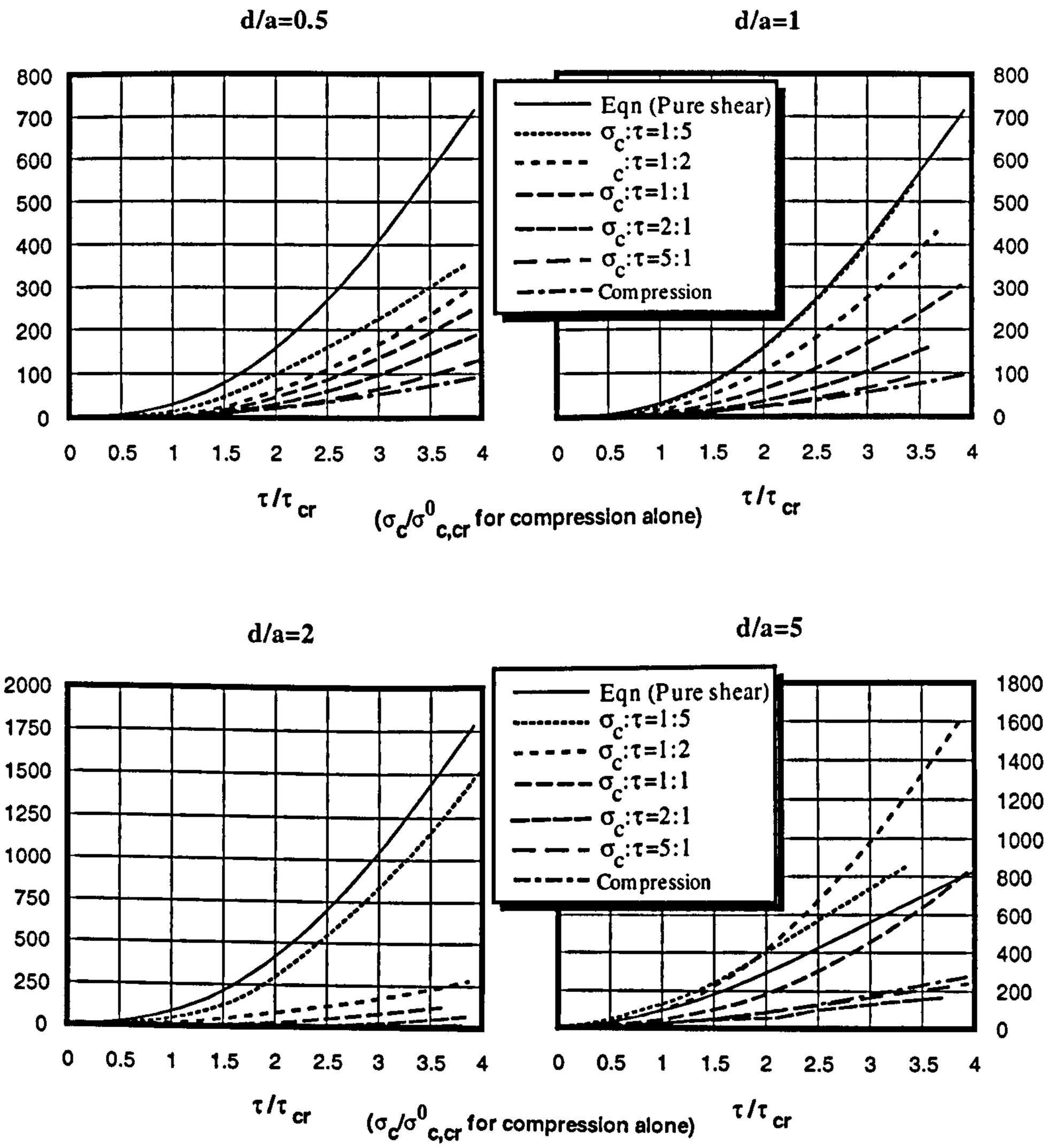


Figure 5.26 The bending moments in the knife edges. Combined shear and compression. Plates with a straight knife edge. w_{0p}/t=0.485. Non-linear elastic FE results.

In Fig. 5.26, the horizontal axis represents the value of τ/τ_{cr} for combined shear and compression, and σ_c/σ^0_{ccr} for compression alone. It is found that in general, as the shear component, τ, becomes predominant, the magnitude of the knife edge moment becomes significantly greater.

It can also be seen in Fig. 5.26 that for different ratios of applied compressive stress to shear stress, σ_c/τ, the variations in the knife edge moment $M_{pk}b/Dt$ with the aspect ratio d/a are quite complicated. The knife edge bending moments calculated from Eqn. 5.3, which has been proposed for predicting M_{pk} for pure shear, are also shown in Fig. 5.26. It is apparent that in most of the cases, the curve of $M_{pk}b/Dt$ versus τ/τ_{cr} obtained for pure shear provides an upper limit of M_{pk} for combined shear and compression conditions. In order to give a reasonably accurate estimation of M_{pk} for combined loading conditions, it is considered that the proposed design formulae for predicting M_{pk} for the pure shear condition, as presented in Eqn. 5.3, may be extended for combined loading conditions, but the ratio of τ/τ_{cr} in Eqn. 5.3 for pure shear (ie., τ/τ^0_{cr}) should be replaced with an equivalent shear stress ratio τ_{eq}/τ^0_{cr}. It is clear from Fig. 5.26 that τ_{eq}/τ^0_{cr} may be taken as a factored τ/τ_{cr}. The definition of the equivalent shear stress τ_{eq} for combined shear and compression conditions is presented in Section 5.3.2.3.

5.3.2.3 Design Formulae for Predicting M_{pk}

For a given ratio of σ_c/τ, the critical shear stress τ_{cr} in the presence of compression can be calculated from Eqn. 5.6. In terms of Eqns. 5.6 and 5.7, the ratio of applied shear stress to the critical shear stress, τ/τ_{cr}, can be written as:

$$\frac{\tau}{\tau_{cr}} = \frac{1}{2}\left(\frac{\sigma_c}{\sigma^0_{c,cr}}\right) + \sqrt{\left(\frac{\tau}{\tau^0_{cr}}\right)^2 + \frac{1}{4}\left(\frac{\sigma_c}{\sigma^0_{c,cr}}\right)^2} \qquad (5.8)$$

It is found in Eqn. 5.8 that as $\tau \rightarrow 0$ (Compression alone), $\tau/\tau_{cr} \rightarrow \sigma_c/\sigma^0_{ccr}$. It can be found in Fig. 5.26 that in order to use Eqn. 5.3 for predicting M_{pk} for compression, an equivalent ratio of τ/τ_{cr}, which is less than σ_c/σ^0_{ccr}, should be used.

By assuming that the knife edge moment at σ_c/σ^0_{ccr} for compression is equal to the knife edge moment at τ_{eq}/τ^0_{cr} for pure shear, an equivalent shear stress τ_{eq} for compression alone can be defined. For reasons of simplicity, it is assumed that the equivalent shear stress τ_{eq} for compression alone can be written as:

$$\frac{\tau_{eq}}{\tau^0_{cr}} = \beta_c \left(\frac{\sigma_c}{\sigma^0_{c,cr}} \right) \tag{5.9}$$

where β_c is a factor introduced to account for the difference in the magnitudes of M_{pk} between compression alone and pure shear loading conditions.

In terms of Eqns. 5.8 and 5.9, it is proposed that for combined shear and compression, the knife edge moment M_{pk} can be calculated using Eqn. 5.3 with τ/τ_{cr} being replaced by the equivalent shear stress ratio:

$$\frac{\tau_{eq}}{\tau^0_{cr}} = \frac{1}{2}\left(\beta_c \frac{\sigma_c}{\sigma^0_{c,cr}} \right) + \sqrt{\left(\frac{\tau}{\tau^0_{cr}} \right)^2 + \frac{1}{4}\left(\beta_c \frac{\sigma_c}{\sigma^0_{c,cr}} \right)^2} \tag{5.10}$$

For compression alone, Eqn. 5.10 reduces to Eqn. 5.9. For pure shear, Eqn. 5.10 gives:

$$\frac{\tau_{eq}}{\tau^0_{cr}} = \frac{\tau}{\tau^0_{cr}} \tag{5.11}$$

By the curve-fitting of the finite element solutions for combined shear and compression conditions with Eqn. 5.3, it is found that the factor β_c may be approximately taken as:

$$\beta_c = \begin{cases} 0.45, & for \quad d/a \le 1 \quad or \quad d/a \ge 3 \\ 0.2 + 0.25 \cdot \left| \frac{d}{a} - 2 \right|, & for \quad \left| \frac{d}{a} - 2 \right| < 1 \\ 0.2, & for \quad d/a = 2 \end{cases} \tag{5.12}$$

In Fig. 5.27, the non-dimensional knife edge moment $M_{pk}b/Dt$, predicted by Eqn. 5.3 using the equivalent shear stress τ_{eq} given by Eqns. 5.10 and 5.12, are compared with the finite element results. In general, the estimated knife edge moments are close to the numerical results, especially for plates of $d/a \le 1$. For $d/a=5$, significant differences between the estimates and FE results can be seen. However, as indicated previously, for tall plates, the accuracy of representing M_{pk} may not be so important as for plates of

d/a≤1. Therefore, it is considered that the approach proposed above may still be acceptable. Alternatively, by examining the diagrams in Fig. 5.26, an additional equation is proposed to supplement Eqn. 5.12:

$$\beta_c = 1, \quad for \quad d/a \geq 5 \quad and \quad \sigma_c/\tau \leq 1 \tag{5.13}$$

Eqn. 5.13 implies that for d/a≥5 and $\sigma_c/\tau \leq 1$, the equivalent shear stress ratio is given by Eqn. 5.8, that is, $\tau_{eq}/\tau_{cr}^0 = \tau/\tau_{cr}$, where τ_{cr} is the critical shear stress in the presence of compression.

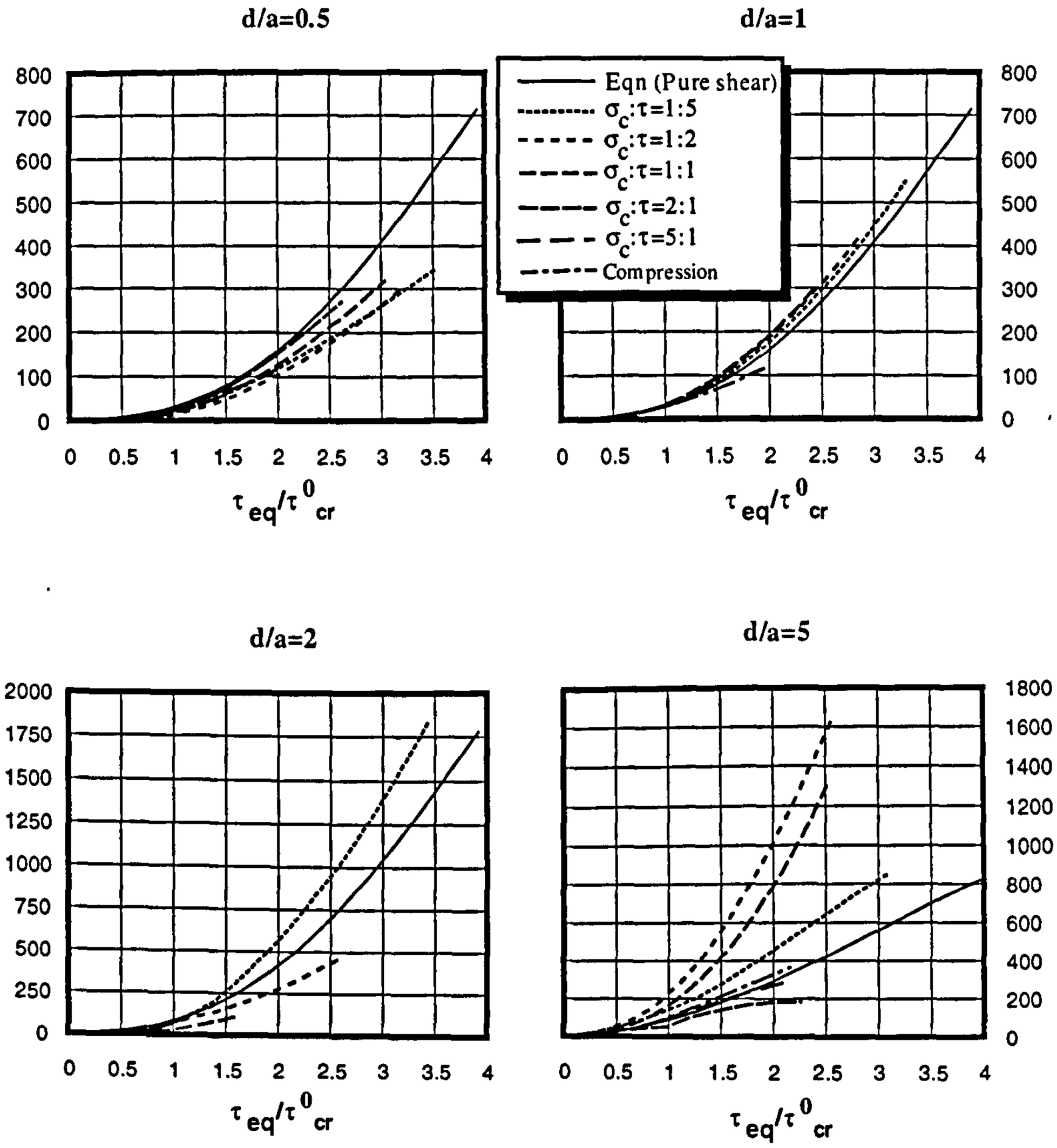


Figure 5.27 Comparisons in the knife edge moments between the proposed equations and FE solutions. Shear and compression. Plates with a straight knife edge. $w_{0p}/t=0.485$. τ_{eq} as in Eqns. 5.10 & 5.12

Based on the above discussion, it is proposed that for plates subjected to coexistent shear and compression, the knife edge bending moment M_{pk} can be calculated using Eqn. 5.3, by assuming that a pure shear stress of τ_{eq} , given by Eqns. 5.10, 5.12 and 5.13, is applied. The design formulae for general loading conditions will be summarized in Section 5.4.

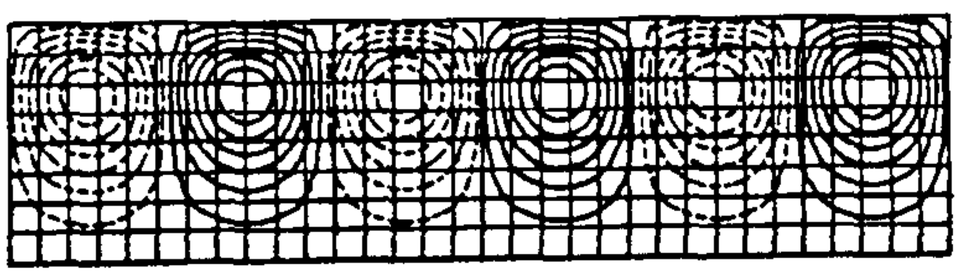
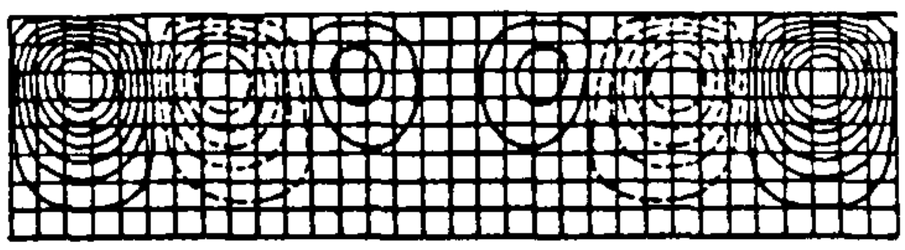
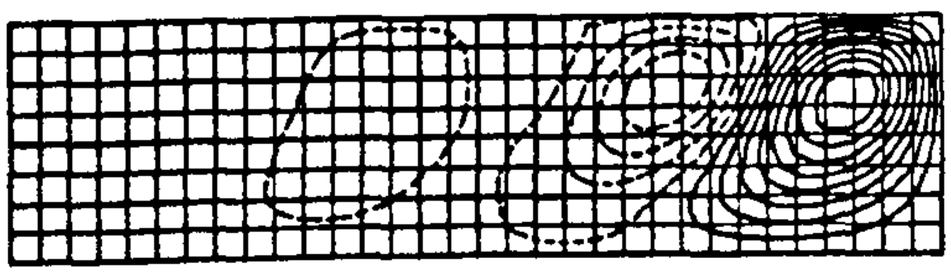
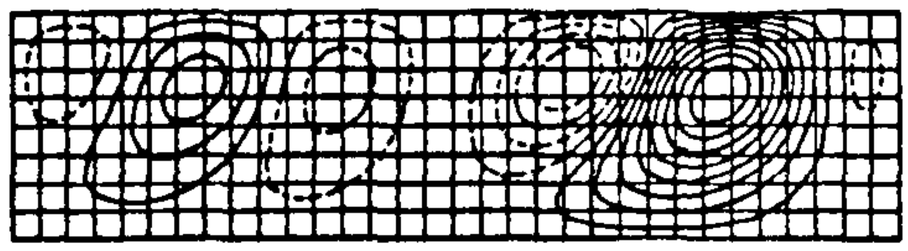
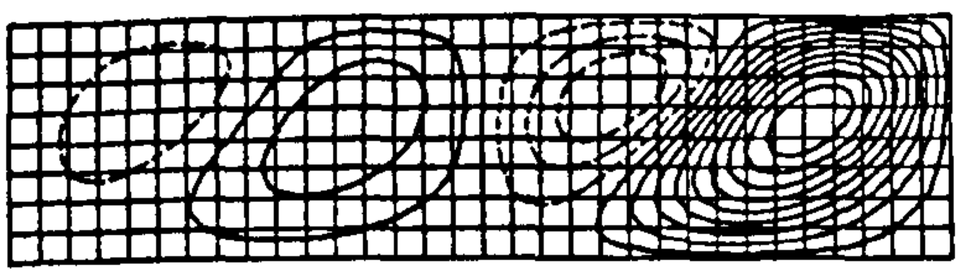
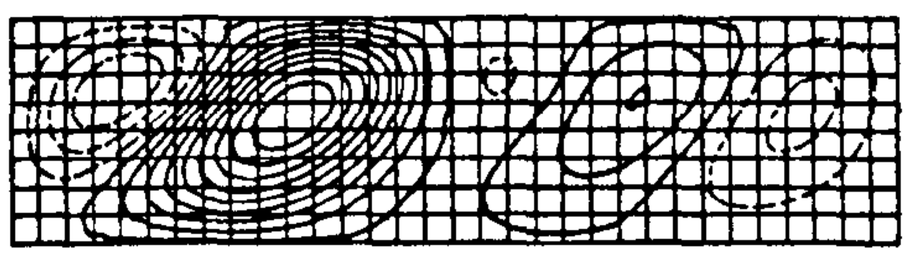
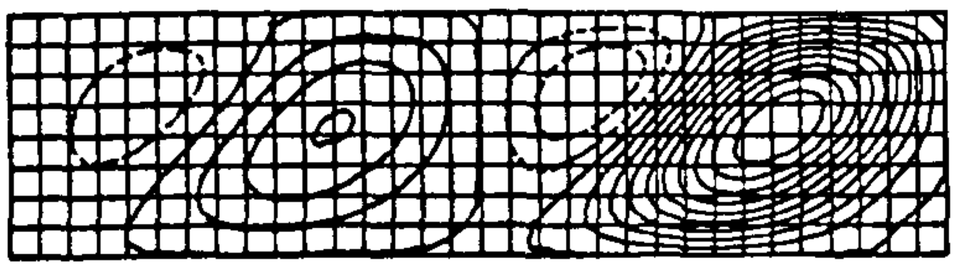
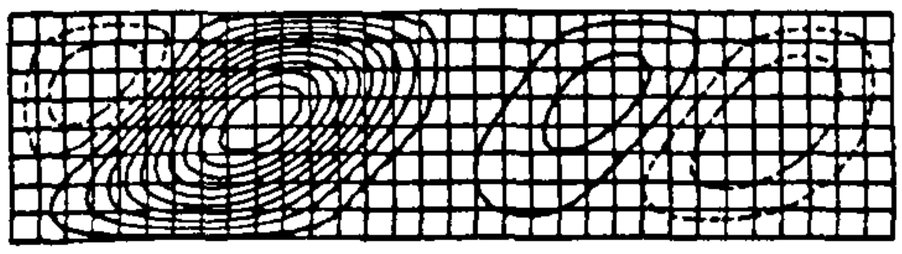
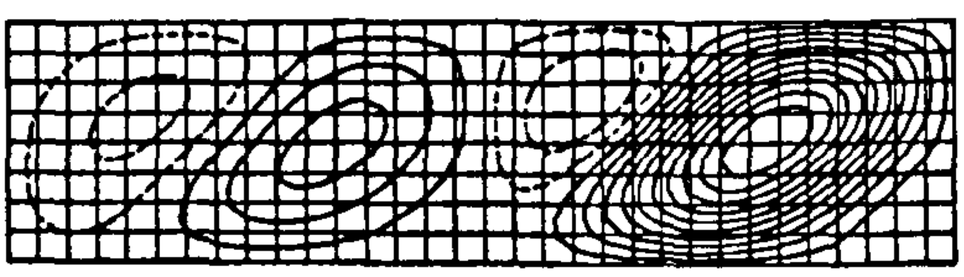
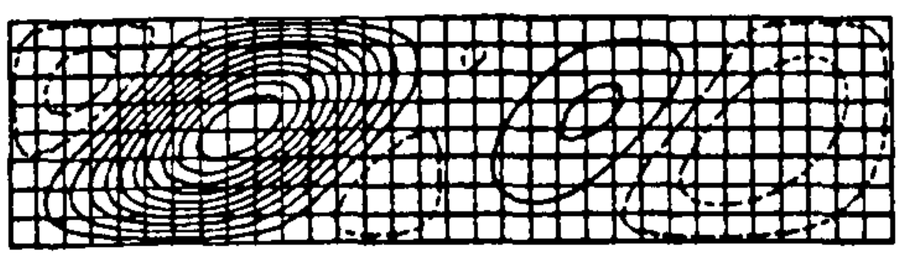
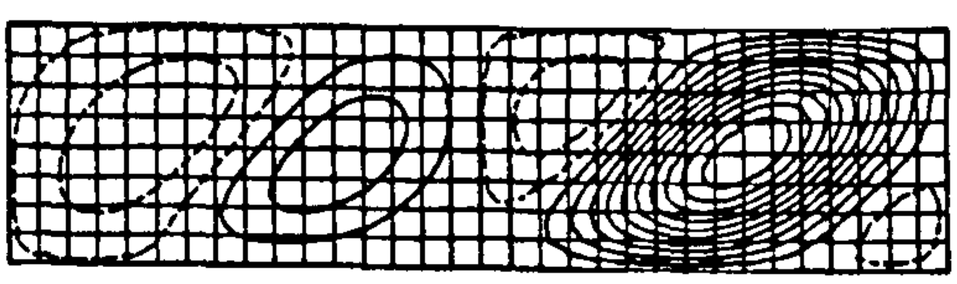
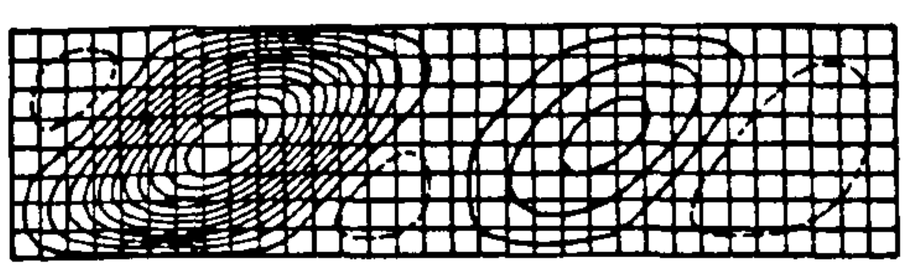
5.3.3 Combined Shear and Bending

5.3.3.1 Critical Buckling Behaviour

The contour plots of the first two critical buckling modes for plates with a straight knife edge, subjected to coexistent shear and bending, are given in Fig. 5.28, covering the range of panel aspect ratios considered in this study, i.e. d/a=0.5, 1, 2, and 5. It can be observed in Fig. 5.28 that the variation in the buckling modes is even more complicated than for combined shear and compression conditions. The applied bending stresses produce compression in the upper part of the panels, and tension in the bottom part, with the result that the main buckles occur at the top of the panels. As the relative magnitude of the applied shear stress τ is increased, the inclined angles of the buckles increase progressively, with the buckling modes changing from the bending (symmetric) modes to the shear (point-symmetric) modes. For tall panels, the buckling modes for different values of the load ratio σ_b/τ differ from each other in both the number and the position of the buckles along the depth of the plate, apart from the buckle inclination.

The interaction curves of the lowest critical buckling stresses for the knife edge plates of d/a=0.5, 1, 2 and 5, subjected to combined shear and bending are presented in Fig. 5.29. It is found in Fig. 5.29 that the interaction curve between shear and bending can be represented approximately by the equation:

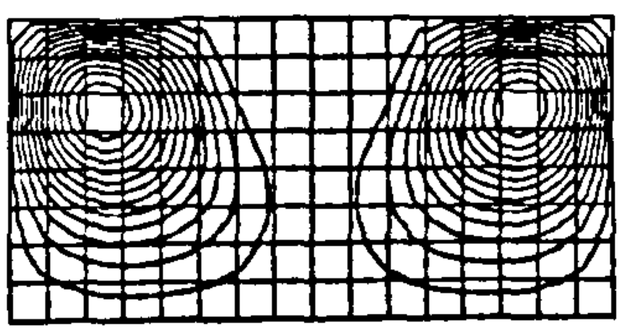
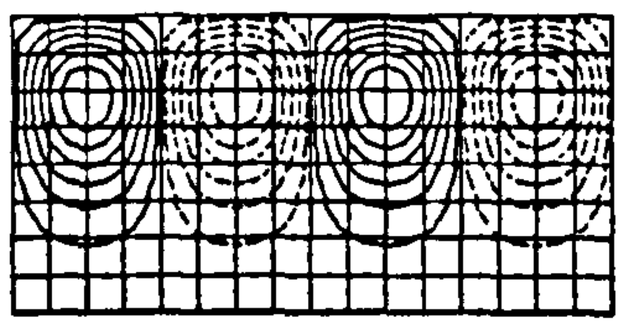
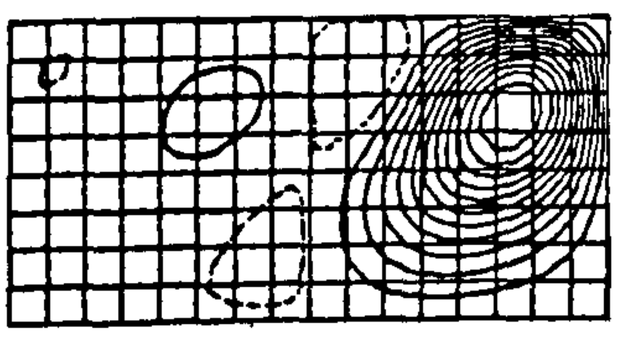
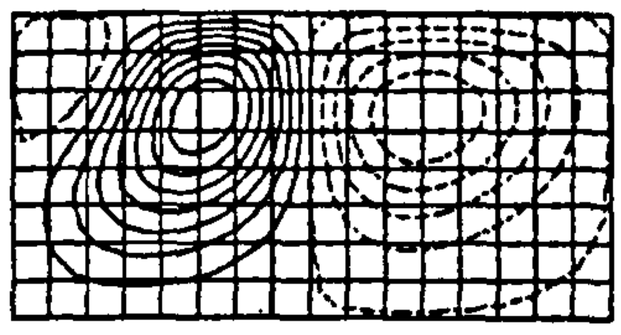
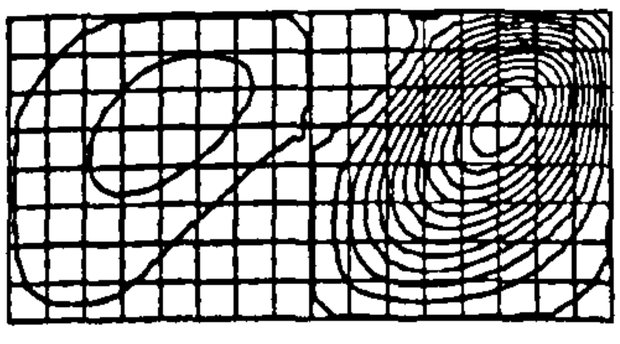
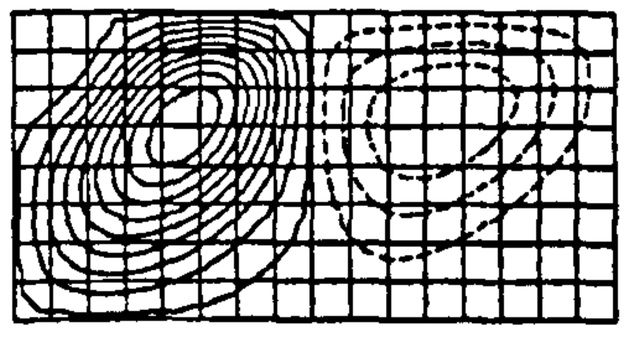
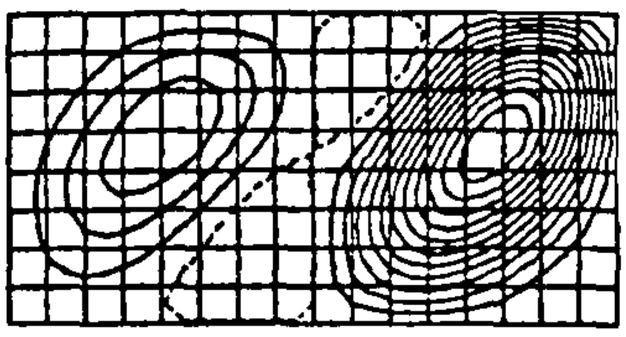
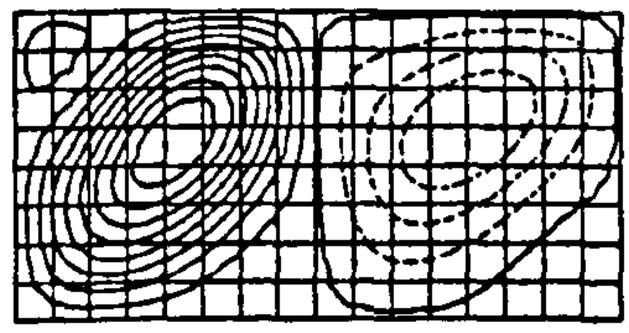
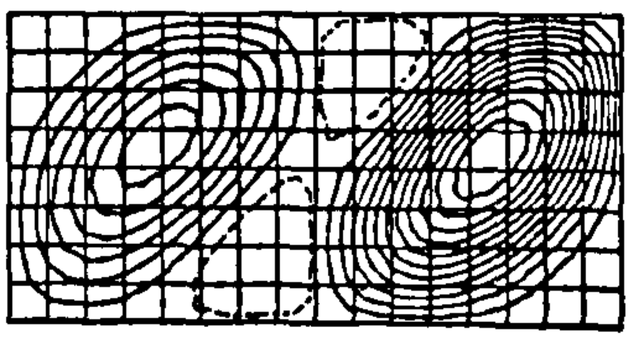
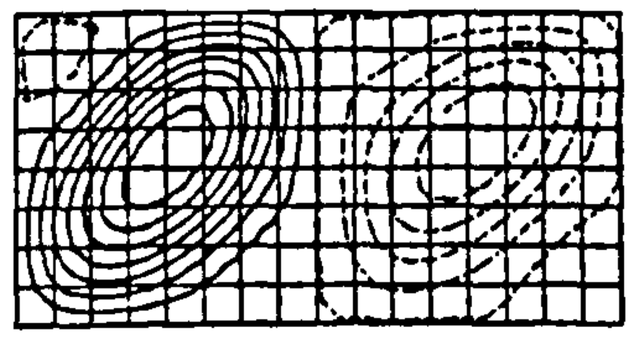
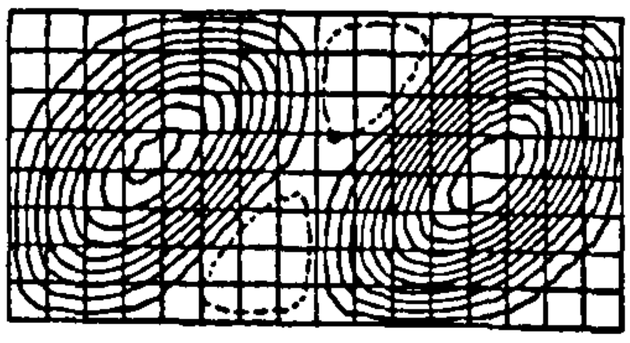
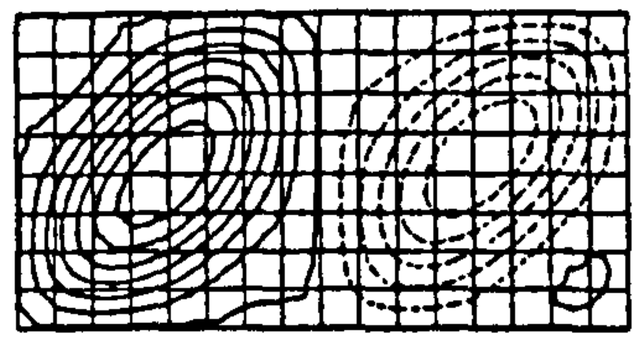
$$\left(\frac{\sigma_{b,cr}}{\sigma^0_{b,cr}}\right)^2 + \left(\frac{\tau_{cr}}{\tau^0_{cr}}\right)^2 = 1 \qquad (5.14)$$

1st Buckling Mode	2nd Buckling Mode
	
σ_b:τ=1:0, $k_{cr,b}$=23.91, $k_{cr,s}$=0	σ_b:τ=1:0, $k_{cr,b}$=24.47, $k_{cr,s}$=0
	
σ_b:τ=5:1, $k_{cr,b}$=19.37, $k_{cr,s}$=3.874	σ_b:τ=5:1, $k_{cr,b}$=21.23, $k_{cr,s}$=4.245 (4th Mode)
	
σ_b:τ=2:1, $k_{cr,b}$=11.40, $k_{cr,s}$=5.701	σ_b:τ=2:1, $k_{cr,b}$=11.72, $k_{cr,s}$=5.862
	
σ_b:τ=1:1, $k_{cr,b}$=6.269, $k_{cr,s}$=6.269	σ_b:τ=1:1, $k_{cr,b}$=6.380, $k_{cr,s}$=6.380
	
σ_b:τ=1:2, $k_{cr,b}$=3.233, $k_{cr,s}$=6.465	σ_b:τ=1:2, $k_{cr,b}$=3.265, $k_{cr,s}$=6.531
	
σ_b:τ=1:5, $k_{cr,b}$=1.308, $k_{cr,s}$=6.538	σ_b:τ=1:5, $k_{cr,b}$=1.313, $k_{cr,s}$=6.567

(a) d/a=0.5

$$Note: \quad k_{cr,b} = \sigma_{b,cr}\frac{b^2 t}{\pi^2 D} \quad , \quad k_{cr,s} = \tau_{cr}\frac{b^2 t}{\pi^2 D}$$

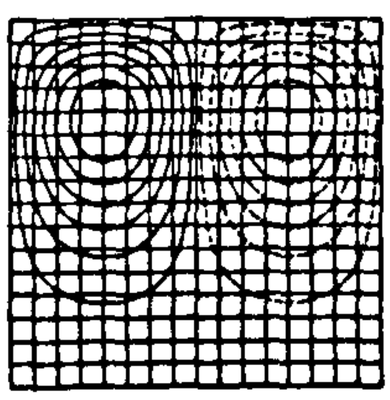
Figure 5.28 Critical buckling modes of plates with a knife edge. Shear and bending

1st Buckling Mode		2nd Buckling Mode	
	σ_b:τ=1:0 $k_{cr,b}$=26.34 $k_{cr,s}$=0 (2nd Mode)		σ_b:τ=1:0 $k_{cr,b}$=25.57 $k_{cr,s}$=0 (1st Mode)
	σ_b:τ=5:1 $k_{cr,b}$=21.73 $k_{cr,s}$=4.346		σ_b:τ=5:1 $k_{cr,b}$=23.23 $k_{cr,s}$=4.646
	σ_b:τ=2:1 $k_{cr,b}$=15.0 $k_{cr,s}$=7.498		σ_b:τ=2:1 $k_{cr,b}$=15.99 $k_{cr,s}$=7.992
	σ_b:τ=1:1 $k_{cr,b}$=9.051 $k_{cr,s}$=9.051		σ_b:τ=1:1 $k_{cr,b}$=9.489 $k_{cr,s}$=9.489
	σ_b:τ=1:2 $k_{cr,b}$=4.831 $k_{cr,s}$=9.661		σ_b:τ=1:2 $k_{cr,b}$=5.019 $k_{cr,s}$=10.04
	σ_b:τ=1:5 $k_{cr,b}$=1.972 $k_{cr,s}$=9.861		σ_b:τ=1:5 $k_{cr,b}$=2.043 $k_{cr,s}$=10.21

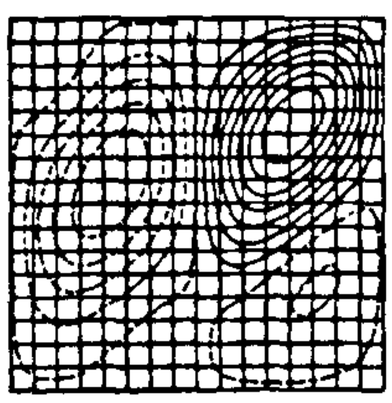
(b) d/a=1

$$Note: \quad k_{cr,b} = \sigma_{b,cr} \frac{b^2 t}{\pi^2 D} \quad , \quad k_{cr,s} = \tau_{cr} \frac{b^2 t}{\pi^2 D}$$

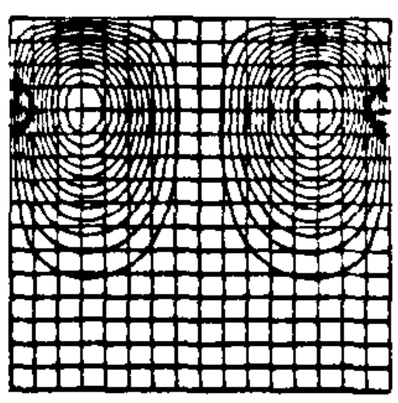
Figure 5.28 (Cont) Critical buckling modes of plates with a knife edge. Shear and bending



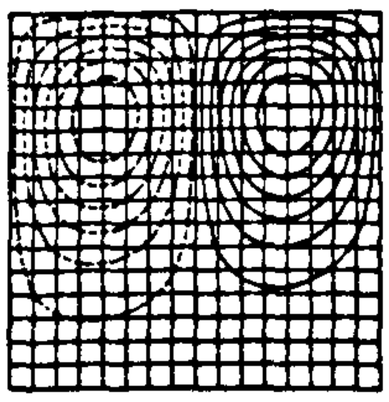
σ_b:τ=1:0, 1st Mode
$k_{cr,b}$=6.383, $k_{cr,s}$=0



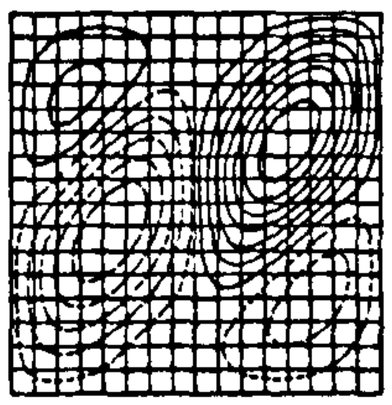
σ_b:τ=1:2, 1st Mode
$k_{cr,b}$=2.935, $k_{cr,s}$=5.871



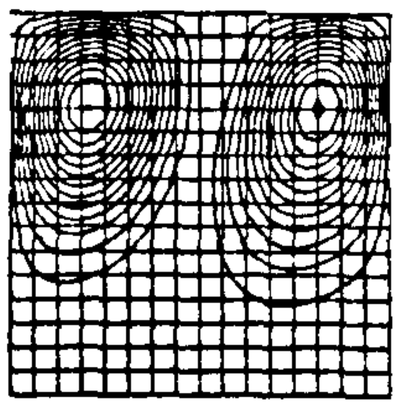
σ_b:τ=1:0, 2nd Mode
$k_{cr,b}$=8.586, $k_{cr,s}$=0



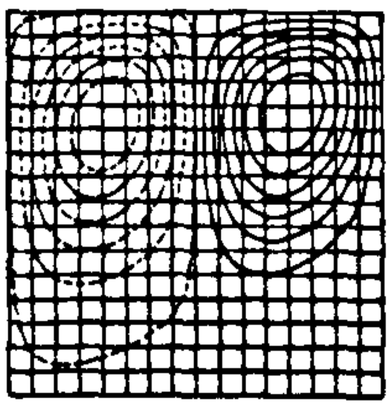
σ_b:τ=5:1, 1st Mode
$k_{cr,b}$=6.259, $k_{cr,s}$=1.252



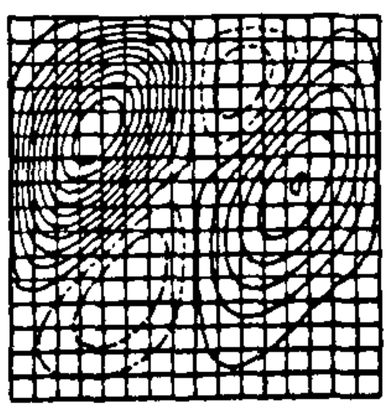
σ_b:τ=1:5, 1st Mode
$k_{cr,b}$=1.290, $k_{cr,s}$=6.452



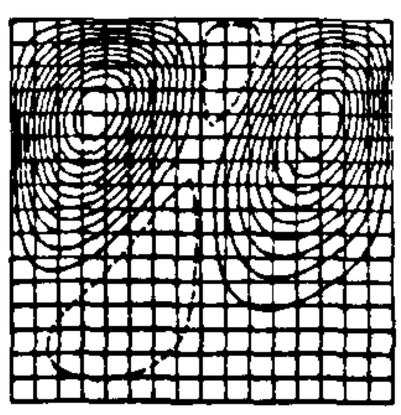
σ_b:τ=5:1, 2nd Mode
$k_{cr,b}$=8.242, $k_{cr,s}$=1.648



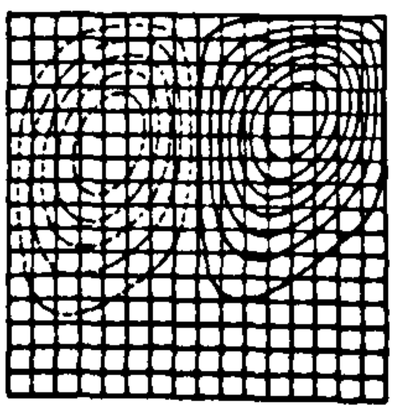
σ_b:τ=2:1, 1st Mode
$k_{cr,b}$=5.720, $k_{cr,s}$=2.860



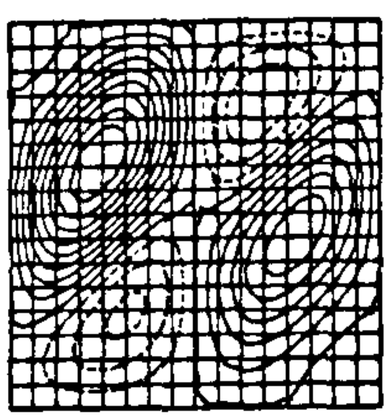
σ_b:τ=1:2, 2nd Mode
$k_{cr,b}$=3.059, $k_{cr,s}$=6.117



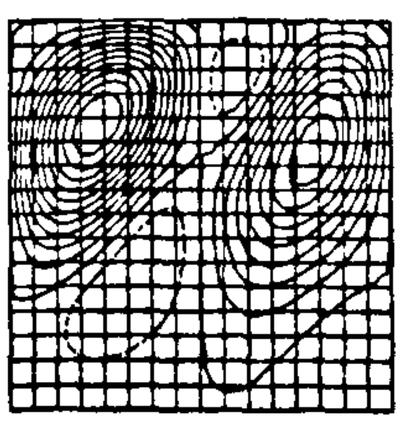
σ_b:τ=2:1, 2nd Mode
$k_{cr,b}$=7.004, $k_{cr,s}$=3.502



σ_b:τ=1:1, 1st Mode
$k_{cr,b}$=4.567, $k_{cr,s}$=4.567



σ_b:τ=1:5, 2nd Mode
$k_{cr,b}$=1.327, $k_{cr,s}$=6.633

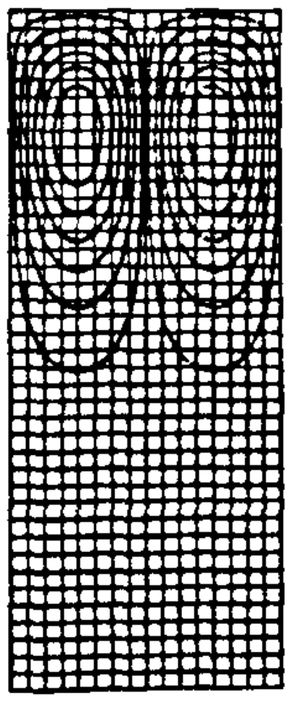


σ_b:τ=1:1, 2nd Mode
$k_{cr,b}$=5.081, $k_{cr,s}$=5.081

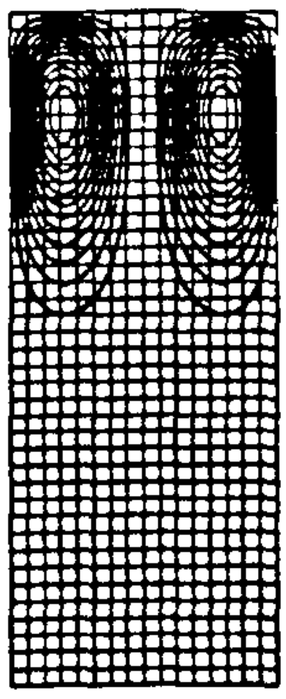
(c) d/a=2

$$Note: \quad k_{cr,b} = \sigma_{b,cr} \frac{b^2 t}{\pi^2 D} \quad , \quad k_{cr,s} = \tau_{cr} \frac{b^2 t}{\pi^2 D}$$

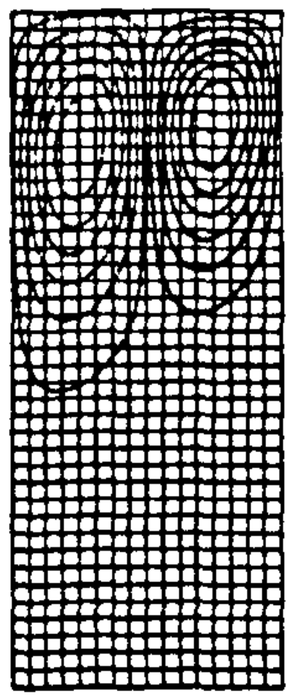
Figure 5.28(Cont) Critical buckling modes of plates with a knife edge. Shear and bending



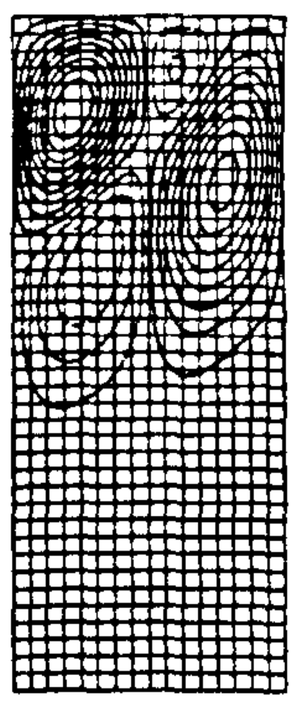
σ_b:τ=1:0, 1st Mode
$k_{cr,b}$=2.413, $k_{cr,s}$=0



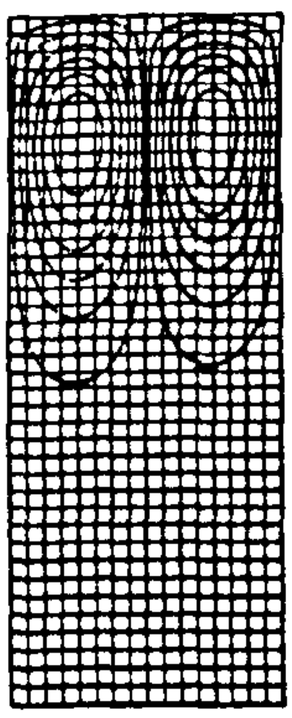
σ_b:τ=1:0, 2nd Mode
$k_{cr,b}$=4.056, $k_{cr,s}$=0



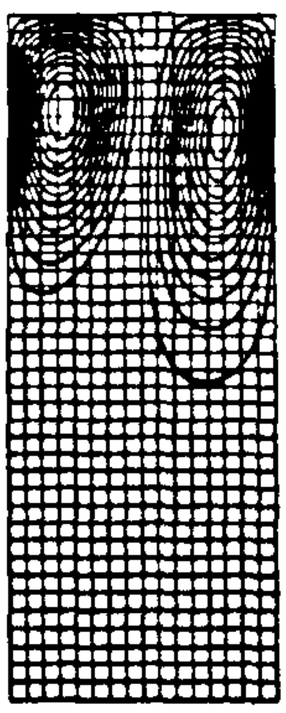
σ_b:τ=1:1, 1st Mode
$k_{cr,b}$=2.243, $k_{cr,s}$=2.243



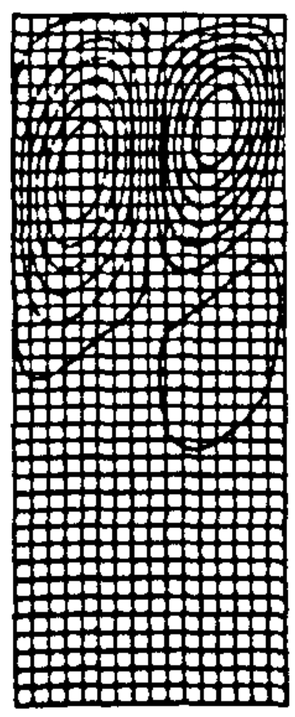
σ_b:τ=1:1, 2nd Mode
$k_{cr,b}$=3.094, $k_{cr,s}$=3.094



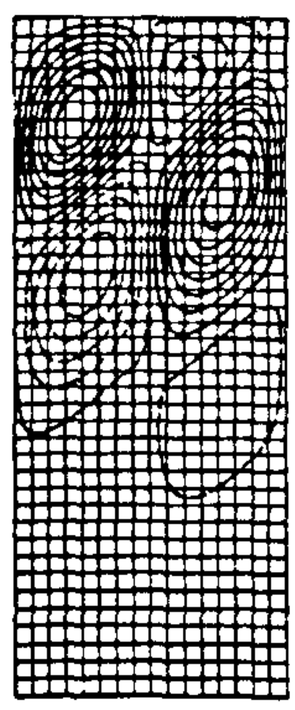
σ_b:τ=5:1, 1st Mode
$k_{cr,b}$=2.406, $k_{cr,s}$=0.481



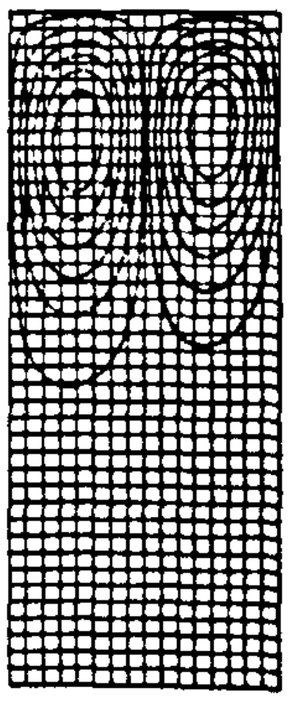
σ_b:τ=5:1, 2nd Mode
$k_{cr,b}$=3.993, $k_{cr,s}$=0.799



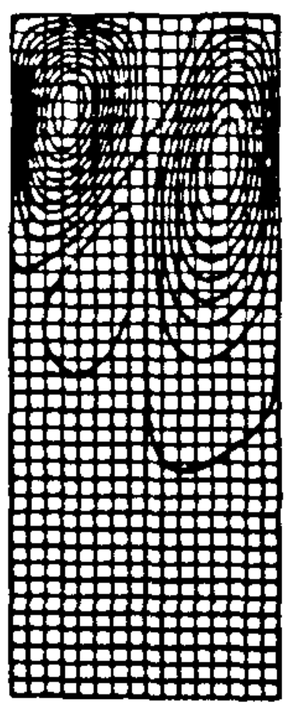
σ_b:τ=1:2, 1st Mode
$k_{cr,b}$=1.871, $k_{cr,s}$=3.742



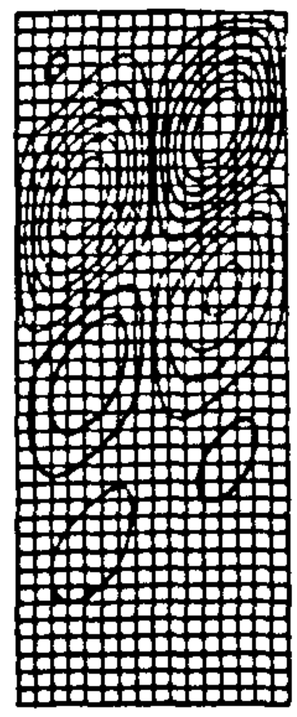
σ_b:τ=1:2, 2nd Mode
$k_{cr,b}$=2.149, $k_{cr,s}$=4.297



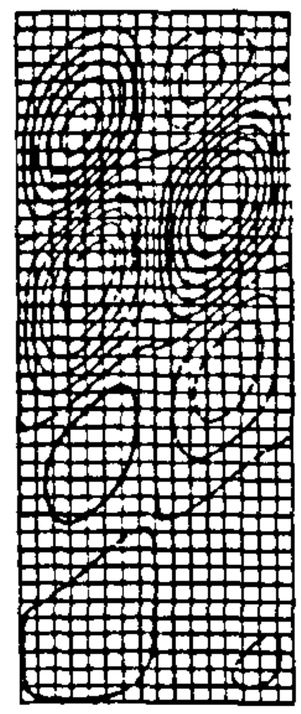
σ_b:τ=2:1, 1st Mode
$k_{cr,b}$=2.368, $k_{cr,s}$=1.184



σ_b:τ=2:1, 2nd Mode
$k_{cr,b}$=3.712, $k_{cr,s}$=1.856



σ_b:τ=1:5, 1st Mode
$k_{cr,b}$=1.019, $k_{cr,s}$=5.095



σ_b:τ=1:5, 2nd Mode
$k_{cr,b}$=1.042, $k_{cr,s}$=5.208

(d) d/a=5

$$Note: \quad k_{cr,b} = \sigma_{b,cr} \frac{b^2 t}{\pi^2 D} \quad , \quad k_{cr,s} = \tau_{cr} \frac{b^2 t}{\pi^2 D}$$

Figure 5.28(Cont) Critical buckling modes of plates with a knife edge. Shear and bending

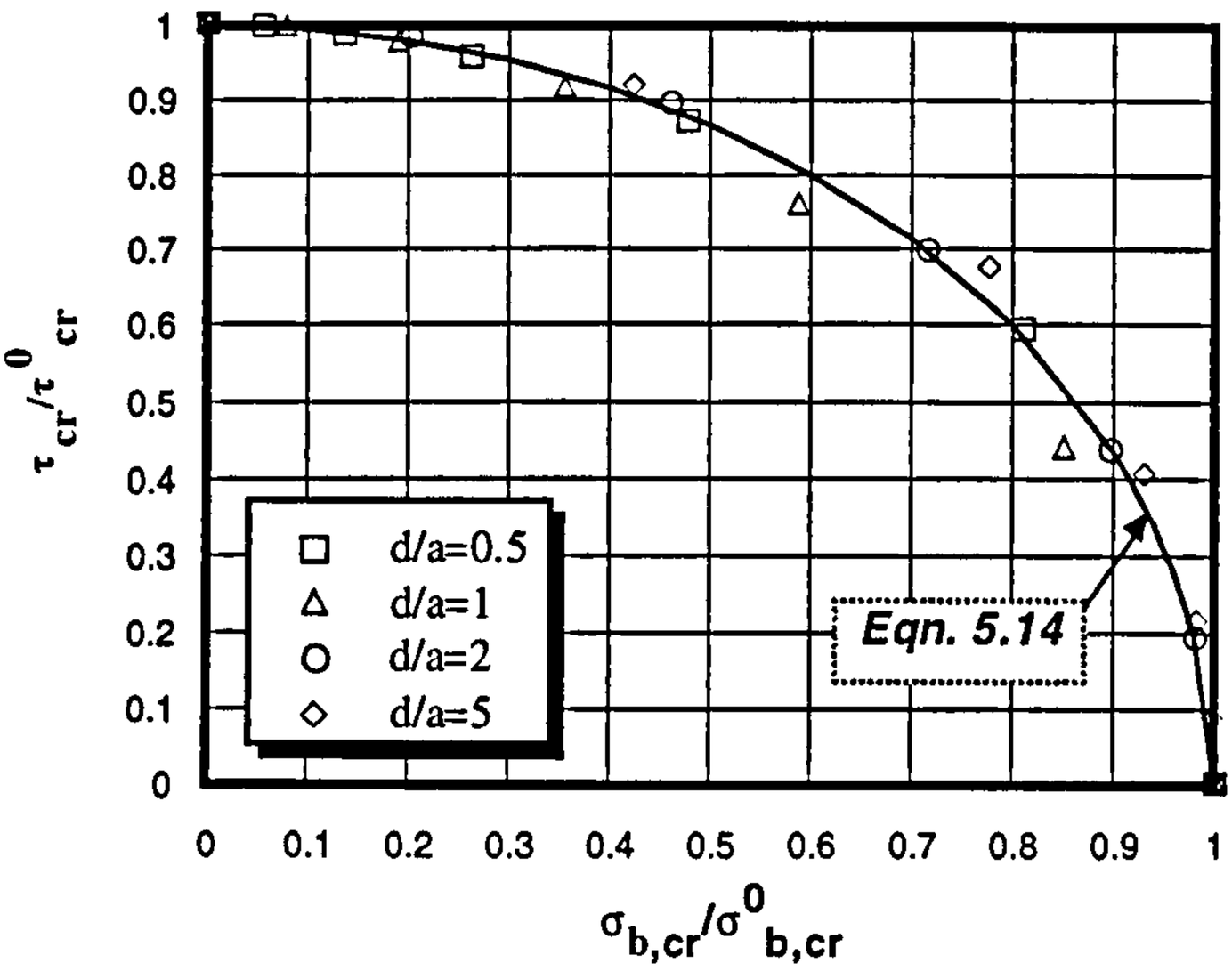


Figure 5.29 Interaction curves of the critical stresses for combined shear and bending. Plates with a straight knife edge. FE results. Eqn. 5.14

As stated previously, the lowest critical buckling stress for plates with a knife edge under pure shear, τ^0_{cr}, may be taken as the simply supported panel buckling stress, as given by Eqn. 5.2. Similarly, it is suggested that the critical bending stress $\sigma^0_{b,cr}$ can be determined by the equation [56]:

$$\sigma^0_{b,cr} = k_{cr}\frac{\pi^2 D}{d^2 t}, \quad k_{cr} = \begin{cases} 24, & for \quad d/a \le 1.5 \\ 24 + 73\left(\frac{2}{3} - \frac{a}{d}\right)^2, & for \quad d/a \ge 1.5 \end{cases} \tag{5.15}$$

For a given ratio of applied bending stress to the shear stress, σ_b/τ, the critical shear stress τ_{cr} in the presence of bending can be obtained from Eqn. 5.14 and expressed as:

$$\frac{\tau_{cr}}{\tau^0_{cr}} = \frac{1}{\sqrt{1 + r_b^2}} \tag{5.16}$$

where r_b represents the ratio of applied bending stress to the shear stress, defined as:

$$r_b = \frac{\sigma_b / \sigma_{b.cr}^0}{\tau / \tau_{cr}^0} \tag{5.17}$$

5.3.3.2 Non-Linear Elastic Buckling Behaviour

- ***Deflection Modes***

Contour plots of out-of-plane deflection from the non-linear elastic buckling analysis are presented in Fig. 5.30, for the different combinations of applied shear and bending stresses investigated. The initial imperfection modes used in the non-linear buckling analysis are the first buckling mode which is, or is close to, a symmetric or point-symmetric buckling mode for each loading combination. The variations in the deflection modes with the load ratio σ_b/τ are similar to those observed in the critical buckling modes, as mentioned in Section 5.3.3.1. It was also found, by means of the ABAQUS POST program, that the deflection modes vary with the magnitudes of applied loads. As the applied load is increased, the panel buckles become progressively sharper. By comparing the modes shown in Figs. 5.30 and 5.28, the differences between the critical buckling modes (or initial imperfection modes) and the elastic large-deflection modes can be seen.

As indicated in Section 5.3.2.2, the knife edge moment M_{pk} for combined loading conditions is too difficult to represent accurately, due to the wide variations in the deflection modes, which are even more complicated for combined shear and bending than for combined shear and compression.

- ***Distribution of the Knife Edge Moment***

For plates subjected to coexistent shear and bending stresses, τ and σ_b, the distributions of the bending moments along the knife edge, obtained from the non-linear elastic finite element analyses, are presented in Fig. 5.31. For each case, the knife edge moments at three different load levels, represented by τ/τ_{cr} for cases in the presence of shear and

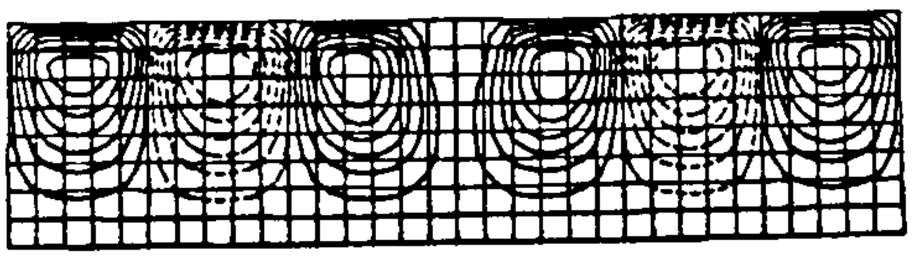
$\sigma_b/\sigma^0_{b,cr}$ for pure bending, are illustrated in Fig. 5.31. Since the main interest in the knife edge moment is its maximum magnitude, the sign of the knife edge moment, shown in Fig. 5.31, has been adjusted to give a positive maximum value of $M_{pk}b/Dt$.

To aid understanding, some non-linear elastic buckling analyses were carried out by replacing the knife edge with a straight stiffener of flexural rigidity Ψ which is great enough to divide the plate. The tendency for the knife edge to deflect, due to the local panel bending effect, can be revealed by observing the direction of the stiffener deflection.

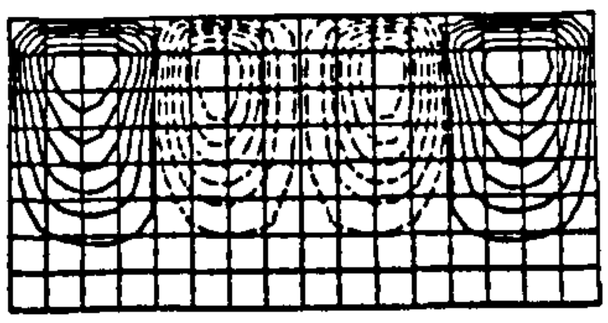
In Fig. 5.32(a), the stiffener deflections relative to the panel deflection for plates subjected pure bending are illustrated. It is found that for d/a=2, the stiff stiffener tends to deflect in the direction opposite to the panel deflection, whereas the reverse is observed for d/a=5. This is because for d/a=2, the preferred mode of the unstiffened plate has two half waves across its width, whereas for d/a=5, the preferred mode for the unstiffened plate has a single half wave across the plate width. Thus for plates under pure bending, the deflected panels may apply a distributed lateral force on the stiffener or the knife edge, in either the same or opposite direction to the panel deflection, depending on the panel aspect ratio.

Fig. 5.32(b) shows the deflection profiles along the depth of the plate, for stiffened plates subjected to combined shear and bending. It can be seen that when the shear stresses are in the presence, in addition to the bending stress, the top of the stiffener is forced to deflect in the direction opposite to the main panel buckles.

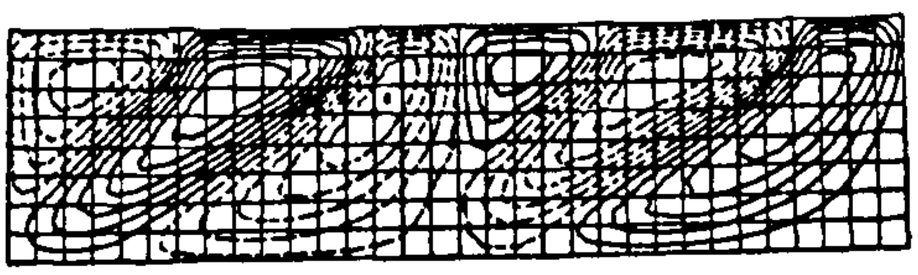
When the action of the buckled panels on the knife edge, due to the applied bending stresses, is in the same direction as that due to the applied shear stresses, as found for d/a=2, the distributions of the knife edge moments are more regular, with the maximum magnitude occurring in the top part of the knife edge. When the actions of the applied shear stresses and bending stresses are in the opposite directions, as found for d/a=5, the maximum magnitude of the knife edge moment may occur in another part of the knife edge, as shown in Fig. 5.31(d).



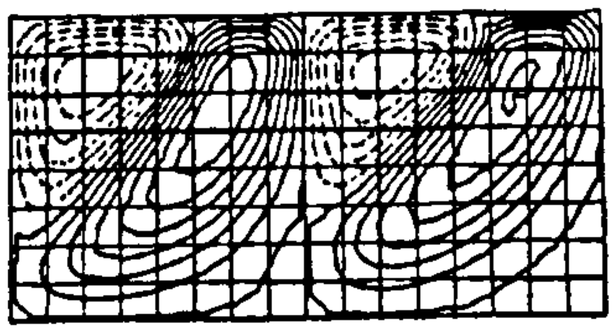
σ_b:τ=1:0



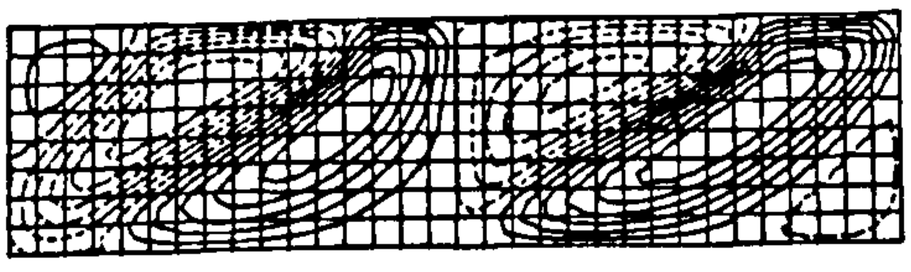
σ_b:τ=1:0



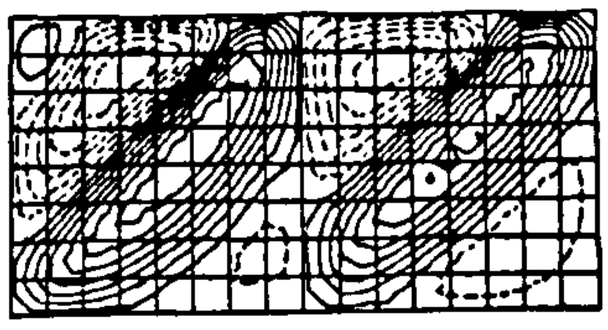
σ_b:τ=5:1



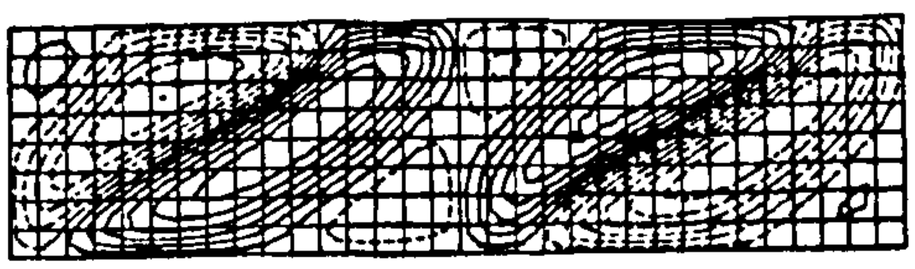
σ_b:τ=5:1



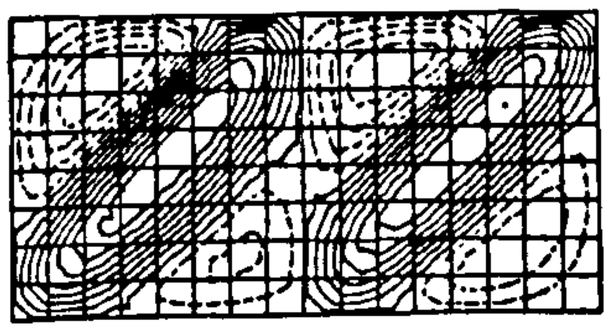
σ_b:τ=2:1



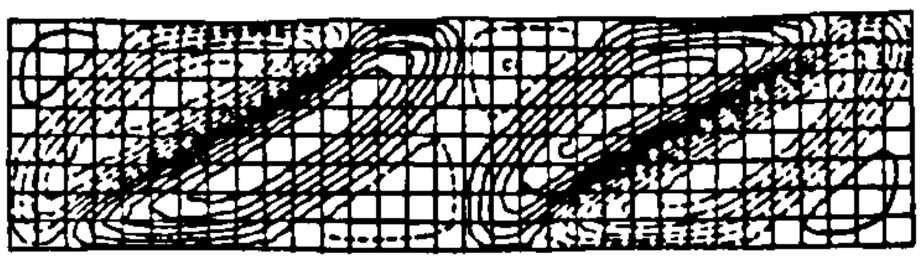
σ_b:τ=2:1



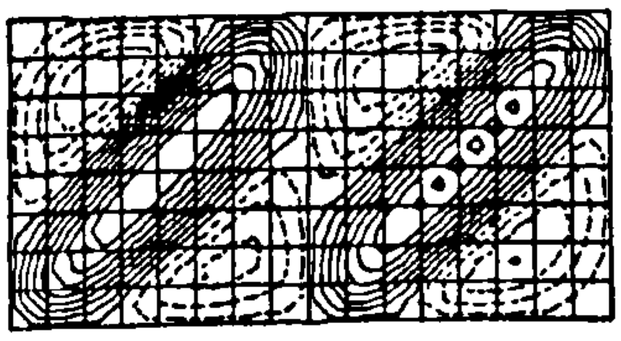
σ_b:τ=1:1



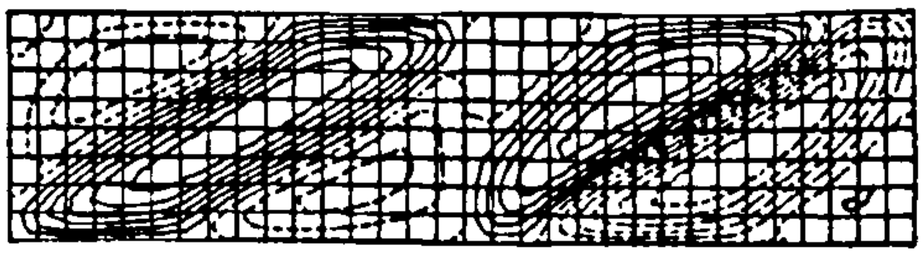
σ_b:τ=1:1



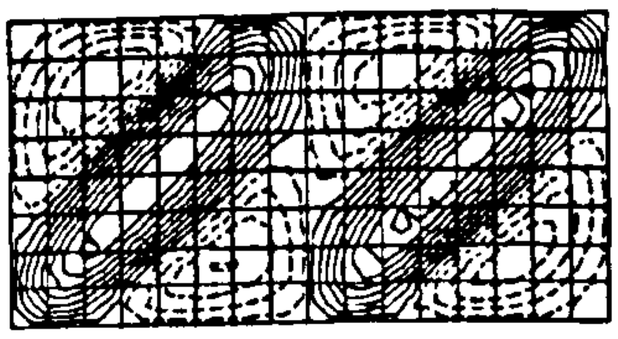
σ_b:τ=1:2



σ_b:τ=1:2



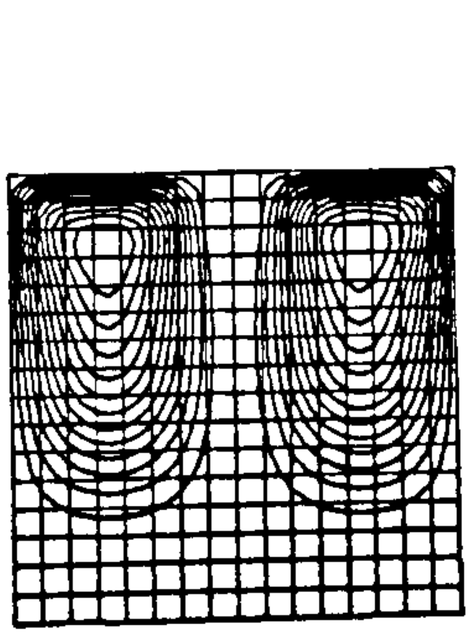
σ_b:τ=1:5



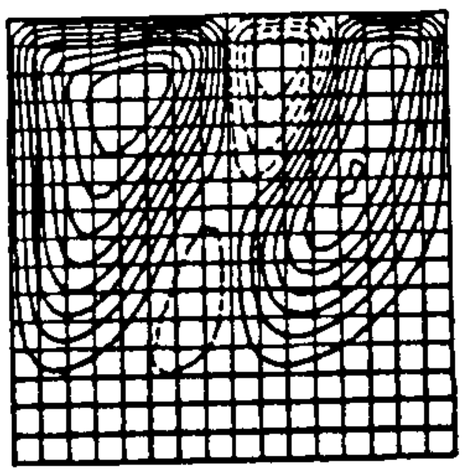
σ_b:τ=1:5

(a) d/a=0.5 **(b) d/a=1**

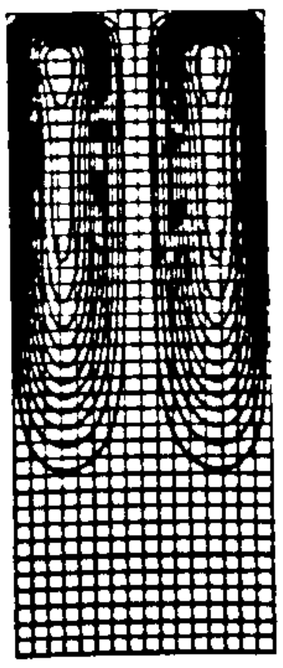
Figure 5.30 Deflection modes of plates with a straight knife edge.
Combined shear and bending. Non-linear elastic FE results. w_{0p}/t=1.091



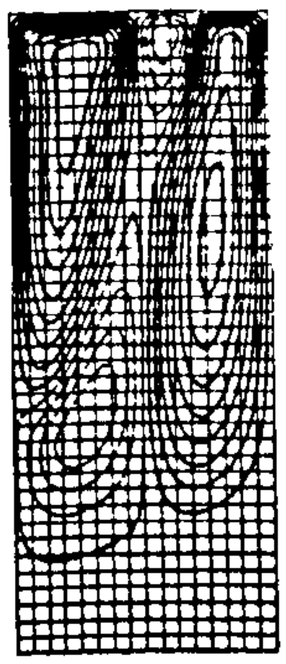
σ_b:τ=1:0



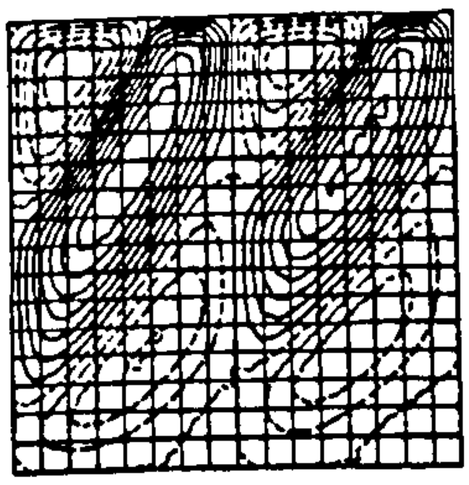
σ_b:τ=5:1



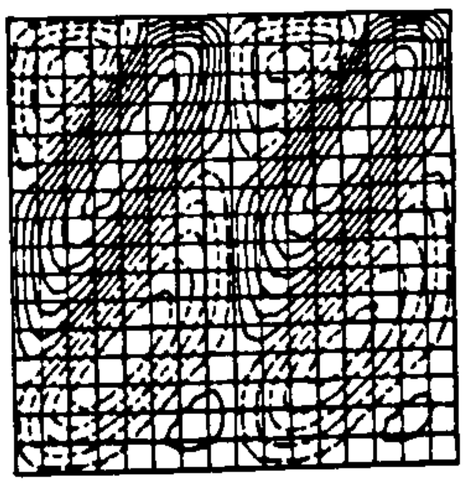
σ_b:τ=1:0



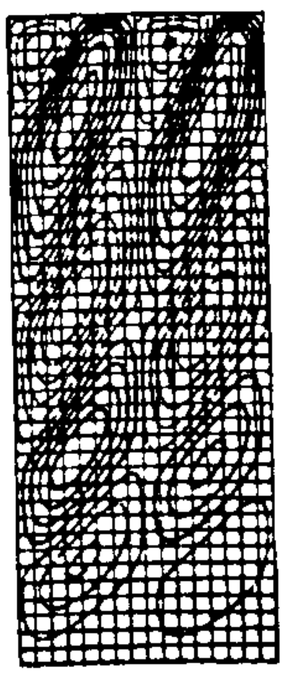
σ_b:τ=5:1



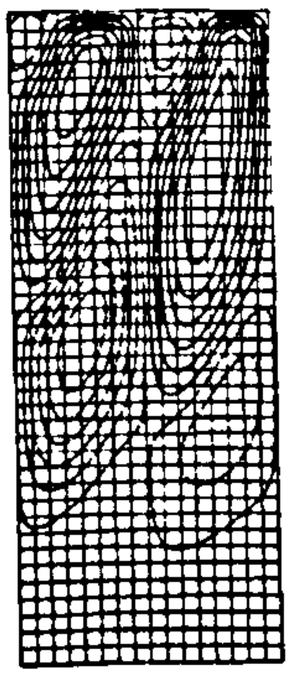
σ_b:τ=2:1



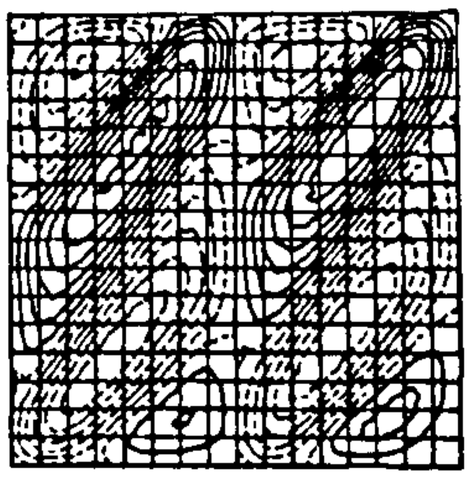
σ_b:τ=1:1



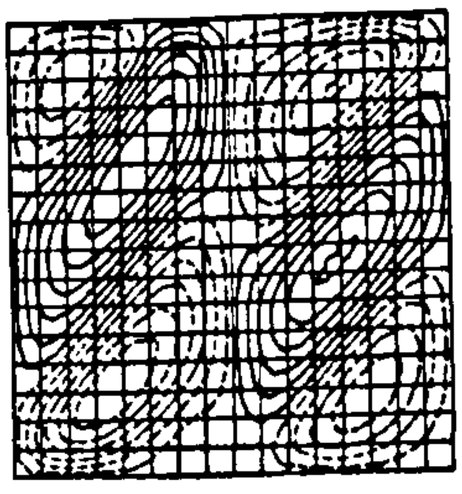
σ_b:τ=2:1



σ_b:τ=1:1



σ_b:τ=1:2



σ_b:τ=1:5



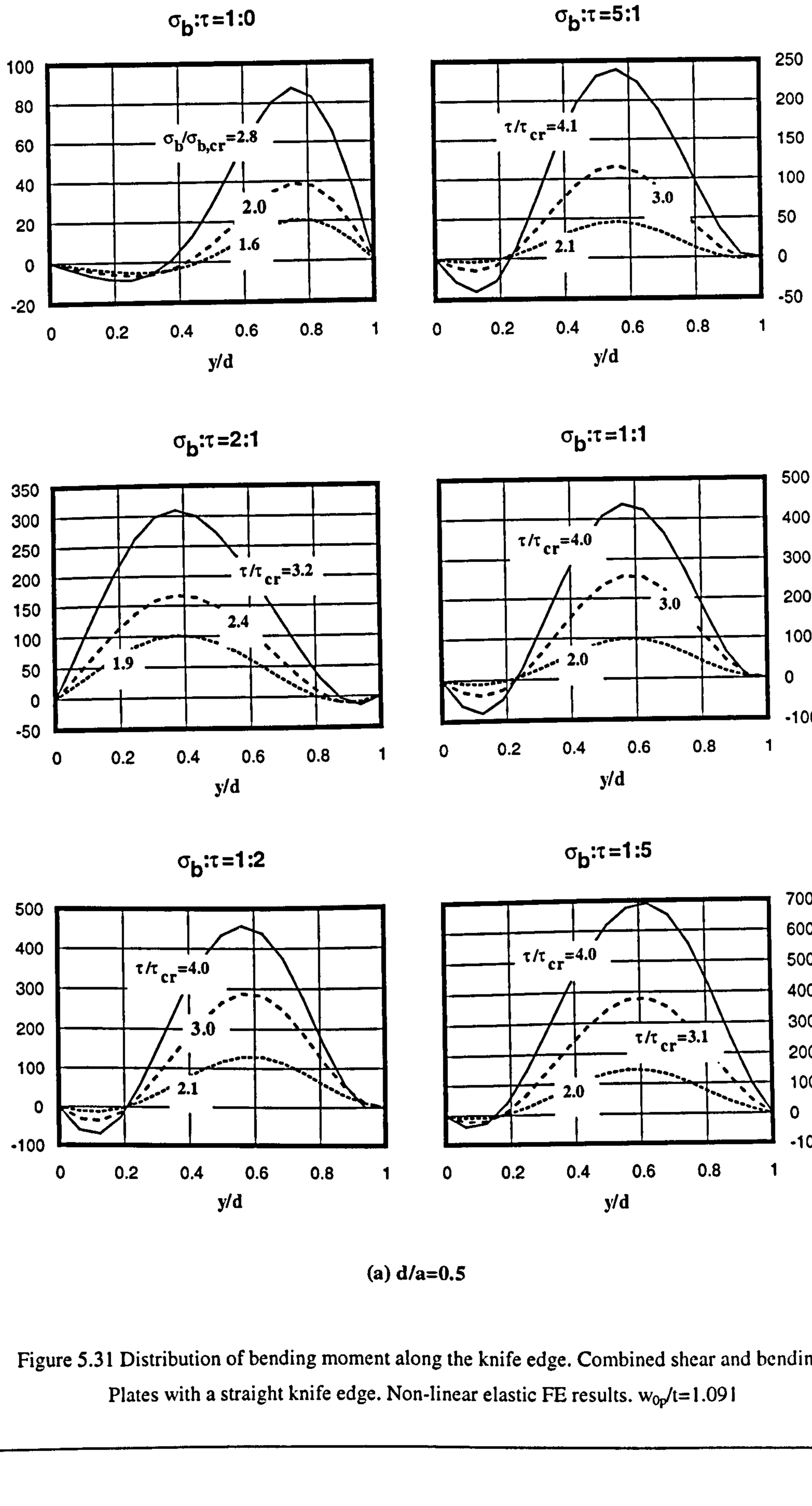
σ_b:τ=1:2



σ_b:τ=1:5

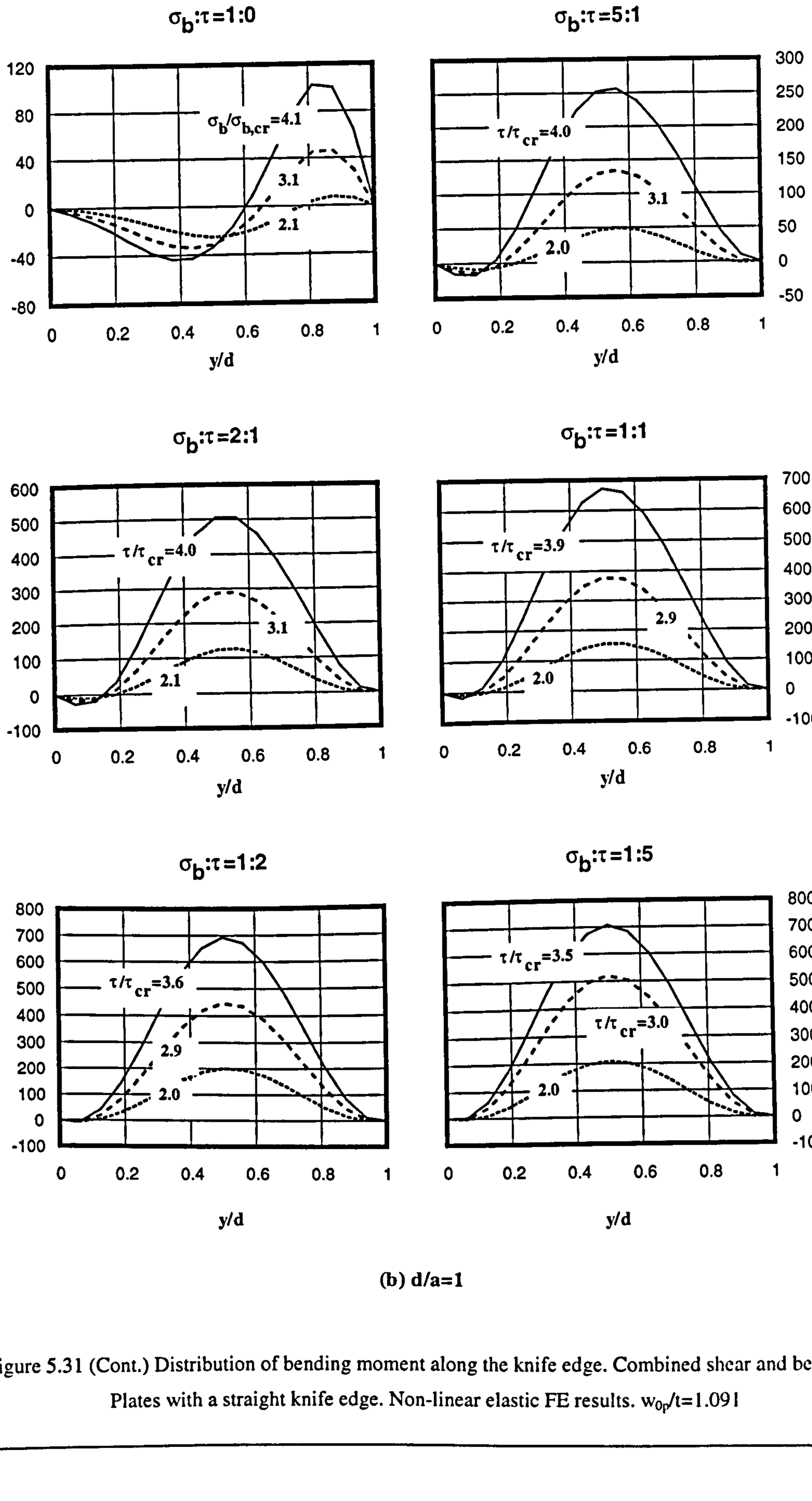
(c) d/a=2 **(d) d/a=5**

Figure 5.30 (Cont) Deflection modes of plates with a straight knife edge.
Combined shear and bending. Non-linear elastic FE results. w_{0p}/t=1.091



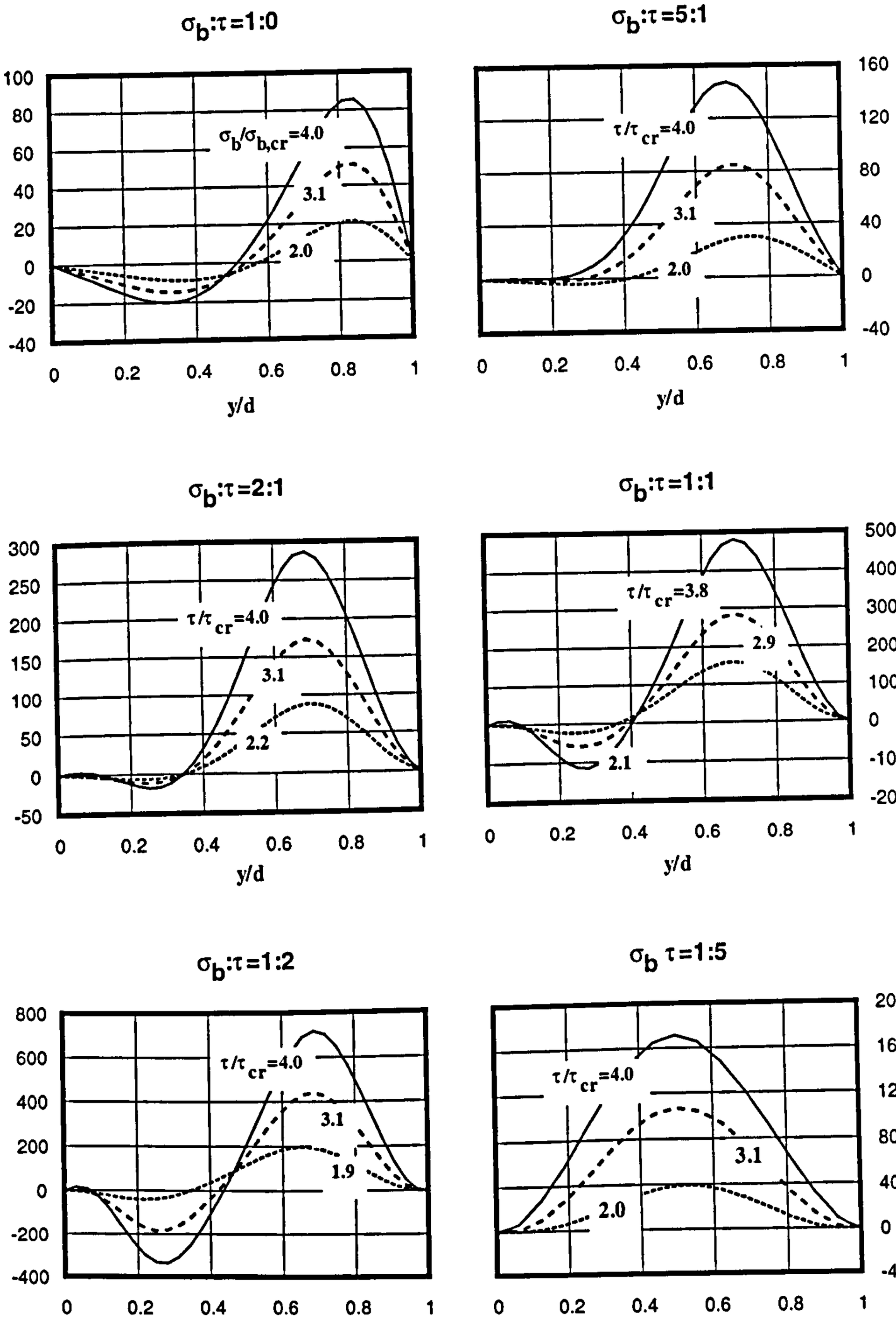
(a) d/a=0.5

Figure 5.31 Distribution of bending moment along the knife edge. Combined shear and bending. Plates with a straight knife edge. Non-linear elastic FE results. $w_{0p}/t=1.091$



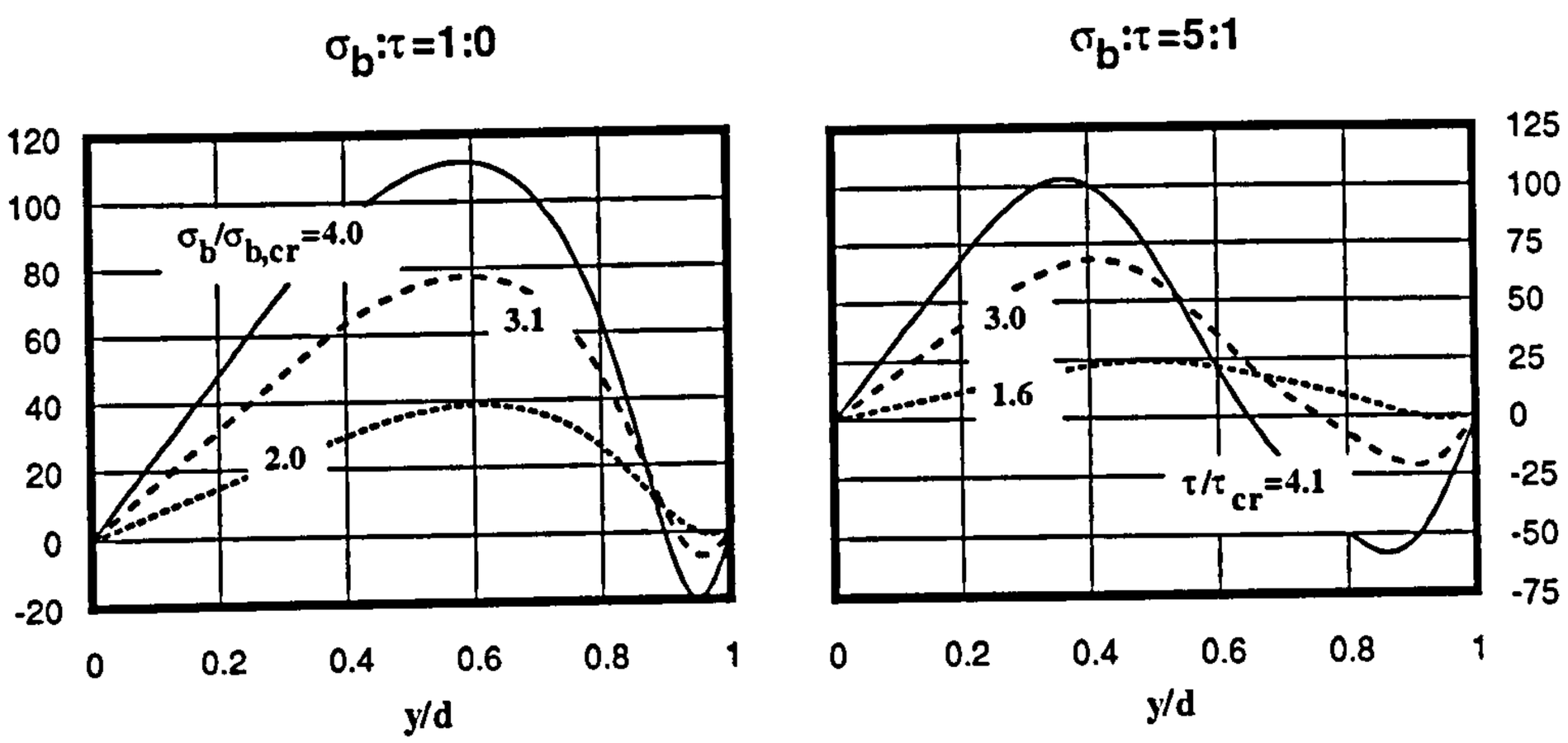
(b) d/a=1

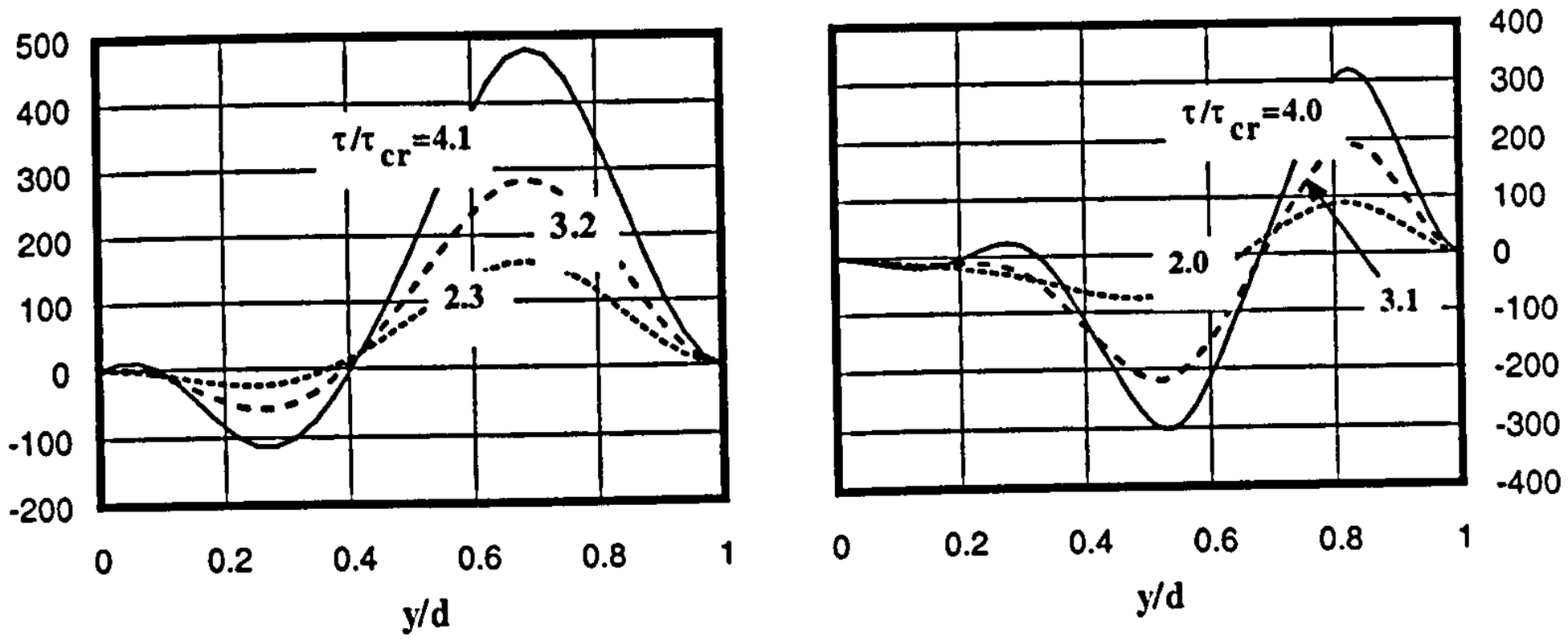
Figure 5.31 (Cont.) Distribution of bending moment along the knife edge. Combined shear and bending. Plates with a straight knife edge. Non-linear elastic FE results. $w_{0p}/t=1.091$

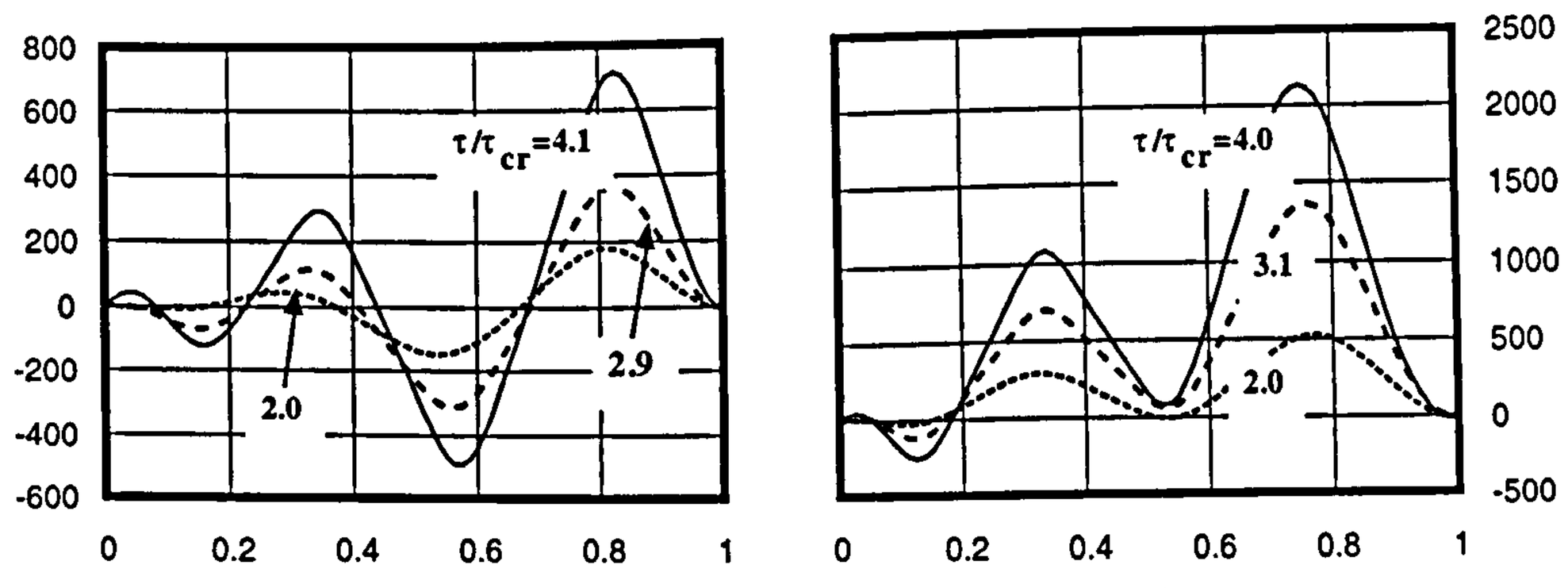


(c) d/a=2

Figure 5.31 (Cont.) Distribution of bending moment along the knife edge. Combined shear and bending. Plates with a straight knife edge. Non-linear elastic FE results. $w_{0p}/t=1.091$

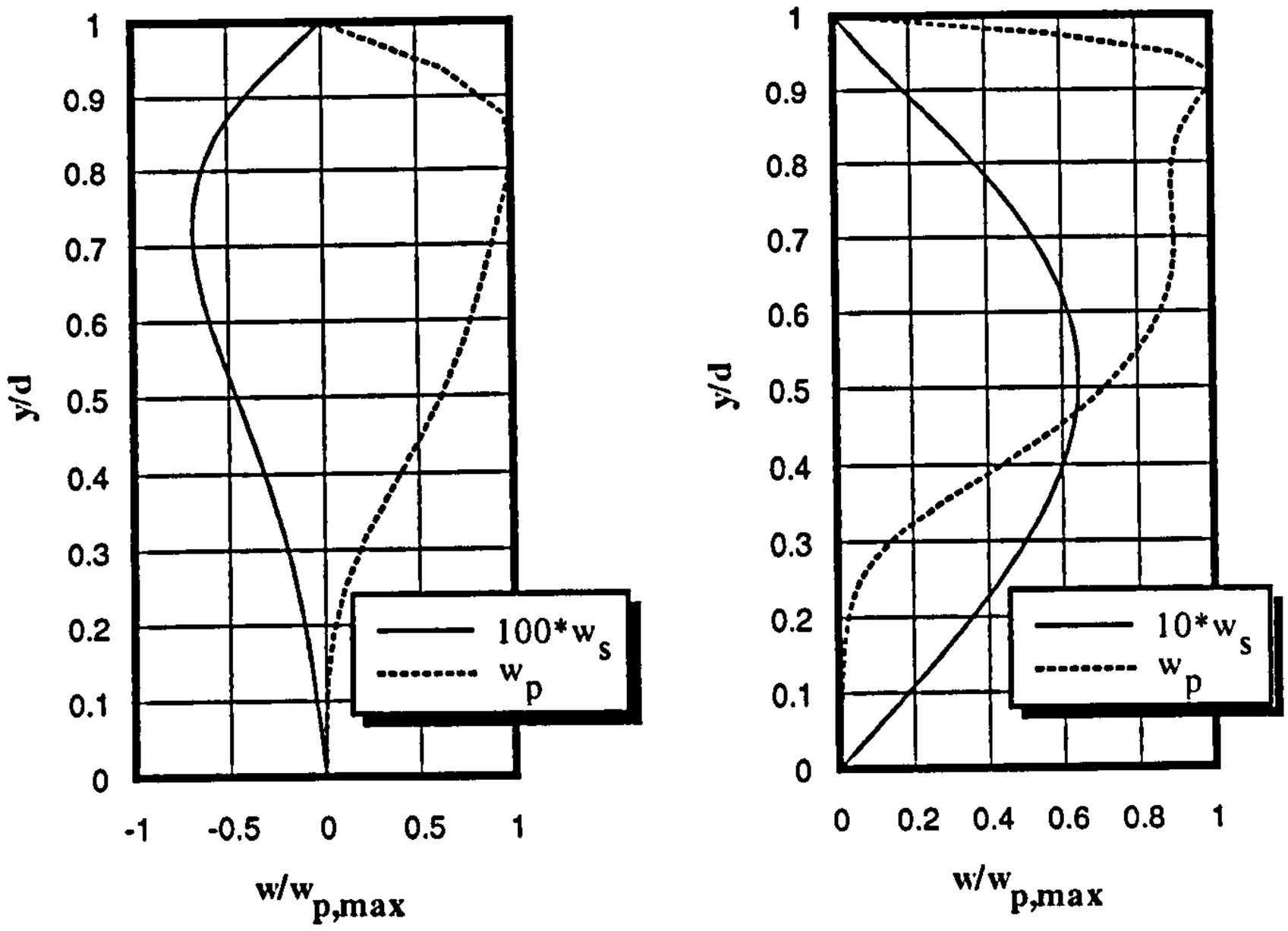




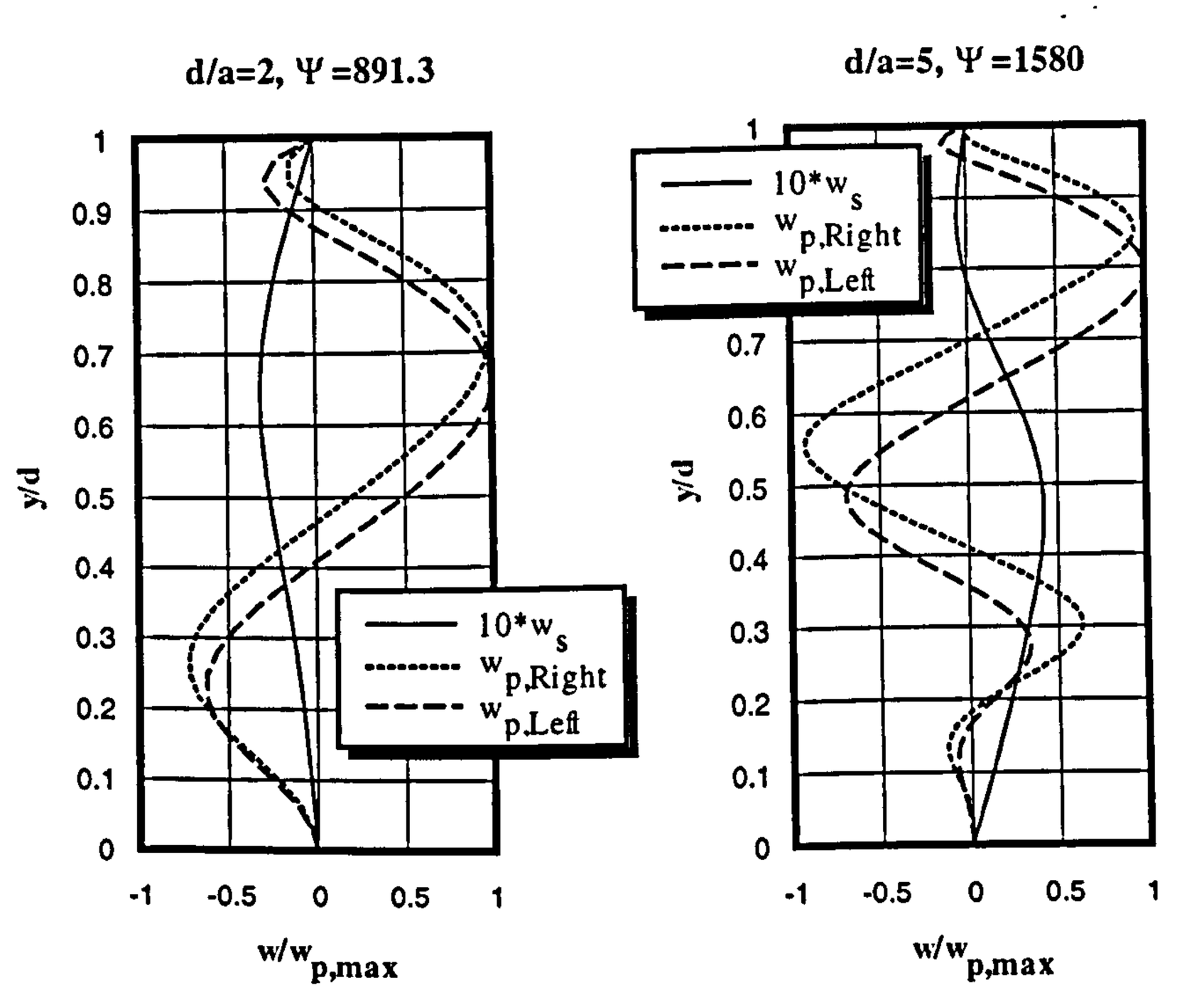


(d) d/a=5

Figure 5.31 (Cont.) Distribution of bending moment along the knife edge. Combined shear and bending. Plates with a straight knife edge. Non-linear elastic FE results. $w_{0p}/t=1.091$



(a) Pure bending



(b) σ_b:τ=1:1

Figure 5.32 Deflection profiles along the stiffener and central lines of sub-panels. w_{0p}/t=1.091. $w_{p.max}$ denotes the maximum deflection of the panel. Combined shear and bending. Plates with a straight stiffener. Non-linear elastic FE results. $\Psi=EI_s/Db$

- ***Magnitude of the Knife Edge Moment, M_{pk}***

With respect to design of the transverse stiffeners, the maximum amplitude of the bending moment along the knife edge is of interest. For the cases of different ratios of σ_b/τ, considered for each aspect ratio d/a, the maximum values of the non-dimensional knife edge moment, $M_{pk}b/Dt$, are plotted in the same diagram, as shown in Fig. 5.33. The horizontal axis represents the value of τ/τ_{cr} for combined shear and bending, and σ_b/σ^0_{bcr} for pure bending. It can be seen in Fig. 5.33 that in general, as the shear component, τ, becomes predominant, the magnitude of the knife edge moment becomes significantly greater.

It can also be seen in Fig. 5.33 that for different ratios of applied bending stress to shear stress, σ_b/τ, the variations in the knife edge moment $M_{pk}b/Dt$ with the aspect ratio d/a do not follow a regular trend. The knife edge bending moments calculated from Eqn. 5.3, which has been proposed for predicting M_{pk} for pure shear, are also shown in Fig. 5.33. It is apparent that in most of the cases, the curve of $M_{pk}b/Dt$ versus τ/τ_{cr} obtained for pure shear, provides an upper limit of M_{pk} for combined shear and bending conditions. However, in order to give a reasonably accurate estimation of M_{pk} for combined shear and bending conditions, it is considered that an approach in parallel to the method proposed for combined shear and compression conditions should be adopted. That is, the design formulae for predicting M_{pk} for the pure shear condition, as presented in Eqn. 5.3, will be extended for combined shear and bending conditions, but the ratio of τ/τ_{cr} in Eqn. 5.3 for pure shear (ie., τ/τ^0_{cr}) will be replaced with an equivalent shear stress ratio τ_{eq}/τ^0_{cr}. It is clear from Fig. 5.33 that τ_{eq}/τ^0_{cr} may be taken as a factored τ/τ_{cr}. The definition of the equivalent shear stress τ_{eq} for combined shear and bending conditions is presented in Section 5.3.3.3.

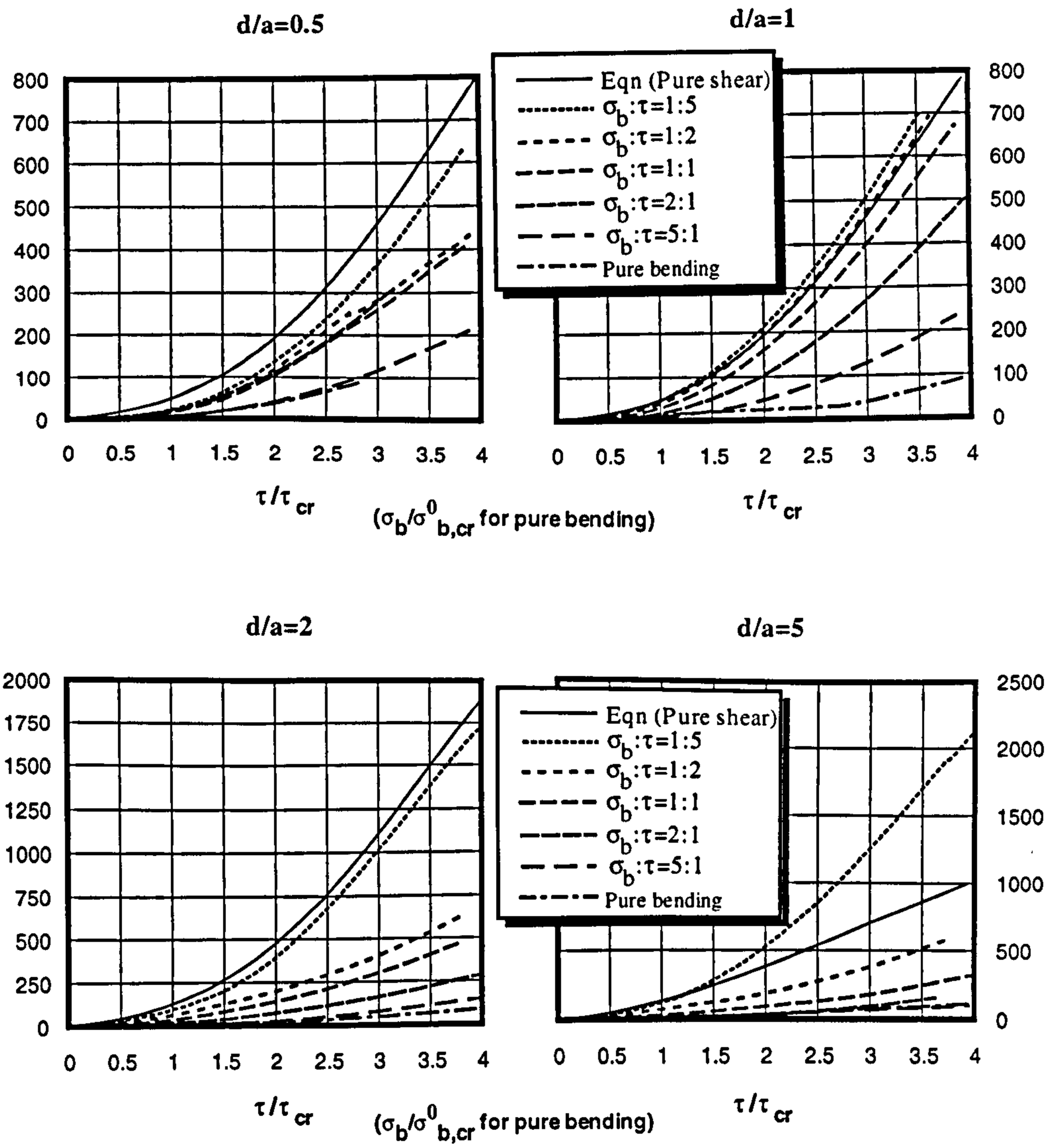


Figure 5.33 The bending moments in the knife edges. Combined shear and bending. Plates with a straight knife edge. w_{0p}/t=1.091. Non-linear elastic FE results

5.3.3.3 Design Formulae for Predicting M_{pk}

For a given ratio of σ_b/τ, the critical shear stress τ_{cr} in the presence of bending can be calculated from Eqn. 5.16. In terms of Eqns. 5.16 and 5.17, the ratio of applied shear stress to the critical shear stress, τ/τ_{cr}, can be written as:

$$\frac{\tau}{\tau_{cr}} = \sqrt{\left(\frac{\tau}{\tau_{cr}^{0}}\right)^{2} + \left(\frac{\sigma_b}{\sigma_{b,cr}^{0}}\right)^{2}} \tag{5.18}$$

It can be seen that in Eqn. 5.18 that as $\tau \rightarrow 0$ (pure bending alone), $\tau/\tau_{cr} \rightarrow \cdot \sigma_b/\sigma^{0}_{bcr}$. It is obvious from Fig. 5.33 that in order to use Eqn. 5.3 for predicting M_{pk} for pure bending, an equivalent ratio of τ/τ_{cr}, which is less than $\sigma_b/\sigma^{0}_{bcr}$, should be used.

By assuming that the knife edge moment at $\sigma_b/\sigma^{0}_{bcr}$ for pure bending is equal to the knife edge moment at τ_{eq}/τ^{0}_{cr} for pure shear, an equivalent shear stress τ_{eq} for pure bending can be defined. For reasons of simplicity, it is assumed that the equivalent shear stress τ_{eq} for pure bending can be written as:

$$\frac{\tau_{eq}}{\tau_{cr}^{0}} = \beta_b \left(\frac{\sigma_b}{\sigma_{b,cr}^{0}}\right) \tag{5.19}$$

where β_b is a factor introduced to account for the difference in the magnitudes of M_{pk} between pure bending and pure shear conditions.

In terms of Eqns. 5.18 and 5.19, it is proposed that for combined shear and bending, the knife edge moment M_{pk} can be calculated using Eqn. 5.3 with τ/τ_{cr} being replaced by the equivalent shear stress ratio:

$$\frac{\tau_{eq}}{\tau_{cr}^{0}} = \sqrt{\left(\frac{\tau}{\tau_{cr}^{0}}\right)^{2} + \left(\beta_b \frac{\sigma_b}{\sigma_{b,cr}^{0}}\right)^{2}} \tag{5.20}$$

For bending alone, Eqn. 5.20 reduces to Eqn. 5.19. For pure shear, Eqn. 5.20 reduces to Eqn. 5.11.

By curve-fitting the finite element solutions for combined shear and bending conditions with Eqn. 5.3, it is found that the factor β_b may be approximately taken as:

$$\beta_b = 0.25 \tag{5.21}$$

In Fig. 5.34, the non-dimensional knife edge moments $M_{pk}b/Dt$, predicted by Eqn. 5.3 using the equivalent shear stress τ_{eq} given by Eqns. 5.20 and 5.21, are compared with the finite element results. In general, the estimated knife edge moments are close to the

numerical results, especially for plates of d/a≤1. Also the curves are in general more compact than in Fig. 5.33.

Based on the above discussion, it is proposed that for plates subjected to coexistent shear and bending, the knife edge bending moment M_{pk} can be calculated using Eqn. 5.3, by assuming that a pure shear stress of τ_{eq}, given by Eqns. 5.20 and 5.21, is applied. The design formulae for general loading conditions will be summarized in Section 5.4.

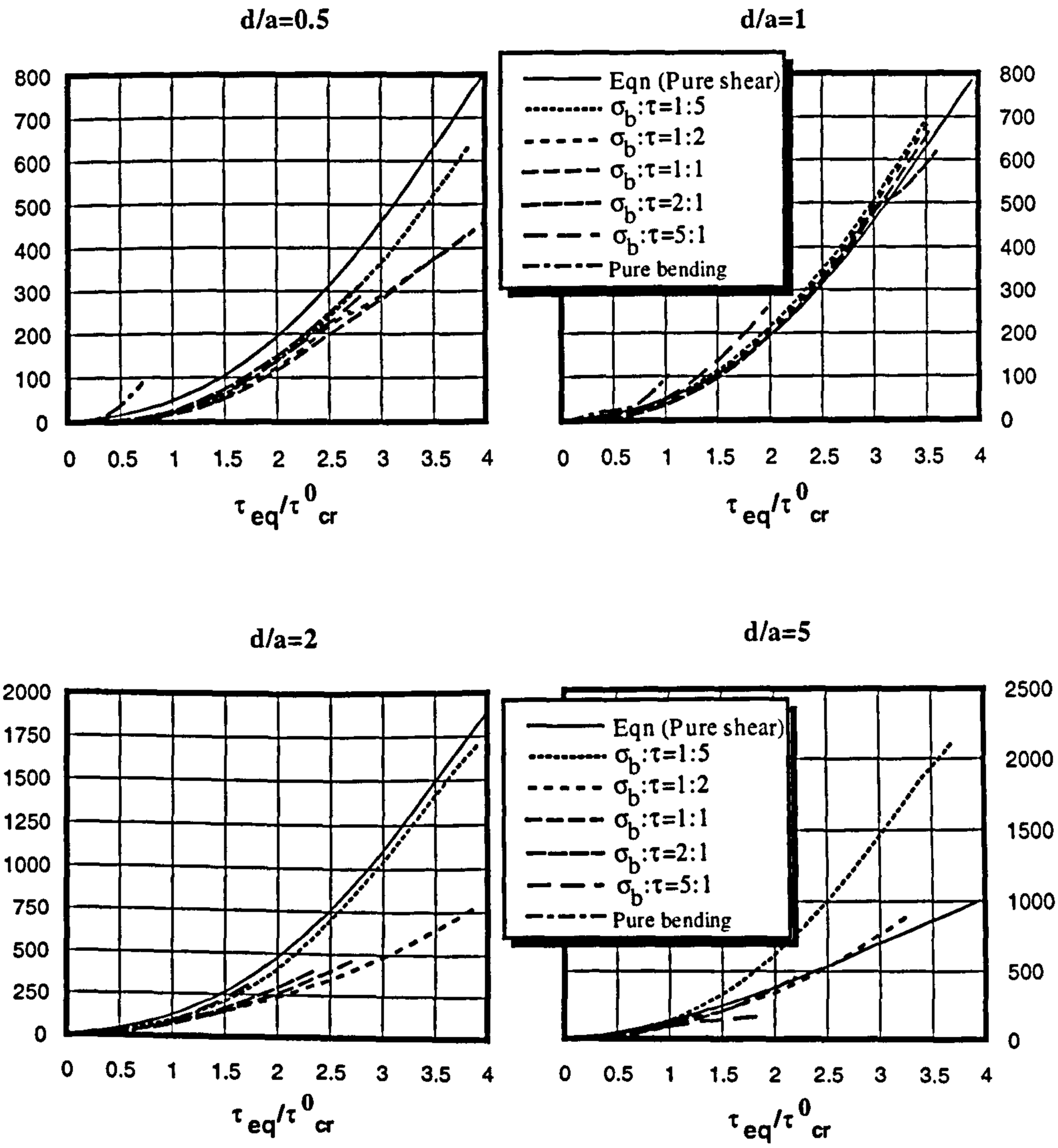


Figure 5.34 Comparisons in the knife edge moments between the proposed equations and FE solutions. Combined shear and bending. Plates with a straight knife edge. $w_{0p}/t=1.091$

5.4 SUMMARY OF THE DESIGN FORMULAE FOR PREDICTING M_{pk}

Based on the above analyses, it is proposed that for plates with a straight knife edge, subjected to general combined shear, compression and bending (Fig. 5.1), the bending moments in the knife edges, M_{pk}, can be estimated by the following equations:

$$\frac{M_{pk}b}{Dt} = 29.71\left(\frac{w_{0p}}{t}\right)\left(\frac{\tau_{eq}}{\tau^0_{cr}}\right) - 0.524\left(\frac{w_{0p}}{t}\right)\left(\frac{\tau_{eq}}{\tau^0_{cr}}\right)^2 \qquad \text{for d/a}\leq 1$$
$$-6.96\left(\frac{\tau_{eq}}{\tau^0_{cr}}\right) + 4.962\left(\frac{\tau_{eq}}{\tau^0_{cr}}\right)^2 + 21.37\left(\frac{\tau_{eq}}{\tau^0_{cr}}\right)^3 - 2.865\left(\frac{\tau_{eq}}{\tau^0_{cr}}\right)^4$$

(5.22a)

$$\frac{M_{pk}b}{Dt} = 83.62\left(\frac{w_{0p}}{t}\right)\left(\frac{\tau_{eq}}{\tau^0_{cr}}\right) - 16.59\left(\frac{w_{0p}}{t}\right)\left(\frac{\tau_{eq}}{\tau^0_{cr}}\right)^2 \qquad \text{for d/a=2}$$
$$-14.03\left(\frac{\tau_{eq}}{\tau^0_{cr}}\right) + 19.70\left(\frac{\tau_{eq}}{\tau^0_{cr}}\right)^2 + 54.99\left(\frac{\tau_{eq}}{\tau^0_{cr}}\right)^3 - 7.676\left(\frac{\tau_{eq}}{\tau^0_{cr}}\right)^4$$

(5.22b)

$$\frac{M_{pk}b}{Dt} = 69.47\left(\frac{w_{0p}}{t}\right)\left(\frac{\tau_{eq}}{\tau^0_{cr}}\right) + 1.942\left(\frac{w_{0p}}{t}\right)\left(\frac{\tau_{eq}}{\tau^0_{cr}}\right)^2 \qquad \text{for d/a}\geq 3$$
$$-16.96\left(\frac{\tau_{eq}}{\tau^0_{cr}}\right) + 80.11\left(\frac{\tau_{eq}}{\tau^0_{cr}}\right)^2 - 7.281\left(\frac{\tau_{eq}}{\tau^0_{cr}}\right)^3 - 0.264\left(\frac{\tau_{eq}}{\tau^0_{cr}}\right)^4$$

(5.22c)

where τ^0_{cr} is the critical shear stress for the simply supported panel, subjected to pure shear alone, and can be determined using Eqn. 5.2. The equivalent shear stress τ_{eq} is given by:

$$\frac{\tau_{eq}}{\tau^0_{cr}} = \frac{1}{2}\left(\beta_c \frac{\sigma_c}{\sigma^0_{c,cr}}\right) + \sqrt{\left(\frac{\tau}{\tau^0_{cr}}\right)^2 + \frac{1}{4}\left(\beta_c \frac{\sigma_c}{\sigma^0_{c,cr}}\right)^2 + \left(\beta_b \frac{\sigma_b}{\sigma^0_{b,cr}}\right)^2} \qquad (5.23)$$

Eqn. 5.23 is a generalized form of Eqns. 5.10 and 5.20. The critical buckling stresses $\sigma^0_{c,cr}$ and $\sigma^0_{b,cr}$ can be calculated using Eqns. 5.5 and 5.15, respectively. The reduction factors β_c and β_b in Eqn. 5.23 are given in Eqns. 5.12, 5.13 and 5.21.

It can be seen that when the applied compressive and bending stresses, σ_c and σ_b, are zero, the above equations reduce to the design formulae for predicting M_{pk}, proposed for pure shear, namely, Eqn. 5.3.

As for the method proposed for pure shear, the values of M_{pk} for $1<d/a<2$ and $2<d/a<3$ can be obtained by linear interpolation, as illustrated in Fig.5.19.

5.5 CONCLUSIONS

In this chapter, the bending moments in the knife edge, due to the lateral forces exerted on the knife edge by the buckled panels, have been investigated. It has been found that the knife edge moment can represent the stiffener moment due to the local panel bending effect. A simple approach for predicting the knife edge moment has been developed, which incorporates the finite element results of non-linear elastic buckling analyses of plates with a straight knife edge, subjected to combined shear, compression and bending. As a result of this study, the following conclusions can be made:

- ***Pure Shear***

(1) The critical buckling shear stress for plates with a knife edge can be approximately taken as the simply supported panel buckling stress, which can be calculated using Eqn. 5.2.

(2) In the non-linear elastic analyses, it is found that as the applied shear stresses are increased, the deflection modes change from the initial imperfection mode to the preferred well-developed sharper mode. For very tall panels, it is also observed that the deflection mode is sensitive to the initial imperfection. For d/a=7 and 10, the deflection modes for different imperfection magnitudes or mode patterns differ

significantly from each other, depending on whether the mode is free to change from the initial mode.

(3) The maximum amplitudes of the lateral force per unit length acting on the knife edge, q_{pk}, do not vary significantly with the panel aspect ratio d/a, but depend mainly on the applied shear stress.

(4) The distributions of the lateral forces along the knife edge vary with the panel aspect ratio d/a. Consequently, both the distribution and amplitude of the resulting knife edge moment vary significantly with d/a. The variations in the distributions of q_{pk} and M_{pk} are due to the differences in the deflection modes.

(5) On the basis of the finite element solutions, a simple formula, given in Eqn. 5.1, is found to be adequate for representing the magnitudes of the knife edge moment M_{pk}.

(6) The finite element results demonstrate that both the distributions and the magnitudes of the bending moments in the straight knife edge and the straight stiff stiffener respectively are quite close to each other. It is therefore considered that the knife edge moment can be taken as an estimate of the stiffener moment due to the panel bending effect.

(7) The axial rigidity of the stiffener, Ω, has a negligible effect on the knife edge moment M_{pk}.

(8) By comparison of the bending moments for a straight knife edge and an imperfect stiff stiffener, it is found that for plates of d/a=1 and 2, the knife edge moment M_{pk} accounts for nearly 92% of the total stiffener moment; and for d/a=5, M_{pk} is equal to about 42% of the total stiffener moment.

(9) For very tall plates, namely, d/a≥7, the knife edge moment may correspond either to the stiffener moment due to the local panel bending effect, or the total stiffener moments, depending on the mode profile and the magnitude of the initial panel

imperfection. Further, it is found that the knife edge moments which agree with the panel bending effect, are close to the values of M_{pk} for d/a=6.

(10) For the design of transverse stiffeners on plates subjected to pure shear, it is proposed that the knife edge moment M_{pk} can be estimated in terms of three equations, presented in Eqn. 5.3.

- ***Shear and Compression***

(11) The interaction curve of the critical buckling compressive and shear stresses for plates with a knife edge, subjected to coexistent shear and compression, can be approximately represented by Eqn. 5.4, which is the same equation as that for the simply supported panel.

(12) The variation in the critical buckling modes with the applied stress ratio σ_c/τ is quite regular, which includes the progressive change in the inclination of the panel buckles, and for tall plates, the change in the number of buckles along the depth of the plate.

(13) The variations in the non-linear elastic deflection modes with the applied stress ratio σ_c/τ and the panel aspect ratio are similar to those observed for the critical buckling modes. In addition, it is found that the deflection modes also vary with the magnitudes of applied loads.

(14) The distribution of the knife edge moment depends on the deflection modes of the panels. It is observed that for combined shear and compression, the knife edge moment distribution generally has a half-wave form, with the maximum amplitude at the mid-length of the knife edge.

(15) The variations in the knife edge moment with the stress ratio σ_c/τ and the panel aspect ratio d/a are quite complicated, especially for tall plates. Therefore, it is considered that an approximation approach for predicting M_{pk} should be developed.

(16) According to the criterion of equal knife edge moments, an equivalent shear stress τ_{eq} is introduced. Based on the interactive equation of the buckling stresses and the non-linear elastic FE solutions, it is proposed that the equivalent shear stress τ_{eq} can be approximately determined in accordance with Eqns. 5.10 and 5.12.

(17) For the design of transverse stiffeners on plates subjected to combined shear and compression, it is proposed that the knife edge moment M_{pk} can be estimated using Eqn. 5.3, by assuming that a pure shear stress of τ_{eq} is applied.

- ***Shear and Bending***

(18) The interaction curve of the critical buckling bending and shear stresses for plates with a knife edge, subjected to coexistent shear and bending, can be approximately represented by Eqn. 5.14, which is the same equation used for the simply supported panel.

(19) The critical buckling modes vary with the applied stress ratio σ_b/τ and the panel aspect ratio d/a, which includes the progressive change in the inclination of the panel buckles, and for tall plates, the changes in both the number and the position of buckles along the depth of the plate.

(20) The variations in the non-linear elastic deflection modes with the applied stress ratio σ_b/τ and the panel aspect ratio are similar to those observed for the critical buckling modes. In addition, it is found that the deflection modes also vary with the magnitudes of applied loads.

(21) For plates subjected to coexistent shear and bending, it is found that the lateral forces on the knife edge, due to the effects of applied shear stress and bending stress respectively, may act in either the same or opposite direction, depending on the panel aspect ratio. As a result, the distribution of the knife edge moment becomes

much more complicated, in comparison with that for combined shear and compression.

(22) The variations in the knife edge moment with the stress ratio σ_b/τ and the panel aspect ratio d/a are irregular, especially for tall plates. Therefore, it is considered that an approximation approach for predicting M_{pk} is necessary.

(23) According to the criterion of equal knife edge moments, an equivalent shear stress τ_{eq} is introduced. Based on the interactive equation of the buckling stresses and the non-linear elastic FE solutions, it is proposed that the equivalent shear stress τ_{eq} can be approximately determined in accordance with Eqns. 5.20 and 5.21.

(24) For the design of transverse stiffeners on plates subjected to combined shear and bending, it is proposed that the knife edge moment M_{pk} can be estimated using Eqn. 5.3, by assuming that a pure shear stress of τ_{eq} is applied.

- ***Combined Shear, Compression and Bending***

(25) For plates subjected to general combined shear, compression and bending, it is proposed that the knife edge moment M_{pk} can be estimated in accordance with Eqns. 5.22a, 5,22b and 5.22c. The equivalent shear stress τ_{eq} can be calculated using Eqns. 5.23, with the factors β_c and β_b given in Eqns. 5.12, 5.13 and 5.21.

CHAPTER 6

AXIAL FORCES IN STIFFENERS

6.1 INTRODUCTION

In the stiffener design model presented in Chapter 9, the axial force resulting from the tension field action is taken into account. The stiffener is designed to withstand the coexistent bending moment and axial force. The purpose of this chapter is to establish the design formulae for predicting the axial forces in the stiffeners.

Different assumptions in respect of the axial forces carried by the stiffeners are made in existing design methods. According to the British Standard BS5400 [3], the stiffeners are designed to resist axial forces, consisting of an in-plane force arising from the tension field action and a hypothetical axial force accounting for the lateral destabilising effects of panel buckling. On the other hand, in the design method proposed by Rahal and Harding [7], the stiffeners were modelled as a simply supported beam subjected to a distributed lateral load, and the action of stiffener axial forces was not taken into account. Based on the numerical parametric results for flat bar stiffeners with a ratio of h_s/t_s=10, Stanway [1] found that the axial forces in the stiffeners are of secondary importance, and were not considered in the design model.

In Chapter 2, the experimental results and FE solutions for the test girders demonstrated that the stiffeners were subjected to both axial forces and bending moments. Therefore, it is considered in this investigation that it is more logical to include the stiffener axial force in the proposed model for designing transverse stiffeners.

It is noted that both in BS5400 and the design method by Rahal and Harding [7], an effective width of web plate is included in the design stiffener section. As indicated in Section 3.3, only the actual stiffener sections are considered in the design model

proposed in this thesis, that is, no effective width of the plate is included. Consequently, the definition of the effective width of the plate, and the resulting wide variation in the position of the neutral axis of the effective stiffener section for various panel slenderness ratios, are avoided. It is recognised that the total vertical force due to the tension field action is resisted together by the actual stiffener and a part of the plate. However, only the axial force carried by the actual stiffener is investigated in this Chapter. It is noted that the axial force acting in the actual stiffener can be more easily obtained from finite element analyses by using truss elements attached to the plate.

In this chapter, the stiffener axial forces obtained from the tension field theory are examined, in comparison with the FE solutions of stiffened plates. The equation derived from the tension field theory is used as a basis to develop a simple formula for the estimation of the axial forces in stiffeners. An extensive parametric study is carried out to examine the non-linear elastic buckling behaviour of plates with a straight non-deflecting stiffener having variable axial stiffness, with particular attention to the in-plane axial forces exerted on the stiffeners. By reference to the finite element results, the coefficients for the proposed design formulae will be established. The effect of the panel plasticity on the stiffener axial force will be examined in Chapter 9.

6.2 STRUCTURAL MODELLING

The two-panel plates under pure shear and combined shear, compression and bending, as shown in Fig. 6.1, are considered in this chapter. The plate is equally divided by a straight non-deflecting stiffener. A finite axial stiffness is assigned to the non-deflecting stiffener, and the stiffener is modelled using truss elements attached to the plate, together with the constraint condition defined by:

$$w\big|_{x=a} = 0 \tag{6.1}$$

Implied in Eqn. 6.1 is the constraint:

$$\theta_x\big|_{x=a} = 0 \tag{6.2}$$

The remaining panel degrees of freedom, u, v, θ_y and θ_z, along the stiffener (x=a), are not specified.

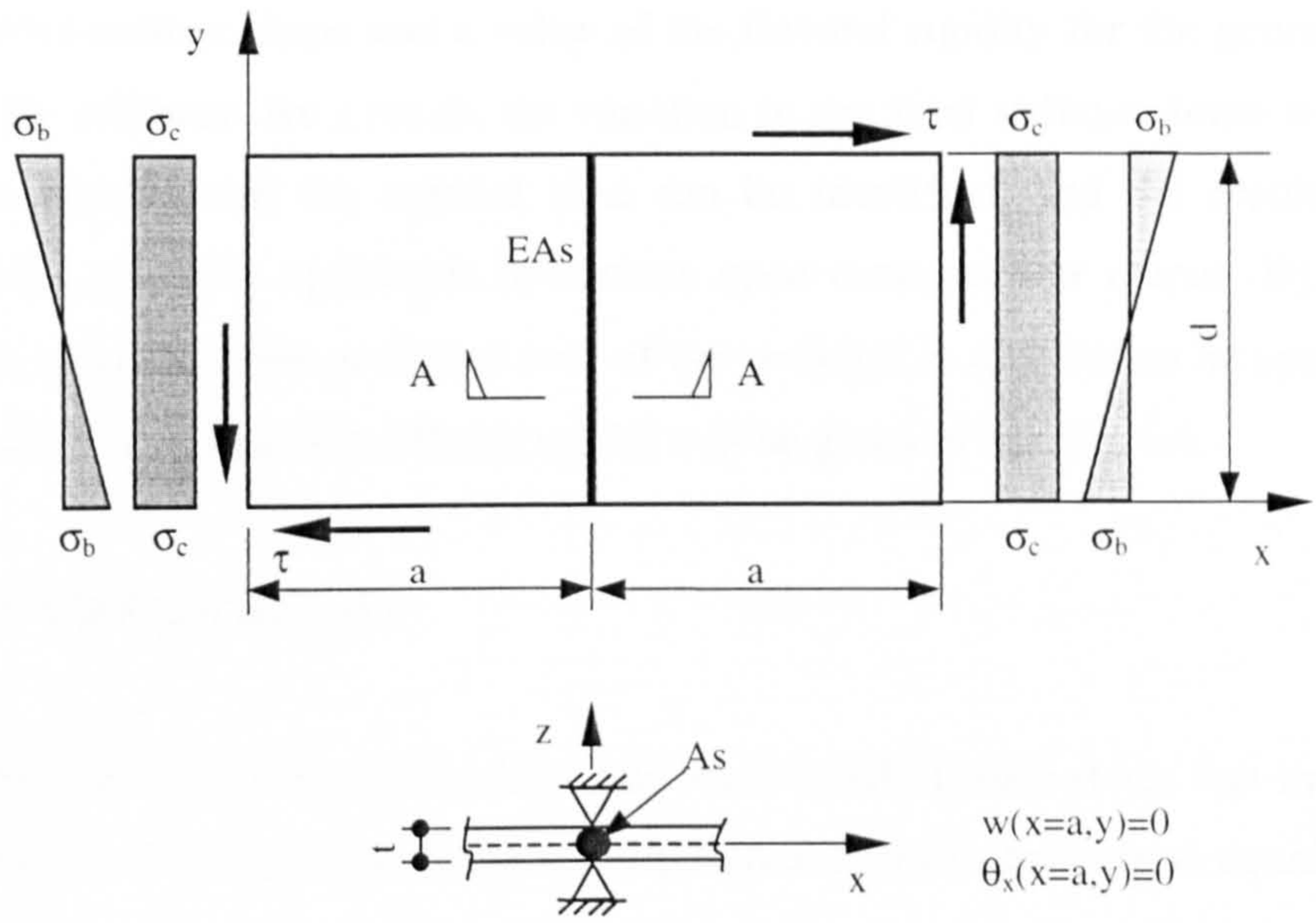


Figure 6.1 Two-panel plate with a straight non-deflecting stiffener, subjected to combined shear, compression and bending

All the boundaries of the plate are simply supported. The in-plane boundary conditions are assumed to be CUCU, as defined in Chapter 2, and the tangential in-plane boundary conditions are taken as being unrestrained.

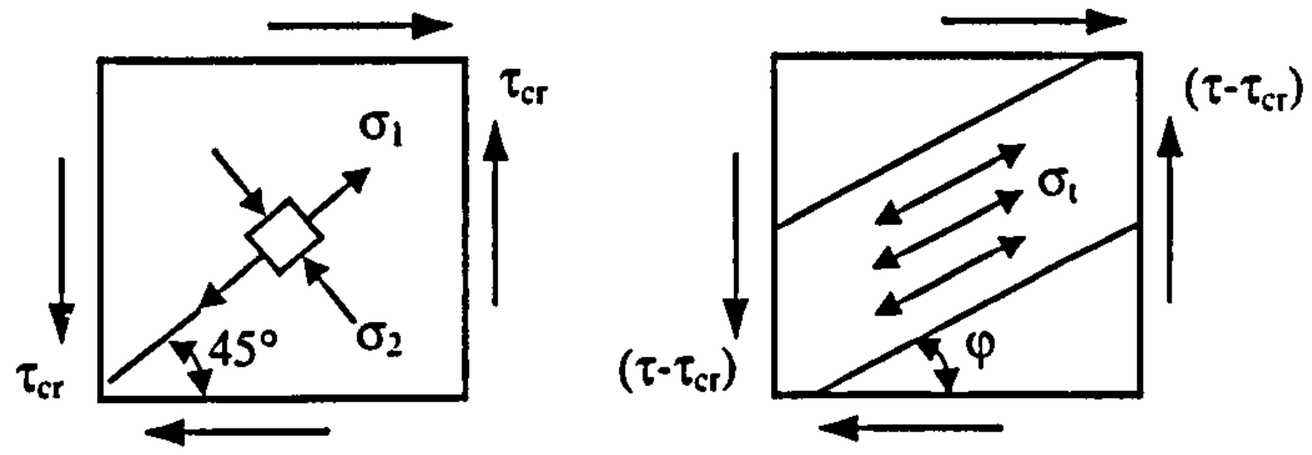
The panel imperfections are fully affine to the first point-symmetric critical buckling modes of the plate, which are presented in Fig. 5.2 for the pure shear condition.

It is noted that when the cross-sectional area of the stiffener is zero, the non-deflecting stiffener model described above will reduce to the finite element model for the knife edge, as presented in Section 4.2. It is recalled that, as illustrated in Fig. 5.16, the knife edge bending moment varies very little with the axial rigidity of the stiffener. Therefore, the models used to evaluate the bending moments and axial forces in the stiffeners are consistent with each other, and this provides a common basis for the proposed design model.

The main reason for adopting a non-deflecting stiffener model in this chapter is to avoid assigning a cross-section shape and a value of the flexural rigidity for the geometrical properties of the stiffener. As a result, the variation in the axial stiffener force with the stiffener axial rigidity and the applied load can be identified, and the results thus obtained will be generally applicable to various open cross-section shapes. By using truss elements, only the cross-sectional area of the stiffener is required to be specified. The basis for the non-deflecting stiffener model will be given in Section 6.4.

6.3 TENSION FIELD THEORY

For a web plate which is subjected to shear, the tension field theory states that the plate panel loaded beyond its critical buckling stress τ_{cr} has a uniform shear stress equal to the critical stress, with a superimposed inclined band of tension such that the equivalent stress within the band is equal to the yield stress (see Fig. 6.2).



(a) Pure shear (b) Tension band

Figure 6.2 Stress distribution in web plate

The alternative tension field models that have been proposed differ in respect of the width, inclination and position of the tension band and in respect of the modified values of τ_{cr}, depending on assumed edge conditions. Among them, the Basler model [32] and the Cardiff model [33] are adopted by the AASHTO specifications and British Standard BS5400, respectively. For a stiffened plate, which can be considered as a girder with flanges of zero stiffness, the Cardiff model produces the same solutions as the true Basler model, namely, the corrected Basler model.

6.3.1 Basler's Model

Basler assumed that the flanges do not possess sufficient flexural rigidity to withstand the lateral loading imposed by the inclined tension field, and therefore the web collapses after development of an off-diagonal yield band (see Fig. 6.3).

By maximizing the vertical component of the inclined force, the angle of inclination, φ, is found to be equal to half the angle of the diagonal, θ. The original formula of the ultimate shear load given by Basler is:

$$V_u = \tau_{cr} dt + \frac{\alpha}{2\sqrt{1+\alpha^2}} \sigma_{0p} dt \left(1 - \frac{\tau_{cr}}{\tau_{0p}}\right) \tag{6.3}$$

where α=d/a, σ_{op} is the yield stress of web plate, and $\tau_{0p} = \sigma_{0p}/\sqrt{3}$.

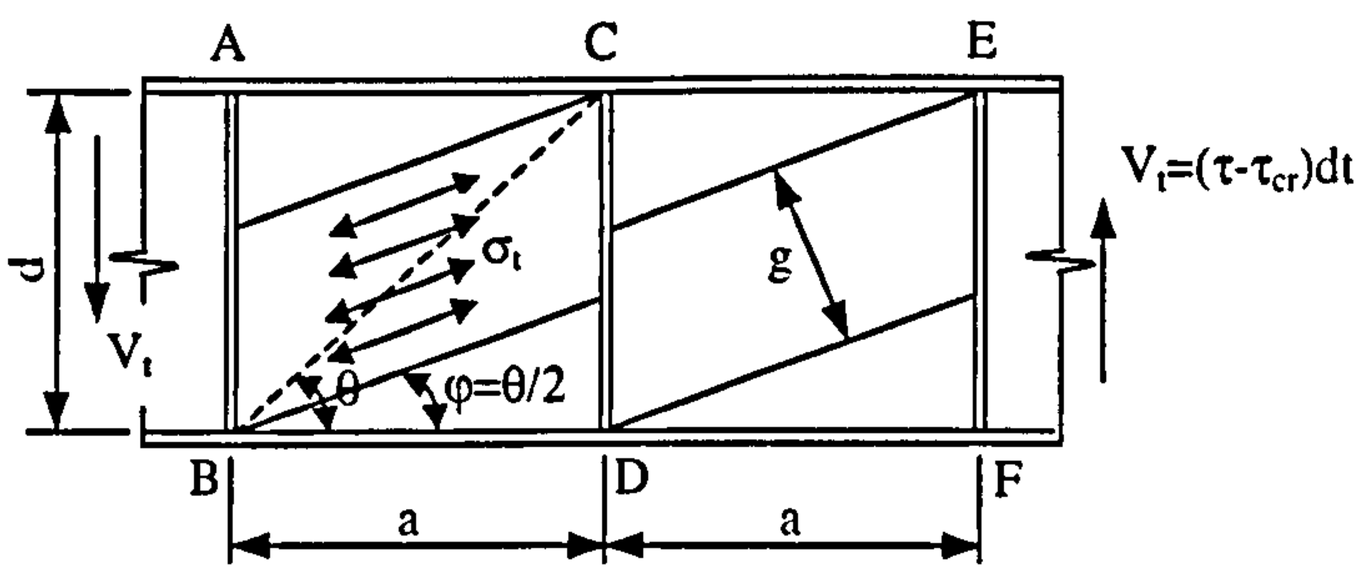


Figure 6.3 Basler's tension field model

It was pointed by Fujii [57] that Eqn. 6.3 does not actually represent the true resistance of the Basler model, which is correctly given by Eqn. 6.4:

$$V_u = \tau_{cr} dt + \frac{\alpha}{2(1+\sqrt{1+\alpha^2})} \sigma_{0p} dt \left(1 - \frac{\tau_{cr}}{\tau_{0p}}\right) \tag{6.4}$$

According to the Basler model, there is no vertical stress at the horizontal boundaries, the horizontal component of the inclined force is reacted by the adjacent panels, while the vertical component is reacted by the stiffeners. The formula for stiffener axial force given by Basler is correct, and can be expressed as:

$$P_s = \frac{1}{2}\sigma_{0p} at \left(1 - \frac{1}{\sqrt{1+\alpha^2}}\right)\left(1 - \frac{\tau_{cr}}{\tau_{0p}}\right) \tag{6.5}$$

6.3.2 Comparison with FE solutions

In order to find out how accurately the tension field theory predicts the stiffener axial force, non-linear elastic finite element analyses were carried out for CUCU stiffened plates of d/a=1 and 2, subjected to pure shear. The stiffener sizes used were great enough to divide the panels. An initial panel imperfection in the form of the first point-symmetric buckling mode was adopted.

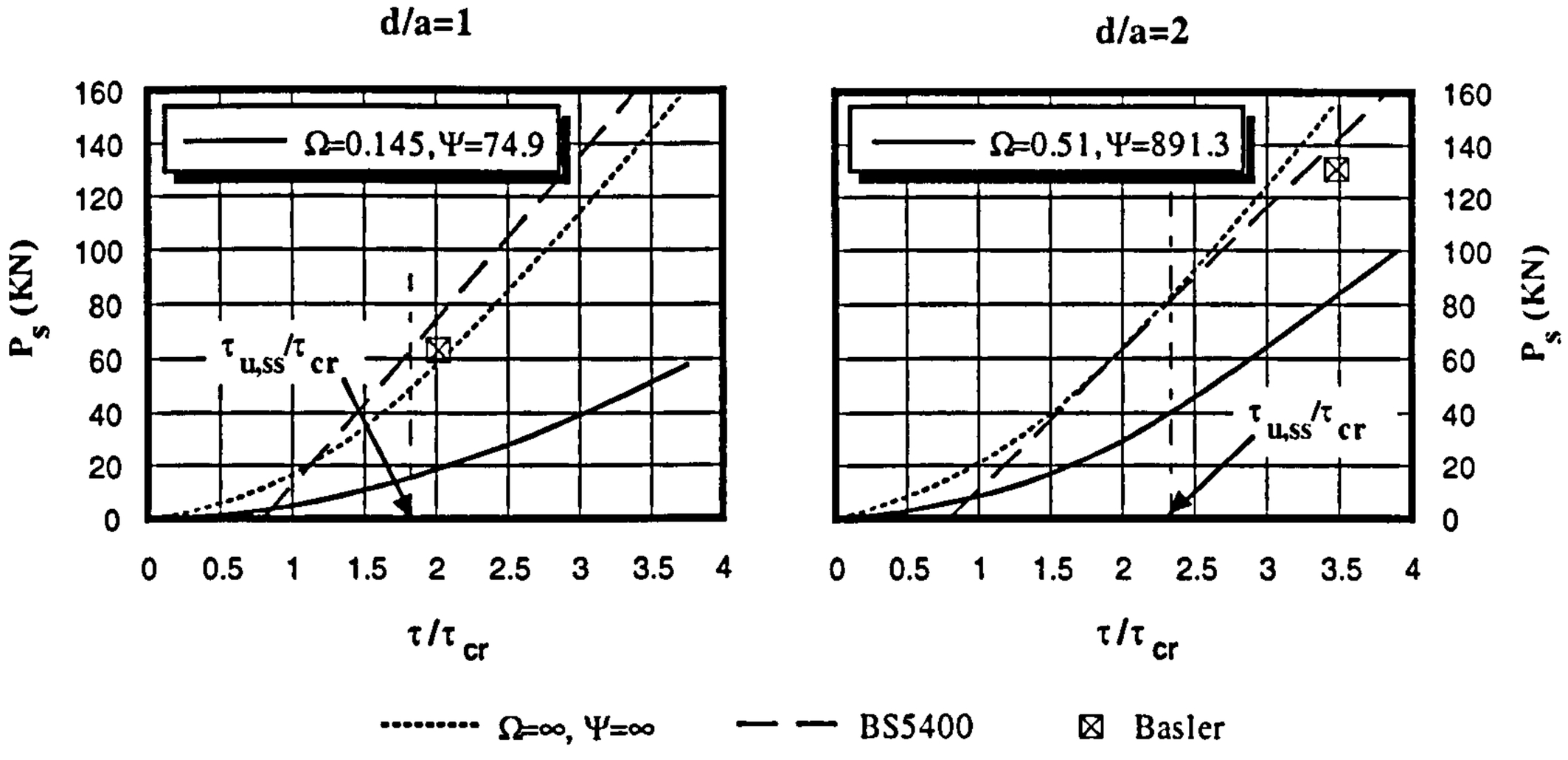


Figure 6.4 Comparison of the stiffener axial force given by tension field theory and by FE solutions. CUCU plates with an initially straight stiffener, a=540mm, t=3mm, σ_0=355Mpa. Pure shear. Initial panel imperfection affine to the 1st PS buckling mode. w_{0p}/t=1.091. $\Psi=EI_s/Db$, $\Omega=A_s/at$

In Fig. 6.4, the axial forces in the stiffeners calculated from Eqn. 6.5 are compared with the finite element solutions. The axial forces due to the tension field action in accordance with BS5400 are also shown in Fig. 6.4. It is noted that in BS5400, an effective width of web plate, *16t* on each side of the stiffener, is assumed to act together with the stiffener. For purposes of comparison, the compressive forces on the segments

of web plate are not included and only the forces carried by the actual stiffener are shown in Fig. 6.4. It was indicated by Basler that the stiffener force P_s given by Eqn. 6.5 is assumed to be resisted only by the actual area of the stiffener, since part of the web is already at the stage of yielding when the tension field has formed.

It is observed in Fig. 6.4 that the axial forces obtained from the tension field theory and BS5400 are considerably greater than the actual force in the stiffener as represented by the FE solutions. This may explain why the stiffener required by these approaches tends to be very conservative, although they do not give sufficient rational recognition to the out-of-plane forces exerted on the stiffener by panel bending.

It can also be seen in Fig. 6.4 that the axial force in a stiffener of infinite rigidity is much greater than the force in a stiffener of finite axial rigidity. Therefore, it may not be adequate to model the real stiffener as a strut having an infinite axial rigidity.

On account of the above observations, it is considered that the approach used for representing the knife edge bending moment could be adopted for the prediction of the stiffener axial forces: that is, the simple equation derived from the tension field theory will be used as a basis to develop a design formula for predicting the axial forces in stiffeners, and the coefficients in the design formula will be determined by means of finite element results.

6.4 PROPOSED EQUATION FOR PREDICTING P_S

6.4.1 Proposed Equation for P_s

Eqn. 6.5 gives the axial force applied to the stiffener when the shear load reaches the ultimate load of the plate, V_u. For an applied shear load $V=\tau dt$ ($\tau_{cr}\leq\tau\leq\tau_u$), the part of shear load carried in the tension band can be obtained according to Fig. 6.3:

$$(\tau-\tau_{cr})\,dt=\sigma_t gt\cdot\sin\varphi=\frac{\sigma_t dt}{2}\tan\frac{\theta}{2} \tag{6.6}$$

By rearranging Eqn. 6.6, the tension band stress σ_t is written as:

$$\sigma_t = 2(\tau - \tau_{cr}) / \tan\frac{\theta}{2} \tag{6.7}$$

The compressive force P_s applied to the stiffener is given by:

$$P_s = \sigma_t a t \cdot \sin^2 \varphi \tag{6.8}$$

Substituting Eqn. 6.7 into Eqn. 6.8, the axial force acting on the stiffener can be obtained as:

$$\frac{P_s}{\tau_{cr}\, dt} = \frac{1}{\sqrt{1+\alpha^2}}\left(\frac{\tau}{\tau_{cr}} - 1\right) \tag{6.9}$$

The approximate solution of P_s given in Eqn. 6.9 is derived from the Basler model which assumes that the angle of inclination, φ, is equal to half the angle of the diagonal for any value of the applied shear load $V \geq V_{cr}$. Also, it is assumed that the P_s does not depend on the cross-sectional area of the stiffener. It is known that a real plate does not act in accordance with the tension field model, since the additional deflections and consequential membrane stresses occur from the first application of load due to the initial imperfections. Also the stiffener axial force P_s varies with the axial rigidity of the stiffener. However, the tension field theory does provide a sound physical description of the failure mechanism, and therefore give a rational basis for the calculation of the axial force in the stiffener.

To be used to represent the actual axial forces in stiffeners, Eqn. 6.9 is modified to include the stiffener axial rigidity as a variable, and coefficients to be determined by the curve-fitting of FE solutions are also introduced. In the light of the FE solutions for some trial cases, the equation for the stiffener axial force is proposed as follows:

$$\frac{P_s}{\tau_{cr}\, dt} = \begin{cases} C_1\left(\dfrac{\tau}{\tau_{cr}} - 1\right) \cdot (1 + C_2 \ln \Omega) & for\ \tau > \tau_{cr} \\ 0 & for\ \tau \leq \tau_{cr} \end{cases} \tag{6.10}$$

where Ω is the stiffener extensional rigidity parameter, defined by $\Omega = A_s/at$, and *ln( )* stands for the natural logarithm function. By comparison with Eqn. 6.9, the coefficients C_1 and C_2 are expected to vary with the panel aspect ratio, $\alpha = d/a$, only.

6.4.2 Discussion on the Proposed Equation

According to Eqns. 6.9 and 6.10, it is expected that the relationship between the non-dimensional stiffener force $P_s/\tau_{cr}dt$ and the applied shear stress ratio τ/τ_{cr} does not vary with the plate slenderness ratio b/t . This is confirmed by the finite element results shown in Fig. 6.5, where the solutions for b/t=80, 180 and 300 are located almost on the same curve. On account of this characteristic, the coefficients in Eqn. 6.10 will be determined in Section 6.5 using the finite element solutions for b/t=180 only.

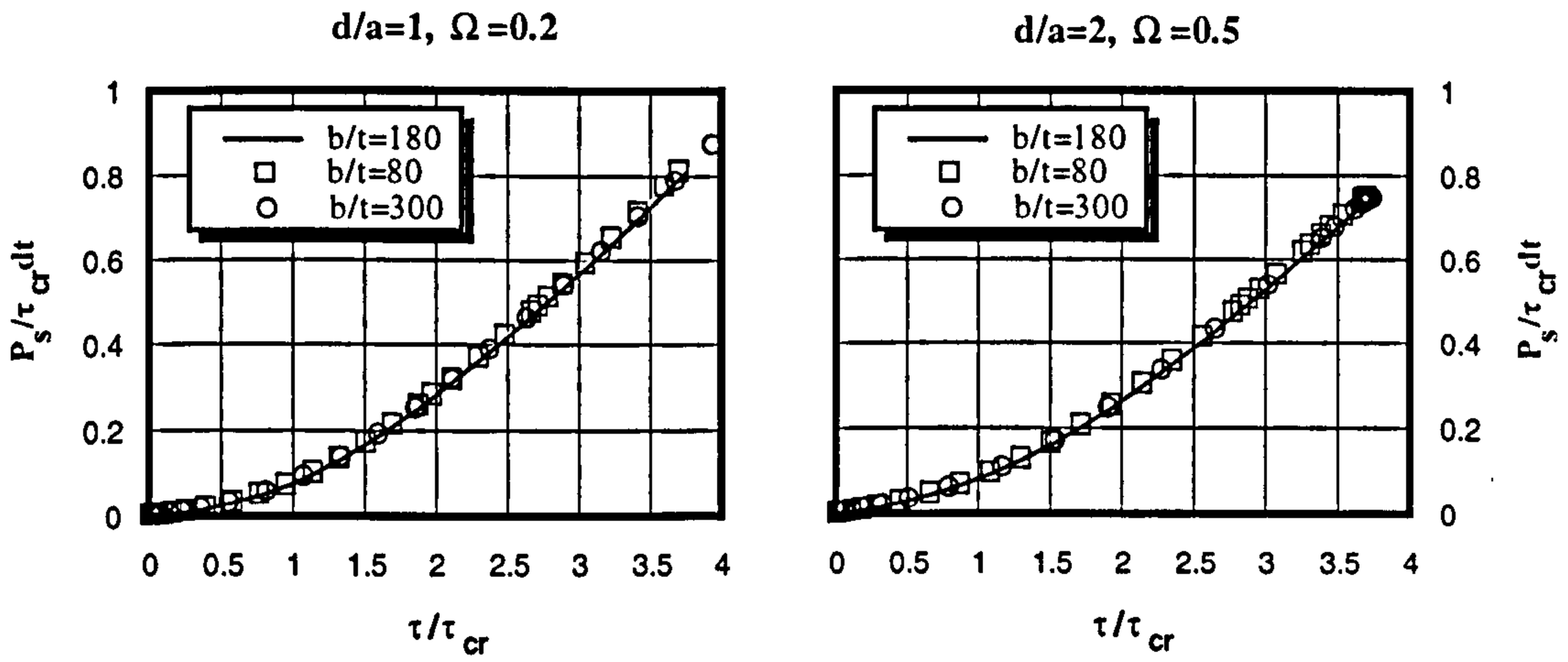


Figure 6.5 Stiffener axial forces for different panel slenderness ratios, b/t. $\Omega=A_s/at$. Non-linear elastic finite element analyses. CUCU Plate with a non-deflecting stiffener. $w_{0p}/t=1.091$. Pure shear

It is also noted that the form of Eqn. 6.10 is developed from the tension field theory, which does not account for the effects of initial imperfections. Owing to the initial deflection, a real plate will develop additional out-of-plane displacement and membrane stresses. To clarify the influences of the initial panel deflection on the stiffener force, a comparative parametric study was carried out on plates with a straight non-deflecting stiffener, subjected to pure shear. The initial imperfection ratio w_{0p}/t varies from 0.485 to 1.818, which correspond to the code tolerance amplitudes for b/t=80~300 for $\sigma_0=355N/mm^2$. Fig. 6.6 shows the finite element results for $P_s/\tau_{cr}dt \sim \tau/\tau_{cr}$ curves. It is

apparent in Fig 6.6 that the magnitude of initial panel imperfection does not affect the stiffener force significantly. Therefore, for the reason of simplicity, the magnitude of initial panel deflection will be taken as $w_{0p}/t=1.091$ in the numerical analyses presented later in this chapter.

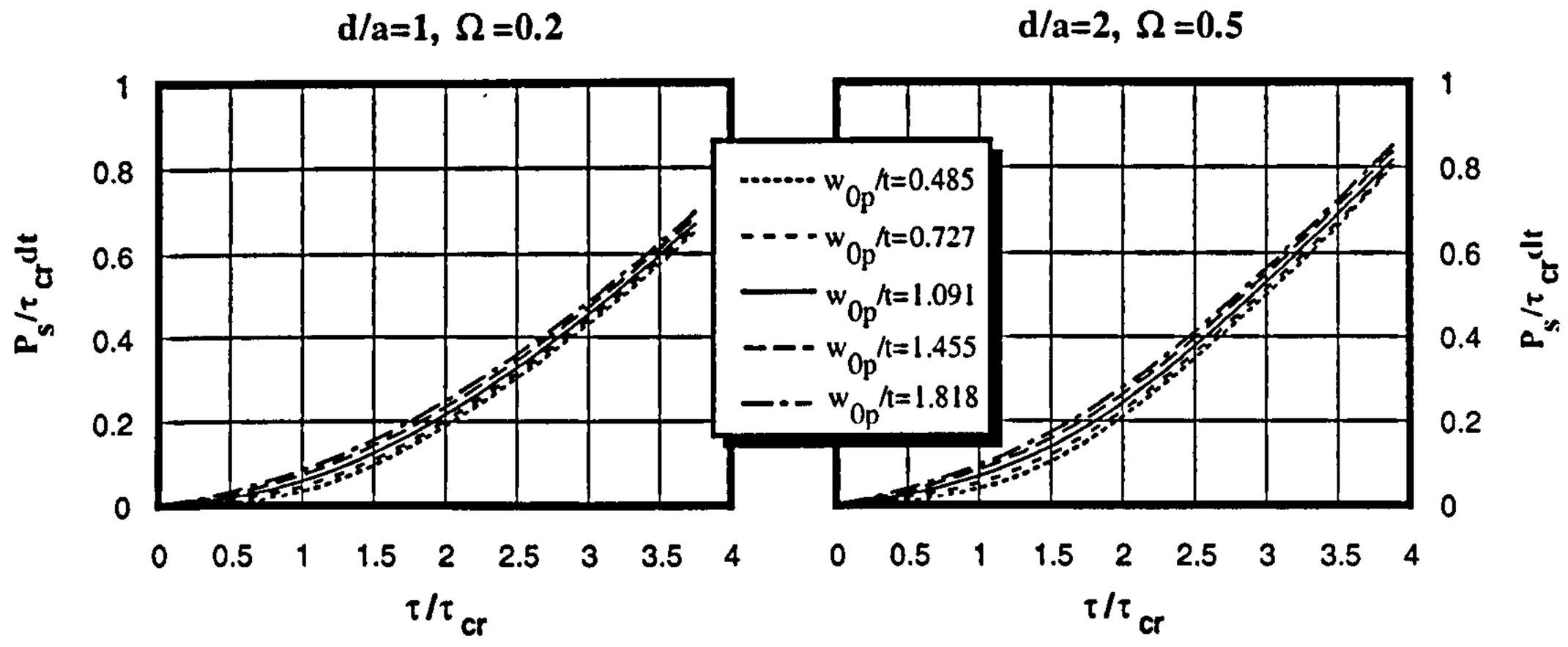


Figure 6.6 Stiffener axial forces for different panel initial imperfections, w_{0p}/t. $\Omega=A_s/at$. Non-linear elastic finite element analyses. CUCU Plate with a non-deflecting stiffener. Pure shear

A further question may arise concerning the modelling of a non-deflecting stiffener in the finite element model. In order to identify any discrepancies in the stiffener axial force between the non-deflecting and real stiffeners, the numerical results for plates with a flat bar stiffener, with or without initial stiffener deflection, are compared with those for plates with a non-deflecting stiffener, as presented in Fig. 6.7. No major differences are found, especially for $d/a\leq 2$. It is also observed in Fig. 6.7 that the axial forces in a straight stiffener are almost identical to the axial forces in an imperfect stiffener. This implies that the stiffener axial force does not vary with the magnitude of the stiffener imperfection w_{0s} for the cases examined.

6.5 PLATES SUBJECTED TO PURE SHEAR

This section presents the numerical results of a non-linear elastic parametric study for plates with a straight non-deflecting stiffener, subjected to pure shear, as shown in Fig. 6.1. Initial imperfection is affine to the first point-symmetric buckling mode, with a

magnitude of $w_{0p}/t=1.091$. On the basis of the finite element solutions, the coefficients in Eqn. 6.10 will be determined.

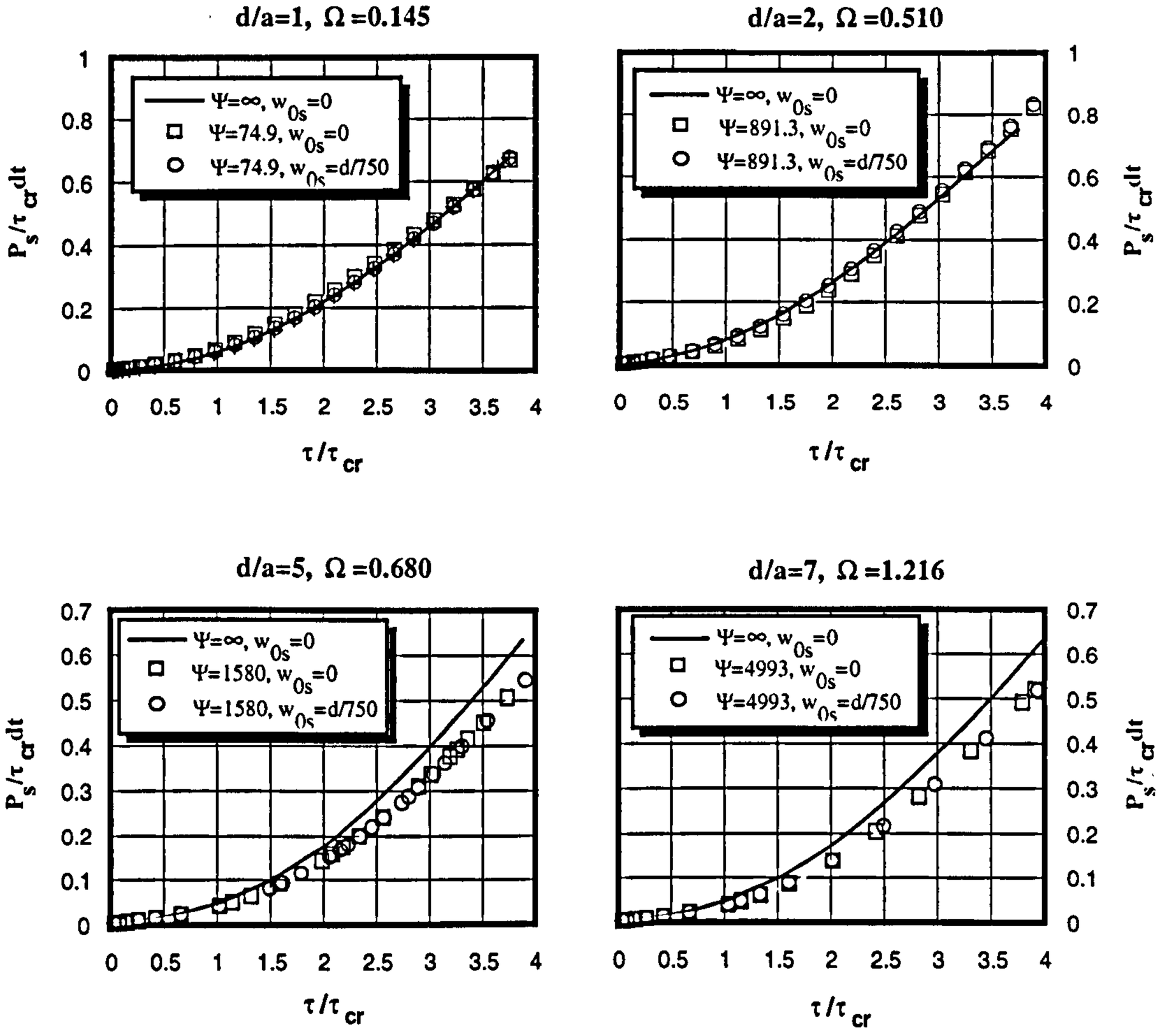


Figure 6.7 Comparison of axial forces in non-deflecting stiffener and real stiffener. Non-linear elastic finite element analyses. $w_{0p}/t=1.091$. $\Omega=A_s/at$. Pure shear

6.5.1 Distribution of the Axial Force in the Stiffener

According to the Basler tension field model shown in Fig. 6.3, it is expected that the compressive stiffener force P_s will reach its maximum value in the centre part of the stiffener, where the tension bands in the adjacent panels overlap each other. The elastic large-deflection finite element analysis results, as presented in Fig. 6.8, confirm that the maximum value of the compressive axial force in a stiffener occurs at the mid-length of

the stiffener, for plates subjected to pure shear. It is noted in Fig. 6.8 that for tall plates, the magnitude of the axial force oscillates in the centre part of the stiffener. This is because the plate panels buckle in several half waves and the tensile principal stress is not constant along the depth of the plate. For purpose of stiffener design, only the maximum value of the stiffener axial force is considered in this thesis.

6.5.2 Magnitude of the Axial Force in the Stiffener

According to the proposed design model for transverse stiffeners, the maximum axial force in the stiffener is required. In this section, the relationship between the magnitudes of normalised stiffener axial force $P_s/\tau_{cr}dt$ and the applied shear stresses are represented in the form of Eqn. 6.10. The coefficients C_1 and C_2 in Eqn. 6.10 are calculated for each aspect ratio considered, by the curve fitting of finite element results using the least squares method. The values of C_1 and C_2 obtained are listed in Table 6.1.

Table 6.1 Coefficients C_1 and C_2 for P_s, Eqn. 6.10

d/a	C_1	C_2
0.333	0.868	0.214
0.5	0.663	0.227
1.0	0.532	0.277
2.0	0.336	0.298
3.0	0.330	0.335
5.0	0.244	0.343
10.0	0.135	0.352

Furthermore, based on the relationship of the coefficients C_1 and C_2 with the panel aspect ratio α=d/a, as defined in Table 6.1, it is found that the two coefficients can be approximately expressed as:

$$C_1 = \frac{1}{2\sqrt{\alpha}} \qquad (6.11)$$
$$C_2 = 0.27 + 0.05 \ln \alpha$$

The variation of C_1 and C_2 with the panel aspect ratio α is shown in Fig. 6.9.

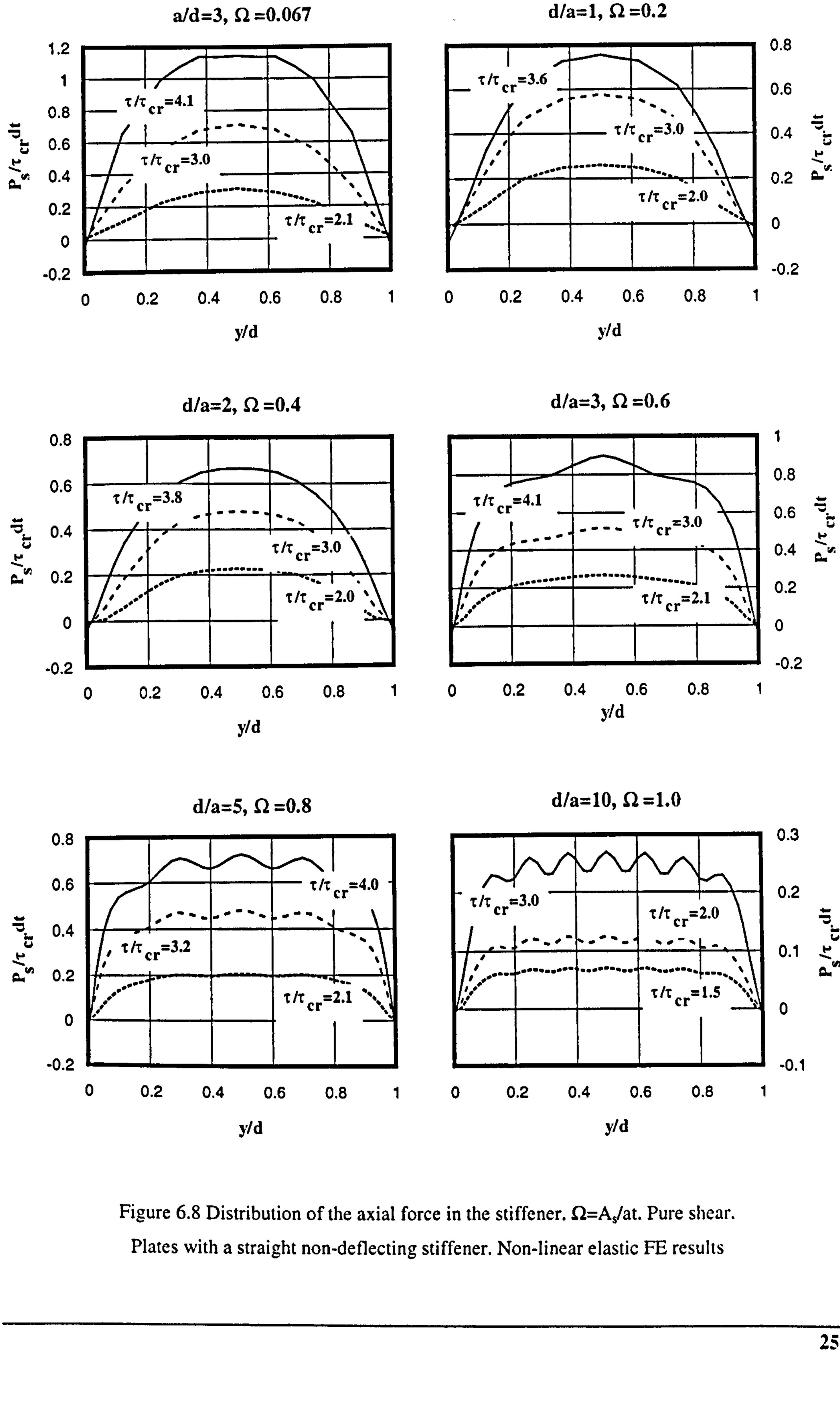


Figure 6.8 Distribution of the axial force in the stiffener. $\Omega=A_s/at$. Pure shear.
Plates with a straight non-deflecting stiffener. Non-linear elastic FE results

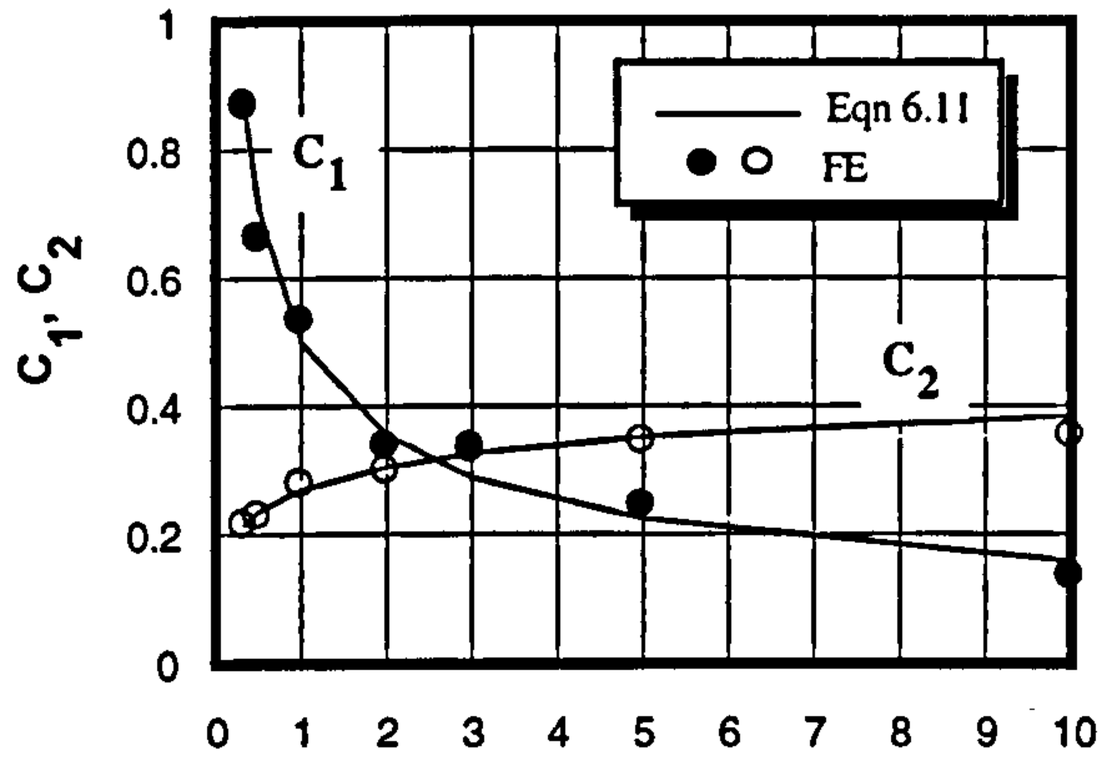


Figure 6.9 Variation of the coefficients C_1 and C_2 in Eqn. 6.10 with the panel aspect ratio d/a. Pure shear

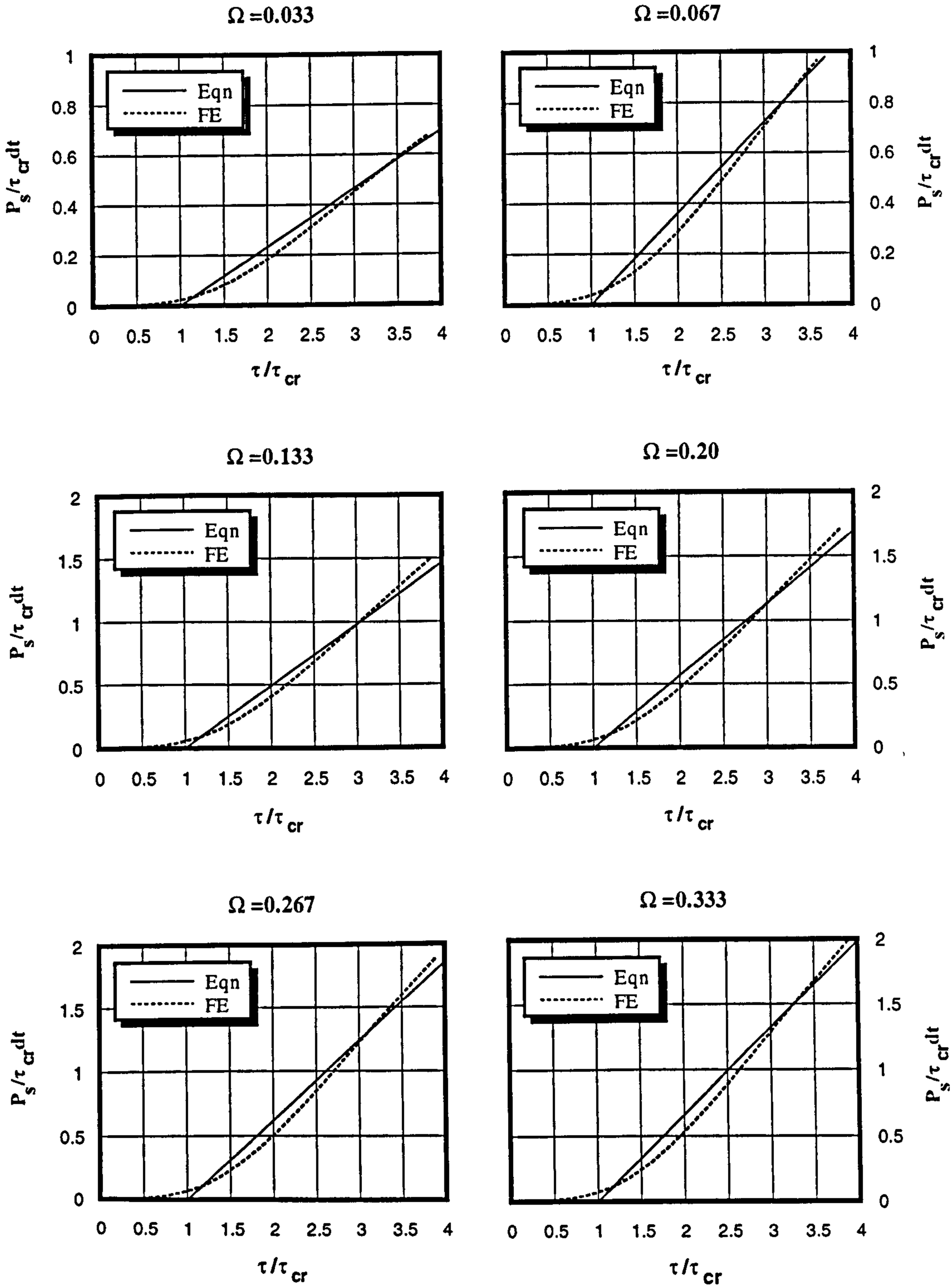
Fig. 6.10 presents a comparison between the numerical results and the values predicted using Eqn. 6.10 with the coefficients given by Eqn. 6.11, and good agreement can be seen. This suggests that for stiffened plates under pure shear, the proposed equation 6.10 with the coefficients defined by Eqn. 6.11 is adequate for presenting the axial force in the stiffener.

6.6 PLATES SUBJECTED TO COMBINED LOADING

6.6.1 General

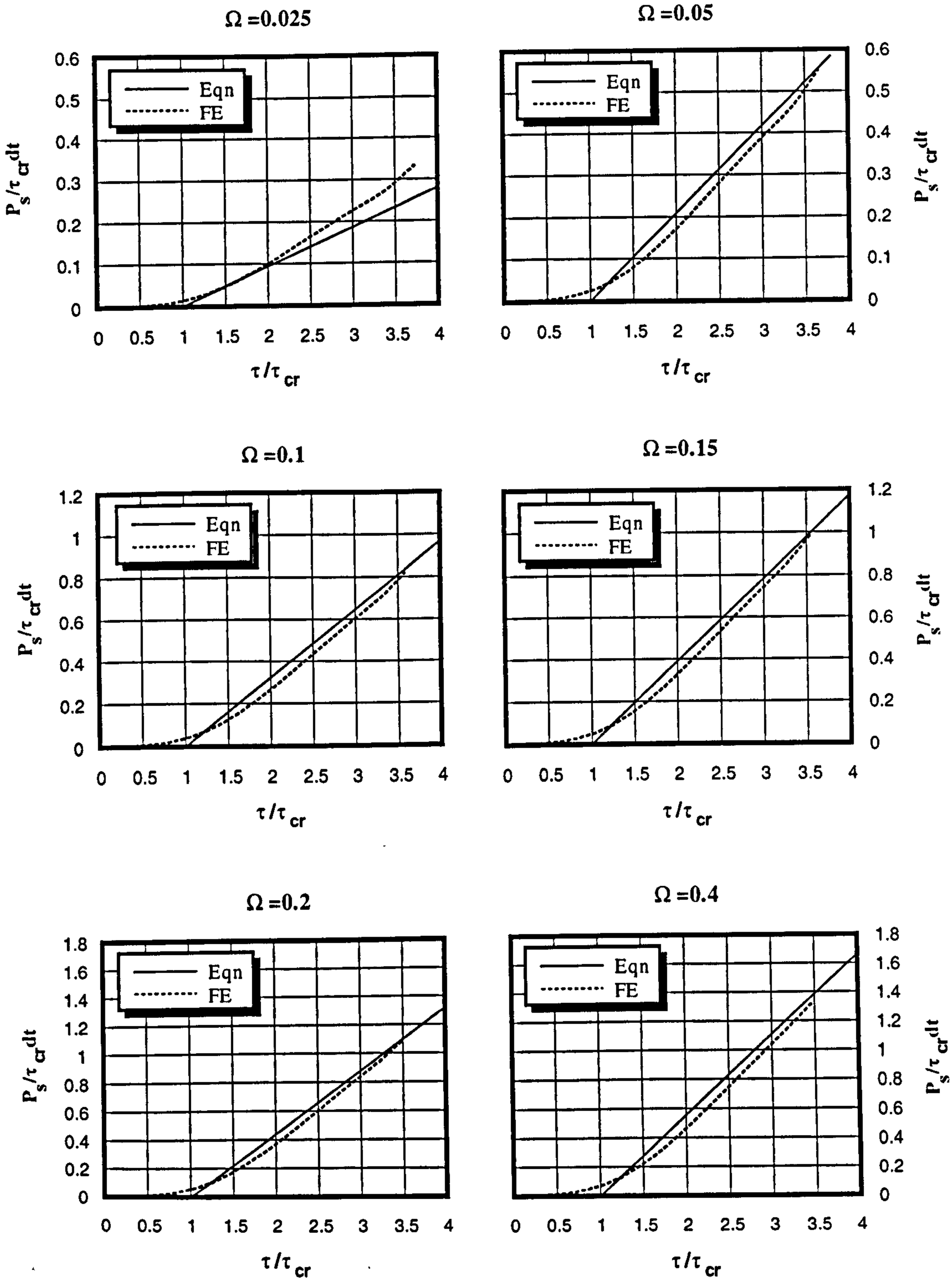
It is known that for plates subjected to combined shear and longitudinal stresses, the plate buckling occurs at a critical shear stress which is less than the critical stress when the shear acts alone. Following the philosophy of the tension field theory, an inclined tension band forms after this reduced critical shear stress.

In Section 6.5, it was found that the stiffener axial force for a plate under pure shear results mainly from the inclined tension field action. This implies that the stiffener force due to the effects of Poisson's ratio and the out-of-plane deflection of panel is relatively



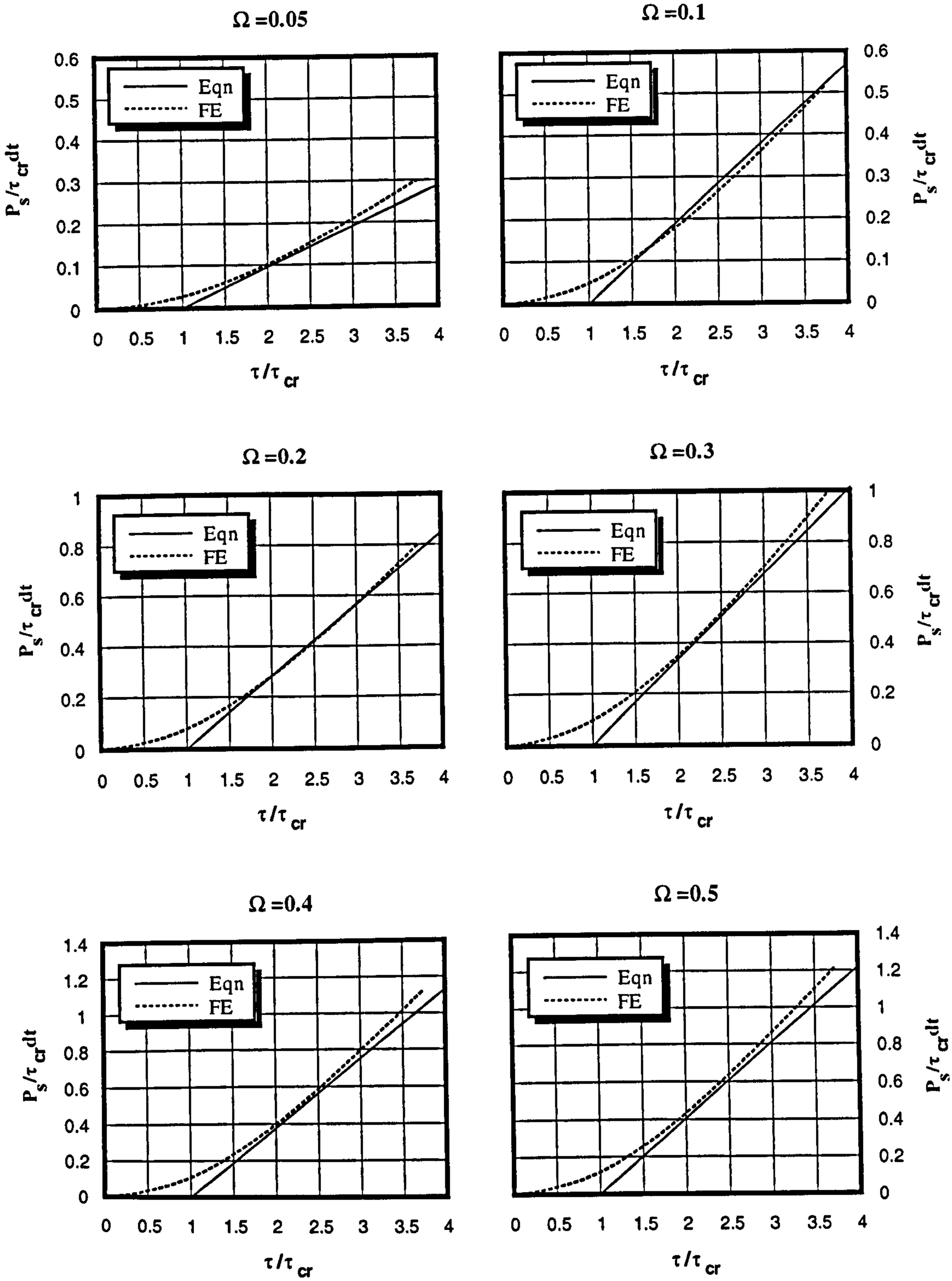
(a) a/d=3

Figure 6.10 The variation in the stiffener axial force with the stiffener area and the applied shear stress. CUCU plates with a straight non-deflecting stiffener. Point-symmetric panel imperfection, $w_{0p}/t=1.091$. $\Omega=A_s/at$. Non-linear elastic FE results. Pure shear



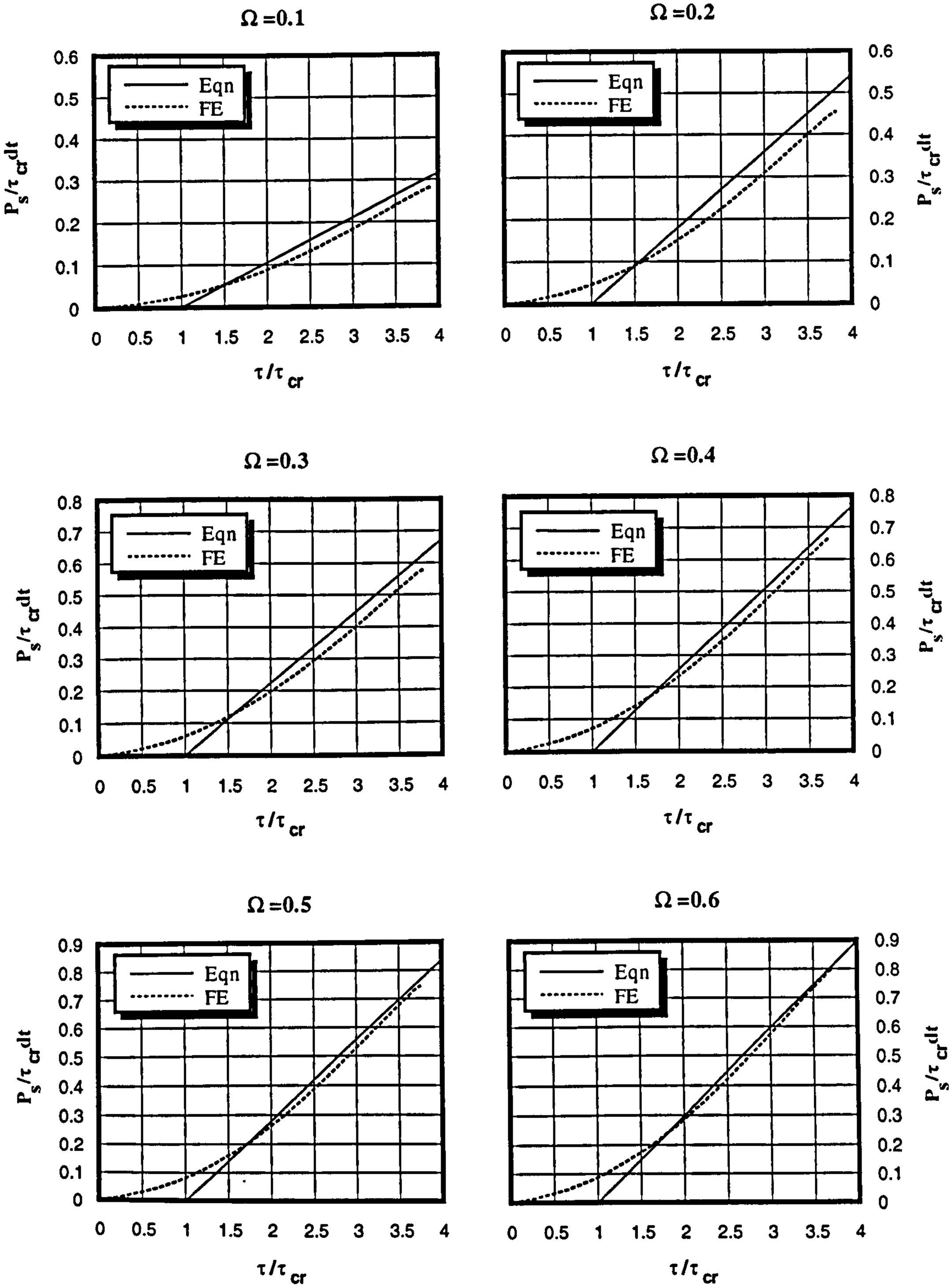
(b) a/d=2

Figure 6.10 (Cont) The variation in the stiffener axial force with the stiffener area and the applied shear stress. CUCU plates with a straight non-deflecting stiffener. Point-symmetric panel imperfection, $w_{0p}/t=1.091$. $\Omega=A_s/at$. Non-linear elastic FE results. Pure shear



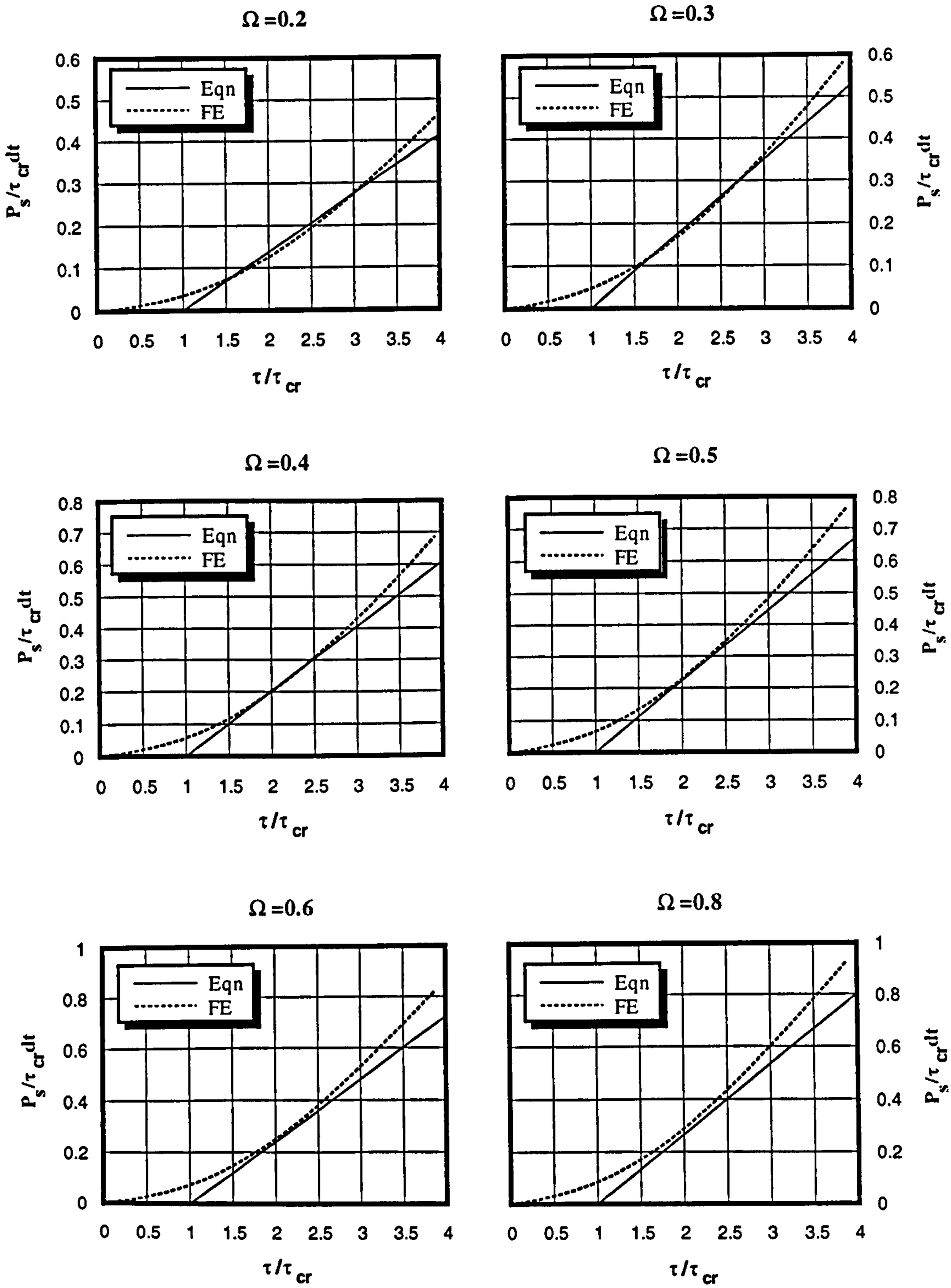
(c) d/a=1

Figure 6.10 (Cont) The variation in the stiffener axial force with the stiffener area and the applied shear stress. CUCU plates with a straight non-deflecting stiffener. Point-symmetric panel imperfection, $w_{0p}/t=1.091$. $\Omega=A_s/at$. Non-linear elastic FE results. Pure shear



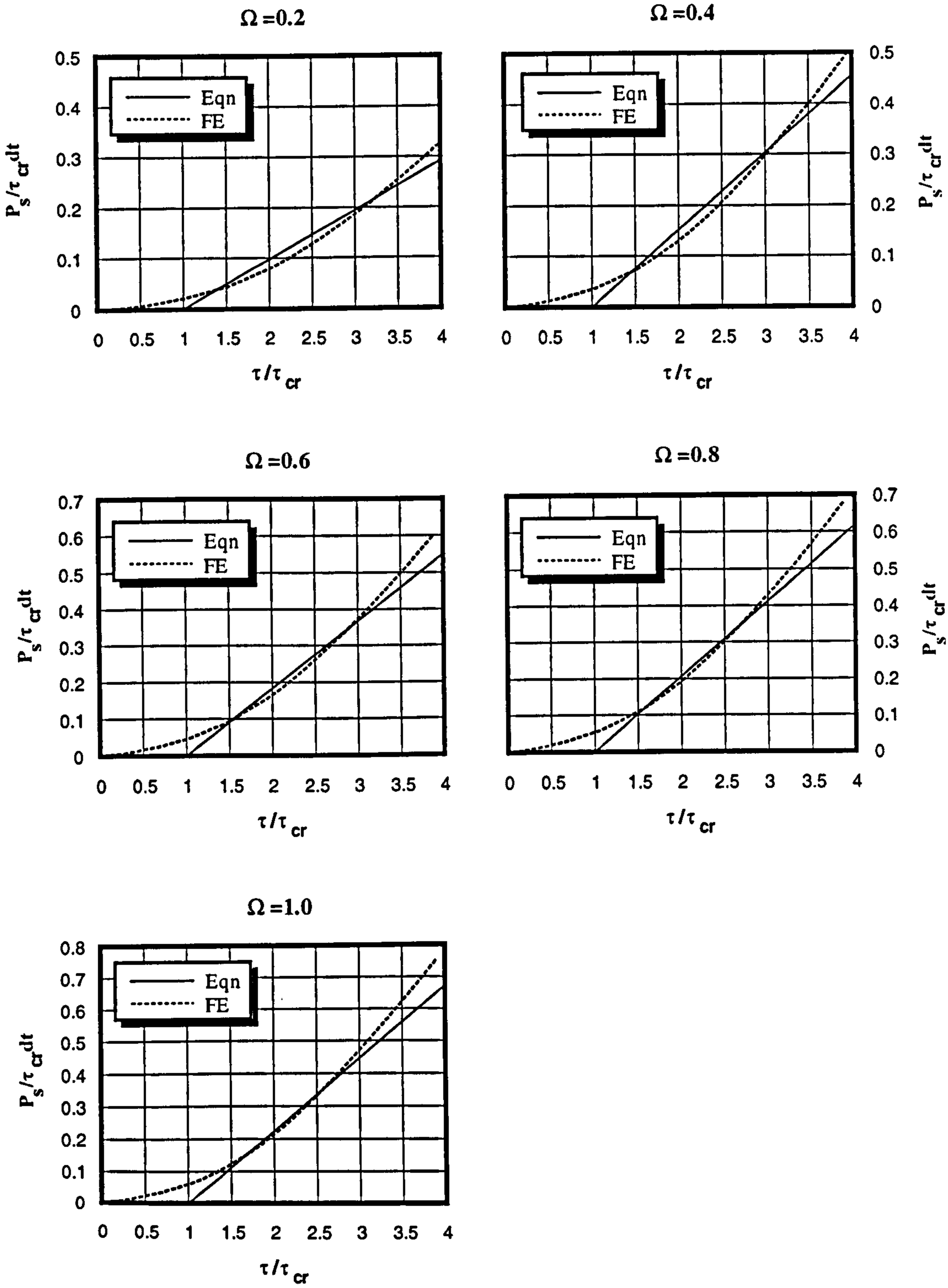
(d) d/a=2

Figure 6.10 (Cont) The variation in the stiffener axial force with the stiffener area and the applied shear stress. CUCU plates with a straight non-deflecting stiffener. Point-symmetric panel imperfection, $w_{0p}/t=1.091$. $\Omega=A_s/at$. Non-linear elastic FE results. Pure shear



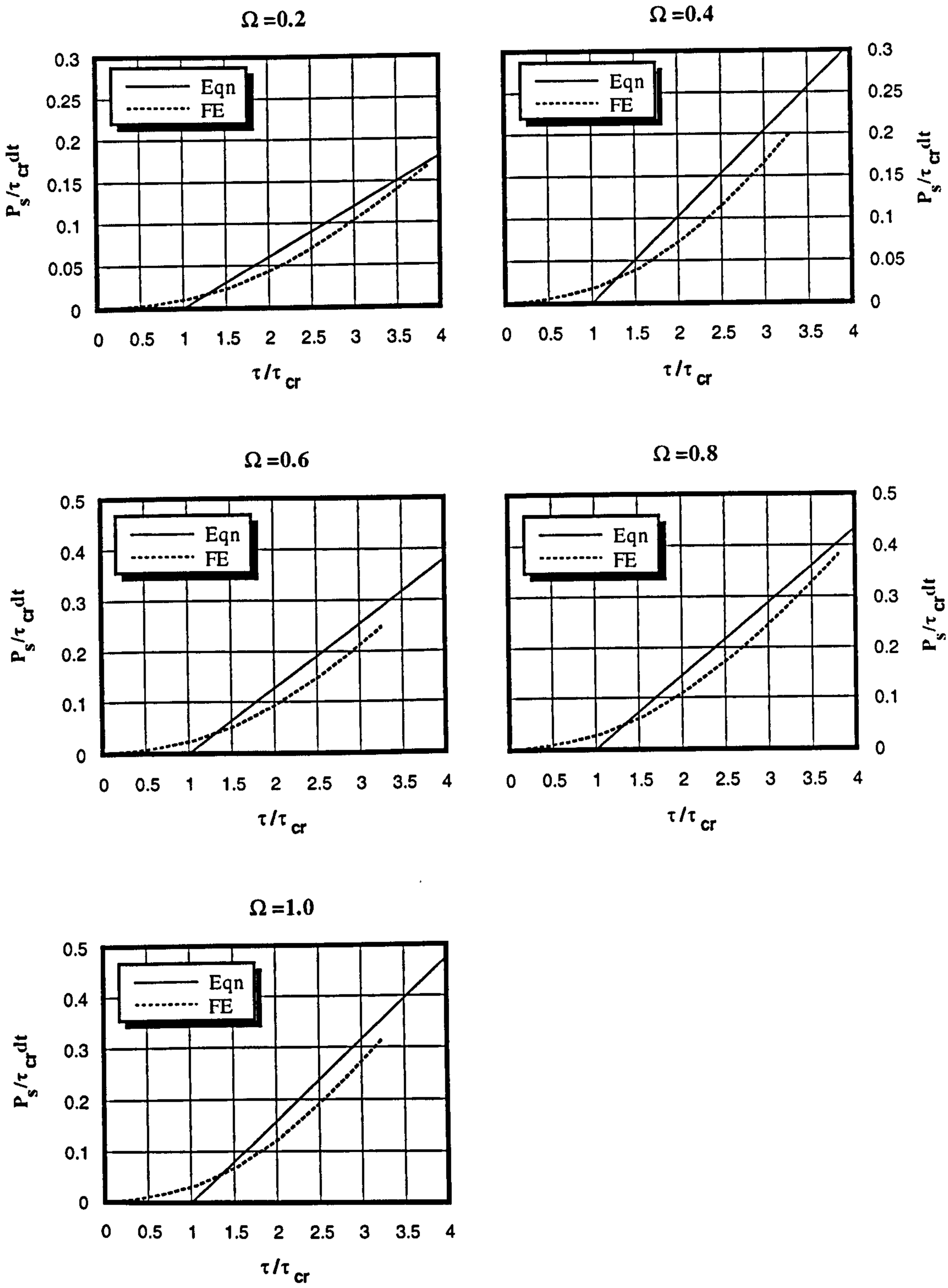
(e) d/a=3

Figure 6.10 (Cont) The variation in the stiffener axial force with the stiffener area and the applied shear stress. CUCU plates with a straight non-deflecting stiffener. Point-symmetric panel imperfection, $w_{0p}/t=1.091$. $\Omega=A_s/at$. Non-linear elastic FE results. Pure shear



(f) d/a=5

Figure 6.10 (Cont) The variation in the stiffener axial force with the stiffener area and the applied shear stress. CUCU plates with a straight non-deflecting stiffener. Point-symmetric panel imperfection, $w_{0p}/t=1.091$. $\Omega=A_s/at$. Non-linear elastic FE results. Pure shear



(g) d/a=10

Figure 6.10 (Cont) The variation in the stiffener axial force with the stiffener area and the applied shear stress. CUCU plates with a straight non-deflecting stiffener. Point-symmetric panel imperfection, $w_{0p}/t=1.091$. $\Omega=A_s/at$. Non-linear elastic FE results. Pure shear

negilible. It is therefore speculated that the stiffener axial force for combined loading conditions would be primarily determined by the shear component, as it is the shear component that produces an inclined tension band. Therefore, the formulae for predicting the stiffener axial force for pure shear, given by Eqns. 6.10 and 6.11, could be extended to the combined loading conditions.

This section considers the cases of a stiffened plate subjected to combined shear, compression and bending. The axial force in the stiffener is investigated by carrying out a non-linear elastic parametric study for plates subjected to different proportions of compression and shear or of bending and shear.

The number of cases corresponding to the different combinations of the factors with which the stiffener force would vary, such as the proportion of individual load components, stiffener area and panel aspect ratio, would be practically inaccessible. However, it is anticipated that the formulae obtained predicting P_s under pure shear could be extended to the combined loading conditions, simply by replacing τ_{cr} in Eqn. 6.10 with the critical shear stress in the presence of compression and bending. To justify the adequacy to use Eqns. 6.10 and 6.11 for predicting the stiffener axial forces for plates subjected to combined shear and longitudinal stresses, the following parameters were considered in the parametric study:

- *d/a=0.5, 1, 2, 5*
- σ_c*:*τ *or* σ_b*:*τ*=1:0, 5:1, 2:1, 1:1, 1:2, 1:5, 0:1*

Only one value of $\Omega=A_s/at$ was considered for each d/a, which was chosen to be around the value of a required stiffener of $h_s/t_s=10$ for the pure shear condition. The initial imperfection is affine to the first point-symmetric buckling mode, with a magnitude of $w_{0p}/t=1.091$. The panel slenderness ratio b/t is taken as 80 for shear and compression, and 180 for shear and bending.

In this section, τ^0_{cr}, $\sigma^0_{c,cr}$ and $\sigma^0_{b,cr}$ stand for the critical stresses of the plate panel, subjected to shear, compression or bending alone, respectively. The stresses which produce buckling when acting simultaneously are denoted as τ_{cr}, $\sigma_{c,cr}$ and $\sigma_{b,cr}$.

6.6.2 Combined Shear and Compression

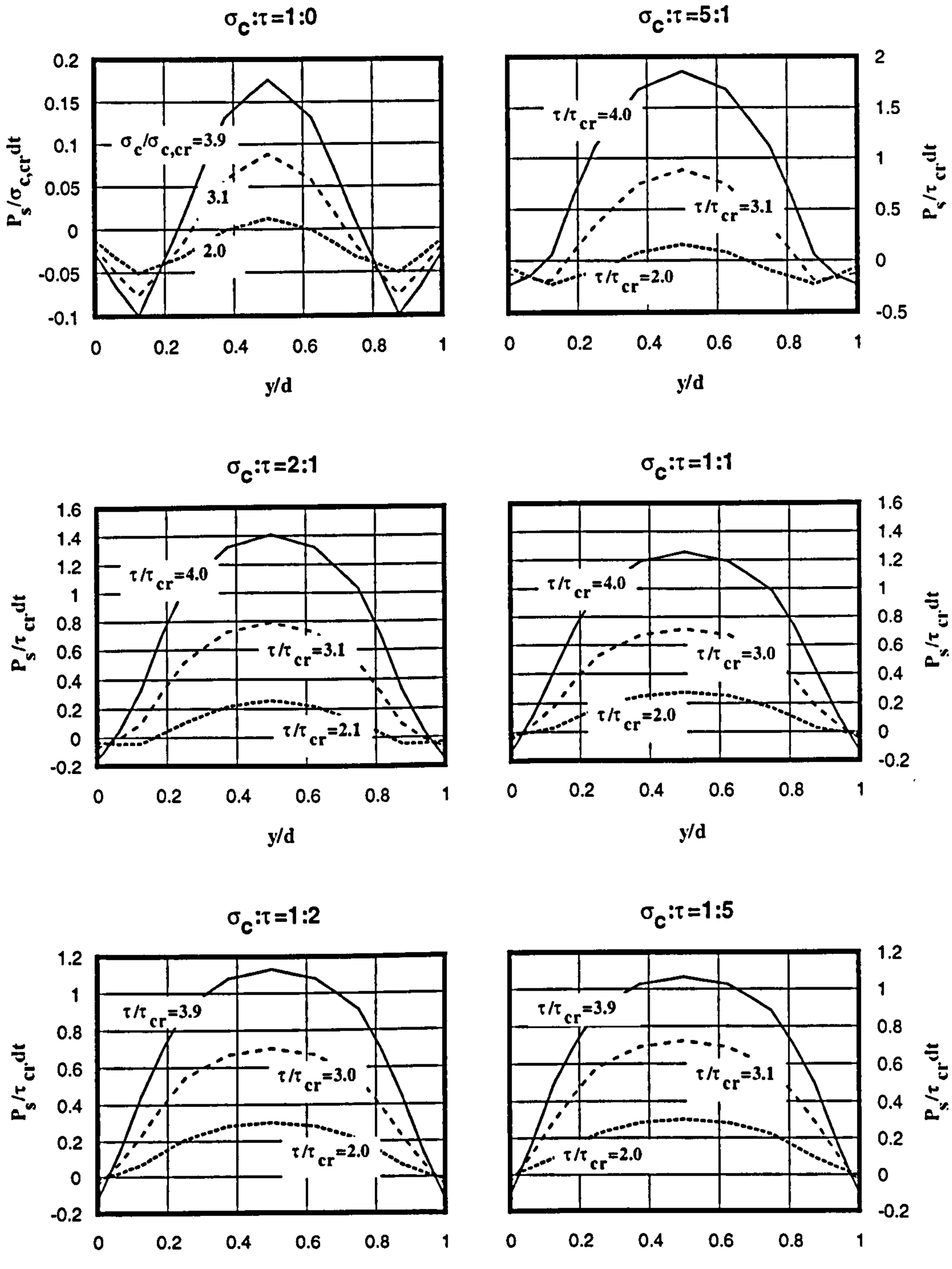
6.6.2.1 Distribution of Axial Force in the Stiffener

For plates subjected to coexistent shear and compressive stresses, τ and σ_c, the distribution curves of the axial forces along the stiffeners, obtained from the non-linear elastic finite element analyses, are illustrated in Fig. 6.11.

It is found that with the increase of the ratio of shear to compression ($\tau:\sigma_c$), the distribution curve gradually adapts to the shape of pure shear, as shown in Fig. 6.8. For the cases of lower ratio of $\tau:\sigma_c$, the distribution profiles are more related to the out-of-plane deflection modes. This is because in these cases the axial forces in the stiffeners result mainly from the effects of Poisson's ratio and the axial constraints provided by the stiffener when the panels produce out-of-plane displacement.

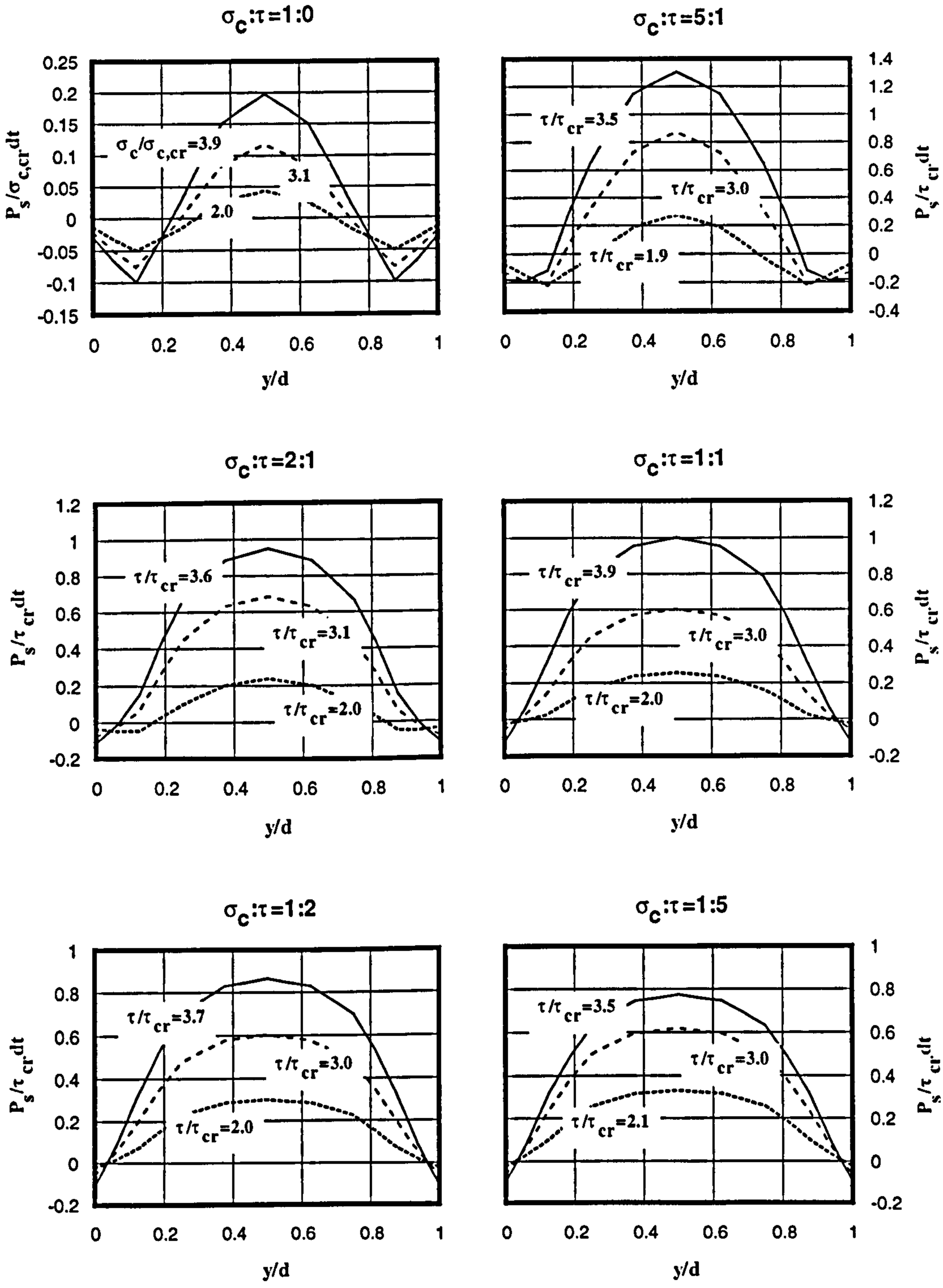
6.6.2.2 Magnitude of Axial Force in the Stiffener

In order to get a feeling of the differences in the stiffener axial forces for the different proportions of shear and compression, the maximum values of the axial force, P_s, given in KN, are shown in Fig. 6.12. The horizontal axis represents the value of τ/τ_{cr} for combined shear and compression, and $\sigma_c/\sigma^0_{c,cr}$ for compression alone. It is seen that as the shear component becomes predominant the magnitude of the axial force becomes much greater. The axial force acting in the stiffener for compression alone is rather small when compared to the pure shear condition. In the next subsection, the maximum values of the stiffener axial forces for plates under combined shear and compression are considered and examined against those estimated using Eqns. 6.10 and 6.11.



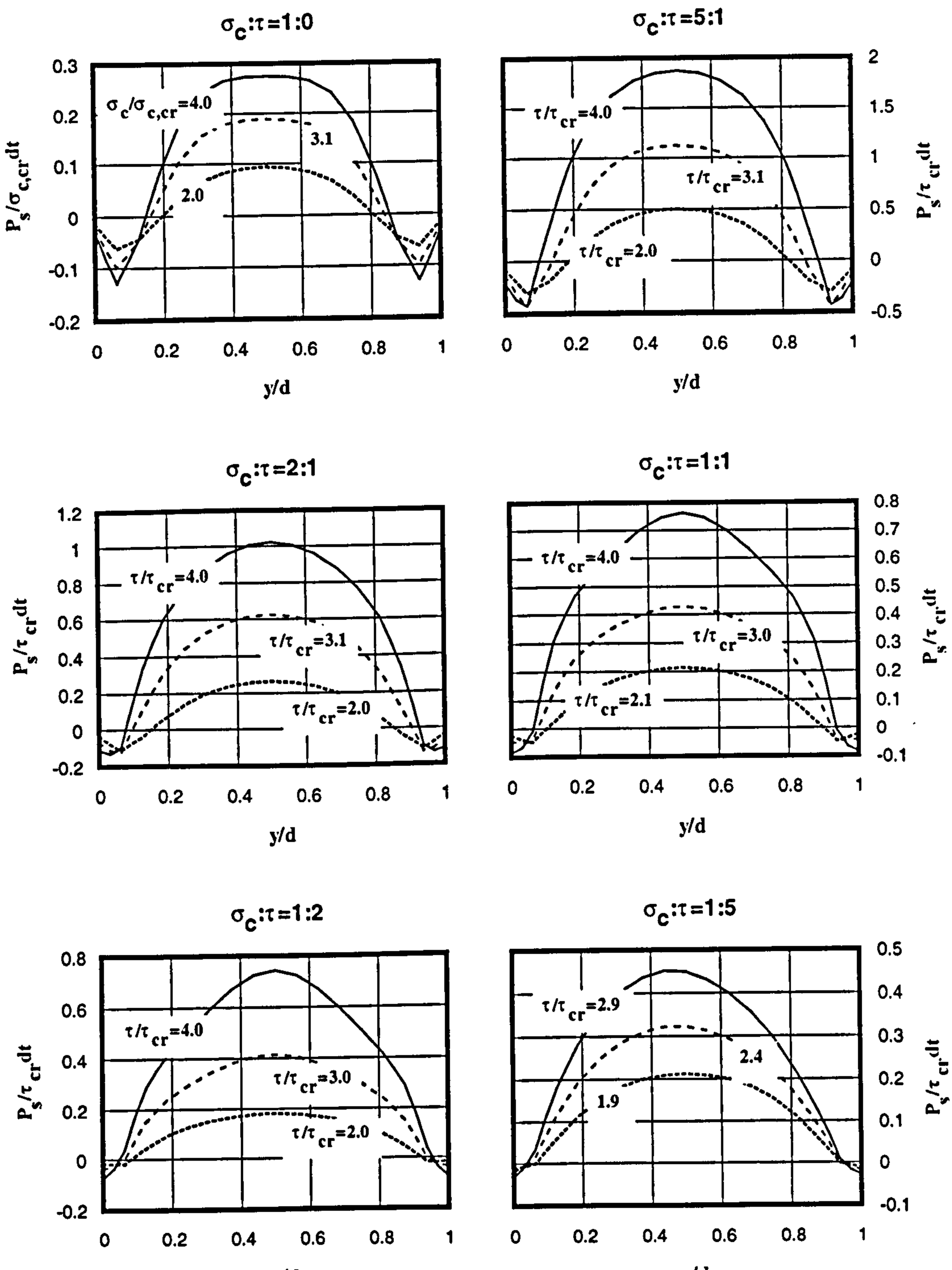
(a) d/a=0.5, Ω =0.1

Figure 6.11 Distribution of the axial force in the stiffener. $\Omega=A_s/at$. Shear and Compression. Plates with a straight non-deflecting stiffener. Non-linear elastic FE results



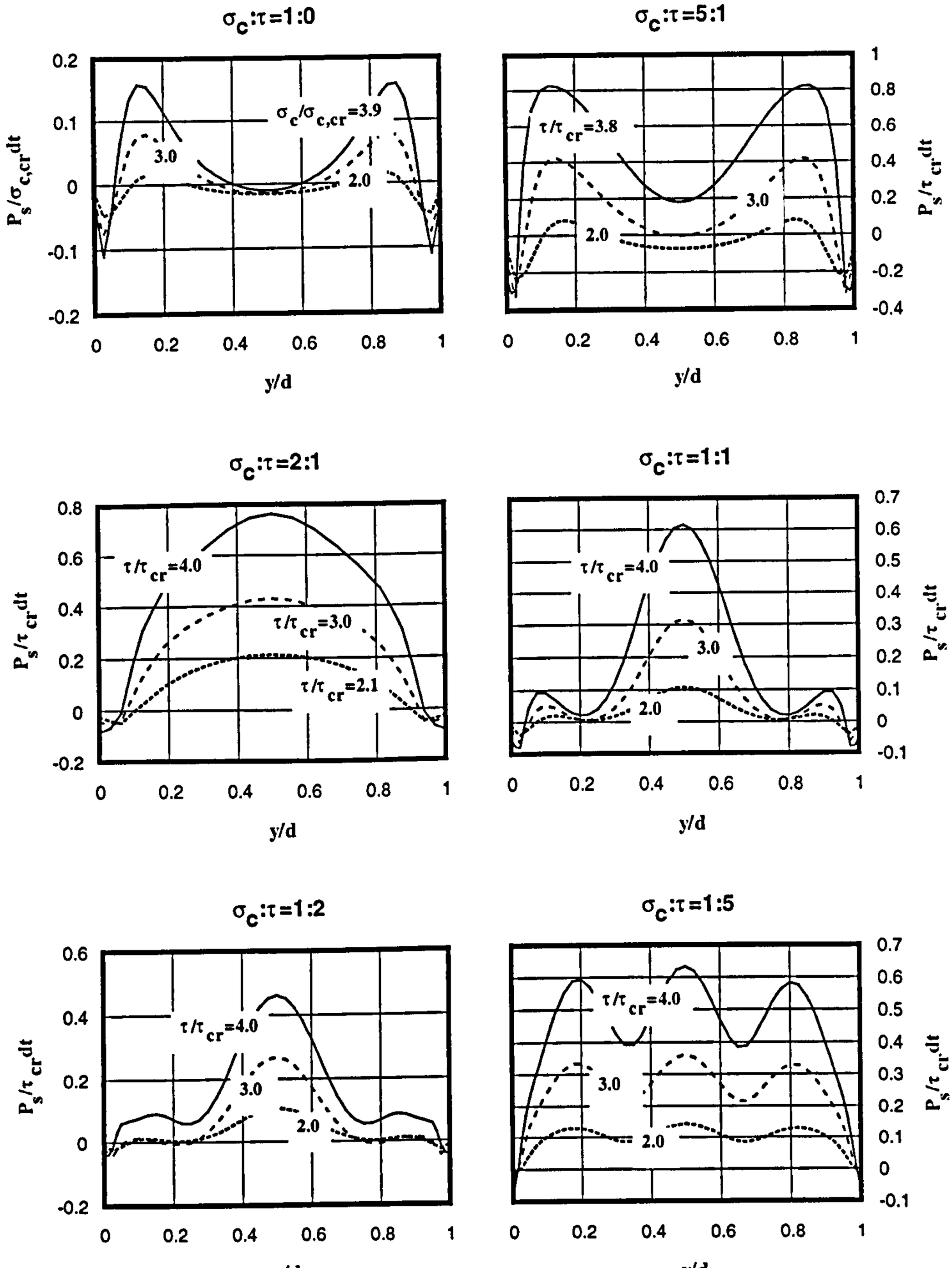
(b) d/a=1, Ω =0.2

Figure 6.11 (Cont) Distribution of the axial force in the stiffener. $\Omega=A_s/at$. Shear and Compression. Plates with a straight non-deflecting stiffener. Non-linear elastic FE results



(c) d/a=2, Ω =0.5

Figure 6.11 (Cont) Distribution of the axial force in the stiffener. $\Omega=A_s/at$. Shear and Compression. Plates with a straight non-deflecting stiffener. Non-linear elastic FE results



(d) d/a=5, Ω =0.6

Figure 6.11 (Cont) Distribution of the axial force in the stiffener. $\Omega=A_s/at$. Shear and Compression. Plates with a straight non-deflecting stiffener. Non-linear elastic FE results

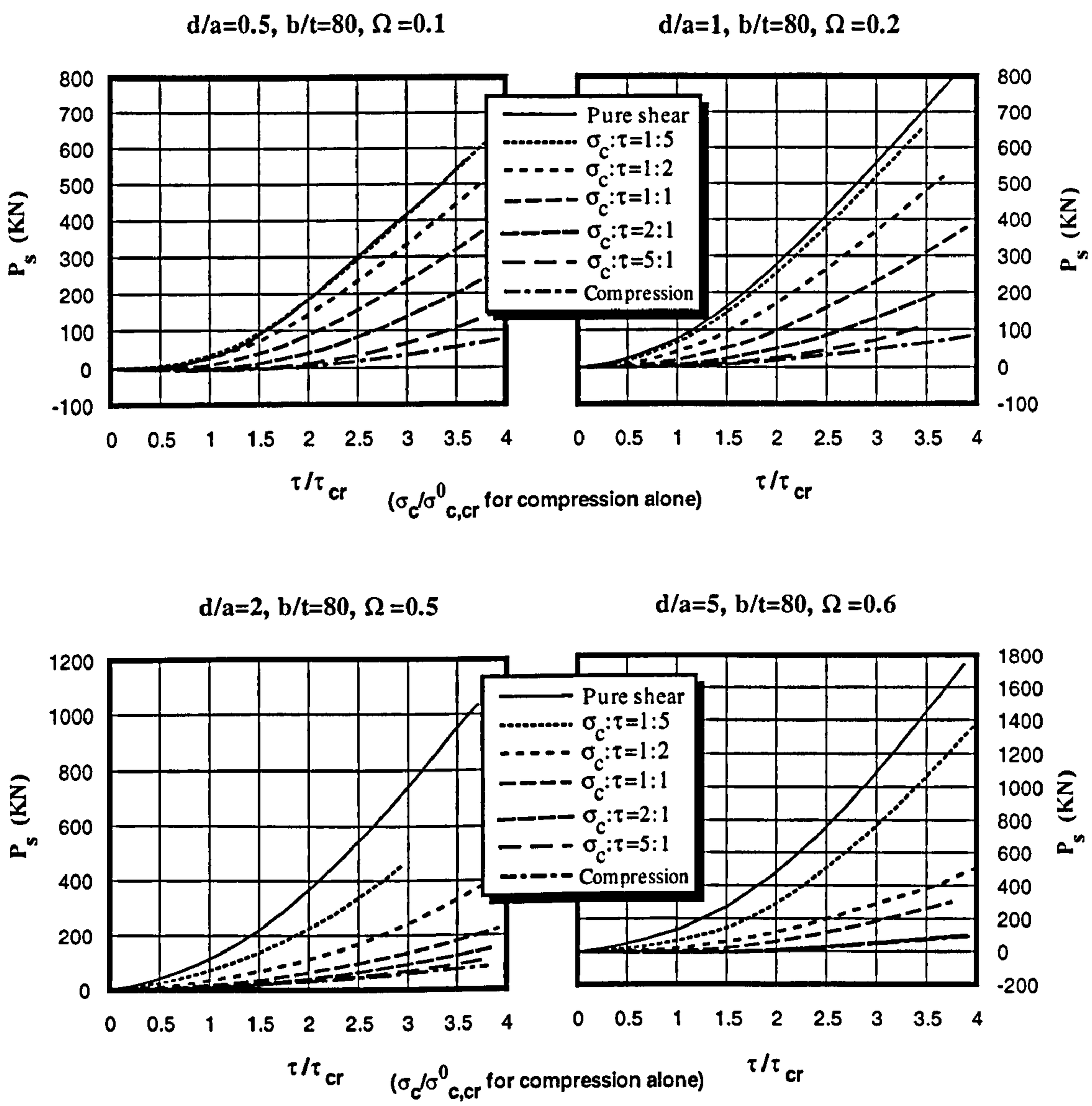


Figure 6.12 The axial forces in the stiffeners. Combined shear and compression. $\Omega=A_s/at$.
Non-linear elastic FE results. CUCU plates with a straight non-deflecting stiffener.
Point-symmetric panel imperfection, $w_{0p}/t=1.091$

6.6.2.3 Comparison of Proposed Equations with FE solutions

It has been found in Section 5.3.2.1 that for plates with a knife edge, the interaction curve between shear and compression can be represented approximately by the equation:

$$\frac{\sigma_{c,cr}}{\sigma^0_{c,cr}}+\left(\frac{\tau_{cr}}{\tau^0_{cr}}\right)^2=1 \qquad (6.12)$$

where τ^0_{cr} and $\sigma^0_{c,cr}$ can be determined by Eqns. 5.2 and 5.5, respectively.

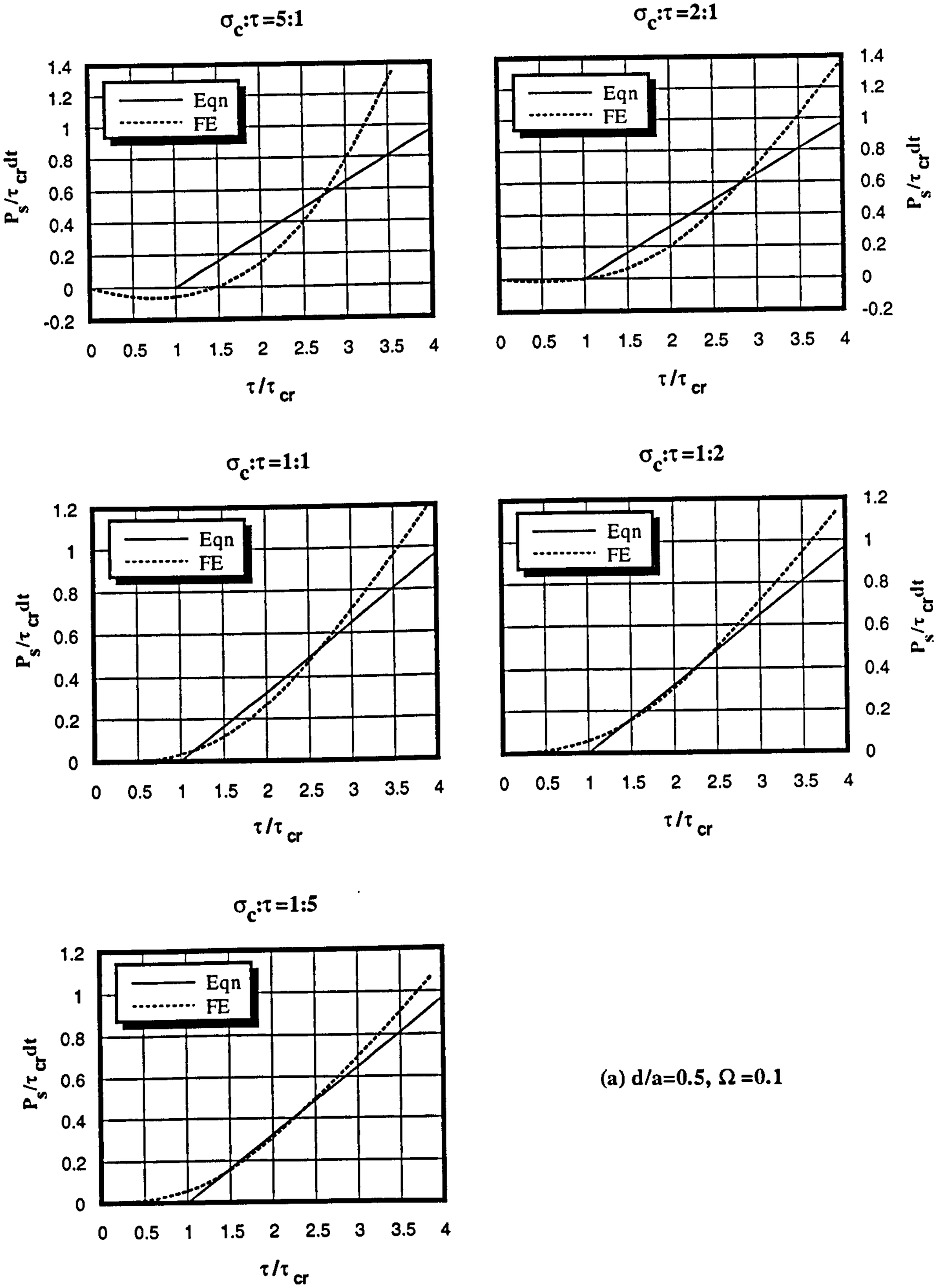
For a given ratio of applied load components, σ_c/τ, the critical shear stress τ_{cr} in the presence of compression can be obtained from Eqn. 6.12, which is given in Eqn. 5.6. By replacing τ_{cr} in Eqn. 6.10 with τ_{cr} from Eqn. 6.12, the maximum value of the axial force in the stiffener, P_s, is obtained. The normalised stiffener axial force $P_s/\tau_{cr}dt$, given by Eqns. 6.10 and 6.11, are compared with the finite element results in Fig. 6.13. It is apparent that there is good agreement between the numerical results and the predicted values, and in most of the cases, the proposed equation provides a conservative estimate of the axial force in the stiffener. Therefore, it is considered that by using the critical shear stress in the presence of compression, the simple formula of Eqn. 6.10, with its associated coefficients given by Eqn. 6.11, can be used directly for predicting the axial force in the stiffener for plates subjected to shear and compression. For the cases of $\sigma_c/\tau>5$, the axial force in the stiffener is taken as zero.

6.6.3 Combined Shear and Bending

6.6.3.1 Distribution of the Axial Force in Stiffener

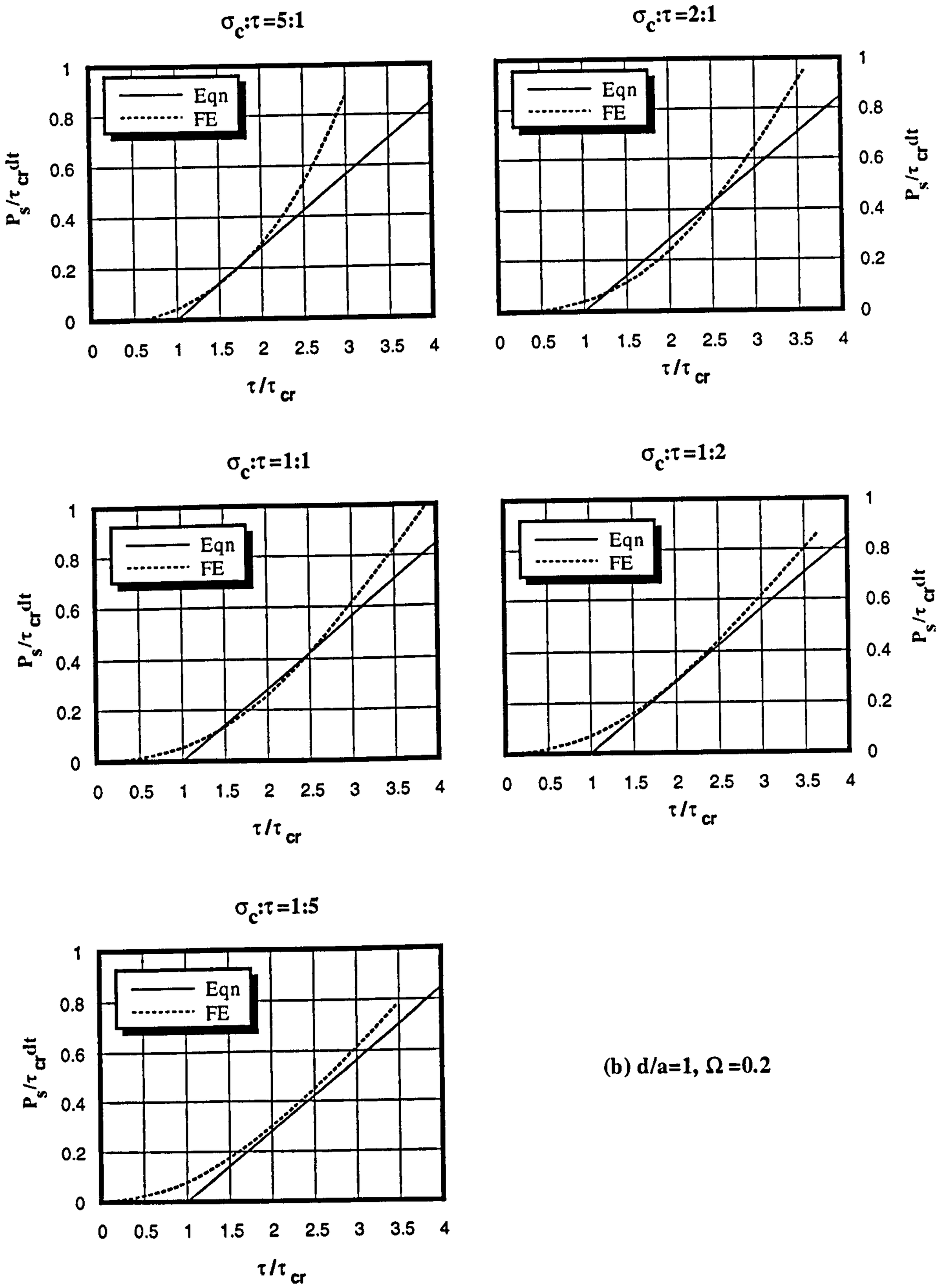
For plates subjected to coexistent shear and bending stresses, τ and σ_b, the distribution curves of the axial forces along the stiffeners, obtained from the non-linear elastic finite element analyses, are illustrated in Fig. 6.14.

Analogous to the combined shear and compression conditions, it is also found that with the increase of the ratio of shear to bending ($\tau:\sigma_b$), the distribution curve gradually adapts to the shape of pure shear, as shown in Fig. 6.8. For tall panels, it is observed that the peak value of the axial force in the stiffener occurs in the upper part of the stiffener. This is because the buckling of the plate is greatest near the top of the panels, where compression is combined with shear.



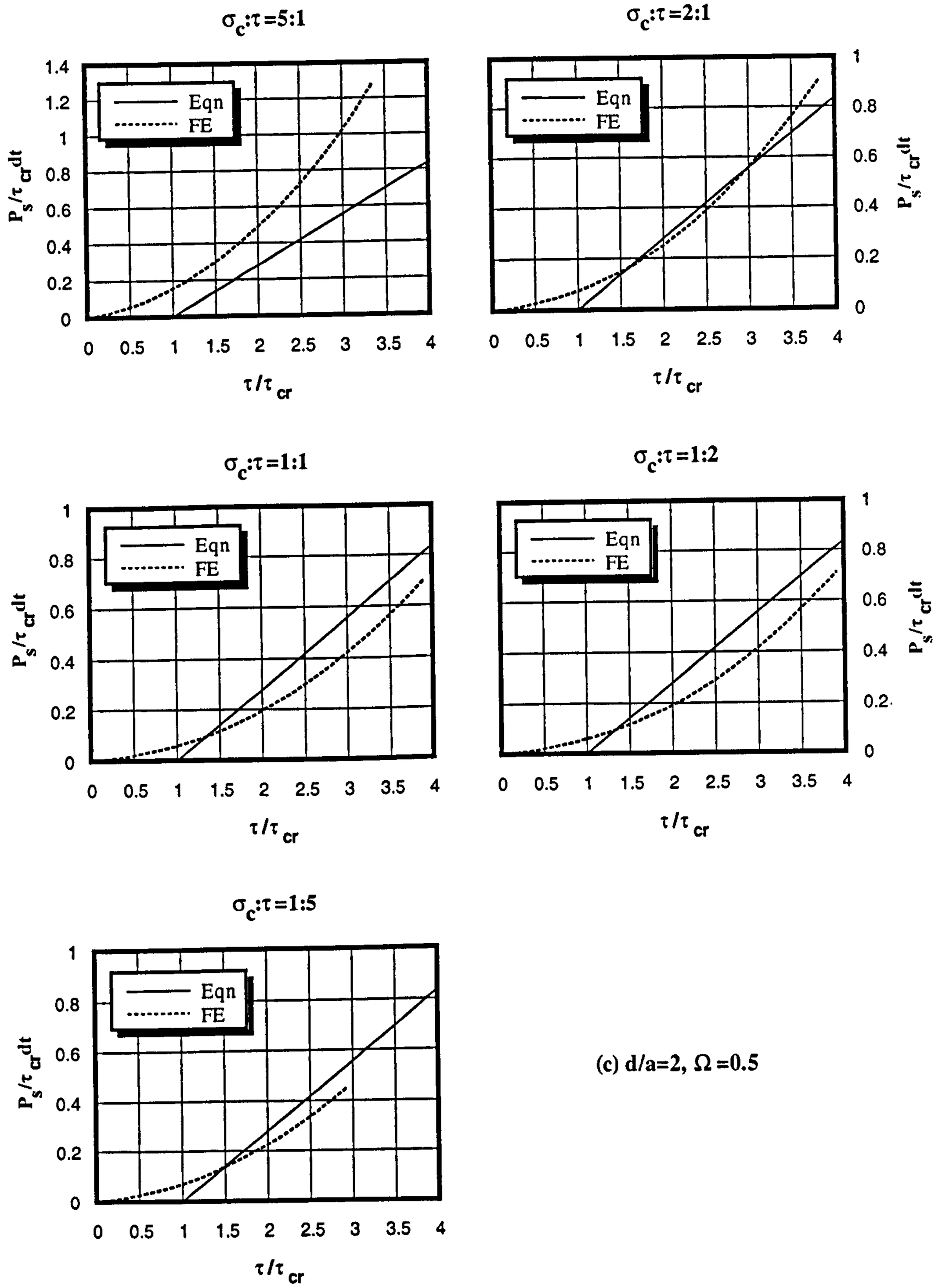
(a) d/a=0.5, Ω =0.1

Figure 6.13 Comparisons in the stiffener axial forces between proposed equations and FE solutions. Combined shear and compression. $\Omega=A_s/at$



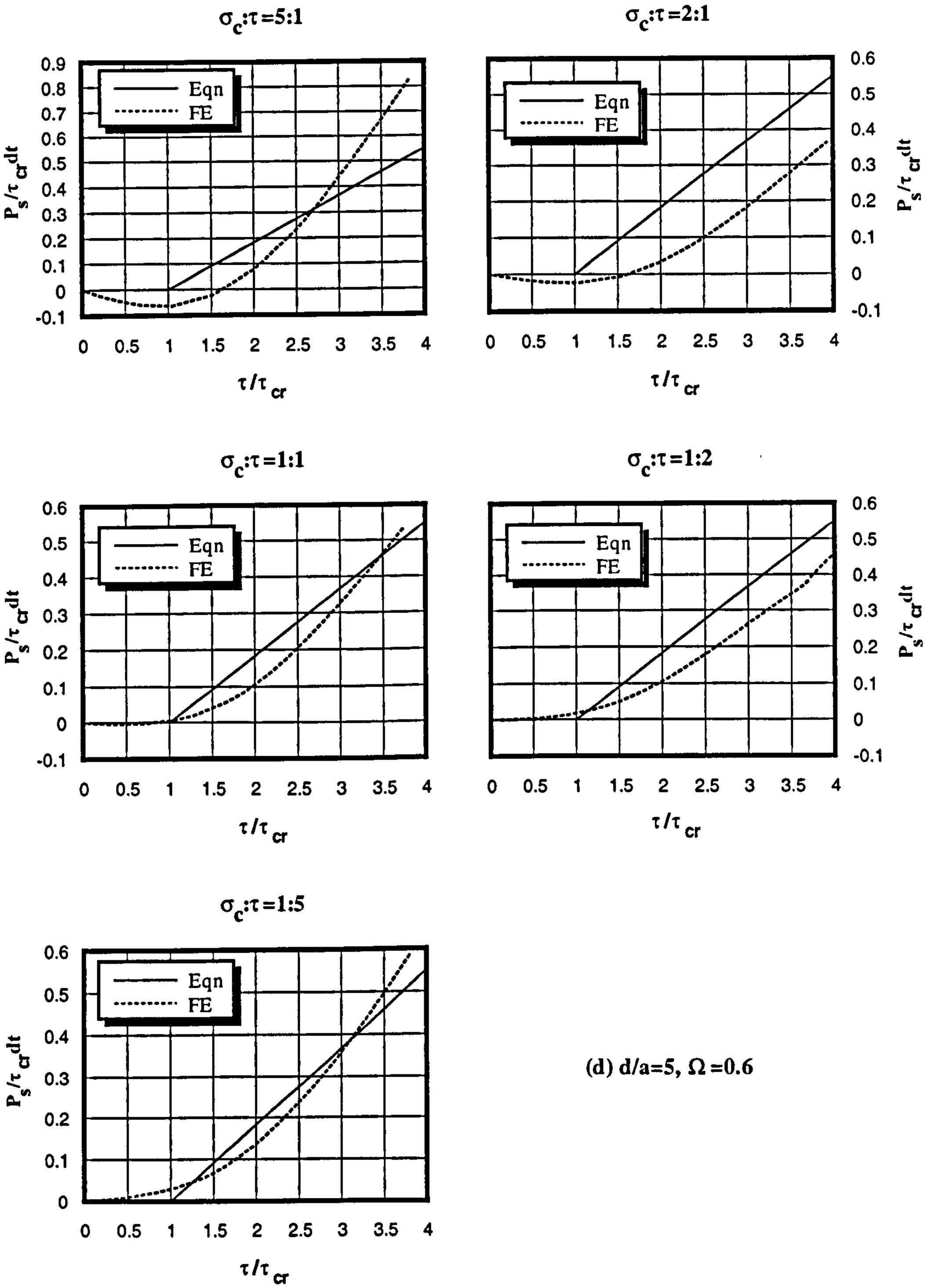
(b) d/a=1, Ω =0.2

Figure 6.13 (Cont) Comparisons in the stiffener axial forces between proposed equations and FE solutions. Combined shear and compression. $\Omega=A_s/at$



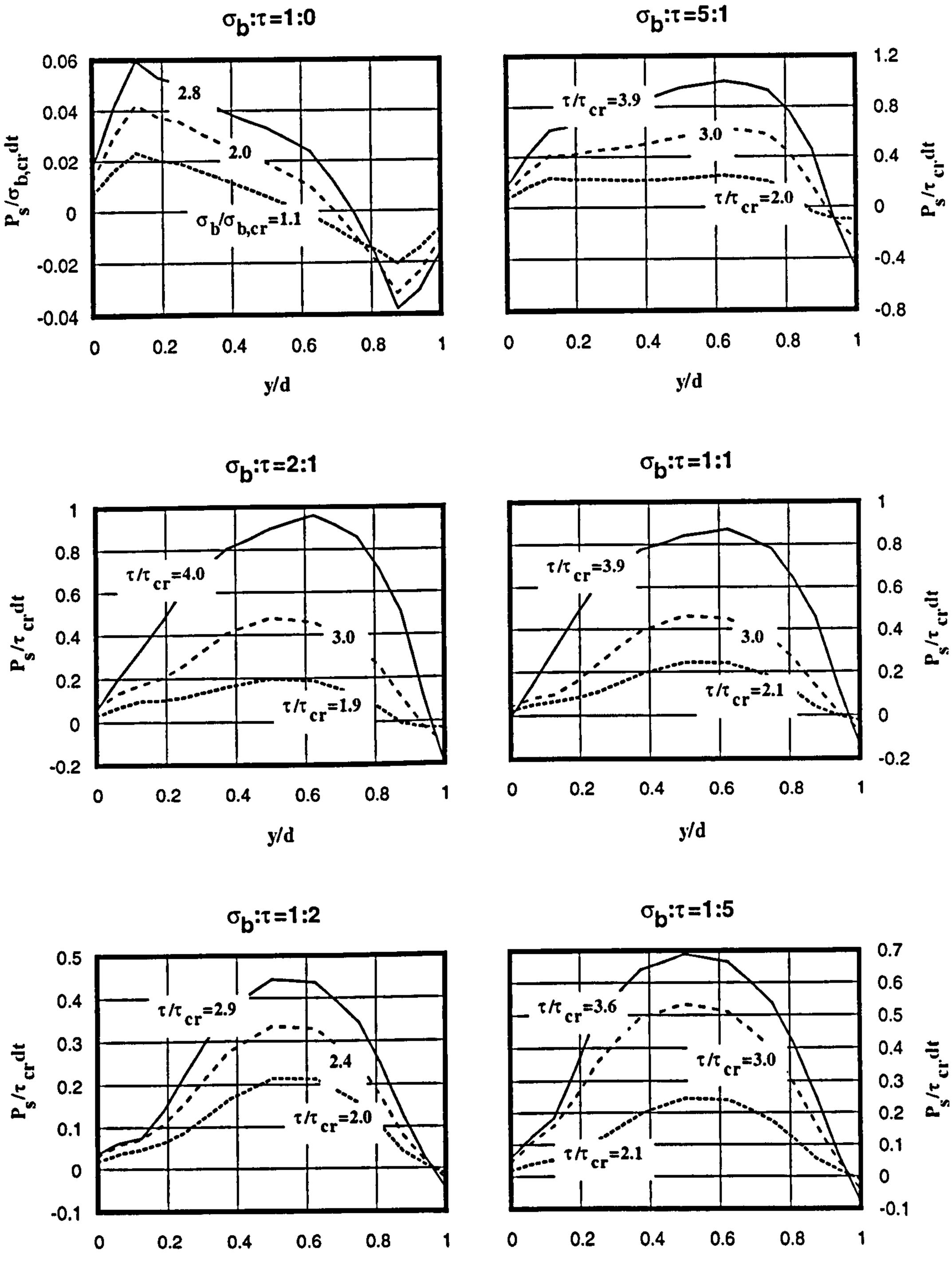
(c) d/a=2, Ω =0.5

Figure 6.13 (Cont) Comparisons in the stiffener axial forces between proposed equations and FE solutions. Combined shear and compression. $\Omega=A_s/at$



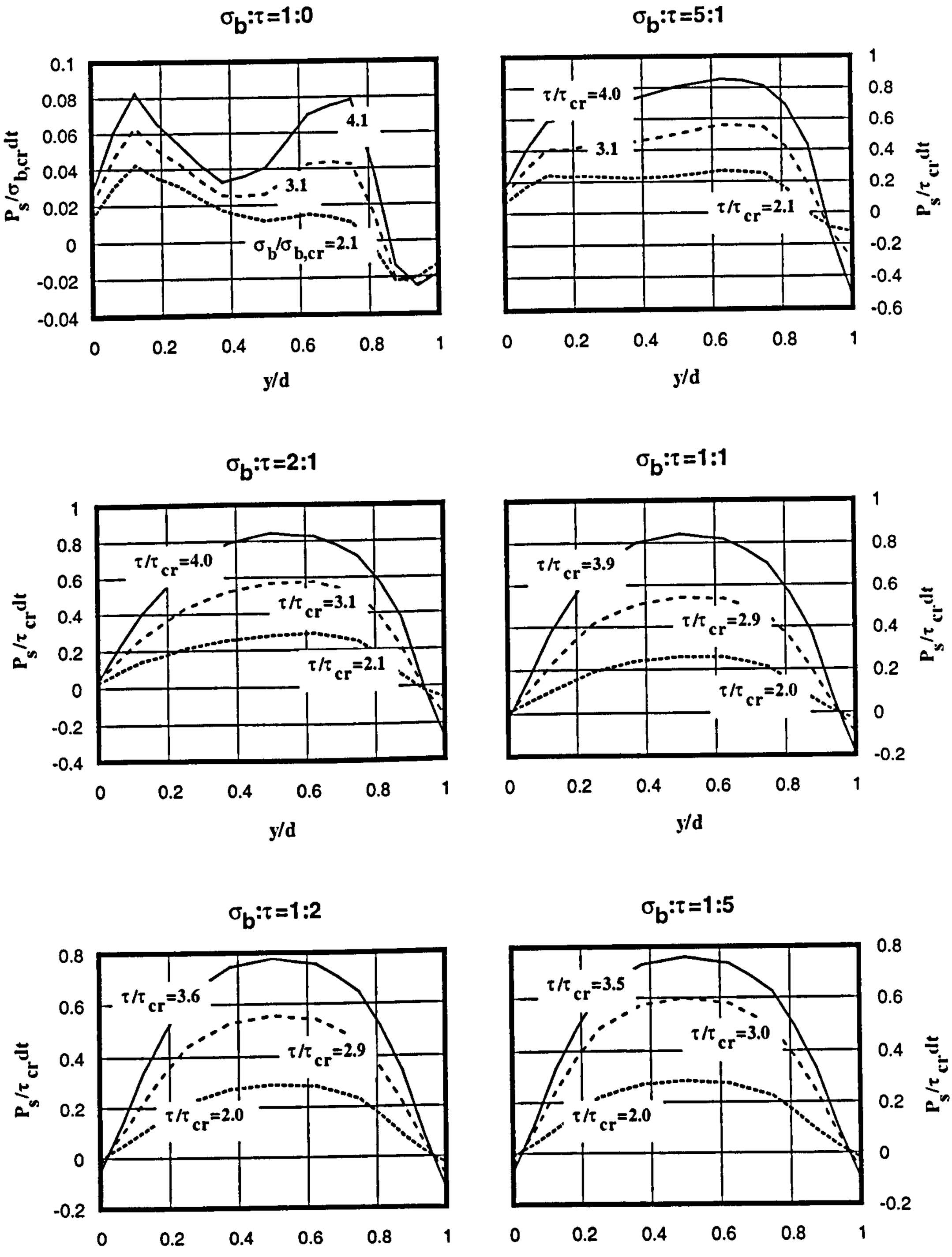
(d) d/a=5, Ω =0.6

Figure 6.13 (Cont) Comparisons in the stiffener axial forces between proposed equations and FE solutions. Combined shear and compression. $\Omega=A_s/at$



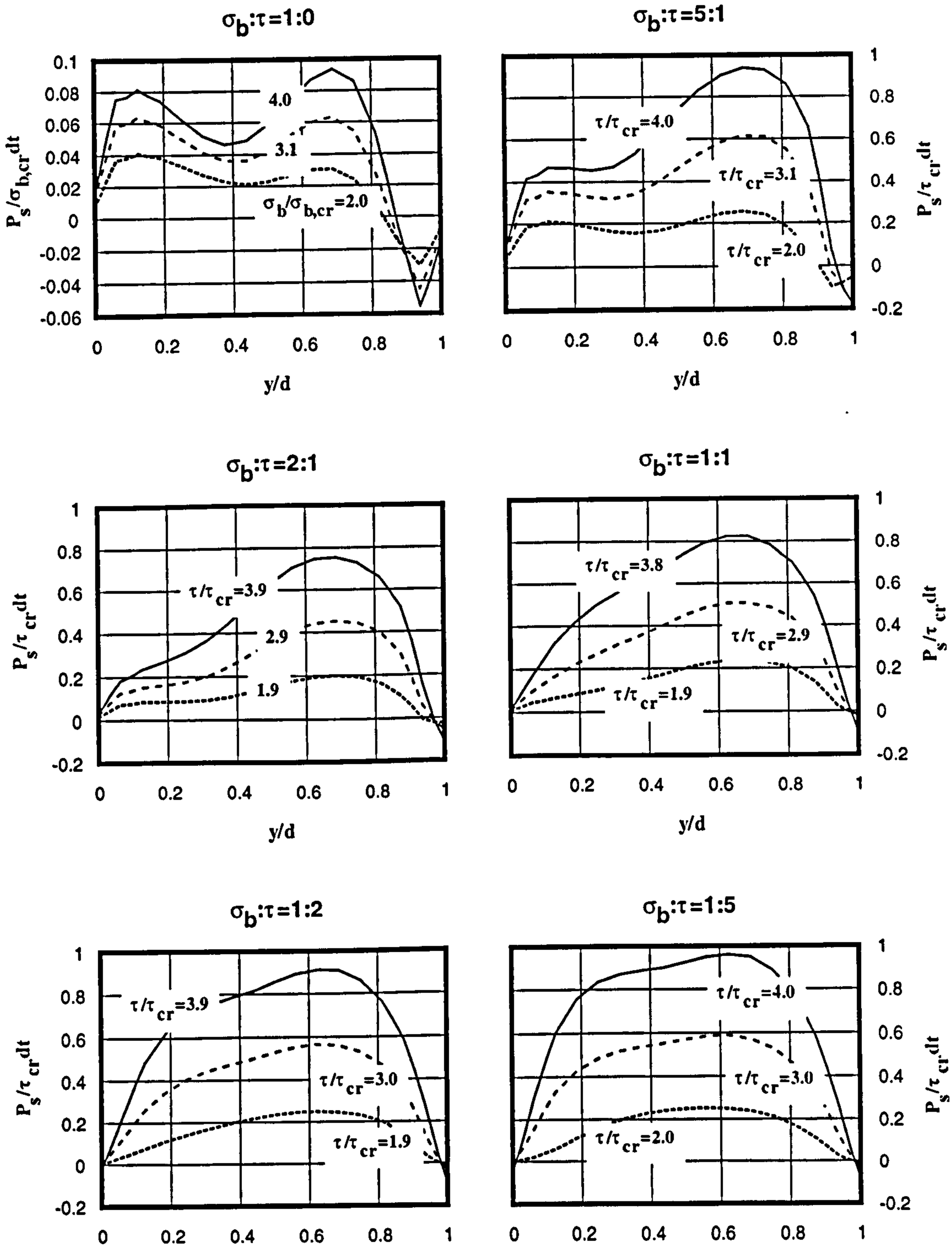
(a) d/a=0.5, Ω =0.1

Figure 6.14 Distribution of the axial force in the stiffener. $\Omega=A_s/at$. Shear and Bending. Plates with a straight non-deflecting stiffener. Non-linear elastic FE results



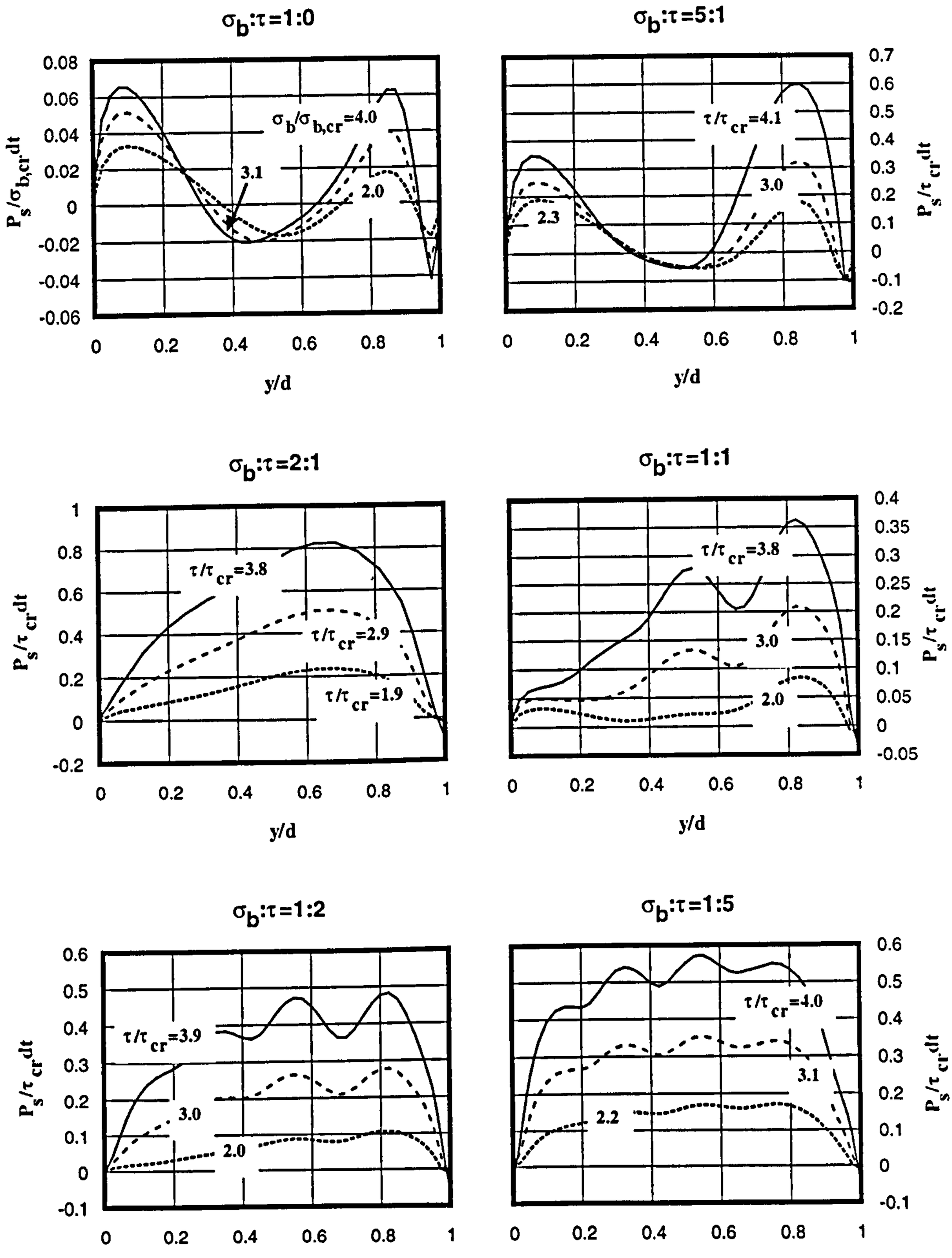
(b) d/a=1, Ω =0.2

Figure 6.14 (Cont) Distribution of the axial force in the stiffener. $\Omega=A_s/at$. Shear and Bending. Plates with a straight non-deflecting stiffener. Non-linear elastic FE results



(c) d/a=2, Ω =0.5

Figure 6.14 (Cont) Distribution of the axial force in the stiffener. $\Omega=A_s/at$. Shear and Bending. Plates with a straight non-deflecting stiffener. Non-linear elastic FE results



(d) d/a=5, Ω =0.6

Figure 6.14 (Cont) Distribution of the axial force in the stiffener. $\Omega=A_s/at$. Shear and Bending. Plates with a straight non-deflecting stiffener. Non-linear elastic FE results

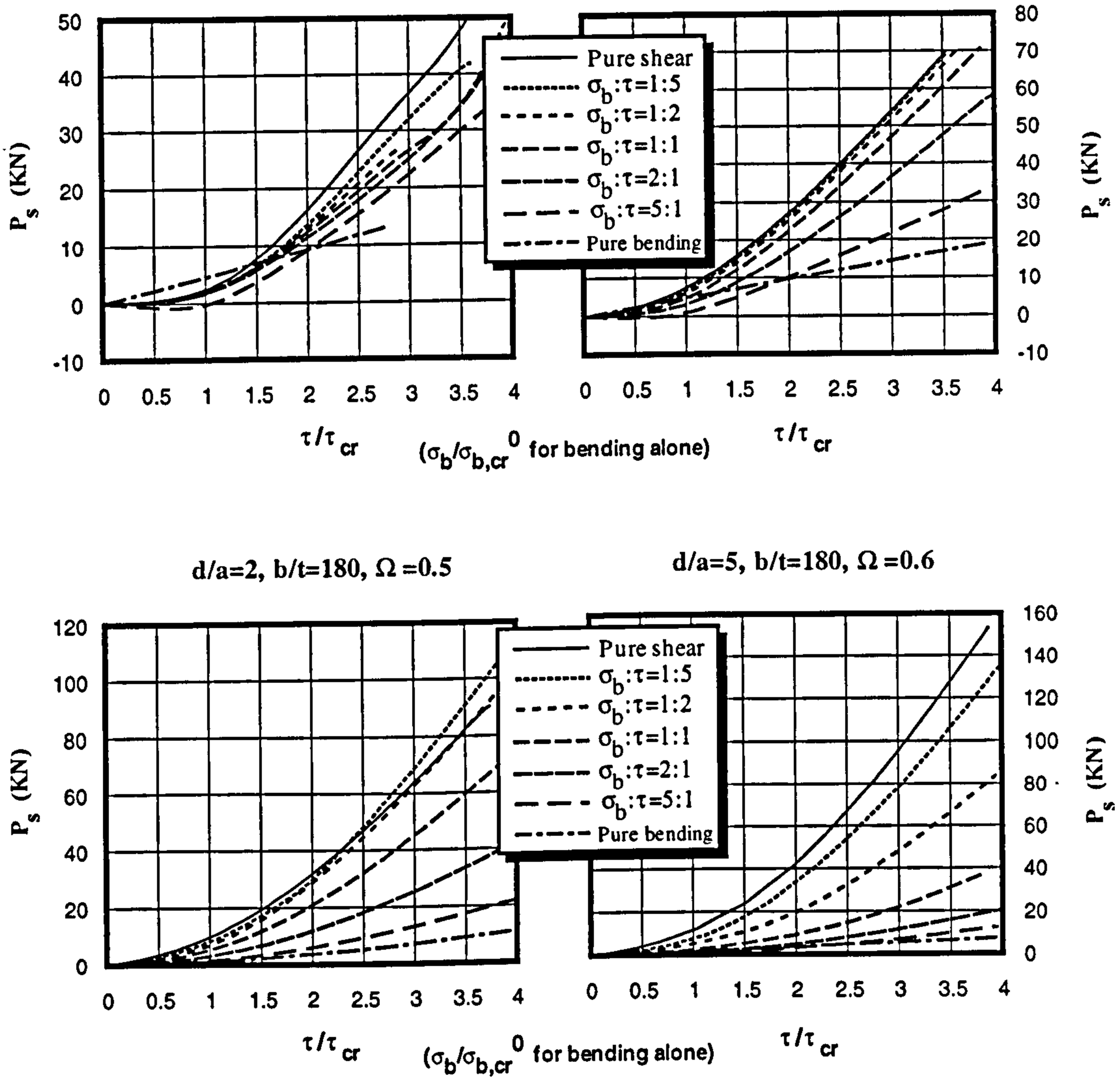


Figure 6.15 The axial forces in the stiffeners. Combined shear and bending. $\Omega=A_s/at$. Non-linear elastic FE results. CUCU plates with a straight non-deflecting stiffener. Point-symmetric panel imperfection, $w_{0p}/t=1.091$

6.6.3.2 Magnitude of the Axial Force in Stiffener

To illustrate the differences in the stiffener axial forces for the different proportions of shear and bending, the maximum values of the axial force, P_s, given in KN, are shown

in Fig. 6.15. The horizontal axis represents the value of τ/τ_{cr} for combined shear and bending, and $\sigma_b/\sigma^0_{b,cr}$ for pure bending alone. It is seen that as the shear component becomes predominant the magnitude of the axial force becomes much greater. The axial force acting in the stiffener for the pure bending condition is rather small when compared to the pure shear condition. In the next subsection, the maximum values of the stiffener axial forces for plates under combined shear and bending are considered and examined against those estimated using Eqns. 6.10 and 6.11.

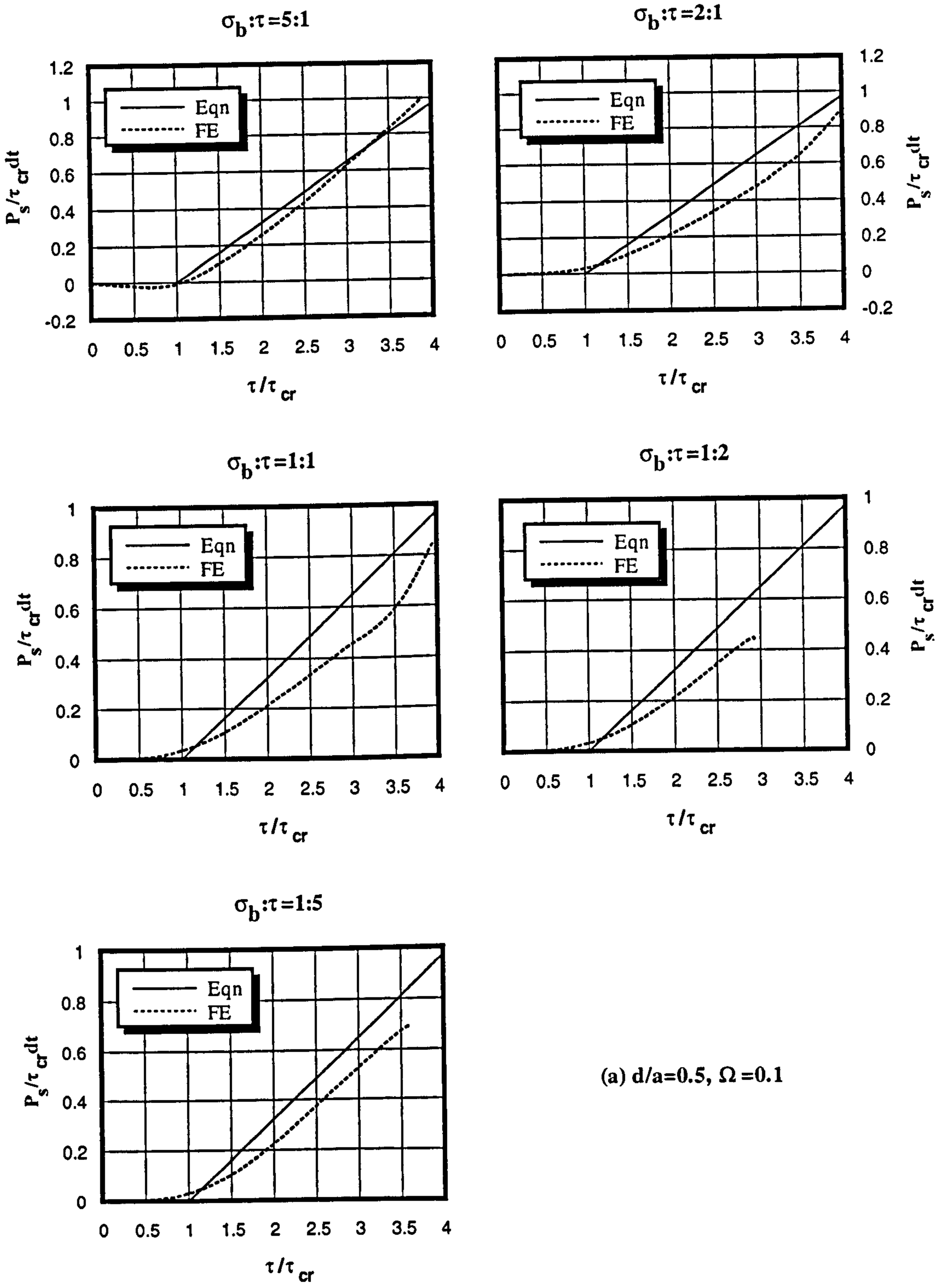
6.6.3.3 Comparison of Proposed Equations with FE solutions

It has been found in Section 5.3.3.1 that for plates with a knife edge, the interaction curve between shear and bending can be represented approximately by the equation:

$$\left(\frac{\sigma_{b,cr}}{\sigma^0_{b,cr}}\right)^2 + \left(\frac{\tau_{cr}}{\tau^0_{cr}}\right)^2 = 1 \qquad (6.13)$$

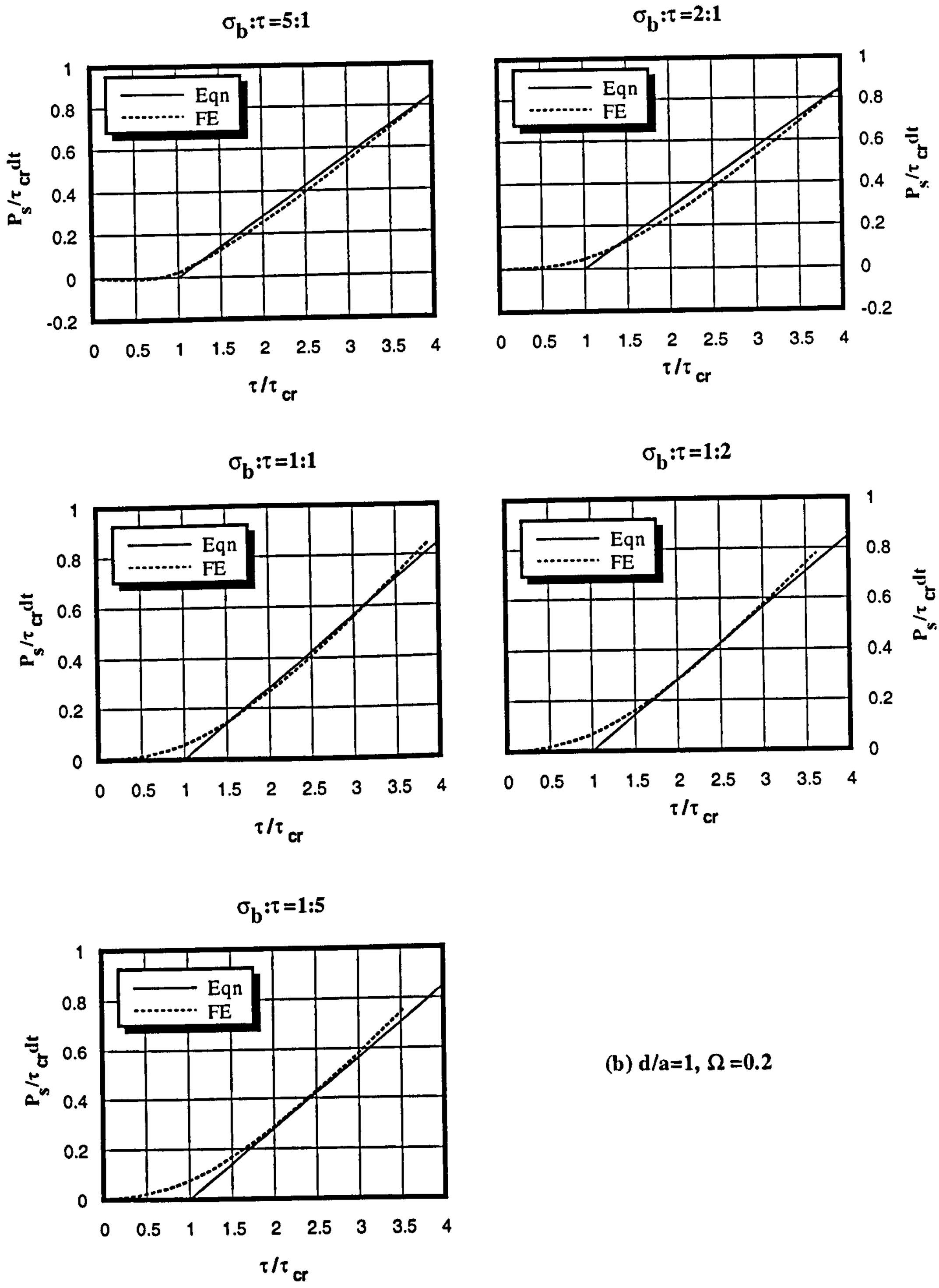
where τ^0_{cr} and $\sigma^0_{b,cr}$ can be determined by Eqns. 5.2 and 5.15, respectively.

For a given ratio of applied bending stress to the shear stress, σ_b/τ, the critical shear stress τ_{cr} in the presence of bending can be obtained from Eqn. 6.13, which is given in Eqn. 5.16. By replacing τ_{cr} in Eqn. 6.10 with τ_{cr} from Eqn. 6.13, the maximum value of the axial force in the stiffener, P_s, is obtained. The normalised stiffener axial force $P_s/\tau_{cr}dt$, given by Eqns. 6.10 and 6.11, are compared with the finite element results in Fig. 6.16. Generally, the predicted axial forces in the stiffeners agree well with the numerical results, and in most of the cases, the proposed equation provides a conservative estimate of the axial force in the stiffener. Therefore, it is considered that by using the critical shear stress in the presence of bending, the simple formula of Eqn. 6.10, with its associated coefficients given by Eqn. 6.11, can be used directly for predicting the axial force in the stiffener for plates subjected to shear and bending. For the cases of $\sigma_b/\tau>5$, the axial force in the stiffener is assumed to be zero.



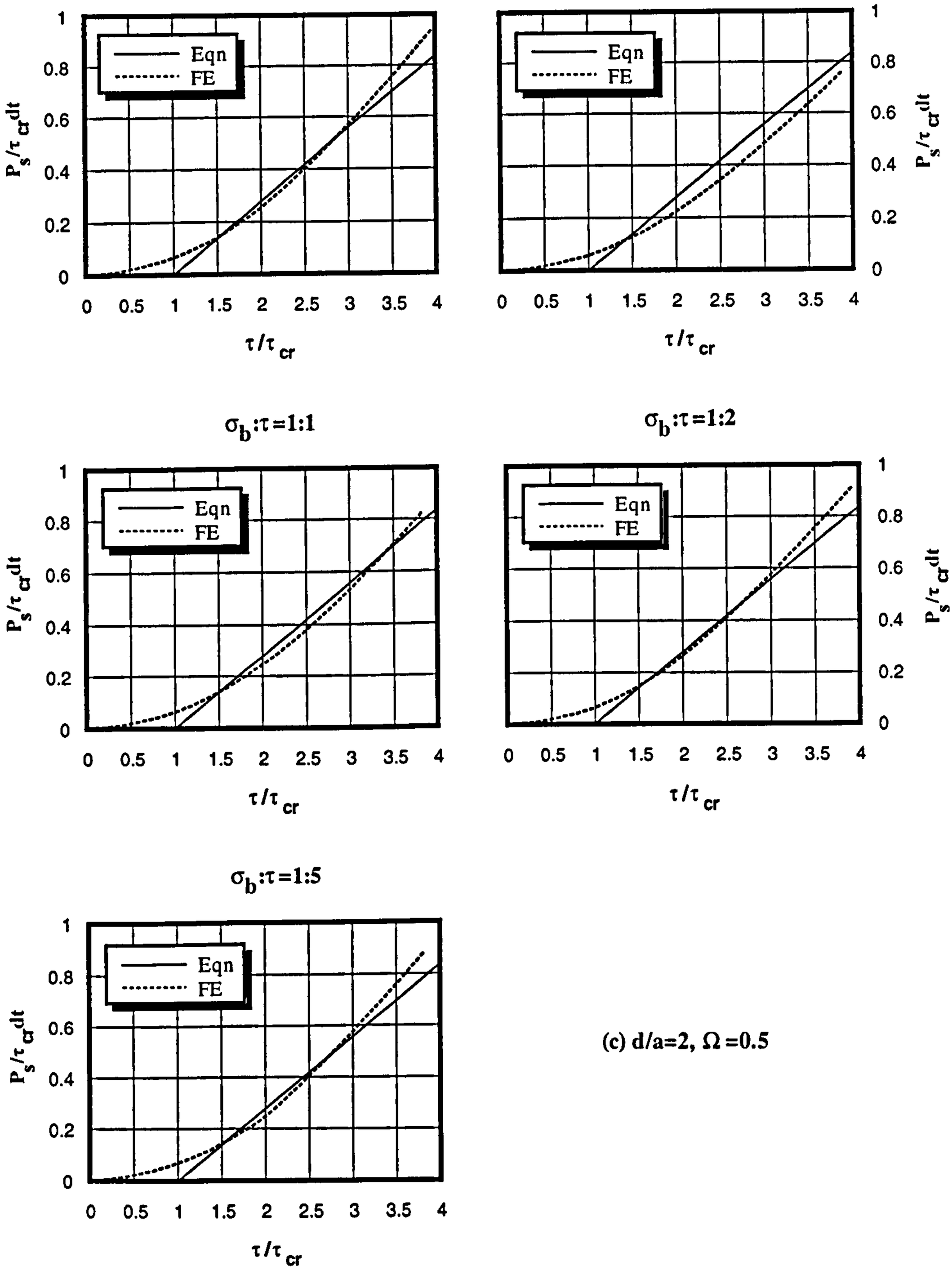
(a) d/a=0.5, Ω =0.1

Figure 6.16 Comparisons in the stiffener axial forces between proposed equations and FE solutions. Combined shear and bending. $\Omega=A_s/at$



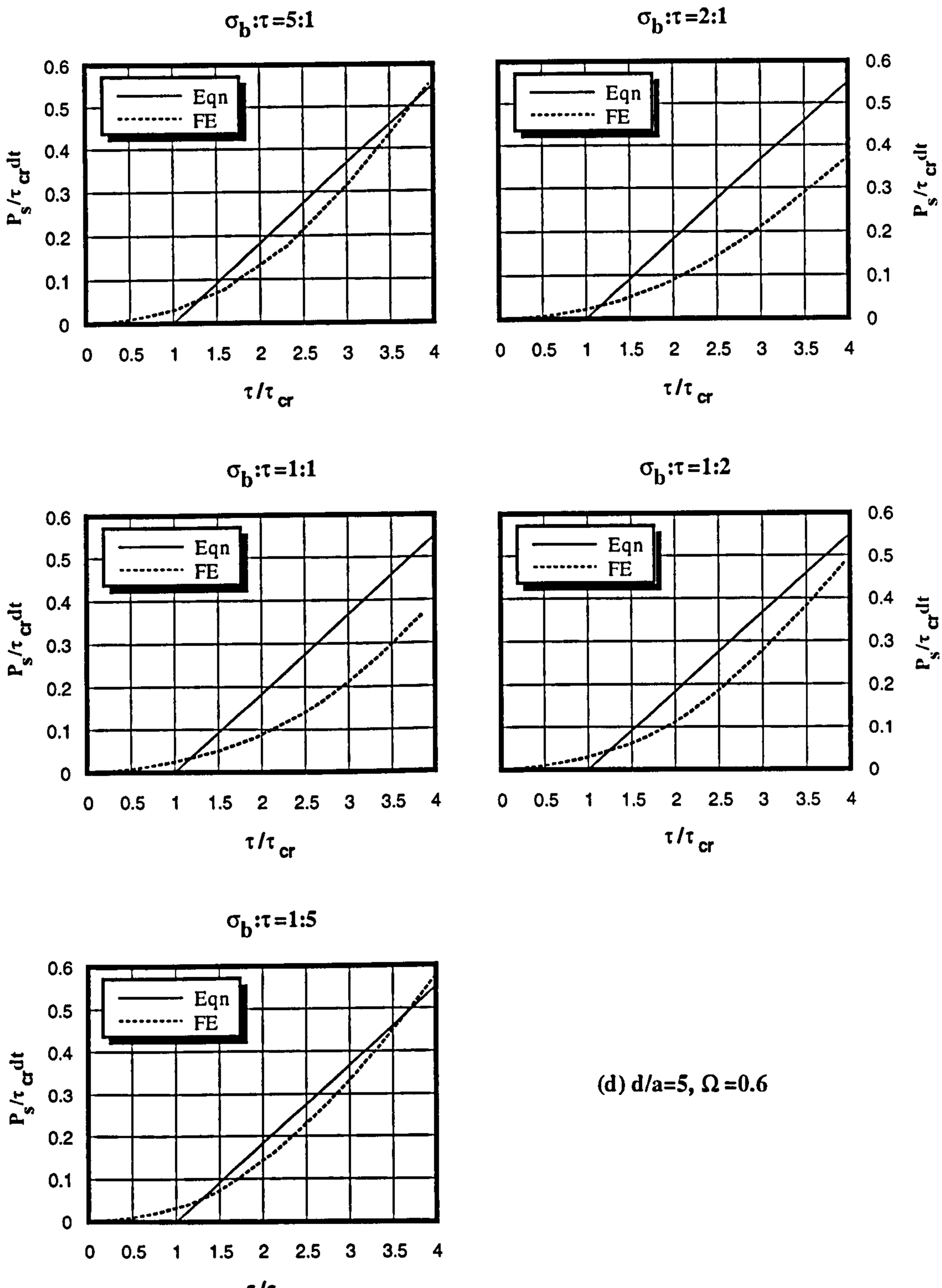
(b) d/a=1, Ω =0.2

Figure 6.16 (Cont) Comparisons in the stiffener axial forces between proposed equations and FE solutions. Combined shear and bending. $\Omega=A_s/at$



(c) d/a=2, Ω =0.5

Figure 6.16 (Cont) Comparisons in the stiffener axial forces between proposed equations and FE solutions. Combined shear and bending. $\Omega=A_s/at$



(d) d/a=5, Ω =0.6

Figure 6.16 (Cont) Comparisons in the stiffener axial forces between proposed equations and FE solutions. Combined shear and bending. $\Omega=A_s/at$

6.7 SUMMARY OF THE DESIGN FORMULAE FOR PREDICTING P_S

Based on the above analyses, it is proposed that for plates subjected to general combined shear, compression and bending, the axial force in the stiffener can be represented by the following equations:

$$\frac{P_s}{\tau_{cr}\, dt} = \begin{cases} C_1\left(\dfrac{\tau}{\tau_{cr}} - 1\right)\cdot(1 + C_2 \ln\Omega) & for\ \tau > \tau_{cr} \\ 0 \quad for\ \tau \le \tau_{cr}, \quad or\ \tau < \sigma_c/5 \quad and \quad \tau < \sigma_b/5 & \end{cases} \tag{6.14}$$

where:

$$C_1 = \frac{1}{2\sqrt{\alpha}}$$
$$C_2 = 0.27 + 0.05 \ln\alpha \tag{6.15}$$

and α=d/a.

The critical shear stress τ_{cr} in the presence of compression and bending can be calculated using Eqn. 6.16:

$$\frac{\sigma_{c,cr}}{\sigma^0_{c,cr}} + \left(\frac{\sigma_{b,cr}}{\sigma^0_{b,cr}}\right)^2 + \left(\frac{\tau_{cr}}{\tau^0_{cr}}\right)^2 = 1 \tag{6.16}$$

Eqn. 6.16 is a generalization of Eqns. 6.12 and 6.13.

6.8 CONCLUSIONS

In this chapter, an investigation has been carried out to examine the in-plane axial forces exerted on the stiffeners. On the basis of the tension field theory, a simple method for the estimation of the stiffener axial force has been developed, which incorporates the finite element results of non-linear elastic buckling analyses of plates with a straight non-deflecting stiffener. As a result of this study, the following conclusions can be made:

(1) The axial forces calculated in accordance with the Basler tension field theory and BS5400 are considerably greater than the actual force in the stiffener as represented by the FE solutions (Fig. 6.4).

(2) The tension field theory provides a rational physical mechanism for the description of the axial force acting in the stiffener. It is found that the Basler model provides a good estimate of the axial force in a stiffener of infinite axial rigidity ($\Omega=\infty$).

(3) The stiffener axial force varies considerably according to the axial rigidity Ω (Figs. 6.4 and 6.10).

(4) A simple and practical method for estimating the stiffener axial force is established by modifying the equation derived from the Basler tension field model, on the basis of finite element solutions.

(5) The non-deflecting stiffener model provides an accurate estimation of the axial force in a real stiffener. The non-deflecting stiffener model can be considered as an extension of the knife edge model, as used in Chapter 5 for developing the design formulae for the knife edge bending moment, except that the stiffener is attached to the plate and has a variable axial stiffness.

(6) The axial force in the stiffener results mainly from the inclined tension field action. It is proposed that the formulae obtained for predicting the stiffener axial force P_s under pure shear (Eqn. 6.10) can be extended to the combined loading conditions, simply by replacing the critical shear stress τ^0_{cr} for pure shear with the critical shear stress τ_{cr} in the presence of compression and bending.

(7) The stiffener axial force due to the effects of Poisson's ratio and the out-of-plane deflection of the panel is relatively small. The magnitudes of initial panel and stiffener imperfections do not affect the stiffener axial force significantly.

(8) For plates subjected to general combined shear, compression and bending, the axial force in the stiffener can be estimated in accordance with the equations 6.14 to 6.16.

CHAPTER 7

OVERALL BUCKLING MODELS

7.1 INTRODUCTION

Stiffened plates can buckle in essentially two basic forms. In overall buckling, the stiffeners buckle along with the plating; in local panel buckling, the plate panels buckle between the stiffeners. For stiffened plates subjected to shear loading, a combination of overall buckling and local panel buckling occurs, provided that the plate is stiffened with non-rigid stiffeners, as the stiffeners are unable to enforce the nodal lines at the position of stiffener. For stiffened plates subjected to compression or pure bending, a stiffener rigid enough will force a nodal line forming at the position of stiffener, but the combination of overall buckling and local panel buckling can still be seen in some higher critical modes.

It was observed that for plates reinforced with stiffeners much less than that required to divide the panels effectively, the critical buckling modes are overall modes. With the increase of the stiffener rigidity Ψ, the component of overall buckling mode reduces, while the component of panel buckling mode becomes dominant gradually. For a rigid stiffener or a knife-edge, only the panel buckling mode appears.

In the work by Stanway et al [9], the tendency for the stiffened plate to buckle overall, as well as the effect of local panel buckling between stiffeners, are distinguished. A rigid–link model was proposed to quantify the overall buckling effect.

In this chapter, the rigid–link model established by Stanway et al for pure shear will be examined, and also extended for compressive and pure bending loading conditions. On account of the inherent disadvantages of the rigid–link model, an overall buckling

model composed of a stiffener and plate panel, referred to as *beam-plate model* later, is presented for the stiffened plate. With the application of an energy method, the buckling analyses are conducted for each loading condition considered, by choosing a simple form of the deflection function for the model. By applying the overall buckling model for plates with an imperfect stiffener, the stiffener bending moment due to the overall buckling effect is derived, which will be used in Chapter 8 to determinate the total bending moment in the stiffener, incorporating with the local panel bending effect.

7.2 RIGID-LINK MODEL

7.2.1 Basis of the Model

The rigid-link model proposed by Stanway et al [9] is shown in Fig.7.1, which is based on the stiffened plate with an intermediate stiffener. In this model, the panels are represented as rigid pin-ended links, inclined at an angle θ to the y-axis, only for the purpose of calculating the overall buckling stress and quantifying the overall effects. The links are also referred to as *Strip elements*, which have an infinitesimal width. The inclined angle θ is chosen to give the minimum buckling load.

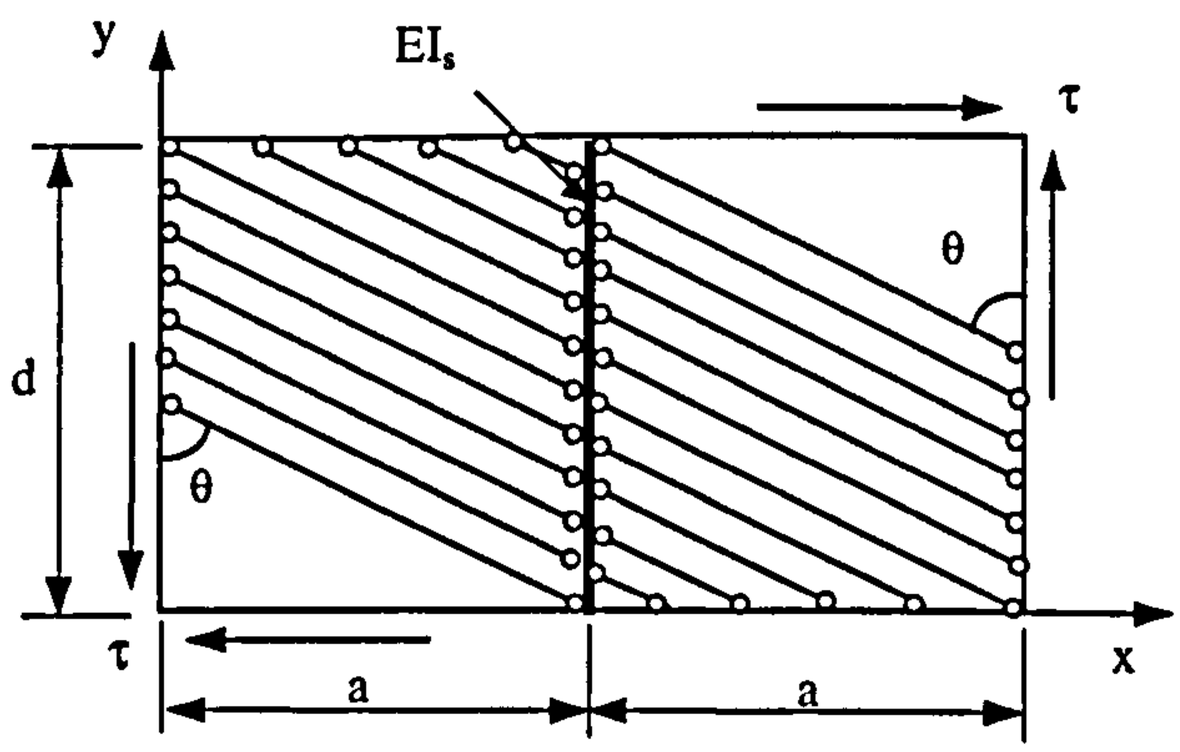


Figure 7.1 Rigid-link model for pure shear

An energy approach is used to calculate the buckling load for the rigid-link model. The overall buckling mode is defined by a deflection shape of the stiffener. In general, the stiffener deflection can be represented by the series:

$$w_s = \sum_{m=1}^{\infty} a_m \sin\frac{m\pi y}{d} \tag{7.1}$$

As a result of w_s, the bending strain energy in the stiffener is given by:

$$U_{sb} = \frac{EI_s}{2}\int_0^d (\frac{\partial^2 w_s}{\partial y^2})^2 dy = \frac{EI_s\pi^4}{4d^3}\sum_{m=1}^{\infty} a_m^2 m^4 \tag{7.2}$$

By denoting the work done by the applied load as T, the total potential energy Π for the rigid-link model can be written as:

$$\Pi = U_{sb} - T \tag{7.3}$$

To minimise the total potential energy, the partial derivative of Π with respect to each of the deflection function amplitude coefficients for the stiffener is set equal to zero

$$\frac{\partial \Pi}{\partial a_m} = 0,\ m=1, 2, \ldots, \infty \tag{7.4}$$

The overall critical stress coefficient k_{cro} and the corresponding buckling mode can be determined from the eigenvalue problem giving by Eqn.7.4. The solutions of Eqn.7.4 for pure shear, compression and pure bending conditions will be discussed in the following sections.

7.2.2 Pure Shear Condition

7.2.2.1 Initially Straight Stiffener, $w_{0s}=0$

It has been found that the overall buckling mode with the lowest buckling load has a stiffener deflection which is closely represented by a half sine wave. Therefore, only the first term in the w_s series 7.1 is considered here for simplicity, that is:

$$w_s = a_1 \sin\frac{\pi y}{d} \tag{7.5}$$

From Eqn.7.2, the strain energy in the stiffener can be expressed as:

$$U_{sb} = \frac{EI_s\pi^4}{4d^3} a_1^2 \tag{7.6}$$

Due to the stiffener deflection w_s, as shown in Fig.7.2, the end of a rigid link at the plate boundary draws in by an amount Δ along the link, and Δ is given by:

$$\Delta = L - \sqrt{L^2 - w_s^2} \approx \frac{1}{2L} w_s^2 \tag{7.7}$$

where L is the length of a rigid link.

The x and y components of the displacement Δ are:

$$\Delta_x = \Delta \cdot \sin\theta \tag{7.8}$$

$$\Delta_y = \Delta \cdot \cos\theta \tag{7.9}$$

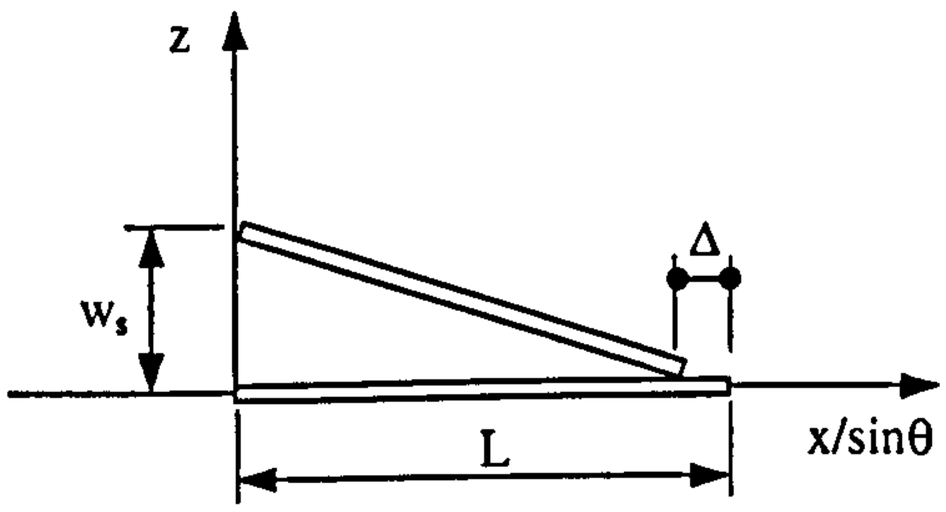


Figure 7.2 Rigid-links, before and after stiffener deflection. Straight stiffener.

Consider in Fig.7.3a, a strip element in the right-hand of the stiffener, which emanates from a point y along the stiffener, where $0 \le y \le y_1$. The work done by the applied shearing force at the end of this strip element is given by:

$$dT_1 = \tau t\, dx \Delta_x = \frac{\tau t}{2} \sin^2\theta \frac{w_s^2}{y} dy \tag{7.10}$$

Similarly, the work done by the applied shearing force at the end of a strip element in the right-hand of the stiffener, which emanates from a point y along the stiffener, where $y_1 \le y \le d$ (Fig.7.3b), may be written as:

$$dT_2 = \tau t\, dy \Delta_y = \frac{\tau t}{2a} \sin\theta \cos\theta\, w_s^2 dy \tag{7.11}$$

Hence, on account of the symmetry of the model, the total work done by the applied shear at the end of the strip elements in both the left and right hands of the stiffener is given by:

$$\begin{aligned} T &= 2(\int_0^{y_1} dT_1 + \int_{y_1}^{d} dT_2) \\ &= \tau t \sin^2\theta \cdot a_1^2 \int_0^{u_1} \frac{\sin^2 u}{u} du + \frac{\tau t d}{\pi a} \sin\theta\cos\theta \cdot a_1^2 \int_{u_1}^{\pi} \sin^2 u du \end{aligned} \tag{7.12}$$

where:

$$u_1 = \begin{cases} \dfrac{\pi a}{d\tan\theta}, & for\ \theta \geq \arctan(\dfrac{a}{d}) \\ \pi, & for\ \theta \leq \arctan(\dfrac{a}{d}) \end{cases} \tag{7.13}$$

$y_1=a/\tan\theta$
$L=y/\cos\theta$
$dx=\tan\theta\,dy$

$y_1=a/\tan\theta$
$L=a/\sin\theta$

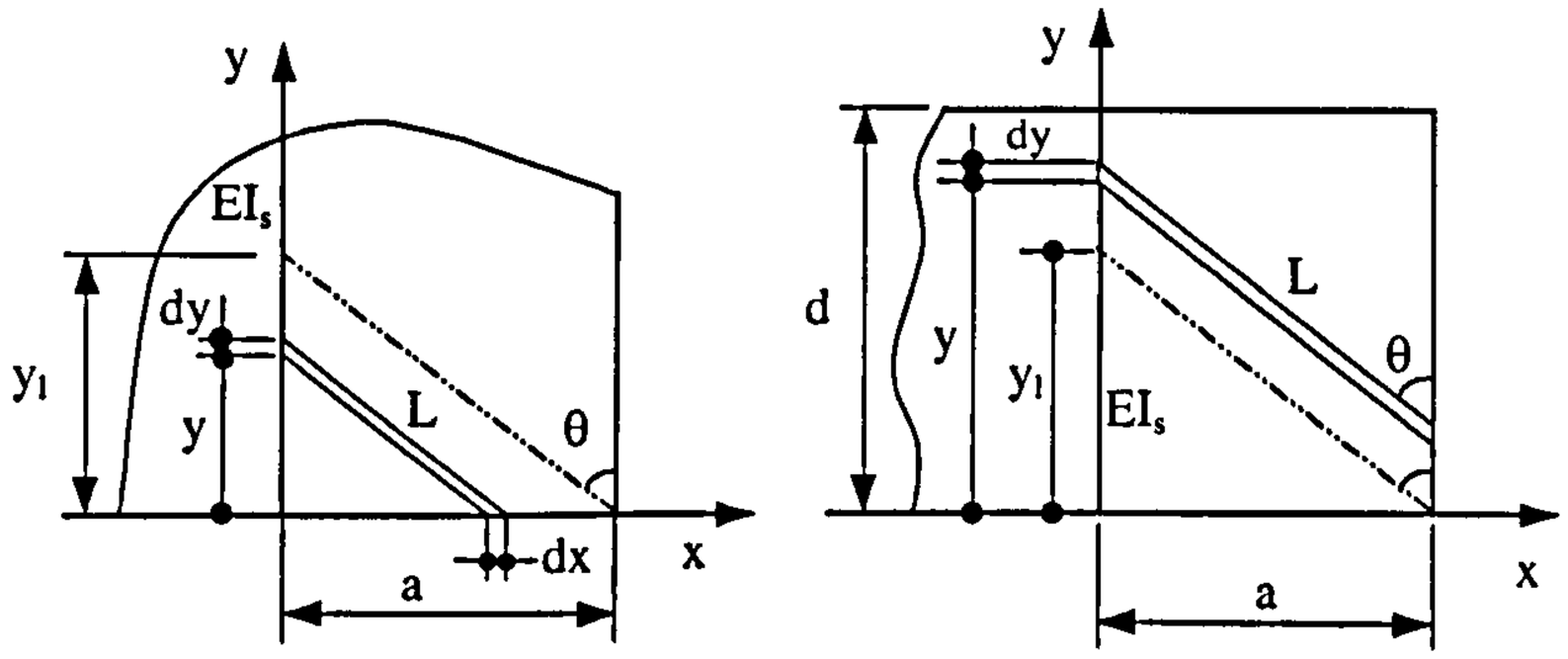


Figure 7.3 Strip Elements

Replacing Eqns.7.3, 7.6 and 7.12 in Eqn.7.4, the following governing equation for overall buckling is obtained:

$$\frac{\pi^4}{2} - 2k_{cro}\sin^2\theta \int_0^{u_1} \frac{\sin^2 u}{u} du - \frac{2k_{cro}}{\pi}\frac{d}{a}\sin\theta\cos\theta \int_{u_1}^{\pi} \sin^2 u du = 0 \tag{7.14}$$

where k_{cro} is the critical stress coefficient defined by:

$$\tau_{cro} = k_{cro} \frac{EI_s}{d^3 t} \tag{7.15}$$

and τ_{cro} is the critical shear stress for the rigid-link model.

k_{cro} from Eqn.7.14 has been presented by Stanway et al [9] in the form of curve fitting equations, where an iteration procedure was employed to search the value of angle θ which gives the minimum k_{cro}. It was demonstrated that as d/a is increased from unity (tall panel) θ tends towards 45°; and as d/a is decreased from unity (long panels) θ is close to the diagonal angle arctan(a/d) of the panels, and tends towards 90°. In order to explore whether an approximate closed-form of k_{cro} could be obtained and simplify the solution procedure, the inclined angle θ is assumed as:

$$\theta = \begin{cases} \arctan(\frac{a}{d}), & for \frac{d}{a} \le 1 \\ 45^\circ, & for \frac{d}{a} \ge 1 \end{cases} \tag{7.16}$$

As a result, the following expressions are obtained for the critical stress coefficient of the rigid-link model:

$$k_{cro} = 20(1+\frac{d^2}{a^2}), \quad for \ \frac{d}{a} \le 1 \tag{7.17a}$$

$$k_{cro} = \left[\sum_{p=1}^{\infty} (-1)^{p+1} \frac{2^{2p}}{(2p)\cdot(2p)!} \cdot \pi^{2p-4} (\frac{a}{d})^{2p} + \frac{1}{\pi^4} \left(\frac{d}{a} - 1 \right) + \frac{d}{2a\pi^5} \sin \frac{2a\pi}{d} \right]^{-1},$$

$$\text{for } \frac{d}{a} \ge 1 \tag{7.17b}$$

By taking 8 terms (*p=8)*, the variation in k_{cro} with aspect ratio of the panels is presented in Fig.7.4, and a good agreement is observed between k_{cro} from Eqn.7.17 and the curves given by Stanway et al [9], especially in the range away from *d/a=1*.

7.2.2.2 Initially Imperfect Stiffener, $w_{0s} \neq 0$

It was concluded by Stanway [1] that the first buckling mode in the rigid-link model is accurately represented by a half sine wave. Therefore, a half sine wave stiffener

imperfection, fully affined to the first buckling mode, is considered, which is expressed as:

$$w_{0s} = w_{0s\,max} \sin \frac{\pi y}{d} \tag{7.18}$$

The stiffener deflection w_s is still represented by Eqn.7.5.

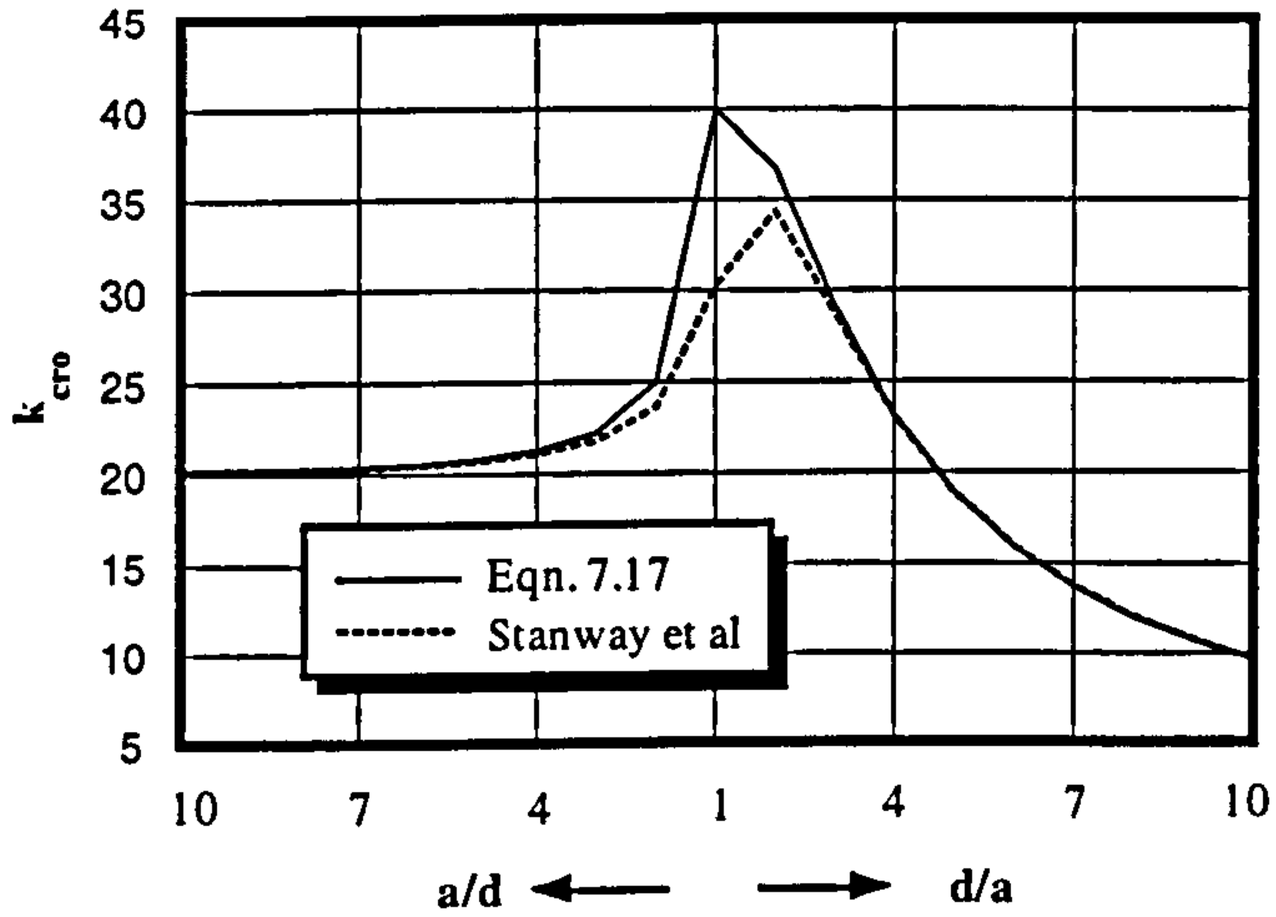


Figure 7.4 Critical buckling stress coefficient for the rigid-link model. Pure shear.

In Fig.7.5, it is shown that the draw-in displacement Δ of the end of a rigid link at the plate boundary, due to the stiffener deflection w_s from the initial position, is given by:

$$\Delta = \sqrt{L^2 - w_{0s}^2} - \sqrt{L^2 - (w_{0s} + w_s)^2} \approx \frac{1}{2L}\left(w_s^2 + 2w_{0s}w_s\right) \tag{7.19}$$

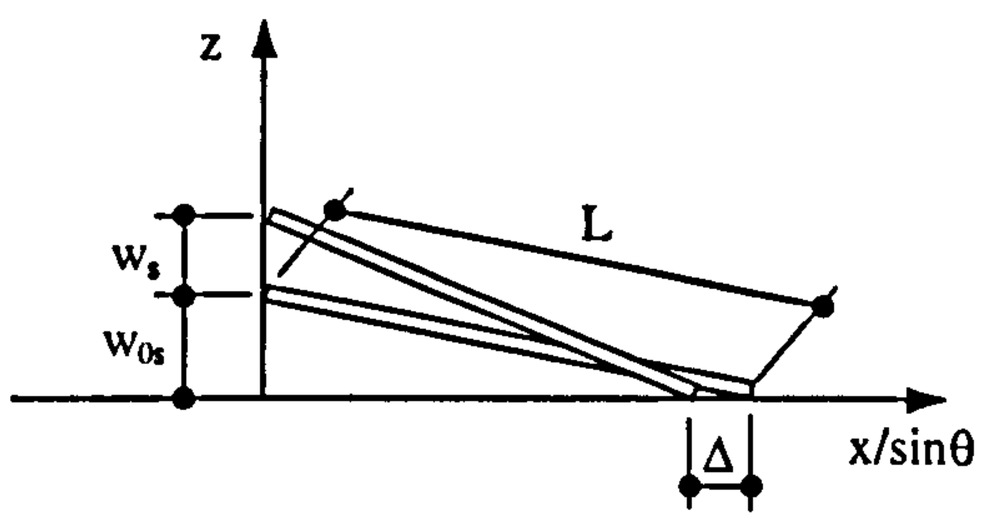


Figure 7.5 Rigid-links, before and after stiffener deflection. Imperfect stiffener.

Using the same procedure as in Section 7.2.2.1, but replacing Δ in Eqn.7.7 with Δ from Eqn.7.19, the following equation for the stiffener deflection w_s is obtained:

$$w_s = \left(\frac{\tau / \tau_{cro}}{1 - \tau / \tau_{cro}} \right) w_{0s\max} \sin \frac{\pi y}{d} \tag{7.20}$$

Using $M_s / EI_s = \partial^2 w_s / \partial y^2$ and Eqn.7.20, the stiffener bending moment for the rigid-link model can be expressed as:

$$M_s = \frac{\pi^2 EI_s w_{0s\max}}{d^2} \left(\frac{\tau / \tau_{cro}}{1 - \tau / \tau_{cro}} \right) \sin \frac{\pi y}{d} \tag{7.21}$$

For the required stiffener, $1 - \tau / \tau_{cro} \approx 1$, and Eqn.7.21 reduces to:

$$M_s = \tau t \left(\frac{d\pi^2 w_{0s\max}}{k_{cro}} \right) \sin \frac{\pi y}{d} \tag{7.22}$$

The result in Eqn.7.22 was used by Stanway et al [9] with the stiffener moment from the straight knife edge to propose a method for predicting the bending moment for design of stiffeners.

7.2.3 Compressive Loading Condition

7.2.3.1 Initially Straight Stiffener, $w_{0s}=0$

Since the applied compressive forces act only on the vertical boundaries of the plate and are in the x direction, as shown in Fig.7.6, the links in the applied stress direction will produce the greatest work done by the applied compressive stresses, and hence the lowest buckling load. Therefore, the inclined angle θ in Fig.7.1 is set to 90° for compressive loading condition.

It is expected that the stiffener will deflect in the form of a half sine wave in the first overall buckling mode of the rigid-link model when subjected to uniaxial compression. Therefore, w_s given in Eqn.7.5 is adopted in this section, and the strain energy in the stiffener is the same as given in Eqn.7.6.

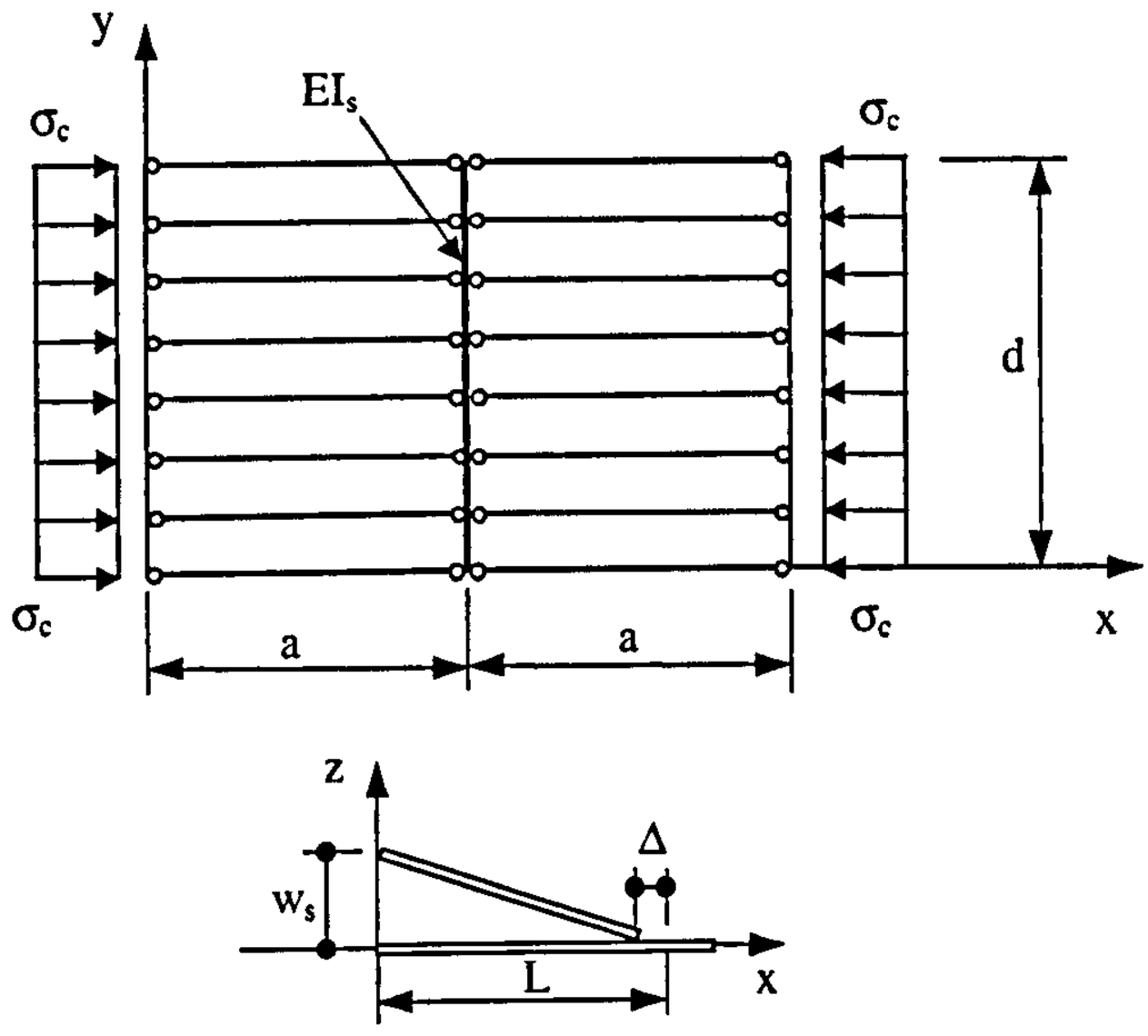


Figure 7.6 Rigid-link model for compression

Due to the stiffener deflection w_s, as shown in Fig.7.6, the end of a rigid link at the plate boundary draws in by an amount Δ along the link, and Δ is given by:

$$\Delta = L - \sqrt{L^2 - w_s^2} \approx \frac{1}{2L} w_s^2 \tag{7.23}$$

where L is the length of a rigid link, L=a.

The work done by the applied compressive force at the end of a rigid link is given by:

$$dT = \sigma_c t\, dy \Delta = \frac{\sigma_c t}{2a} \cdot w_s^2 dy \tag{7.24}$$

Hence, the total work done by the applied compression stress at the end of the strip elements in both the left and right hands of the stiffener is given by:

$$T = 2\int_0^d dT = \frac{\sigma_c t d}{2a} \cdot a_1^2 \tag{7.25}$$

Replacing Eqns.7.3, 7.6 and 7.25 in Eqn.7.4, the following overall buckling stress coefficient k_{cro} is obtained:

$$k_{cro} = \frac{\pi^4}{2}\frac{a}{d} \tag{7.26}$$

where k_{cro} is defined by:

$$\sigma_{c,cro} = k_{cro}\frac{EI_s}{d^3 t} \tag{7.27}$$

and $\sigma_{c,cro}$ is the critical compressive stress for the rigid-link model.

7.2.3.2 Initially Imperfect Stiffener, $w_{0s} \neq 0$

A half sine wave stiffener imperfection as given in Eqn.7.18 is considered, which is fully affined to the first buckling mode of the rigid-link model. The stiffener deflection w_s is represented by Eqn. 7.5.

In Fig.7.5, it is shown that the draw-in displacement Δ of the end of a rigid link at the plate boundary, due to the stiffener deflection w_s from the initial position, is given by:

$$\Delta = \sqrt{L^2 - w_{0s}^2} - \sqrt{L^2 - (w_{0s} + w_s)^2} \approx \frac{1}{2L}\left(w_s^2 + 2w_{0s}w_s\right) \tag{7.28}$$

where L is the length of a rigid link, $L=a$.

Using the same procedure as in Section 7.2.3.1, but replacing Δ in Eqn.7.23 with Δ from Eqn.7.28, the following equation for the stiffener deflection w_s is obtained:

$$w_s = \left(\frac{\sigma_c/\sigma_{c,cro}}{1-\sigma_c/\sigma_{c,cro}}\right) w_{0s\,\max} \sin\frac{\pi y}{d} \tag{7.29}$$

Using $M_s/EI_s = \partial^2 w_s/\partial y^2$ and Eqn.7.29, the stiffener bending moment for the rigid-link model can be written as:

$$M_s = \frac{\pi^2 EI_s w_{0s\,\max}}{d^2}\left(\frac{\sigma_c/\sigma_{c,cro}}{1-\sigma_c/\sigma_{c,cro}}\right)\sin\frac{\pi y}{d} \tag{7.30}$$

For the required stiffener, $1-\sigma_c/\sigma_{c,cro} \approx 1$, and Eqn.7.30 reduces to:

$$M_s = \sigma_c t\left(\frac{d\pi^2 w_{0s\,\max}}{k_{cro}}\right)\sin\frac{\pi y}{d} \tag{7.31}$$

where k_{cro} is given by Eqn.7.26.

7.2.4 Pure Bending Condition

7.2.4.1 Initially Straight Stiffener, $w_{0s}=0$

As shown in Fig.7.7, the applied bending stresses can be written as:

$$\sigma = \sigma_b(2y/d - 1) \tag{7.32}$$

where σ_b is the compressive bending stress at $y=d$, and σ is positive for compression, and vice versa. The inclined angle θ in Fig.7.1 is taken as 90° for pure bending loading condition.

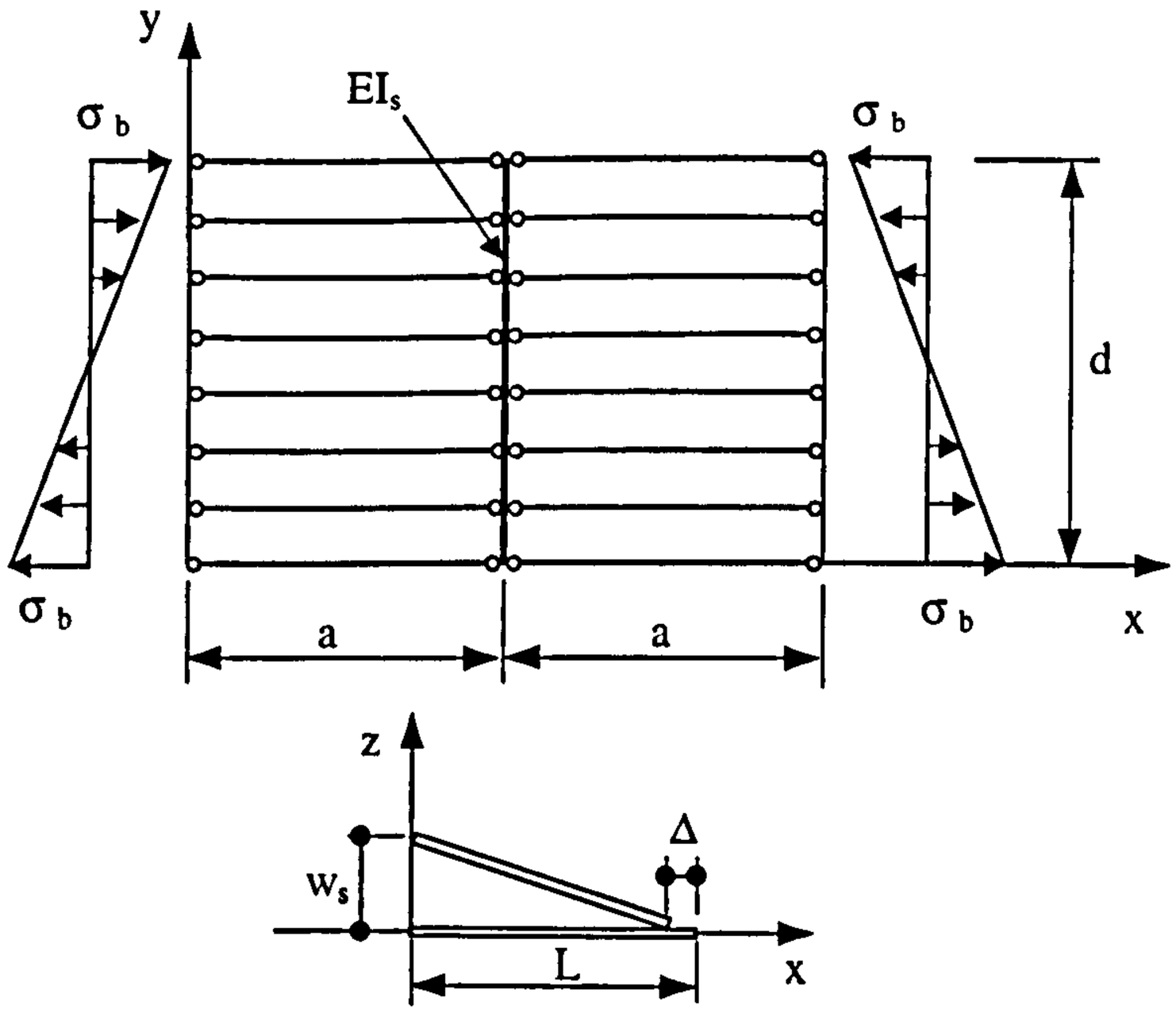


Figure 7.7 Rigid-link model for pure bending

For the rigid-link model subjected to pure bending, the deflection shape of the stiffener will not be in a half sine wave in the first overall buckling mode. Initially, the first four terms in the w_s series 7.1 are considered here, that is:

$$w_s = \sum_{m=1}^{4} a_m \sin\frac{m\pi y}{d} \tag{7.33}$$

The draw-in displacement Δ of the end of a rigid link at the plate boundary is in the x–axis direction and takes the same form as Eqn.7.23.

The work done by the applied bending load at the end of a rigid link is given by:

$$dT = \sigma t dy\Delta = \frac{\sigma_b t}{2a}\cdot(2y/d-1)w_s^2 dy \tag{7.34}$$

Consequently, the total work done by the applied bending stress at the end of the strip elements in both the left and right hands of the stiffener is given by:

$$T = 2\int_0^d dT = -\frac{32\sigma_b t d}{\pi^2 a}\left(\frac{1}{9}a_1a_2 + \frac{3}{25}a_2a_3 + \frac{6}{49}a_3a_4 + \frac{2}{225}a_1a_4\right) \tag{7.35}$$

The bending strain energy in the stiffener may be written as:

$$U_{sb} = \frac{EI_s\pi^4}{4d^3}\left(a_1^2 + 16a_2^2 + 81a_3^2 + 256a_4^2\right) \tag{7.36}$$

Replacing Eqns.7.3, 7.35 and 7.36 in Eqn.7.4, the following overall buckling stress coefficient k_{cro} is obtained:

$$k_{cro} = 533.908\frac{a}{d} \tag{7.37}$$

where k_{cro} is defined by:

$$\sigma_{b,cro} = k_{cro}\frac{EI_s}{d^3 t} \tag{7.38}$$

and $\sigma_{b,cro}$ is the critical bending stress for the rigid-link model.

For the first overall buckling mode of the rigid-link model subjected to pure bending, the relative ratios of the deflection function amplitude coefficients are found to be:

$$a_1 : a_2 : a_3 : a_4 = 1 : (-0.2508) : 0.01491 : (-0.03) \tag{7.39}$$

It is apparent from Eqn.7.39 that the first two terms in the w_s series are dominant. If only the first two terms are considered, the Eqns.7.37 and 7.39 becomes:

$$k_{cro} = \frac{9\pi^6}{16} \cdot \frac{a}{d} \approx 540.781 \frac{a}{d} \tag{7.37a}$$

$$a_1 : a_2 = 1 : (-0.25) \tag{7.39a}$$

7.2.4.2 Initially Imperfect Stiffener, $w_{0s} \neq 0$

A stiffener imperfection fully affine to the first buckling mode of the rigid-link model is considered. For simplicity, only the first two terms are taken in the w_s series 7.1. Correspondingly, the stiffener imperfection w_{0s} is represented by:

$$w_{0s} = a_{01} \sin \frac{\pi y}{d} + a_{02} \sin \frac{2\pi y}{d} \tag{7.40}$$

where $a_{01} = -4a_{02}$.

Using the same procedure as in the above sections, the stiffener deflection w_s is found to be:

$$w_s = \left(\frac{\sigma_b / \sigma_{b,cro}}{1 - \sigma_b / \sigma_{b,cro}} \right) w_{0s} \tag{7.41}$$

Using $M_s / EI_s = \partial^2 w_s / \partial y^2$ and Eqn.7.41, the stiffener bending moment for the rigid-link model can be written as:

$$M_s = \frac{\pi^2 EI_s}{d^2} \left(\frac{\sigma_b / \sigma_{b,cro}}{1 - \sigma_b / \sigma_{b,cro}} \right) w_{0s} \tag{7.42}$$

For a stiffener required, $1 - \sigma_b / \sigma_{b,cro} \approx 1$, and Eqn.7.42 reduces to:

$$M_s = \sigma_b t \left(\frac{d\pi^2}{k_{cro}} \right) w_{0s} \tag{7.43}$$

where k_{cro} is given in Eqn.7.37a.

7.2.5 Discussion

The rigid-link model enables the overall buckling tendency of stiffened plates to be distinguished and quantified, which is otherwise difficult to quantify for the stiffened plates owing to the presence, in varying proportions, of both overall and local buckling in critical modes. Further, by applying the lateral distributed force from the straight knife edge on the stiffener, the rigid-link model can be used to represent the combination of the overall effects and the panel bending effects. Nevertheless, as the panels are modelled as a series of rigid pin-ended links, the overall buckling capacity of the panels is not taken into account. As a result, the critical buckling stress coefficient k_{cro} is only a function of panel aspect ratio d/a, and the critical buckling stress increases linearly with the stiffener rigidity Ψ, starting from zero as $\Psi=0$. However, for $\Psi=0$, k_{cro} should be equal to the overall critical buckling stress coefficient for the unstiffened plate.

In the presence of shear loading, the rigid links should be at an angle θ inclined to the plate boundary, which varies to give the minimum buckling load and can not be expressed in a closed-form function. In fact, an iteration procedure is required for each value of d/a to find the inclined angle θ which gives the minimum k_{cro}. This leads to a large number of numerical calculations to be involved in finding k_{cro}. An attempt is made for pure shear loading condition by assigning a prescribed value to θ, and the results show a certain difference when d/a is about unity, where the overall effects are not important [9]. Furthermore, there is no apparent physical meaning of the angle θ, although it is close to the direction of the principal compressive stress.

On account of the presence of a uniform stress field, it is expected that the rigid-link model may be applicable in the loading conditions of combined shear and compression. On the other hand, due to the presence of a non-uniform stress field, it seems impossible for the rigid-link model to represent the stiffened plates subjected to combined shear and in-plane bending. A possible alternative approach is to establish the rigid-link models for each loading component separately, and then to combine them together using some interaction equations.

Based on the above consideration, an alternative overall buckling model consisting of a stiffener and plate panels, referred to as *beam-plate model*, is proposed in the following section.

7.3 BEAM-PLATE MODEL

7.3.1 Basis of the Model

The proposed beam-plate model is also based on the two-panel stiffened plate. The model, as shown in Fig.7.8, is identical to the configuration of the stiffened plates. The plate is assumed to be simply supported along all four edges.

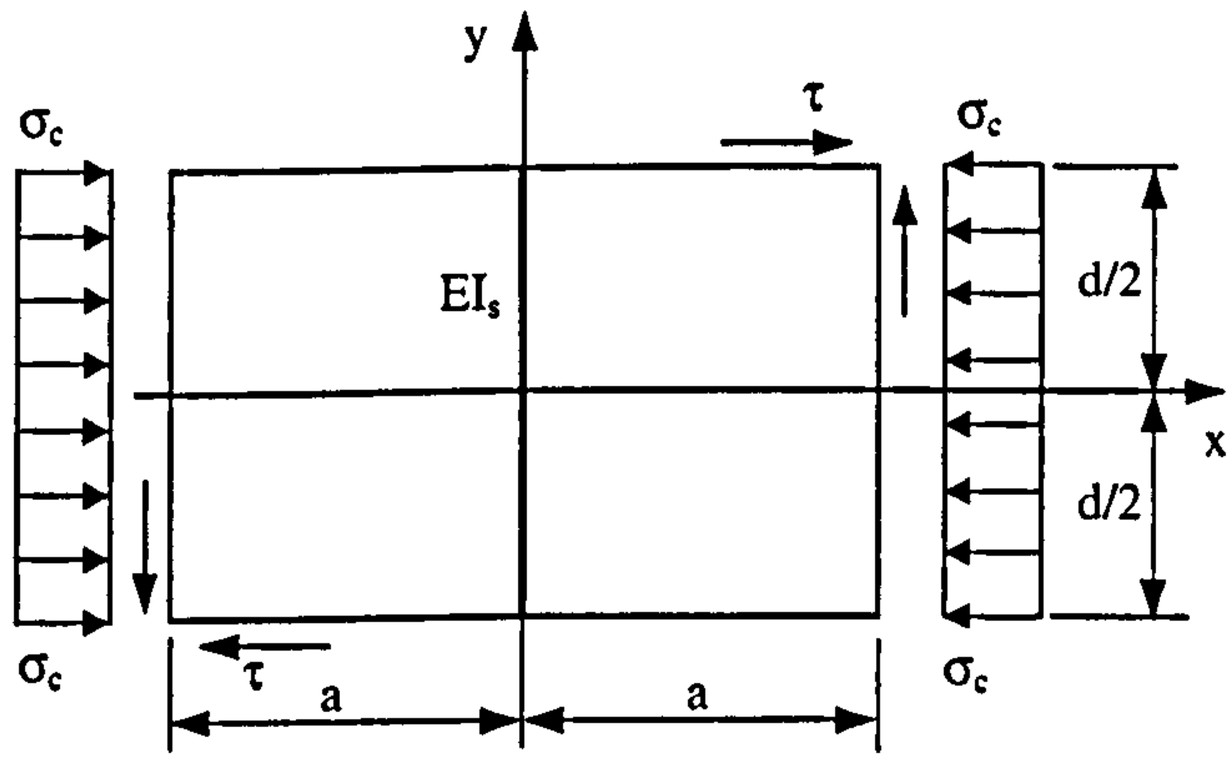


Figure 7.8 Beam-plate model, shear and compression

The proposed overall buckling model assumes a buckling mode by choosing the following deflection function:

$$w = \left(A_1 + A_2 \frac{x}{a}\frac{y}{d} \right) \cos\frac{\pi x}{2a} \cos\frac{\pi y}{d} \qquad (7.44)$$

or:

$$w = A_1 \left(1 + C \frac{x}{a}\frac{y}{d} \right) \cos\frac{\pi x}{2a} \cos\frac{\pi y}{d} \qquad (7.44a)$$

where A_1 and A_2 are coefficients to be determined to give a minimum critical buckling load, and $C=A_2/A_1$.

The reason for choosing the deflection function giving in Eqn. 7.44 is that the preferred overall buckling mode for a stiffened plate under shear has inclined and curved nodal lines. The bracket term in Eqn.7.44a is introduced to take account of this fact observed in the numerical buckling analysis, and it generates a buckle which is symmetrical about a line oblique to the plate boundaries, and not symmetrical about the diagonal line of the plate. A further consideration is that by using this simple deflection function, the results of critical buckling load and the corresponding buckling modes may be expressed in closed-form equations.

The overall buckling mode is assumed to be the same as for the unstiffened plates. Consequently, the overall critical buckling load is derived by an energy method in two steps:

1) Find the overall buckling mode for the plate without stiffener ($\Psi=0$). The deflection function in Eqn.7.44 is adopted, and a relationship between the coefficients A_1 and A_2 is obtained which defines the overall buckling mode.

2) Determine the overall critical buckling load for the stiffened plate having the same plate panels but the stiffener rigidity $\Psi\neq0$. The deflection function is in the same form of Eqn.7.44, but the relationship obtained between the coefficients A_1 and A_2 is imposed. Therefore, there is only one independent coefficient in the deflection function in this step.

From Eqn.7.44, the deflection of the stiffener can be obtained:

$$w_s = w\big|_{x=0} = A_1 \cos\frac{\pi y}{d} \tag{7.45}$$

which is in the same form as assumed in the rigid-link model, that is, the stiffener deflects into a half sine wave in the overall buckling mode.

The strain energy of bending in the panels, due to the deflection w, is given by:

$$U_{pb} = \frac{D}{2}\int_{-a}^{a}\int_{-\frac{d}{2}}^{\frac{d}{2}}\left\{\left(\frac{\partial^2 w}{\partial x^2}+\frac{\partial^2 w}{\partial y^2}\right)^2 - 2(1-\nu)\left[\frac{\partial^2 w}{\partial x^2}\cdot\frac{\partial^2 w}{\partial y^2}-\left(\frac{\partial^2 w}{\partial x \partial y}\right)^2\right]\right\}dxdy \quad (7.46)$$

By substituting Eqn.7.44 into Eqn.7.46, we obtain:

$$U_{pb} = \frac{Dad\pi^4}{4}\left(\frac{1}{4a^2}+\frac{1}{d^2}\right)^2 A_1^2 + \frac{D}{8ad}\left(\frac{\pi^2}{6}+1\right)^2 A_2^2$$
$$+\frac{Dad}{4}\left(\frac{\pi^2}{6}+11\right)\left(\frac{\pi^2}{6}-1\right)\left(\frac{1}{16a^4}+\frac{1}{d^4}\right)A_2^2 \quad (7.47)$$

The strain energy of the stiffener due to bending is:

$$U_{sb} = \frac{EI_s}{2}\int_{-\frac{d}{2}}^{\frac{d}{2}}\left(\frac{\partial^2 w_s}{\partial y^2}\right)^2 dy = \frac{EI_s\pi^4}{4d^3}A_1^2 \quad (7.48)$$

The twisting strain energy in the stiffener is not considered.

By denoting the work done by the applied load as T, the total potential energy Π for the beam-plate model can be written as:

$$\Pi = U_{pb} + U_{sb} - T \quad (7.49)$$

To minimise the total potential energy, the partial derivative of Π with respect to each of the deflection function amplitude coefficients is set equal to zero:

$$\frac{\partial \Pi}{\partial A_m} = 0, \text{ m=1, 2} \quad (7.50)$$

The overall critical stress coefficient, denoted by k_{ov} to distinguish from k_{cro} used for the rigid-link model, and the corresponding buckling mode, can be determined from the eigenvalue problem giving by Eqn.7.50. The solutions of Eqn.7.50 for pure shear, compression, pure bending, and external stiffener force loading conditions will be discussed in the following sections.

7.3.2 Pure Shear Condition

7.3.2.1 Initially Straight Stiffener, $w_{0s}=0$

- **STEP 1.** ***Find the overall buckling mode, $\Psi=0$:***

The total potential energy for a plate without a stiffener is given by:

$$\Pi = U_{pb} - T_\tau \tag{7.51}$$

The work done by the applied shearing forces is:

$$T_\tau = -\tau t \int_{-a}^{a} \int_{-\frac{d}{2}}^{\frac{d}{2}} \frac{\partial w}{\partial x}\frac{\partial w}{\partial y} dxdy = \frac{\tau t}{4} A_1 A_2 \tag{7.52}$$

Replacing Eqns.7.46, 7.51 and 7.52 in Eqn.7.50, the following governing equations for overall buckling are obtained:

$$\frac{Dad\pi^4}{2}\left(\frac{1}{4a^2}+\frac{1}{d^2}\right)A_1 - \frac{\tau_{cr} t}{4} A_2 = 0 \tag{7.53}$$

$$-\frac{\tau_{cr} t}{4} A_1 + \left\{\frac{Dad}{2}\left(\frac{\pi^2}{6}+11\right)\left(\frac{\pi^2}{6}-1\right)\left(\frac{1}{16a^4}+\frac{1}{d^4}\right)+\frac{D}{4ad}\left(\frac{\pi^2}{6}+1\right)^2\right\}A_2 = 0$$

(7.54)

From these equations, the overall critical stress coefficient k_{ov} for the plate without stiffener ($\Psi=0$) is obtained:

$$k_{ov}^0 = \frac{b^2}{d^2}\left(\frac{d^2}{4a^2}+1\right)\sqrt{\left(\frac{\pi^2}{6}+11\right)\left(\frac{\pi^2}{6}-1\right)\left(\frac{d^2}{4a^2}+\frac{4a^2}{d^2}\right)+2\left(\frac{\pi^2}{6}+1\right)^2}$$
$$\approx \frac{b^2}{d^2}\left(\frac{d^2}{4a^2}+1\right)\sqrt{8.155\left(\frac{d^2}{4a^2}+\frac{4a^2}{d^2}\right)+13.99}$$

(7.55)

where the Poisson ratio $\nu=0.3$, and k_{ov} is defined by:

$$\tau_{ov} = k_{ov} \frac{\pi^2 D}{b^2 t} \tag{7.56}$$

and τ_{ov} is the critical shear stress for the beam-plate model. The superscript "*0*" in Eqn.7.55 stands for Ψ=0.

The overall critical stress coefficient k^0_{ov} given in Eqn.7.55 is compared in Fig.7.9 with the numerical results and the critical shear stress given by Stanway et al [9]. It should be indicated that the latter is given for the minimum buckling load, and the corresponding buckling mode may not be a full overall mode. It is shown that the beam-plate model produces a good estimation of the overall buckling stress for the plate panels.

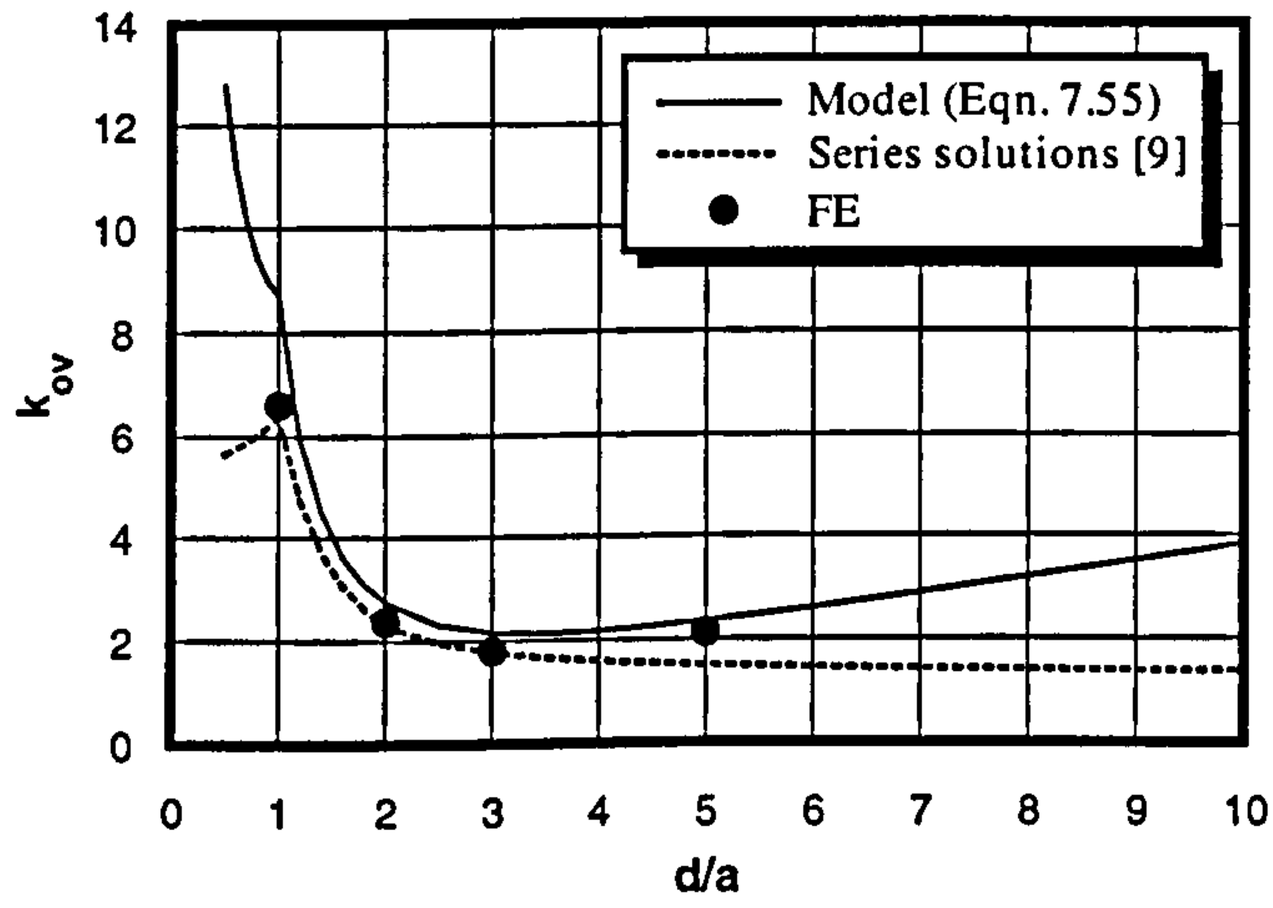


Figure 7.9 Comparison of the critical buckling stress coefficients. Pure Shear, Ψ=0

The relation between the coefficients A_1 and A_2 is giving by:

$$A_2 = \frac{2\pi^2}{k^0_{ov}} \cdot \frac{ab^2}{d^3} \left(\frac{d^2}{4a^2} + 1 \right)^2 A_1 \tag{7.57}$$

Therefore, the overall buckling mode for the stiffened plate can be written as:

$$w = A_1 \cos\frac{\pi x}{2a} \cos\frac{\pi y}{d} \left(1 + C \frac{x}{a} \frac{y}{d} \right), \tag{7.58}$$

where:

$$C=\frac{A_2}{A_1}=\frac{2\pi^2}{k_{ov}^0}\cdot\frac{ab^2}{d^3}\left(\frac{d^2}{4a^2}+1\right)^2 \tag{7.59}$$

- **STEP 2.** ***Determine the critical stress of stiffened plates, $\Psi\neq 0$:***

For a stiffened plate with a stiffener $\Psi\neq 0$, the deflection function is taken as that given in Eqns.7.58 and 7.59. By substituting Eqn.7.58 into Eqns.7.47, and 7.52 separately, and using Eqns.7.48 and 7.49,we obtain the total potential energy:

$$\begin{aligned}\Pi=&\frac{Dad\pi^4}{4}\left(\frac{1}{4a^2}+\frac{1}{d^2}\right)^2A_1^2+\frac{Dad}{4}\left(\frac{\pi^2}{6}+11\right)\left(\frac{\pi^2}{6}-1\right)\left(\frac{1}{16a^4}+\frac{1}{d^4}\right)C^2A_1^2\\&+\frac{D}{8ad}\left(\frac{\pi^2}{6}+1\right)^2C^2A_1^2+\frac{EI_s\pi^4}{4d^3}A_1^2-\frac{\tau t}{4}CA_1^2\end{aligned} \tag{7.60}$$

In terms of equation $\frac{\partial\Pi}{\partial A_1}=0$, the overall critical stress coefficient k_{ov} can be found:

$$\begin{aligned}k_{ov}=&\frac{b^2}{d^2}\sqrt{\left(\frac{\pi^2}{6}+11\right)\left(\frac{\pi^2}{6}-1\right)\left(\frac{d^2}{4a^2}+\frac{4a^2}{d^2}\right)+2\left(\frac{\pi^2}{6}+1\right)^2}\\&\cdot\left[\left(\frac{d^2}{4a^2}+1\right)^2+\frac{b}{2a}\Psi\right]\Big/\left(\frac{d^2}{4a^2}+1\right)\\\approx&\frac{b^2}{d^2}\sqrt{8.155\left(\frac{d^2}{4a^2}+\frac{4a^2}{d^2}\right)+13.99}\cdot\left[\left(\frac{d^2}{4a^2}+1\right)^2+\frac{b}{2a}\Psi\right]\Big/\left(\frac{d^2}{4a^2}+1\right)\end{aligned} \tag{7.61}$$

The variation in k_{ov} with respect to the stiffener rigidity Ψ is presented in Fig.7.10, where the results for the rigid-link model given by Stanway et al [9] are shown for comparison. For d/a=5, the numerical results for the overall buckling modes are also included.

7.3.2.2 Initially Imperfect Stiffener, $w_{0s}\neq 0$

An imperfection fully affine to the overall critical buckling mode of the beam-plate model is considered, which can be expressed as:

$$w_0 = A_{01}\cos\frac{\pi x}{2a}\cos\frac{\pi y}{d}\left(1+C\frac{x}{a}\frac{y}{d}\right) \tag{7.62}$$

and the stiffener imperfection is:

$$w_{0s} = w\big|_{x=0} = A_{01}\cos\frac{\pi y}{d} \tag{7.63}$$

where the amplitude coefficient A_{01} is taken as w_{0smax} envisaged in BS5400. The additional deflection w is still represented by Eqn.7.58.

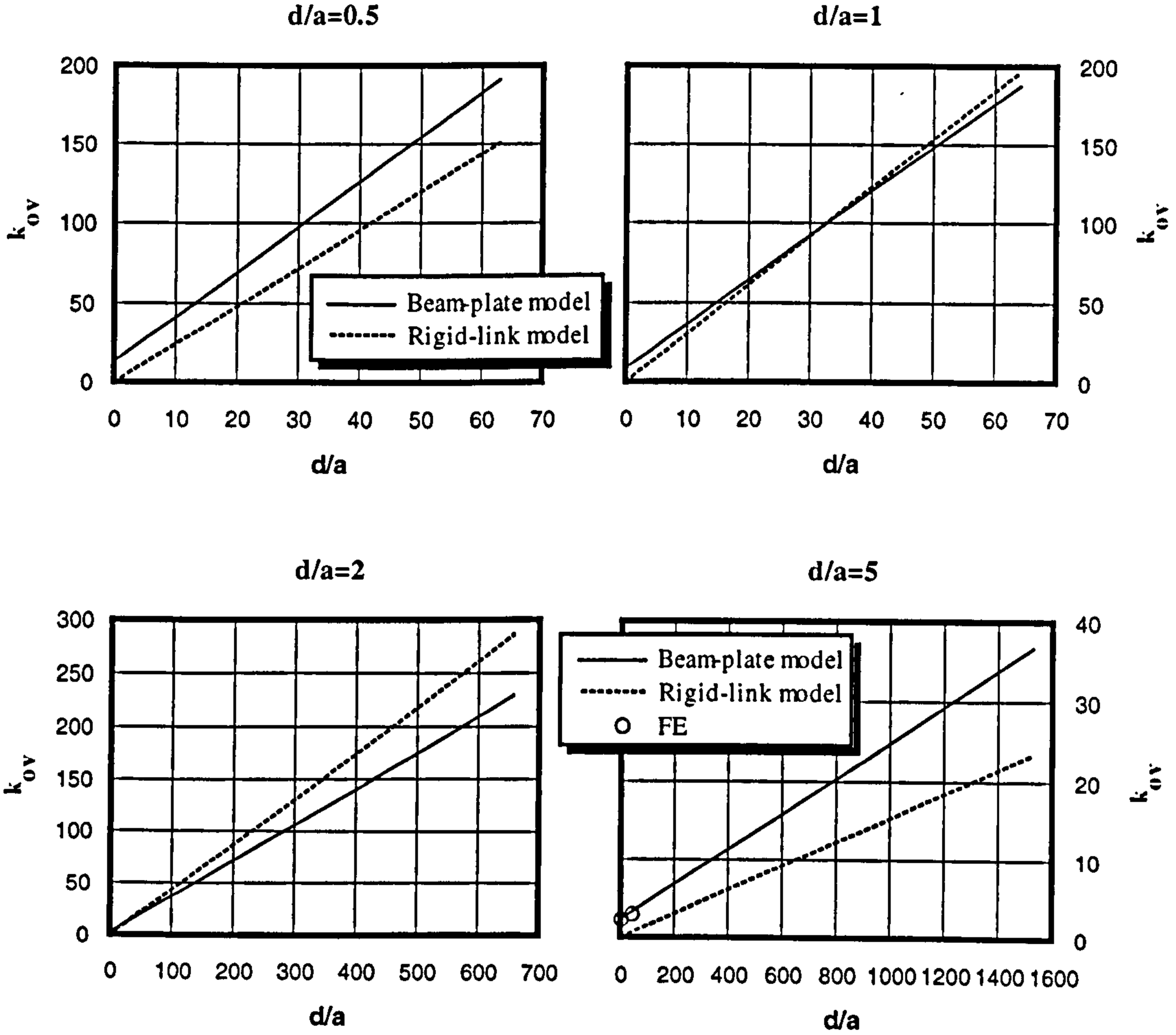


Figure 7.10 Overall buckling stress coefficients. Pure shear

The effect of forces acting in the middle plane of the plate on bending depends not only on w but also on w_0. For linear buckling analysis, the work done by the applied shearing forces can be expressed as:

$$T_\tau = -\tau t \int_{-a}^{a} \int_{-\frac{d}{2}}^{\frac{d}{2}} \left[\left(\frac{\partial w}{\partial x} + \frac{\partial w_0}{\partial x} \right) \left(\frac{\partial w}{\partial y} + \frac{\partial w_0}{\partial y} \right) - \frac{\partial w_0}{\partial x} \frac{\partial w_0}{\partial y} \right] dxdy \tag{7.64}$$
$$= \frac{\tau t}{4} C \left(A_1^{\,2} + 2 A_{01} A_1 \right)$$

Using the same procedure as in Section 7.3.2.1, but replacing T_τ in Eqn.52 with T_τ from Eqn.7.64, the following equation for the additional deflection w is obtained:

$$w = \left(\frac{\tau / \tau_{ov}}{1 - \tau / \tau_{ov}} \right) w_0 \tag{7.65}$$

Therefore, the additional stiffener deflection w_s is:

$$w_s = \left(\frac{\tau / \tau_{ov}}{1 - \tau / \tau_{ov}} \right) w_{0s\,\max} \cos \frac{\pi y}{d} \tag{7.66}$$

Using $M_s / EI_s = \partial^2 w_s / \partial y^2$ and Eqn.7.66, the maximum bending moment along the stiffener for the beam-plate model can be found:

$$M_s = \frac{\pi^2 E I_s w_{0s\,\max}}{d^2} \left(\frac{\tau / \tau_{ov}}{1 - \tau / \tau_{ov}} \right) \tag{7.67}$$

The bending moment M_s from the beam-plate model represents the component of the stiffener moment due to the overall buckling effect, denoted as M_{ov}. The result in Eqn.7.67 will be incorporated in Section 7.4 with the stiffener moments for other loading components to formulate an interaction equation for predicting the bending moment due to the overall buckling effect.

7.3.3 Compressive Loading Condition

7.3.3.1 Initially Straight Stiffener, $w_{0s}=0$

- **STEP 1.** ***Find the overall buckling mode, $\Psi=0$:***

The work done by the applied compressive forces is:

$$T_c = \frac{1}{2}\sigma_c t \int_{-a}^{a}\int_{-\frac{d}{2}}^{\frac{d}{2}} \left(\frac{\partial w}{\partial x}\right)^2 dxdy \tag{7.68}$$

Using the deflection function giving in Eqn. 7.44, the above equation becomes:

$$T_c = \frac{\pi^2 d\,t}{16a}\sigma_c A_1^2 + \frac{d\,t}{16\pi^2 a}\left(\frac{\pi^4}{36}-1\right)\sigma_c A_2^2 \tag{7.69}$$

Using the same procedure as in Section 7.3.2.1, but replacing T_τ with T_c, the following solution for the critical buckling load is obtained:

$$\sigma^0_{c,ov1} = \frac{\pi^2 D}{d^2 t}\left(\frac{d}{2a}+\frac{2a}{d}\right)^2 \tag{7.70}$$

$$\sigma^0_{c,ov2} = \frac{\pi^2 D}{d^2 t}\left\{\left(\frac{\pi^2}{6}+11\right)\left(\frac{\pi^2}{6}-1\right)\left(\frac{d^2}{4a^2}+\frac{4a^2}{d^2}\right)+2\left(\frac{\pi^2}{6}+1\right)^2\right\}\Big/\left(\frac{\pi^4}{36}-1\right) \tag{7.71}$$

It is apparent that the critical stress $\sigma^0_{c,ov1}$ is the correct solution, and $\sigma^0_{c,ov2}$ should be discarded.

The overall buckling mode corresponding to the critical stress $\sigma^0_{c,ov1}$ is:

$$w = A_1 \cos\frac{\pi x}{2a}\cos\frac{\pi y}{d} \tag{7.72}$$

The overall critical stress coefficient k_{ov} for the plate without stiffener (Ψ=0) is:

$$k^0_{ov} = \frac{b^2}{d^2}\left(\frac{d}{2a}+\frac{2a}{d}\right)^2 \tag{7.73}$$

- **STEP 2.** ***Determine the critical stress of stiffened plates, $\Psi\neq 0$:***

For a stiffened plate with a stiffener $\Psi\neq 0$, the deflection function is taken as that given in Eqn.7.72. By substituting Eqn.7.72 into Eqns.7.47 and 7.69 separately, and using Eqns.7.48 and 7.49,we obtain the total potential energy:

$$\Pi = \frac{Dad\pi^4}{4}\left(\frac{1}{4a^2}+\frac{1}{d^2}\right)^2 A_1^2 + \frac{EI_s\pi^4}{4d^3}A_1^2 - \frac{\pi^2 dt}{16a}\sigma_c A_1^2 \tag{7.74}$$

In terms of equation $\frac{\partial \Pi}{\partial A_1} = 0$, the overall critical stress coefficient $k_{c,ov}$ can be found:

$$k_{ov} = \frac{b^2}{d^2}\left[\left(\frac{d}{2a}+\frac{2a}{d}\right)^2+\frac{4ab}{d^2}\Psi\right] \tag{7.75}$$

where k_{ov} is defined by:

$$\sigma_{c,ov} = k_{ov}\frac{\pi^2 D}{b^2 t} \tag{7.76}$$

The variation in k_{ov} with respect to the stiffener rigidity Ψ is presented in Fig.7.11, where the results for the rigid-link model, given by Eqns.7.26 and 7.27, are shown for comparison. For d/a=5, the numerical results for the overall buckling modes are also included.

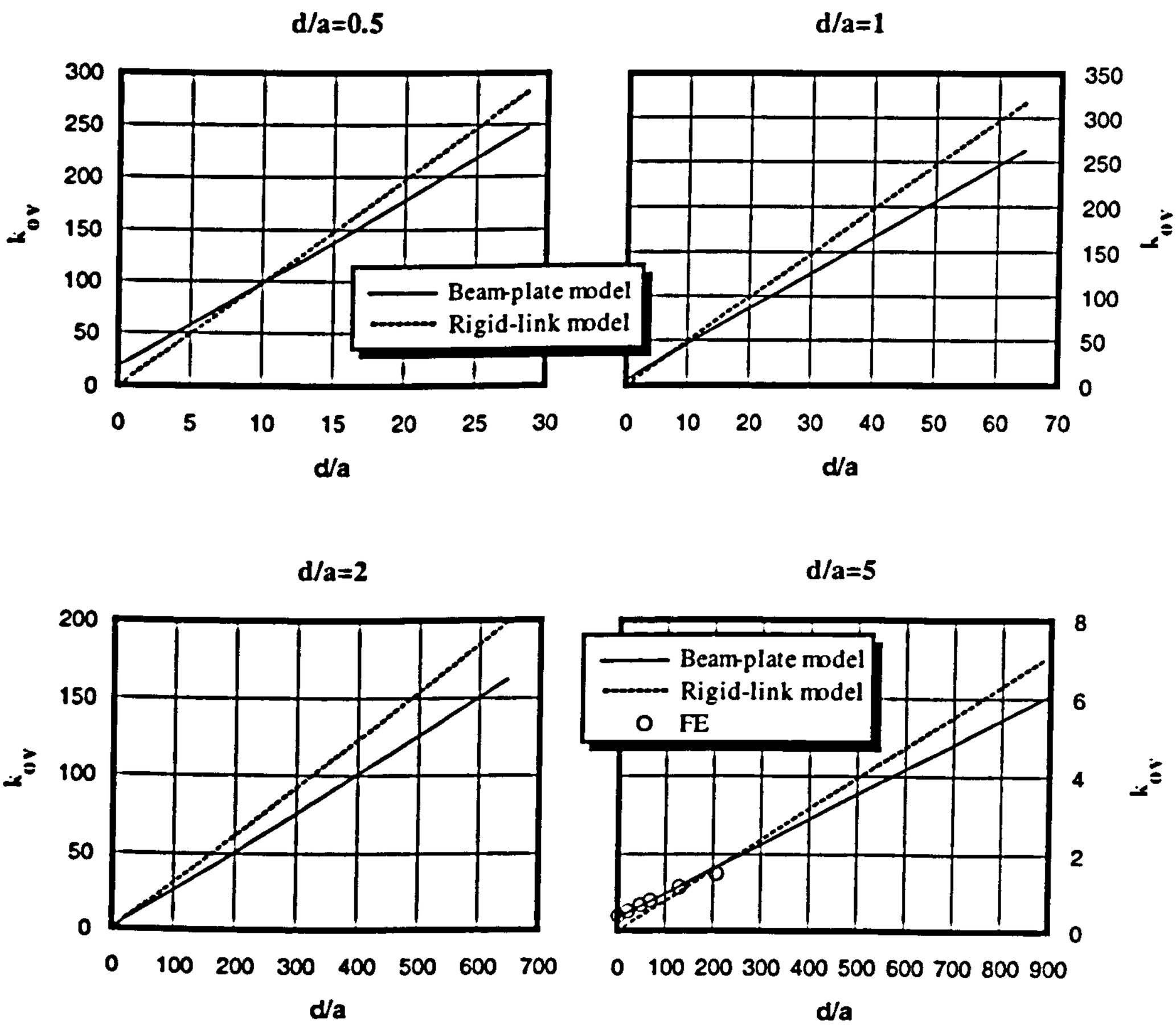


Figure 7.11 Overall buckling stress coefficients. Compression

7.3.3.2 Initially Imperfect Stiffener, $w_{0s} \neq 0$

An imperfection fully affine to the overall critical buckling mode of the beam-plate model is considered, which can be expressed as:

$$w_0 = A_{01} \cos\frac{\pi x}{2a} \cos\frac{\pi y}{d} \tag{7.77}$$

and the stiffener imperfection is in the form of a half sine wave:

$$w_{0s} = w\big|_{x=0} = A_{01} \cos\frac{\pi y}{d} \tag{7.78}$$

where the amplitude coefficient A_{01} is taken as w_{0smax} envisaged in BS5400. The additional deflection w is represented by Eqn.7.72.

For linear buckling analysis, the work done by the applied compressive forces can be expressed as:

$$T_c = \frac{1}{2}\sigma_c t \int_{-a}^{a}\int_{-\frac{d}{2}}^{\frac{d}{2}}\left[\left(\frac{\partial w}{\partial x}+\frac{\partial w_0}{\partial x}\right)^2 - \left(\frac{\partial w_0}{\partial x}\right)^2\right] dxdy = \frac{\pi^2 dt}{16a}\sigma_c\left(A_1^{\,2} + 2A_{01}A_1\right) \tag{7.79}$$

Using the same procedure as in Section 7.3.3.1, but replacing T_c in Eqn.7.69 with T_c from Eqn.7.79, the following equation for the additional deflection w is obtained:

$$w = \left(\frac{\sigma_c/\sigma_{c,ov}}{1-\sigma_c/\sigma_{c,ov}}\right) w_{0s\,max} \cos\frac{\pi x}{2a}\cos\frac{\pi y}{d} \tag{7.80}$$

Using $M_s / EI_s = \partial^2 w_s / \partial y^2$ and Eqn.7.80, the maximum bending moment along the stiffener for the beam-plate model can be obtained:

$$M_s = \frac{\pi^2 EI_s w_{0s\,max}}{d^2}\left(\frac{\sigma_c/\sigma_{c,ov}}{1-\sigma_c/\sigma_{c,ov}}\right) \tag{7.81}$$

The bending moment M_s given in Eqn. 7.81 represents the component of the stiffener moment due to the overall buckling effect, M_{ov}. The result in Eqn.7.81 will be incorporated in Section 7.4 with the stiffener moments for other loading components to formulate an interaction equation for predicting the bending moment due to the overall buckling effect.

7.3.4 Pure Bending Condition

7.3.4.1 Initially Straight Stiffener, $w_{0s}=0$

The deflection function given in Eqn.7.44 can not be used for the pure bending condition, since the work done by the applied bending forces would be zero. In Section 7.2.4.1, it is found that the stiffener deflection can be represented approximately by a sinusoidal series with the first two terms. Similarly, the following deflection function is adopted for the beam-plate model under pure bending:

$$w=\left(a_1 \sin\frac{\pi y}{d}+a_2 \sin\frac{2\pi y}{d}\right)\sin\frac{\pi x}{2a} \tag{7.82}$$

The coordinate system is shown in Fig.7.12.

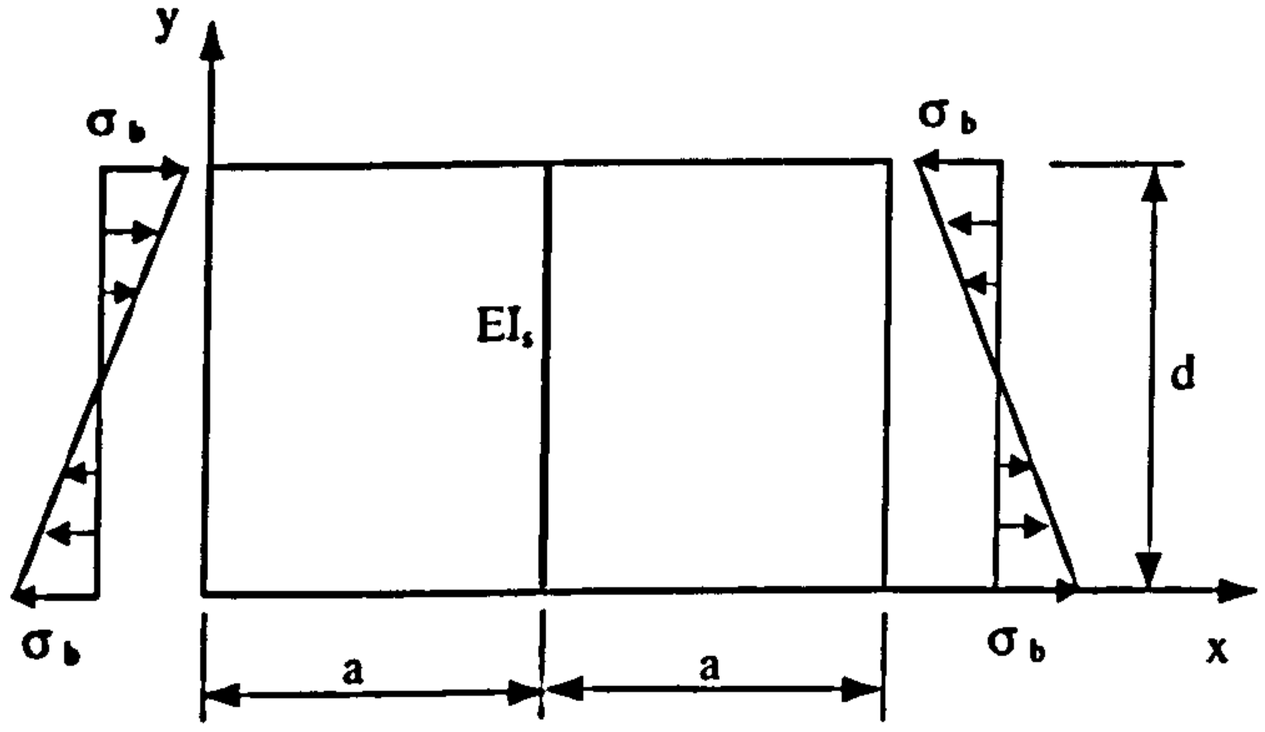


Figure 7.12 Beam-plate model for pure bending

The work done by the applied bending stresses is:

$$T_b=\frac{1}{2}\sigma_b t\int_0^{2a}\int_0^{d}\left(\frac{2y}{d}-1\right)\left(\frac{\partial w}{\partial x}\right)^2 dxdy \tag{7.83}$$

Using the deflection function giving in Eqn.7.82, the above equation becomes:

$$T_b=-\frac{4dt}{9a}\sigma_b a_1 a_2 \tag{7.84}$$

Replacing Eqn.7.82 in Eqn.7.46, the strain energy of bending in the panels, due to the deflection w, is obtained:

$$U_{pb} = \frac{Dad\pi^4}{4}\left(\frac{1}{4a^2}+\frac{1}{d^2}\right)^2 a_1^2 + \frac{Dad\pi^4}{4}\left(\frac{1}{4a^2}+\frac{4}{d^2}\right)^2 a_2^2 \qquad (7.85)$$

The strain energy of the stiffener due to bending is:

$$U_{sb} = \frac{EI_s}{2}\int_0^d \left(\frac{\partial^2 w}{\partial y^2}\right)_{x=a}^2 dy = \frac{EI_s\pi^4}{4d^3}\left(a_1^2 + 16a_2^2\right) \qquad (7.86)$$

The total potential energy is:

$$\Pi = U_{pb} + U_{sb} - T_b \qquad (7.87)$$

In terms of the equations:

$$\frac{\partial \Pi}{\partial a_m} = 0,\ \mathrm{m}=1,2 \qquad (7.88)$$

the overall buckling coefficient is obtained:

$$k_{ov} = \frac{9a^2b^2\pi^2}{2d^4}\sqrt{\left[\left(\frac{d^2}{4a^2}+1\right)^2+\frac{b}{a}\Psi\right]\left[\left(\frac{d^2}{16a^2}+1\right)^2+\frac{b}{a}\Psi\right]} \qquad (7.89)$$

The overall buckling bending stress $\sigma_{b,ov}$ is given by:

$$\sigma_{b,ov} = k_{ov}\frac{\pi^2 D}{b^2 t} \qquad (7.90)$$

The overall buckling mode can be represented by Eqn.7.82, with:

$$a_2 = -\frac{a_1}{4}\sqrt{\left[\left(\frac{d^2}{4a^2}+1\right)^2+\frac{b}{a}\Psi\right]\Big/\left[\left(\frac{d^2}{16a^2}+1\right)^2+\frac{b}{a}\Psi\right]} \qquad (7.91)$$

For a stiffener with $\Psi >> (d/a)^4$, the above equation may reduce to:

$$a_2 = -\frac{1}{4}a_1 \qquad (7.92)$$

Eqn.7.92 is identical to Eqn.7.39a that represents the overall buckling mode of the rigid-link model for pure bending.

In Fig.7.13, the overall critical stress coefficient k_{ov} for unstiffened plates (Ψ=0) is compared with the finite element analysis results for the overall buckling modes. It is demonstrated that good agreement is achieved between the beam-plate model and the numerical analysis.

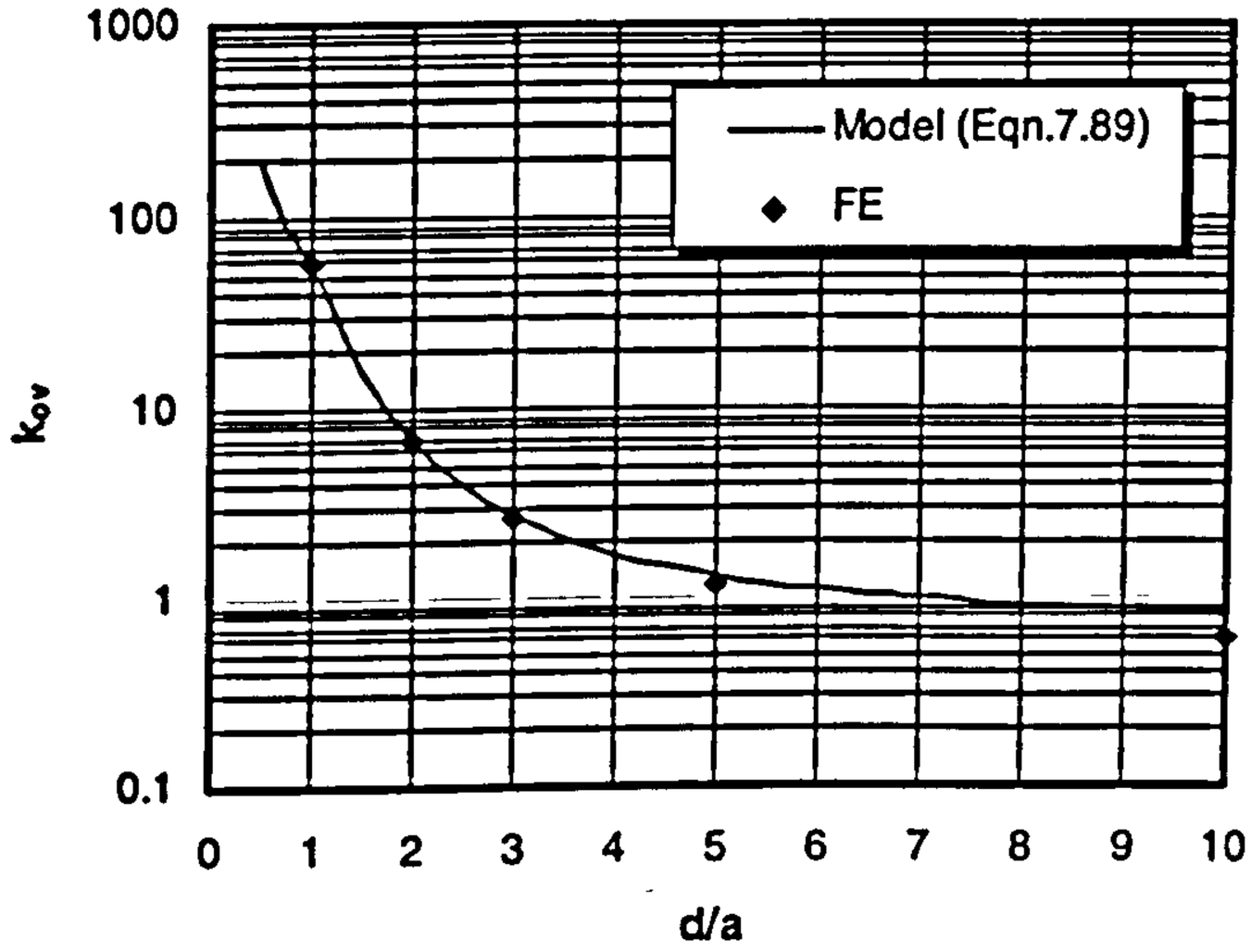


Figure 7.13 Comparison of the critical buckling stress coefficients. Pure Bending, Ψ=0

The variation in k_{ov} with respect to the stiffener rigidity Ψ is presented in Fig.7.14, where the results for the rigid-link model, given by Eqns.7.37a and 7.38, are shown for comparison. For d/a=5, the numerical results for the overall buckling modes are also included. The significant differences between the beam-plate model and the rigid-link model are resulted from the overall buckling capacity of the panels. In addition, the stiffeners in these two models may deflect in different shapes, due to the interaction between the stiffener and the panels, which contributes to the different slopes of k_{ov} vs. Ψ curves in Fig.7.14.

7.3.4.2 Initially Imperfect Stiffener, $w_{0s}\neq 0$

An imperfection fully affined to the overall critical buckling mode of the beam-plate model is considered, which can be expressed as:

$$w_0 = \left(a_{01} \sin\frac{\pi y}{d} + a_{02} \sin\frac{2\pi y}{d} \right) \sin\frac{\pi x}{2a} \tag{7.93}$$

and the stiffener imperfection is:

$$w_{0s} = w_0\big|_{x=a} = a_{01} \sin\frac{\pi y}{d} + a_{02} \sin\frac{2\pi y}{d} \tag{7.94}$$

where the relation between the amplitude coefficients a_{01} and a_{02} is giving by:

$$a_{02} = -\frac{a_{01}}{4} \sqrt{\left[\left(\frac{d^2}{4a^2} + 1 \right)^2 + \frac{b}{a}\Psi \right] \Big/ \left[\left(\frac{d^2}{16a^2} + 1 \right)^2 + \frac{b}{a}\Psi \right]} \tag{7.95}$$

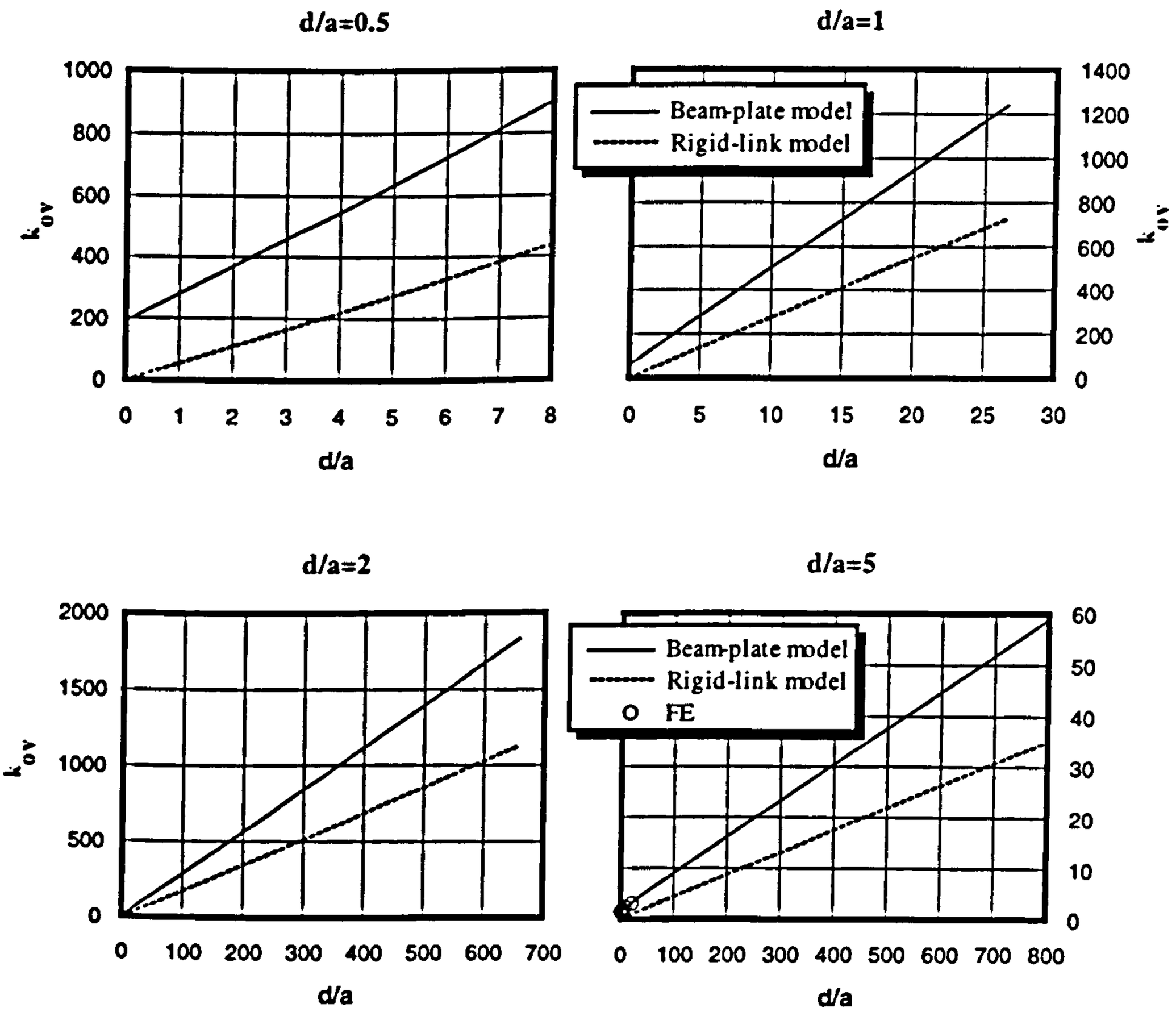


Figure 7.14 Overall buckling stress coefficients. Pure bending

Using the same procedure as in Section 7.3.3.2, the following equation for the additional deflection w is obtained:

$$w = \left(\frac{\sigma_b / \sigma_{b.ov}}{1 - \sigma_b / \sigma_{b.ov}} \right) w_0 \tag{7.96}$$

Using $M_s / EI_s = \partial^2 w_s / \partial y^2$ and Eqn.7.90, the maximum bending moment along the stiffener for beam-plate model can be written as:

$$M_s = \frac{\pi^2 EI_s}{d^2} \left(\frac{\sigma_b / \sigma_{b.ov}}{1 - \sigma_b / \sigma_{b.ov}} \right) \left(a_{01} \sin \frac{\pi y}{d} + 4 a_{02} \sin \frac{2\pi y}{d} \right) \tag{7.97}$$

The bending moment M_s given in Eqn. 7.97 represents the component of the stiffener moment due to the overall buckling effect, M_{ov}. The result in Eqn.7.97 will be incorporated in Section 7.4 with the stiffener moments for other loading components to formulate an interaction equation for predicting the bending moment due to the overall buckling effect.

7.3.5 External Stiffener Forces

7.3.5.1 External Forces at Both Ends, Q_2

The beam-plate model can be used for a straight stiffener subjected to equal external forces at both ends (Fig.7.15). The deflection function given in Eqn.7.82 may reduce to:

$$w = a_1 \sin \frac{\pi x}{2a} \sin \frac{\pi y}{d} \tag{7.98}$$

where it is assumed that the stiffener buckles into a half sine wave. This is based on the fact that a beam on elastic foundation may buckle into a half sine wave when subjected to two equal axial end forces [25].

The work done by the end forces is:

$$T_q = Q_2 \cdot \frac{1}{2} \int_0^d \left(\frac{\partial w}{\partial y} \right)_{x=a}^2 dy = \frac{\pi^2 Q_2}{4d} a_1^2 \tag{7.99}$$

Using Eqns.7.85, 7.91 and 7.99, the total potential energy can be obtained:

$$\Pi = U_{pb} + U_{sb} - T_q$$
$$= \frac{Dad\pi^4}{4}\left(\frac{1}{4a^2}+\frac{1}{d^2}\right)a_1^2 + \frac{EI_s\pi^4}{4d^3}a_1^2 - \frac{\pi^2 Q_2}{4d}a_1^2 \qquad (7.100)$$

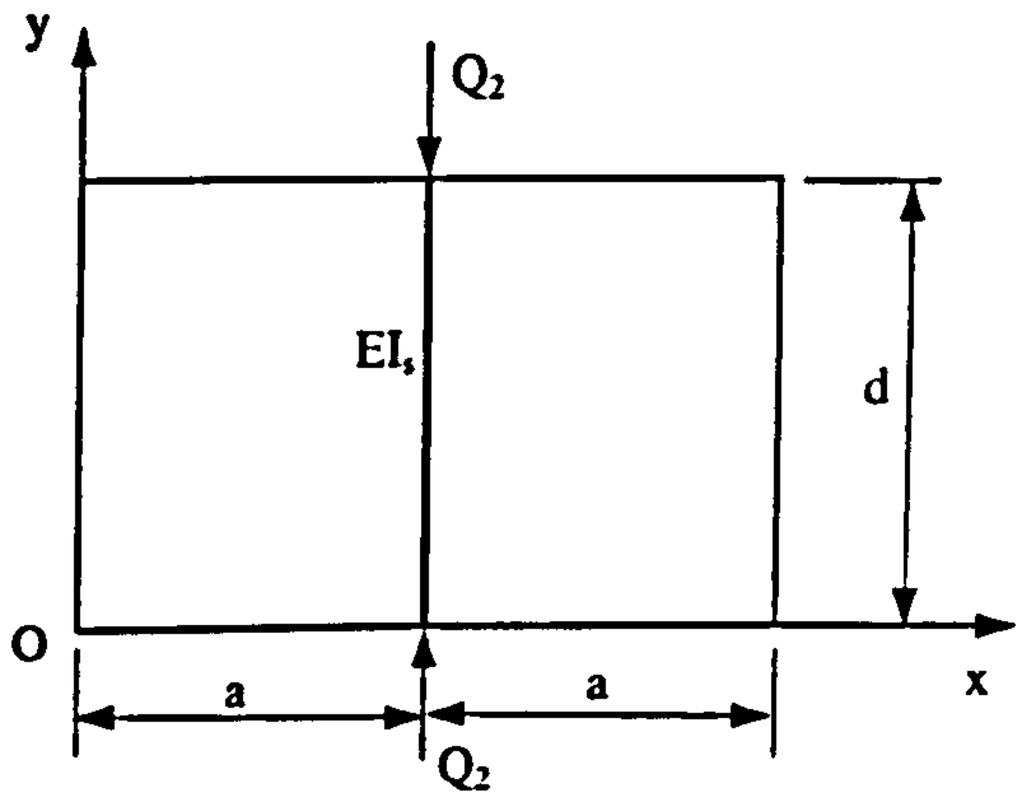


Figure 7.15 Beam-plate model for external forces at both ends, Q_2

In terms of equation $\frac{\partial \Pi}{\partial a_1} = 0$, the overall critical load coefficient k_{Qov} can be found:

$$k_{Qov} = \frac{b}{a}\Psi + \left(\frac{d^2}{4a^2}+1\right)^2 \qquad (7.101)$$

where k_{Qov} is defined by:

$$Q_{2,ov} = k_{Qov}\frac{\pi^2 Da}{d^2} \qquad (7.102)$$

In Fig.7.16, the critical load coefficient k_{Qov} given in Eqn.7.101 is compared with the numerical results for stiffened plates with an aspect ratio of d/a=5. The numerical values in Fig.7.16 are related to the full overall buckling modes. It is observed that the model proposed gives a reasonable estimation for the overall buckling load.

If the stiffener has an initial imperfection in the form of half sine wave, as given in Eqn.7.18, the additional stiffener deflection w_s can be found:

$$w_s = \left(\frac{Q_2 / Q_{2.ov}}{1 - Q_2 / Q_{2.ov}} \right) w_{0s\max} \sin \frac{\pi y}{d} \tag{7.103}$$

Therefore, the maximum bending moment along the stiffener can be obtained:

$$M_s = \frac{\pi^2 E I_s w_{0s\max}}{d^2} \left(\frac{Q_2 / Q_{2.ov}}{1 - Q_2 / Q_{2.ov}} \right) \tag{7.104}$$

The bending moment M_s given in Eqn. 7.104 represents the component of the stiffener moment due to the overall buckling effect, M_{ov}. The result in Eqn.7.104 will be incorporated in Section 7.4 with the stiffener moments for other loading components to formulate an interaction equation for predicting the bending moment due to the overall buckling effect.

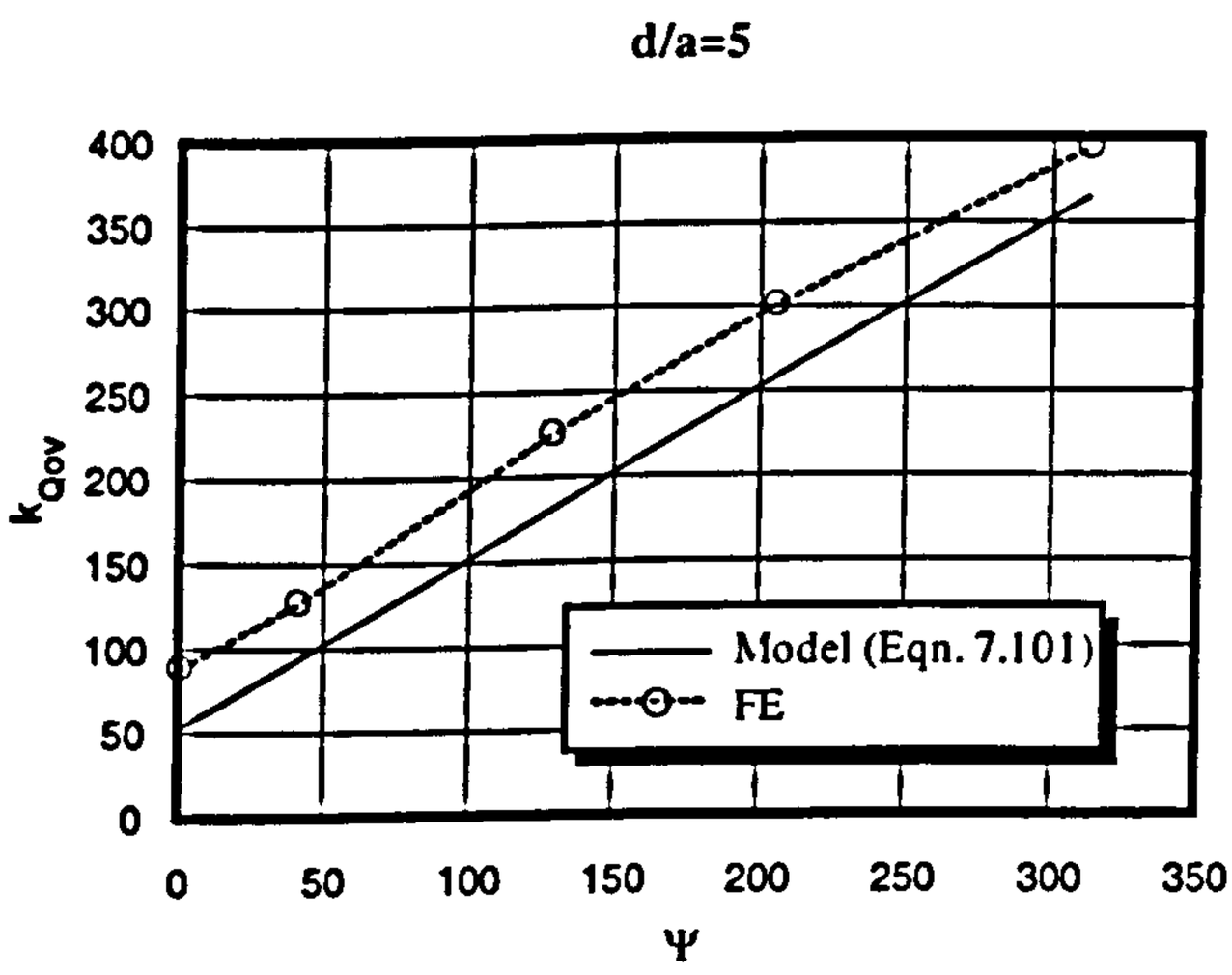


Figure 7.16 Critical load coefficient k_{Qov}. External stiffener forces at both ends, Q_2

7.3.5.2 External Force at One End, Q_1

When the beam-plate model is used for a straight stiffener subjected to external force at one end, the load applied is considered to be supported by the shear stresses on the two vertical edges, as shown in Fig.7.17. The shear stress is assumed to have a parabolic

distribution along the vertical edges. This assumption is as the same as that used by Khan and Walker [52] for a rectangular plate loaded along part of the top edge. Further, the shear stress distribution over the plate is taken as:

$$\tau_{xy} = \frac{3Q_1 y}{d^2 t}\left(\frac{y}{d} - 1\right), \quad for\ x < a$$
$$\tau_{xy} = \frac{3Q_1 y}{d^2 t}\left(1 - \frac{y}{d}\right), \quad for\ x > a \qquad (7.105)$$

Some preliminary numerical critical analyses demonstrated that the overall critical mode for this loading case is close to that for pure bending. Therefore, the deflection function given in Eqn.7.82 is taken for the beam-plate model loaded by an external force at one end.

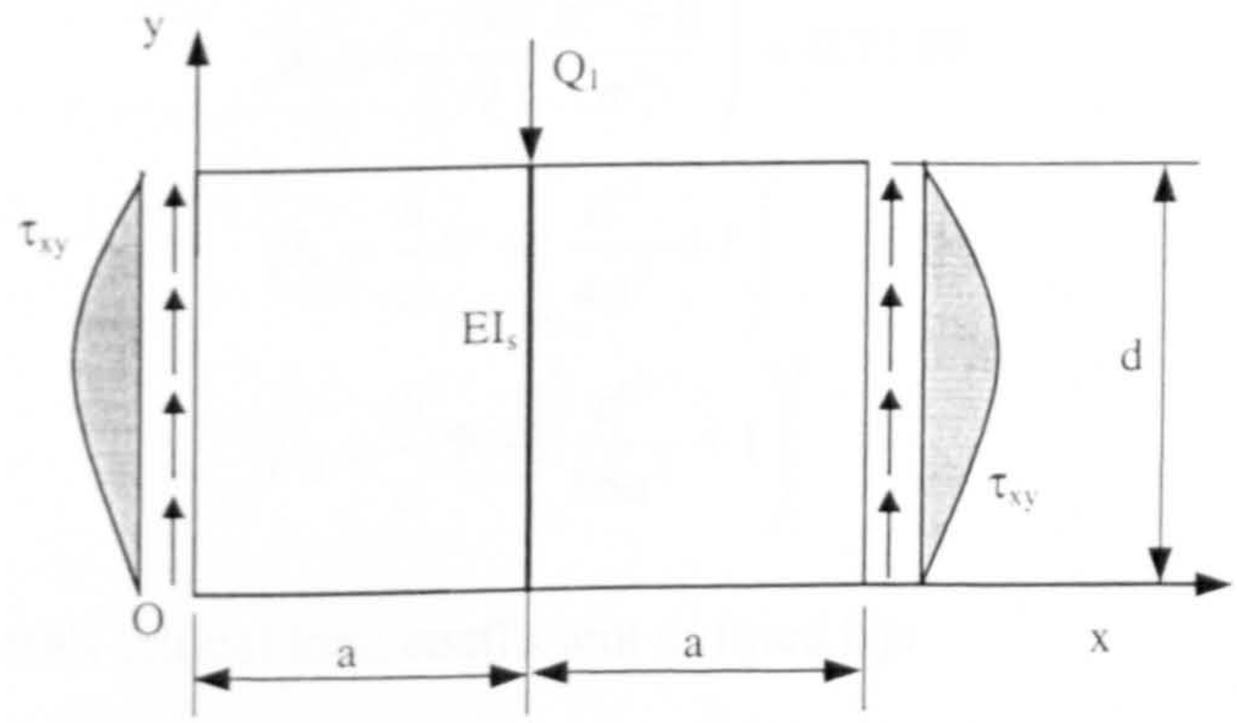


Figure 7.17 Beam-plate model for external stiffener force at one end, Q_1

The work done by the shear stresses can be expressed as:

$$T_\tau = -t\int_0^{2a}\int_0^{d} \tau_{xy}\frac{\partial w}{\partial x}\frac{\partial w}{\partial y}dxdy \qquad (7.106)$$

By replacing Eqns7.82 and 7.105 into Eqn.7.106, the work T_τ can be obtained:

$$T_\tau = -\frac{16Q_1}{3\pi^2 d}\cdot a_1 a_2 \qquad (7.107)$$

Based on the assumption of inextensional buckling and that the centre of the plate does not move vertically, the work done by the external force Q_1 can be written as:

$$T_q = Q_1 \cdot \frac{1}{2}\int_0^d \left(\frac{\partial w}{\partial y}\right)_{x=a}^2 dy = \frac{\pi^2 Q_1}{8d}a_1^2 + \frac{\pi^2 Q_1}{2d}a_2^2 - \frac{2\pi Q_1}{3d}a_1 a_2 \qquad (7.108)$$

The total potential energy can be expressed as:

$$\Pi = U_{pb} + U_{sb} - T_q - T_r \qquad (7.109)$$

where U_{pb} and U_{sb} are given in Eqns.7.85 and 7.91 respectively. In terms of the Eqn.7.87, the following governing equations for overall buckling are obtained:

$$\beta_1 k_{q.ov}^2 - 2(\beta_2 + 4\beta_3)k_{q.ov} + 16\beta_2\beta_3 = 0 \qquad (7.110)$$

where:

$$\beta_1 = 1 - \frac{16}{9}\left(\frac{\pi^3 + 8}{\pi^4}\right)^2 \approx 0.7149$$

$$\beta_2 = \frac{b}{a}\Psi + \left(\frac{d^2}{4a^2} + 1\right)^2 \qquad (7.111)$$

$$\beta_2 = \frac{b}{a}\Psi + \left(\frac{d^2}{16a^2} + 1\right)^2$$

and k_{Qov} is the overall critical load coefficient defined by:

$$Q_{1.ov} = k_{Qov}\frac{\pi^2 D a}{d^2} \qquad (7.112)$$

From Eqn.7.110, the overall critical load coefficient k_{Qov} can be found:

$$k_{Qov} = \left(\frac{\beta_2 + 4\beta_3}{\beta_1}\right) - \sqrt{\left(\frac{\beta_2 + 4\beta_3}{\beta_1}\right)^2 - \frac{16\beta_2\beta_3}{\beta_1}} \qquad (7.113)$$

In order to find a more simple equation for k_{Qov}, a relation between the deflection function amplitude coefficients a_1 and a_2 is introduced:

$$a_2 = -Ca_1 \qquad (7.114)$$

where C is a constant.

Substituting Eqn.7.114 into Eqn.7.109, and in terms of equation $\frac{\partial \Pi}{\partial a_1}=0$, the overall critical load coefficient k_{Qov} can be written as:

$$k_{Qov}=\left[\left(1+16C^2\right)\frac{b}{a}\Psi+\left(\frac{d^2}{4a^2}+1\right)^2+16C^2\left(\frac{d^2}{16a^2}+1\right)^2\right]\Bigg/\left[\frac{1+4C^2}{2}+\frac{8C}{3\pi^4}\left(8+\pi^3\right)\right] \tag{7.115}$$

Assuming C=0.25, as given in Eqns.7.39a and 7.92, Eqn.7.115 becomes:

$$k_{Qov}=1.121\left[\frac{2b}{a}\Psi+\left(\frac{d^2}{4a^2}+1\right)^2+\left(\frac{d^2}{16a^2}+1\right)^2\right] \tag{7.116}$$

The variation in k_{Qov} with respect to the stiffener rigidity Ψ is presented in Fig.7.18, where the numerical results corresponding to the critical modes with a single wave stiffener deflection are also shown for comparison. It is apparent that Eqn7.116 agrees well with the finite element analysis results. It is noted that the two FE points with a higher value of Ψ are associated with a buckling mode which also involves certain local panel deflection.

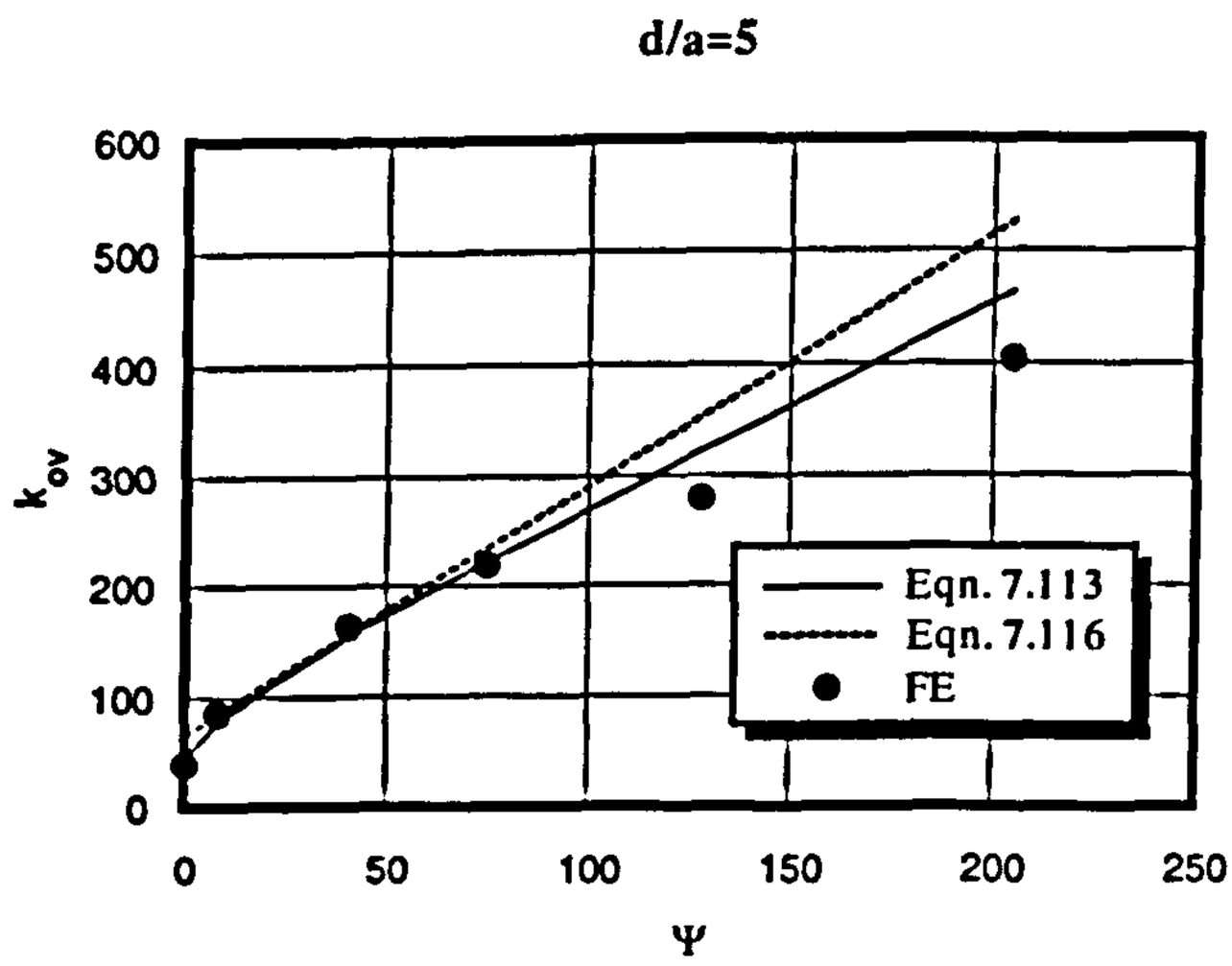


Figure 7.18 Overall critical load coefficient k_{Qov}. External stiffener force at one end, Q_1

An initial imperfection fully affine to the overall buckling mode is considered. and the stiffener imperfection can be expressed as:

$$w_{0s} = a_{01} \sin\frac{\pi y}{d} + a_{02} \sin\frac{2\pi y}{d} \tag{7.117}$$

where:

$$a_{02} = -Ca_{01} \tag{7.118}$$

and C is the constant as defined in Eqn.7.114.

Using the same approach as the above, the additional stiffener deflection w_s can be found:

$$w_s = \left(\frac{Q_1/Q_{1.ov}}{1-Q_1/Q_{1.ov}}\right) w_{0s} \tag{7.119}$$

Using $M_s/EI_s = \partial^2 w_s/\partial y^2$ and Eqn.7.119, the maximum bending moment along the stiffener can be found:

$$M_s = \frac{\pi^2 EI_s\, w_{0s.max}}{d^2}\left(\frac{Q_1/Q_{1.ov}}{1-Q_1/Q_{1.ov}}\right) \tag{7.120}$$

The bending moment M_s given in Eqn. 7.120 represents the component of the stiffener moment due to the overall buckling effect, M_{ov}. The result in Eqn.7.120 will be incorporated in Section 7.4 with the stiffener moments for other loading components to formulate an interaction equation for predicting the bending moment due to the overall buckling effect.

7.4 PROPOSED INTERACTION EQUATIONS FOR COMBINED LOADING

By adopting an appropriate deflection function for the plate, the applied shear stress, compressive stress and bending stress, as well as the external stiffener forces, may be incorporated simultaneously into the beam-plate model. Referring to the coordinate system shown in Fig. 7.12, a possible function which may be used for this purpose is:

$$w = \left(A_1 \sin\frac{\pi y}{d} + A_2 \sin\frac{2\pi y}{d}\right)\sin\frac{\pi x}{2a} + A_3\left(\frac{x}{a}-1\right)\left(\frac{y}{d}-\frac{1}{2}\right)\sin\frac{\pi x}{2a}\cdot\sin\frac{\pi y}{d} \tag{7.121}$$

Eqn. 7.121 is a generalised form of the deflection functions used in Section 7.3 for each loading component, given in Eqns. 7.44 and 7.82.

By using Eqn. 7.121 and following the same procedures as those used in Section 7.3, the overall buckling stresses (or loads) and the bending moment in an imperfect stiffener for stiffened plates subjected to combined loading might be found, which take into account the interaction between the different components of applied loading. However, such a solution is anticipated to be quite complicated, and may not be expressed in a closed-form equation. Therefore, in order to develop a rational but also practical design method for transverse stiffeners, the interaction between the different components of applied loading, is not studied by applying the beam plate model. Instead, simple interaction equations are proposed below, based on the analytical solutions obtained in Section 7.3 for each loading component.

For stiffened plates subjected to coexistent shear stress τ, compressive stress σ_c and bending stress σ_b, it is proposed that the stiffener moment due to the overall buckling effect, denoted as M_{ov}, can be determined by:

$$M_{ov} = \frac{\pi^2 E I_s w_{0s}}{d^2}\left(\frac{\tau/\tau_{ov} + \sigma_c/\sigma_{c,ov} + \sigma_b/\sigma_{b,ov}}{1-\tau/\tau_{ov} - \sigma_c/\sigma_{c,ov} - \sigma_b/\sigma_{b,ov}}\right) \tag{7.122}$$

where w_{0s} denotes the maximum magnitude of the initial stiffener deflection. Eqn. 7.122 is a generalized form of Eqns. 7.67, 7.81 and 7.97.

To include the destabilising effect caused by the external force Q_1 applied to one end of the stiffener, it is proposed that Eqn. 7.122 should be modified as:

$$M_{ov} = \frac{\pi^2 E I_s w_{0s}}{d^2}\left(\frac{\tau/\tau_{ov} + \sigma_c/\sigma_{c,ov} + \sigma_b/\sigma_{b,ov} + Q_1/Q_{1,ov}}{1-\tau/\tau_{ov} - \sigma_c/\sigma_{c,ov} - \sigma_b/\sigma_{b,ov} - Q_1/Q_{1,ov}}\right) \tag{7.123}$$

It can be seen that when $\tau=\sigma_c=\sigma_b=0$, Eqn. 7.123 reduces to Eqn. 7.120.

For cases where the external force Q_2 is applied to both ends, it is proposed that Eqn. 7.122 should be modified as:

$$M_{ov} = \frac{\pi^2 E I_s w_{0s}}{d^2}\left(\frac{\tau/\tau_{ov} + \sigma_c/\sigma_{c,ov} + \sigma_b/\sigma_{b,ov} + Q_2/Q_{2,ov}}{1-\tau/\tau_{ov} - \sigma_c/\sigma_{c,ov} - \sigma_b/\sigma_{b,ov} - Q_2/Q_{2,ov}}\right) \qquad (7.124)$$

It can be seen that when $\tau=\sigma_c=\sigma_b=0$, Eqn. 7.124 reduces to Eqn. 7.104.

In Chapter 8, the stiffener moment due to the overall buckling effect, M_{ov}, will be used with the bending moment from the straight knife edge to propose a method for predicting the total bending moment in the stiffener.

7.5 CONCLUSIONS

In this chapter, the overall buckling behaviour of transversely stiffened plates has been studied by using an energy method. The stiffened plates are represented by two different overall buckling models, referred to as the *rigid-link model* and the *beam-plate model.* The buckling analyses are carried out respectively for shear, compression, bending, and the external force applied to one or both ends of the stiffener. Different deflection functions are chosen to represent the overall buckling mode for each loading component. As a result of this study, the following conclusions can be made:

(1) The overall buckling models enable the overall buckling tendency of stiffened plates to be distinguished and quantified, which is otherwise difficult to quantify for the stiffened plates owing to the presence, in varying proportions, of both overall and local buckling in the deflection modes.

(2) The rigid-link model proposed by Stanway et al [9], in which the panels are modelled as a series of rigid pin-ended links at an inclined angle to the stiffener, does not take into account the overall buckling capacity of the panels. The inclined angle is taken as that which gives the minimum buckling load.

(3) For pure shear, no closed-form solutions can be derived from the rigid-link model. An approximate solution is obtained by assigning a prescribed value to the inclined angle of the links (Eqn. 7.16). In comparison with the accurate solutions by Stanway

[1], the approximate solutions show a certain difference when d/a is about unity, where the overall buckling effect is not important.

(4) The rigid-link model is extended to compression and pure bending, respectively. However, for loading conditions where bending is in the presence of shear or compression, the stress field in the panels is non-uniform, and hence it is not adequate to represent the panels by the parallel rigid links dispersed over the whole panel.

(5) The beam-plate model, so called to distinguish it from the rigid-link model, consists of a beam and two plate panels, which are identical to the structures considered. By choosing appropriate deflection functions, the beam-plate model can be used for different loading conditions. In addition, the overall buckling capacity of the panels is taken into account.

(6) The deflection functions proposed in this chapter represent the basic features of the overall buckling modes for each loading component considered. For example, the deflection function for pure shear takes account of the inclined buckling mode. It is found that the overall buckling stresses or loads from the beam-plate model agree well with the finite element results.

(7) The buckling analyses are carried out for both initially straight and imperfect stiffeners. By assuming an imperfection fully affine to the overall critical buckling mode, the stiffener moment due to the overall buckling effect is derived. All the analytical results from the beam-plate model can be expressed as closed-form equations.

(8) Based on the analytical solutions for each individual loading component, interaction equations are proposed for predicting the stiffener moment due to the overall buckling effect, M_{ov}, for combined shear, compression and bending, as well as external forces applied to one or both ends of the stiffener.

CHAPTER 8

PROPOSED DESIGN MODEL FOR TRANSVERSE STIFFENERS

8.1 INTRODUCTION

It has been known for many years that web buckling causes inclined tension field forces. These forces are reacted by the edge regions of the web panel, and the adjacent stiffeners [32], and by the flanges [33]. For stiffened plates subjected to pure shear, Stanway et al [1,9] found that the stiffener moment is the most important factor to be considered in designing transverse stiffeners, and the same conclusions had been independently reached by Rahal & Harding [6], and by Horne & Grayson [45]. However, the experimental results and FE solutions for the test girders, presented in Chapter 2, confirmed that the stiffeners were subjected to both axial forces and bending moments. The magnitudes of the stiffener axial force have been quantified in Chapter 6 on the basis of a parametric study, and it can be seen that the significance of the stiffener axial force depends on the panel slenderness ratio, which is recognised in the Basler model [32]. It can be expected that for single-sided stiffeners, the axial force due to the tension field action may become an important factor, because of the eccentricity of the axial force.

In the proposed design model for transverse stiffeners, the stiffener forces to be considered consist of the axial force due to the tension field action, and the components of the stiffener moment due to the local panel bending effect and the tendency for the stiffened plate to buckle overall. External forces applied at the ends of the stiffener are also included in the design model.

The forces acting in the transverse stiffeners have been investigated separately in the preceding chapters by carrying out non-linear elastic parametric studies on the idealised simple structures (e.g. the non-deflecting stiffener model). In this chapter, the calculation of the total stiffener bending moment will be discussed, and the effects of panel plasticity on the stiffener forces will be examined by conducting non-linear elasto-plastic buckling analyses, so that the stiffener forces at the ultimate load of stiffened plates can be estimated. For design of the stiffener, it is usual to approximate the strength of the stiffened plate by the strength of the individual panels, which are assumed to be simply supported. The stiffeners are then designed to enable the panels to act independently.

Transverse stiffeners are introduced mainly to increase the plate strength, but they also help to achieve the intended geometry of the girder section. An adequate stiffener should satisfy the following requirements:

(1) The chosen stiffener should enable the ultimate strength of the stiffened plate to be at least equal to the strength of the individual panel, assuming it is simply supported. The minimum flexural rigidity which satisfies this criterion will be denoted as Ψ_{ssir}

(2) The chosen stiffener should effectively divide the plating; that is, an effectively divided panel deflection mode should be maintained until the ultimate load of the stiffened plate is reached.

(3) The chosen stiffener should not be unnecessarily large. The stiffener size adopted should ideally be such that a further significant increase in the stiffener size results in only a very small relative increase in the ultimate strength, while a significant reduction in the stiffener size results in a significant reduction in the ultimate strength.

(4) The chosen stiffener should prevent a rapid reduction in the load carrying capacity of the stiffened plate in the post-ultimate region. It is therefore desirable that stiffener failure does not occur before panel failure: it is assumed that this will be achieved if the stiffener does not yield at the maximum resistance of the stiffened plate.

For plates subjected to pure shear, Stanway [1] found that stiffeners at the start of the plateau in the ultimate shear stress against the stiffener flexural rigidity (τ_u' vs. Ψ) curves would reasonably satisfy the above requirements, and to ensure that the design

stiffener occurs within this region, both strength and stiffness criteria were introduced in the design model [1,9]. In this chapter, the design criteria that satisfy the above requirements are established based on the numerical results for plates under pure shear, and then extended for the combined shear and in-plane longitudinal loading. The resulting design stiffeners are validated against the ultimate strength versus stiffener rigidity Ψ curves. Special features and design requirements for single-sided stiffeners are discussed.

8.2 EFFECTS OF PANEL PLASTICITY

8.2.1 General

It has been found in Chapter 5 that the stiffener moment due to the local panel bending effect can be represented by the knife edge moment, and the coefficients in the formulae for predicting the knife edge moment M_{pk} have been established based on the non-linear elastic finite element solutions. In Chapter 6, the non-linear elastic parametric results for plates with a non-deflecting stiffener were used to develop the design formulae for predicting the axial force in the stiffener, resulting from the panel tension field action. In this section, the effects of panel plasticity on the knife edge moment and the stiffener axial force will be examined, and taken into account in the design formulae.

For the stiffener moment due the overall buckling effect, the effects of panel plasticity will not be accounted for. This is because the overall buckling model, from which the stiffener moment due to the overall stiffener buckling deflection, M_{ov}, is derived, is developed to represent the potential tendency for the stiffened plate to buckle overall, but of course the buckling stress is much greater than the design stress. Also, it is a design criterion that the stiffener should remain elastic up to the ultimate load.

8.2.2 Bending Moment due to the Local Panel Bending Effect

The effects of panel plasticity on the knife edge moment can be found by comparison of the finite element solutions obtained for the plate with a straight knife edge, with and

without introducing plasticity of the panels. For this reason, non-linear elasto-plastic buckling analyses were carried out for two-panel plates with a straight knife edge, subjected to pure shear, with the panel yield stress varying from 245N/mm^2 to 500N/mm^2. By reference to the results of Stanway [1], it is expected that a simple unique equation may be introduced to account approximately for the panel plasticity effects on the knife edge moment for various geometrical parameters. Therefore, only a group of geometrical parameters are selected for the numerical analyses presented in this section, which include b/t=180, w_{0p}/t=1.091, and d/a=1, 2, 5 and 7.

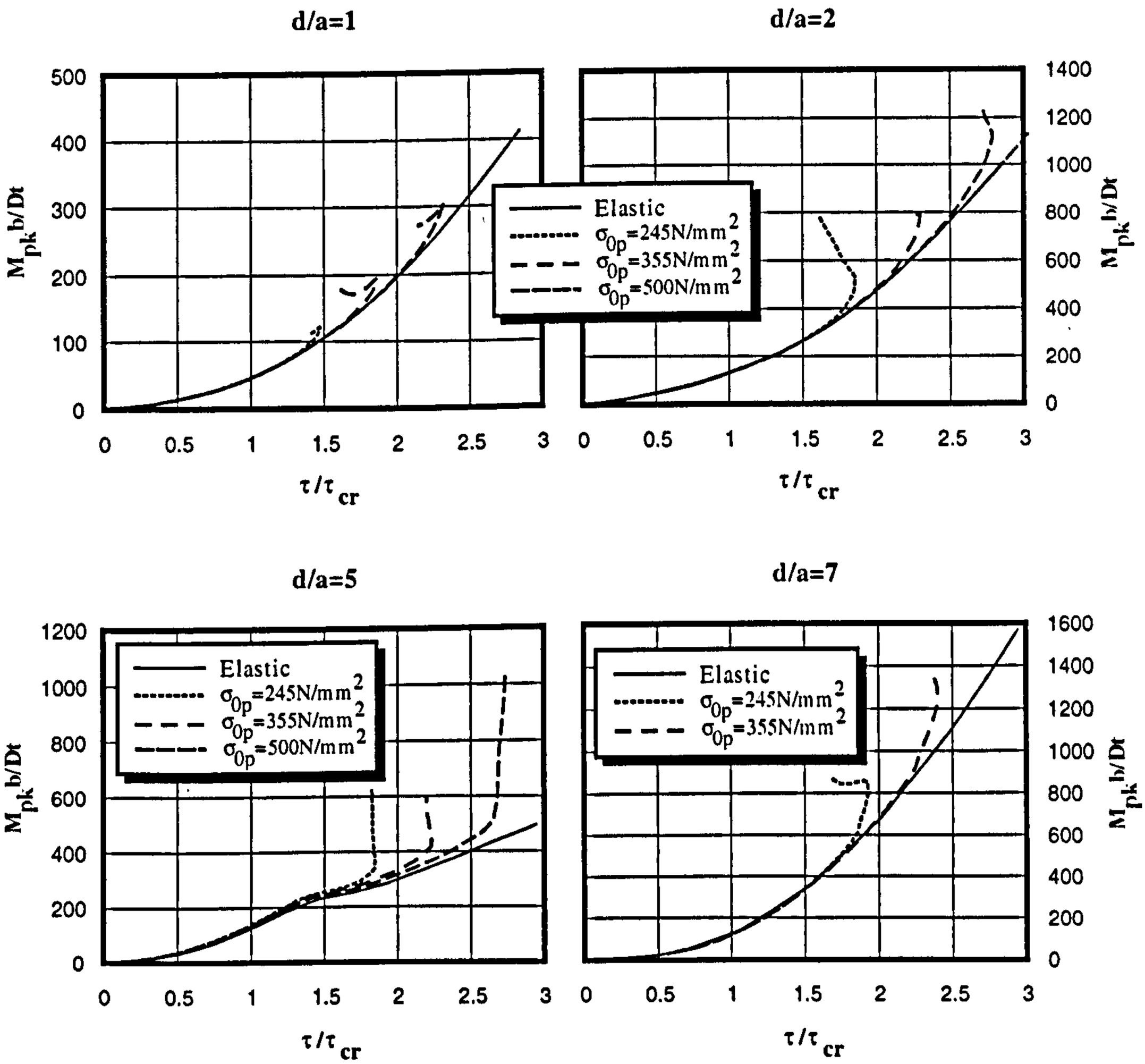


Figure 8.1 Comparison of the knife edge moments from the non-linear elastic and elasto-plastic analyses. CUCU plates with a straight knife edge. Point symmetric imperfection, w_{0p}/t=1.091. b/t=180. Pure shear

Fig. 8.1 presents the non-dimensional knife edge moment $M_{pk}b/Dt$ vs. τ/τ_{cr} curves obtained from the non-linear elastic and elasto-plastic analyses. It can be seen in Fig. 8.1 that in the region of the ultimate load, M_{pk} increases significantly with a small change in the applied shear stress. The reason for this is that as the applied shear stress approaches the ultimate shear strength, the plastic deformation in the panels increases rapidly, which in turn results in a significant increase in the panel deflection, and hence in the knife edge moment.

In the proposed design model, the bending moment in a straight knife edge at the ultimate load of the plate, taking account of the effects of panel plasticity, will be taken as the stiffener bending moment due to the panel bending effect. To distinguish this stiffener moment from the bending moment M_{pk} from the elastic solutions, the stiffener bending moment due to the panel bending effect is denoted as M_{pb}, as illustrated in Fig. 8.2. The component of the stiffener moment due to the overall stiffener buckling deflection is denoted as M_{ov}.

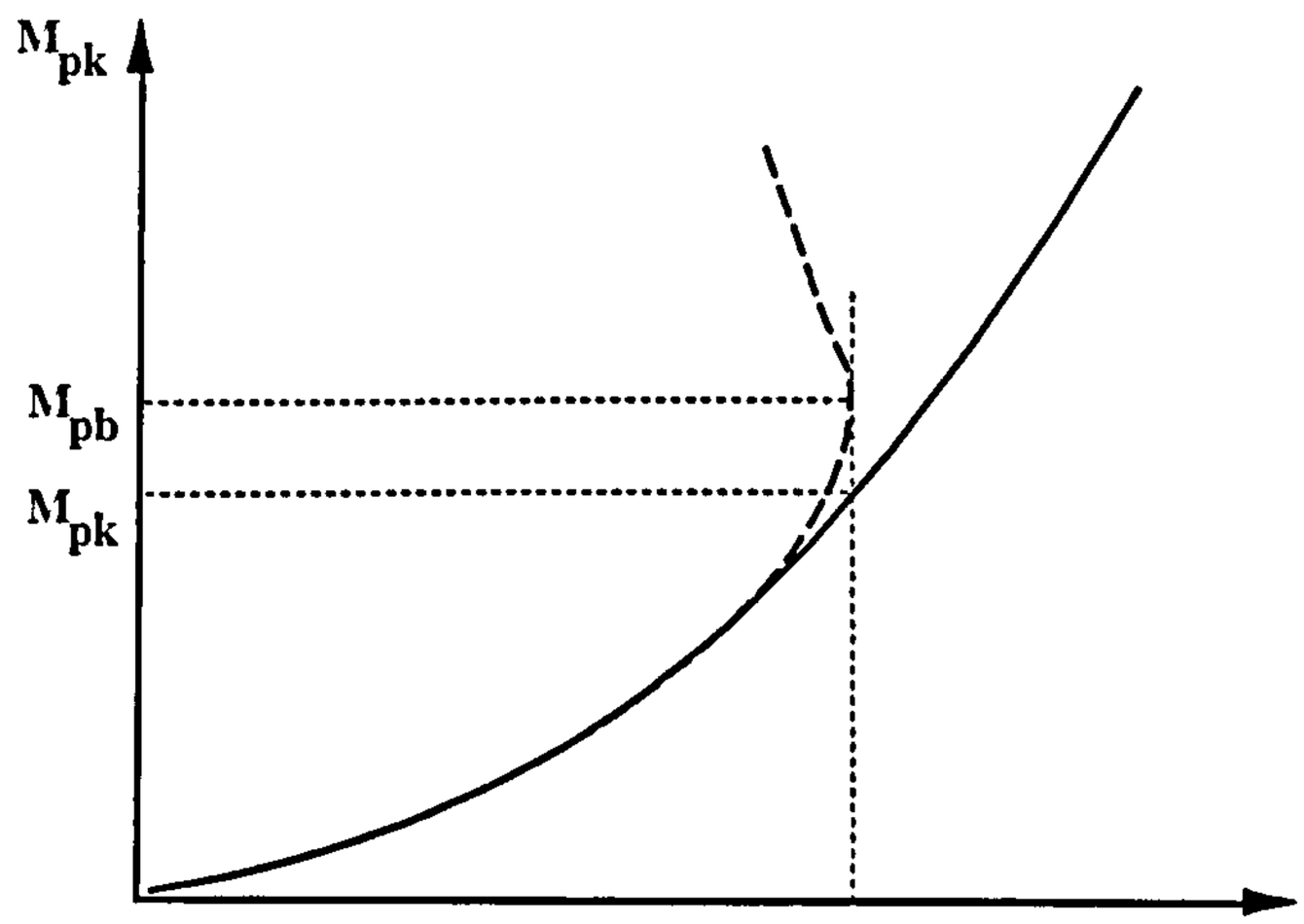


Figure 8.2 Schematic representation of the knife edge moments, with or without considering panel plasticity

In Table 8.1, the values of the knife edge moment at the ultimate load for different panel yield stresses are compared with the elastic solution at the same applied load. It can be observed in Table 8.1 that the ratio of M_{pb}/M_{pk} does not vary substantially, the average value being equal to 1.22.

Table 8.1 Ratios of the knife edge moments from elastic and elasto-plastic analyses

d/a	σ_{0p}=245N/mm^2		σ_{0p}=355N/mm^2		σ_{0p}=500N/mm^2	
	τ_u/τ_{cr}	M_{pb}/M_{pk}	τ_u/τ_{cr}	M_{pb}/M_{pk}	τ_u/τ_{cr}	M_{pb}/M_{pk}
1	1.471	1.191	1.866	1.164	2.319	1.134
2	1.854	1.271	2.297	1.231	2.787	1.167
5	1.843	1.264	2.232	1.207	2.654	1.167
7	1.928	1.390	2.401	1.291	—	—
Average	N/A	1.279	N/A	1.223	N/A	1.156

In Fig. 8.3, the variation of M_{pb}/M_{pk} with the yield stress of the panel is illustrated. It is found that the ratio of M_{pb}/M_{pk}, denoted as F_{pl}, may be approximately represented by:

$$F_{pl} = 1.6 - 0.35\sqrt{\sigma_{0p}/355} \quad and \quad F_{pl} \geq 1.0 \tag{8.1}$$

Eqn. 8.1 is based on the numerical results for pure shear. However, it has been found in Chapter 5 that for combined shear, compression and bending, the elastic knife edge moment can be represented by the same $M_{pk}b/Dt$ vs. τ/τ_{cr} curves as established for shear alone, with the applied shear stress τ being replaced with an equivalent shear stress τ_{eq}. It is therefore reasonable to assume that the relation between the knife edge moments from elastic and elasto-plastic analyses for combined loading conditions is similar to that for pure shear; that is, it is assumed that Eqn. 8.1 may also be applied for the combined loading conditions.

In summary, it is proposed that the stiffener bending moment due to the panel bending effect, M_{pb}, can be calculated as follows:

$$M_{pb} = F_{pl} M_{pk} \tag{8.2}$$

where F_{pl} is given by Eqn. 8.1, and M_{pk} is the knife edge moment from the non-linear elastic analysis. For plates subjected to combined shear and longitudinal loading, M_{pk} can be determined using Eqn. 5.22.

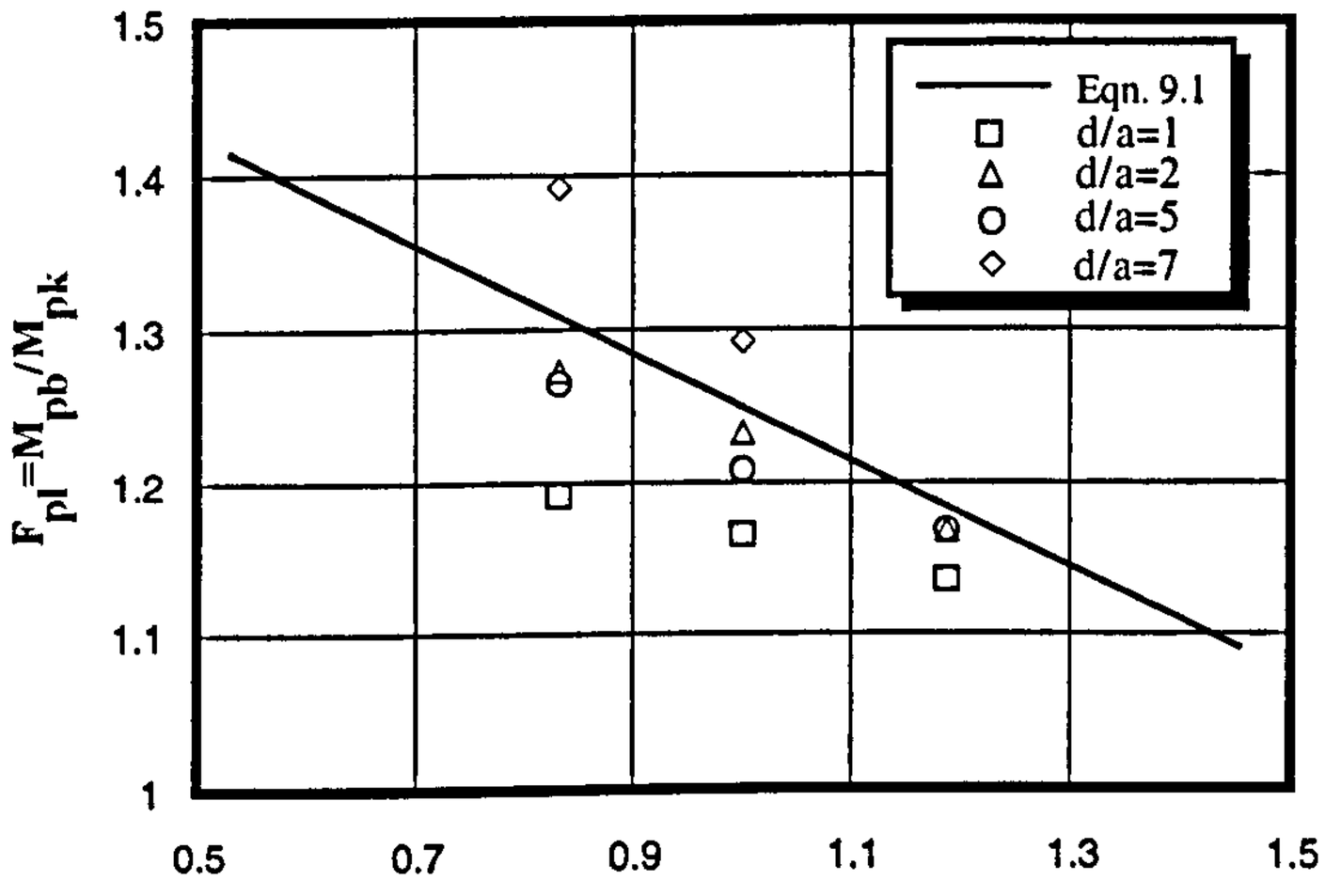


Figure 8.3 Ratios of M_{pb}/M_{pk} , varying with the panel yield stress σ_{0p}. Pure shear

8.2.3 Axial Force in the Stiffener

For a stiffened plate under pure shear, when the applied shear stress approaches the ultimate shear strength, the plastic deformation in the panels increases rapidly, which in turn results in a significant increase in the panel deflection with a small change in the applied shear stress. Nevertheless, it has been found in Chapter 6 that the axial force acting in the stiffener results mainly from the inclined tension field action, which depends mainly on the applied shear stress, and the magnitude of panel out-of-plane deflection does not affect the stiffener axial force significantly. Therefore, it is contemplated that the effects of the panel plasticity on the stiffener axial force may be

much less than that for the knife edge moment. That is, the stiffener axial force at the ultimate load from the non-linear elasto-plastic analysis may be quite close to the axial force at the same load level, obtained from the non-linear elastic analysis. To verify this speculation, non-linear elasto-plastic analyses were carried out for plates with an imperfect stiffener, subjected to pure shear. The stiffener sizes used are great enough to divide the panels. The non-linear elastic solutions for the same plates have been presented in Fig. 6.7 of Chapter 6.

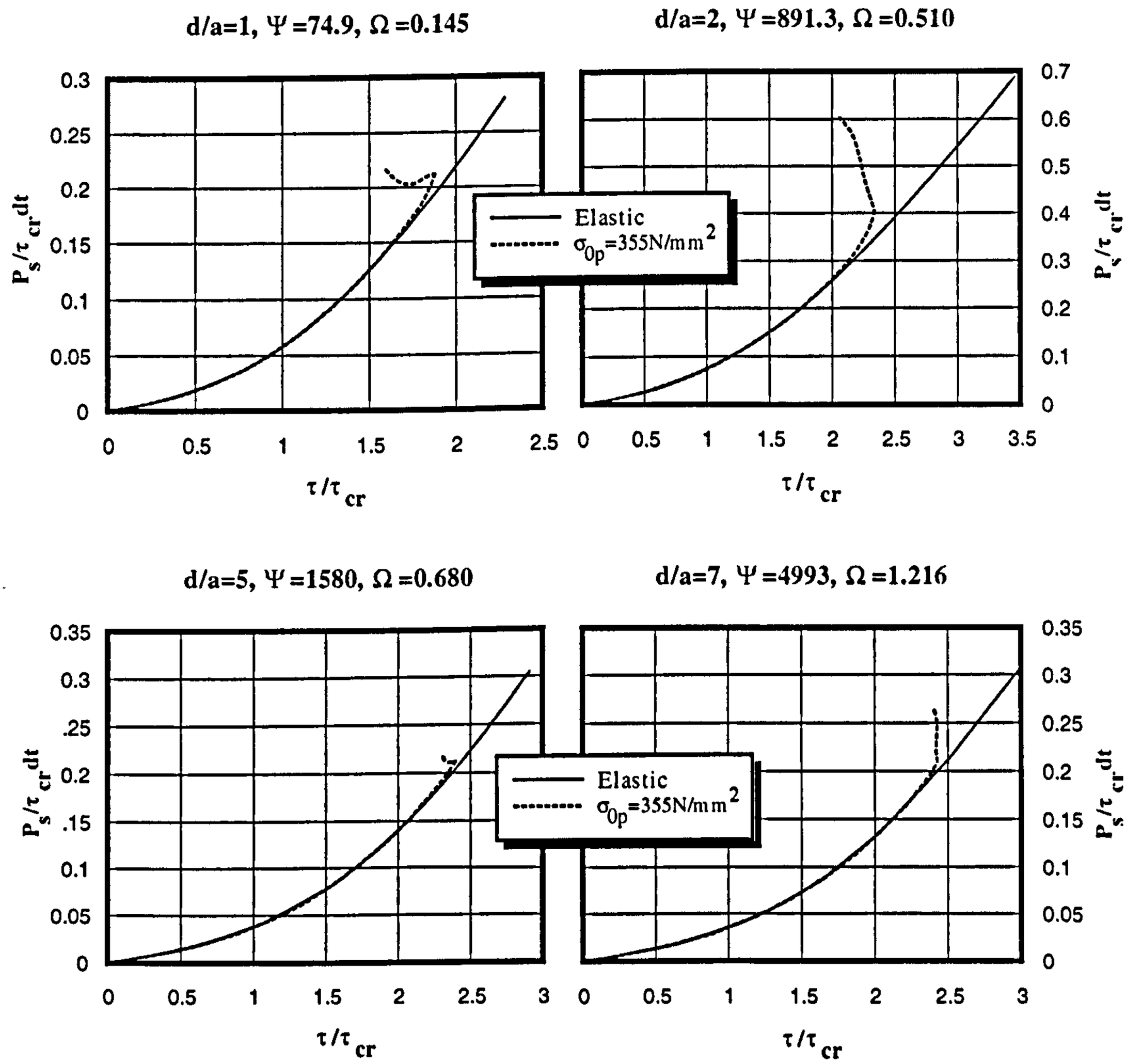


Figure 8.4 Comparison of the stiffener axial forces from the non-linear elastic and elasto-plastic analyses. Initial imperfection (see Fig. 3.5): Type B for d/a=1, 2 & 7; Type A for d/a=7, w_{0p}/t=1.091, w_{0s}=d/750. CUCU plates with an imperfect stiffener. b/t=180. $\sigma_{0p}=\sigma_{0s}=355N/mm^2$. Pure shear

In Fig. 8.4, a comparison in the stiffener axial forces is made between non-linear elastic and elasto-plastic FE solutions for plates with an imperfect stiffener of great rigidity (great enough to divide the plate), subjected to pure shear. By reference to Fig. 8.4, it is considered that for an applied shear stress up to the ultimate shear strength, the differences in the stiffener axial forces from elastic and elasto-plastic analyses may reasonably be neglected. Therefore, no further modification will be made on the proposed design formulae for predicting the stiffener axial force P_s, which are given in Eqns. 6.14 to 6.16.

8.3 DETRMINATION OF FORCES IN STIFFENERS

The stiffener forces to be included in the proposed design model have been studied separately in the previous chapters, and the corresponding predictive formulae have been developed. The purpose of this section is to propose a method for predicting the total stiffener forces which take account of the combination of different effects.

In the design model proposed by Stanway et al [9] for pure shear, the panels were represented as rigid pin-ended links, inclined to the edge of the plate; this was referred to as "rigid-link" model (Section 7.2). The panel bending effect was incorporated in the model by applying a lateral distributed force to the stiffener, which was assumed to be taken as the lateral force acting on the straight knife edge. The rigid-link model enables the effects of the local panel bending and overall buckling of the stiffened plate to be combined. With the terms adopted in this thesis, the total stiffener moment derived from the rigid-link model may be approximately expressed as [9]:

$$M_s = M_{ov} + \frac{M_{pb}}{1-\tau/\tau_{ov}} \tag{8.3}$$

It is noted that the second term on the right-hand side of Eqn. 8.3 is a conservative approximation. Further, for an adequate stiffener, the ratio of τ/τ_{ov} is much less than 1.0. Therefore, it is reasonable to simplify Eqn. 8.3 as:

$$M_s = M_{ov} + M_{pb} \tag{8.4}$$

According to Eqn. 8.4, the total stiffener bending moment M_s can be approximately calculated by adding the components of stiffener moment due to the local panel bending effect and the tendency for the stiffened plate to buckle overall. Such a simplification is especially useful for the combined loading conditions, where the interaction is much more complicated.

The beam-plate model developed in Chapter 7 may be used to derive the total stiffener moment which takes account of the interaction of the panel bending and overall buckling effects. This can be done in a similar way to that for the rigid-link model; that is, the panel bending effect can be represented by a distributed lateral force acting on the stiffener, which may be taken as the lateral knife edge force q_{pk}. By adopting an appropriate deflection function for the plate, the applied shear stress τ, compressive stress σ_c and bending stress σ_b, as well as the external stiffener forces, may be incorporated simultaneously into the model. Consequently, the model may produce an equation which accounts for not only the interaction between the panel bending and overall buckling effects, but also the interaction between different components of applied loading. However, such a solution is anticipated to be quite complicated, and may not be expressed in a closed-form equation. Therefore, in order to develop a rational but also practical design method for transverse stiffeners, the interaction between the panel bending and overall buckling effects, incorporating different components of applied loading, is not studied further in this thesis.

Based on the above discussion, it is proposed that the stiffener should be designed to resist the coexistent bending moment M_s and axial force P_s, with the stiffener cross-section consisting of the actual stiffener area only. It is reiterated that the axial force P_s is determined using Eqn. 6.14, while the stiffener bending moment M_s is calculated using Eqn. 8.4, where M_{pb} and M_{ov} are given in Eqns 8.2 and 7.122, respectively.

In Fig. 8.5, the elastic stiffener moment (i.e., $M_s=M_{pk}+M_{ov}$), estimated using the proposed method but without introducing the factor F_{pl} for the effect of panel plasticity, is compared with the finite element solutions.

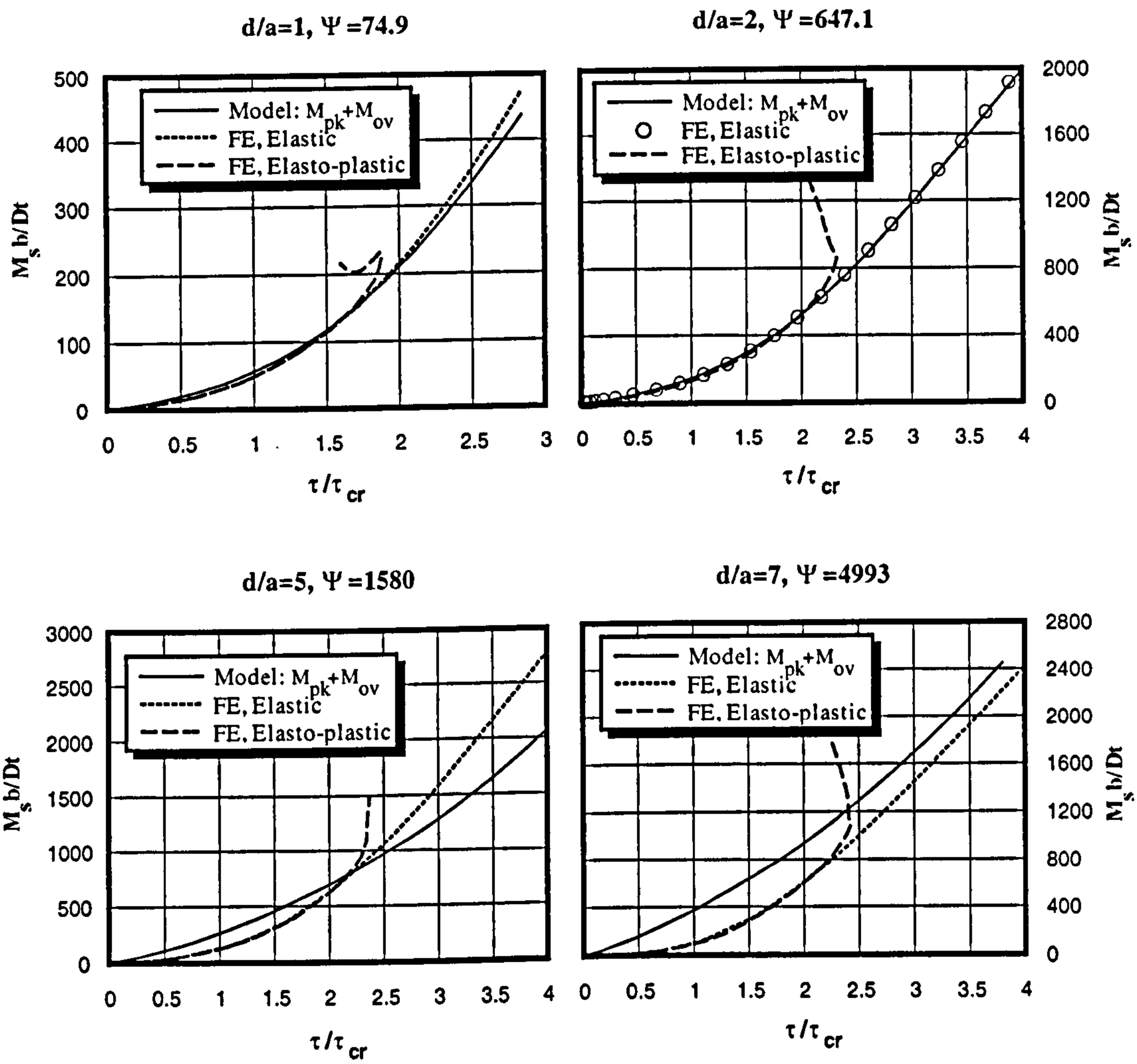


Figure 8.5 Comparison of the elastic stiffener moment from the proposed model with the FE solutions.

Initial imperfection (see Fig. 3.5): Type B for d/a=1, 2 & 7; Type B for d/a=5. $\Psi=EI_s/Db$

CUCU plates with an imperfect stiffener. b/t=180. $\sigma_{0p}=\sigma_{0s}=355N/mm^2$. Pure shear

For b/t=180 and $\sigma_{0p}=\sigma_{0s}=355N/mm^2$, a comparison of the total stiffener moments at the ultimate shear stress is made in Table 8.2 between the proposed method and FE results. The values of M_s in Table 8.2 from the proposed model were calculated using Eqn. 8.4, that is, the factor F_{pl} for the effect of panel plasticity was included. It is observed that the stiffener moments calculated from the proposed method agree well with the numerical results. It is noted in Table 8.2 that for d/a=7, the estimated stiffener moment

is about 42% greater than that from FE solutions, which may be due to the overestimation in the panel plasticity effect and the overall buckling effect. Nevertheless, it is found in the subsequent sections that the stiffeners for d/a=7 calculated in accordance with the proposed model are satisfactory. Therefore, the discrepancy shown in Table 8.2 is considered to be acceptable.

Table 8.2 Stiffener bending moments at the ultimate shear stress. CUCU plates with an imperfect stiffener b/t=180. $\sigma_{0p}=\sigma_{0s}=355N/mm^2$. Pure shear

d/a	Ψ	τ_u/τ_{cr}	$M_s b/Dt$		$\frac{M_s^{Model}}{M_s^{FE}}$
			FE	Model	
1	74.9	1.827	229.8	230.3	1.0
2	647.1	2.342	865	883	1.02
5	1580	2.227	1087	1093	1.01
7	4993	2.229	1084	1543	1.42

8.4 ULTIMATE STRENGTH OF SIMPLY SUPPORTED PANELS

As indicated previously, one requirement of the stiffener is that the chosen stiffener should provide an ultimate strength for the stiffened plate which is at least as great as the ultimate strength for the individual panel, assuming it is simply supported. Therefore, it is proposed that for design of the stiffener, the ultimate load for the simply supported panel is taken as the load applied on the stiffened plate.

The ultimate strength of individual panels subjected to pure shear has been treated by Chapman and Davidson [39]. Formulae for the panel shear strength are given by Davidson [40], which are based on a parametric study using the finite element program FINASIC [39,40], with initial panel imperfections assumed to be double sinusoidal in form. Recently, by means of the finite element program ABAQUS, Fortune [58] has obtained numerical results for the ultimate strength for both individual panels and stiffened plates, subjected to pure shear. In the parametric study carried out by Fortune

[58], initial panel imperfection is affine to the first point-symmetric buckling mode. It is found that the numerical solutions given by Fortune are about 3~4% less than the values predicted by using the formulae proposed by Davidson [40]. Since it is intended that the ultimate shear strength τ_u' versus stiffener flexural rigidity Ψ curves provided by Fortune [58] will be used to validate the proposed design model, it is decided that the values of the panel shear strength given by Fortune will be taken as the applied shear stress for designing a transverse stiffener.

The ultimate shear strengths for simply supported panels in shear given by Fortune [58] are presented in Table 8.3, for which the panel yield stress is equal to 245N/mm^2.

To validate the proposed design model for other yield stresses of material and other loading conditions, namely, combined shear and compression, as well as combined shear and bending, similar elasto-plastic analyses were carried out in the present investigation for simply supported panels, with selected geometrical parameters and load ratios. The reason for choosing those values is stated in Sections 8.5.3.2 and 8.5.3.3. The ultimate strengths obtained from ABAQUS are listed in Tables 8.4~8.6, respectively.

Table 8.3 Strength data for simply supported panels subjected to pure shear, from Ref. 58.
Initial panel imperfection affine to the first PS buckling mode, w_{0p} as given in Eqn. 3.8.
CUCU boundary conditions. σ_{0p}=245N/mm^2. Finite element results

d/a	τ_u'		
	b/t=80	b/t=120	b/t=180
0.5	0.819	0.591	0.411
1	0.920	0.739	0.547
2	0.877	0.651	0.462
3	0.866	0.639	0.445
5	0.861	0.619	0.418
7	0.847	0.618	0.404

Table 8.4 Strength data for simply supported panels subjected to pure shear. σ_{0p}=355N/mm^2. Initial panel imperfection affine to the first PS buckling mode, w_{0p} as given in Eqn. 3.8. CUCU boundary conditions. Finite element results

b/t	τ_u'		
	d/a=2	d/a=5	d/a=7
180	0.428	0.344	0.339

Table 8.5 Strength data for simply supported panels subjected to combined shear and compression. σ_{0p}=355N/mm^2. d/a=2, b/t=80. w_{0p} as given in Eqn. 3.8. CUCU boundary conditions. FE results

σ_c : τ	σ_{cu}'	τ_u'
1:0	0.286	0.0
1:2	0.149	0.515
1:5	0.0634	0.549
0:1	0.0	0.849

Table 8.6 Strength data for simply supported panels subjected to combined shear and bending. σ_{0p}=355N/mm^2. d/a=2, b/t=180. w_{0p} as given in Eqn. 3.8. CUCU boundary conditions. FE results

σ_b : τ	σ_{bu}'	τ_u'
1:0	0.369	0.0
2:1	0.245	0.212
1:1	0.166	0.287
0:1	0.0	0.428

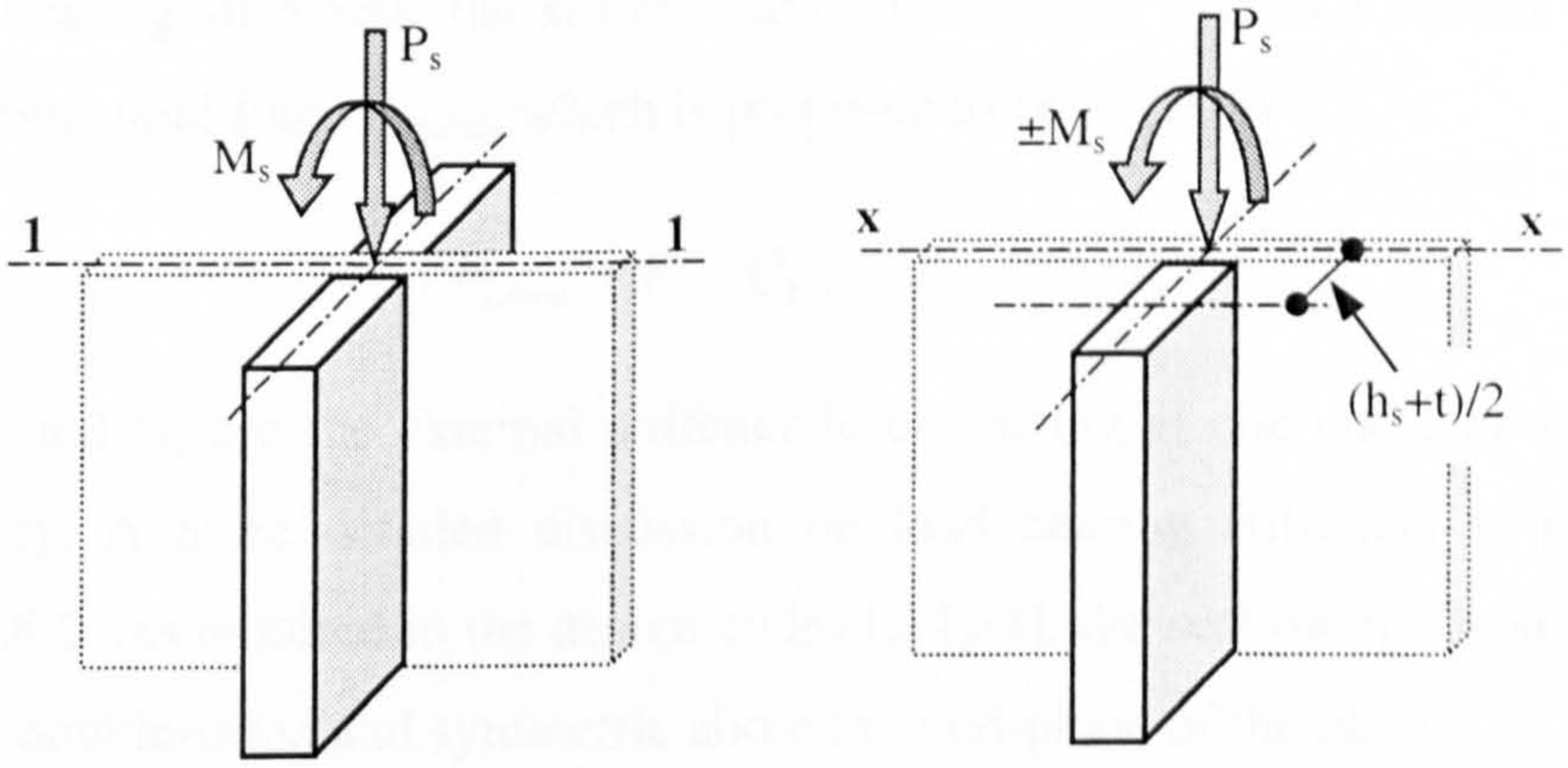
8.5 STRENGTH CRITERION FOR STIFFENER DESIGN

In this section, strength design of the transverse stiffener is examined. The strength requirement, together with the stiffness requirement (Section 8.6), is used to size the

stiffener in the proposed design model. In Sections 8.5 and 8.6, attention is paid mainly to double-sided stiffeners, while special considerations required for single-sided stiffeners are presented in Section 8.7.

8.5.1 Calculation of Stiffener Stresses

As stated in Section 8.3, in the proposed design model, a stiffener is assumed to be subjected to the coexistent bending moment M_s and axial force P_s, with the stiffener cross-section consisting of the actual stiffener area A_s only. It is noted that the predictive formulae for the axial force in the stiffener are developed from the non-deflecting stiffened plate model, in which the stiffener is modelled using truss elements which lie in the mid-plane of the plate. Therefore, the axial force P_s should be taken as acting in the mid-plane of the plate, as illustrated in Fig. 8.6.



(a) Double-sided stiffener (b) Single-sided stiffener

Figure 8.6 Design forces acting in the stiffener

It is demonstrated in Fig. 8.6 that for double-sided stiffeners, the stiffener can be designed as a simple beam loaded by an axial force equal to P_s acting at the centroid of the stiffener cross-section, and a bending moment M_s about the centroidal axis *1–1*. For single-sided flat bar stiffeners, the stiffener can be designed as a simple beam loaded by a bending moment M_s and an eccentric axial load P_s acting at a distance $(h_s+t)/2$ from

the centroidal axis *1–1* of the stiffener cross-section (Fig. 8.6). It is apparent that for the single-sided stiffener, an additional bending moment resulting from the eccentricity of the axial load P_s should be included, and the possible combinations of the stiffener forces should be considered for the design of the eccentric stiffener.

In the later part of this section and Section 8.6, the design method is developed for double-sided stiffeners, and special considerations required for the design of single-sided stiffeners will be discussed in Section 8.7.

It is proposed that for double-sided (concentric) stiffeners, the maximum stress in the stiffener can be calculated as follows:

$$\sigma_{s,\max} = \frac{P_s}{A_s} + \frac{M_s}{Z_s} \tag{8.5}$$

For load bearing stiffeners, the stiffener axial force P_s in Eqn. 8.5 should be replaced with the total axial force $P_{s,total}$, which is proposed to be as follows:

$$P_{s,total} = P_s + Q_1 \,, \quad or \quad P_s + Q_2 \tag{8.6}$$

where Q_1 and Q_2 are the external stiffener forces acting at one end and at both ends, respectively. A more detailed discussion on load bearing stiffeners is presented in Section 8.8.2. As required in the design codes [3,4,34], the section of a bearing stiffener should be double-sided and symmetric about the mid-plane of the plate.

8.5.2 Strength Requirement

The purpose of the strength requirement is to ensure that stiffener failure does not occur before panel failure. This is necessary because otherwise the stiffener deflection might be such that the panel strength would not be mobilized, and because stiffener failure causes a rapid reduction in resistance of the stiffened plate.

Stiffener failure may be prevented in design by providing a stiffener for which the yield stress is not exceeded, referred to as "the no yield criterion" in this thesis. The no yield

criterion has been adopted in the design methods proposed by Stanway et al [9], and by Rahal and Harding [6]. Another criterion, as adopted in the method by Rockey et al [47], is to provide a stiffener for which the plastic moment capacity is not exceeded, refered to as "plastic collapse criterion". It is noted that after yielding, the stiffener stiffness will diminish, the deflection will increase, and the analytical assumptions may be violated.

For the strength design of the transverse stiffener, the no yield criterion is adopted. It is proposed that the maximum stress in the stiffener, calculated using Eqn. 8.5, should not exceed the yield stress of the stiffener; that is:

$$\sigma_{s,\max} \leq \sigma_{0s} \tag{8.7}$$

It has been pointed out in Section 8.4 that for design of the stiffener the ultimate load for a simply supported panel is taken as the load applied on the stiffened plate. However, the actual plate strength is often greater than the strength for the simply supported panel, and therefore it is desirable that the required stiffener size according to the strength criterion would ensure the stiffener remains elastic at the actual ultimate load of the stiffened plate, and this will be checked in the next subsection.

8.5.3 Required Stiffener Size According to the Strength Criterion

In this section, the flexural rigidity of the smallest stiffener (double-sided, $h/t_s=10$) which satisfies the strength criterion in Eqn. 8.7, denoted as Ψ_{dZ}, is compared with the ultimate strength results from the non-linear elasto-plastic finite element analyses. The stiffener forces were determined in accordance with the method summarised in Section 8.3. The applied load was taken as the ultimate load of the simply supported panel, presented in Section 8.4. Stiffener sizes for plates under different loading conditions were determined, which are presented in the subsequent sections.

The purpose of the comparison is to show to what extent the forces given by the proposed method result in a stiffener which satisfies the strength criterion that the stiffener does not yield at the ultimate load of the plate. This will be indicated by the position of Ψ_{dZ} in relation to Ψ_p (the largest value of Ψ, of those considered, for which

yielding of the stiffener occurs at the ultimate load) and Ψ_e (the smallest value of Ψ, of those considered, for which yielding of the stiffener does not occur at the ultimate load). The value of Ψ for which the stiffener just remains elastic at the ultimate load lies between Ψ_p and Ψ_e.

8.5.3.1 Plates subjected to pure shear

The latest parametric results for stiffened plates subjected to pure shear are given by Fortune [58], obtained from ABAQUS. In his work, the yield stress of stiffener and panel material was taken as 245N/mm^2, panel aspect ratio d/a varies from 0.5 to 7, and the panel slenderness ratios of 80, 120 and 180 were considered. The τ_u' vs. Ψ results given by Fortune [58] are used to validate the required stiffener size Ψ_{dZ} calculated according to the method proposed in this thesis, as presented in Fig. 8.7, where the flexural rigidity of the smallest stiffener (double-sided, h/t_s=10) which satisfies the stiffness criterion (Section 8.6), denoted as Ψ_{dI}, is also indicated.

In Fig. 8.8, the required stiffener size Ψ_{dZ} is also compared with the τ_u' vs. Ψ results from finite element analyses, with the yield stress of stiffener and panel material being equal to 355N/mm^2.

According to the strength criterion (Eqn. 8.7), the stiffener with a rigidity of Ψ_{dZ} should remain elastic at the ultimate load. Two stiffener sizes are marked on the curves in Figs. 8.7 and 8.8; namely, Ψ_p and Ψ_e. It has been pointed out that the value of Ψ for which the stiffener just remains elastic at the ultimate load lies between Ψ_p and Ψ_e. It can be seen in Figs. 8.7 and 8.8 that for all the cases considered, the required stiffener rigidity Ψ_{dZ} according to the strength criterion is in close proximity to the region bounded by Ψ_p and Ψ_e, and mostly greater than Ψ_p. Implied by this observation is that the stiffener forces determined in accordance with the method proposed in this thesis are satisfactory.

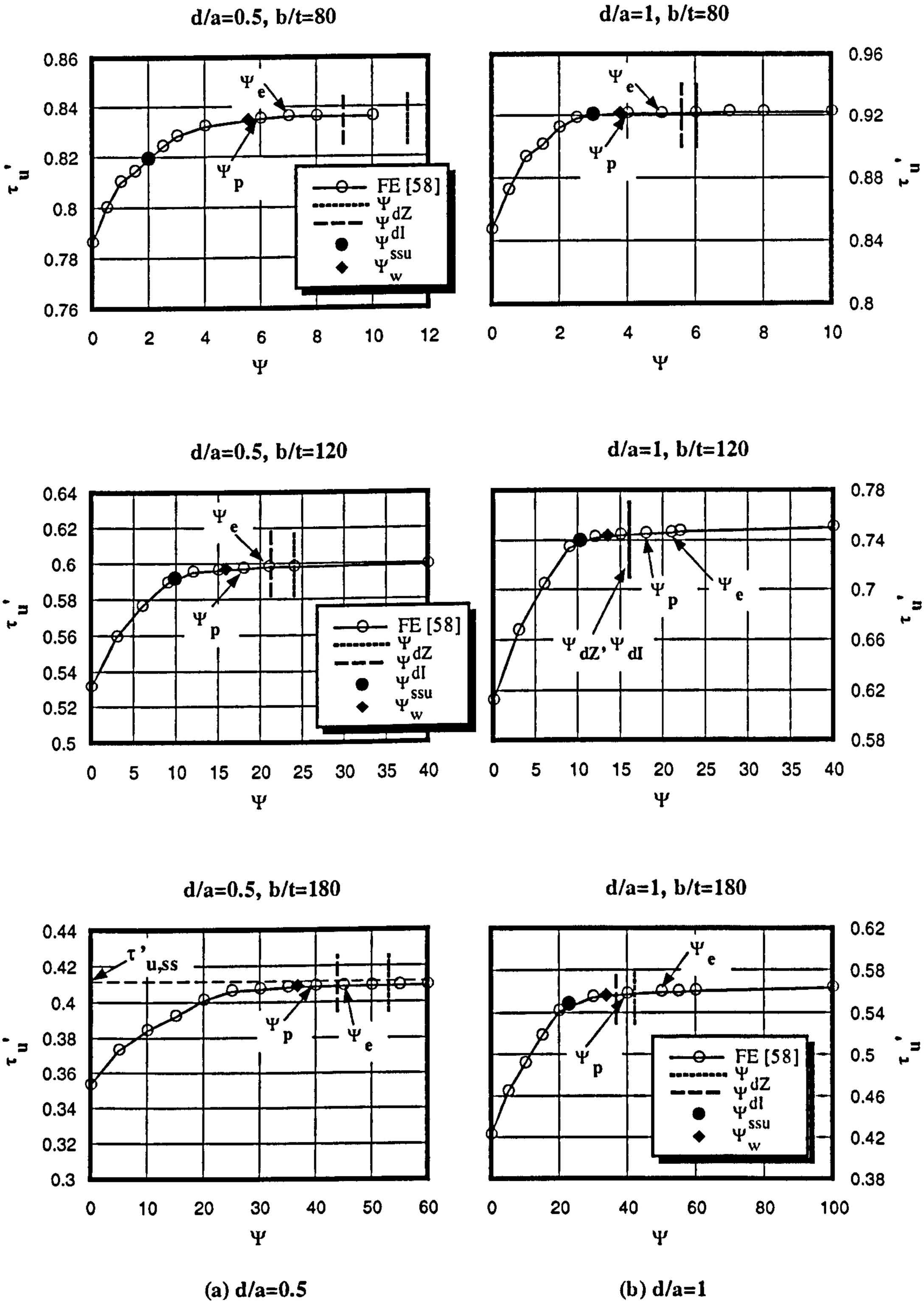
For a stiffener design model, the basic requirement is that it should provide a stiffener which will ensure that the ultimate load for the stiffened plate is at least as great as the

ultimate load for the simply supported panel. The minimum flexural rigidity which satisfies this criterion is denoted as Ψ_{ssu}. In Figs. 8.7 and 8.8, Ψ_{ssu} is also indicated on the τ_u' vs. Ψ results curves. For the calculation of Ψ_{dZ} to be satisfactory in sizing the required stiffener, it should be equal to or greater than Ψ_{ssu}; that is:

$$\Psi_{dZ} \geq \Psi_{ssu} \tag{8.8}$$

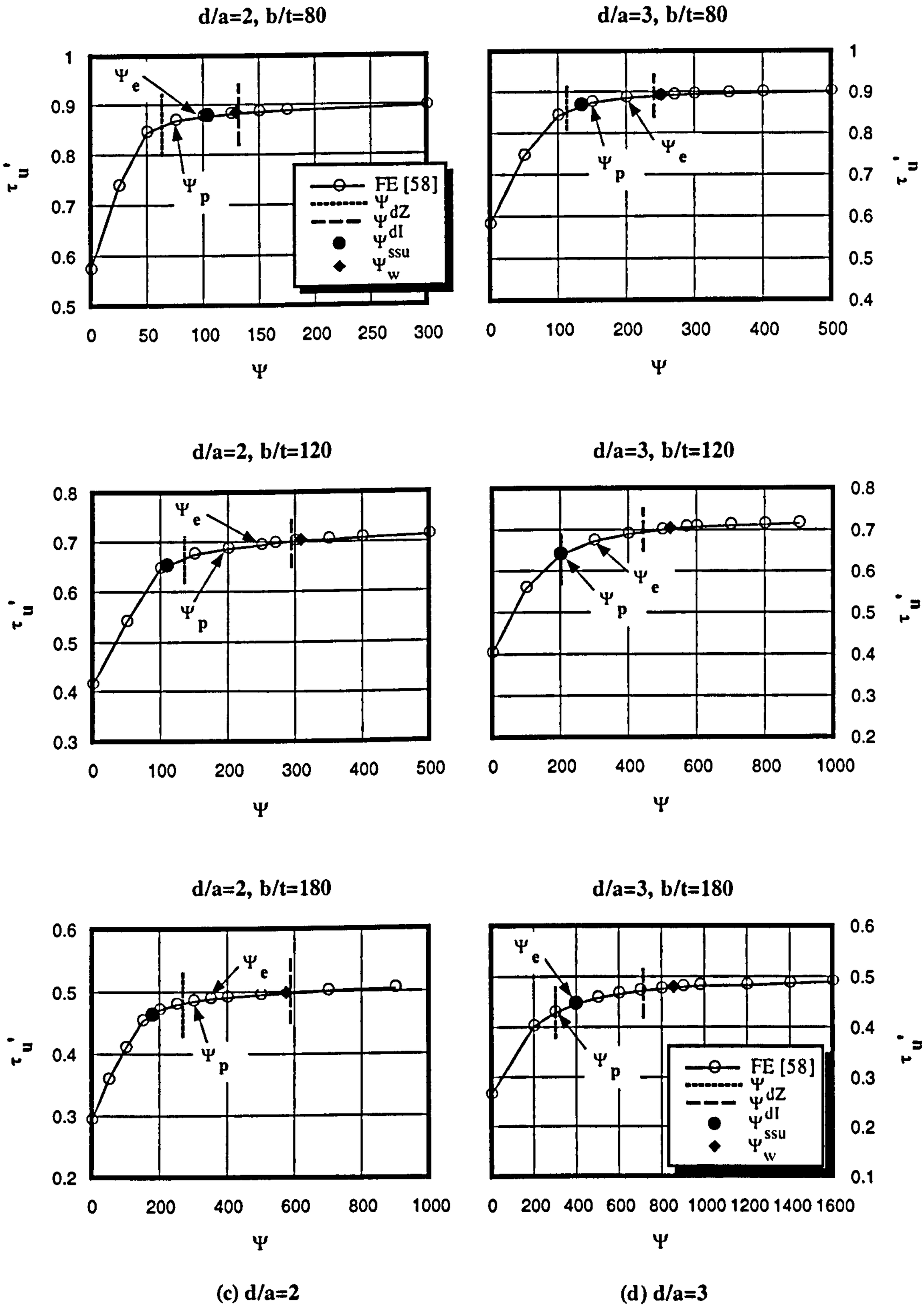
In Figs. 8.7 (a) and (b), it can be observed that Eqn. 8.8 can be satisfied for all cases considered for d/a=0.5 and 1 (except for d/a=0.5, b/t=180). For d/a=0.5, b/t=180, it is found that the ultimate strength of the stiffened plates is negligibly less than the panel strength (about 0.5%), even for a stiffener of great rigidity Ψ. However, the design stiffener Ψ_{dZ} for this case is considered to be adequate, because any increase in Ψ from Ψ_{dZ} will not result in appreciable increase in τ_u' for the stiffened plate. It is noted that for d/a=0.5 and 1, the region bounded by Ψ_p and Ψ_e is at a significant distance along the plateau of the τ_u' vs. Ψ curve, and this means that a stiffener which just remains elastic at the ultimate load will represent the required stiffener size. By comparison with the required stiffener rigidity according to the stiffness criterion, Ψ_{dI}, it is found that for all cases considered for d/a=0.5 and 1, an adequate design size of the stiffener is obtained from the strength criterion.

In Figs. 8.7 (c) to (f) and Fig. 8.8, it can be seen that the required stiffener rigidity Ψ_{dZ} is in close proximity to Ψ_{ssu}, and in most of the cases, is equal to or greater than Ψ_{ssu}. Therefore, as far as the requirement given in Eqn. 8.8 is concerned, the stiffener rigidity Ψ_{dZ} according to the proposed strength criterion is still satisfactory for d/a≥2. However, it is observed that for d/a≥2, the stiffener corresponding to the strength criterion is not on the plateau of the τ_u' vs. Ψ curve, and therefore cannot be taken as an adequate stiffener. It is noted that for these cases, the stiffener which remains fully elastic at the ultimate load is relatively small, and deflects to a degree which would not provide adequate subdivision of the plate, and would result in a reduction in the plate resistance. For this reason, a stiffness criterion is also necessary to ensure that the design stiffener is adequate, and the stiffness criterion is presented in Section 8.6.



(a) d/a=0.5 (b) d/a=1

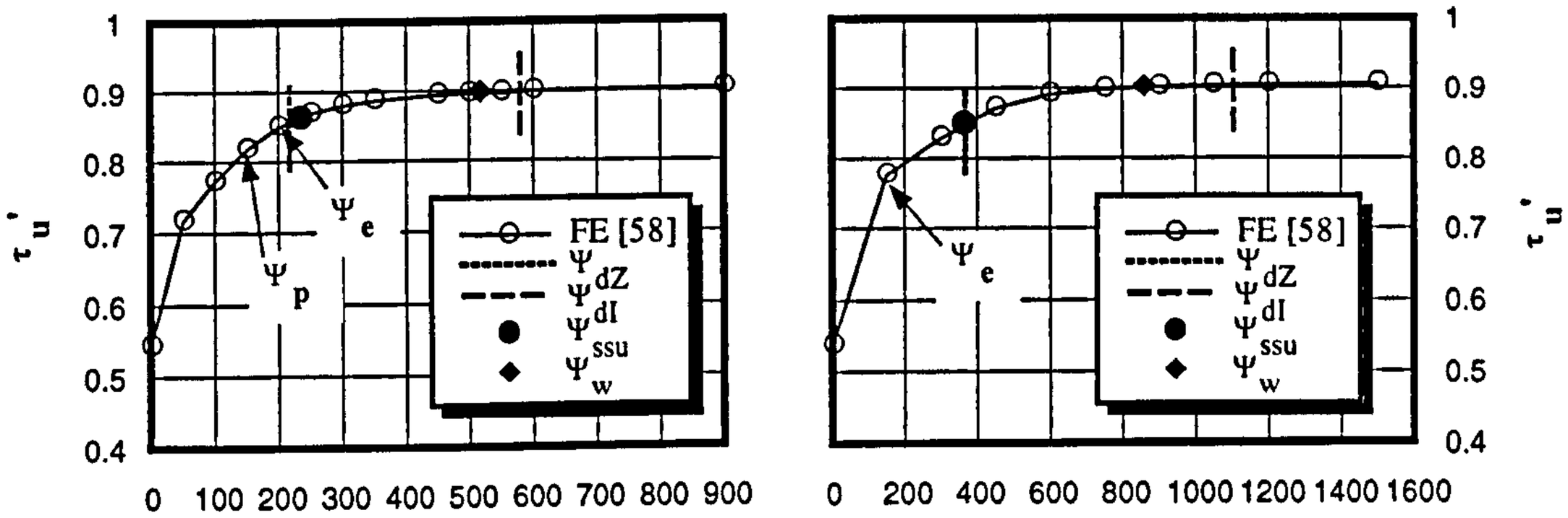
Figure 8.7 Comparison of stiffener requirements from the proposed model, with the τ_u' vs. Ψ results from FE analyses, given by Fortune [58], with $\sigma_{0p}=\sigma_{0s}=245N/mm^2$. w_0 as in Fig. 3.5. $\Psi=EI_s/Db$. Pure shear

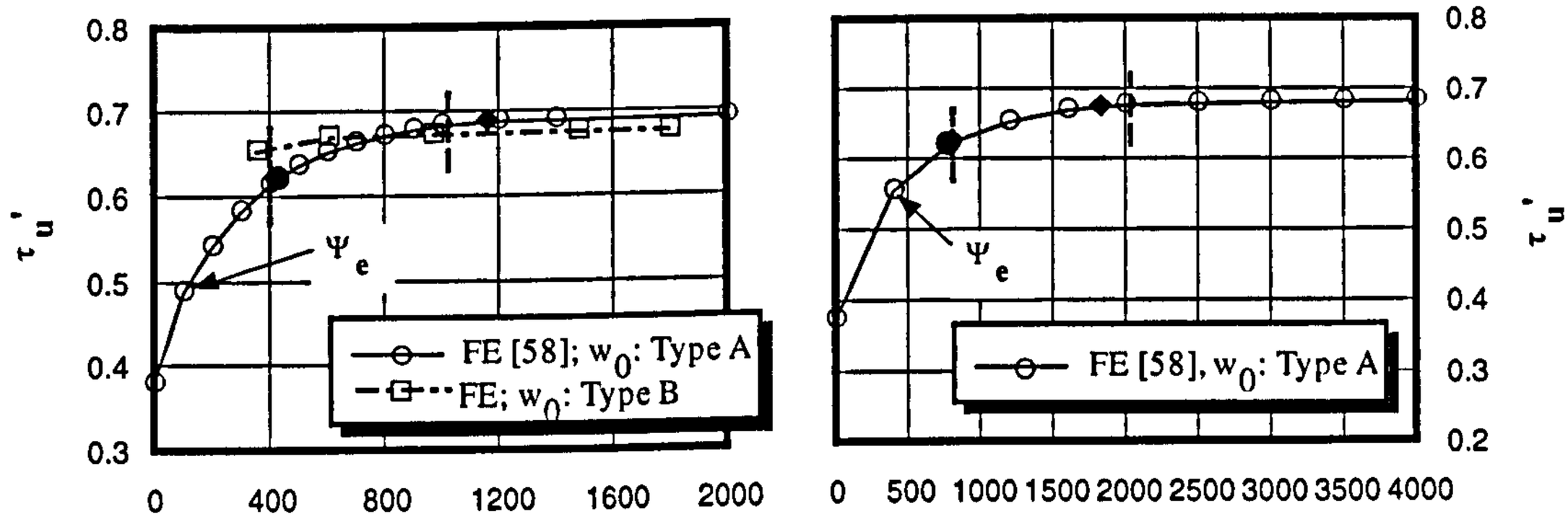


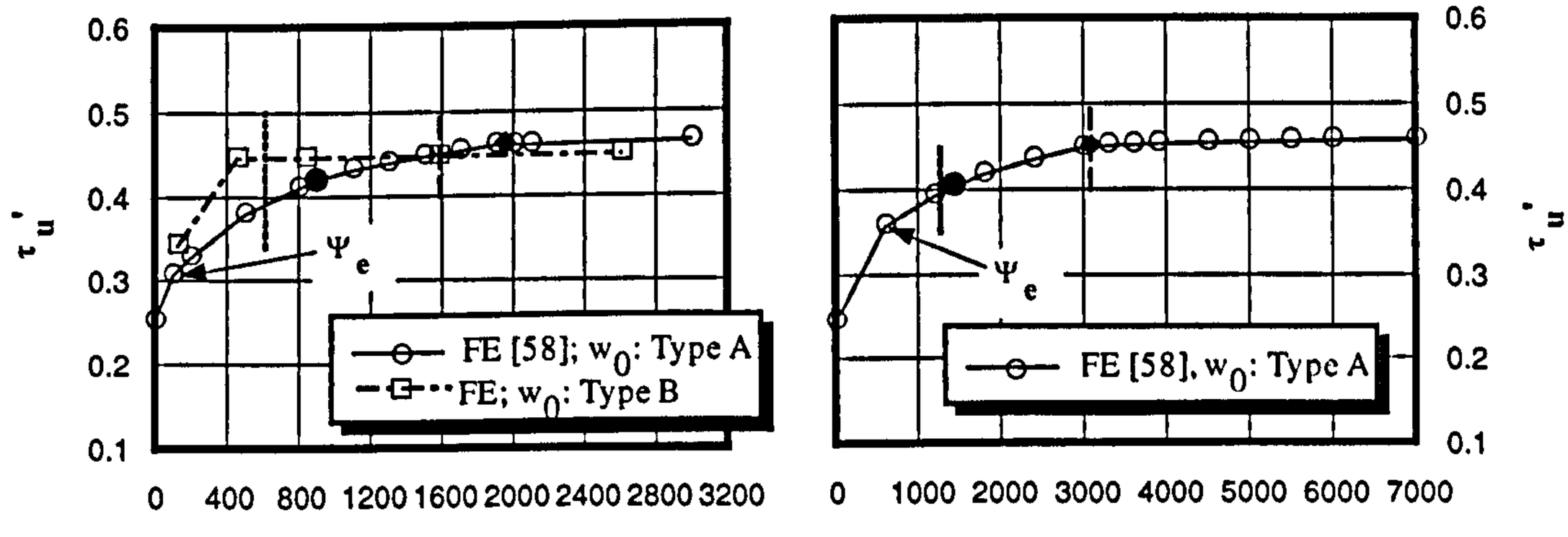
(c) d/a=2

(d) d/a=3

Figure 8.7 (Cont.) Comparison of stiffener requirements from the proposed model, with the τ_u' vs. Ψ' results from FE analyses, given by Fortune [58], with $\sigma_{0p}=\sigma_{0s}=245N/mm^2$. w_0 as in Fig. 3.5. $\Psi'=EI_s/Db$.

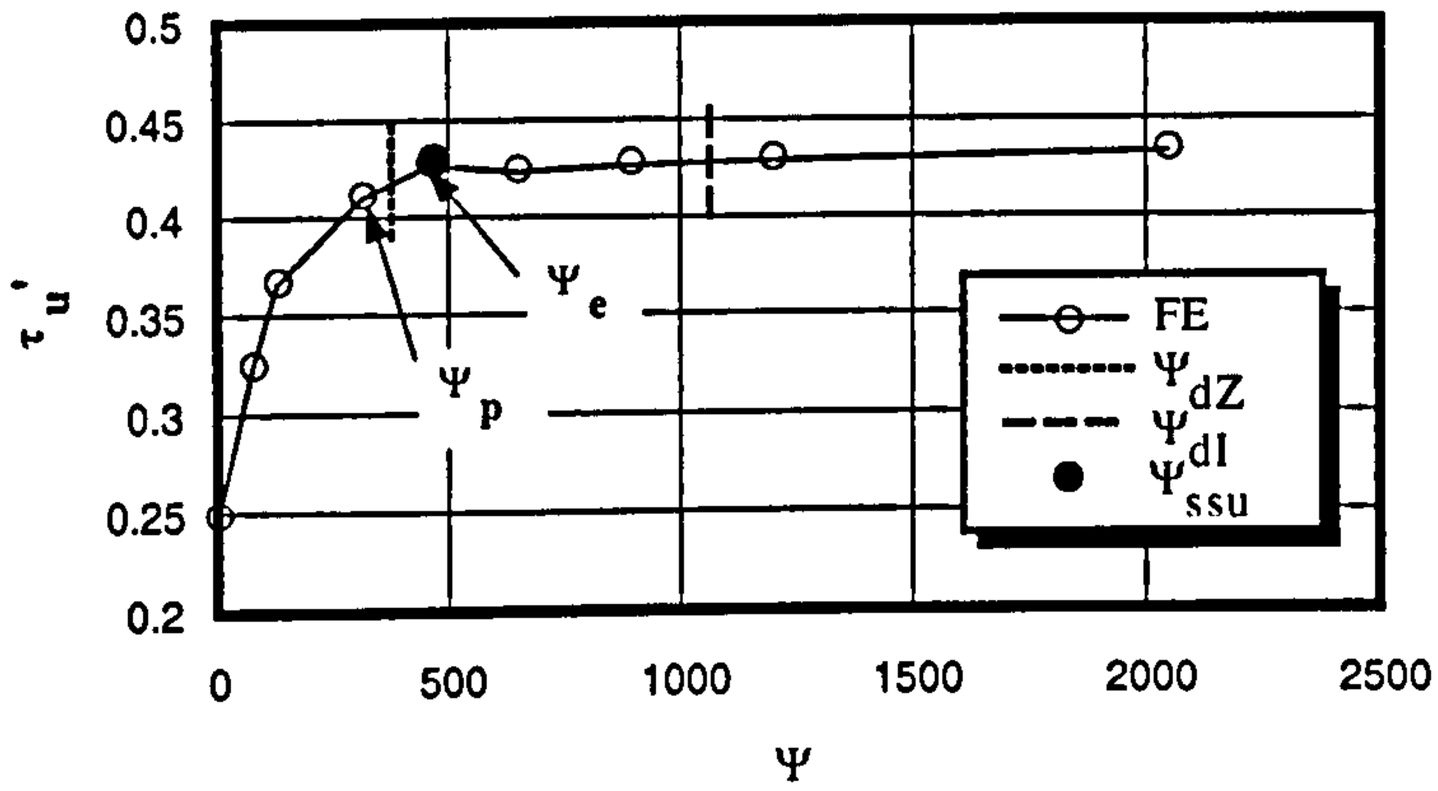


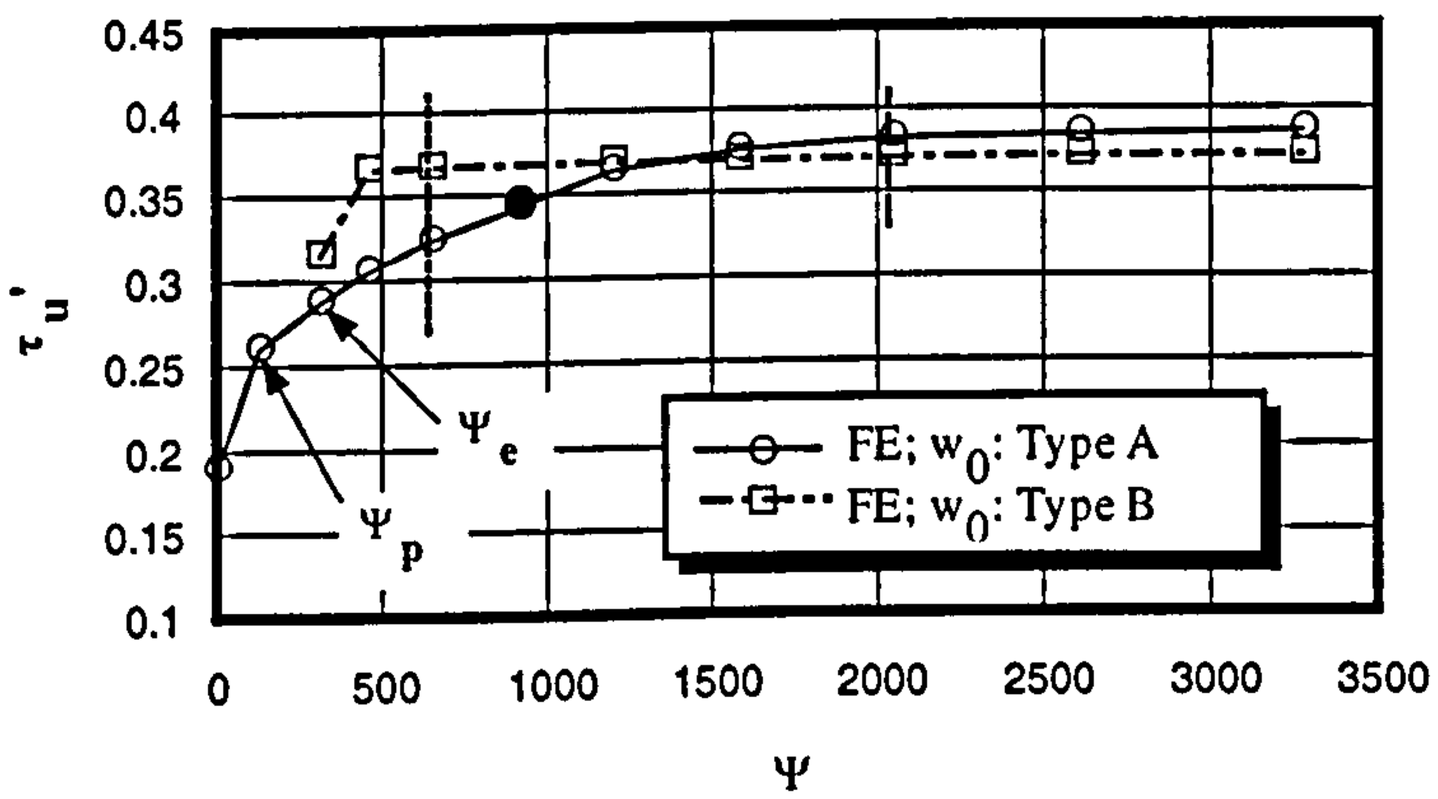


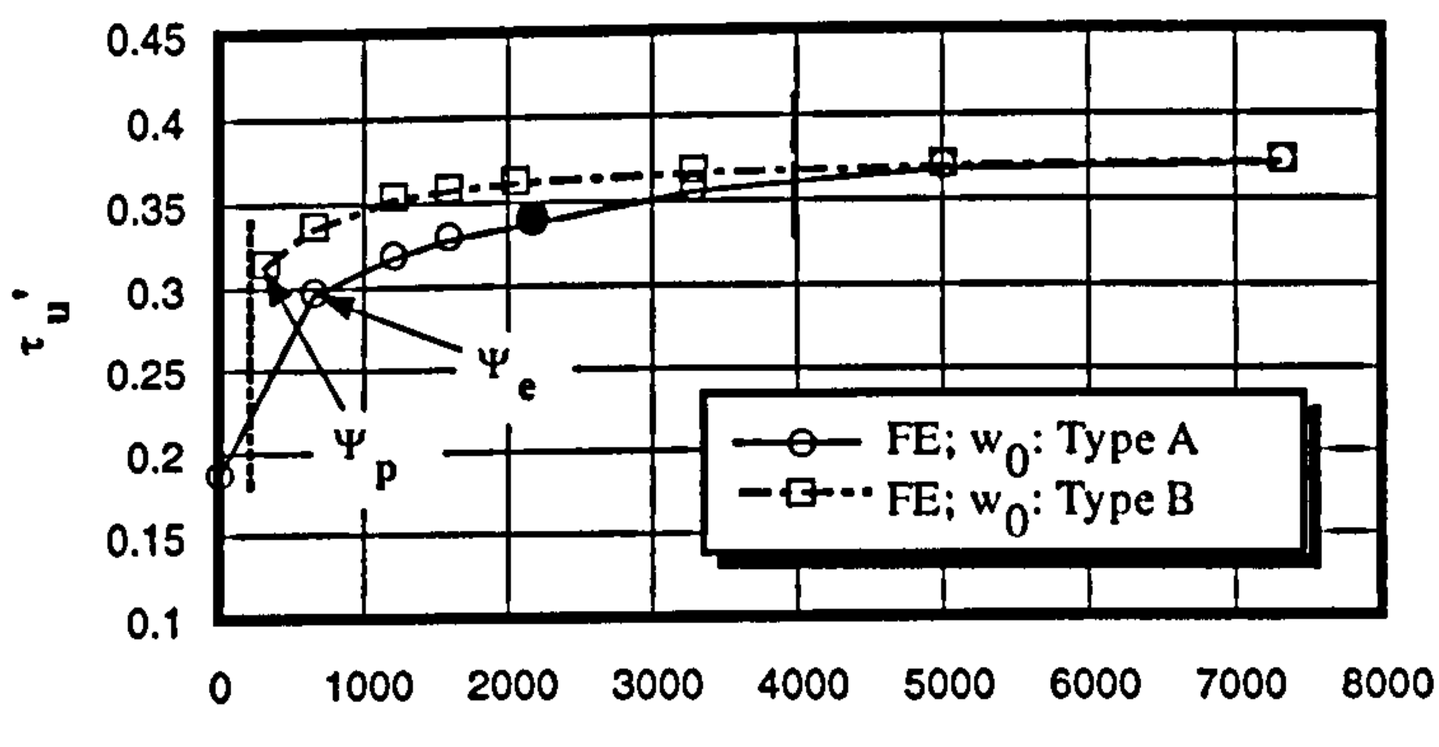


(e) d/a=5 **(f) d/a=7**

Figure 8.7 (Cont.) Comparison of stiffener requirements from the proposed model, with the τ_u' vs. Ψ results from FE analyses, with $\sigma_{0p}=\sigma_{0s}=245N/mm^2$. w_0 as in Fig. 3.5. $\Psi=EI_s/Db$.







* $\sigma_{0p}=\sigma_{0s}=355$ N/mm^2, w_0 as in Fig. 3.5

Figure 8.8 Comparison of stiffener requirements from the proposed model, with the τ_u' vs. Ψ results from finite element analyses, with $\sigma_{0p}=\sigma_{0s}=355$N/mm^2. $\Psi=EI_s/Db$. Pure shear

It should also be pointed out that the proposed method for predicting the stiffener forces is developed for stiffeners whose sizes are within the practical range; that is, the stiffener should be great enough to effectively divide the plate. For a weak stiffener, the knife edge model (also the non-deflecting stiffener model) is not valid, and neither is the equation for estimating the bending moment due to the overall buckling effect. This is because the bending moment due to the overall buckling effect is derived from the overall buckling model by assuming that the applied stress is much less than the overall buckling. However, for a weak stiffener, the overall buckling stress may be close to or less than the ultimate stress of the simply supported panel, which is the assumed applied stress for designing a stiffener.

8.5.3.2 Plates subjected to combined shear and compression

This and the next sections consider the required stiffener rigidity Ψ_{dZ} for combined shear and longitudinal loading. It is noted that the proposed design method is based on theoretical solutions and extensive numerical results, and has been verified at each stage of model development. Therefore, on account of the time limit for this investigation, only a group of typical cases are analysed to provide a basis for the validation of the proposed design model when used for the combined loading conditions.

For combined shear and compression, the plates of d/a=2 were considered, on account of the analysis cost and the irregularity in the knife edge moment. The ratios of individual loading components examined are: σ_c:τ=1:0, 1:2, 1:5. It is noted in Fig. 5.27 that for d/a=2, the possible maximum errors in estimating the knife edge moment according to the proposed method may be associated with the loading conditions σ_c:τ =1:2, 1:5, while σ_c:τ=1:0 represents a limiting loading condition, namely, longitudinal compression alone.

In Fig. 8.9(a), the required stiffener size Ψ_{dZ} according to the proposed strength criterion is compared with the ultimate strength results from finite element analyses. It is apparent that for the cases considered, the ultimate load corresponding to the stiffener

rigidity Ψ_{dZ} is well above the ultimate load of the simply supported panel, that is, the requirement given in Eqn. 8.8 is satisfied.

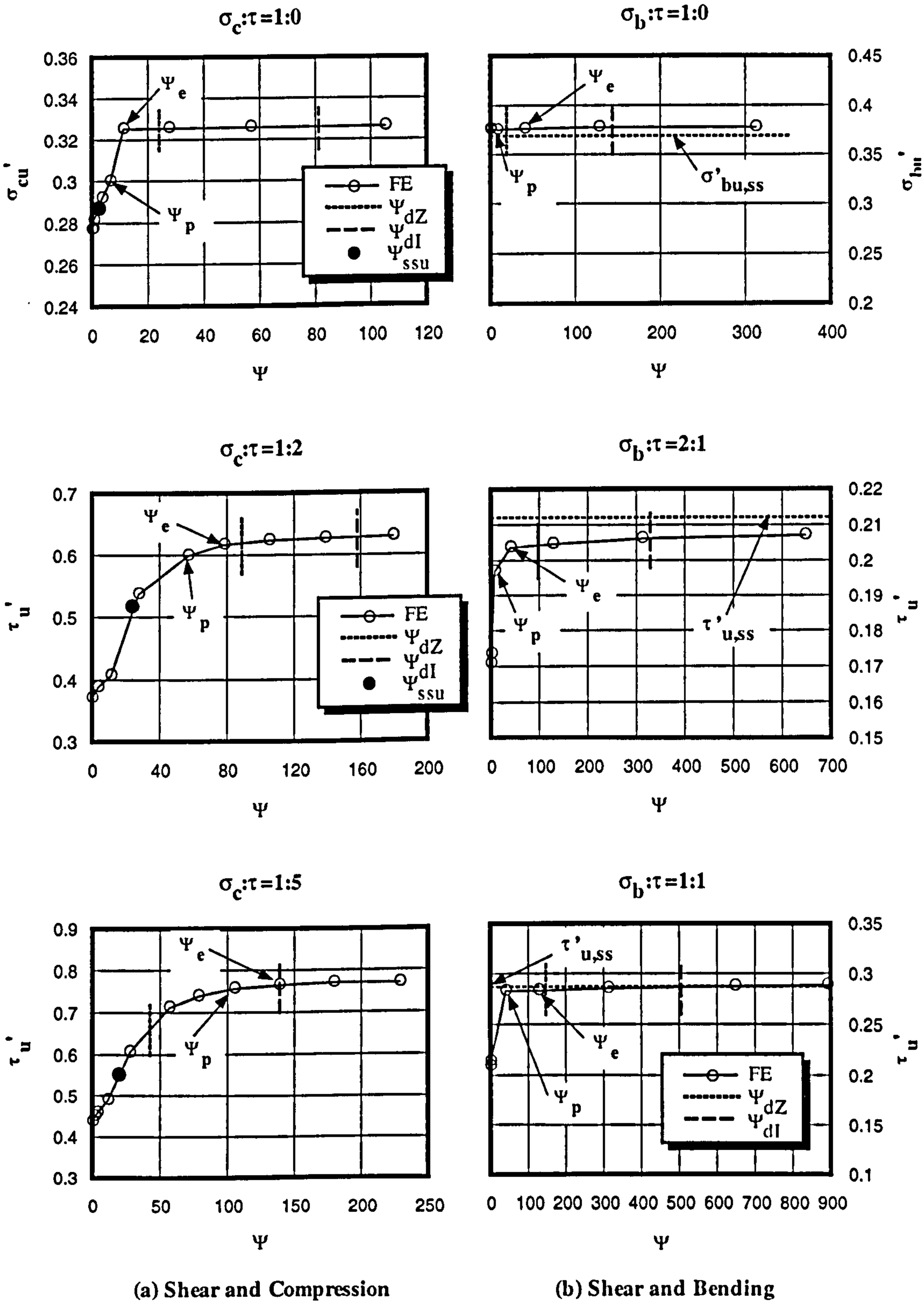
It is found that for σ_c:τ=1:5, Ψ_{dZ} is less than Ψ_p, because the assumed applied load, which is taken as the ultimate load for the simply supported panel (Table 8.5), is considerably less than the ultimate load of the stiffened plates. The difference in the ultimate loads is due to the assumed boundary conditions and the initial panel imperfection modes adopted (Chapter 3). Considering the case of compression alone, the initial panel imperfection mode is taken to be affine to the first symmetric buckling mode, and the resulting deflection mode is also symmetric. For the two-panel plates, the symmetric mode implies that one of the vertical edges of the panel is restrained against rotation (at the stiffener position), whereas for individual panels, simply supported conditions are assumed. It has been pointed out in Section 3.6.1 that the critical buckling stress for the first symmetric buckling mode is also considerably greater than that for the simply supported condition.

Nevertheless, for the purpose of validating the required stiffener size according to the proposed design model, a symmetric imperfection mode is adopted. This is because for the symmetric deflection mode, the stiffener required to divide the plate would be considerably greater than that for other imperfection modes. Therefore, a stiffener which is proved to be adequate for the symmetric deflection mode can ensure that the requirements for the stiffener are satisfied for other deflection modes.

By reference to the position of Ψ_{dZ} along the plateau of the ultimate strength curves, it is considered that a stiffness criterion is also necessary for the combined loading conditions, in order to ensure that the design stiffener is adequate. In Section 8.6, the stiffness criterion derived for pure shear is also applied for the combined loading.

8.5.3.3 Plates subjected to combined shear and bending

For combined shear and bending, the plates of d/a=2, b/t=180 were considered. The ratios of individual loading components examined are: σ_b:τ=1:0, 2:1, 1:1. It can be seen



(a) Shear and Compression **(b) Shear and Bending**

Figure 8.9 Comparison of stiffener requirements from the proposed model, with the τ_u' vs. Ψ results from FE analyses, with $\sigma_{0p}=\sigma_{0s}=355N/mm^2$. d/a=2, b/t=180. $\Psi=EI_s/Db$. Combined loading conditions.

in Fig. 5.34 that for d/a=2, significant errors in estimating the knife edge moment according to the proposed method may occur for the loading conditions σ_b:τ =2:1, 1:1, while σ_b:τ=1:0 represents a limiting loading condition, namely, pure bending.

In Fig. 8.9(b), the required stiffener size Ψ_{dZ} according to the proposed strength criterion is compared with the finite element results for the ultimate strengths of plates subjected to combined shear and bending. It is found that for the cases considered the difference in the ultimate loads for the stiffened plate and the unstiffened plate is very small, especially for the pure bending condition, and the ultimate load for the stiffened plate is also very close (about ±2%) to the ultimate load for the simply supported individual panel. Considering the limiting case of pure bending, by referring to the deflection contour diagrams presented in Fig. 8.14, it is seen that the deflection mode of the stiffened plate is close to the mode for the unstiffened plate.

It is observed that the required stiffener rigidity Ψ_{dZ} is within or beyond the region bounded by Ψ_p and Ψ_e, that is, the stiffener determined in accordance with the proposed strength criterion will remain elastic at the ultimate load. However, by reference to Fig. 8.14, it is observed that the stiffener having a rigidity of Ψ_{dZ} does not always effectively divide the plate into panels.

8.6 STIFFNESS CRITERION FOR STIFFENER DESIGN

It has been found in Section 8.5 that the proposed strength criterion may not be sufficient to provide an adequate stiffener which can effectively divide the plating into panels. For plates subjected to pure shear, it was found by Stanway et al [8] that if the stiffener effectively divides the plate, then a plate strength within the plateau of the τ_u' vs. Ψ curve, and greater than that for simply supported panels, will be attained. To ensure that the plate is effectively divided, the deflection of the stiffener at the ultimate load, denoted as w_{su}, must be sufficiently small. The approach adopted in the proposed design model is therefore to specify a maximum allowable stiffener deflection which will ensure that the plate is effectively divided, and hence the plate strength is within the plateau of the strength against Ψ curve.

In this section, a formula for estimating the stiffener deflection is presented. Based on the non-linear elasto-plastic finite element solutions for plates with a double-sided stiffener, subjected to pure shear, given by Fortune [58], a design limit for the maximum stiffener deflection at the ultimate load (stiffness criterion) is proposed for double-sided stiffeners. The smallest stiffener which satisfies the stiffness criterion, denoted as Ψ_{dl}, is then compared with the ultimate strength results from the non-linear elasto-plastic finite element analyses. The stiffener deflection limit for single-sided stiffeners is discussed in Section 8.7.

8.6.1 Calculation of Stiffener Deflection

For stiffened plates subjected to pure shear, it has been found that the stiffener deflection may be closely represented by a half sine wave [1,8]. For stiffness design of the stiffener, the deflected shape of the stiffener is assumed to be a half sine wave. This assumption is consistent with that made in the overall buckling model (Section 7.3.2), from which the stiffener moment due to the overall buckling effect is derived.

As implied in the no yield strength criterion, the stiffener is considered to be elastic in the proposed design model. Therefore, by using $M_s/EI_s=\partial^2 w_s/\partial y^2$, the stiffener deflection w_s can be written as:

$$w_s = \frac{M_s d^2}{\pi^2 E I_s} \tag{8.9}$$

where w_s and M_s are the maximum values along the stiffener length, and the calculation of the stiffener moment M_s is discussed in Section 8.3.

In Fig. 8.10, the stiffener deflection given by Eqn. 8.9 is compared with the finite element solutions. The point corresponding to the ultimate load is indicated on the elasto-plastic w_s/t vs. M_s/M_{ps} curve. It can be observed in Fig. 8.10 that the variation in w_s with M_s is basically linear, which would be expected if the sine wave prevails, especially prior to the ultimate load, and the agreement between Eqn. 8.9 and the finite

element results is considered to be satisfactory. Similar comparisons were made by Stanway [1] for different values of Ψ, with the material yield stress being taken as 245N/mm^2. In the design model by Stanway et al [9], the stiffener deflection is also estimated by means of Eqn. 8.9.

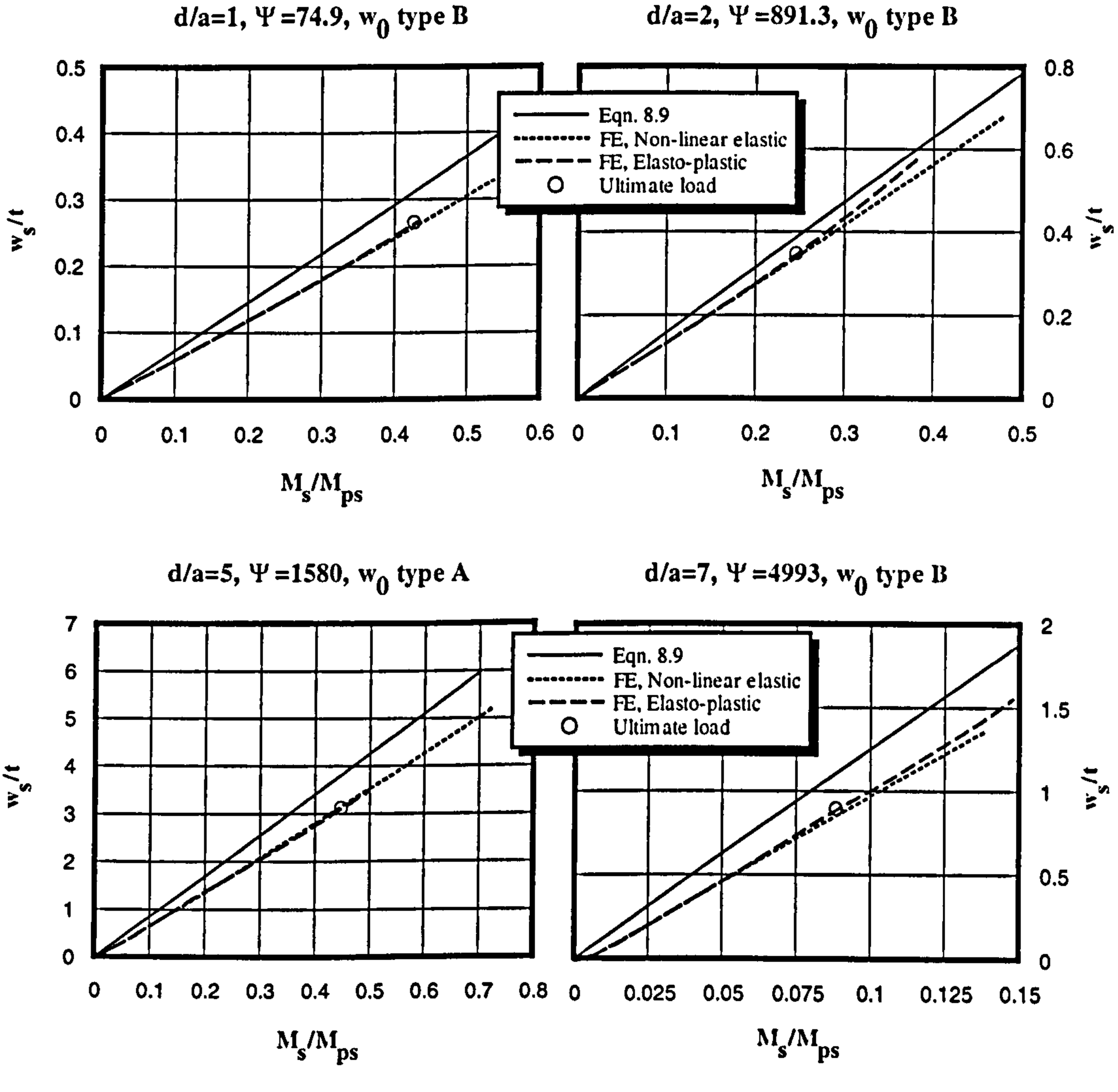


Fig. 8.10 Comparison of w_s vs. M_s curves from finite element analyses with Eqn. 8.9. Pure shear. Initial imperfection w_0 as in Fig. 3.5. $\sigma_{0p}=\sigma_{0s}=355N/mm^2$. $\Psi=EI_s/Db$

8.6.2 Design Limit of Stiffener Deflection

The stiffness criterion originally developed by Stanway et al [9] is that the stiffener deflection measured over a panel buckle half wavelength should be small in relation to the amplitude of the panel buckle for a rigid stiffener, and the panel deflection is assumed to be that given by non-linear elastic analyses for a simply supported panel. This approach is logical in introducing a quantitative means to define the subdivision of the plate. However, it involves the estimation of the panel deflection, which has been found to be quite complicated even for pure shear, due to the variation of the deflection mode with the applied load (see Section 4.6). For plates subjected to combined shear and longitudinal loading, the estimation of the panel deflection will be much more difficult.

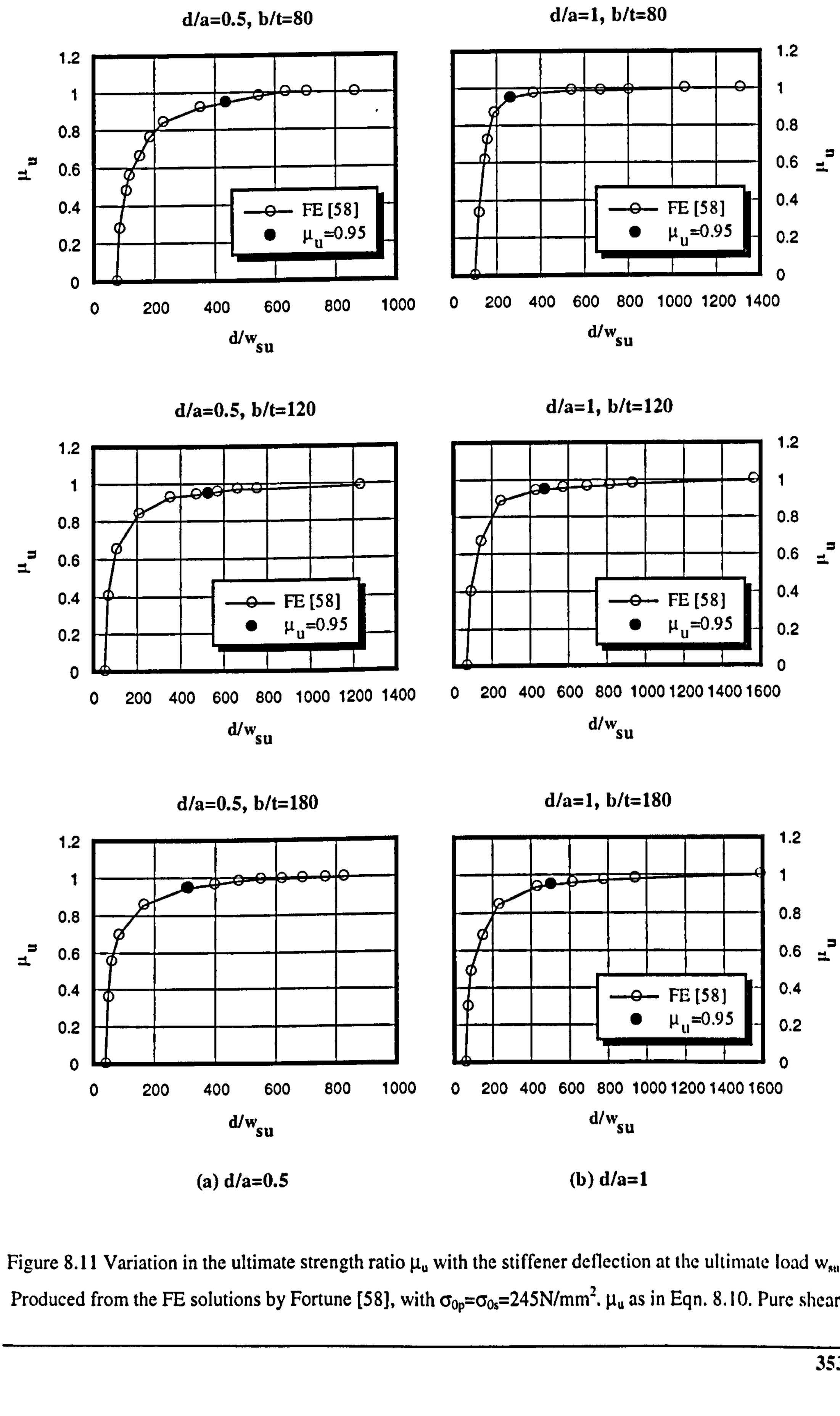
An alternative approach to ensure the subdivision of the plate is to limit the straightness of the stiffener. Assuming that the deflected shape of the stiffener is a half sine wave, the straightness of the stiffener may be represented by the ratio of w_s/d.

The stiffener deflection ratio w_s/d must be small enough to ensure that the effectively divided panel mode and the required plate strength are achieved. For plates subjected to pure shear, this means that a plate strength within the plateau of the τ_u' vs. Ψ curve should be attained. In order to define consistently a point of reference for the start of the plateau, the following parameter is introduced:

$$\mu_u = \frac{\tau_u(\Psi) - \tau_u(\Psi = 0)}{\tau_u(\Psi = \Psi_{max}) - \tau_u(\Psi = 0)} \tag{8.10}$$

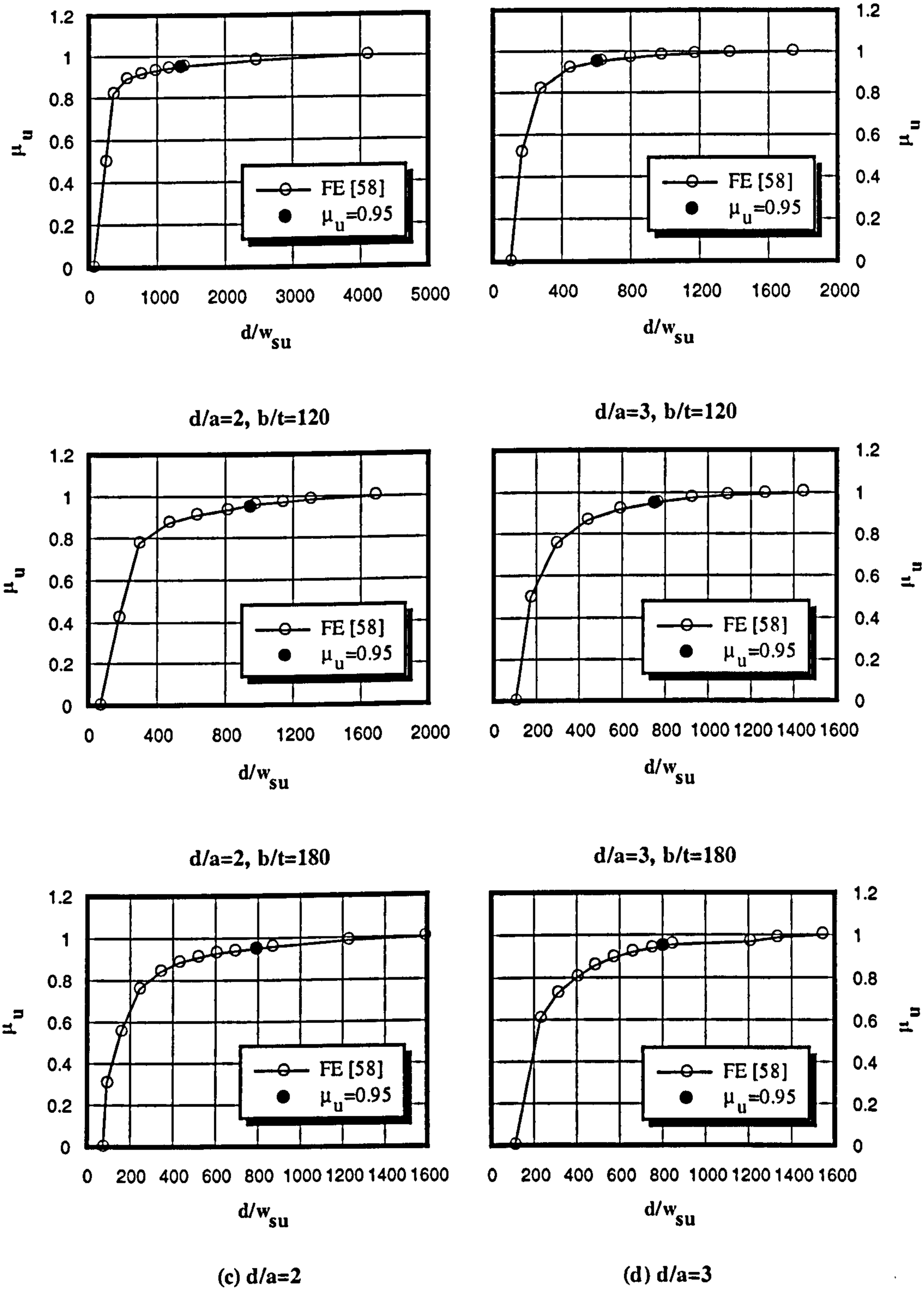
where Ψ_{max} denotes the maximum finite stiffener rigidity considered in the parametric analyses.

Fig. 8.11 presents the μ_u vs. d/w_{su} results derived from the finite element solutions given by Fortune [58] for plates subjected to pure shear. Marked on the μ_u vs. d/w_{su} curves are the positions for μ_u=0.95. It can be seen in Fig. 8.11 that the d/w_{su} for μ_u=0.95 remains at the start of the plateau of the μ_u vs. d/w_{su} curve.



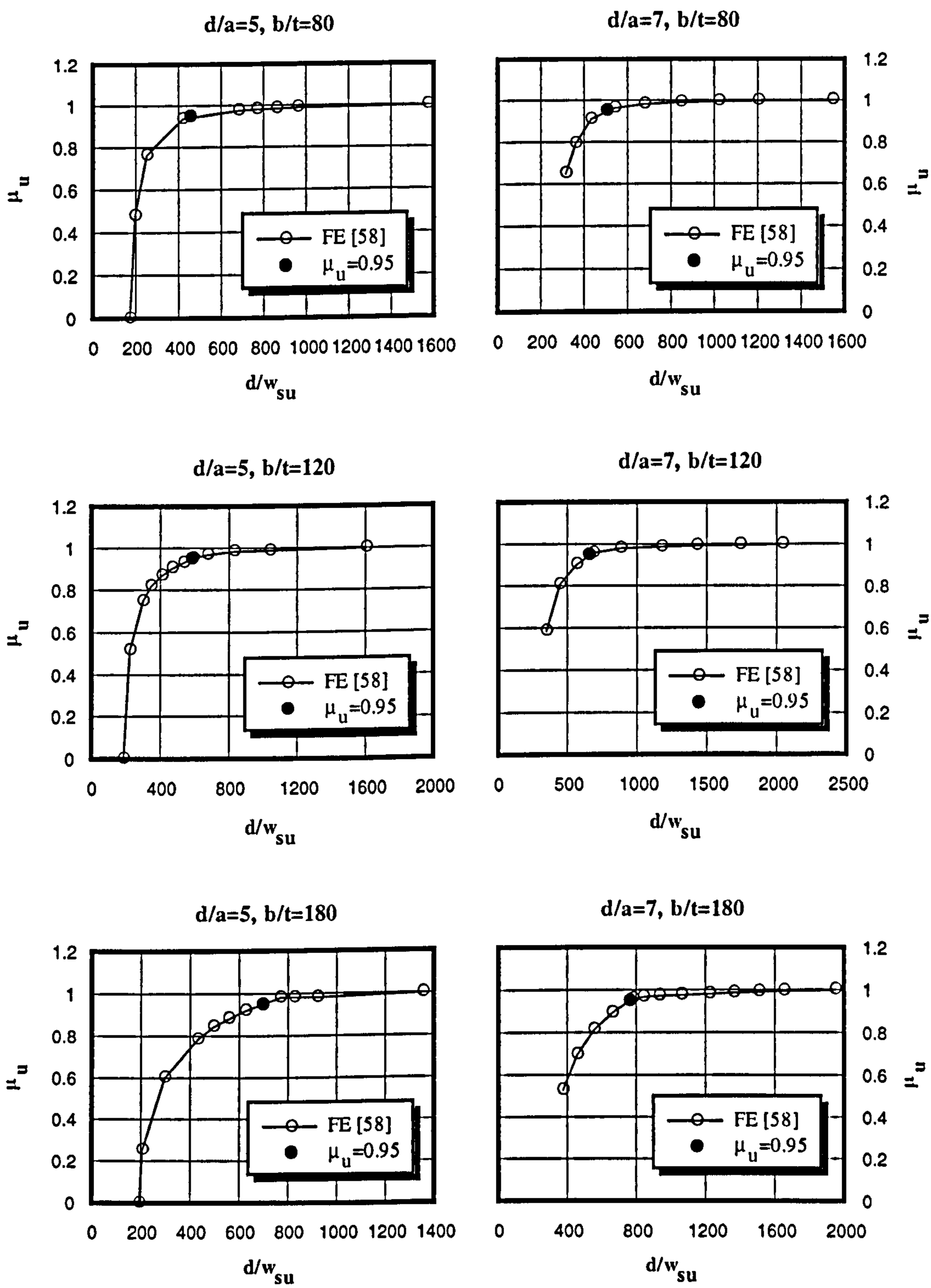
(a) d/a=0.5 (b) d/a=1

Figure 8.11 Variation in the ultimate strength ratio μ_u with the stiffener deflection at the ultimate load w_{su}. Produced from the FE solutions by Fortune [58], with $\sigma_{0p}=\sigma_{0s}=245N/mm^2$. μ_u as in Eqn. 8.10. Pure shear



(c) d/a=2 (d) d/a=3

Figure 8.11 (Cont) Variation in the strength ratio μ_u with the stiffener deflection at the ultimate load w_{su}. Produced from the FE solutions by Fortune [58], with $\sigma_{0p}=\sigma_{0s}=245N/mm^2$. μ_u as in Eqn. 8.10. Pure shear



(e) d/a=5 (f) d/a=7

Figure 8.11 (Cont) Variation in the strength ratio μ_u with the stiffener deflection at the ultimate load w_{su}. Produced from the FE solutions by Fortune [58], with $\sigma_{0p}=\sigma_{0s}=245N/mm^2$. μ_u as in Eqn. 8.10. Pure shear

Values of d/w_{su} corresponding to μ_u=0.95, interpolated from the FE results, are listed in Table 8.7, and shown against the panel aspect ratio d/a in Fig. 8.12. It is found in Fig. 8.12 that a single value of the limit of d/w_{su} may be specified for a given d/a and different values of b/t.

Table 8.7 Values of d/w_{su} corresponding to μ_u=0.95. $\sigma_{0p}=\sigma_{0s}$=245N/mm^2. FE results (from [58])

d/a	b/t=80	b/t=120	b/t=180	Average	Design Limit (Eqn.8.12)
0.5	434	525	310	423	500
1	262	475	503	413	500
2	1342	945	791	1026	1000
3	603	750	800	718	800
5	456	585	697	579	800
7	506	658	763	642	800

For design of transverse stiffeners, it is proposed that the stiffener deflection at the ultimate load, w_{su}, calculated using Eqn. 8.9, should be less than the design limit of the stiffener deflection, denoted as w_{sd}, that is:

$$w_{su} \leq w_{sd} \tag{8.11}$$

where w_{sd} for double-sided (concentric) stiffeners is given by:

$$\frac{w_{sd}}{d}=\begin{cases} \dfrac{1}{500}\left(\dfrac{b}{d}\right), & for \quad \dfrac{d}{a}\leq 2 \\ \dfrac{1}{4000}\left(7-6\dfrac{a}{d}\right), & for \quad 2<\dfrac{d}{a}<3 \\ \dfrac{1}{800}, & for \quad \dfrac{d}{a}\geq 3 \end{cases} \tag{8.12}$$

The value of w_{sd} for single-sided stiffeners is studied in Section 8.7, and is proposed to be taken as the twice the value given in Eqn. 8.12.

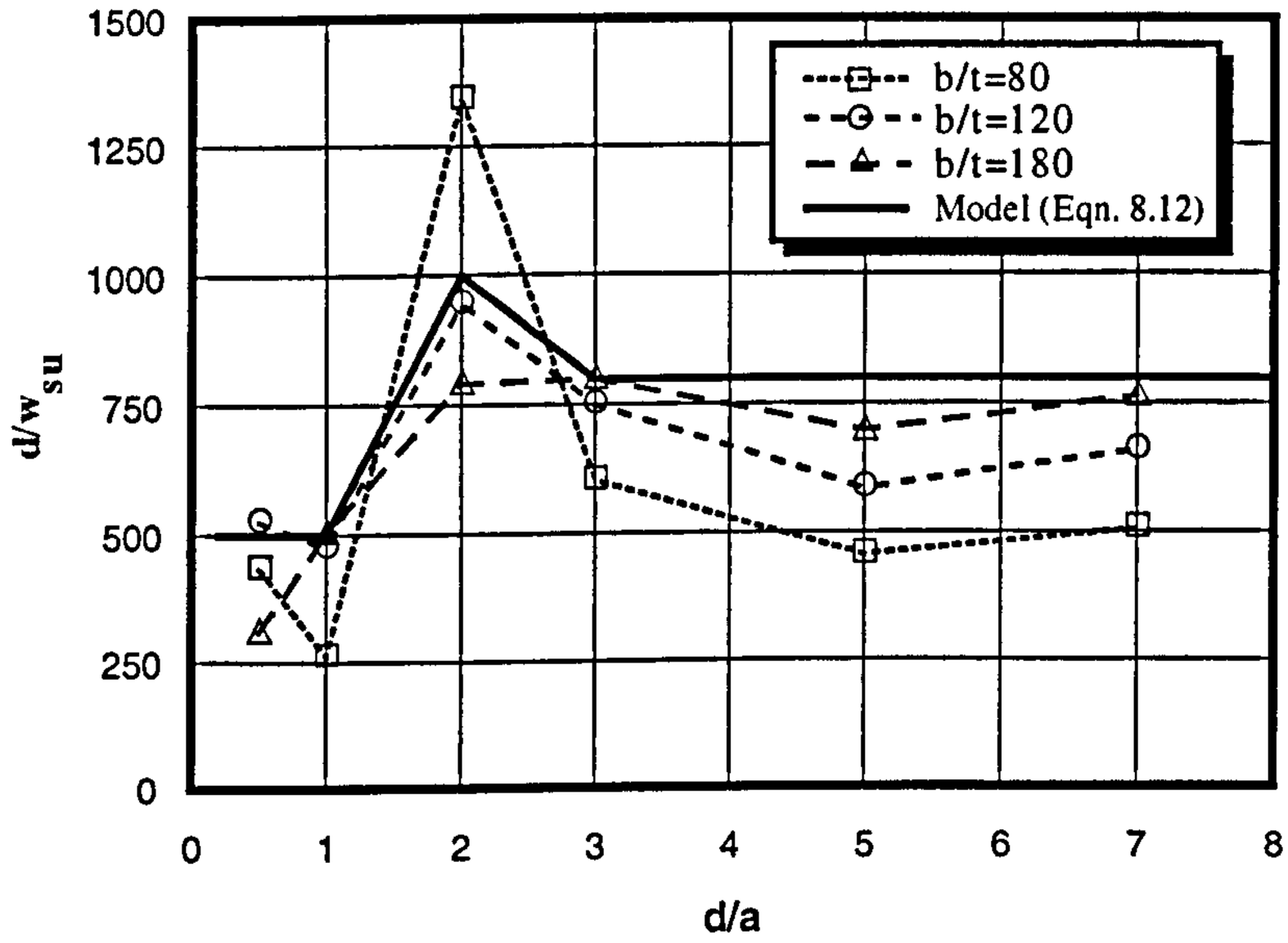


Figure 8.12 Values of the stiffener deflection at the ultimate load w_{su} for μ_u=0.95. Pure shear. Proposed design limit of the stiffener deflection as given in Eqn. 8.12. μ_u as in Eqn. 8.10

The proposed design limit of w_{su}/d given by Eqn. 8.12 is also shown in Fig. 8.12. It is noted that for d/a=2, b/t=80, the proposed value (w_{su}/d=1/1000) is less than that for μ_u=0.95. Nevertheless, it can be found in Fig. 8.11(c) that a plate strength within the plateau of the μ_u vs. d/w_{su} curve can still be achieved for w_{su}/d=1/1000.

In Fig 8.7, the stiffener rigidity for which the stiffener deflection at the ultimate load is equal to the deflection limit specified in Eqn. 8.12, denoted as Ψ_w, is also indicated. The value of Ψ_w is estimated by the interpolation of the finite element solutions. It can be seen in Fig. 8.7 that Ψ_w lies within the plateau of the τ_u' vs. Ψ curve. It should be noted that Ψ_w is from finite element solutions, not from the design model.

It is also proposed that the design limit of w_{su}/d given by Eqn. 8.12 is valid for plates subjected to combined shear and longitudinal loading, because the ratio of w_{su}/d

specified in Eqn. 8.12 represents the requirement of the stiffener straightness for the effective subdivision of the plate for double-sided stiffeners.

8.6.3 Required Stiffener Size According to the Stiffness Criterion

In this section, the flexural rigidity of the smallest stiffener (double-sided, h/t_s=10) which satisfies the proposed stiffness criterion in Eqns. 8.11 and 8.12, denoted as Ψ_{dI}, is compared with the ultimate strength results from the non-linear elasto-plastic finite element analyses. The stiffener moment M_s was determined in accordance with the method summarised in Section 8.3. The applied load was taken as the ultimate load of the simply supported panel, presented in Section 8.4. Stiffener sizes for plates under different loading conditions were determined, which are presented in the subsequent sections.

8.6.3.1 Plates subjected to pure shear

The smallest stiffener which satisfies the stiffness criterion given in Eqns. 8.11 and 8.12 is compared with the finite element results of τ_u' vs. Ψ in Figs. 8.7 and 8.8, for plates subjected to pure shear. Also shown in Figs. 8.7 and 8.8 is the flexural rigidity of the smallest stiffener (double-sided, h/t_s=10) which satisfies the strength criterion (Section 8.5), denoted as Ψ_{dZ}.

According to the stiffness criterion (Eqns. 8.11 and 8.12), the stiffener deflection at the ultimate load w_{su} should be restricted to ensure that the plate is effectively divided, and consequently to ensure that a plate strength within the plateau of the τ_u' vs. Ψ curve, and greater than the strength for simply supported panels, is attained. Referring to Figs. 8.7 and 8.8, it is found that for the cases considered, the stiffener with a rigidity of Ψ_{dI}, determined in accordance with the proposed stiffness criterion, satisfy this requirement.

By comparison of the required stiffener rigidities Ψ_{dZ} and Ψ_{dI}, it is found that for the cases examined for d/a=0.5 and 1, the adequate design size of the stiffener, denoted as

Ψ_d (Ψ_d=max{Ψ_{dZ}, Ψ_{dI}}), is governed by the strength criterion, whereas for all the other cases, the stiffness criterion governs.

The above observation suggests that in order to provide an adequate design stiffener, both the strength and stiffness criteria are required. The two criteria are necessary when considering the possible combinations of stiffener properties. For example, if the ratio Z_s/I_s is increased, or if the yield stress of stiffener is increased, the strength criterion is more likely to produce an unsatisfactory stiffener. On the other hand, if the ratio Z_s/I_s is reduced, for example, by replacing a flat bar stiffener with a Tee stiffener, the stiffness criterion is more likely to result in an unsatisfactory stiffener. In the proposed design model, both the strength and stiffness criteria are used to quantify the required stiffener.

It is observed in Figs. 8.7 and 8.8 that the design stiffener rigidity Ψ_d is in general at a satisfactory distance along the plateau of the τ_u' vs. Ψ curve.

8.6.3.2 Plates subjected to combined shear and compression

In Fig. 8.9(a), the required stiffener size Ψ_{dI} according to the proposed stiffness criterion is compared with the ultimate strength results from finite element analyses for the cases discussed in Section 8.5.3.2. It is apparent that for the cases considered, for the required stiffener Ψ_{dI}, the plate strength is within the plateau region of the strength curve, and greater than the strength for simply supported panels.

By comparison of the required stiffener rigidities Ψ_{dZ} and Ψ_{dI}, it is found that for the cases examined for combined shear and compression, the adequate design size of the stiffener Ψ_d is governed by the stiffness criterion, and Ψ_d is at a reasonable distance along the plateau of the strength curve.

According to the stiffness criterion (Eqns. 8.11 and 8.12), the stiffener with a rigidity of Ψ_{dI} should ensure that the plate is effectively divided at the ultimate load of the stiffened plate. In Fig. 8.13, the contour plots of the out-of-plane deflection at the

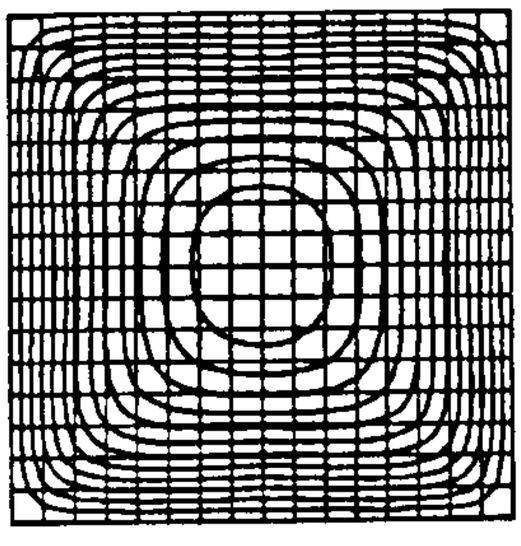
ultimate load are presented for some cases examined. It can be seen that for the stiffener rigidity Ψ_{dl}, an effectively divided panel mode can be achieved.

In Table 8.8, the numerical values of Ψ_{dZ} and Ψ_{dl} required for the combined loading are compared with those for pure shear. It is observed that for the same stiffener type, the design stiffener rigidity Ψ_d for the combined loading conditions may be considerably less than that required for the same plate to achieve its pure shear strength. This suggests that it would be considerably conservative if the stiffener designed to develop the maximum shear capacity of the panel is used for other combinations of shear and compression.

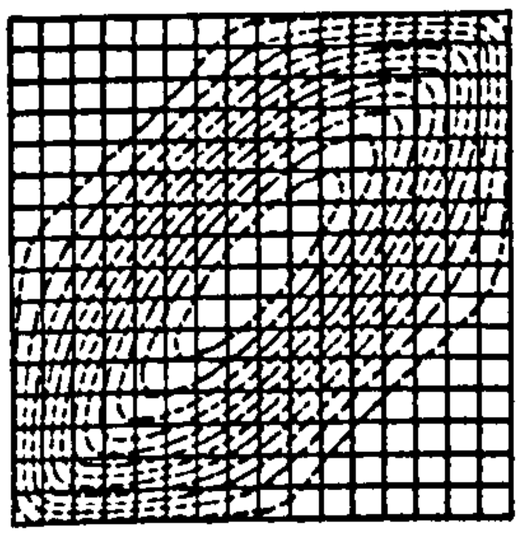
Table 8.8 Comparison of the required stiffener rigidities Ψ_{dZ} and Ψ_{dl} for combined shear and compression conditions. d/a=2, a/t=80, $\sigma_{0p}=\sigma_{0s}=355N/mm^2$

$\sigma_c:\tau$	Ψ_{dZ}	Ψ_{dl}	Ψ_d	$\Psi_d/\Psi_{d.\ shear}$
1:0	23.9	81.2	81.2	0.306
1:2	88.9	157.9	157.9	0.594
1:5	42.4	138.8	138.8	0.522
0:1	98.3	265.7	265.7	1.0

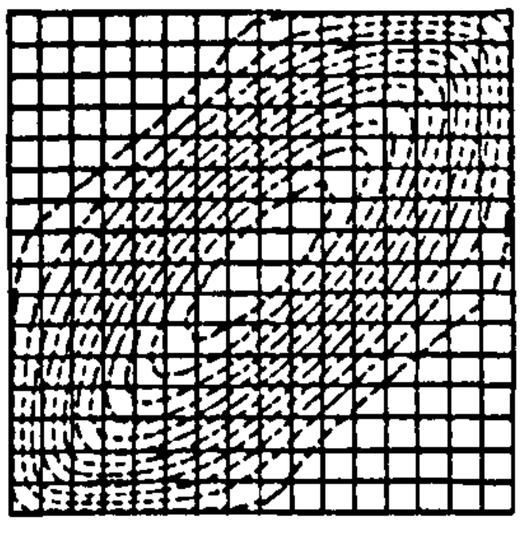
It is noted in Table 8.8 that the design stiffener rigidity Ψ_d for $\sigma_c:\tau=1:5$ is slightly less than that for $\sigma_c:\tau=1:2$. This may not be the case, and the reason for this can be found in Fig. 5.27. It is observed in Fig. 5.27 that the knife edge moment M_{pk} for $\sigma_c:\tau=1:5$ is underestimated according to the proposed design formulae, while M_{pk} for $\sigma_c:\tau=1:2$ is overestimated. Nevertheless, as stated before, the design stiffener Ψ_d for these two cases can satisfy the design requirements, although Ψ_d is marginally satisfactory for $\sigma_c:\tau=1:5$. Therefore, the simple approach proposed in this thesis for combined shear and compression is considered to be satisfactory. Alternatively, for cases where shear is predominant, such as $\sigma_c/\tau\leq 1/5$, the stiffener rigidity needed for pure shear may be used as a safe estimate of the required stiffener rigidity; for cases where compression is predominant, it would be even safer.



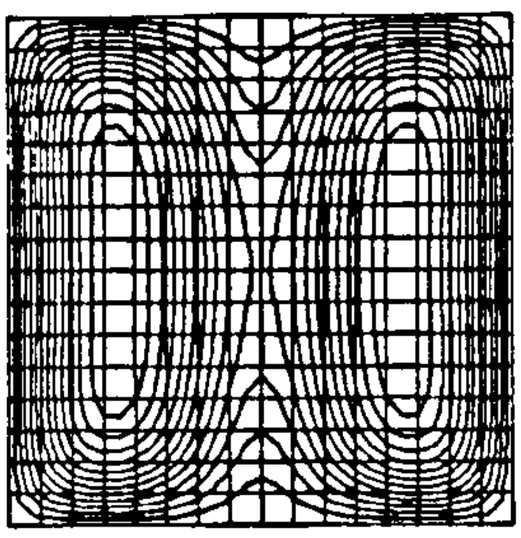
Ψ=0



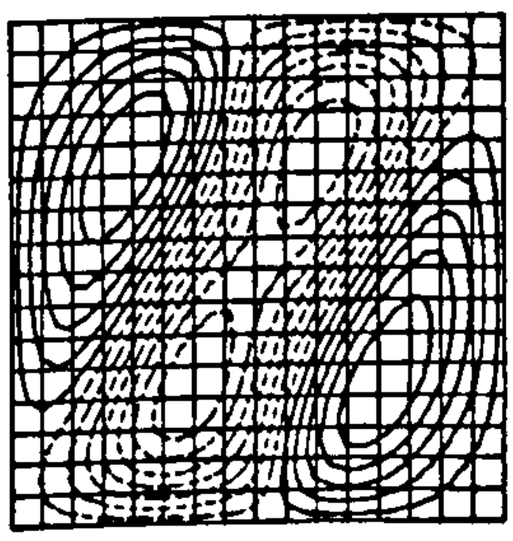
Ψ=0



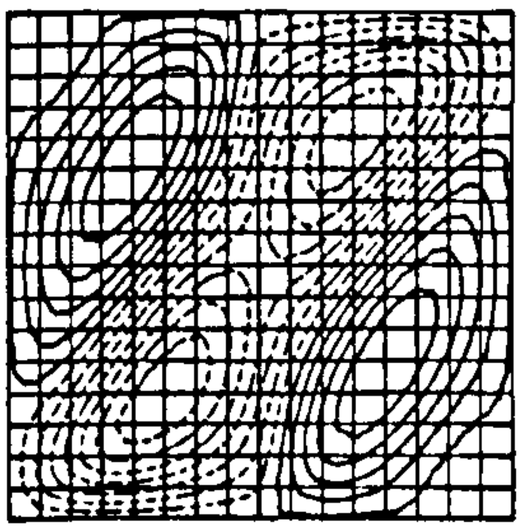
Ψ=0



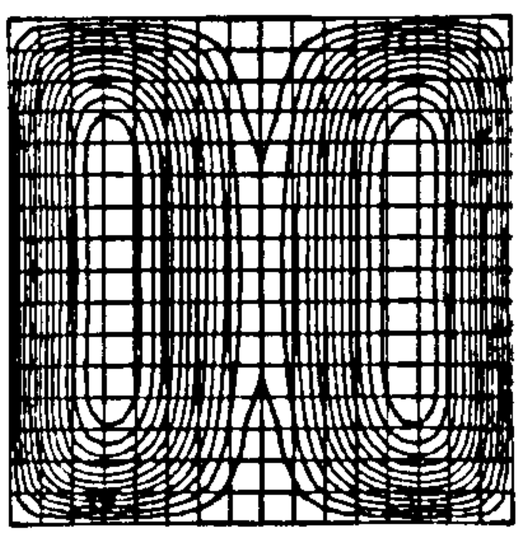
Ψ=11.22



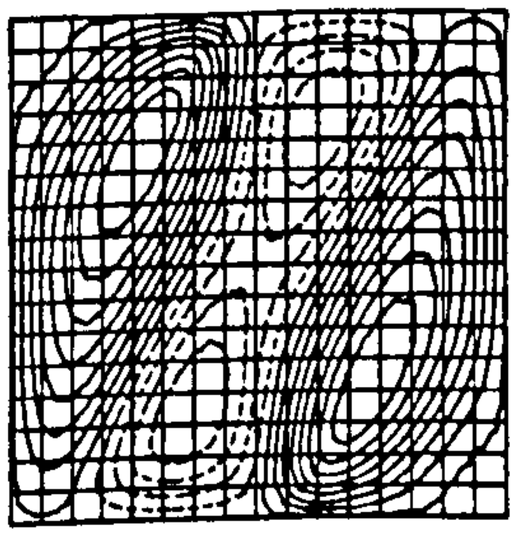
Ψ=27.39



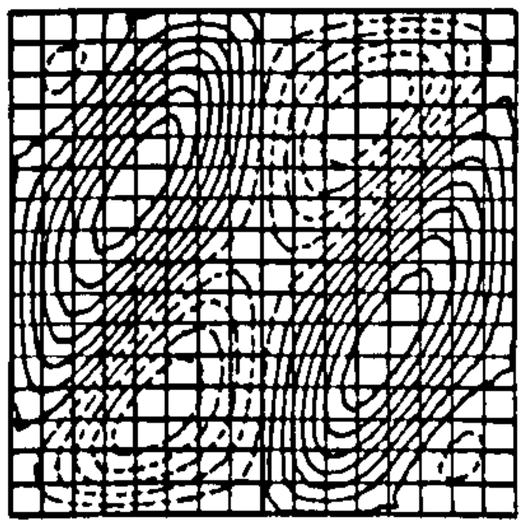
Ψ=56.80



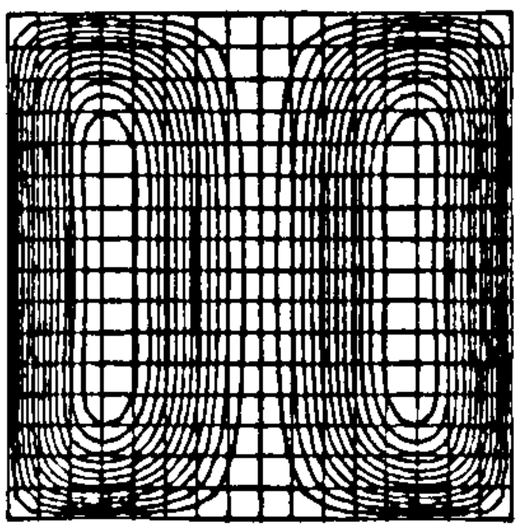
Ψ=27.39



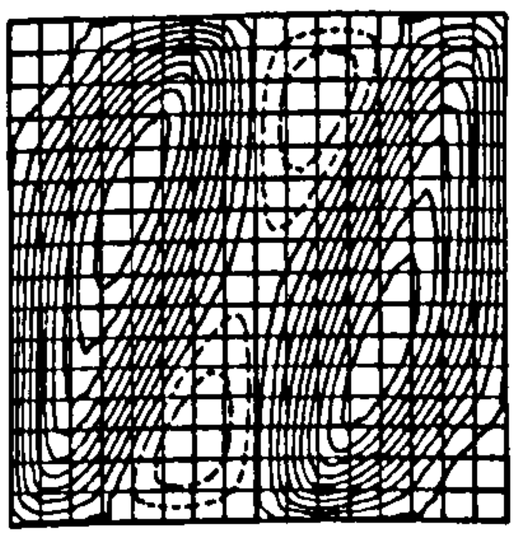
Ψ=56.80



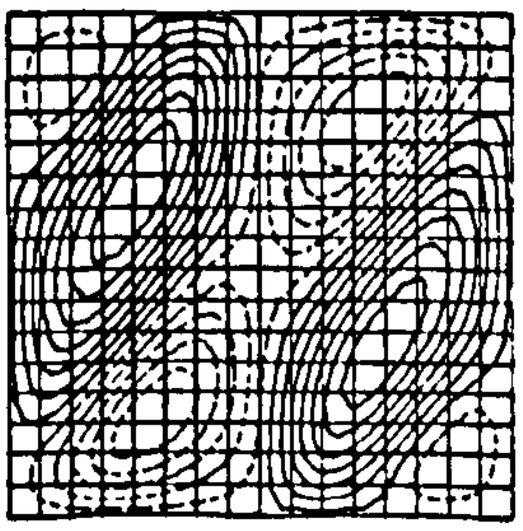
Ψ=138.7



Ψ=56.80



Ψ=105.2



Ψ=179.5

(a) Compression **(b) σ_c:τ=1:2** **(c) σ_c:τ=1:5**

Figure 8.13 Comparison of the deflection modes at the ultimate load for varying stiffener rigidities. Stiffened plates subjected to combined shear and compression. w_0 type A as in Fig. 3.5. $\Psi=EI_s/Db$

It has been pointed out in Section 8.5.3.2 that the strength curve presented in Fig. 8.9(a) for compression alone is from ABAQUS by adopting a symmetric imperfection mode. For the symmetric deflection mode, the ultimate load of the stiffened plate is significantly greater than the applied load assumed for the stiffener design, which is taken as the ultimate load for the simply supported panel (Table 8.5), due to the constraint implied by the symmetric deflection mode.

8.6.3.3 Plates subjected to combined shear and bending

In Fig. 8.9(b), the required stiffener size Ψ_{dI} according to the proposed stiffness criterion is compared with the ultimate strength results from finite element analyses for the cases discussed in Section 8.5.3.3. It is observed that for the cases considered, for the required stiffener Ψ_{dI}, the plate strength is within the plateau region of the strength curve, and is very close ($\approx \pm 2\%$, as indicated in Section 8.5.3.3) to the ultimate load for the simply supported individual panel. Also, it is found that for the cases examined for combined shear and bending, the design size of the stiffener, $\Psi_d = \max\{\Psi_{dZ}, \Psi_{dI}\}$, is governed by the stiffness criterion.

According to the stiffness criterion (Eqns. 8.11 and 8.12), the stiffener with a rigidity of Ψ_{dI} should ensure that the plate is effectively divided at the ultimate load of the stiffened plate. In Fig. 8.14, the contour plots of the out-of-plane deflection at the ultimate load are presented for some cases examined. It can be seen that for the stiffener rigidity Ψ_{dI}, an effectively divided panel mode can be achieved.

In Table 8.9, the numerical values of Ψ_{dZ} and Ψ_{dI} required for the combined loading are compared with those for pure shear. It is observed that for the same stiffener type, the design stiffener rigidity Ψ_d for the combined loading conditions may be considerably less than that required for the same plate but subjected to pure shear alone. This suggests that it would be considerably conservative if the stiffener designed to develop the maximum shear strength of the panel is used for other combinations of shear and bending.

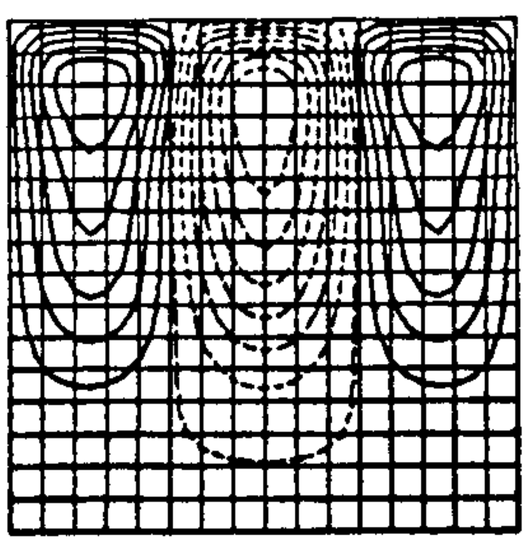
Table 8.9 Comparison of the required stiffener rigidities Ψ_{dZ} and Ψ_{dI} for combined shear and bending conditions. d/a=2, a/t=180, $\sigma_{0p}=\sigma_{0s}=355N/mm^2$

σ_b:τ	Ψ_{dZ}	Ψ_{dI}	Ψ_d	$\Psi_d/\Psi_{d.\ shear}$
1:0	19.15	143.6	143.6	0.135
2:1	97.93	328.9	328.9	0.309
1:1	146.95	505.8	505.8	0.476
0:1	375.1	1063.5	1063.5	1.0

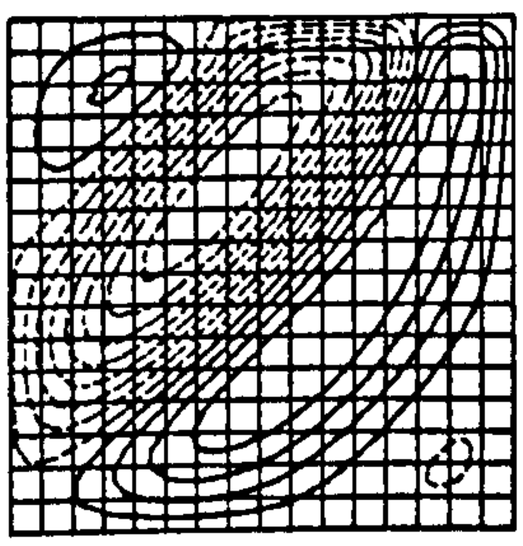
8.7 DESIGN OF SINGLE-SIDED STIFFENERS

For single-sided stiffeners, different assumptions in respect of the neutral axis and the effective section of the stiffener are made in existing design methods. According to BS5400 [3] and Eurocode 3 [4], the effective cross-section of the stiffener consists of stiffener section itself and a width of plate. In some other methods, as that proposed by Horne and Grayson [45], only the actual stiffener section is considered, but the neutral axis of the stiffener section is taken to be at the surface of the plate. It was suggested that with the moment of inertia I_s calculated about an axis at the surface of the plate, the single-sided stiffener can be designed to achieve the same flexural rigidity Ψ as required for double-sided stiffeners.

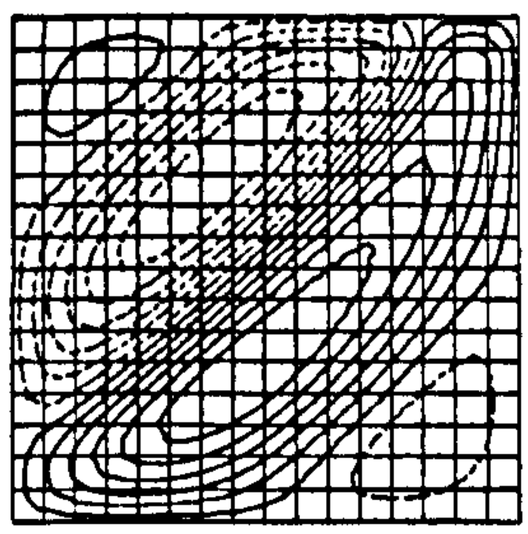
In this section, numerical results are presented for plates with a single-sided flat bar stiffener (h_s/t_s=10). The stress distribution along the width of the stiffener, indicated by the finite element solutions, is examined. As a result, the adequacy of the assumption made by Horne and Grayson [45] regarding the neutral axis of the stiffener cross section can be examined. Also, the stiffener forces predicted by the method now proposed (Section 8.3) can be verified. Based on these analyses, the method for calculating the stresses in the single-sided stiffener is proposed. Special design requirements for single-sided stiffeners are discussed in this section.



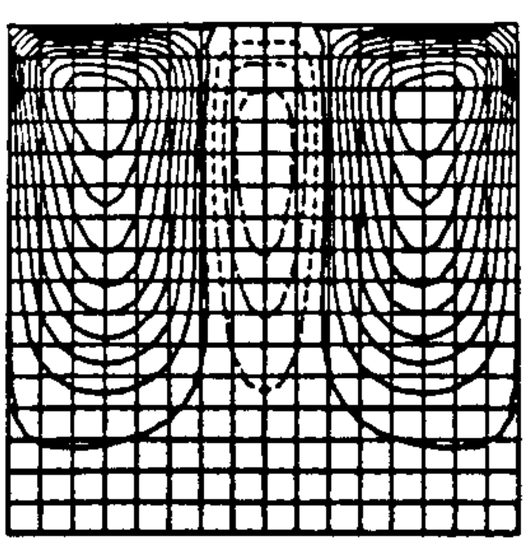
Ψ=0



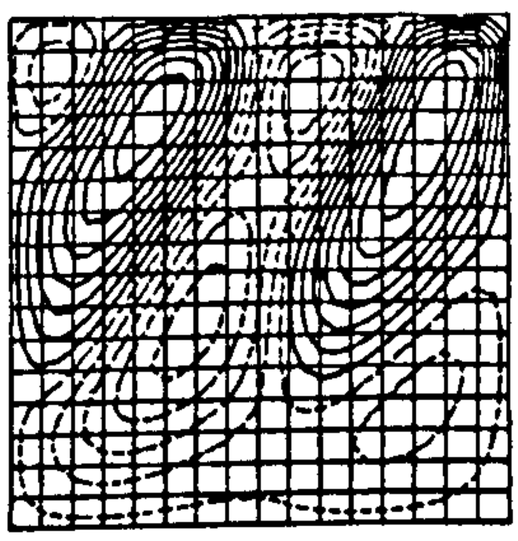
Ψ=0



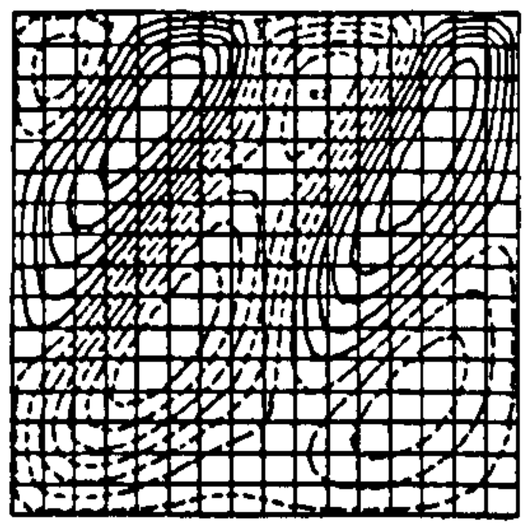
Ψ=0



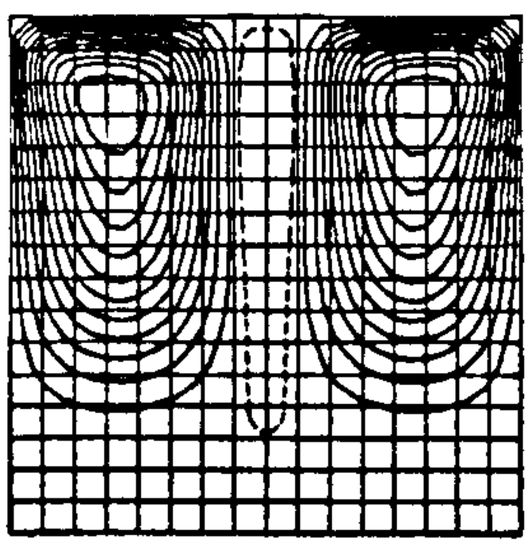
Ψ=7.986



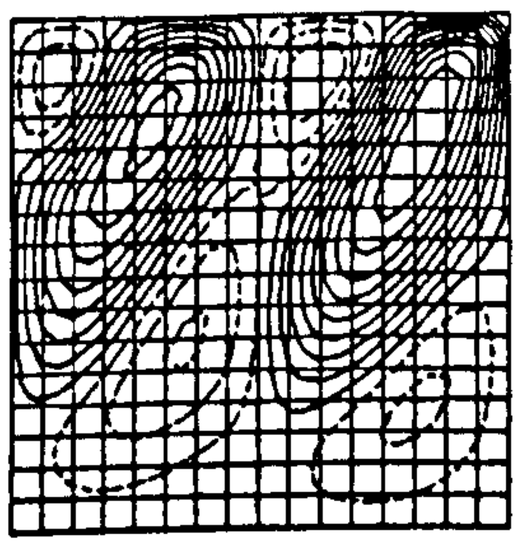
Ψ=40.44



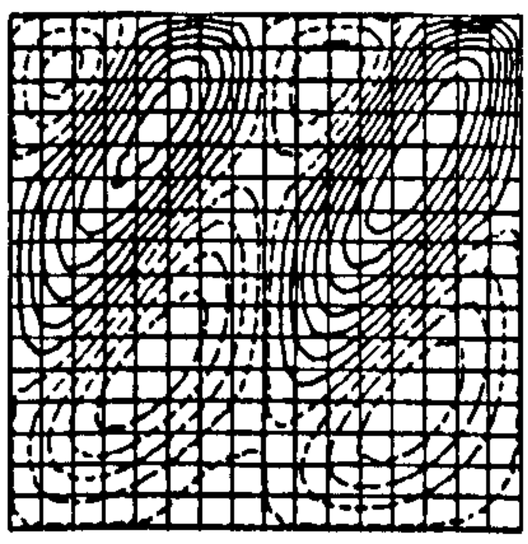
Ψ=40.44



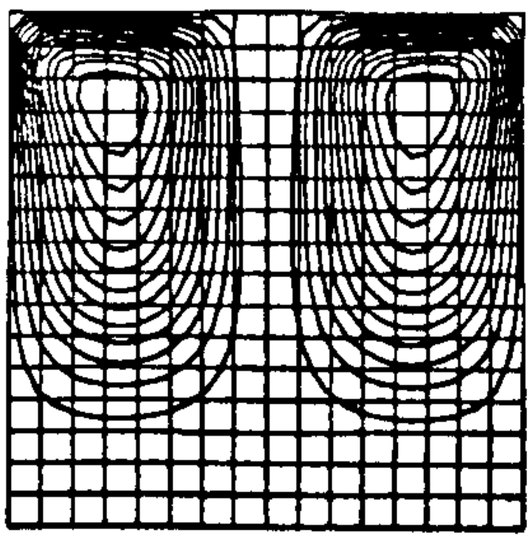
Ψ=40.44



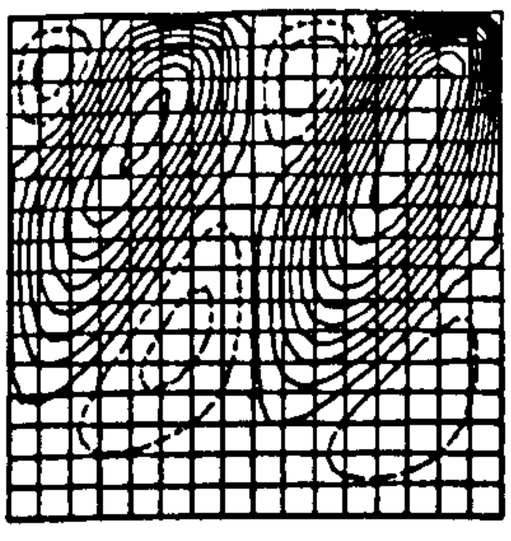
Ψ=127.8



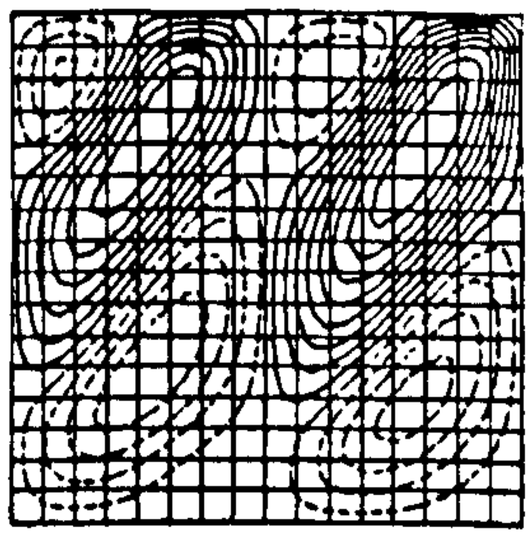
Ψ=127.8



Ψ=127.8



Ψ=312.1



Ψ=312.1

(a) Pure bending **(b) σ_b:τ=2:1** **(c) σ_b:τ=1:1**

Figure 8.14 Comparison of the deflection modes at the ultimate load for varying stiffener rigidities. Stiffened plates subjected to combined shear and bending. w_0 type A as in Fig. 3.5. $\Psi=EI_s/Db$

8.7.1 Modelling of Single-sided Stiffener

For double-sided (concentric) stiffeners, the centroid of the stiffener lies on the mid-plane of the plate (modelled by shell elements), and therefore the stiffener can be modelled as a beam which shares the same nodes with the shell elements.

For single-sided (eccentric) stiffeners, the general method of using a beam as a stiffener on a plate is to define the beam and shell elements with separate nodes, and these nodes can then be constrained to each other using a rigid beam. However, a more economical way is provided in ABAQUS for certain beam section types (TRAPEZOID, I and ARBITRARY). In this approach, the same node for the beam node and the shell node is used, and the offset of the centroid of the cross-section of the beam is defined in the beam section data.

In the ensuing finite element analyses for plates with a single-sided stiffener, the latter approach is adopted, and the section of a flat bar stiffener is defined using the ABAQUS beam section type TRAPEZOID. The forces in the stiffener and the stresses at the four corners of the stiffener section are requested as a part of the ABAQUS output results.

8.7.2 Stress Distribution along the Width of Stiffener

To illustrate the stress distribution on the stiffener cross-section, a non-linear elastic finite element analysis was carried out for a plate of d/a=2, b/t=180 with an intermediate single-sided stiffener Ψ=255.6 (with I_s calculated using Eqn. 3.6), subjected to pure shear. The values of the axial stress at τ/τ_{cr}=2.45 (τ_u/τ_{cr}=2.354 for σ_{0p}= σ_{0s}=355N/mm^2) are shown in Fig. 8.15. Also indicated in Fig. 8.15 are the axial force and bending moment with respect to the centroid of the stiffener section, denoted as $P_{s,1}$ and $M_{s,1}$ respectively, obtained from the ABAQUS solutions.

It is demonstrated in Fig. 8.15 that the axial stress at the surface in contact with the plate has a significant value, instead of the zero stress as implied in the assumption that the

neutral axis of the stiffener cross-section occurs at the surface of the plate. It is also observed that a single-sided stiffener is subjected to coexistent bending and axial compression, and the contribution of the axial force to the total maximum stress is substantial (for the case examined, the ratio is *69.92/95.0 = 73.6%*).

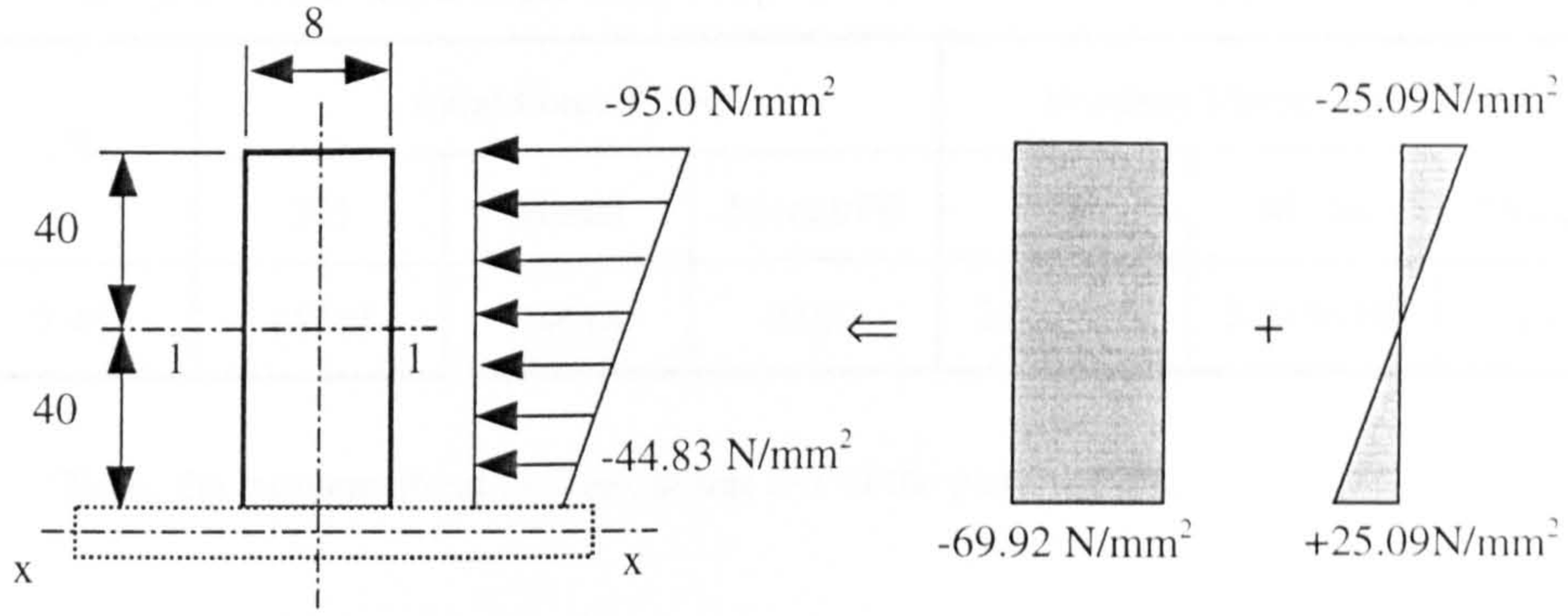


Figure 8.15 Axial stress distribution along the width of the stiffener. Non-linear FE solutions. Plates with a single-sided stiffener. d/a=2, a/t=180, Ψ=255.6 (with I_s given by Eqn. 3.6). Pure shear, τ/τ_{cr}=2.45. w_0 type B as in Fig. 3.5. $\Psi=EI_s/Db$

It has been pointed out in Section 8.5.1 that the axial force P_s predicted using the proposed design formulae (Eqns. 6.14 to 6.16) should be taken as acting in the mid-plane of the plate, as illustrated in Fig. 8.6. In Table 8.10, the axial force and bending moment, with respect to the central line x-x of the plate section, are compared with the corresponding values derived from the FE results. It can be seen in Table 8.10 that for the case considered, the stiffener forces calculated using the proposed design method (Section 8.3) are also valid for single-sided stiffeners.

It was found in the elasto-plastic finite element analyses that for plates of d/a=2, the tip of the single-sided stiffener is always more compressed than the plate edge at the ultimate load, even if it is initially in tension. However, for tall plates as d/a=5, it was found that the tip of the stiffener is in tension, while the edge in contact with the plate is

in compression. It is noted that several factors may affects the direction in which the stiffener deflects, which include the eccentricity of the tension field action, the panel bending effects, initial imperfections and the Poisson effect.

Table 8.10 Comparison of the estimated stiffener forces with the FE solutions. Non-linear elastic analyses. Plate with a single-sided stiffener. d/a=2, a/t=180. w_0: type B as in Fig. 3.5

τ/τ_{cr}	Axial Force P_s (N)			Bending Moment M_s^* (N*mm)		
	FE	Model	Model/FE	FE	Model	Model/FE
2.45	44747	44614	0.997	2.071×10^6	2.219×10^6	1.071

*Note: the moment about the central line x-x of the plate section.

8.7.3 Calculation of Stiffener Stresses

It has been pointed out in Section 8.5.1 that a single-sided stiffener is to be designed as a simple beam loaded by a bending moment M_s (from the lateral distributed force) and an eccentric axial load P_s acting at a distance e, $e=(h_s+t)/2$ for flat bar stiffeners, from the centroidal axis *1–1* (Fig. 8.6) of the stiffener cross-section. The eccentric load P_s is statically equivalent to a force P_s applied at the centroid plus a couple equal to $P_s \cdot e$. To calculate the maximum stress in the stiffener, the possible combinations of the stiffener forces should be considered for the design of the eccentric stiffener. It is recalled that according to the proposed design model, the stiffener cross-section consists of the actual stiffener section only.

An adequate stiffener should be rigid enough to divide the plate, and the axial force in such a stiffener is always a compressive force, which has been quantified in Chapter 6. In Fig. 8.16, two possible combinations of the axial force P_s and the bending moment M_s are illustrated. For the case 1 (Fig. 8.16a), where the tip of the stiffener is in compression, the stiffener forces with respect to the centroidal axis *1–1* is given by:

$$P_{s,1} = P_s \,, \quad M_{s,1} = M_s - P_s \cdot e \tag{8.13}$$

and the maximum compressive and tensile stress can be calculated by:

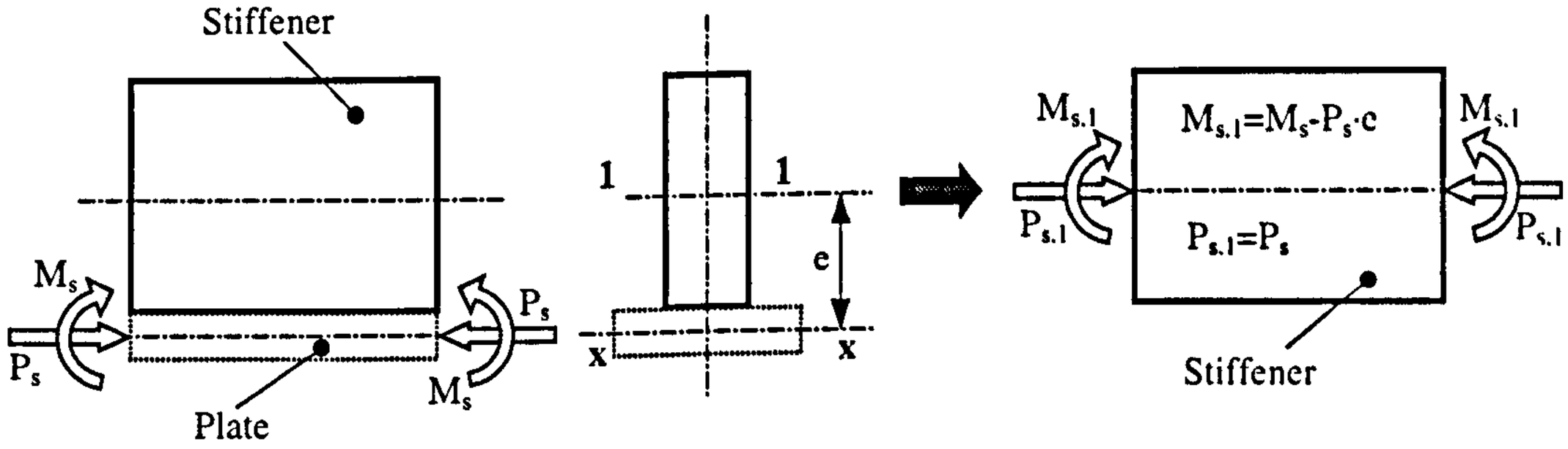
$$\sigma_{s,C} = \frac{P_s}{A_s} + \frac{(M_s - P_s \cdot e)}{Z_{s,C}} \tag{8.14}$$

$$\sigma_{s,T} = -\frac{P_s}{A_s} + \frac{(M_s - P_s \cdot e)}{Z_{s,T}} \tag{8.15}$$

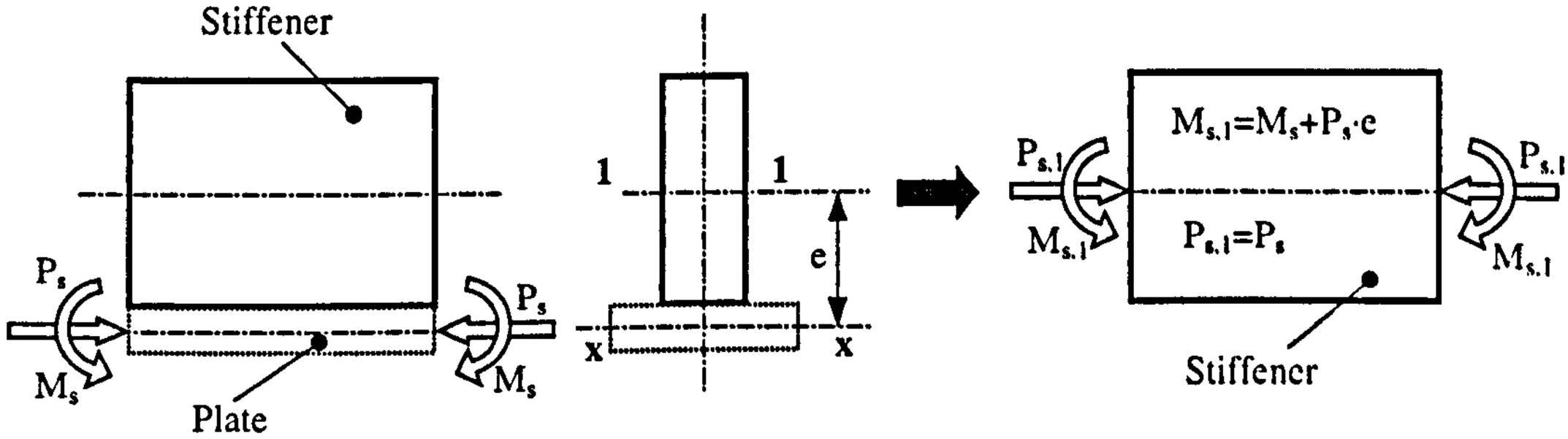
where $Z_{s,C}$ and $Z_{s,T}$ are the section moduli for the compressive and tensile edges of the stiffener, respectively.

For the case 2 (Fig. 8.16b), where the tip of the stiffener may be in tension, the stiffener forces with respect to the centroidal axis *1–1* can be written as:

$$P_{s,1} = P_s\ , \quad M_{s,1} = M_s + P_s \cdot e \tag{8.16}$$



(a) Case 1, for d/a≤2



(b) Case 2, for d/a>2

Figure 8.16 Possible combinations of the axial force and the bending moment in a single-sided stiffener.

and the maximum compressive and tensile stress can be calculated by:

$$\sigma_{s,C} = \frac{P_s}{A_s} + \frac{(M_s + P_s \cdot e)}{Z_{s,C}} \tag{8.17}$$

$$\sigma_{s,T} = -\frac{P_s}{A_s} + \frac{(M_s + P_s \cdot e)}{Z_{s,T}} \tag{8.18}$$

As indicated in Section 8.7.2, it was found from the FE solutions that for plates of d/a=2, the stress at the tip of the stiffener is always more compressive than at the plate edge at the ultimate load, while for plates of d/a=5 the tip of the stiffener is in tension, and the edge in contact with the plate is in compression. It is also noted that the stiffener bending moment $M_{s,1}$ of the case 2 is greater than that of the case 1 (Fig. 8.16).

In view of the above discussion, it is suggested that for the calculation of the maximum stresses in the single-sided stiffener, Eqns. 8.13 to 8.15 should be used for plates of $d/a \leq 2$, while for plates of $d/a > 2$, Eqns. 8.16 to 8.18 should be used.

It is recognised that this suggestion is based on a small number of cases, and it is necessary that further verification should be made over a wide range of d/a and b/t.

8.7.4 Stiffener Deflection and Its Design Limit

8.7.4.1 Calculation of Stiffener Deflection

For single-sided stiffeners, the stiffener deflection can still be estimated using Eqn. 8.9, which is derived from the simple beam theory by assuming that the stiffener deflects in a half sine wave. The moment of inertia of the stiffener section I_s should be taken about the centroidal axis of the stiffener section. For flat bar stiffeners, I_s is given by Eqn. 3.6. The bending moment M_s in Eqn. 8.9 should be replaced with the moment about the centroid axis *1–1* of the stiffener section, $M_{s,1}$. It is proposed in Section 8.7.3 that for $d/a \leq 2$, $M_{s,1}$ is given by Eqn. 8.13, while for $d/a > 2$, $M_{s,1}$ is given by Eqn. 8.16. For reasons of clarification, the formulae for calculating the stiffener deflection of the single-sided stiffener at the ultimate load, w_{su}, are quoted below:

$$w_{su} = \frac{M_{s,1}\, d^2}{\pi^2 E I_s} \tag{8.19}$$

$$M_{s,1} = \begin{cases} M_s - P_s \cdot e, & for \quad d/a \le 2 \\ \\ M_s + P_s \cdot e, & for \quad d/a > 2 \end{cases} \tag{8.20}$$

where e is the distance between the central line (x-x) of the plate section and the centroidal axis (*1–1*) of the cross-section of the stiffener, as depicted in Fig. 8.16.

8.7.4.2 Design Limit of Stiffener Deflection

In Section 8.6.2, a design limit of the stiffener deflection is established for double-sided stiffeners, to ensure that the plate is effectively divided by the stiffener and that the plate strength is within the plateau of the graph of the ultimate strength against the stiffener rigidity. This principle can also be used to derive a deflection limit for the single-sided stiffeners.

To investigate the buckling behaviour and validate the proposed design model for single-sided stiffeners, non-linear elasto-plastic finite element analyses were carried out for plates of d/a=2, 5 and b/t=180, with a single-sided flat bar stiffener (h_s/t_s=10) of varying flexural rigidity Ψ, subjected to pure shear. Fig. 8.17 presents the τ_u vs. d/w_{su} curves obtained from the finite element solutions. It is observed that by taking d/w_{su}=500 for d/a=2 and 400 for d/a=5 respectively, the required plate strength can be achieved. It is noted that these two values of d/w_{su} are equal to the twice the limit specified in Eqn. 8.12.

For design of the single-sided stiffeners, it is proposed that the design limit of the stiffener deflection, w_{sd}, can be taken as the twice the value proposed for the double-sided stiffeners (Eqn. 8.12). That is, the value of w_{sd} for the single-sided stiffener can be expressed as:

$$\frac{w_{sd}}{d}=\begin{cases}\dfrac{1}{250}\left(\dfrac{b}{d}\right), & for \quad \dfrac{d}{a}\le 2\\[2ex] \dfrac{1}{2000}\left(7-6\dfrac{a}{d}\right), & for \quad 2<\dfrac{d}{a}<3\\[2ex] \dfrac{1}{400}, & for \quad \dfrac{d}{a}\ge 3\end{cases} \tag{8.21}$$

In the next section, the design limit of w_{sd} given in Eqn. 8.21, together with the no yield requirement, will be used to determine the required stiffener size, which will then be compared with the finite element results.

Similar to the suggestions made in Section 8.7.3, it is recognised that Eqn. 8.21 is also based on a small number of cases, and further verification over a wide range of d/a and b/t is needed.

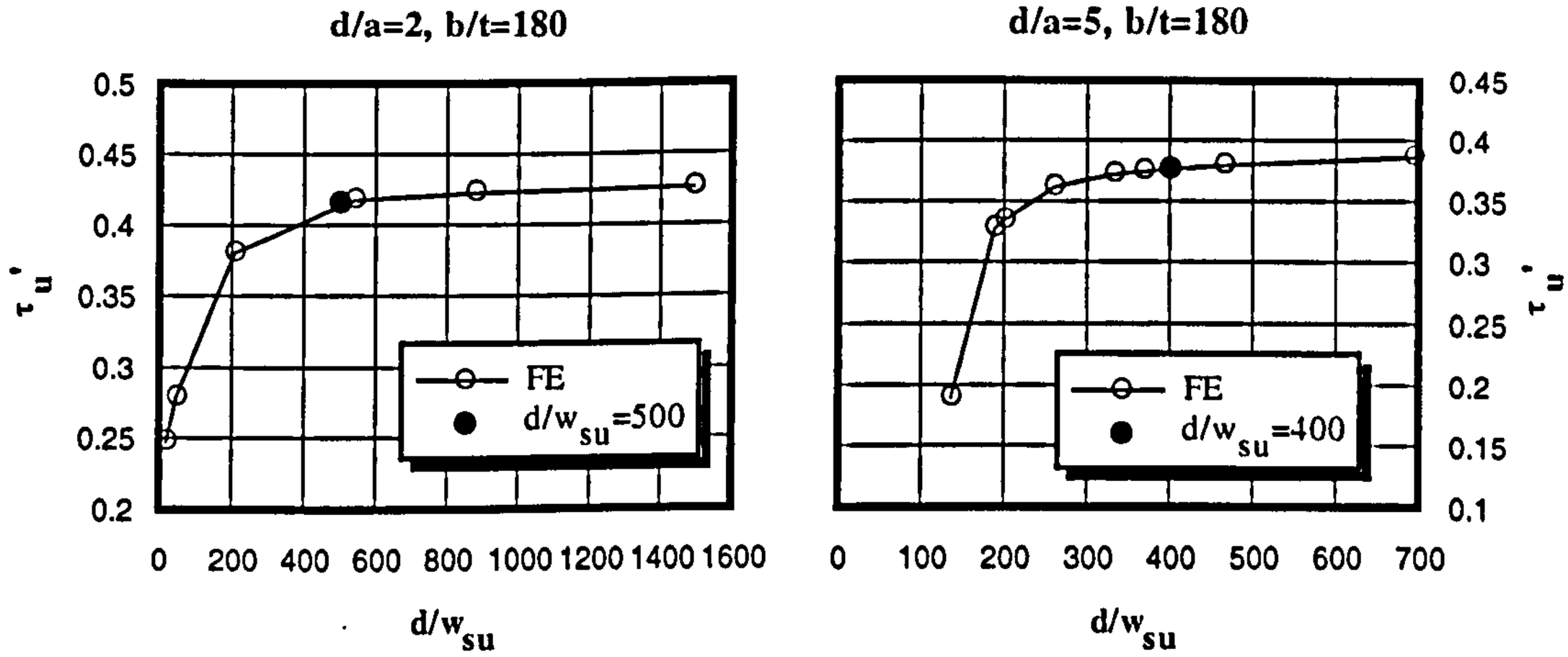


Figure 8.17 Relationship of the ultimate shear strength with the stiffener deflection at the ultimate load. Plates with a single-sided stiffener. b/t=180. w_0: type B for d/a=2; type A for d/a=5, as in Fig. 3.5

8.7.5 Required Stiffener Size

Plates subjected to pure shear were considered in this section. Table 8.11 presents the smallest stiffeners (single-sided, h_s/t_s=10) which satisfy the proposed strength criterion

(Eqn. 8.7) and the stiffness criterion (Eqns. 8.11 and 8.21), represented by Ψ_{dZ} and Ψ_{dI} respectively. In Fig. 8.18, Ψ_{dZ} and Ψ_{dI} are compared with the finite element results of τ_u' vs. Ψ. It is reiterated that for design of the stiffener, the applied load was taken as the ultimate load of the simply supported panel, given in Table 8.4.

Table 8.11 Required stiffener rigidities Ψ_{dZ} and Ψ_{dI} for single-sided stiffeners.
Pure shear. b/t=180, $\sigma_{0p}=\sigma_{0s}=355N/mm^2$. $\Psi=EI_s/Db$, I_s as in Eqn. 3.6

d/a	Ψ_{dZ}	Ψ_{dI}
2	131.4	213.7
5	897.6	3488

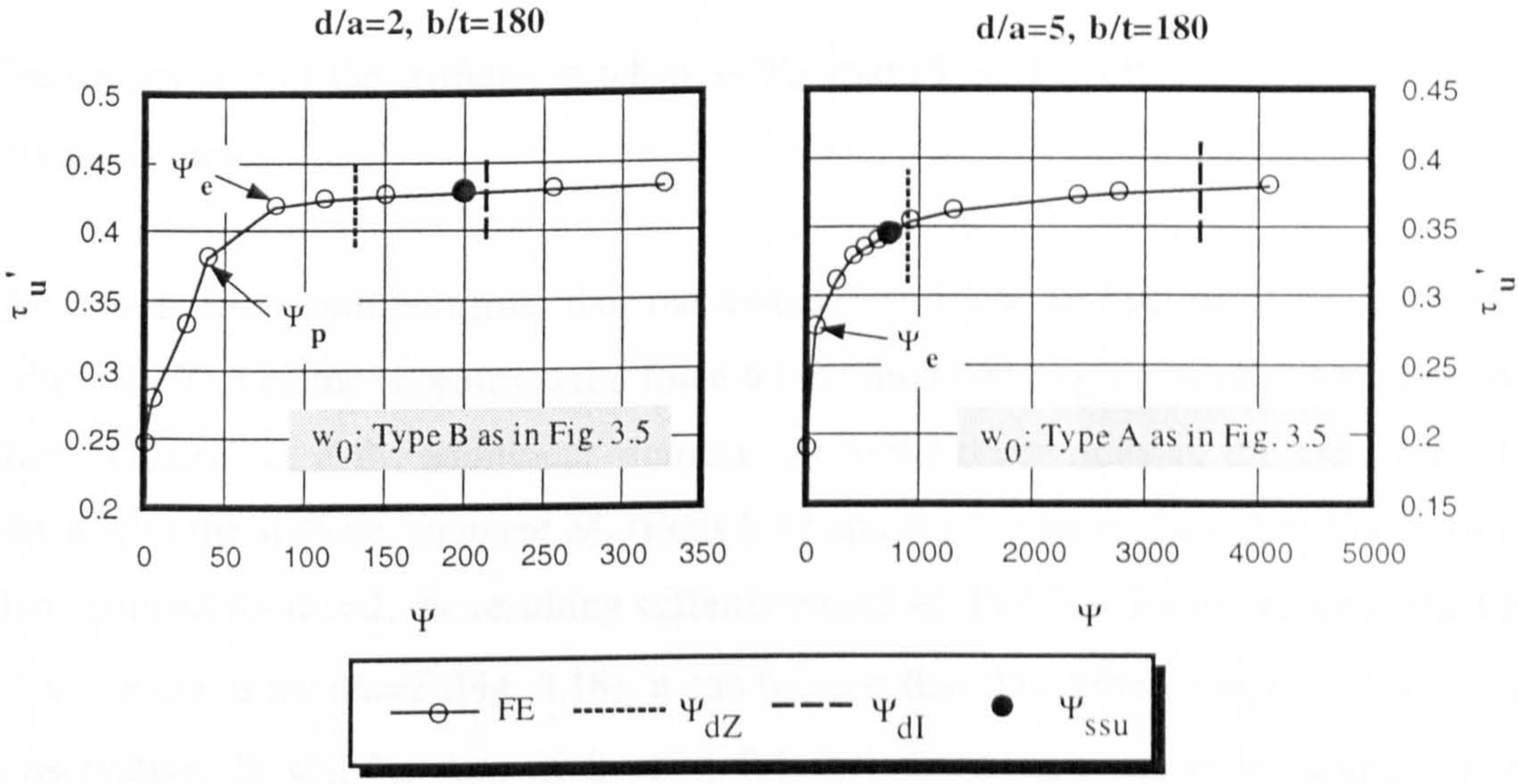


Figure 8.18 Comparison of stiffener requirements from the proposed model, with the τ_u' vs. Ψ results from FE analyses. $\sigma_{0p}=\sigma_{0s}=355N/mm^2$. Single-sided stiffeners, $\Psi=EI_s/Db$, I_s as in Eqn. 3.6. Pure shear

It can be observed in Fig. 8.18 that the required stiffener rigidity Ψ_{dZ} is greater than Ψ_e for both cases considered, which implies that the stiffener of Ψ_{dZ} does not yield at the ultimate load. It is also seen that the required stiffener Ψ_{dZ} can ensure the plate strength to be greater or nearly equal to the panel strength. It is noted that for d/a=2, Ψ_{dZ} is

smaller than Ψ_{ssu}, but the difference in the plate strengths for the two stiffener rigidities is negligible. However, by reference to the contour diagrams of the deflection modes at the ultimate load, shown in Fig. 8.19, it can be found that the required stiffener according to the strength criterion, Ψ_{dZ}, does not produce an effectively divided panel mode.

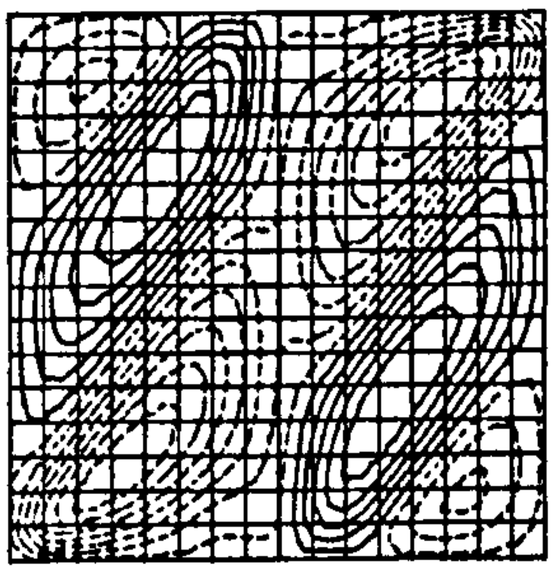
As for the required stiffener in accordance with the stiffness criterion, it is apparent in Fig. 8.18 that the stiffener with a rigidity of Ψ_{dI} can ensure that the plate strength lies within the plateau of the τ_u' vs. Ψ curve, and is greater than the strength for simply supported panels. By referring to the contour plots in Fig. 8.19 and the values of Ψ_{dI} given in Table 8.11, it can be seen that the stiffener with a rigidity of Ψ_{dI} results in an effectively divided panel mode.

The design size of the stiffener is taken as $\Psi_d=\max\{\Psi_{dZ}, \Psi_{dI}\}$, which is considered to be satisfactory.

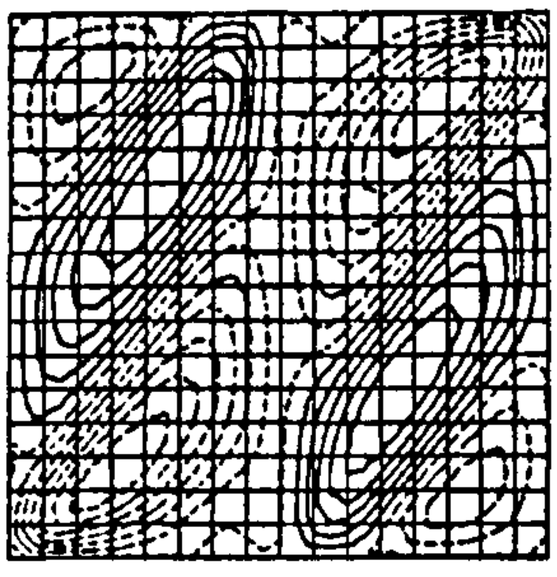
The above discussion confirms that the assumption made in Section 8.7.3 about the reducing effect of the eccentric axial force on the total bending moment is adequate for d/a=2. Otherwise, if the additional moment due to the eccentricity of the axial force is added with the stiffener moment M_s (Eqns 8.17 and 8.18), that is, Case 2 in Fig. 8.16 is also assumed for d/a=2, the resulting stiffener would be Ψ=1212. By reference to the FE τ_u' vs. Ψ curve for d/a=2 (Fig. 8.18), it can be seen that this stiffener rigidity is unduly conservative. It will be seen in Section 9.4 that the design equations suggested in Sections 8.7.3 and 8.7.4 also give satisfactory single-sided stiffeners for the test girder GII, where d/a≈1 and b/t≈300. Nevertheless, the design equations proposed for single-sided stiffeners should be further validated.

8.7.6 Comparison with Double-sided Stiffeners

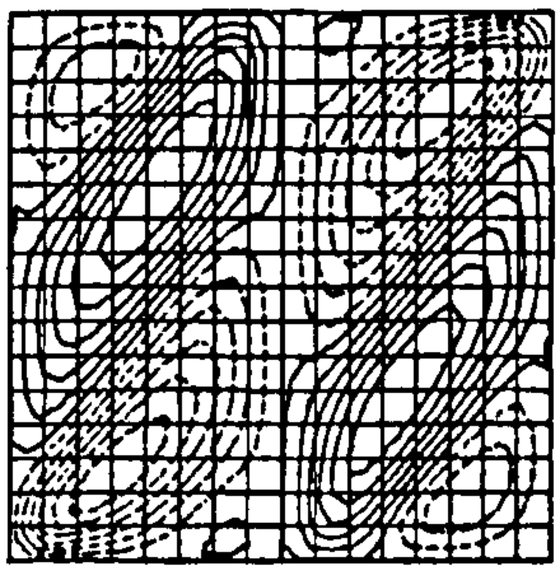
In this section, the moment of inertia I_s, and correspondingly the flexural rigidity Ψ, of a single-sided stiffener are calculated by assuming that the neutral axis of the stiffener section locates at the surface of the plate. That is:



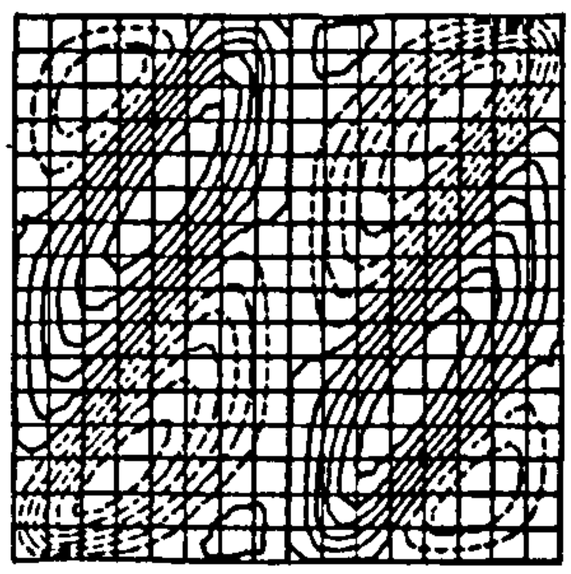
Ψ=80.89, τ_u'=0.418



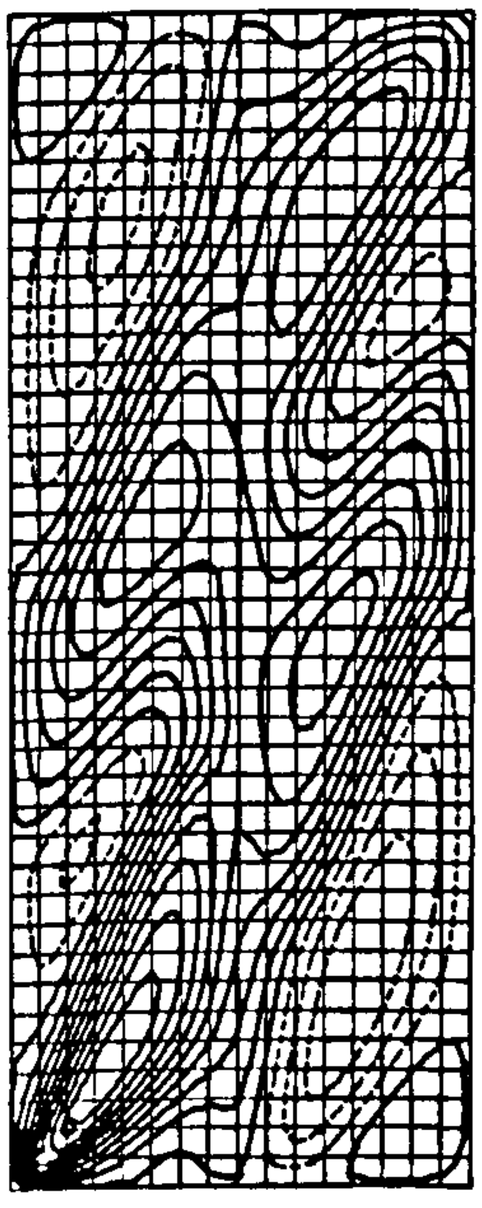
Ψ=149.9, τ_u'=0.426



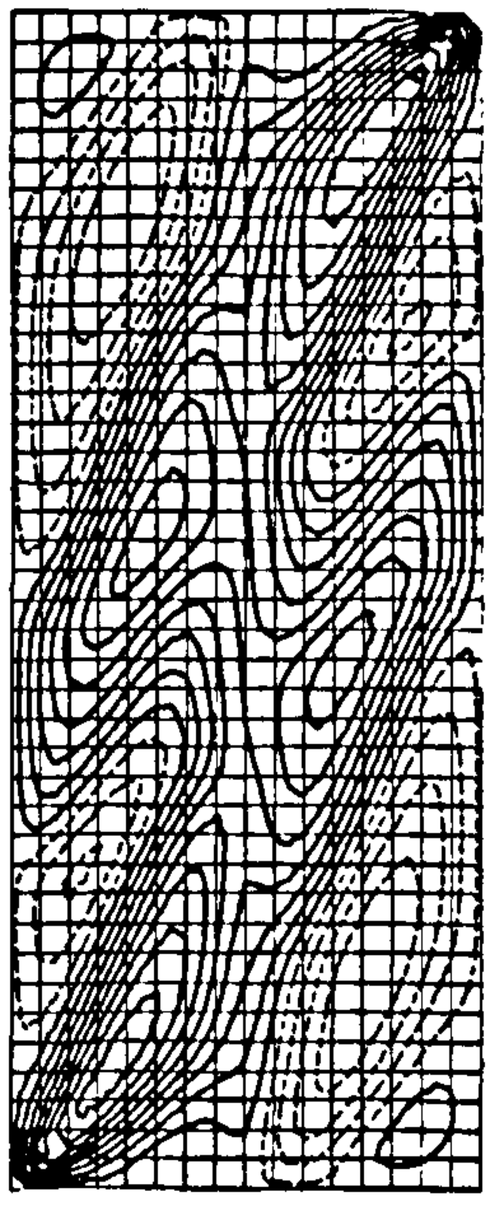
Ψ=197.5, τ_u'=0.428



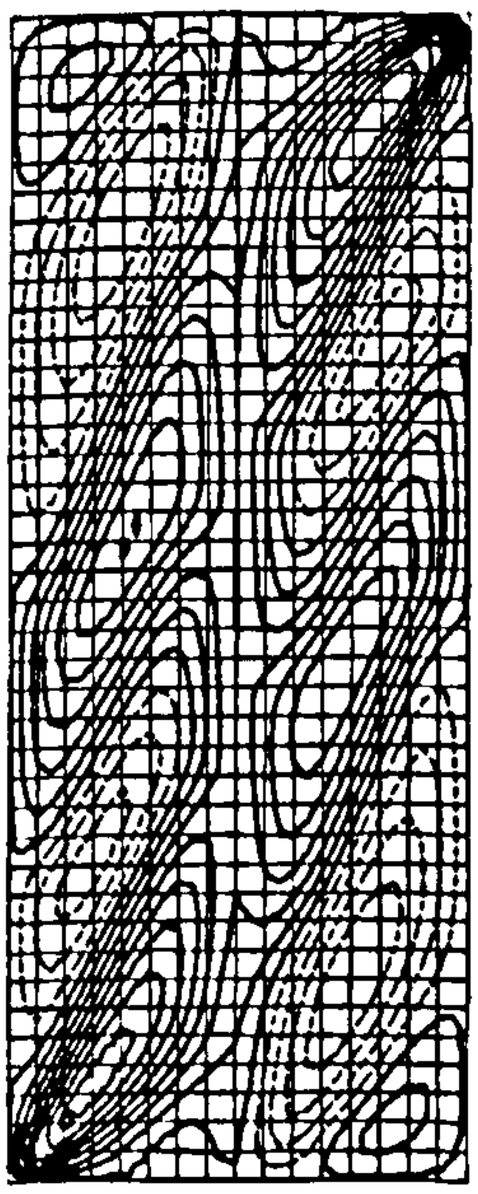
Ψ=325.8, τ_u'=0.433



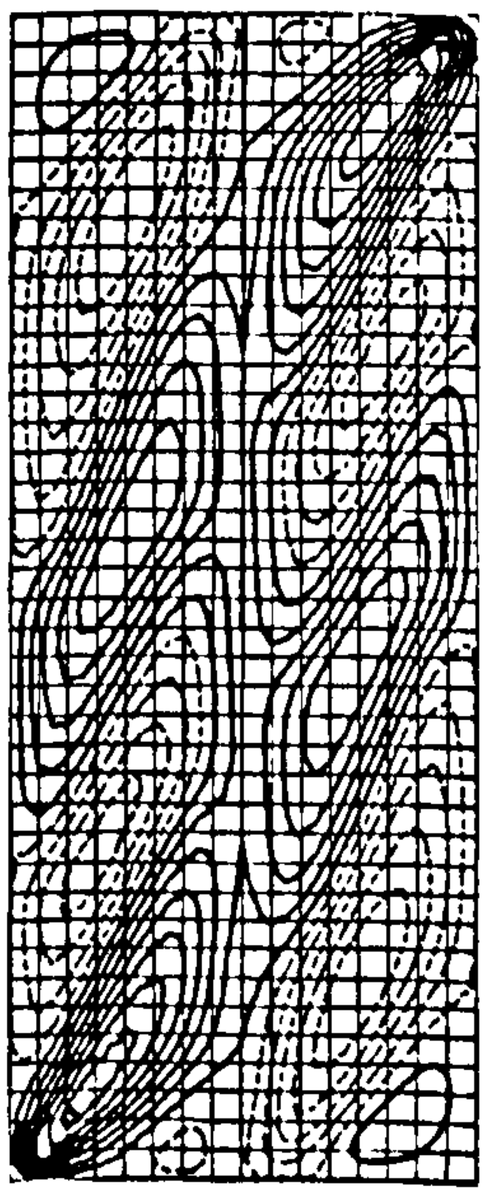
Ψ=624.1, τ_u'=0.339



Ψ=913.8, τ_u'=0.354



Ψ=2759, τ_u'=0.374



Ψ=4090, τ_u'=0.379

(a) d/a=2

(b) d/a=5

Figure 8.19 Comparison of the deflection modes at the ultimate load for varying stiffener rigidities. Plates with a single-sided stiffener, subjected to pure shear. b/t=180. $\Psi=EI_s/Db$, I_s as given by Eqn. 3.6.

$$I_s = \frac{1}{3} t_s h_s^3 , \quad \Psi = \frac{E I_s}{D b} \tag{8.22}$$

The stiffener rigidities shown in Fig. 8.18, including the required stiffener rigidities given in Table 8.11, are converted using Eqn. 8.22. In Fig. 8.20, the converted values of Ψ_{dZ} and Ψ_{dI} and the finite element curve of τ_u' vs. Ψ for the single-sided stiffeners are compared with those for the double-sided stiffeners (see Fig. 8.8).

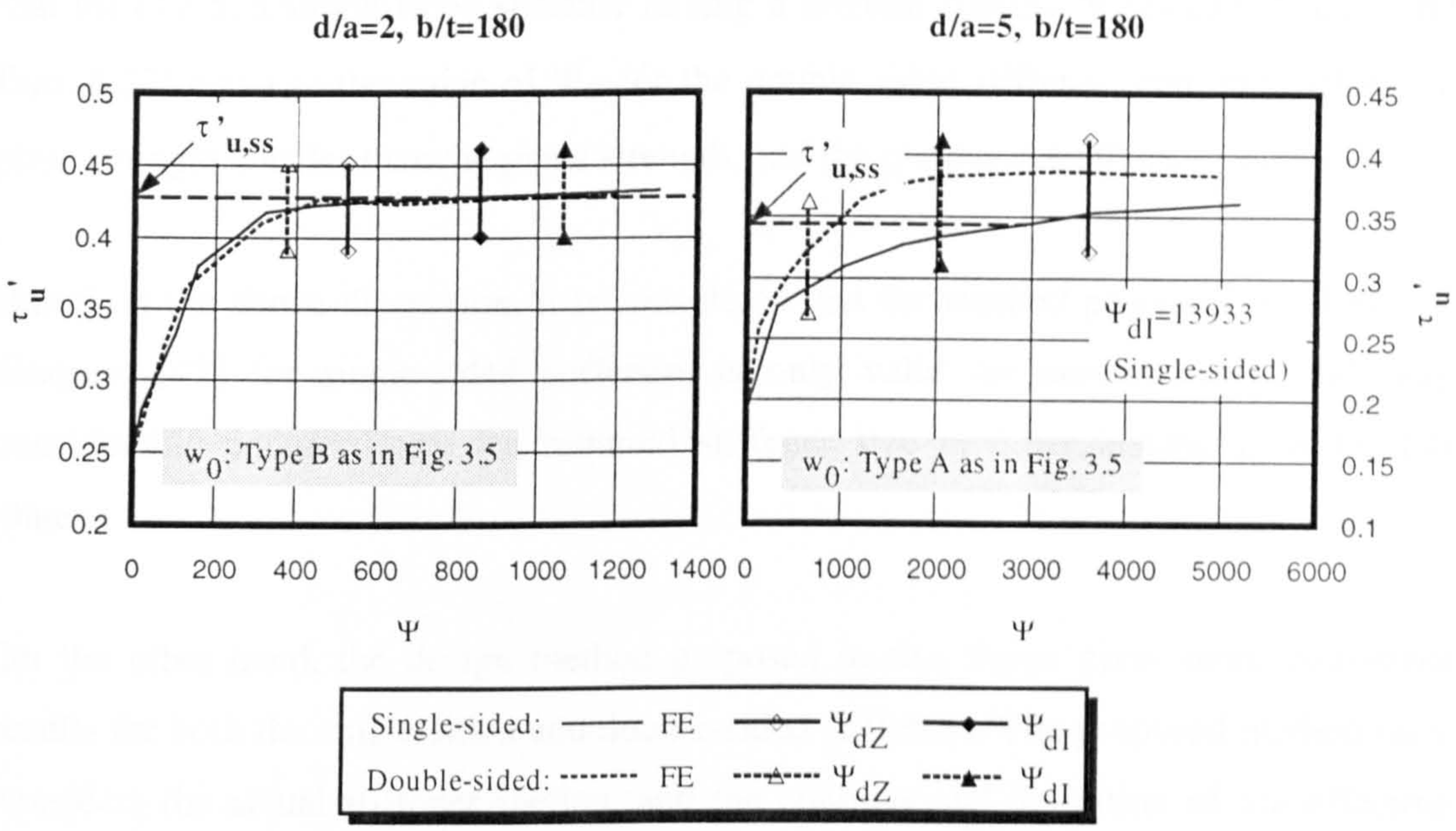


Figure 8.20 Comparison of plate strength and stiffener requirements between single-sided and double-sided stiffeners. $\sigma_{0p}=\sigma_{0s}=355N/mm^2$. $\Psi=EI_s/Db$, I_s of the single-sided stiffener as in Eqn. 8.22. Pure shear

It has been proposed by Horne and Grayson [45] that with the moment of inertia I_s calculated about an axis at the surface of the plate, the single-sided stiffener can be designed to attain the same flexural rigidity Ψ as required for double-sided stiffeners. Therefore, the comparison presented in Fig. 8.20 may establish whether this proposal is adequate.

It can be seen in Fig. 8.20 that for d/a=2, by calculating the stiffener rigidity using Eqn. 8.22, the finite element curves of τ_u' vs. Ψ for the single-sided and double-sided

stiffeners almost coincide with each other. This suggests that an adequate estimate of the required single-sided stiffener size can be obtained for this case by using the simple method proposed by Horne & Grayson [45].

However, it is observed that for d/a=5, significant difference exists between the two τ_u' vs. Ψ curves, and a value of Ψ which is adequate for the double-sided stiffener is much less than the required rigidity for the single-sided stiffener. It is apparent in Fig. 8.20 that for d/a=5, a single-sided stiffener having a flexural rigidity Ψ (as calculated using Eqn. 8.22) equal to the value of Ψ_{dl} for the double-sided stiffener, can only achieve a plate strength smaller than the panel strength, and the plate is not effectively divided.

Based on the above discussion, it is considered that the method proposed by Horne & Grayson [45] for single-sided stiffeners is only valid for certain cases, and may considerably underestimate the required stiffener size in other instances, as for tall plates.

On the other hand, the design method proposed in this thesis gives more consistent results for both the single-sided and double-sided stiffeners. The proposed method only considers the actual stiffener section, and the controversial definition of the effective width of the plate is avoided. This is achieved by considering the forces acting in the stiffener itself, and therefore the stiffener can be analysed using the simple beam theory, without introducing the assumption that the neutral axis of a single-sided stiffener occurs at the surface of the plate. The proposed design method is based on analytical studies, incorporated with extensive parametric results for idealised structures. In this section, the model is validated for single-sided stiffeners with a small number of cases, and further validation should ideally be undertaken in the future.

8.8 PROPOSED DESIGN PROCEDURE

In this section, the procedure proposed for designing a transverse stiffener for a plate subjected to coexistent shear and direct in-plane loading (Fig. 3.1) is given. The variable parameters used in the design procedure are:

- *Components of the ultimate strength for CUCU simply supported panels: τ_u, σ_{cu}, σ_{bu};*
- *External stiffener forces for load bearing stiffeners: Q_1 (at one end), Q_2 (at both ends);*
- *Panel dimensions: a, d, t;*
- *Initial imperfections: w_{0p}, w_{0s}, measured as in Fig. 3.5;*
- *Yield stresses of panel and stiffener material: σ_{0p}, σ_{0s};*
- *Cross-sectional properties of the stiffener: A_s, I_s, Z_s (see Section 3.3) and e (see Fig. 8.16);*

The calculation of the ultimate strength of simply supported panels is not within the scope of the present study. Formulae for predicting the strength of individual panels subjected to shear and compressive loading have been given by Davidson [40]. For the panel shear strength τ^0_u (τ_u for pure shear), as indicated in Section 8.4, the predicted values are about 3~4% greater than the finite element solutions [58]. Therefore, it is recommended that in the proposed stiffener design method, the shear strength of CUCU panels may be calculated using the formulae given by Davidson [40]. For panels subjected to combined loading, the components of the ultimate panel strength (τ_u, σ_{cu}, σ_{bu}) may be evaluated by using the known ratio between the applied stresses and an available method in the design codes, such as the interaction equation in BS5400.

The design method proposed for intermediate stiffeners is summarized in Section 8.8.1. Special features and design requirements for load bearing stiffeners are discussed in Section 8.8.2.

8.8.1 Intermediate Stiffeners

The proposed design method for intermediate transverse stiffeners is summarized below, and each step in the design procedure is explained.

(1) Calculate the critical buckling stresses for a simply supported panel, subjected to shear, compression and bending alone, using Eqns. 5.2 (p.162), 5.5 (p.196) and 5.15 (p.219), respectively.

(2) Calculate the critical shear stress τ_{cr} in the presence of compression and bending using the known ratio between the applied stresses and the interaction equation 6.16 (p.282).

(3) Calculate the equivalent shear stress τ_{eq} using Eqn. 5.23 (p.233), with the reduction factors β_c and β_b given by Eqns.5.12, 5.13 (pp.212-213) and 5.21 (p.231).

(4) Calculate the elastic knife edge moment M_{pk} using Eqns. 5.22a to 5.22c (p.233), with τ_{eq} obtained in Step (3). The method for calculating M_{pk} is summarized in Section 5.4.

(5) Calculate the plastic factor F_{pl} using Eqn. 8.1 (p.328), and the stiffener bending moment due to the panel bending effect M_{pb} using Eqn. 8.2 (p.329).

(6) Calculate the design limit of the stiffener deflection, w_{sd}, using Eqn. 8.12 (p.356) for double-sided stiffeners, and Eqn. 8.21 (p.371) for single-sided stiffeners.

(7) Choose a trial stiffener section and calculate A_s, I_s, Z_s, and e (for single-sided stiffeners). The calculation of stiffener properties is discussed in Section 3.3. The trial stiffener size may be chosen in terms of experience. Otherwise, it is proposed that the trial stiffener may be determined approximately by considering the stiffener required for the plate subjected to pure shear, with the component of stiffener moment due to the overall effect being taken as the value for $\Psi=\infty$, denoted as M_{ov}^{KE}. M_{ov}^{KE} can be obtained by replacing Eqns. 7.55 and 7.56 (pp.301-302) in Eqn. 7.67 (p.305), and then calculating the limit of M_{ov} as $\Psi\rightarrow\infty$. It is found that M_{ov}^{KE} can be expressed as:

$$M_{ov}^{KE} = \lim_{\Psi\rightarrow\infty} M_{ov}$$
$$= 2a\left(\frac{d^2}{4a^2}+1\right)\cdot\tau t w_{0s} \Big/ \sqrt{8.155\left(\frac{d^2}{4a^2}+\frac{4a^2}{d^2}\right)+13.99} \qquad (8.23)$$

A suggested trial stiffener is the smallest stiffener which satisfy the following criteria:

$$Z_s \geq \frac{M_{pk} + M_{ov}^{KE}}{0.8\sigma_{0s}} \tag{8.24}$$

$$I_s \geq \left(M_{pk} + M_{ov}^{KE}\right)\frac{d^2}{\pi^2 E w_{asu}} \tag{8.25}$$

In Eqn. 8.24, the stiffener axial force P_s is not included, but allowance for P_s is made for the trial by reducing the stiffener yield stress σ_{0s} by 20%.

(8) Calculate the axial force P_s in the stiffener using Eqns. 6.14 and 6.15 (p.277), with the applied shear stress τ and the buckling shear stress τ_{cr} obtained in Step (2).

(9) Calculate the stiffener bending moment due to the overall buckling effect M_{ov}, using Eqn. 7.122 (p.320), with the overall buckling stresses τ_{ov}, $\sigma_{c,ov}$ and $\sigma_{b,ov}$ given by Eqns. 7.61 (p.303), 7.75 (p.307) and 7.89 (p.310), respectively.

(10) Calculate the total stiffener moment $M_s=M_{pb}+M_{ov}$ (Eqn. 8.4, p.331).

(11) Calculate the maximum stress in the stiffener $\sigma_{s,max}$. For double-sided stiffeners, Eqn. 8.5 (p.338) is used. For single-sided stiffeners, Eqns. 8.13 to 8.15 (pp.367-368) should be used for $d/a \leq 2$, and Eqns. 8.16 to 8.18 (pp.368-369) for $d/a > 2$.

(12) Calculate the stiffener deflection at the ultimate load, w_{su}, using Eqn. 8.9 (p.350) for double-sided stiffeners, and Eqns.8.19 and 8.20 (p.370) for single-sided stiffeners.

(13) Check the strength and stiffness criteria, given in Eqns. 8.7 (p.339) and 8.11 (p.356), respectively.

(14) If either the strength criterion (Eqn. 8.7) or the stiffness criterion (Eqn. 8.11) is not satisfied, then the chosen stiffener size must be increased. Conversely, if both criteria are more than satisfied, then the chosen stiffener size may be reduced.

Subsequent stiffener sizes may be checked by returning to step (8) in the design procedure.

The above procedure may be converted into a computer program. Appendix D presents a sample FORTRAN program, from which the optimum stiffener size can be obtained. An optimum stiffener is defined by the optimal model:

$$\begin{aligned} &\min \quad A_s \\ &\textit{subjected to}: \quad \sigma_{s,\max} \le \sigma_{0s} \\ &\qquad\qquad\quad w_{su} \le w_{sd} \\ &\qquad\qquad\quad A_s > 0 \end{aligned} \tag{8.26}$$

8.8.2 Special Considerations for Load Bearing Stiffeners

For a stiffener loaded by external forces, either at one end or both ends, special considerations should be given, which are presented below.

(1) The section of a load bearing stiffener should preferably be chosen to be double-sided and symmetric about the mid-plane of the plate as required in BS5400.

(2) The applied external force is resisted by the stiffener itself and by part of the plate together. For slender plates, the amount of the force resisted by the plate may be negligible, but for stocky plates, the contribution of the plate to the total resistance is appreciable. A possible approach to dealing with the effect of the plate is to establish a formula for predicting the component of the external force resisted by the stiffener itself. This may be achieved by employing an approach similar to what is used in Chapter 6 to develop a design formula for predicting the stiffener axial force due to the tension field action. Nevertheless, since the panel is not designed to resist the external force applied at the end of the stiffener, it is consistent to assume that the external force is taken by the stiffener itself. Therefore, it is suggested that when designing a load bearing stiffener, only the stiffener section should be considered.

(3) For stiffeners subjected to equal external forces at both ends, Q_2, as shown in Fig. 8.21, the stiffener can be sized by following the design procedure proposed for an intermediate stiffener (double-sided), given in Section 8.8.1. However, the stiffener axial force P_s obtained in Step (8) should be replaced with the total stiffener axial force $P_{s,total}$ given by:

$$P_{s,total} = P_s + Q_2 \tag{8.27}$$

In addition, in Step (9), the stiffener bending moment due to the overall buckling effect M_{ov} should be calculated using Eqn. 7.124, which is proposed to include the destabilising effect caused by the external force Q_2:

$$M_{ov} = \frac{\pi^2 E I_s w_{0s}}{d^2}\left(\frac{\tau/\tau_{ov} + \sigma_c/\sigma_{c,ov} + \sigma_b/\sigma_{b,ov} + Q_2/Q_{2,ov}}{1-\tau/\tau_{ov} - \sigma_c/\sigma_{c,ov} - \sigma_b/\sigma_{b,ov} - Q_2/Q_{2,ov}}\right) \tag{8.28}$$

where the overall buckling load $Q_{2,ov}$ can be calculated using Eqn. 7.101 (p.314).

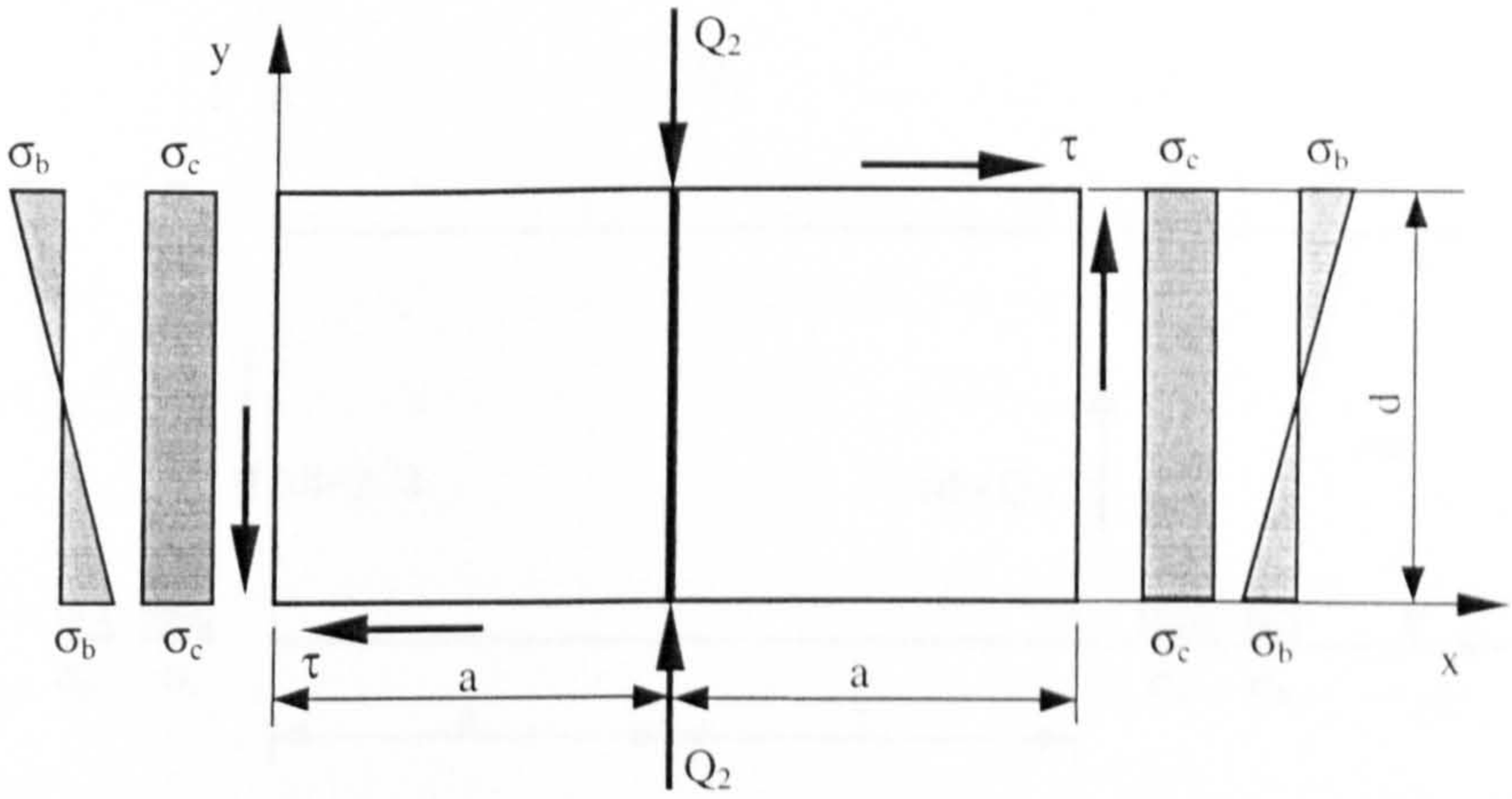


Figure 8.21 Stiffener subjected to equal external forces at both ends

(4) For stiffeners subjected to an external force directly applied at one end, Q_1, as shown in Fig. 8.22, the stiffener can be sized also by following the design procedure proposed for intermediate stiffeners (double-sided), given in Section 8.8.1. However, the stiffener axial force P_s obtained in Step (8) should be substituted with the total stiffener axial force $P_{s,total}$ given by:

$$P_{s,total} = P_s + Q_1 \tag{8.29}$$

The axial force due to the tension field action, P_s, should be calculated using the average shear stress τ in the two adjacent panels. This is because the axial force resulting from the tension bands due to the shear stress component corresponding to the applied external force Q_1 is balanced by Q_1 itself, as illustrated in Fig. 8.22.

Also, in Step (9), the stiffener bending moment due to the overall buckling effect M_{ov} should be calculated using Eqn. 7.123, which takes into account the destabilising effect caused by the external force Q_1:

$$M_{ov} = \frac{\pi^2 E I_s w_{0s}}{d^2}\left(\frac{\tau/\tau_{ov} + \sigma_c/\sigma_{c,ov} + \sigma_b/\sigma_{b,ov} + Q_1/Q_{1,ov}}{1-\tau/\tau_{ov} - \sigma_c/\sigma_{c,ov} - \sigma_b/\sigma_{b,ov} - Q_1/Q_{1,ov}}\right) \tag{8.30}$$

where the overall buckling load $Q_{1,ov}$ can be calculated using Eqn. 7.116 (p.318).

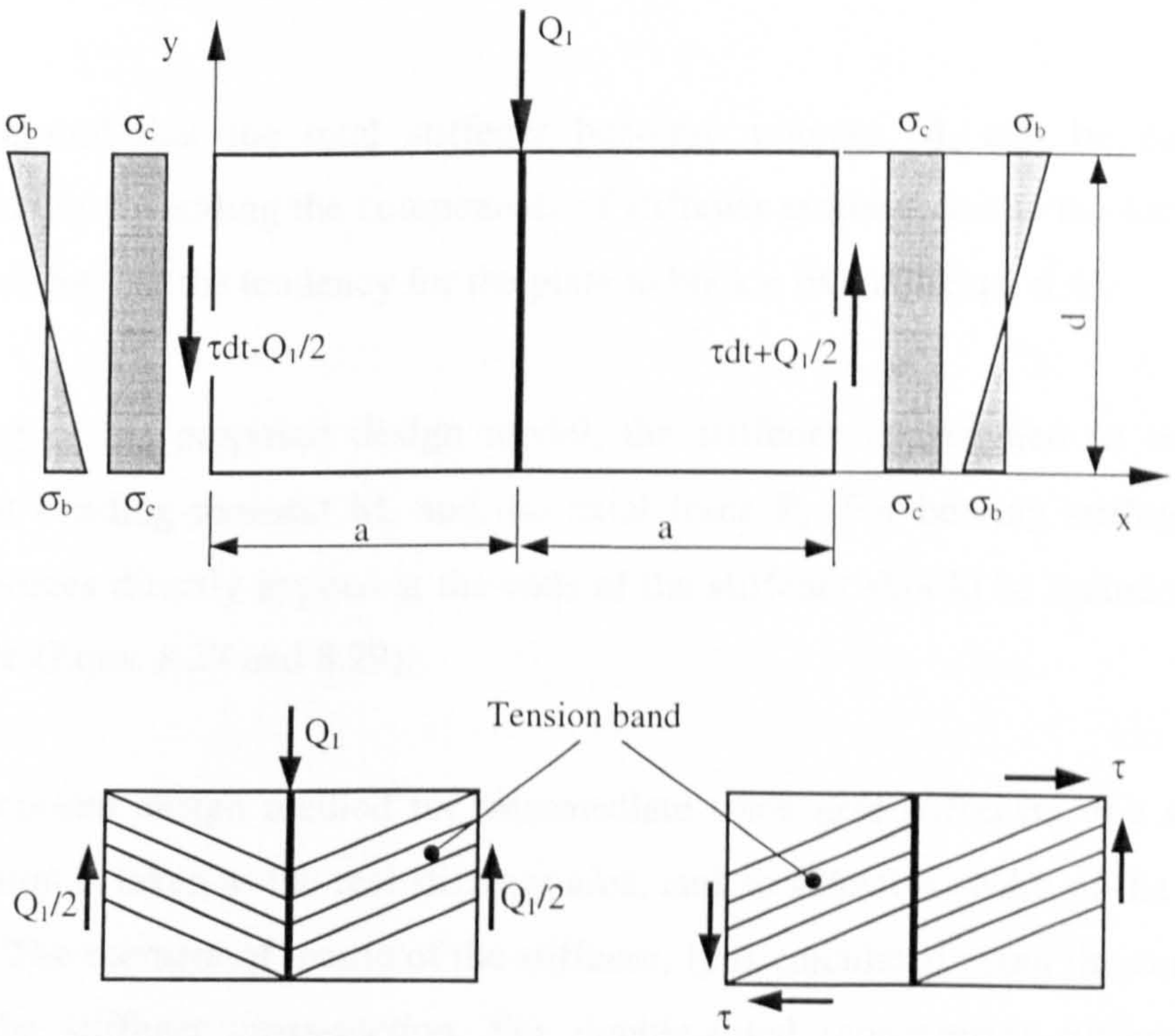


Figure 8.22 Stiffener subjected to external force at one end

8.9 CONCLUSIONS

In this chapter, a design model for transverse stiffeners has been developed for plates subjected to coexistent shear and direct in-plane loading, including the external forces applied directly to the ends of the stiffener. Both concentric and eccentric stiffeners are considered. As a result of this study, the following conclusions can be made:

(1) Due to the effects of panel plasticity, the knife edge moment M_{pk} increases significantly in the region of the ultimate load, and such an increase can be accounted for approximately by introducing a factor F_{pl}, which may be expressed as a simple function of the panel yield stress σ_{0p} (Eqn. 8.1).

(2) Panel plasticity has negligible effect on the stiffener axial force P_s, because the axial force in the stiffener results mainly from the inclined tension field action, which depends on the applied shear stress.

(3) It is proposed that the total stiffener bending moment M_s can be calculated approximately by adding the components of stiffener moment due to the local panel bending effect and the tendency for the plate to buckle overall (Eqn. 8.4).

(4) According to the proposed design model, the stiffener is designed to resist the coexistent bending moment M_s and the axial force P_s. For bearing stiffeners, the external forces directly applied at the ends of the stiffener should be included in the axial force (Eqns. 8.27 and 8.29).

(5) In the proposed design method for intermediate transverse stiffeners, the stiffener cross-section is taken as the real stiffener area, and no effective width of the plate is included. The moment of inertia of the stiffener, I_s, is calculated about the centroidal axis of the stiffener cross-section. For double-sided (concentric) stiffeners, the centroidal axis of the stiffener section coincides with the center line of the plate section.

(6) The stiffener axial force is assumed to act in the mid-plane of the plate. Therefore, for single-sided stiffeners, an additional bending moment due to the eccentricity of the axial force must be included (Eqns. 8.13 and 8.16, or Eqn. 8.20).

(7) For the strength design of the stiffener, it is proposed that the maximum stress in the stiffener must not exceed the yield stress of the stiffener (Eqn. 8.7), that is, the no yield criterion is adopted in the proposed design model.

(8) For the stiffness design of the stiffener, it is proposed that the stiffener deflection at the ultimate load, w_{su}, must be less than the deflection limit w_{sd}, which may be expressed as a fraction of the stiffener length (Eqn. 8.12 for concentric stiffeners, Eqn. 8.21 for single-sided stiffeners).

(9) The proposed design limit of the stiffener deflection w_{sd} represents the required straightness of the stiffener, and is derived from the finite element solutions for plates subjected to pure shear by assuming that the required strength of the stiffened plate is attained. It is found that the specified deflection limit is also adequate for combined loading conditions. Further verification is needed for the value of w_{sd} proposed for single-sided stiffeners over a wide range of d/a and b/t.

(10) It is found that the stiffener deflection can be estimated from the bending moment using the simple elastic beam theory and by assuming that the deflected shape of the stiffener is a half sine wave.

(11) In order to produce an adequate design stiffener, both strength and stiffness requirements are necessary. In the proposed design model, both the strength and stiffness criteria are used to quantify the required stiffener.

(12) The proposed design model ensures that the strength of the stiffened plate is within the plateau region of the graph of the ultimate load against the stiffener rigidity Ψ, and equal to or greater than the strength of simply supported panels.

(13) The proposed design model ensures that the stiffener remains elastic at the ultimate load, and hence the stiffener failure does not occur before panel failure.

(14) The proposed design model also ensures that the plate is effectively divided. For the design stiffener, an effectively divided panel deflection mode can be achieved.

(15) It is found that it may be considerably conservative if the stiffener designed to develop the maximum shear capacity of the panel is used for other combinations of shear and longitudinal loading, especially when the other loading components are predominant. However, when the shear component is predominant, the stiffener needed for developing the maximum shear capacity of the panel may be used as a satisfactory estimate of the required stiffener.

(16) The proposed design model has been validated against finite element solutions for plates with a double-sided flat bar stiffener, subjected to pure shear, shear and compression, and shear and bending, respectively. The proposed model has also been validated for some plates with a single-sided flat bar stiffener, subjected to pure shear. It is found that the proposed design model gives consistent results for both single-sided and double-sided stiffeners.

(17) For single-sided stiffeners, it is found that the design method proposed by Horne & Grayson [45] and other researchers is only valid for certain cases, and may considerably underestimate the required stiffener size in other instances, as for tall plates.

(18) A detailed design procedure for intermediate stiffeners is given (Section 8.8.1). As part of the proposed design model, a design method for load bearing stiffeners is suggested but not validated.

(19) The proposed design model is based on analytical studies, incorporated with extensive parametric results for idealised structures. There are no restrictions on

stiffener shape inherent in the proposed design model, except that they should not be prone to lateral torsional buckling and that they are not closed sections.

(20) Further validation of the proposed model is needed for different shapes of the stiffener cross-section, load bearing stiffeners, as well as more extensive cases of different loading and geometrical combinations, especially for combined loading and for stiffeners on one side of the plate.

CHAPTER 9

COMPARISONS OF THE PROPOSED MODEL WITH EXISTING METHODS AND RESULTS FOR TEST GIRDERS

9.1 INTRODUCTION

For stiffened plates subjected to pure shear, Stanway [1] has compared several existing design methods for transverse stiffeners with the finite element results, and it was found that the existing design methods differ widely in the stiffener size which results.

In this chapter, the basis of the existing design methods is described. The transverse stiffener required according to the proposed design model (Chapter 8) is compared with those from the existing methods, and also with the results for the test girders. Comparisons are made mainly for plates with a double-sided stiffener, subjected to pure shear, but single-sided flat bar stiffeners are also considered. Since most of the existing design methods do not consider combined loading conditions, the comparison is not made for plates subjected to combined loading. In Chapter 8, the proposed model has been validated against the finite element results for plates subjected to combined shear and compression, as well as to combined shear and bending. For the comparisons with the test results, combined shear and bending is considered.

The existing design methods considered in this chapter include three design codes (namely, BS5400 [3], Eurocode 3 [4] and AASHTO [34]) and the methods proposed by Horne & Grayson [45], by Rahal & Harding [6,7], and by Stanway, Chapman & Dowling [9].

9.2 EXISTING DESIGN METHODS

9.2.1 BS5400

BS5400 [3] uses a strut model for design of the transverse stiffener. The effective cross-section of the strut consists of the real stiffener and a width of plate equal to *32t*, and the buckling length of the strut is taken to be equal to the depth of the plate d. For intermediate transverse stiffeners, the code requires that the strut is capable of resisting the following compressive forces:

(1) Axial force due to tension field action F_{tw}, given by:

$$F_{tw} = bt(\tau - \tau_1) \tag{9.1}$$

where

b is the small panel dimension

τ is the average shear stress in the panel, which is taken as the ultimate shear stress of the panel as calculated from BS5400.

τ_1 is 80% of the critical buckling stress of the panel, and is given by:

$$\tau_1 = \begin{cases} 3.6E\left[1+\left(\frac{d}{a}\right)^2\right]\left(\frac{t}{d}\right)^2 \sqrt{1-\frac{\sigma_c}{2.9E}\left(\frac{d}{t}\right)^2} & for \quad \sigma_c < 2.9E\left(\frac{t}{d}\right)^2 \\ 0 & for \quad \sigma_c \geq 2.9E\left(\frac{t}{d}\right)^2 \end{cases} \tag{9.2}$$

and σ_c is the compressive stress in the plate.

The force F_{tw} is to be taken as acting in the mid-plane of the plate. In deriving Eqn. 9.1, the tension field stresses are assumed to act over the whole plate, and the inclination of the tension field stresses φ (see Fig. 6.2b) is assumed to be no greater than 45°.

(2) Axial force representing the destabilizing influence of the plate F_{wi}, given by:

$$F_{wi} = \frac{d^2}{a} t k_s \sigma_R \tag{9.3}$$

where

σ_R $=\tau_R+\sigma_c+\sigma_b/6$

τ_R $=\min\{\tau, \tau_1\}$

σ_c, σ_b are the compressive and bending stress in the plate, respectively

k_s is a parameter depending on the slenderness of the plate

F_{wi} is obtained by considering a "saw tooth" stiffened plate buckling model, originally proposed by Richmond [48], subjected to a longitudinal compressive stress σ_R. The derivation of Eqns 9.1 and 9.3 was described in detail by Chatterjee [49].

The buckling resistance of the strut, which must be as great as $F_{tw}+F_{wi}$, is determined using the standard procedure for compression members described in BS5400. It is also required that the maximum stress in the stiffener due to the compressive F_{tw} should not exceed the yield stress of the stiffener.

In BS5400, a load bearing stiffener is designed as a strut to resist the reactive force and the axial force representing the destablizing effect of the plate, F_{wi}.

9.2.2 Eurocode 3

Eurocode 3 [4] also uses a strut model for design of the transverse stiffener. The effective cross-section of the strut consists of the real stiffener and a width of plate equal to $30t\sqrt{235/\sigma_{0p}}$. It is specified in Eurocode that the buckling length of the stiffener should be "not less than 0.75d", depending on the conditions of restraint. For the comparisons presented in Section 9.3, the buckling length of the strut is taken as the depth of the plate d, because there is no external rotational restraint at the ends of the stiffener in the FE model (Section 3.5).

For intermediate transverse stiffeners, the Eurocode requires that the strut is capable of resisting the following compressive force:

$$N_s = V - d\,t\,\tau_{bb} \tag{9.4}$$

where

τ_{bb} is the "initial shear buckling resistance", which ranges from τ_{cr} (panel) for slender panels to τ_{0p} for stocky panels.

V is the "shear buckling resistance", which may be calculated using either the simple post-critical method ($V_{ba,Rd}$) or the tension field method ($V_{bb,Rd}$). For the comparison in Section 9.3, the greater value of $V_{ba,Rd}$ and $V_{bb,Rd}$ is assumed.

The buckling resistance of the strut, which must be as great as N_s, is determined using the standard procedure for compression members described in Eurocode, using buckling curve C.

In addition, Eurocode requires that the moment of inertia of the stiffener about the centre line of the plate, I_s, should satisfy the following requirements:

$$\begin{aligned} I_s &\geq 1.5 d^3 t^3 / a^2 \quad for \quad a/d < \sqrt{2} \\ I_s &\geq 0.75 d t^3 \quad for \quad a/d \geq \sqrt{2} \end{aligned} \tag{9.5}$$

For load bearing stiffeners, Eurocode requires that in addition to checking the buckling resistance, the cross-section resistance should be checked adjacent to the loaded flange, and the width of web plate included in the effective cross-section should be limited to s_y, which is related to the sizes of the flanges.

9.2.3 AASHTO

For intermediate transverse stiffeners, AASHTO [34] requires that the area A_s and moment of inertia I_s of the actual stiffener cross-section satisfy the following criteria:

$$A_s \geq \left[0.15 B d t (1-C) \frac{V}{V_u} - 18 t^2 \right] \frac{\sigma_{0p}}{\sigma_{0s}} \tag{9.6}$$

$$\begin{aligned} I_s &\geq [2.5(d/a)^2 - 2] a t^3 \\ I_s &\geq 0.5 a t^3 \end{aligned} \tag{9.7}$$

where:

B =1.0 for double-sided stiffeners, and 2.4 for single-sided flat bar stiffeners.

C is a parameter representing the ratio of the shear buckling stress of the panel to the shear yield stress, and $C \leq 1$.

V/V_u is the ratio of the applied shear force to the shear strength, and is taken as 1 (i.e., $\tau=\tau_{u,ss}$) for the comparisons presented in this Chapter.

When stiffeners are double-sided, the moment of inertia I_s is taken about the center line of the plate. When single-sided stiffeners are used, I_s should be taken about the edge in contact with the plate.

The value of the moment of inertia I_s given in Eqn. 9.7 is based on critical buckling results for stiffened plates, with a magnification factor being introduced to allow for post-buckling behaviour and the detrimental effect of initial imperfections. The stiffener area A_s is required to be great enough to resist the compressive force in the stiffener due to tension field action. In deriving Eqn. 9.6, an effective width of plate equal to 18t is assumed to act in combination with the stiffener.

AASHTO requires the bearing stiffener to be designed as a column to resist the bearing force, The effective section of the column is taken as the stiffener section plus a strip of plate extending not more than 9t on each side of the stiffener.

9.2.4 Horne & Grayson

Horne and Grayson [45] proposed that the design value of the stiffener flexural rigidity Ψ can be determined by the following empirical formula:

$$\Psi^* = 0.6(\lambda - 50)(d/a) \tag{9.8}$$

with

$$\Psi^* \leq 0.8(\lambda - 50) \tag{9.9}$$

where:

$$\lambda = \frac{d}{t}\sqrt{\frac{\sigma_{0p}}{355}} \tag{9.10}$$

$$\Psi^* = \frac{E I_s}{D a} \tag{9.11}$$

When calculating the moment of inertia I_s in Eqn. 9.11, only the actual stiffener section is considered. For double-sided stiffeners, the moment of inertia I_s is calculated about the center line of the plate. For single-sided stiffeners, I_s is calculated about the edge in contact with the plate.

Eqns. 9.8 and 9.9 are empirically derived from elasto-plastic finite element results, such that the ultimate strength of the stiffened plate is not less than that of the individual simply supported panels.

9.2.5 Rahal & Harding

Rahal and Harding [6,7] proposed that the transverse stiffener could be designed as a simply supported beam subjected to the lateral distributed force q given by:

$$q\,(N/mm) = \frac{\lambda^{\frac{1}{3}} a}{35.5}\left(\frac{\sigma_{0p}}{355}\right)^{\frac{3}{2}}\left[\left(\frac{\tau}{\tau_{0p}} + \psi\frac{\sigma_c}{\sigma_{0p}}\right)^3 + \left(\psi'\frac{\sigma_b}{\sigma_{0p}}\right)^3\right]\sin\left(\frac{\pi y}{d}\right) \tag{9.12}$$

where:

τ, σ_c, σ_b are the applied shear, compressive and bending stresses, respectively, and should be taken as the ultimate values of the stresses, applied in combination, for the individual simply supported panels. For the comparison presented in this Chapter, the ultimate strengths from the FE solutions, as given in Section 8.4, are used.

y is the distance along the stiffener.

$\lambda = \frac{d}{t}\sqrt{\frac{\sigma_{0p}}{355}}$

ψ is the reduction coefficient for compressive stresses, $\psi = 0.12\sqrt{\lambda\frac{d}{a}}$

ψ' is the reduction coefficient for bending stresses, $\psi' = 0.415$

Eqn. 9.12 was developed from a curve-fitting operation of the elasto-plastic finite element results for plates of d/a=1 & 2, stiffened with a non-deflecting stiffener. It should be noted that when using Eqn. 9.12 to calculate q, all force and length dimensions must be in *N* and *mm*, respectively.

The maximum bending stress in the stiffener, resulting from the lateral distributed force q, can be calculated using the simple beam theory. The adequate stiffener flexural rigidity is determined by applying the "first yield criterion" (or *no yield criterion*, as referred to in this thesis).

It is proposed that the beam cross-section consists of the stiffener section and a width of plate equal to 32t.

9.2.6 Stanway, Chapman & Dowling

For intermediate transverse stiffeners on plates subjected to pure shear, Stanway et al [9] proposed that the stiffener should be designed to resist a stiffener bending moment M_s which takes account of the effects of out-of-plane forces due to local panel bending and the tendency for the stiffened plate to buckle overall.

The stiffener moment caused by panel bending, M_{pb}, is given by:

$$M_{pb} = \left(\frac{M_{pbcr}}{w_{pcr}} \right) w_p F_{nl} \qquad (9.13)$$

where:

M_{pbcr} denotes M_{pb} from critical buckling analysis.

w_p is the maximum panel out-of-plane deflection.

w_{pcr} is w_p in critical buckling analysis.

F_{nl} is the non-linear moment factor defined as $F_{nl}=q_{pb}/q_{pbcr}$, where q_{pb} is the lateral distributed force on the stiffener, derived from non-linear FE results for the reaction on a straight knife edge, and q_{pbcr} represents q_{pb} from critical buckling analysis.

The predictive formulae for M_{pbcr}/w_{pcr} is derived from critical buckling analyses for plates with a straight knife edge. The panel deflection w_p is calculated using an equation developed by curve-fitting the non-linear elastic finite element solutions.

The stiffener moment resulting from the overall buckling effect, M_o, is given by:

$$M_o = \frac{\tau t d \pi^2 w_{0s}}{k_{cro}} \tag{9.14}$$

where:

τ is the applied shear stress, taken as $\tau_{u,ss}$.

w_{0s} is the stiffener imperfection.

k_{cro} is the overall buckling stress coefficient, derived from the proposed rigid-link model.

Based on the theoretical analysis of the rigid-link model, the total stiffener moment M_s is proposed to be approximately given by:

$$M_s = \frac{M_o + M_{pb}}{1 - \tau/\tau_{cro}} \tag{9.15}$$

where:

$$\tau_{cro} = k_{cro} \frac{E I_s}{d^3 t} \tag{9.16}$$

The stiffener is quantified by the two criteria given below:

(1) The chosen stiffener must satisfy the strength criterion given by:

$$\frac{M_s}{Z_s} \leq \sigma_{0s} \tag{9.17}$$

where Z_s is the section modulus of the stiffener, and σ_{0s} is the stiffener yield stress.

(2) The chosen stiffener must satisfy the stiffness criterion defined as:

$$w_s \leq w_{sd} \tag{9.18}$$

where w_s is the stiffener deflection calculated using:

$$w_s = \frac{M_s d^2}{\pi^2 E I_s} \tag{9.19}$$

and w_{sd} is the proposed design limit of the stiffener deflection given by:

$$w_{sd} = \frac{0.125 w_p}{1-\cos\left(\frac{\pi k_\lambda b}{2d}\right)}, \quad and \quad \frac{d}{1000} \le w_{sd} \le \frac{d}{200} \tag{9.20}$$

with:

$$k_\lambda = \begin{cases} 0.375 d/b + 0.625 & for \quad d/a < 3 \\ 1.75 & for \quad d/a \ge 3 \end{cases} \tag{9.21}$$

In calculating I_s and Z_s, only the stiffener section is used. For a concentric stiffener, I_s and Z_s are calculated by assuming that the neutral axis occurs at the mid-plane of the plate. For an eccentric stiffener, it is suggested that I_s and Z_s may be calculated by assuming that the neutral axis occurs at the face in contact with the plate.

9.3 COMPARISON WITH EXISTING DESIGN METHODS

9.3.1 Required Stiffener Sizes

In this section, comparisons of the required stiffener sizes are made between the proposed model and the existing design methods discussed in Section 9.2. Comparisons are made mainly for plates with a double-sided stiffener, subjected to pure shear, but single-sided flat bar stiffeners are also considered. For all the results described in this section, a flat bar stiffener with a side ratio of $h_s/t_s=10$ (for both double-sided and single-sided, as shown in Fig. 3.1) is assumed.

9.3.1.1 Double-sided Stiffeners

Table 9.1 lists the minimum values of the stiffener flexural rigidity, denoted as Ψ_d, required according to the proposed model and the existing design methods for stiffened plates with a double-sided flat bar stiffener. Plates having a panel aspect ratio d/a=0.5, 1, 2, 3, 5 & 7, and a slenderness ratio b/t=80, 120 &180, respectively, are considered.

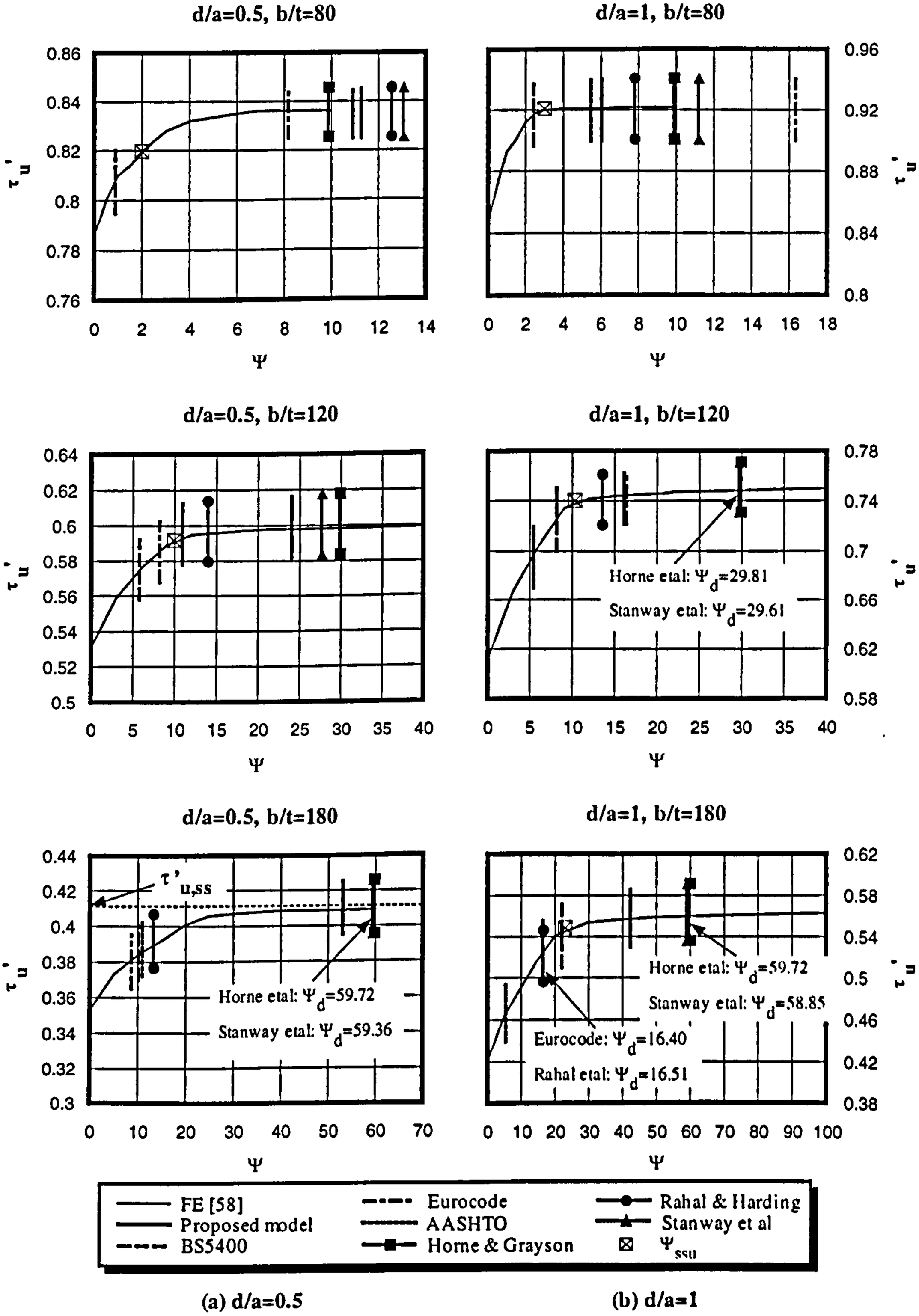
Table 9.1 Required stiffener flexural rigidities Ψ_d. Double-sided flat bar stiffeners (h_s/t_s=10)

Pure shear. $\sigma_{0p}=\sigma_{0s}$=245N/mm^2. $\Psi=EI_s/Db$, I_s as in Eqn. 3.4

b/t	d/a	Proposed Model (Note 1)	BS5400 (Note 2)	Eurocode (Note 2)	AASHTO (Note 2)	Horne & Grayson	Rahal & Harding (Note 1)	Stanway et al (Note 1)
80	0.5	11.27	0.888	8.183	10.92	9.876	12.57	13.07
	1	6.037	2.422	16.33	5.460	9.876	7.793	11.17
	2	131.9	45.39	130.8	87.36	66.34	57.85	150.9
	3	240.7	233.2	442.5	223.9	119.5	194.4	431.0
	5	580.4	1838	2055	660.7	225.8	999.5	700.2
	7	1105	7000	5617	1316	332.2	2619	1774
120	0.5	24.04	5.757	8.187	10.92	29.81	13.94	27.62
	1	16.10	8.180	16.38	5.460	29.81	13.51	29.61
	2	294.7	96.84	130.9	87.36	119.5	71.06	309.4
	3	444.3	388.1	442.1	223.9	199.3	232.7	648.8
	5	1024	2308	2447	660.7	358.8	1001	1019
	7	2037	7911	6685	1316	518.3	2976	2622
180	0.5	53.09	10.12	8.645	10.92	59.72	13.23	59.36
	1	42.25	22.04	16.40	5.460	59.72	16.51	58.85
	2	587.9	192.5	494.6	87.36	199.3	72.84	609.2
	3	714.6	598.4	2149	230.0	318.9	221.0	1022
	5	1588	2796	9946	869.9	558.1	841.0	1554
	7	3090	8645	24677	1903	797.4	2088	3888

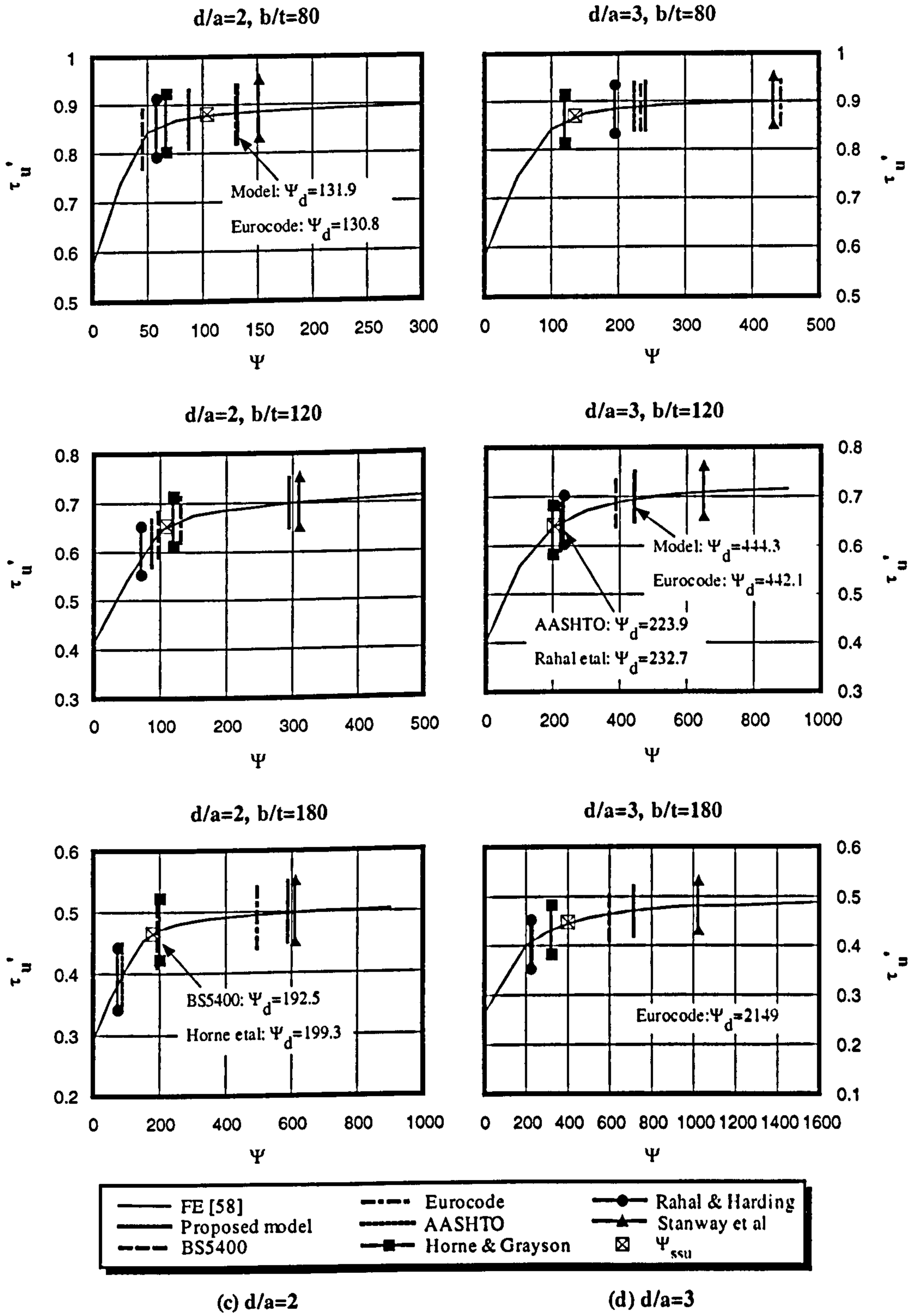
Note 1: Applied shear taken as the panel strength τ_u from Table 8.3.

Note 2: Applied shear taken as the panel strength τ_u, calculated from the same code.



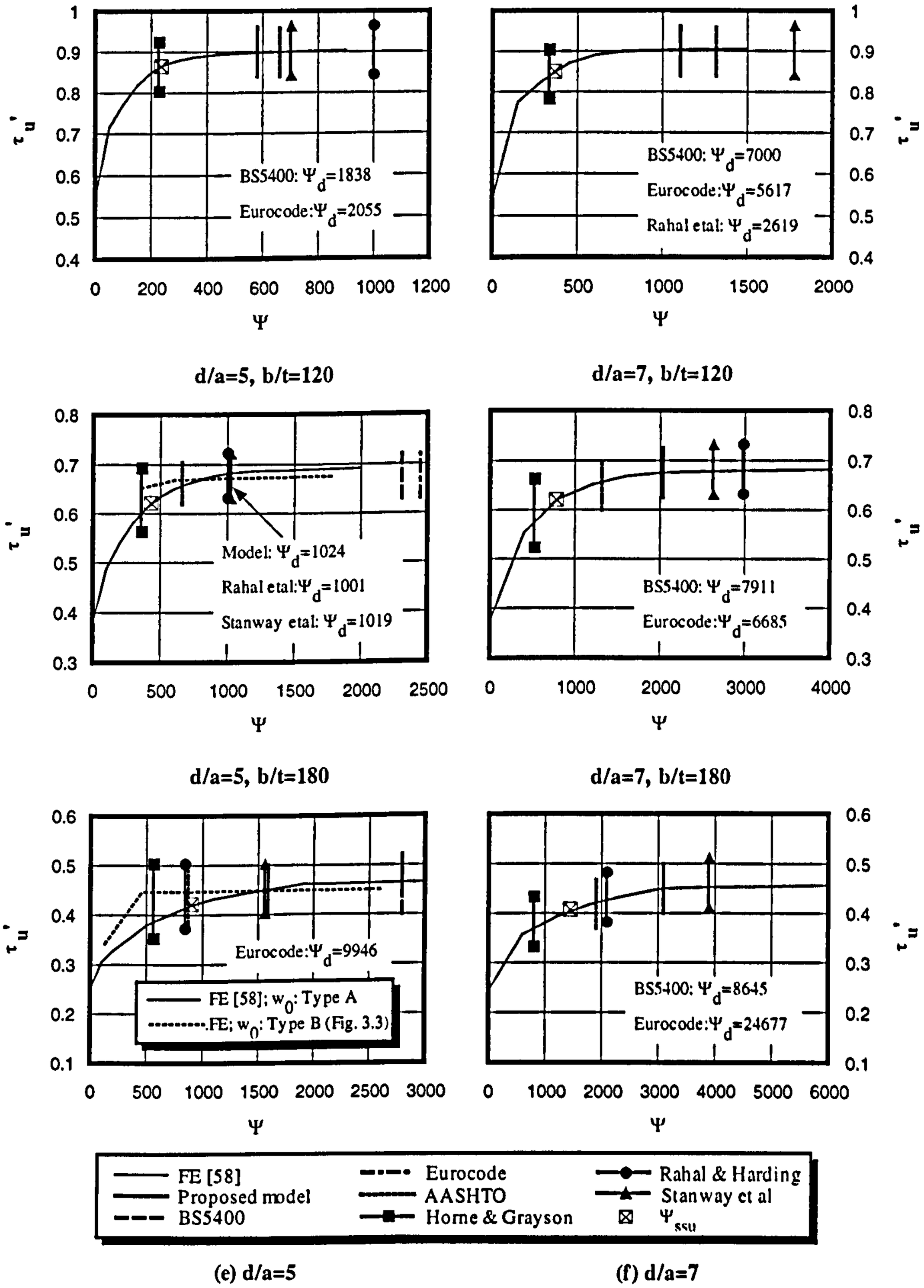
(a) d/a=0.5 (b) d/a=1

Figure 9.1 Comparison of the stiffener flexural rigidity Ψ_d required by the proposed model and the existing methods, with the FE τ_u' vs. Ψ results from [58]. Double-sided flat bar stiffeners (h_s/t_s=10) $\sigma_{0p}=\sigma_{0s}=245N/mm^2$. $\Psi=EI_s/Db$, I_s as in Eqn. 3.4. Pure shear



(c) d/a=2 (d) d/a=3

Figure 9.1 (Cont) Comparison of the stiffener flexural rigidity Ψ_d required by the proposed model and the existing methods, with the FE τ_u' vs. Ψ results from [58]. Double-sided flat bar stiffeners (h_s/t_s=10) $\sigma_{0p}=\sigma_{0s}$=245N/mm^2. $\Psi=EI_s/Db$, I_s as in Eqn. 3.4. Pure shear



(e) d/a=5 (f) d/a=7

Figure 9.1 (Cont) Comparison of the stiffener flexural rigidity Ψ_d required by the proposed model and the existing methods, with the FE τ_u' vs. Ψ results from [58]. Double-sided flat bar stiffeners ($h_s/t_s=10$) $\sigma_{0p}=\sigma_{0s}=245N/mm^2$. $\Psi=EI_s/Db$, I_s as in Eqn. 3.4. Pure shear

Table 9.2 Values of $100\Omega_d$ ($\Omega=A_sd/adt$) for the proposed model and the existing design methods. Double-sided flat bar stiffeners ($h_s/t_s=10$). Pure shear. $\sigma_{0p}=\sigma_{0s}=245N/mm^2$.

b/t	d/a	Proposed Model (Note 1)	BS5400 (Note 2)	Eurocode (Note 2)	AASHTO (Note 2)	Horne & Grayson	Rahal & Harding (Note 1)	Stanway et al (Note 1)
80	0.5	3.868	0.965	3.407	3.802	3.605	4.098	4.183
	1	5.538	3.371	9.779	5.245	7.210	6.350	7.695
	2	28.10	16.13	28.60	22.69	19.66	18.31	30.11
	3	38.32	37.70	53.27	36.91	26.69	34.31	51.69
	5	60.15	108.5	116.1	64.36	37.07	79.54	66.27
	7	83.69	213.8	192.9	91.45	45.22	129.8	106.5
120	0.5	4.765	2.236	2.809	3.143	5.333	3.576	5.125
	1	7.721	5.393	8.062	4.346	10.67	7.041	10.63
	2	34.90	19.68	23.47	18.66	21.94	16.77	35.80
	3	43.08	40.20	43.62	30.32	28.55	30.92	52.28
	5	65.97	99.77	103.7	52.77	38.61	65.21	65.81
	7	93.53	186.2	172.3	74.95	46.61	113.4	106.4
180	0.5	5.928	2.496	2.380	2.596	6.301	2.874	6.281
	1	10.53	7.507	6.632	3.597	12.60	6.457	12.51
	2	40.76	23.03	37.82	15.34	23.45	13.97	41.50
	3	45.01	41.13	79.49	25.23	29.82	24.72	54.01
	5	67.57	90.0	172.0	49.75	39.69	48.91	66.80
	7	94.67	159.3	271.7	74.06	47.59	77.62	106.3

Note 1: Applied shear taken as the panel strength τ_u from Table 8.3.

Note 2: Applied shear taken as the panel strength τ_u, calculated from the same code.

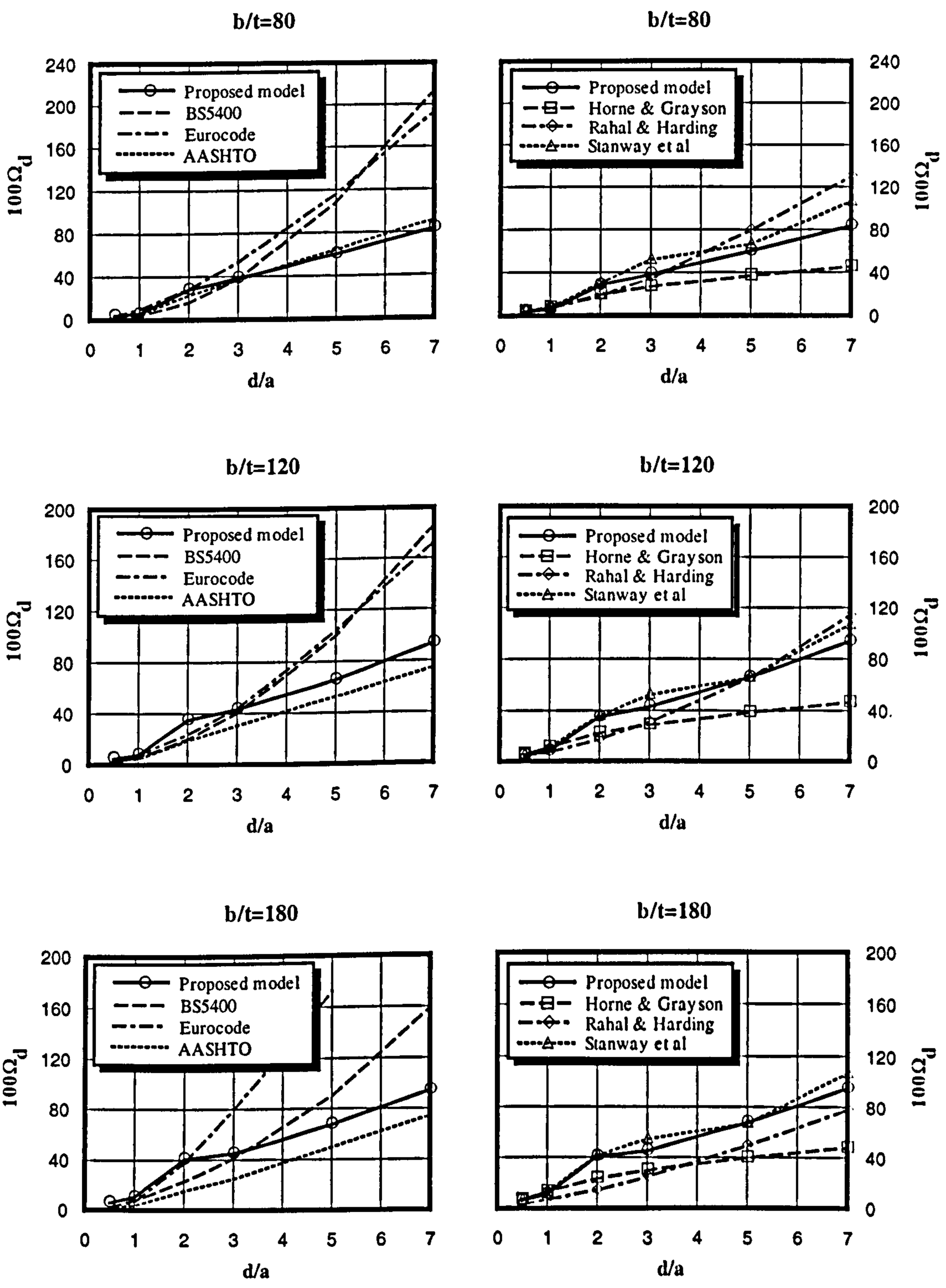


Figure 9.2 Minimum values of the stiffener extensional rigidity Ω_d required by the proposed model and the existing methods. Double-sided flat bar stiffeners (h_s/t_s=10). $\sigma_{0p}=\sigma_{0s}$=245N/mm^2. $\Omega=A_s/at$. Pure shear

It has been pointed out in Chapter 8 that the basic requirement for an adequate stiffener is to ensure that the ultimate strength for the stiffened plate is at least as great as the strength for the associated simply supported panel, represented by:

$$\Psi_d \geq \Psi_{ssu} \tag{9.22}$$

Also, an adequate stiffener should ensure that the plate strength is within the plateau of the τ_u' vs. Ψ curve.

To demonstrate the adequacy of the stiffeners given by the various design methods considered, the Ψ_d values are compared with the FE τ_u' vs. Ψ curves in Fig. 9.1.

Presented in Table 9.2 are the minimum values of the stiffener extensional rigidity, denoted as Ω_d ($\Omega=A_s d/adt$), for the proposed model and the existing design methods considered. The variations in Ω_d with the panel aspect ratio d/a according to the various design methods are illustrated in Fig. 9.2. It is noted that Ω_d represents the ratio of the weight of the stiffener to the weight of the panel ($A_s d/adt$), and therefore is a measure of cost. The value of Ω_d may indicate whether it is economical to introduce stiffening, or simply to increase the plate thickness, to achieve the required strength. It is observed in Fig. 9.2 that according to the proposed model, an approximately linear relation between Ω_d and d/a, for $h_s/t_s=10$, may be assumed, as shown in Fig. 9.3. This simple relation may be used to give an estimate of the required stiffener size for initial design.

9.3.1.2 Single-sided Stiffeners

In this section, the proposed model and the existing design methods are used to estimate the stiffener size required for stiffened plates of d/a=2, 5 and b/t=180 with a single-sided flat bar stiffener having $h_s/t_s=10$, subjected to pure shear. In Table 9.3, the minimum values of the stiffener flexural rigidity, Ψ_d, required according to the various design methods are listed. In Fig. 9.4, the values of Ψ_d for different design methods are compared with the finite element results of τ_u' vs. Ψ. Also shown in Fig. 9.4 are the values of Ψ_{ssu}.

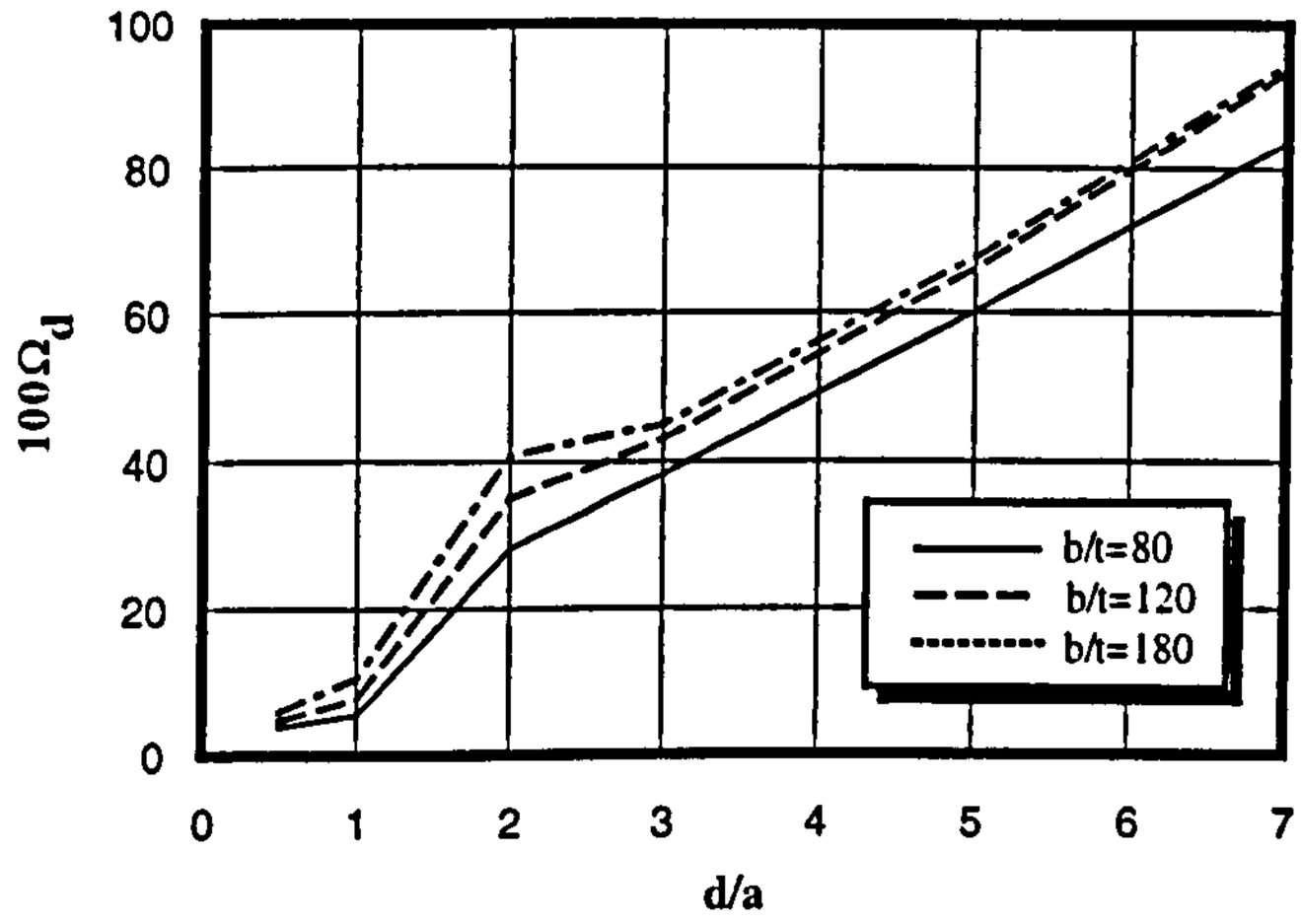


Figure 9.3 Minimum values of the stiffener extensional rigidity Ω_d required by the proposed model. Double-sided flat bar stiffeners (h_s/t_s=10). $\sigma_{0p}=\sigma_{0s}$=245N/mm^2. $\Omega=A_s/at$. Pure shear

Table 9.3 Required stiffener flexural rigidities Ψ_d. Single-sided flat bar stiffeners (h_s/t_s=10) Pure shear. $\sigma_{0p}=\sigma_{0s}$=355N/mm^2. $\Psi=EI_s/Db$, I_s as in Eqn. 3.6

b/t	d/a	Proposed Model (Note 1)	BS5400 (Note 2)	AASHTO (Note 2)	Horne & Grayson	Rahal & Harding (Note 1)	Stanway et al (Note 1)
180	2	213.7	346.2	407.3	62.0	25.78	217.5
	5	3488	3821	3429	170.0	813.4	453.2

Note 1: Applied shear taken as the panel strength τ_u from Table 8.4.

Note 2: Applied shear taken as the panel strength τ_u, calculated from the same code.

Presented in Table 9.4 are the minimum values of the stiffener extensional rigidity, Ω_d, for the proposed model and the existing design methods.

The results presented above demonstrate that there is a wide difference in the stiffeners required by the various existing design methods for a given plate geometry. In the next section, the results for each method considered are discussed.

Table 9.4 Values of $100\Omega_d$ ($\Omega=A_sd/adt$) for the proposed model and the existing design methods. Single-sided flat bar stiffeners ($h_s/t_s=10$). Pure shear. $\sigma_{0p}=\sigma_{0s}=355N/mm^2$.

b/t	d/a	Proposed Model (Note 1)	BS5400 (Note 2)	AASHTO (Note 2)	Horne & Grayson	Rahal & Harding (Note 1)	Stanway et al (Note 1)
180	2	36.13	45.97	49.87	19.45	12.54	36.44
	5	145.8	152.7	144.7	32.21	38.36	52.60

Note 1: Applied shear taken as the panel strength τ_u from Table 8.4.

Note 2: Applied shear taken as the panel strength τ_u, calculated from the same code.

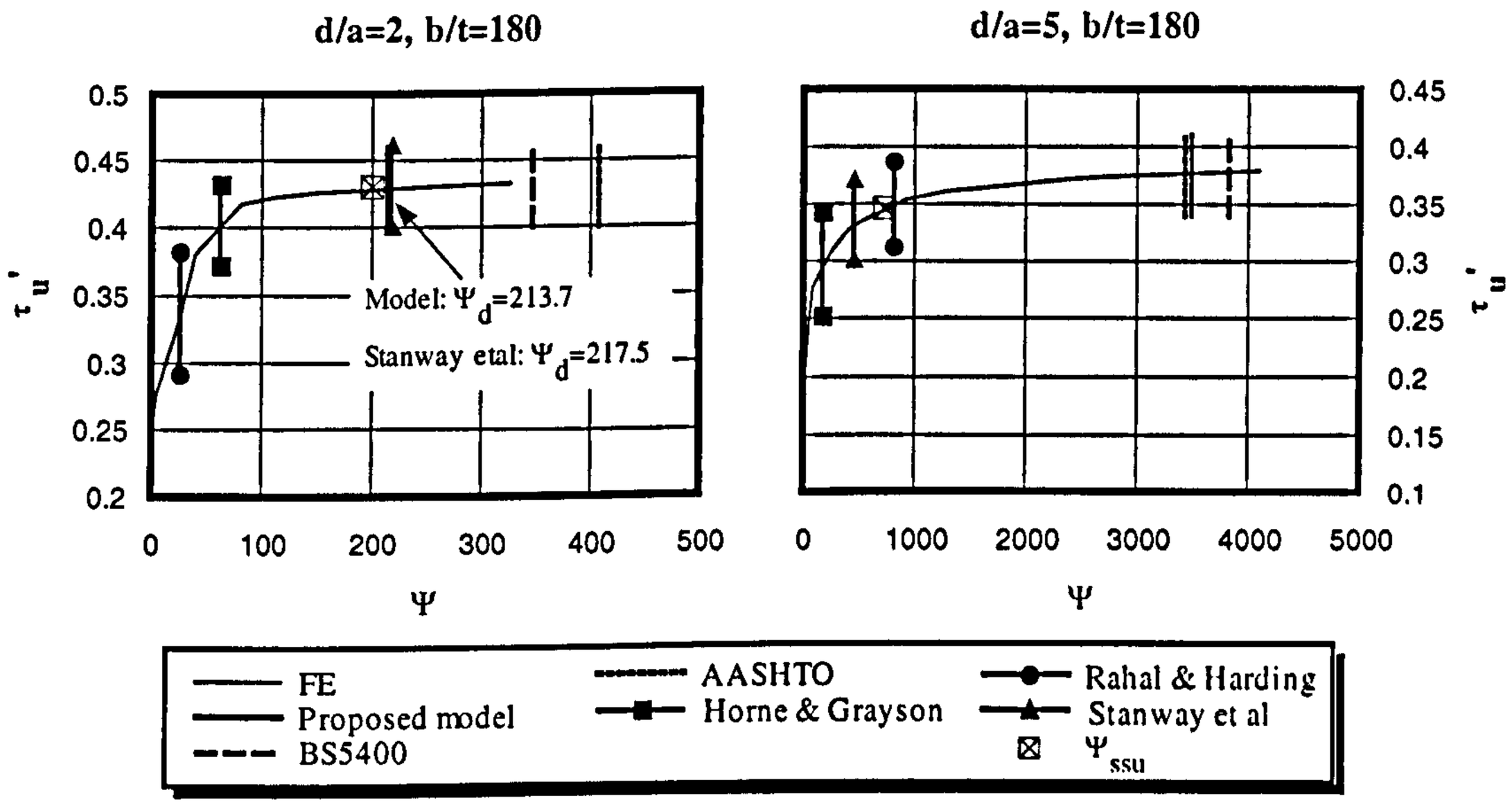


Figure 9.4 Comparison of the stiffener flexural rigidity Ψ_d required by the proposed model and the existing methods, with the FE τ_u' vs. Ψ results. Single-sided flat bar stiffeners ($h_s/t_s=10$) $\sigma_{0p}=\sigma_{0s}=355N/mm^2$. $\Psi=EI_s/Db$, I_s as in Eqn. 3.6. Pure shear

9.3.2 Comments

9.3.2.1 BS5400

Referring to Fig. 9.1, it is observed that for d/a≤2, BS5400 gives stiffeners which occur prior to the start of the plateau in the τ_u' vs. Ψ curve, and does not give a value of τ_u' as

great as that for the simply supported panel (except for d/a=2, b/t=180). That is, BS5400 gives inadequate stiffeners for these cases. However, for very tall plates (e.g. d/a≥5), BS5400 becomes unduly conservative. It can be seen in Fig. 9.2 that as d/a increases, the stiffener extensional rigidity parameter Ω increasingly exceeds the model requirement.

The preceding observations indicate that BS5400 does not give a correct account of the trend in the stiffener required as d/a is varied. This is because in BS5400, the stiffener is designed as a strut, subjected to axial loading only, and the lateral force exerted on the stiffener, resulting from the effect of local panel bending, is not taken into account. The imaginary axial force F_{wi} attempts only to account for the effect of stiffener imperfection. It has been found in Section 5.2.5 that for d/a≤2, the panel bending effect is dominant. Therefore for d/a≤2, although BS5400 may overestimate the stiffener axial force due to the tension field action (see Fig. 6.4), the total forces on the stiffener are underestimated. For very tall plates, the panel bending effect becomes less important, and the overestimation in the axial force results in an overly conservative estimate of the required stiffener.

It is seen in Fig. 9.4 that for the two cases considered, BS5400 gives satisfactory results for single-sided stiffeners. As stated in Section 8.7, an additional bending moment results from the eccentricity of the stiffener axial force due to the tension field action. This additional moment is considered in BS5400.

9.3.2.2 Eurocode 3

For d/a≤1, b/t=180 (Fig. 9.1a & b), Eurocode underestimates the stiffener size required to attain a plate strength τ_u' which is at least as great as that for the simply supported panel. In fact, for these cases, the stiffeners from Eurocode fall below the plateau of the τ_u' vs. Ψ curve. As d/a increases from 5, the required stiffener size given by Eurocode increases rapidly, and becomes unduly conservative. The reason for these trends is similar to that pointed out for BS5400 (Section 9.3.2.1).

It is observed in Fig. 9.2 that for tall plates with b/t≤120, the required stiffeners given by Eurocode and BS5400 are quite close. However, for tall plates with b/t=180, Eurocode gives stiffeners which are considerably greater than those from BS5400. This is because for b/t=180, the tension field is well developed, and the compressive force N_s in Eurocode (Eqn. 9.4) is greater than the axial force F_{tw} (Eqn. 9.1) from the tension field action in BS5400 by a factor of approximately d/a, for tall plates.

9.3.2.3 AASHTO

It is seen in Fig. 9.1 that for b/t=80 and each d/a value, AASHTO gives stiffeners which lie within the plateau of the τ_u' vs. Ψ curve, although for d/a=2 the plate strength is slightly less than that for the simply supported panel. Therefore, the stiffeners given by AASHTO for b/t=80 can be considered to be satisfactory.

As the panel slenderness ratio b/t increases, the degree to which AASHTO underestimates the required stiffener increases progressively. For b/t=180 (Fig. 9.1), AASHTO gives stiffeners which occur prior to the start of the plateau in the τ_u' vs. Ψ curve, and severely underestimates the required stiffener. The inadequacy of the stiffeners given by AASHTO for b/t=180 is also shown in Fig. 9.2.

It has been pointed out in Section 9.2.3 that the stiffener rigidity requirement in AASHTO given by Eqn. 9.7 is based on critical buckling results for stiffened plates. This can explain why the stiffener required by AASHTO is sufficient for b/t=80, but insufficient for b/t=180 where the post-buckling behaviour of the plate becomes more important. Although a constant magnification factor is introduced in AASHTO to account for the post-buckling behaviour and the effect of initial imperfections, the above observations demonstrate that this constant factor does not give a correct account of these effects as b/t is varied.

It is seen in Fig. 9.4 that for d/a=2 & 5 and b/t=180, AASHTO gives satisfactory results for single-sided stiffeners. It is found that in these cases, the strength requirement given in Eqn. 9.6 controls. It is noted that as implied in Eqn. 9.6, AASHTO assumes that for

stiffeners made of flat bars, the single-sided stiffener requires at least 2.4 times the total area of the double-sided stiffeners. It may be due to this empirical factor that sufficient results are given for single-sided stiffeners for the cases examined.

9.3.2.4 Horne & Grayson

As shown in Fig. 9.1, Horne & Grayson's approach gives satisfactory results for d/a≤1, where the stiffener given locates within the plateau of the τ_u' vs. Ψ curve. As d/a increases from 2, the stiffener given by Horne & Grayson's approach moves gradually toward the transition region of the τ_u' vs. Ψ curve, which is either only marginally sufficient or insufficient. For d/a≥3, Horne & Grayson's approach underestimates the required stiffener. It is observed in Fig. 9.2 that for d/a≥4, Horne & Grayson's approach gives stiffeners which are the smallest among all the design methods considered.

In Fig. 9.4, it is shown that the single-sided stiffeners given by Horne & Grayson's approach for the two cases examined are inadequate.

9.3.2.5 Rahal & Harding

It is observed in Fig. 9.1 that as b/t increases from 80 to 180, the stiffener given by Rahal & Harding's approach moves progressively towards a position prior to the start of the plateau in the τ_u' vs. Ψ curve. For d/a=0.5, 1 and b/t=80, 120, Rahal & Harding's approach gives stiffeners which lie within the plateau of the τ_u' vs. Ψ curve, and the corresponding strength of the stiffened plates is greater than that for the simply supported panel. However, for d/a≤5 and b/t=180, the stiffener given by Rahal & Harding's approach is inadequate, whereas for d/a=7 and b/t=80, it is overly conservative.

For single-sided stiffeners, it is apparent in Fig. 9.4 that for d/a=2 and b/t=180, Rahal & Harding's approach severely underestimates the required stiffener. For d/a=5 and b/t=180, the single-sided stiffener given by Rahal & Harding's approach is slightly

greater than Ψ_{ssu}, but cannot give an effectively divided panel mode (see Fig. 8.19), and hence is still insufficient.

9.3.2.6 Stanway, Chapman & Dowling

For double-sided stiffeners, it is observed in Fig. 9.1 that the approach by Stanway et al is the only one of all the existing methods considered that gives sufficient stiffeners for all d/a and b/t examined. That is, the stiffener from this approach is within the plateau of the τ_u' vs. Ψ curve, and gives a plate strength at least as great as that for the simply supported panel. The position of the stiffener along the plateau of the τ_u' vs. Ψ curve varies with b/t, but is not unduly conservative.

For single-sided stiffeners (Fig. 9.4), for which the suggested approach by Stanway et al was not validated, an adequate stiffener is given by this approach for d/a=2, b/t=180, but an inadequate stiffener for d/a=5, b/t=180. The reason for this is that as adopted in Horne & Grayson's approach, the neutral axis of the single-sided stiffener is assumed to be at the face in contact with the plate, and no direct account is taken for the axial force in the stiffener due to the tension field action. It has been found in Section 8.7.6 that the method proposed by Horne & Grayson [45] for single-sided stiffeners is only valid for certain cases, and may considerably underestimate the required stiffener size in other instances, as for tall plates.

9.3.2.7 Proposed Model

The stiffeners given by the proposed model have been discussed in detail in Chapter 8. It has been found that the proposed model gives satisfactory results for all cases examined, including double-sided and single-sided stiffeners, and for plates subjected to combined shear and compression, as well as shear and bending. That is, the proposed model ensures that the strength of the stiffened plate is within the plateau region of the graph of the ultimate load against the stiffener rigidity Ψ, and is equal or greater than the strength of simply supported panels.

In comparison with BS5400 and Eurocode, the proposed design model gives heavier stiffeners for d/a≤2 plates (Fig. 9.1, except for d/a=1, b/t=80 for Eurocode), and considerably lighter stiffeners for d/a≥5 plates (Fig. 9.2). For single-sided stiffeners (Fig. 9.4), the stiffener given by the proposed model is lighter than that from BS5400.

Compared to AASHTO, the proposed model gives heavier double-sided stiffener for all cases considered except for d/a=7 and b/t=80, but a lighter single-sided stiffener for d/a=2 and b/t=180.

In comparison with the approach by Horne & Grayson, the proposed model gives lighter double-sided stiffeners for d/a≤1 plates and heavier stiffeners for d/a≥2 (Fig. 9.1). and heavier single-sided stiffeners for the two cases examined.

It is seen in Figs. 9.1 and 9.2 that in comparison with Rahal & Harding's approach, the proposed model gives heavier double-sided stiffeners for b/t=180 and each d/a considered, and lighter double-sided stiffeners for b/t=80 and all d/a considered except for d/a=2 & 3. The single-sided stiffener given by Rahal & Harding's approach is much less than that from the proposed model (Fig. 9.4).

By reference to Fig. 9.2, it is observed that for concentric stiffeners the trend in the stiffener required as d/a is varied is very similar for the proposed model and the approach by Stanway et al. In Fig. 9.1, it is seen that the stiffener given by the proposed model is in general less conservative than that from the Stanway et al approach, but still locates at a reasonable distance along the plateau of the τ_u' vs. Ψ curve.

9.4 COMPARISON WITH RESULTS FOR TEST GIRDERS

In Section 2.6.1, the finite element results for the ultimate shear strength V_u' vs. stiffener rigidity Ψ have been given for the I-section test girders (GI and GII) and associated CUCU two-panel stiffened plates. For the CUCU plates, the loading conditions considered include pure shear and combined shear and bending. The applied stress ratio was taken as $\tau:\sigma_b=1:0.52$, which was the stress ratio at the position of the

intermediate stiffener in the test girders GI and GII. It is noted that in the parametric study carried out for the test girders GI and GII, the stiffener thickness was kept constant as t_s=5mm, but the stiffener depth h_s varied, and the panel dimensions were taken as a=590mm, d=600mm, t=2mm.

In this section, the minimum values of the stiffener flexural rigidity Ψ_d required according to the proposed model and some of the existing design methods are compared with the experimental and numerical results for the test girders.

9.4.1 Proposed Model

According to the proposed design model, the transverse stiffener required for an I-section girder is determined by considering the associated web plate, assuming its in-plane boundary conditions to be CUCU, that is, the flanges are not included. It has been found in Chapter 2 that the stiffener that is adequate for the CUCU plate is also adequate for the plates with flanges.

To calculate the required stiffener sizes using the proposed model, the ultimate strength for CUCU simply supported panels should be given. For this purpose, finite element analyses were carried out, and the values of the ultimate shear strength are listed in Table 9.5.

Table 9.5 Strength data for simply supported panels. σ_{0p}=300N/mm^2. a=590mm, d=600mm, t=2mm. w_{0p} as given in Eqn. 3.8. CUCU boundary conditions. FE results

$\sigma_b : \tau$	τ_u'	σ_{bu}'
0.52:1	0.318	0.0954
0:1	0.351	0.0

By using the panel strength data given in Table 9.5, the required stiffener sizes are calculated for plates subjected to shear alone and to combined shear and bending (τ:σ_b=1:0.52), respectively, and the values of Ψ_d and Ω_d are tabulated in Table 9.6.

Fig. 9.5 presents a comparison of the stiffener flexural rigidity Ψ_d required by the proposed model with the experimental and FE V_u' vs. Ψ results for the test girders GI & GII and the associated CUCU plates. Also shown in Fig. 9.5 are the values of Ψ_{ssu}, Ψ_p and Ψ_e. It has been pointed out that the value of Ψ for which the stiffener just remains fully elastic at the ultimate load lies between Ψ_p and Ψ_e.

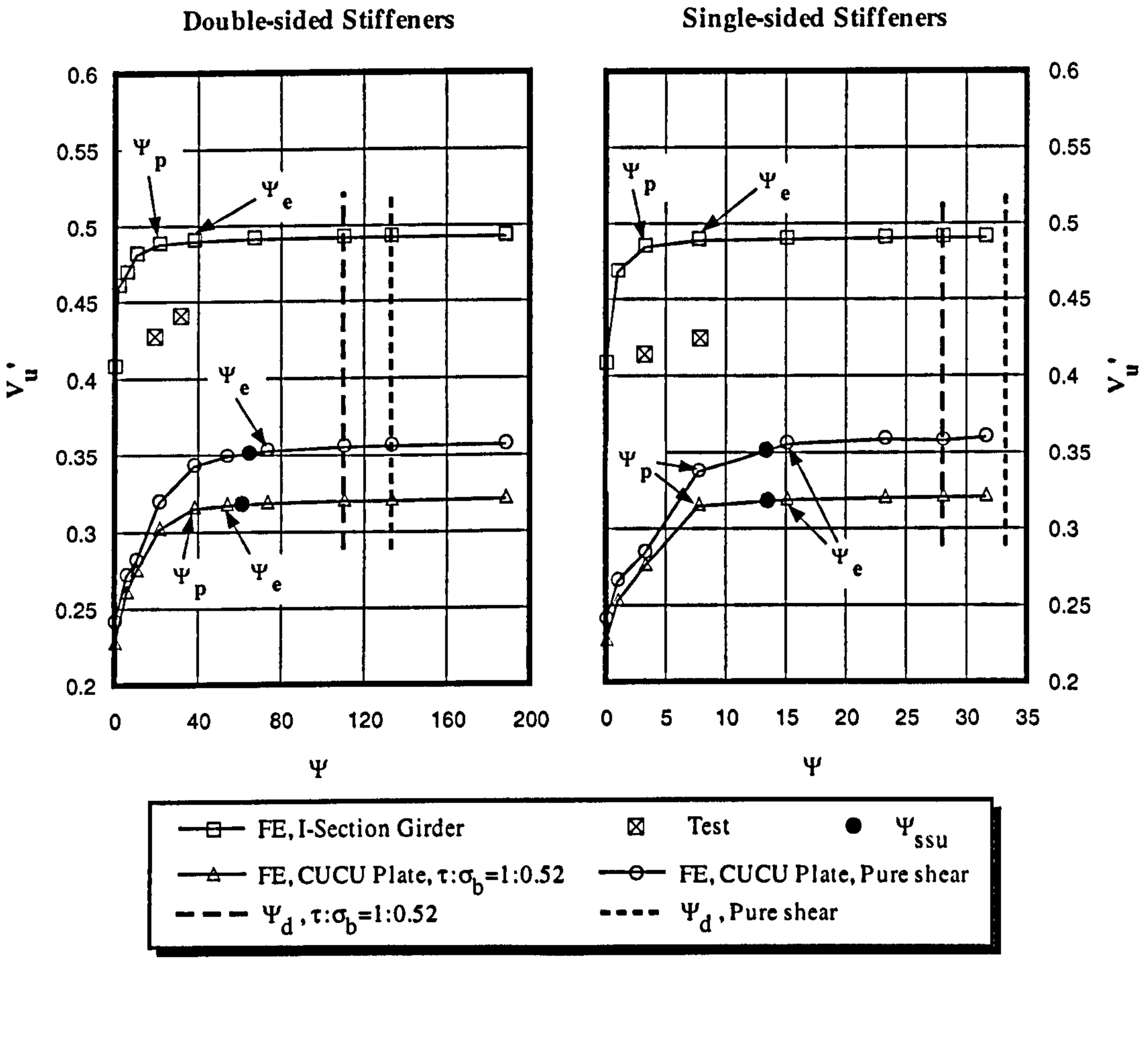


Figure 9.5 Comparison of the stiffener flexural rigidity Ψ_d required by the proposed model with the experimental and FE V_u' vs. Ψ results for the test girders and the associated CUCU plates. a=590mm, d=600mm, t=2mm. t_s=5mm. σ_{0p}=300N/mm^2, σ_{0s}=320N/mm^2. Ψ=EI$_s$/Db, I$_s$ as in Eqns. 3.4 and 3.6.

It can be seen in Fig. 9.5 that the stiffener rigidity Ψ_d required by the proposed model is greater than the values of Ψ of the test stiffeners, which failed either by yielding or deflecting in the physical tests. It is also observed that the proposed model ensures that the strength of the stiffened plate with or without flanges is within the plateau region in the V_u' vs. Ψ curve, and that Ψ_d is greater than Ψ_{ssu}. It is apparent that the required stiffener from the proposed model remains fully elastic at the ultimate strength.

For the cases shown in Fig. 9.5, the stiffener rigidity Ψ_d for plates subjected to shear alone is greater than the rigidity needed for combined shear and bending (τ:σ_b=1:0.52), but the difference is not significant. This agrees with the tendency indicated by the V_u' vs. Ψ curves from the finite element analyses.

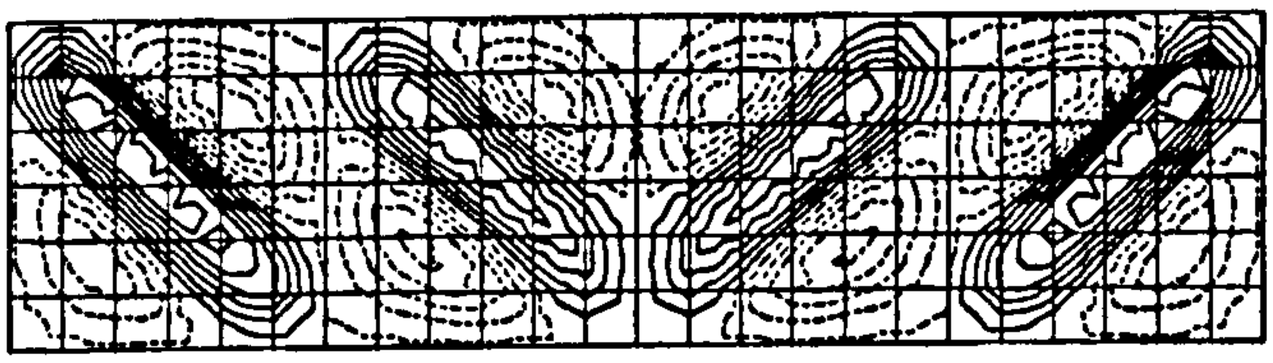
In Fig. 9.6, the contour plots of the out-of-plane deflection at the ultimate load are presented for the intermediate stiffeners required by the proposed model. It is evident in Fig. 9.6 that for the required stiffener rigidity Ψ_d, an effectively divided panel mode can be achieved.

In view of the above observations, it can be concluded that the proposed design model gives satisfactory results for the test girders and their associated plates considered, including both double-sided and single-sided stiffeners, and shear alone and combined shear and bending.

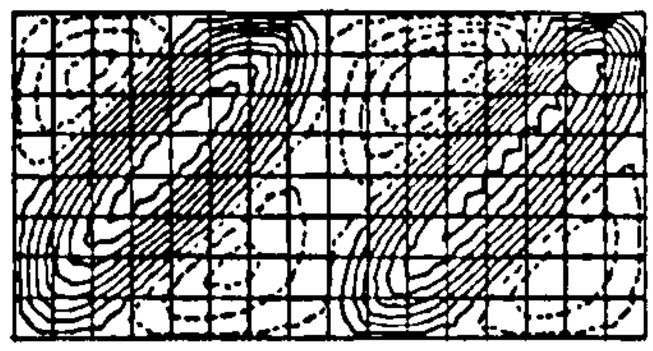
9.4.2 Existing Design Methods

The cases shown in Fig. 9.5 are beyond the range of panel geometry examined in Section 9.3 for the comparison of the existing design methods. Therefore, it would be interesting to know how the existing design methods work for these cases. For this reason, the minimum values of Ψ_d and Ω_d for stiffened plates subjected to pure shear are calculated using the existing design method, and listed in Table 9.6. In Fig. 9.7, the values of Ψ_d for different design methods are compared with the finite element results of τ_u' vs. Ψ. By reference to Fig. 9.5, the position of the required stiffener along the V_u' vs. Ψ curve for I-section girders can be identified.

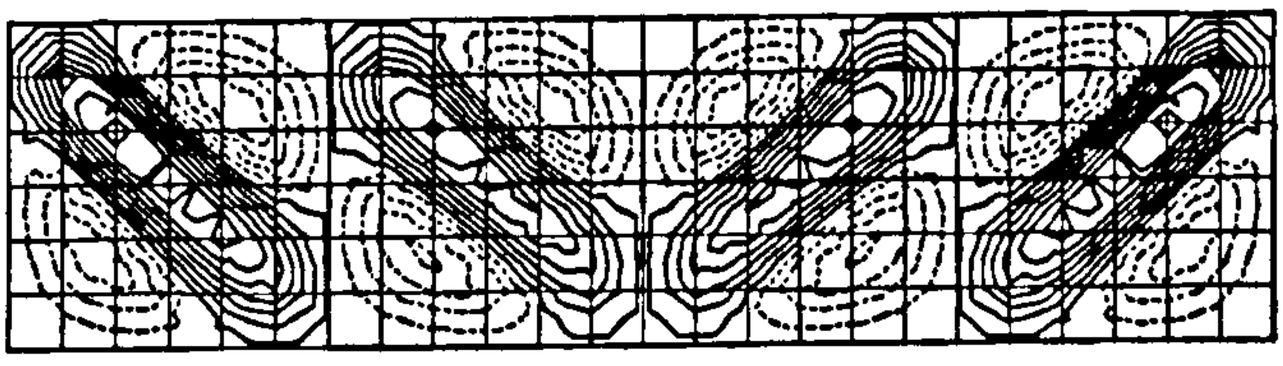
Double-sided Stiffener, Ψ=110.1, V_u'=0.492



Double-sided Stiffener
Ψ=110.1, V_u'=0.320



Single-sided Stiffener, Ψ=28.06, V_u'=0.491



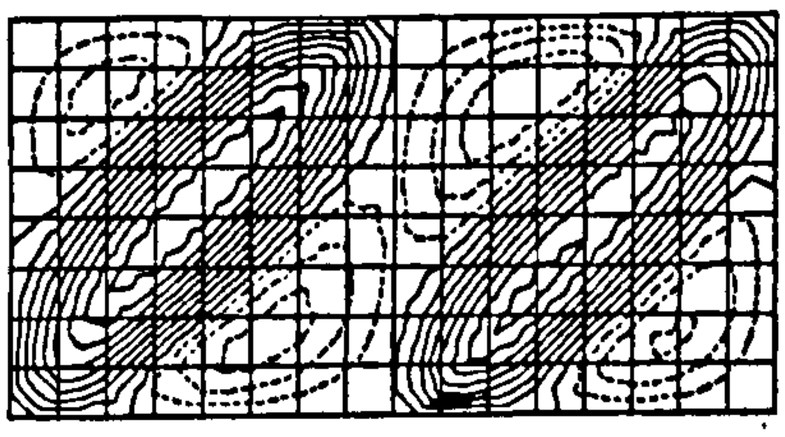
Single-sided Stiffener
Ψ=28.06, V_u'=0.320



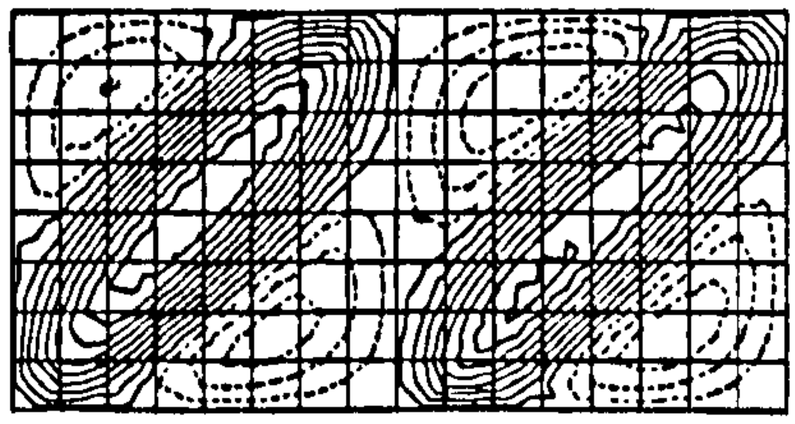
(a) I-section girders under central loading

(b) CUCU Plates, τ : σ_b=1:0.52

Double-sided Stiffener
Ψ=133.0, V_u'=0.356



Single-sided Stiffener
Ψ=33.24, V_u'=0.358



(c) CUCU Plates, Pure shear

Figure 9.6 Contour plots of the out-of-plane deflection at the ultimate load for the test girders and the associated CUCU plates. a=590mm, d=600mm, t=2mm. t_s=5mm. σ_{0p}=300N/mm^2, σ_{0s}=320N/mm^2. Ψ=EI_s/Db, I_s as in Eqns. 3.4 and 3.6. V_u'=V/(τ_{0p}dt)

Table 9.6 Required stiffener flexural rigidity parameters Ψ_d and Ω_d. a=590mm, d=600mm, t=2mm. t_s=5mm. σ_{0p}==300N/mm^2, σ_{0s}=320N/mm^2. Ψ=EI$_s$/Db, I$_s$ as in Eqns. 3.4 and 3.6.

Design Method	Double-sided Stiffeners			Single-sided stiffeners		
	h_s (mm)	Ψ_d	$100\Omega_d$	h_s (mm)	Ψ_d	$100\Omega_d$
Proposed Model (Note 1) (Pure shear)	24.84	133.0	20.70	32.55	33.24	13.56
Proposed Model (Note 1) (τ:σ_b=1:0.52)	23.26	110.1	19.38	30.76	28.06	12.82
BS5400 (Note 2)	19.47	66.19	16.23	60.74	216.0	25.31
AASHTO (Note 2)	8.398	6.393	6.998	57.94	187.5	24.14
Horne & Grayson	25.13	137.6	20.94	32.92	34.39	13.72
Rahal & Harding (Note 1)	10.10	10.53	8.417	15.79	3.795	6.579
Stanway et al (Note 1)	26.13	153.9	21.78	34.18	38.49	14.24

Note 1: Applied shear taken as the panel strength τ_u from Table 9.5.

Note 2: Applied shear taken as the panel strength τ_u, calculated from the same code.

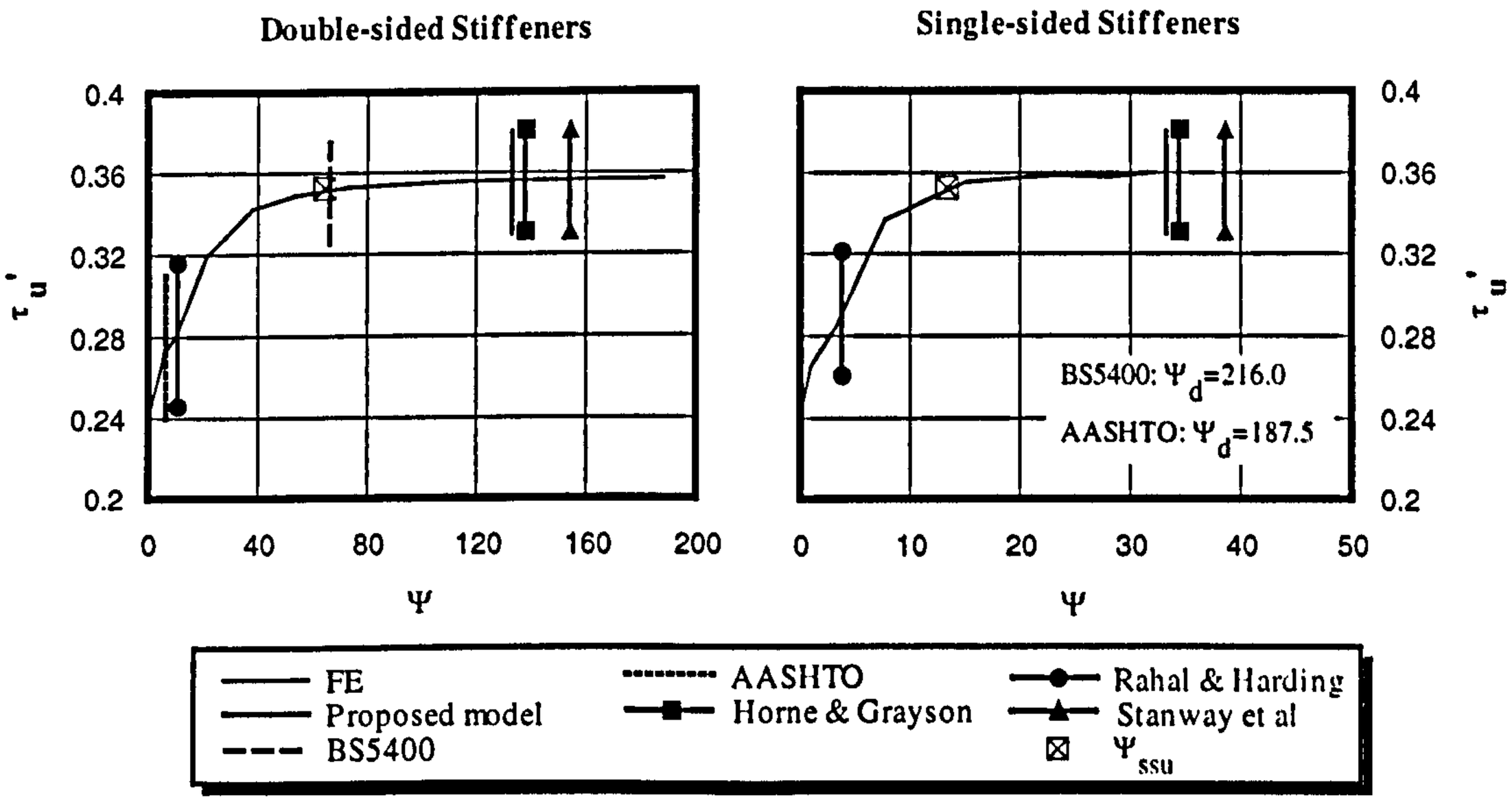


Figure 9.7 Comparison of the stiffener flexural rigidity Ψ_d required by the proposed model with the FE τ_u' vs. Ψ results for CUCU plates subjected to pure shear. a=590mm, d=600mm, t=2mm, t_s=5mm. σ_{0p}==300N/mm^2, σ_{0s}=320N/mm^2. Ψ=EI$_s$/Db, I$_s$ as in Eqns. 3.4 and 3.6

It is observed in Fig. 9.7 that for d/a=1.017, b/t=295, the approaches by Horne & Grayson and by Stanway et al produce adequate stiffeners. It can be seen in Fig. 9.7 that for double-sided stiffeners, AASHTO and Rahal & Harding's approach severely underestimate the required stiffener. For single-sided stiffeners, the stiffener given by Rahal & Harding's approach is also inadequate, whereas the stiffeners given by AASHTO and BS5400 are overly conservative.

It is pointed out in Section 9.2.5 that the approach by Rahal & Harding considered coexistent shear and in-plane longitudinal compression and bending. However, this approach is not used for the combined shear and bending condition examined in Fig. 9.5. This is because the stiffener given by this approach for slender plates b/t=180 under shear alone is already underestimated, and it is expected that the stiffener given for combined loading would be even smaller.

9.5 CONCLUSIONS

In this chapter, the transverse stiffener required by the proposed model is compared with those given by the existing design methods, in conjunction with the finite element and experimental results. Detailed comments on each method have been presented in Section 9.3. In this section, some of the main observations are summarized below.

- ***General***

(1) There is a wide difference in the stiffeners required by the various existing design methods for a given plate geometry. This in itself is one of the strong reasons for carrying out the investigation presented in this thesis.

(2) In comparison with BS5400 and Eurocode, the proposed model gives in general heavier stiffeners for d/a≤2 plates, and considerably lighter stiffeners for d/a≥5 plates.

(3) According to the proposed model, an approximate linear relation of the stiffener extensional rigidity required Ω_d with d/a may be assumed for various b/t, with the side ratio of the stiffener h_s/t_s=10. This simple relation may be useful for estimating the required stiffener size in initial design.

(4) It is found that the proposed model gives adequate stiffeners for the test girders. According to the proposed design model, the transverse stiffener required for an I-section girder is determined by considering the associated web plate, assuming its in-plane boundary conditions to be CUCU, that is, the flanges are not included. It is desirable that the proposed design model is validated in the future for plates with various boundary conditions, such as restrained edges.

(5) The proposed model gives consistently satisfactory stiffeners for all the cases examined, including the case of combined shear and bending (τ:σ_b=1:0.52), without being overly conservative. Of all the design methods considered, the proposed model is the only approach which gives adequate results for both double-sided and single-sided stiffeners.

- ***Double-sided Stiffeners***

(6) BS5400 gives inadequate stiffeners for d/a≤2, but unduly conservative stiffeners for very tall plates (e.g. d/a≥5).

(7) Eurocode underestimates the stiffeners required for d/a≤1 and b/t=180. For d/a≥5 plates, the stiffener from Eurocode is unduly conservative. For tall plates with b/t=180, Eurocode gives stiffeners which are considerably greater than those from BS5400, due to the difference in the magnitude of the axial force caused by tension field action.

(8) AASHTO gives satisfactory stiffeners for b/t=80, where the post-buckling behaviour of the plate is not important. For slender plates (e.g. b/t≥180), AASHTO severely underestimates the required stiffeners.

(9) Horne & Grayson's approach gives satisfactory stiffeners for d/a≤1, and inadequate stiffeners for d/a≥3.

(10) Rahal & Harding's approach gives satisfactory stiffeners for d/a=0.5 & 1 and b/t=80 & 120. For d/a≤5 and b/t≤180, the stiffener given by Rahal & Harding's approach is inadequate, whereas for d/a=7 and b/t=80, it is overly conservative.

(11) The approach by Stanway et al is the only one of all the existing methods considered that gives satisfactory, but not unduly conservative, double-sided stiffeners for all d/a and b/t examined.

- ***Single-sided Stiffeners***

(12) For the single-sided stiffener cases examined, the proposed model gives satisfactory results, while the approach by Rahal & Harding gives inadequate stiffeners. It is hoped that more cases can be studied in the future.

(13) BS5400 and AASHTO give satisfactory stiffeners for b/t=180, but overly conservative stiffeners for b/t=295.

(14) The stiffener given by Horne & Grayson's approach is satisfactory for d/a<2, but inadequate for d/a=5. The suggested approach by Stanway et al gives satisfactory stiffeners for d/a≤2, but inadequate stiffeners for d/a=5. It has been indicated that in these two approaches, the neutral axis of the single-sided stiffener is assumed to be at the face in contact with the plate, and the inadequacy of this assumption has been discussed in Section 8.7.2.

CHAPTER 10

CONCLUSIONS AND RECOMMENDATIONS FOR FUTURE WORK

10.1 RECAPITULATION AND CONCLUSIONS

The overall objective of this thesis has been to develop a rational and usable design model for transverse stiffeners, based on the non-linear buckling theory. Particular objectives are to take account of coexistent shear, compression, bending, and external forces applied to the ends of the stiffener. In Chapter 1, Section 1.3, more detailed objectives for this research project were stated.

Chapter 1 also provided a review of relevant background material. Previous researches on the buckling behaviour of transversely stiffened plates were summarized; these covered the buckling of individual panels and stiffened plates, existing design methods for transverse stiffeners, and published experimental work conducted specially to investigate the behaviour of transverse stiffeners.

In Chapter 2, laboratory tests conducted on plate girders with transversely stiffened webs were reported and discussed in relation to non-linear elasto-plastic finite element solutions from ABAQUS. The tests provided validation of the finite element program ABAQUS, which was used to carry out the extensive parametric study presented in this thesis. The tests also demonstrated that satisfactory stiffeners could be designed without taking into account the effects of residual stresses. The finite element analyses for the test girders also confirmed that the design method for transverse web stiffeners could be based on a simplified structural model, in which flanges were not included.

The simplified structural model, namely, CUCU plates, was defined in Chapter 3. The general features concerning finite element modelling used in this investigation were described, including structural configuration, material properties, initial imperfections and boundary conditions. The finite element meshes adopted were based on a mesh convergence study.

In order to develop a rational design approach for transverse stiffeners, forces in stiffeners were studied by analytical and numerical analyses, as described in Chapters 4 and 5. Rational approaches were established to estimate transverse forces and bending moments on straight knife-edge stiffeners. The approach adopted was to formulate design equations based on simple theoretical solutions, and then to introduce coefficients, based on non-linear finite element solutions, which take account of behavioural complexities not represented by the simplifying assumptions on which the analytical equations were based. Separate and combined effects of shear, compression and bending applied to the stiffened plates, and the effect of external force applied to one or both ends of a stiffener were considered. It was confirmed that forces on a non-deflecting knife edge can be used to find the forces on a stiffener, which is adequate to divide the plate, due to the effect of local panel bending of the stiffened plates. The lateral distributed forces on the knife edge depend on the magnitude and mode of the panel deflection, and the resulting knife edge moment varies with the applied stresses, initial panel imperfection and panel aspect ratio d/a.

For plates subjected to combined shear and longitudinal direct loading, it was found that the panel deflection modes vary greatly depending on the relative magnitudes of the applied stress components. For tall plates the deflection mode can vary between one and several half waves, depending on the applied stresses and panel side ratios. The behaviour of plates under combined loading is extremely complex so various approximations have been introduced.

The design formulae for predicting the knife edge moment are based on non-linear elastic theory, incorporating coefficients based on non-linear elastic and elasto-plastic finite element solutions. The proposed design formulae treat combined shear,

compression and bending by introducing an equivalent shear stress which will cause the same knife edge moment as for pure shear. The greatest difficulty occurs for very tall panels ($d/a \geq 7$), when the panel bending effect does not dominate.

In Chapter 6, the axial force in the stiffener was investigated by using a non-deflecting stiffener model, which can be considered as an extension of the knife edge model used to study the stiffener forces caused by the panel bending effect, except that the stiffener is attached to the plate and has a variable axial stiffness. It is found that the axial force in the stiffener results mainly from the inclined tension field action, whereas the effects of Poisson's ratio and panel deflection are small enough to be neglected. The axial force in a finite stiffener is found to be considerably smaller than that given by Basler's tension field model and by BS5400. However, the Basler model gives a satisfactory estimate of axial force for incompressible stiffeners.

It is found from the experiments and the finite element analyses for the test girders that for concentric stiffeners, the stiffener stress due to the axial force varies between 10~20% of the total stress. For eccentric stiffeners the axial force may contribute to about 60% of the total stress.

The proposed design formulae for predicting the axial force in the stiffener is based on the Basler model, which has been modified by reference to the non-linear elastic finite element solutions and also to take account of the compressibility of the stiffener. Applied compressive and bending stresses are taken into account by replacing the critical shear stress for pure shear with the critical shear stress in the presence of compression and bending. The proposed method is simple to apply, and agrees well with forces given by finite element analyses.

The overall buckling behaviour of the stiffened plate was studied in Chapter 7 by using an energy method. The overall buckling model developed in this thesis is based on a stiffener between two plate panels. By adopting appropriate deflection functions, the model was used for stiffened plates subjected to shear, compression, bending and external force applied to one or both ends of the stiffener, respectively. The deflection

functions were chosen to represent the overall buckling modes for each loading component. For pure shear, the deflection function takes account of the inclined buckling mode.

The critical buckling analysis led to the overall buckling stress and mode, by solving the eigenvalue problem formed by minimising the total potential energy of the system. By assuming an imperfection fully affine to the overall buckling mode, the stiffener moment caused by the overall buckling effect was derived, based on the assumption that the applied stress is much smaller than the overall buckling stress, which is true for a stiffener that is sufficient to divide the plate. The importance of the overall buckling effect increases with d/a; for d/a=5, for concentric stiffeners, the overall buckling effect contributes about 60% of the total moment.

The design model described in Chapter 8 requires that the transverse stiffener be designed to resist the coexistent bending moment and axial force in the stiffener. The bending moment is determined by adding the components of stiffener moment due to the local panel bending effect and the tendency for the stiffened plate to buckle overall. The axial force caused by the tension field action acts in the mid-plane of the plate, resulting in an additional bending moment for eccentric stiffeners due to the eccentricity of this axial force. For eccentric stiffeners the axial force may contribute up to about 70% of the total stress. This occurs when the plate bending effect acts in opposition to the eccentricity moment. For bearing stiffeners, the external forces applied to the ends of the stiffener are included in the axial force. The proposed method gives forces acting in the stiffener itself, which does not require the effective width of the plate to be considered. The moment of inertia is calculated about the centroidal axis of the actual stiffener section for both concentric and eccentric stiffeners.

Both strength and stiffness criteria were developed to quantify the required stiffener. The strength criterion requires that the maximum stress in the stiffener must not exceed the yield stress of the stiffener. The stiffness criterion requires that the stiffener deflection is sufficiently small to ensure that the stiffened plate is effectively divided. It is found from the experiments and the finite element analyses that the transverse

stiffeners fail to perform their functions either by yielding or by deflecting rapidly without yielding, depending on the geometry and the yield stresses of the web plate and the stiffener.

The proposed design model is based on analytical studies, incorporating coefficients based on finite element solutions for idealised structures. There are no restrictions on stiffener shape inherent in the proposed design model, except that they should not be prone to lateral torsional buckling and that they are not closed sections.

The proposed design model has been validated against experimental results and finite element solutions for stiffened plates and girders. The required transverse stiffener is determined by considering the associated web plate, assuming its in-plane boundary conditions to be CUCU, that is, the flanges are not included. It is found that the proposed design model gives satisfactory stiffeners for concentric and eccentric stiffeners, and for pure shear, shear and compression, and shear and bending, respectively. When compared with existing design methods, it is found that the proposed model gives more consistent stiffener sizes in relation to those required to satisfy the design criteria. The extent of the variability of existing methods can be seen in Tables 9.1 and 9.2, and Figures 9.1 and 9.2.

10.2 RECOMMENDATIONS FOR FUTURE WORK

The proposed design model takes account of the effects of shear, compression and bending applied to the stiffened plates, and has been validated by using the finite element solutions for a number of cases. Further verification, including verifying the proposed model for a wider range of loading and geometrical combinations, is required.

In the proposed method, the forces acting in the stiffener are assumed to be resisted by the stiffener alone, that is, no effective width of the plate is included. Although the reduction in the Basler tension field force does imply a transfer of axial force from stiffener to plate, only the axial force resisted by the stiffener is taken into account. For eccentric (single-sided) stiffeners, an additional bending moment exists due to the

eccentricity of the stiffener axial force caused by the tension field action. Based on the finite element results for a small number of cases, the direction of this additional bending moment relative to the bending moment due to the panel bending and overall buckling effects was determined. Also, the design limit of stiffener deflection was given on the basis of these cases. Depending on the geometry, these bending moments might or might not be additive. Perhaps it would be prudent to assume that they are always additive, but the resulting stiffener might become overly conservative, as discussed in Section 8.7.5.

In the proposed model it has been assumed for simplicity that the plate does not contribute to the bending resistance of the single-sided stiffener. Depending on the outcome of the numerical results it might be shown that an effective width of plate should be taken into account. As a result, the moment of inertia I_s for eccentric stiffeners may increase considerably, however the effect on the section modulus Z_s may be much less. It should be remarked that depending on the direction of the stiffener deflection, the plate is either stabilised or destabilised when acting as a flange to the stiffener.

Although for the cases examined (including plates and girders), the design equations give satisfactory eccentric stiffeners, it is necessary to provide further verification over a wide range of d/a and b/t.

Based on the analytical results for the overall buckling model developed in this thesis, design equations for load bearing stiffeners have been suggested, but not validated. These design equations should be checked using finite element solutions for load bearing stiffeners.

As pointed out in Section 10.1, there are no restrictions on stiffener shape inherent in the proposed design model, except that they should not be prone to lateral torsional buckling and that they are not closed sections. It is desirable that the proposed design model is further validated for other open stiffener sections; that would also give useful information on the relative efficiency of different sections.

The proposed design model is developed by using a CUCU plate model (defined in Fig. 3.2). By comparison of the finite element results for I-section girders and CUCU plates, it has been found that the stiffener that is adequate for the CUCU plate is also adequate for the plate with flanges. It would be desirable to verify that this assumption is still valid for other boundary restraints. These can arise for example as a result of lengthwise variations in loading with consequential variation in panel and stiffener dimensions.

The proposed model is based on a single stiffener plate, and has been compared with finite element solutions for single stiffener plates and for the test girders. It is desirable that the proposed model should be compared with the finite element results for multi-stiffener plates. If necessary, the proposed model could be extended to take account of multi-stiffener plates. It is expected that for multi-stiffener plates, the stiffener axial force and the bending moment due to the panel bending effect would be the same as those for single stiffener plates. The bending moment caused by the overall buckling effect could be modified by analysing the beam-plate model (Section 7.3) using appropriate deflection functions which represent the basic features of the overall buckling mode for the multi-stiffener plate.

A methodology has been developed for deriving design equations based on simple theoretical solutions, incorporating coefficients based on finite element solutions. This methodology may be used to develop a design model for longitudinal stiffeners, or to take account of lateral pressure on the stiffened plate.

REFERENCES

1. **Stanway, G.,** *The Behaviour and Design of Transversely Stiffened Plates Subject to In-plane Shear Forces,* Ph.D Thesis, Civil Engineering Dept., Imperial College, London, 1990.
2. **Skaloud, M.,** Optimum rigidity of stiffeners of webs and flanges, *Plated Structures: Stability and Strength*, Narayanan, R. ed., Applied Science Publishers, London, 1983, pp.103-134.
3. **British Standard Institution,** *Steel, Concrete and Composite Bridges, BS5400: Part 3. Code of Practice for Design of Steel Bridges*, BSI, London, 1982.
4. **European Committee for Standardization,** *Design of Steel Structures, Eurocode 3: Part 1-1. General – General Rules and rules for buildings,* Brussels, 1994.
5. **Rahal, K. N. and Harding, J. E.,** Transversely stiffened girder webs subjected to shear loading – part 1: behaviour, *Proc. Instn Civ. Engrs,* Part 2, Vol.89, 1990, pp.47-65.
6. **Rahal, K. N. and Harding, J. E.,** Transversely stiffened girder webs subjected to shear loading – part 2: stiffener design, *Proc. Instn Civ. Engrs,* Part 2, Vol.89, 1990, pp.67-87.
7. **Rahal, K. N. and Harding, J. E.,** Transversely stiffened girder webs subjected to combined in-plane loading, *Proc. Instn Civ. Engrs,* Part 2, Vol.91, 1991, pp.237-258.
8. **Stanway, G. S., Chapman, J. C. and Dowling, P. J.,** Behaviour of a web plate in shear with an intermediate stiffener, *Proc. Instn Civ. Engrs Structs & Bldgs,* Vol.99, 1993, pp.327-344.
9. **Stanway, G. S., Chapman, J. C. and Dowling, P. J.,** A design model for intermediate web stiffeners, *Proc. Instn Civ. Engrs Structs & Bldgs,* Vol.116, 1996, pp.54-68.
10. **Boobnov, I. G.,** On the stresses in a ship's bottom plating due to water pressure, *Transactions of the Institute of Naval Architects*, Vol.44, 1902, and Theory of Structures of Ships, Vols.1 and 2, St. Petersburg, 1912-1914.

11. **Timoshenko, S. P.**, *Stability of Rectangular Plates with Stiffeners*, Memoirs of the Institute of Engineers of Ways and Communications, St. Petersburgh (in Russian), Vol.89, 1915, p.23.
12. **Timoshenko, S. P.**, On the stability of the stiffened plates, *Der Eisenbau (in German)*, Vol.12, 1921, pp.147-163.
13. **Wagner, H.**, Flat sheet metal girder with very thin metal web, *NACA, Tech. Memo., 1931, pp.604-606.*
14. **Koiter, W. T.**, *On the Stability of Elastic Equilibrium*, Thesis, Delft, 1945. English translation NACA Tech. Trans. F-10, Vol.833, 1967.
15. **Massonnet, Ch.**, Essais de voilement sur poutres à âme raidie, *Mémoires AIPC*, Vol.14, Zurich 1954, pp.125-186.
16. **Djahani, P. and Dowling, P. J.**, *Inelastic Analysis of Discretely Stiffened Plates*, CESLIC Report BG45, Imperial College, London, England, 1977.
17. **Crisfield, M. A.**, Full-range analysis of steel plates and stiffened plating under uniaxial compression, *Proc. Instn. Civ. Engrs.*, Vol.59, Dec. 1975, pp.595-624.
18. **Saint Venant, B. de.**, Discussion in *Théorie de l'élasticité des corps solids*, by Clebsch, 1883, p.704.
19. **Bryan, G. H.**, On the stability of a plane plate under thrusts in its own plane, with applications to the "buckling" of the sides of a ship, *Proceedings of the London Mathematical Society*, Vol.22, 1891, pp.54-67.
20. **Southwell, R. U. and Skan, S. W.**, On the stability under shearing forces of a flat elastic strip, *Proc. Roy. Soc. London*, Ser.A, Vol.105, 1924, pp.582.
21. **Stein, M. and Neff, J.**, Buckling stresses of simply supported rectangular flat plates in shear, *NACA, Technical Note 1222*, 1947.
22. **Budiansky, B. and Connor, R. W.**, Buckling stresses of clamped rectangular flat plates in shear, *NACA, Tech. Note 1559*, 1948.
23. **Batdorf, S. B. and Stein, M.**, *NACA, Tech. Note 1223*, 1947.
24. **Way, S.**, Stability of rectangular plates under shear and bending forces, *Journal of Applied Mechanics*, Vol.3, No.4, Dec. 1936, p.A.131.
25. **Timoshenko, S. P. and Gere, J. M.**, *Theory of Elastic Stability*, 2nd edition, McGraw-Hill, New York, 1961.

26. **von Kármán, Th.**, Festigkeitsprobleme im maschinenbau, *Encyklopadie der Mathematischen Wissenschaften,* Teilband IV.4, Teubner, Leipzig, 1910.
27. **Marguerre, K.**, Zur theorie der gekrümmten platte grosser formänderung, *Proc. 5th Int. Congress for Appl. Mech.*, John Wiley & Sons, New York, 1939, pp.93-101.
28. **Skaloud, M. and Donea, J.,** Comportement post-critique des âmes à tensions résiduelles, *Mémoires AIPC*, Vol.23, Zurich 1963, pp.293-320.
29. **Bulson, P.**, *The Stability of Flat Plates*, Chatto & Windus, London, 1970.
30. **Moxham, K. E.**, Theoretical prediction of the strength of welded steel plates in compression, *Report CUED C-Struct. TR2*, Dept. of Engrg., University of Cambridge, England, 1971.
31. **Frieze, P. A., Dowling, P. J. and Hobbs, R. E.**, Ultimate load behaviour of plates in compression, *Steel Plated Structures*, Dowling, P. J. et al ed., Crosby Lockwood Staples, 1977, pp.24-50.
32. **Basler, K.**, Strength of plate girders under combined bending and shear, J. *Struct. Div., ASCE,* Vol.87, No.2, 1961, pp.181-197.
33. **Porter, D. M., Rockey, K. C. and Evans, H. R.**, The collapse behaviours of plate girders loaded in shear, *The Structural Engineer*, Vol.53, No.9, 1975, pp.313-325.
34. **American Association of State Highway and Transportation Officials**, *Standard Specifications for Highway Bridges*, 16th Ed., AASHTO, Washington, D.C., 1996.
35. **Harding, J. E., Hobbs, R. E. and Neal, B. G.**, Ultimate load behaviour of plates under combined direct and shear in-plane loading, *Steel Plated Structures*, Dowling, P. J. et al ed., Crosby Lockwood Staples, 1977, pp.369-403.
36. **Horne, M. R., Dowling, P. J. and Ogle, M. H.**, *Report to Steering Group on Plated Structures*, Committee B116/3, British Standards Inst., London, 1976.
37. **Harding, J. E.**, The interaction of direct and shear stresses on plate panels, *Plated Structures: Stability and Strength,* Narayanan, R. ed., Applied Science Publishers, London, 1983, pp.221-255.
38. **Harding, J. E. and Dowling, P. J.**, The basis of the proposed new design rules for the strength of web plates and other panels subject to complex edge loading, *Stability Problems in Engineering Structures and Components*, Richards, T. H. and Stanley, P. ed., Applied Science Publishers, Barking, 1979, pp.355-376.

39. **Chapman, J. C. and Davidson, P. C.**, Behaviour and design of full-depth web panels in shear, *The Structural Engineer*, Vol.65B, No.4, 1987, pp.65-71.

40. **Davidson, P. C.**, *Design of Plate Panels under Biaxial Compression, Shear and Lateral Pressure*, Ph.D Thesis, Civil Engineering Dept., Imperial College, London, 1989.

41. **Davidson, P. C., Chapman, J. C., Smith, C. S. and Dowling, P. J.**, The design of plate panels subject to in-plane shear and biaxial compression, *Transactions of Royal Institution of Naval Architects (RINA)*, London, 1989, pp.267-280.

42. **Klöppel, K. and Scheer, J.**, *Beulwerte Ausgesteifter Rechteckplatten*, Band 1, W. Ernst & Sohn, Berlin, 1960.

43. **Klöppel, K. and Möller, K. H.**, *Beulwerte Ausgesteifter Rechteckplatten*, Band 2, W. Ernst & Sohn, Berlin, 1968.

44. **Skaloud, M., Donea, J. and Massonnet, Ch.**, Comportement postcritique d'une plaque carrée raidie cisaillée uniformément – lère partie: solution générale et déformée de la plaque, *Mémoires AIPC*, Zurich, Vol.27, 1967, pp.187-210.

45. **Horne, M. R. and Grayson, W. R.**, Parametric finite element study of transverse stiffeners for webs in shear, *Instability and Plastic Collapse of Steel Structures*, Morris, L. J. ed., Granada Publishing, London, 1983.

46. **Grayson, W. R.**, *Behaviour and Design of Stiffened Web Panels*, Ph.D Thesis, University of Manchester, England, 1981.

47. **Rockey, K. C., Valtinat, G. and Tang, K. H.**, The design of transverse stiffeners on webs loaded in shear —an ultimate approach, *Proc. Instn Civ. Engrs*, Part 2, Vol.71, 1981, pp.1069-1099.

48. **Richmond, B.**, Parametric Study of Web Panels, *Report for Department of the Environment*, Maunsell and Partners, London, 1972.

49. **Chatterjee, S.**, Design of webs and stiffeners in plate and box girders, *The Design of Steel Bridges*, Rockey, K. C. and Evans, H. R. ed, Granada Publishing, St. Albans, 1981, paper 11.

50. ***Tang, K. H. and Evans, H. R.**, Transverse stiffeners for plate girder webs: an experimental study, Journal of Constructional Steel Research, No.4, 1984, pp.253-280.*

51. **British Standard Institution,** *Steel, Concrete and Composite Bridges, BS5400: Part 6. Specification for Materials and Workmanship*, Steel, BSI, London, 1980.

52. **Timoshenko, S. P. and Woinowsky-Krieger, S.,** *Theory of Plates and Shells*, 2nd edition, McGraw-Hill, New York, 1981.

53. **Jirousek, J. and Bouberguig, A.,** A contribution to evaluation of shear forces and reactions of Mindlin plates by using isoparametric elements, *Computers and Structures*, Vol.19, No.5/6, 1984, pp.793-800.

54. **Williams, D. G. and Walker, A. C.,** Explicit solutions for plate buckling analysis, *J. Engineering Mechanics Division, ASCE,* Vol.103, No.EM4, 1977, pp.549-197568.

55. **Khan, M. Z. and Walker, A. C.,** Buckling of plates subjected to localized edge loading, *The Structural Engineer*, Vol.50, No.6, 1972, pp.225-232.

56. **Bleich, F.,** *Buckling Strength of Metal Structures*, McGraw-Hill, New York, 1952.

57. **Fujii, T.,** On an improved theory for Dr. Basler's theory, *Proc. 8th*, IABSE, New York, September 1968, pp.477-487.

58. **Fortune, L. H.,** *Design of Intermediate Stiffeners for Girder Webs Subject to Shear*, Ph.D Thesis, Dept. of Civil and Environmental Engineering, Imperial College, London, 2000.

APPENDICES

APPENDIX A

FINITE ELEMENT PROGRAM ABAQUS

A.1 DESCRIPTION OF ABAQUS

The numerical analyses presented in this thesis are carried out by means of the commercial general-purpose finite element program ABAQUS, which runs on a UNIX platform. The ABAQUS element library provides a wide range of geometric modelling capacity. All elements use numerical integration to allow the generality in material behaviour. Shell and beam element properties may be defined as general section behaviours, or each cross-section of the element may be integrated numerically, so that non-linear response can be tracked accurately when needed. Especially, shell element properties allow layers of different materials to be used through the cross-section.

The material library in ABAQUS contains both linear and non-linear, isotropic and anisotropic material models. The simplest form is linear elasticity. The classical metal plasticity models in ABAQUS use standard Mises (for isotropic materials) or Hill (for anisotropic materials) yield surface models with associated plastic flow. Associated plastic flow means that, as the material is yielding, the inelastic deformation rate is in the direction of the normal to the yield surface. Three possibilities of work hardening are provided in ABAQUS: perfect plasticity, isotropic hardening, and kinematic hardening.

Both linear and non-linear constraint conditions may be specified when using ABAQUS. Linear constraints include supports of structure, fixed displacements at nodal points, and linear multi-point constraints given in the form of an equation. Non-linear constraints allow relations to be imposed between different degrees of freedom of the

model. These relations can either be the default multi-point constraint (MPC) types that are provided in ABAQUS or can be coded in the form of a user subroutine. In the numerical analyses presented in this thesis, the default MPC type *SLIDER* is used to model constrained edges — ones that are constrained to remain straight. SLIDER keeps a node on a straight line defined by two other nodes, but allows the possibility of moving along the line, and the line to change length.

External loading may be specified in ABAQUS as distributed loads, point loads, or prescribed displacements. The last of these approaches is required for displacement control of incrementation.

ABAQUS is based on the concept of analysis steps. Each step either involves non-linear response, or is a linear perturbation analysis. The latter allows general application of linear analysis techniques. Non-linear static analysis requires the solution of non-linear equilibrium equations, for which ABAQUS generally uses Newton's method, and the solution is usually obtained as a series of increments, with iteration within each increment to obtain equilibrium. ABAQUS offers both direct user control and automatic control of increment size. As it is hard to predict the response ahead of time, the automatic control is used in most cases.

Non-linear static problems frequently involve buckling or collapse behaviour, where the load-displacement response shows a negative stiffness, and the structure must release strain energy to remain in equilibrium. In some cases displacement control can provide a solution. More generally, static equilibrium states during the unstable phase of the response can be found by using the modified Riks method. It is applicable for cases where the loading is proportional. The basic algorithm remains the Newton method, but the equilibrium solution is obtained by controlling the path length along the load-displacement curve within each increment, rather than controlling the load or displacement increment alone.

A.2 NUMERICAL STUDY ON SHELL ELEMENTS

A.2.1 Shell Elements

ABAQUS provides a wide range of shell element types, which have already been checked by means of a large number of test cases [i]. These investigations provide good starting points when choosing an element type for a specific problem. In order to decide which element type to be used to model the plate for all analysis to be performed, some numerical tests are carried out for the following shell element types choosing from ABAQUS element library:

- S4R: 4-node doubly curved thin or thick shell, reduced integration, hourglass control, finite membrane strains;
- S8R: 8-node doubly curved thick shell, reduced integration;
- S8R5: 8-node doubly curved thin shell, reduced integration, using five degrees of freedom per node;
- S9R5: 9-node doubly curved thin shell, reduced integration, using five degrees of freedom per node;

The element type S8R allows proper modelling of shear flexible behaviour, but its formulation has the disadvantage that spurious (hourglass) displacement patterns may occur. The other elements are formulated to prevent the occurrence of the hourglass mode. In these elements, the transverse shear strains become essentially transverse shear constraints, numerically enforcing the Kirchhoff constraint.

The general shell elements may use either five degrees of freedom or six degrees of freedom at all nodes. When five degrees of freedom are used, ABAQUS will automatically switch to using six degrees of freedom under particular circumstances. In the elements that use six degrees of freedom at all nodes, there is a singularity at any node where the surface is assumed to be continuously curved, because three rotation

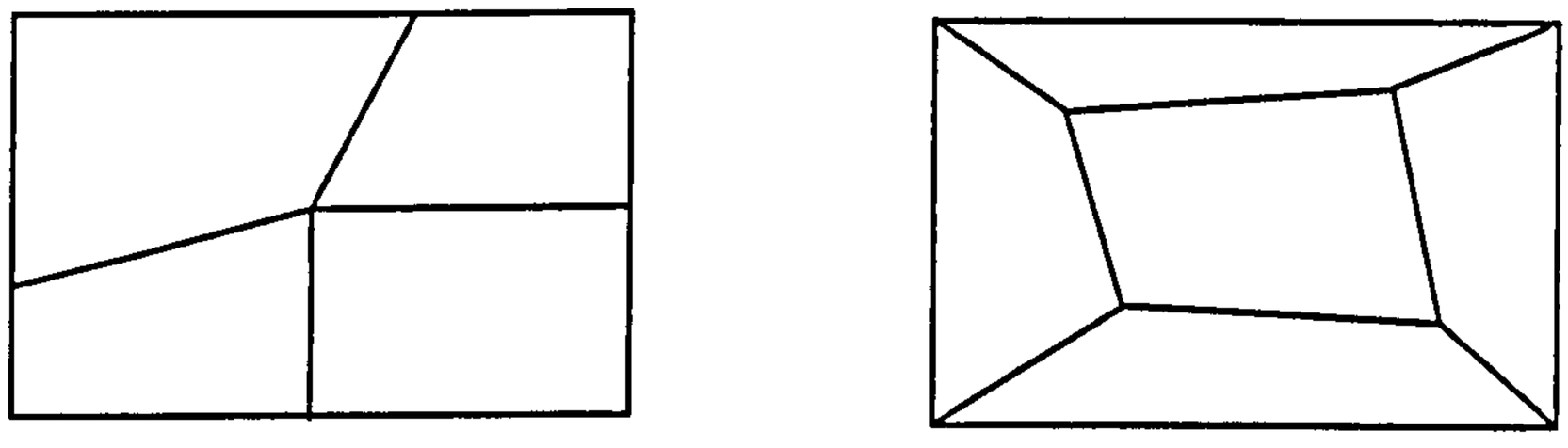
[i] ABAQUS/Standard Verification Manual, Version 5.5, 1995.

components are used, but only two are actively associated with stiffness. A small stiffness is associated with the normal rotation to avoid this difficulty.

In thin shells, reduced integration tends to soften an element, and may thus countering the overly stiff behaviour associated with an assumed displacement field.

A.2.2 The Patch Test

As a test to investigate whether an assemblage of finite elements is complete, the patch test has been proposed[ii,iii]. In this test a constant stress or strain is applied to a patch of elements. If the computed element stresses actually represent the constant stress conditions for the physical problem modelled, then the element passes the patch test, and convergence is ensured. Therefore, when this type of element is used to model any other structure, mesh refinement will produce a sequence of approximate solutions that converges to the exact solution. In other words, the patch test serves as a necessary and sufficient condition for correct convergence of a finite element formulation.



(a) (b)

Figure A.1 Patch test meshes

Figure A.1(a) shows a patch test mesh used in numerical investigations for ABAQUS shell element types S4R, S8R, S8R5, and S9R5. All element types are patch-tested for constant stress states of σ_X, σ_Y, and τ_{XY}, and for constant bending moments M_X, M_Y

[ii] Irons, B. M. and Razzaque, A., Experience with the patch test for convergence of finite elements, in *The Mathematical Foundations of the Finite Element Method with Applications to Partial Differential Equations*, Aziz, A.K. ed., Academic Press, New York, pp.557-587, 1972.
[iii] Taylor, R. L., Simo, J. C., Zienkiewicz, O. C., and Chan, A. C. H., The patch test -- A condition for assessing FEM convergence, Int. J. Num. Meth. Engng., Vol.22, No.1, 1986, pp.39-62.

and constant twisting moment M_{xy}. It is found that all elements tested can pass these tests.

In ABAQUS/Standard Verification Manual[i], a 5-element (quadrilateral) mesh (Fig. A.1b) was used in the patch test for plate bending, and all ABAQUS shell elements pass the test except S8R. It was said that the element type S8R would pass the patch test if the element shapes are rhombic, but it fails the test for general quadrilaterals.

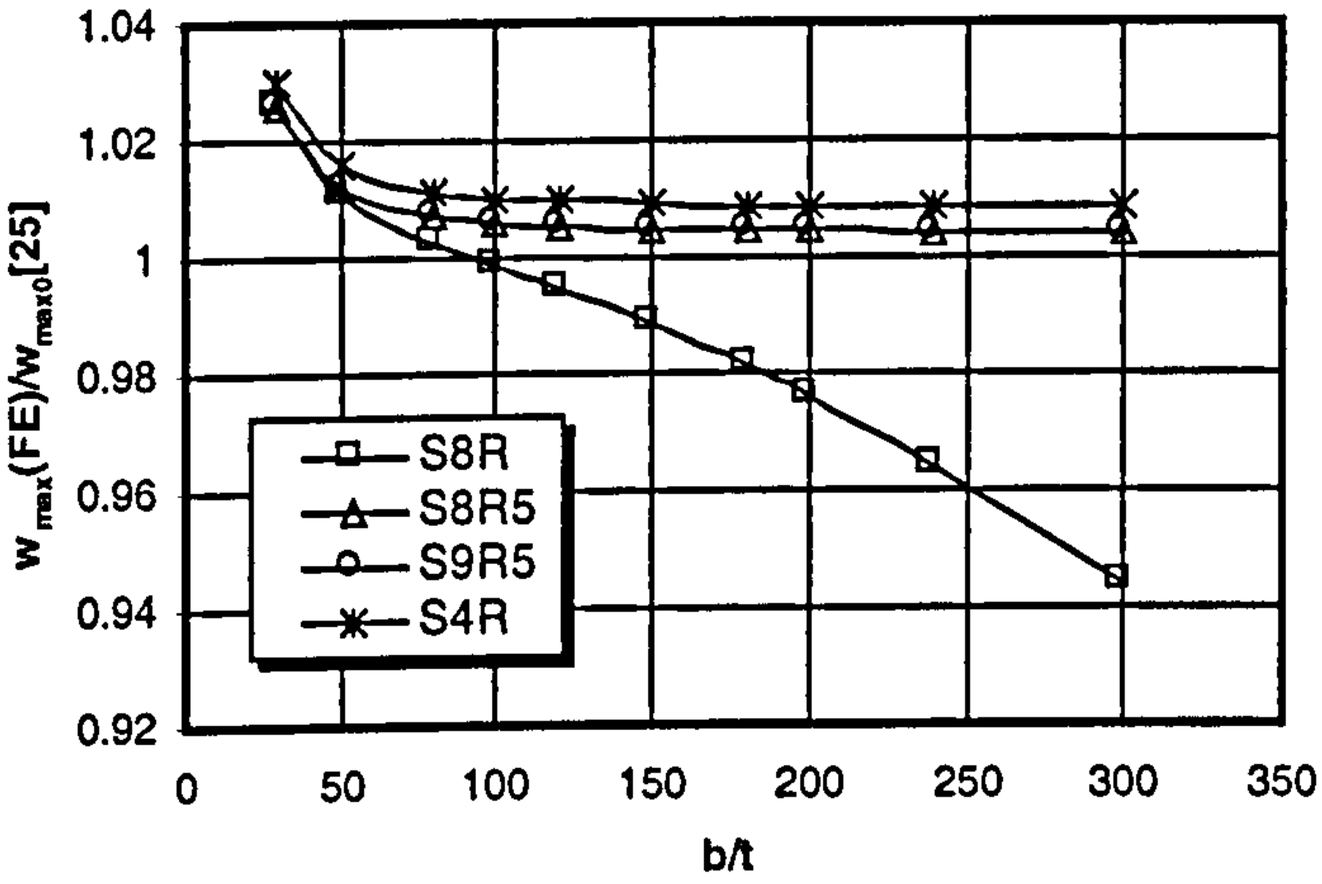
A.2.3 The Sensitivity Test on Plate Slenderness Ratio b/t

A square plate with clamped edges (edge immovable), subjected to a uniformly distributed lateral load, is used to investigate the sensitivity of shell elements to the plate slenderness ratio. Both linear elastic analysis and geometrically non-linear elastic analysis are carried out using ABAQUS with an 8 by 8 mesh. The numerical results of the deflection at the centre of plate are compared in Fig. A.2 with the analytical solutions [25]. It is necessary to state that the analytic solution presented in Fig. A.2(b) is only an approximate solution which was obtained by a simple method consisting of a combination of the known solutions given by the theory of small deflections and the membrane theory.

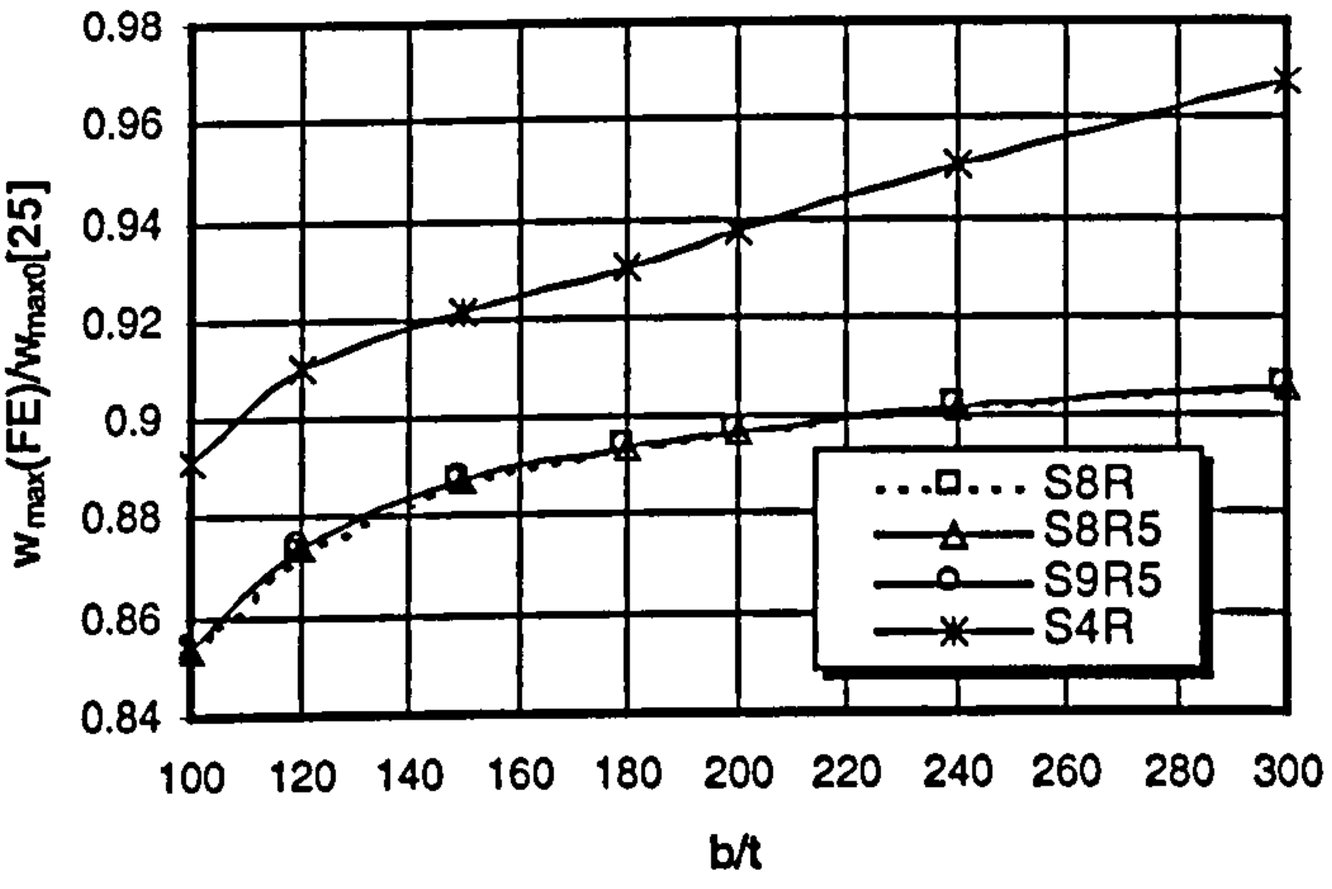
As can be seen in Fig.A.2(a) where linear elastic results are shown, the shell elements S8R5 and S9R5 are the best of the element types tested. Both of them give a high accuracy over the range of slenderness ratio examined (b/t=30—300). The four-node doubly curved element type S4R also responds properly over this range of slenderness ratios. It gives less accurate results than the element type S8R5 or S9R5 does. For the eight-node doubly curved shell element type S8R, its accuracy is acceptable only for small slenderness ratios, that is, thick plates. With the increase of slenderness ratio b/t, the discrepancy increases rapidly.

For the large deflection analysis, it is demonstrated in Fig. A2(b) that the shell elements S8R5 and S9R5 still produce the same results, which can be expected to be the converged results. It is observed that some discrepancies exist between the numerical

results obtained from the element types S4R and S8R5 (or S9R5). It is noted that the element type S8R, which has been verified to be suitable only for thick plates in linear analysis, agrees well with the element type S8R5 (or S9R5) for the whole range of slenderness ratios examined in the geometrically non-linear elastic analysis.



(a) Linear elastic analysis



(b) Large deflection elastic analysis

Figure A.2 Uniformly loaded square plate with clamped edges

A.2.4 Further Comparative Studies on the Elements S8R5, S9R5 and S4R

Since critical buckling analysis and elasto-plastic analysis are parts of the main subjects to be investigated, it is reasonable to carry out further studies on the behaviour of shell

elements for these analyses. On account of the cost and the above discussion, three element types, namely, S8R5, S9R5 and S4R are chosen to be further tested for critical buckling analysis and elasto-plastic analysis.

The critical stresses of a square plate subjected to uniaxial compressive loading and shear loading, respectively, are predicted using ABAQUS. The numerical values are given in Table A.1, together with the series solutions. It is evident that the element types S8R5 and S9R5 produce more accurate results. When the mesh becomes finer, the results for S4R converge towards those for S8R5 (or S9R5). It is also observed that shear buckling requires a finer mesh than compressive buckling, and the possible reason is that the wavelength in shear buckling is smaller.

Table A.1 Critical stress coefficient k_{cr} for a square plate

Eigenmode	**S8R5, S9R5 4*4 mesh**	**S4R 4*4 mesh**	**S4R 8*8 mesh**	**Series Solution**
Uniaxial compressive loading				
1st	4.004	4.460	4.105	4.0
2nd	6.312	8.923	6.736	6.25
3rd	11.750	26.262*	13.691	11.111
Shear loading				
1st	9.459	—	10.384	9.345
2nd	11.884	—	13.619	11.549

* Real 3rd mode has been lost.

The geometrically non-linear elasto-plastic analysis is conducted for a square plate with an initial imperfection subjected to uniaxial compressive stresses. The imperfection is in the form of the first eigenmode, whose magnitude is taken as 10% of the plate thickness (or 0.1% of the side length). The results obtained from ABAQUS are shown in Fig. A.3, where the values of normalised ultimate stress $\sigma_u'=\sigma_u/\sigma_0$ are given, and σ_0 is the yield stress of material. It is demonstrated that with the refinement of mesh, the numerical values for S4R converge towards the solution for S8R5 or S9R5.

A.2.5 Comments

(1) The shell element types S4R, S8R5 and S9R5 can pass the patch tests. Therefore, it is ensured for these types of elements that mesh refinement will produce approximate solutions that converge to the exact solution. On the contrary, the element type S8R is found to fail the patch tests when a mesh consisting of general quadrilaterals is used.

(2) The element types S4R, S8R5 and S9R5 are appropriate to model the bending plate with a slenderness ratio b/t from 30 to 300, while the element type S8R seems to be suitable mainly for thick plates with a small slenderness ratio.

(3) The comparative studies show that the element types S8R5 and S9R5 produces more accurate results than the element type S4R, and they are acceptable for buckling analysis and geometrically non-linear elasto-plastic analysis.

(4) Finally, it is decided that the shell element type S8R5 will be used in all analysis to be conducted, on account of the fact that S8R5 is more cost-effective than S9R5.

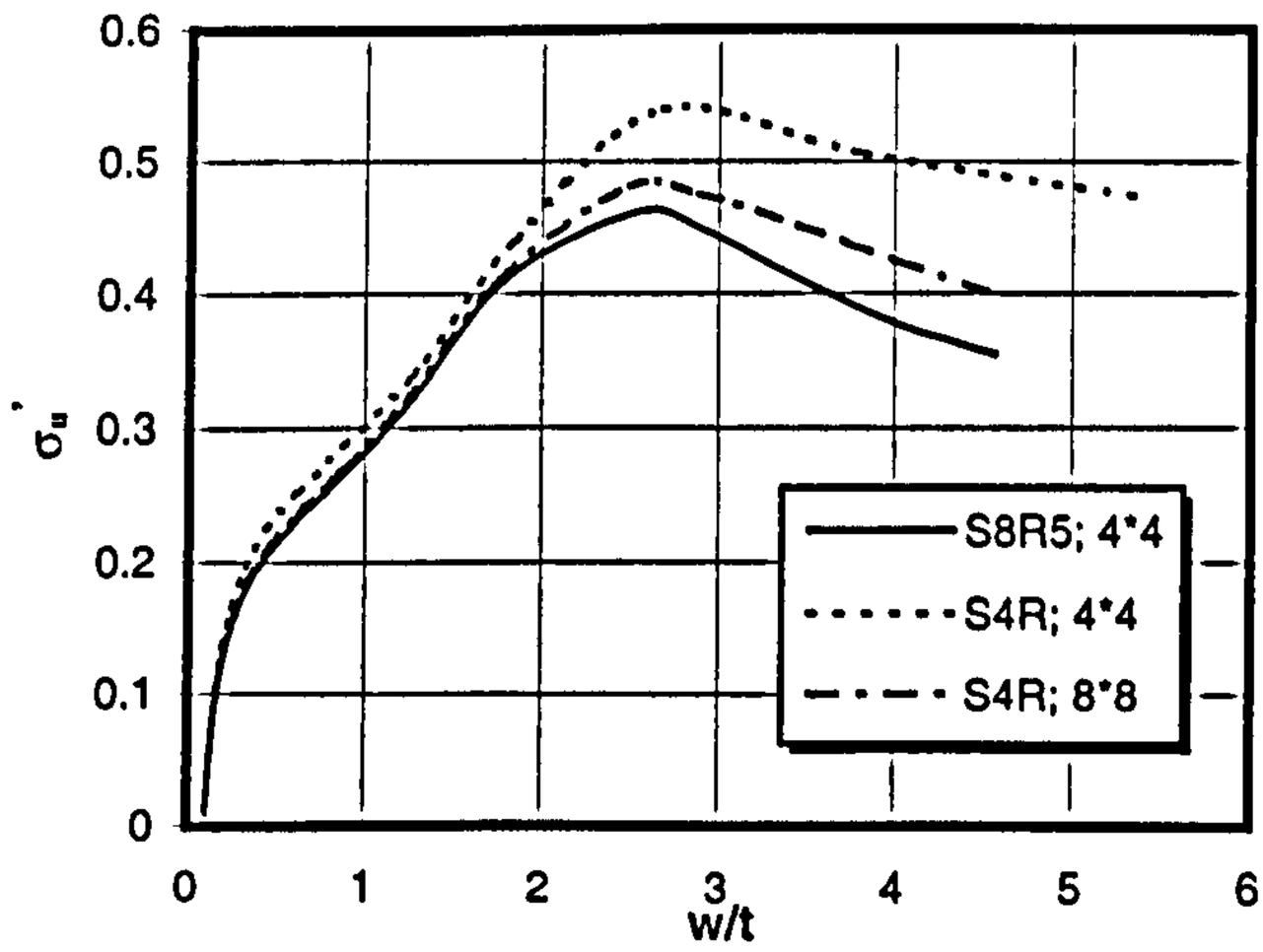


Figure A.3 Square plate under uniaxial compression

A.3 NUMERICAL STUDY ON BEAM ELEMENTS

A.3.1 Beam Elements

Euler-Bernoulli beams and Timoshenko beams are available in ABAQUS beam element library. Euler-Bernoulli beams (B23, B33, etc.) do not allow for transverse shear deformation. These beam elements use cubic interpolation functions. Since the cubic beam elements are written for small strain, they may not be appropriate for torsional stability problems due to the approximations in the underlying formulation, and they cannot be used in analyses involving very large rotations.

Timoshenko beams allows for transverse shear deformation, that is, the cross-section may not necessarily remain normal to the beam axis. ABAQUS provides shear flexible beams with linear interpolation (B21, B31, etc.) and with quadratic interpolation (B22, B32, etc).

When modelling beams in space, a further consideration arises from the possible warping of the beam cross-section under torsional loading. ABAQUS includes a library of open section beam elements (B31OS, B32OS, etc.) for modelling such cases. In these elements, the open section warping theory is used, and the warping magnitude is an additional degree of freedom.

A.3.2 Beam Cross Section Behaviour

Non-solid sections are treated in ABAQUS as *thin-walled* sections. This assumption allows ABAQUS to treat the shear in the section wall as constant through the wall thickness.

In a solid section ABAQUS assumes that warping of the section is small enough so that it can be neglected in computing the axial strains in the section. It is treated locally, by using St. Venant warping theory, to construct a single component of shear strain at each integration point in the section. The St. Venant warping functions are used to define the

shear strain even when the response in the section is no longer purely elastic. This limits the accuracy of the modelling for cases involving non-circular solid beam sections subjected to torsional loadings that cause large amounts of inelastic deformation.

A.3.3 Critical Buckling Analysis

To illustrate the behaviour and the accuracy of beam elements for critical buckling analysis, especially for the lateral and torsional buckling of beams, a slender, elastic straight beam with I-section, subjected to an axial load or a distributed lateral load respectively, is considered. The beam is modelled by the following beam elements chosen from ABAQUS beam element library:

- B31: 2-node general linear beam,
- B32: 3-node general quadratic beam,
- B31OS: 2-node linear open section beam,
- B32OS: 3-node quadratic open-section beam.

The critical buckling load estimates provided by ABAQUS are compared with theoretical results, and shown in Tables A.2.

Table A.2 Ratios of buckling load estimate to the theoretical value

Number	B31	B32	B31OS	B32OS	Mode
Flexural and torsional buckling					
1	0.9869	0.9859	0.9869	0.9859	flexural
2	0.6613	0.6613	1.0041	1.0027	torsional
3	—	—	0.9842	0.9806	flexural
4	—	—	1.0086	0.9977	torsional
Lateral buckling					
1	0.8070	0.8041	0.9981	0.9940	lateral
2	0.5570	0.5509	1.0	0.9844	lateral

It is evident in Table A.2 that there is no significant difference between the regular beam elements (B31, B32) and the open section beam elements (B31OS, B32OS) for flexural buckling. For lateral and torsional buckling, the regular beam elements result in significant errors, so the open section beam elements should be used.

Furthermore, the same beam but with a narrow rectangular section is used to examine the performance of the above beam elements for a non-warping section. The torsional buckling loads obtained are compared with theoretical results, and shown in Table A.3.

Table A.3 Ratios of torsional buckling load estimate to the theoretical value

Beam Element	Section Definition	Critical Load
B31	RECT, or GENERAL	0.9922
B32	RECT, or GENERAL	0.9922
B31OS	GENERAL	0.9979
B32OS	GENERAL	0.9979

It is observed in Table A.3 that the regular beam elements can produce satisfactory torsional buckling load estimates for narrow rectangular section beams.

A.3.4 Comments

The regular beam elements B31 and B32 are suitable for solid beam sections (e.g. rectangular), but may give significant errors for torsional and lateral buckling when used to represent open sections, especially open thin-walled sections. In the later cases, the accurate estimates can only be obtained from open section beam elements.

In the numerical analyses presented in this thesis, the quadratic beam element B32 is used for modelling flat bar stiffeners, and this is consistent with the shell element S8R5 used for modelling plate panels.

APPENDIX B

POST-BUCKLING ANALYSIS OF SIMPLY SUPPORTED PLATES IN UNIAXIAL COMPRESSION

This appendix presents the derivation of a non-linear elastic buckling analysis of simply supported constrained plates subjected to uniaxial compression, as illustrated in Fig. B.1. The analysis of rectangular plates under compression was carried out by Abdel-Sayed [i], using the von Kármán equations and Galerkin's method. The approximate analytical solutions obtained for this simple case are used in Chapter 4 to develop explicit equations for the knife edge forces, which will incorporate finite element analysis results.

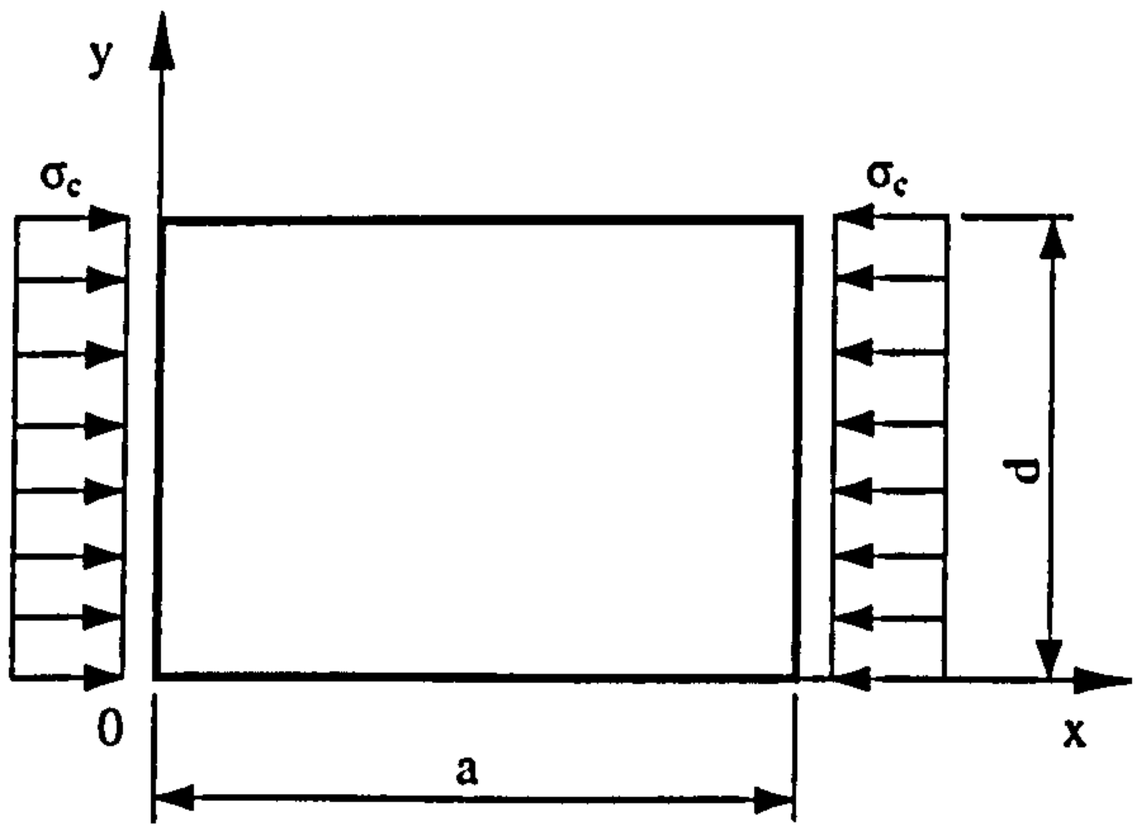


Figure B.1 Simply supported rectangular plates subjected to uniaxial compression

[i] **Abdel-Sayed, G.**, Effective width of thin plates in compression, *J. of Structural Division, ASCE*, Vol.95, No.ST10, 1969, pp.2183-2203.

The von Kármán large deflection equations of a thin elastic isotropic plate, in the presence of initial geometric imperfections can be expressed as:

$$D\nabla^4 w = q + \frac{\partial^2 \Phi}{\partial y^2}\cdot\frac{\partial^2 (w+w_0)}{\partial x^2} + \frac{\partial^2 \Phi}{\partial x^2}\cdot\frac{\partial^2 (w+w_0)}{\partial y^2} - 2\frac{\partial^2 \Phi}{\partial x \partial y}\cdot\frac{\partial^2 (w+w_0)}{\partial x \partial y} \quad \text{(B.1)}$$

$$\frac{1}{Et}\nabla^4 \Phi = \left[\frac{\partial^2 (w+w_0)}{\partial x \partial y}\right]^2 - \frac{\partial^2 (w+w_0)}{\partial x^2}\cdot\frac{\partial^2 (w+w_0)}{\partial y^2} - \left[\left(\frac{\partial^2 w_0}{\partial x \partial y}\right)^2 - \frac{\partial^2 w_0}{\partial x^2}\cdot\frac{\partial^2 w_0}{\partial y^2}\right] \quad \text{(B.2)}$$

where w is the additional out-of-plane deflection due to the applied load; w_0 is the initial geometric imperfection; E is Young's modulus; t is the thickness of the plate; D is the plate flexural rigidity given by $Et^3/12(1-\nu^2)$; ∇^4 denotes the two-dimensional Laplacian operator:

$$\nabla^4 = \frac{\partial^4 \Phi}{\partial x^4} + 2\frac{\partial^4 \Phi}{\partial x^2 \partial y^2} + \frac{\partial^4 \Phi}{\partial y^4}$$

and Φ is the stress function defined as:

$$\sigma_x t = \frac{\partial^2 \Phi}{\partial y^2} \quad , \quad \sigma_y t = \frac{\partial^2 \Phi}{\partial x^2} \quad , \quad \tau_{xy} t = -\frac{\partial^2 \Phi}{\partial x \partial y} \quad \text{(B.3)}$$

where σ_x, σ_y and τ_{xy} are the stresses in the x-y plane. For the post buckling analysis, the geometric relationship between strain and displacement is given by:

$$\varepsilon_x = \frac{\partial u}{\partial x} + \frac{1}{2}\left(\frac{\partial w}{\partial x}\right)^2 + \frac{\partial w}{\partial x}\cdot\frac{\partial w_0}{\partial x}$$

$$\varepsilon_y = \frac{\partial v}{\partial y} + \frac{1}{2}\left(\frac{\partial w}{\partial y}\right)^2 + \frac{\partial w}{\partial y}\cdot\frac{\partial w_0}{\partial y} \quad \text{(B.4)}$$

$$\gamma_{xy} = \frac{\partial u}{\partial y} + \frac{\partial v}{\partial x} + \frac{\partial w}{\partial x}\cdot\frac{\partial w}{\partial y} + \frac{\partial w}{\partial x}\cdot\frac{\partial w_0}{\partial y} + \frac{\partial w}{\partial y}\cdot\frac{\partial w_0}{\partial x}$$

in which ε_x and ε_y are the middle surface membrane strains in the x and y directions, respectively; γ_{xy} is the middle surface shear strain, and u, v are the in-plane displacements in the x and y directions.

The out-of-plane boundary conditions along the plate edges are simply supported, i.e.:

$$[w]_{x=0,a}=0 \quad , \quad \left[\frac{\partial^2 w}{\partial x^2}+\nu\frac{\partial^2 w}{\partial y^2}\right]_{x=0,a}=0 \tag{B.5}$$

$$[w]_{y=0,d}=0 \quad , \quad \left[\frac{\partial^2 w}{\partial y^2}+\nu\frac{\partial^2 w}{\partial x^2}\right]_{y=0,d}=0 \tag{B.6}$$

The in-plane boundary conditions along the loaded and unloaded edges are constrained to remain straight and free of shear stresses, as given by:

$$[u]_{x=0}=0 \quad , \quad [u]_{x=a}=\text{constant} \quad , \quad [\tau_{xy}]_{x=0,a}=0 \tag{B.7}$$

$$[v]_{y=0}=0 \quad , \quad [v]_{y=d}=\text{constant} \quad , \quad [\tau_{xy}]_{y=0,d}=0 \tag{B.8}$$

The analysis assumes that both the initial imperfection, w_0, and the additional deflection due to the applied load, w, are given by a single sinusoidal function:

$$w=A\cdot\sin\frac{\pi x}{a}\sin\frac{\pi y}{d} \tag{B.9}$$

$$w_0=A_0\cdot\sin\frac{\pi x}{a}\sin\frac{\pi y}{d} \tag{B.10}$$

It is noted that such deflection functions can satisfy the boundary conditions of Eqns. B.5 and B.6.

Substituting Eqns. B.9 and B.10 into Eqn. B.2, results in the form:

$$\nabla^4\Phi=\frac{\pi^4 E t}{2a^2d^2}\left(A^2+2A_0A\right)\cdot\left(\cos\frac{2\pi x}{a}+\cos\frac{2\pi y}{d}\right) \tag{B.11}$$

Eqn. B.11 can be satisfied by considering that:

$$\Phi=\frac{Et}{32}\left(A^2+2A_0A\right)\cdot\left(\frac{a^2}{d^2}\cos\frac{2\pi x}{a}+\frac{d^2}{a^2}\cos\frac{2\pi y}{d}\right)+\Phi_1(x,y) \tag{B.12}$$

where $\Phi_1(x,y)$ is a function which fulfils the biharmonic equation:

$$\nabla^4\Phi_1=0 \tag{B.13}$$

Replacing Eqn. B.12 into Eqn. B.3, the stresses in the x-y plane can be written as:

$$\sigma_x = -\frac{\pi^2 E}{8a^2}\left(A^2 + 2A_0 A\right)\cos\frac{2\pi y}{d} + \frac{1}{t}\cdot\frac{\partial^2 \Phi_1}{\partial y^2}$$

$$\sigma_y = -\frac{\pi^2 E}{8d^2}\left(A^2 + 2A_0 A\right)\cos\frac{2\pi x}{a} + \frac{1}{t}\cdot\frac{\partial^2 \Phi_1}{\partial x^2} \qquad \text{(B.14)}$$

$$\tau_{xy} = -\frac{1}{t}\cdot\frac{\partial^2 \Phi_1}{\partial x \partial y}$$

The boundary conditions along the loaded and unloaded edges can be expressed as:

$$\frac{1}{d}\int_0^d [\sigma_x]_{x=0,a}\, dy = -\sigma_c \quad , \quad \int_0^d [\sigma_x]_{x=0,a}\,(y - d/2)\, dy = 0$$

$$\frac{1}{a}\int_0^a [\sigma_y]_{y=0,d}\, dx = 0 \quad , \quad \int_0^a [\sigma_y]_{y=0,d}\,(x - a/2)\, dx = 0 \qquad \text{(B.15)}$$

where σ_c is the applied compressive stresses, taken as a positive value for compression. Incorporating Eqns. B.13–B.15, a solution of $\Phi_1(x,y)$ can be found:

$$\Phi_1 = -\frac{\sigma_c t}{2} y^2 \qquad \text{(B.16)}$$

Accordingly, the stress function and the stresses in the middle surface become:

$$\Phi = \frac{Et}{32}(A^2 + 2AA_0)\cdot\left(\frac{a^2}{d^2}\cos\frac{2\pi x}{a} + \frac{d^2}{a^2}\cos\frac{2\pi y}{d}\right) - \frac{\sigma_c t}{2} y^2 \qquad \text{(B.17)}$$

$$\sigma_x = -\frac{\pi^2 E}{8a^2}(A^2 + 2A_0 A)\cos\frac{2\pi y}{d} - \sigma_c$$

$$\sigma_y = -\frac{\pi^2 E}{8d^2}(A^2 + 2A_0 A)\cos\frac{2\pi x}{a} \qquad \text{(B.18)}$$

$$\tau_{xy} = 0$$

In terms of the elastic relationship for a plane state of stresses, the middle surface strains can be obtained:

$$\varepsilon_x = \frac{1}{E}(\sigma_x - \nu\sigma_y) = -\frac{\pi^2}{8}(A^2 + 2A_0 A)\left(\frac{1}{a^2}\cos\frac{2\pi y}{d} - \nu\frac{1}{d^2}\cos\frac{2\pi x}{a}\right) - \frac{\sigma_c}{E}$$

$$\varepsilon_y = \frac{1}{E}(\sigma_y - \nu\sigma_x) = -\frac{\pi^2}{8}(A^2 + 2A_0 A)\left(\frac{1}{d^2}\cos\frac{2\pi x}{a} - \nu\frac{1}{a^2}\cos\frac{2\pi y}{d}\right) + \nu\frac{\sigma_c}{E} \qquad \text{(B.19)}$$

$$\gamma_{xy} = \frac{2(1+\nu)}{E}\tau_{xy} = 0$$

Incorporating Eqns. B.9, B.10 and B.19 into Eqn. B.4 and carrying out integration, the in-plane displacements are found as follows:

$$u=-\frac{\pi a}{16}(A^2+2A_0A)\left[\frac{1}{a^2}\left(1-\cos\frac{2\pi y}{d}\right)-\nu\frac{1}{d^2}\right]\cdot\sin\frac{2\pi x}{a}-\frac{\pi^2}{8a^2}(A^2+2A_0A)x-\frac{\sigma_c}{E}x$$

$$v=-\frac{\pi d}{16}(A^2+2A_0A)\left[\frac{1}{d^2}\left(1-\cos\frac{2\pi x}{a}\right)-\nu\frac{1}{a^2}\right]\cdot\sin\frac{2\pi y}{d}-\frac{\pi^2}{8d^2}(A^2+2A_0A)y+\nu\frac{\sigma_c}{E}y \qquad \text{(B.20)}$$

The displacements given in Eqn. B.20 satisfy the displacement boundary conditions presented in Eqns. B.7 and B.8.

An approximate solution to the equilibrium differential equation B.1 can now be obtained by the Galerkin method, which leads to the following equation:

$$D\int_0^a\int_0^d(\nabla^4 w)\cdot\sin\frac{\pi x}{a}\sin\frac{\pi y}{d}\,dxdy=\int_0^a\int_0^d(q+q_1)\cdot\sin\frac{\pi x}{a}\sin\frac{\pi y}{d}\,dxdy \qquad \text{(B.21)}$$

where q=0, and q_1 is given by:

$$q_1=\frac{\partial^2\Phi}{\partial y^2}\cdot\frac{\partial^2(w+w_0)}{\partial x^2}+\frac{\partial^2\Phi}{\partial x^2}\cdot\frac{\partial^2(w+w_0)}{\partial y^2}-2\frac{\partial^2\Phi}{\partial x\partial y}\cdot\frac{\partial^2(w+w_0)}{\partial x\partial y} \qquad \text{(B.22)}$$

Substituting Eqns. B.9, B.10 and B.17 into Eqn. B.22 and rearranging, leads to the following post-buckling equilibrium path:

$$\frac{\sigma_c}{\sigma_{c,cr}}=\frac{w_p}{w_p+w_{0p}}+\frac{3(1-\nu^2)(\alpha^2+\alpha^{-2})}{4(\alpha+\alpha^{-1})^2}\cdot\left[\left(\frac{w_p+w_{0p}}{t}\right)^2-\left(\frac{w_{0p}}{t}\right)^2\right] \qquad \text{(B.23)}$$

where $\alpha=d/a$, $w_p=A$, $w_{0p}=A_0$, and $\sigma_{c,cr}$ is the critical compressive stress of the plate panel given by:

$$\sigma_{c,cr}=\frac{\pi^2 D}{d^2 t}\left(\frac{d}{a}+\frac{a}{d}\right)^2 \qquad \text{(B.24)}$$

The transverse shearing force per unit length of plate section perpendicular to the x axis is:

$$Q_x=-D\frac{\partial}{\partial x}\left(\frac{\partial^2 w}{\partial x^2}+\frac{\partial^2 w}{\partial y^2}\right) \qquad \text{(B.25)}$$

By replacing Eqn. B.9 into Eqn. B.25 and taking x=0 and a, the shearing forces along the loaded edges can be obtained:

$$[Q_x]_{x=0,a} = \pm\frac{\pi^3 D}{a^3}\left(1+\frac{a^2}{d^2}\right)\cdot w_p \sin\frac{\pi y}{d} \tag{B.26}$$

The approximate analytical solutions, given by Eqns. B.23 and B.26, will be used in Chapter 4 as the basis to explore explicit equations for the non-linear elastic behaviour of plates subjected to pure shear.

APPENDIX C

COMPARISONS OF ABAQUS SOLUTION WITH FINASIC SOLUTION

C.1 INTRODUCTION

In the present investigation, the general-purpose finite element program ABAQUS is used to carry out a parametric study. The basic phenomena for stiffened plates under pure shear have been extensively investigated by Stanway [1] using the finite element program FINASIC, developed at Imperial College. In this appendix, a comparative validation between ABAQUS and FINASIC is made.

For the purpose of comparison, the cases studied are chosen from those examined by Stanway [1]. The structural configuration is shown in Fig. 3.1, with the stiffener being double-sided flat bars of h/t_s=10. The panel aspect ratios considered are d/a=1 and 2 only. The plates are simply supported, with CUCU in-plane boundary conditions (Fig. 3.2). The initial imperfection shape adopted by Stanway [1] consists of the most significant deflection function term in the buckling mode, and was referred to as the "part affined" mode, which is summarised in Table C.1.

Table C.1 Part affined imperfection modes (from Ref. [1])

d/a	Panel Component	Stiffener Component
1	$-a_0\left(\sin\frac{\pi x}{2a}+\sin\frac{3\pi x}{2a}\right)\sin\frac{\pi y}{d}$	$w_{0s}\sin\frac{\pi x}{2a}\sin\frac{\pi y}{d}$ *where* $w_{0s}=d/750$
2	$-a_0\sin\frac{\pi x}{a}\sin\frac{2\pi y}{d}$	

The coefficient a_0 in Table C.1 is calculated so that the panel imperfection magnitude w_{0p} is equal to the code tolerances, as given by Eqn. 3.8, and the measurement of w_{0p} is shown in Fig. 3.5.

The yield stresses of the panel and the stiffener are equal to 245N/mm^2, and the other material properties are given in Section 3.4.

In the numerical analyses, ABAQUS shell element S8R5 and beam element B32 are used to model the panel and the stiffener, respectively. The finite element meshes adopted are identical to those used by Stanway [1].

C.2 CRITICAL BUCKLING STRESS

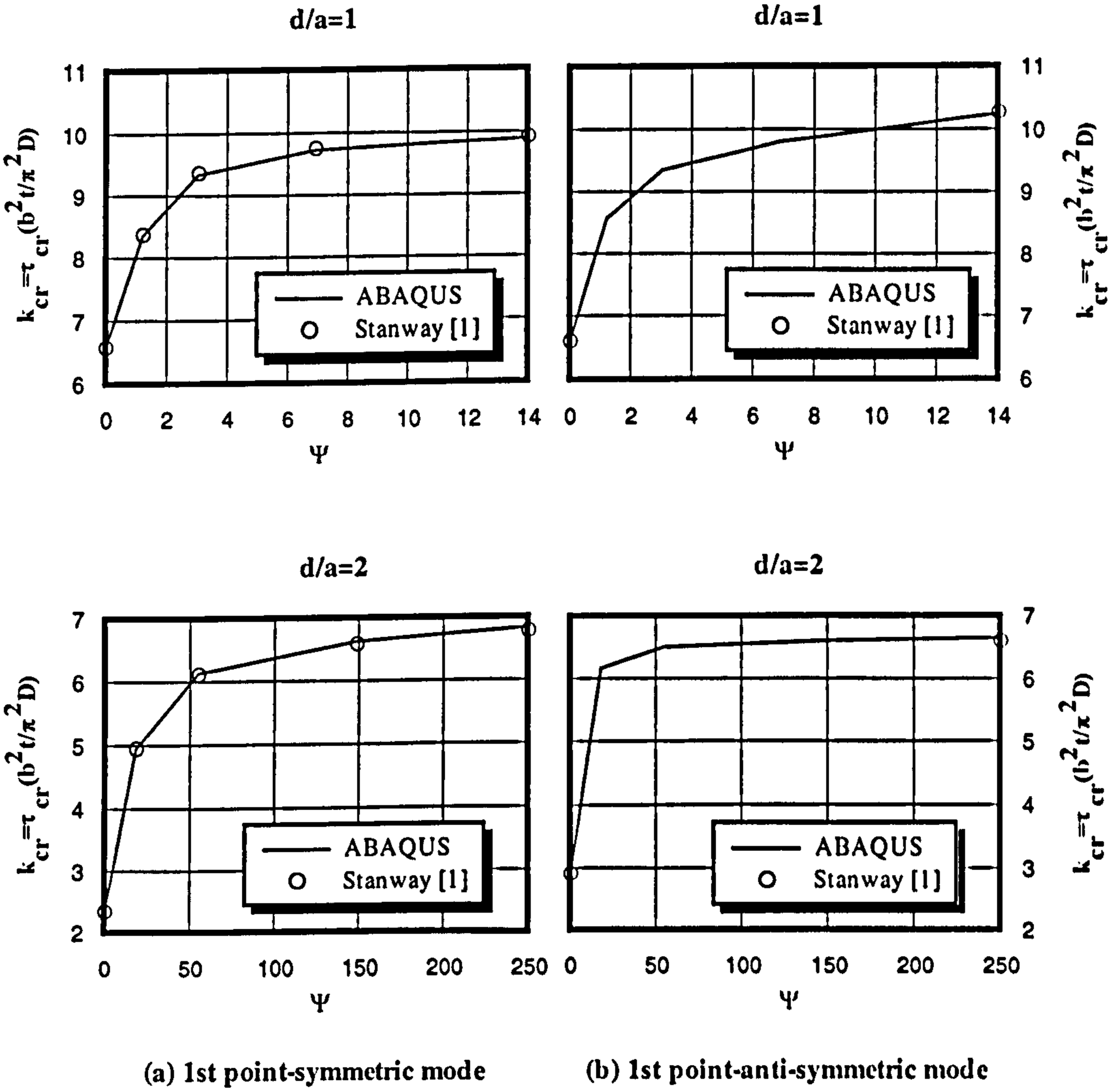
The values of the critical buckling stress parameter k_{cr} given in Ref. [1] were from the series solutions. However, it was pointed out by Stanway [1] that both FINASIC and the series solution give k_{cr} values which are negligibly different (<1%), provided a sufficiently fine mesh (or number of terms) is taken in each case. Therefore, the comparison of ABAQUS solution with the series solution can provide an indirect comparison between ABAQUS and FINASIC, and also the accuracy of the ABAQUS solution can be validated.

Fig. C.1 presents a comparison of the critical buckling stress parameter k_{cr} from ABAQUS for the first point-symmetric and point-anti-symmetric buckling modes, with the converged series solutions, for plates with a Γ=0 stiffener, subjected to pure shear. It is apparent that the values of k_{cr} predicted by ABAQUS agree closely with the series solution.

C.3 ULTIMATE STRENGTH

In Fig. C.2, the ultimate shear stress ratio τ_u' obtained by carrying out non-linear elasto-plastic buckling analyses using ABAQUS, are compared with the FINASIC solution given by Stanway [1].

It can be seen in Fig. C.2 that the ABAQUS solution for τ_u' is less than the FINASIC solution, except for the case of d/a=1 and a/t=80, and the greatest difference occurs after the stiffener flexural rigidity Ψ becomes great enough for the Ψ vs. τ_u' curve to reach its plateau. For stiffeners which correspond to a point located in the plateau of the Ψ vs. τ_u' curve, the deflection mode of the plate at ultimate load is a divided panel mode, which means the bending curvature of the panels becomes much greater, especially for the more slender plates.



(a) 1st point-symmetric mode **(b) 1st point-anti-symmetric mode**

Figure C.1 Comparison of the critical buckling stress factor from ABAQUS with the series solution, Given by Stanway [1]. Number of square elements across the small panel dimension is N=8. Pure shear

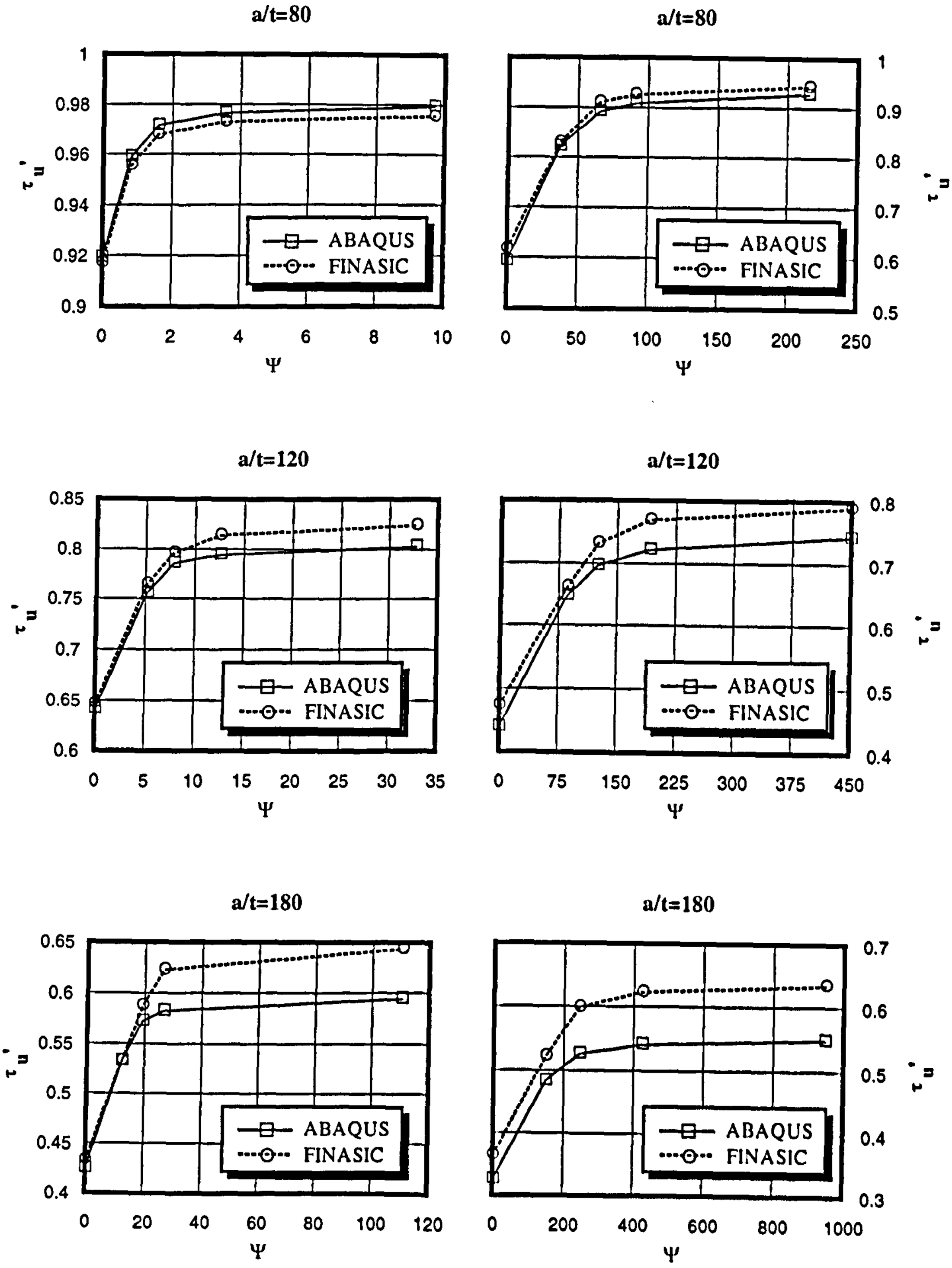


Figure C.2 Comparison of the ultimate shear strength from ABAQUS with the FINASIC solution [1]. CUCU stiffened plated under pure shear. FE mesh size as adopted by Stanway (Table 3.1)

It is also observed in Fig. C.2 that the difference between these two numerical solutions increases with the panel slenderness ratio a/t. For d/a=1, the relative difference in τ_u' increases from 0.4% for a/t=80 to 8% for a/t=180; whereas for d/a=2, the relative difference is 1.6% and 15% for a/t=80 and 180, respectively. The difference may be due to the different shell element types adopted in the finite element models. It is noted that the FINASIC shell element is an 8-node doubly-curved isoparametric element, which has the full six degrees of freedom per node and employs reduced integration [1]. By reference to the ABAQUS element library, the FINASIC shell element may be similar or equivalent to the ABAQUS shell element S8R, which is designed mainly for thick plates. However, the ABAQUS solution presented above was obtained by employing ABAQUS shell element S8R5, which is specially designed for thin shells.

Another factor which may contribute to the differences between ABAQUS and FINASIC solutions is the modelling of constrained edges, for which shear springs of high stiffness were used in FINASIC analyses, whereas geometrical constrained equations were employed in ABAQUS to keep the constrained edge straight.

Nevertheless, it is apparent in Fig. C.2 that although significant differences between ABAQUS and FINASIC solutions exist for plates of a/t≥180, the stiffener flexural rigidities at which the plateau of the Ψ vs. τ_u' curve starts are nearly identical according to the two finite element programs. Therefore, the basic phenomena of stiffener behaviour, revealed in the previous parametric study by Stanway [1] using FINASIC, are still valid, and will be used as the basis of the present investigation.

APPENDIX D

FORTRAN PROGRAM FOR TRANSVERSE STIFFENER DESIGN

The FORTRAN program presented in this appendix is written for determining the smallest stiffener required by the design model proposed in this thesis. The program can be used for both concentric and eccentric flat bar stiffeners. Stiffened plates subjected to combined shear, compression and bending are considered. The data required by the program are:

Panel width a (mm)

Panel deight d (mm)

Panel thickness t (mm)

Panel yield stress σ_{0p} (N/mm^2)

Stiffener yield stress σ_{0s} (N/mm^2)

Stiffener type: single-sided (=1) or double-sided (=2)

Ultimate shear stress ratio of the panel, τ_u/τ_{0p}

Ultimate compressive stress ratio of the panel, σ_{cu}/σ_{0p}

Ultimate bending stress ratio of the panel, σ_{bu}/σ_{0p}

The program calculates the maximum shear resistance of the CUCU panel using the formulae given by Davidson [40], and the estimated value is provided for reference before asking for the input of applied stress ratios. For plates subjected to combined loading, the components of the ultimate panel strength (τ_u, σ_{uc} and σ_{ub}) should be used.

The thickness of the stiffener, t_s, can be specified, and the program will then output the minimum stiffener depths h_{sZ} and h_{sI} which satisfy the strength and stiffness criteria, respectively. Alternatively, by assigning "-1" to t_s, the smallest stiffener with a side ratio h_s/t_s=10 will be given.

```
C=======================================================
C
C   Stiffener Design for Combined Shear, Compression and Bending
C  (Shear Resistance of CUCU Panels is based on Davidson's Model)
C
C          E=20500MPa, V=0.3, Single Flat Bar Stiffeners
C
C=======================================================
C
C
      PROGRAM MXIE_CL
      IMPLICIT REAL*8 (A-H,O-Z)
      CHARACTER STYPE, STATUS
C
      STATUS='y'
C
      DO WHILE (STATUS.EQ.'y')
      CALL INPUT(A,D,T,NUMSTFN,E,SIGYP,SIGYS,DWOS,BWOP,STYPE)
      DA=D/A
      AD=A/D
      B=A
      IF (D.LT.A) B=D
      WOPT=B/(BWOP*T)
      WOS=D/DWOS
      CALL TDUCALC(DA,AD,B,T,E,SIGYP,TDU)
      WRITE(6,5) TDU
5     FORMAT(//1X,'Calculated Tu/Ty (pure shear)= ',F12.6)
      WRITE(6,7)
7     FORMAT(//11X,'Enter the Magnitudes of the Applied Loads'//)
      WRITE(6,*) '====>> Shear stress ratio Tu/Ty : '
      READ(5,*) TDU
      WRITE(6,*) '====>> Compressive stress ratio SIGCu/SIGy : '
      READ(5,*) SIGCU
      WRITE(6,*) '====>> Bending stress ratio SIGBu/SIGy : '
      READ(5,*) SIGBU
C
      TAO=TDU*(1.0/(3**0.5))*SIGYP
      SIGC=SIGCU*SIGYP
      SIGB=SIGBU*SIGYP
C
      CALL TCRCALC(DA,AD,B,T,E,TCR)
      CALL SCCRCALC(DA,D,T,E,SCCR)
      CALL SBCRCALC(DA,D,T,E,SBCR)
C
      IF (DA.LE.1.) THEN
        BELTAC=0.45
      ELSE IF (DA.EQ.2.) THEN
        BELTAC=0.2
      ELSE IF (DA.GE.3.) THEN
        BELTAC=0.45
      ELSE
        BELTAC=0.2+0.25*ABS(DA-2.)
      END IF
      BELTAB=0.25
      TTCR=0.5*BELTAC*SIGC/SCCR+SQRT((TAO/TCR)**2
     +            +(BELTAB*SIGB/SBCR)**2+(BELTAC*SIGC/SCCR)**2/4.)
C
      WRITE(6,30) TAO,SIGC,SIGB
30    FORMAT(//1X,'Applied Loads TAO,SIGc,SIGb (MPa) = ',3F12.6)
```

```
      WRITE(6,40) TCR,SCCR,SBCR
40    FORMAT(/1X,'Critical Stresses TCR,SCCR,SBCR (MPa) = ',3F12.6)
      WRITE(6,50) TTCR
50    FORMAT(/1X,'Shear Stress Ratio for Combined Loading TEQ/TCR = '
     +           ,F12.6)
C
      CALL MPK(DA,AD,WOPT,TTCR,ZMPKND)
      C=1.6-0.35*SQRT(SIGYP/355)
      IF (C.LT.1.) C=1.0
      ZMPKND=C*ZMPKND
      ZMPK=ZMPKND*T*E*(T**3)/(B*12*(1-(.3**2)))
C
      CALL TRIALSIZE(A,D,T,E,SIGYP,SIGYS,WOS,ZMPK,STYPE,TS,HS0)
C
      CALL STRENGTH(A,D,T,E,NUMSTFN,SIGYS,ZMPK,WOS,TAO,SIGC,
     +           SIGB,STYPE,TS,HS0,HSZ,YZ,PSZ,ZMOVZ,ZMSZ)
C
      CALL STIFFNESS(A,D,T,E,NUMSTFN,WOS,ZMPK,TAO,SIGC,SIGB,
     +           STYPE,TS,HS0,HSI,YI,PSI,ZMOVI,ZMSI,WSA)
C
      CALL OUTPUT(ZMPKND,ZMPK,STYPE,TS,HSZ,YZ,PSZ,ZMOVZ,ZMSZ,HSI,
     +           YI,PSI,ZMOVI,ZMSI,WSA,TDU,SIGCU,SIGBU)
      WRITE(6,10)
10    FORMAT(//,2X,'Do you want another calculation (y/n)')
      READ(5,'(A)') STATUS
      END DO
C
      STOP
      END
C
      SUBROUTINE INPUT(A,D,T,NUMSTFN,E,SIGYP,SIGYS,DWOS,BWOP,STYPE)
      IMPLICIT REAL*8(A-H,O-Z)
      CHARACTER STYPE
      WRITE(6,10)
10    FORMAT(//15X,'*** Web Stiffener Design ***'//)
      WRITE(6,*) '====>> Panel Width a (mm):'
      READ(5,*) A
      WRITE(6,* ) '====>> Panel Height d (mm):'
      READ(5,*) D
      WRITE(6,*) '====>> Panel Thickness t (mm):'
      READ(5,*) T
C     WRITE(6,*) '====>> Single (=1) of Muti (=2) Stiffener Plate :'
C     READ(5,*) NUMSTFN
      NUMSTFN=1
C     WRITE(6,*) '====>> Elastic Modulus E (N/mm2):'
C     READ(5,*) E
      E=205000.
      WRITE(6,*) '====>> Panel Yield Stress (N/mm2):'
      READ(5,*) SIGYP
C     SIGYP=245.
      WRITE(6,*)'====>> Stiffener Yield Stress (N/mm2):'
      READ(5,*) SIGYS
C     SIGYS=245.
C     WRITE(6,*) '====>> Stiffener Imperfection  d/wos:'
C     READ(5,*) DWOS
      DWOS=750.
C     WRITE(6,*) '====>> Panel Imperfection b/wop'
C     READ(5,*) BWOP
      BWOP=165.*SQRT(355./SIGYP)
```

```
      WRITE(6,20)
20    FORMAT(1X,'====>> Single-Sided (=1) or Double-Sided (=2)',1X,
     +                'Flat Bar Stiffeners :')
      READ(5,'(A)') STYPE
      END
C
      SUBROUTINE KCRCALC(DA,AD,ZKCR)
      IMPLICIT REAL*8   (A-H,O-Z)
      ALPHA=DA
      IF (AD.GT.ALPHA) THEN
      ALPHA=AD
      END IF
      ZKCR=5.34+4/ALPHA/ALPHA
C     ZKCR=5.386+(0.121/ALPHA)+(3.727/(ALPHA**2))
      END
C
      SUBROUTINE KCRSCALC(DA,AD,ZKCR)
      IMPLICIT REAL*8   (A-H,O-Z)
      ALPHA=DA
      IF (AD.GT.ALPHA) THEN
      ALPHA=AD
      END IF
      ZKCR=5.34+4/ALPHA/ALPHA
C     ZKCR=5.386+(0.121/ALPHA)+(3.727/(ALPHA**2))
      END
C
      SUBROUTINE KCRCCALC(DA,ZKCR)
      IMPLICIT REAL*8   (A-H,O-Z)
      IF (DA.GT.1) THEN
        ZKCR=(DA+1./DA)**2
      ELSE
        ZKCR=4.
      END IF
      END
C
      SUBROUTINE KCRBCALC(DA,ZKCR)
      IMPLICIT REAL*8   (A-H,O-Z)
      IF (DA.GT.1.5) THEN
        ZKCR=24.+73.*(2./3.-1./DA)**2
      ELSE
        ZKCR=24.
      END IF
      END
C
      SUBROUTINE TCRCALC(DA,AD,B,T,E,TCR)
      IMPLICIT REAL*8 (A-H,O-Z)
      PARAMETER(PI=3.14159265358)
      CALL KCRSCALC(DA,AD,ZKCR)
      TCR=(E*(T**3)/(12*(1-(.3**2))))*(PI**2)*ZKCR/(T*(B**2))
      END
C
      SUBROUTINE SCCRCALC(DA,D,T,E,SCCR)
      IMPLICIT REAL*8 (A-H,O-Z)
      PARAMETER(PI=3.14159265358)
      CALL KCRCCALC(DA,ZKCR)
      SCCR=(E*(T**3)/(12*(1-(.3**2))))*(PI**2)*ZKCR/(T*(D**2))
      END
C
      SUBROUTINE SBCRCALC(DA,D,T,E,SBCR)
```

```
      IMPLICIT REAL*8 (A-H,O-Z)
      PARAMETER(PI=3.14159265358)
      CALL KCRBCALC(DA,ZKCR)
      SBCR=(E*(T**3)/(12*(1-(.3**2))))*(PI**2)*ZKCR/(T*(D**2))
      END
C
      SUBROUTINE TDUCALC(DA,AD,B,T,E,SIGYP,TDU)
      IMPLICIT REAL*8 (A-H,O-Z)
      PARAMETER(PI=3.14159265358)
      BELTA=B/T*SQRT(SIGYP/E)
      ALPHA=DA
      IF (AD.GT.ALPHA) THEN
        ALPHA=AD
      END IF
C     CALL KCRCALC(DA,AD,ZKCR)
      ZKCR=5.34+4/ALPHA/ALPHA
      ZLAMBDA=0.8*BELTA/SQRT(ZKCR)
C
C   Tu for CCCC Panels
      IF (ALPHA.LE.5.) THEN
        C1=1.3-0.05*ALPHA
      ELSE
        C1=1.05
      END IF
      C2=0.85-C1
      C3=-4.+6.*C1+7.*C2
      C4=24.-29.*C1-34.*C2
      C5=-36.+44.*C1+52.*C2
      C6=16.-20.*C1-24.*C2
      IF (ZLAMBDA.GE.1.) THEN
        TCC=C1/ZLAMBDA+C2/ZLAMBDA/ZLAMBDA
      ELSE IF (ZLAMBDA.LT.0.5) THEN
        TCC=1.0
      ELSE
        TCC=C3+C4*ZLAMBDA+C5*ZLAMBDA**2+C6*ZLAMBDA**3
      END IF
C
C   Tu for UUUU Panels
      IF (ALPHA.LT.3.) THEN
        C1=1.12-0.15*ALPHA
      ELSE
        C1=0.67
      END IF
      IF (ALPHA.LT.3.) THEN
        C2=0.14*ALPHA-0.3
      ELSE
        C2=0.12
      END IF
      C3=-4.+6.*C1+7.*C2
      C4=24.-29.*C1-34.*C2
      C5=-36.+44.*C1+52.*C2
      C6=16.-20.*C1-24.*C2
      IF (ZLAMBDA.GE.1.) THEN
        TUU=C1/ZLAMBDA+C2/ZLAMBDA/ZLAMBDA
      ELSE IF (ZLAMBDA.LT.0.5) THEN
        TUU=1.0
      ELSE
        TUU=C3+C4*ZLAMBDA+C5*ZLAMBDA**2+C6*ZLAMBDA**3
      END IF
```

```
C
C    Tu for CUCU Panels
       IF (DA.LE.1) THEN
         TDU=(TCC-TUU)/(1+ALPHA**3)+TUU
       ELSE
         TDU=(TCC-TUU)/(1+1/ALPHA)+TUU
       END IF
       END
C
       SUBROUTINE MPK(DA,AD,WOPT,TTCR,ZMPK)
       IMPLICIT REAL*8 (A-H,O-Z)
       IF (DA.GE.3.) THEN
         C1=69.47
         C2=1.942
         C3=-16.96
         C4=80.11
         C5=-7.281
         C6=-0.264
      ELSE IF (DA.GT.2.) THEN
         C1=83.62+(DA-2.)*(69.47-83.62)
         C2=-16.59+(DA-2.)*(1.942+16.59)
         C3=-14.03+(DA-2.)*(-16.96+14.03)
         C4=19.70+(DA-2.)*(80.11-19.70)
         C5=54.99+(DA-2.)*(-7.281-54.99)
         C6=-7.676+(DA-2.)*(-0.264+7.676)
      ELSE IF (DA.EQ.2.) THEN
         C1=83.62
         C2=-16.59
         C3=-14.03
         C4=19.70
         C5=54.99
         C6=-7.676
      ELSE IF (DA.GT.1.)THEN
         C1=29.71+(DA-1.)*(83.62-29.71)
         C2=-0.524+(DA-1.)*(-16.59+0.524)
         C3=-6.960+(DA-1.)*(-14.03+6.960)
         C4=4.962+(DA-1.)*(19.70-4.962)
         C5=21.37+(DA-1.)*(54.99-21.37)
         C6=-2.865+(DA-1.)*(-7.676+2.865)
      ELSE IF (DA.LE.1.)THEN
         C1=29.71
         C2=-0.524
         C3=-6.960
         C4=4.962
         C5=21.37
         C6=-2.865
      END IF
      ZMPK=C1*WOPT*TTCR+C2*WOPT*TTCR**2+C3*TTCR
     +                 +C4*TTCR**2+C5*TTCR**3+C6*TTCR**4
       END
C
       SUBROUTINE TRIALSIZE(A,D,T,E,SIGYP,SIGYS,WOS,ZMPK,STYPE,TS,HS)
       IMPLICIT REAL*8 (A-H,O-Z)
       CHARACTER STYPE
       DA=D/A
       AD=A/D
       B=A
       IF (D.LT.A) B=D
       CALL TDUCALC(DA,AD,B,T,E,SIGYP,TDU)
```

```
      TAOPURE=TDU*(1.0/(3**0.5))*SIGYP
      YSKOV=2*A*(DA**2/4.+1)/SQRT(8.155*(DA**2/4.+4./DA**2)+13.99)
      ZMOVK=YSKOV*TAOPURE*T*WOS
      ZMIK=ZMPK+ZMOVK
C
C   Assuming Ps/As=0.2*SIGYS & TS=HS/10
C
      IF (STYPE.EQ.'2') THEN
          HS=((ZMIK*15.)/0.8/SIGYS)**(1/3.0)
      ELSE IF (STYPE.EQ.'1') THEN
        HS=((ZMIK*30.)/0.8/SIGYS)**(1/3.0)
      END IF
      TS=HS/10.
      WRITE(6,10) TS, HS
10    FORMAT(//1X,'Suggested Stiffener: ts=',F8.3,'mm, hs=',F8.3,'mm')
C
      WRITE(6,20)
20    FORMAT(/1X,'=====>>Stiffener Thickness ts(=-1
     +        for hs/ts=10, mm): ')
      READ(5,*) TS
      IF (TS.GT.0) THEN
        IF (STYPE.EQ.'2') THEN
            HS=SQRT(3*ZMIK/2./TS/0.8/SIGYS)
          ELSE IF (STYPE.EQ.'1') THEN
            HS=SQRT(3*ZMIK/TS/0.8/SIGYS)
        END IF
      END IF
      WRITE(6,30) TS, HS
30    FORMAT(//1X,'Trial Stiffener Size: ts=',F8.3,'mm,
     +       hs=',F8.3,'mm')
      END
C
      SUBROUTINE STIFPROP(B,T,E,STYPE,TS,HS,AS,ZIS,ZZS,YS)
      IMPLICIT REAL*8   (A-H,O-Z)
      CHARACTER STYPE
      IF (TS.LT.0.) THEN
        IF (STYPE.EQ.'2') THEN
          AS=2*HS*HS/10.
          ZIS=HS*(HS+T/2.)**3/15.-HS*T**3/120.
          ZZS=ZIS/(HS+T/2.)
        ELSE IF (STYPE.EQ.'1') THEN
          AS=HS*HS/10.
          ZIS=(HS**4)/120.
          ZZS=ZIS/HS*2.
        END IF
      ELSE
        IF (STYPE.EQ.'2') THEN
          AS=2*HS*TS
          ZIS=2*TS*(HS+T/2.)**3/3.-TS*T**3/12.
            ZZS=ZIS/(HS+T/2.)
          ELSE IF (STYPE.EQ.'1') THEN
          AS=HS*TS
            ZIS=TS*HS**3/12.
            ZZS=ZIS/HS*2.
        END IF
      END IF
      YS=E*ZIS/(B*E*(T**3)/(12.*(1-.3**2)))
      END
C
```

```
      SUBROUTINE AXIALF(A,D,T,E,TAO,SIGC,SIGB,AS,PS)
      IMPLICIT REAL*8   (A-H,O-Z)
      PI=3.141592654
      DA=D/A
      AD=A/D
      B=A
      IF (D.LT.A) B=D
      CALL TCRCALC(DA,AD,B,T,E,TCR)
      CALL SCCRCALC(DA,D,T,E,SCCR)
      CALL SBCRCALC(DA,D,T,E,SBCR)
      IF (TAO.NE.0.) THEN
        RC=(SIGC/SCCR)/(TAO/TCR)
        RB=(SIGB/SBCR)/(TAO/TCR)
        TEQCR=2./(SQRT(4*RB**2+RC**2+4.)+RC)
        TEQCR=TEQCR*TCR
        TTCR=TAO/TEQCR
        IF ((SIGC/TAO.GT.5.).OR.(SIGB/TAO.GT.5.)) TTCR=0.
      ELSE
        TTCR=0.
      END IF
C
      IF (TTCR.GT.1.) THEN
        C=0.27+0.05*LOG(DA)
        PS=0.5/SQRT(DA)*(TTCR-1)*(1+C*LOG(AS/A/T))
      ELSE
        PS=0.0
      END IF
      PS=PS*TCR*D*T
      END
C
      SUBROUTINE KOVS(A,D,T,NUMSTFN,YS,ZKOVS)
      IMPLICIT REAL*8 (A-H,O-Z)
      PI=3.141592654
      DA=D/A
      B=A
      IF (D.LT.A) B=D
C
      IF (NUMSTFN.EQ.1) THEN
        ZKOVS=SQRT(8.155*(DA**2/4.+4./DA**2)+13.99)*(B/D)**2
        ZKOVS=ZKOVS*((DA**2/4.+1)**2+YS*B/2./A)/(DA**2/4.+1)
      ELSE
C       (Multi-stidffeners)
      END IF
      END
C
      SUBROUTINE KOVC(A,D,T,NUMSTFN,YS,ZKOVC)
      IMPLICIT REAL*8 (A-H,O-Z)
      PI=3.141592654
      DA=D/A
      B=A
      IF (D.LT.A) B=D
C
      IF (NUMSTFN.EQ.1) THEN
        ZKOVC=(B/D)**2*((DA/2.+2./DA)**2+4.*A*B*YS/D/D)
      ELSE
C       (Multi-stidffeners)
      END IF
      END
C
```

```
      SUBROUTINE KOVB(A,D,T,NUMSTFN,YS,ZKOVB)
      IMPLICIT REAL*8 (A-H,O-Z)
      PI=3.141592654
      DA=D/A
      B=A
      IF (D.LT.A) B=D
C
      IF (NUMSTFN.EQ.1) THEN
        ZKOVB=((DA**2/4.+1.)**2+B/A*YS)*((DA**2/16.+1.)**2+B/A*YS)
        ZKOVB=4.5*(PI*A*B/D)**2*SQRT(ZKOVB)
      ELSE
C       (Multi-stidffeners)
      END IF
      END
C
      SUBROUTINE MOMENT(A,D,T,E,NUMSTFN,TAO,SIGC,SIGB,
     +                  WOS,YS,ZMPK,ZMOV,ZMS)
      IMPLICIT REAL*8   (A-H,O-Z)
      PI=3.141592654
      B=A
      IF (D.LT.A) B=D
C
      DPLT=E*(T**3)/(12.*(1-.3**2))
      CALL KOVS(A,D,T,NUMSTFN,YS,ZKOVS)
      TOV=ZKOVS*PI*PI*DPLT/(B**2*T)
      CALL KOVC(A,D,T,NUMSTFN,YS,ZKOVC)
      SOVC=ZKOVC*PI*PI*DPLT/(B**2*T)
      CALL KOVB(A,D,T,NUMSTFN,YS,ZKOVB)
      SOVB=ZKOVB*PI*PI*DPLT/(B**2*T)
C
      RLOAD=TAO/TOV+SIGC/SOVC+SIGB/SOVB
      ZMOV=RLOAD/(1.-RLOAD)*PI**2*DPLT*B*YS/D/D*WOS
C
      IF (ZMOV.LT.0.) ZMOV=0.
      ZMS=ZMPK+ZMOV
      END
C
      SUBROUTINE STRENGTH(A,D,T,E,NUMSTFN,SIGYS,ZMPK,WOS,TAO,
     +      SIGC,SIGB,STYPE,TS,HS0,HS,YS,PS,ZMOV,ZMS)
      IMPLICIT REAL*8 (A-H,O-Z)
      CHARACTER STYPE
      B=A
      IF (D.LT.A) B=D
      ERROR=.0001
      HSI0=HS0
C
34    HSI=HSI0
      HSJ=2*HSI
      HSINC=HSI
33    CALL STIFPROP(B,T,E,STYPE,TS,HSJ,ASJ,ZISJ,ZZSJ,YSJ)
      CALL AXIALF(A,D,T,E,TAO,SIGC,SIGB,ASJ,PSJ)
      CALL MOMENT(A,D,T,E,NUMSTFN,TAO,SIGC,SIGB,
     +            WOS,YSJ,ZMPK,ZMOVJ,ZMSJ)
      SUMPSJ=PSJ
      CALL STRESS(A,D,T,STYPE,SUMPSJ,ZMSJ,TS,HSJ,ASJ,ZZSJ,SIGSJ)
C
      IF (SIGSJ.EQ.SIGYS) GO TO 31
      IF (SIGSJ.LT.SIGYS) GO TO 32
      HSJ=HSJ+HSINC
```

```
      GOTO 33
32    HSK=(HSJ+HSI)/2.0
      CALL STIFPROP(B,T,E,STYPE,TS,HSK,ASK,ZISK,ZZSK,YSK)
      CALL AXIALF(A,D,T,E,TAO,SIGC,SIGB,ASK,PSK)
      CALL MOMENT(A,D,T,E,NUMSTFN,TAO,SIGC,SIGB,
     +            WOS,YSK,ZMPK,ZMOVK,ZMSK)
      SUMPSK=PSK
      CALL STRESS(A,D,T,STYPE,SUMPSK,ZMSK,TS,HSK,ASK,ZZSK,SIGSK)
C
      IF (SIGSK.LT.SIGYS) THEN
        HSJ=HSK
        ZISJ=ZISK
      ELSE IF(SIGSK.GT.SIGYS)THEN
        HSI=HSK
        ZISI=ZISK
      END IF
      HSACC=(HSJ-HSI)*100/HSJ
      IF (HSACC.LT.ERROR) GO TO 31
      GO TO 32
31    IF (HSJ.GT.(HSI0+ERROR)) THEN
        HS=HSJ
        YS=E*ZISJ/(B*E*(T**3)/(12*(1-.3**2)))
        CALL STIFPROP(B,T,E,STYPE,TS,HS,AS,ZIS,ZZS,YS)
        CALL AXIALF(A,D,T,E,TAO,SIGC,SIGB,AS,PS)
        CALL MOMENT(A,D,T,E,NUMSTFN,TAO,SIGC,SIGB,
     +              WOS,YS,ZMPK,ZMOV,ZMS)
        RETURN
      ELSE
        HSI0=HSI0/2.
        GO TO 34
      END IF
      END
C
      SUBROUTINE STRESS(A,D,T,STYPE,PS,ZMS,TS,HS,AS,ZZS,SIGS)
      IMPLICIT REAL*8 (A-H,O-Z)
      CHARACTER STYPE
      DA=D/A
      IF (STYPE.EQ.'2') THEN
          SIGS=ZMS/ZZS+PS/AS
      ELSE IF (STYPE.EQ.'1') THEN
        ZE=(HS+T)/2.
        IF (DA.LE.2.) THEN
          SIGS=PS/AS+(ZMS-PS*ZE)/ZZS
        ELSE
          SIGSC=PS/AS+(ZMS+PS*ZE)/ZZS
          SIGST=-PS/AS+(ZMS+PS*ZE)/ZZS
          SIGS=SIGSC
          IF (SIGS.LT.SIGST) SIGS=SIGST
        END IF
      END IF
      END
C
      SUBROUTINE STIFFNESS(A,D,T,E,NUMSTFN,WOS,ZMPK,TAO,SIGC,
     +            SIGB,STYPE,TS,HS0,HS,YS,PS,ZMOV,ZMS,WSA)
      IMPLICIT REAL*8(A-H,O-Z)
      CHARACTER STYPE
      PI=3.141592654
      B=A
      IF (D.LT.A) B=D
```

```
      CALL WSALLOW(A,D,STYPE,WSA)
      ERROR=.0001
      HSI0=HS0
44    HSI=HSI0
      HSJ=2*HSI
      HSINC=HSI
43    CALL STIFPROP(B,T,E,STYPE,TS,HSJ,ASJ,ZISJ,ZZSJ,YSJ)
      CALL AXIALF(A,D,T,E,TAO,SIGC,SIGB,ASJ,PSJ)
      CALL MOMENT(A,D,T,E,NUMSTFN,TAO,SIGC,SIGB,
     +            WOS,YSJ,ZMPK,ZMOVJ,ZMSJ)
      CALL STIFFDEF(A,D,T,E,STYPE,PSJ,ZMSJ,HSJ,ZISJ,WSJ)
      IF (WSJ.EQ.WSA) GO TO 41
      IF (WSJ.LT.WSA) GO TO 42
      HSJ=HSJ+HSINC
      GOTO 43
42    HSK=(HSJ+HSI)/2.0
      CALL STIFPROP(B,T,E,STYPE,TS,HSK,ASK,ZISK,ZZSK,YSK)
      CALL AXIALF(A,D,T,E,TAO,SIGC,SIGB,ASK,PSK)
      CALL MOMENT(A,D,T,E,NUMSTFN,TAO,SIGC,SIGB,
     +            WOS,YSK,ZMPK,ZMOVK,ZMSK)
      CALL STIFFDEF(A,D,T,E,STYPE,PSK,ZMSK,HSK,ZISK,WSK)
      IF (WSK.LT.WSA) THEN
        HSJ=HSK
        ZISJ=ZISK
      ELSE IF(WSK.GT.WSA) THEN
        HSI=HSK
        ZISI=ZISK
      END IF
      HSACC=(HSJ-HSI)*100./HSJ
      IF(HSACC.LT.ERROR) GO TO 41
      GO TO 42
41    IF (HSJ.GT.(HSI0+ERROR)) THEN
        HS=HSJ
          YS=E*ZISJ/(B*E*(T**3)/(12.*(1-.3**2)))
        CALL STIFPROP(B,T,E,STYPE,TS,HS,AS,ZIS,ZZS,YS)
        CALL AXIALF(A,D,T,E,TAO,SIGC,SIGB,AS,PS)
        CALL MOMENT(A,D,T,E,NUMSTFN,TAO,SIGC,SIGB,
     +              WOS,YS,ZMPK,ZMOV,ZMS)
        RETURN
      ELSE
        HSI0=HSI0/2.
        GO TO 44
      END IF
      END
C
      SUBROUTINE STIFFDEF(A,D,T,E,STYPE,PS,ZMS,HS,ZIS,WS)
      IMPLICIT REAL*8 (A-H,O-Z)
      CHARACTER STYPE
      PI=3.141592654
      DA=D/A
      IF (STYPE.EQ.'1') THEN
        ZE=(HS+T)/2.
C       ZMS1=ZMS-PS*ZE
        IF (DA.LE.2.) THEN
          ZMS1=ZMS-PS*ZE
        ELSE
          ZMS1=ZMS+PS*ZE
        END IF
      ELSE IF (STYPE.EQ.'2') THEN
```

```
        ZMS1=ZMS
      END IF
      WS=ZMS1*(D**2)/(E*ZIS*(PI**2))
      END
C
      SUBROUTINE WSALLOW(A,D,STYPE,WSA)
      IMPLICIT REAL*8   (A-H,O-Z)
      CHARACTER STYPE
      DA=D/A
      AD=A/D
      B=A
      IF (D.LT.A) B=D
      IF (DA.LE.2.) THEN
        WSA=D/500.*(B/D)
      ELSE IF ((DA.GT.2.).AND.(DA.LT.3.)) THEN
        WSA=D/4000.*(7.-6.*AD)
      ELSE IF (DA.GE.3.) THEN
        WSA=D/800.
      END IF
      IF (STYPE.EQ.'1') WSA=WSA*2.
      END
C
      SUBROUTINE OUTPUT(ZMPKND,ZMPK,STYPE,TS,HSZ,YZ,PSZ,ZMOVZ,ZMSZ,
     +            HSI,YI,PSI,ZMOVI,ZMSI,WSA,TDU,SIGCU,SIGBU)
      IMPLICIT REAL*8   (A-H,O-Z)
      CHARACTER STYPE
      WRITE(6,50) TDU
50    FORMAT(//'         Tu/Ty = ',E20. 12)
      WRITE(6,60) SIGCU
60    FORMAT('       SIGcu/SIGy = ',E20. 12)
      WRITE(6,70) SIGBU
70    FORMAT('       SIGbu/SIGy = ',E20. 12)
C
      WRITE(6,130) ZMPKND
130   FORMAT(/'        Mpkb/Dt = ',E20. 12)
      WRITE(6,140) ZMPK
140   FORMAT('       Mpk (N.mm) = ',E20. 12)
      WRITE(6,180) WSA
180   FORMAT('       Wsu,a (mm) = ',E20. 12)
C
      IF (STYPE.EQ.'2') THEN
        WRITE(6,200)
200     FORMAT(//6X,'Double-sided flat bar stiffeners 2hs*ts :')
      ELSE IF (STYPE.EQ.'1') THEN
        WRITE(6,210)
210     FORMAT(//6X,'Single-sided flat bar stiffeners hs*ts :')
      END IF
      IF (TS.GT.0) THEN
        WRITE(6,220) TS
220     FORMAT(/'         TS (mm) = ',E20. 12)
      ELSE
        WRITE(6,230)
230     FORMAT(/'         TS = hs/10')
      END IF
      WRITE(6,240) HSZ
240   FORMAT(/'       HSz (mm) = ',E20. 12)
      WRITE(6,250) YZ
250   FORMAT('        PSIz = ',E20. 12)
      WRITE(6,260) PSZ
```

```
260   FORMAT('          Psz (N) = ',E20. 12)
      WRITE(6,270) ZMOVZ
270   FORMAT('          Movz (N*mm) = ',E20. 12)
      WRITE(6,280) ZMSZ
280   FORMAT('          Msz (N*mm) = ',E20. 12)
      WRITE(6,290) HSI
290   FORMAT(/'          HSi (mm) = ',E20. 12)
      WRITE(6,300) YI
300   FORMAT('          PSIi = ',E20. 12)
      WRITE(6,310) PSI
310   FORMAT('          Psi (N) = ',E20. 12)
      WRITE(6,320) ZMOVI
320   FORMAT('          Movi (N*mm) = ',E20. 12)
      WRITE(6,350) ZMSI
350   FORMAT('          Msi (N*mm) = ',E20. 12)
      END
```

BRIT. LONDON UNIV.